

UNCLASSIFIED

AD NUMBER
ADB212813
NEW LIMITATION CHANGE
TO Approved for public release, distribution unlimited
FROM Distribution authorized to U.S. Gov't. agencies and their contractors; Critical Technology; Jan 1996. Other requests shall be referred to WL/FIGC, 2210 Eight St., Suite 11, WPAFB, OH 45433
AUTHORITY
AFRL Ltr., 14 Sep 99

THIS PAGE IS UNCLASSIFIED

WL-TR-96-3043



INNOVATIVE CONTROL EFFECTORS (ICE)

Kenneth M. Dorsett
David R. Mehl

*Lockheed Martin Tactical Aircraft Systems
P.O. Box 748
Fort Worth TX 76101-0748*

JANUARY 1996

FINAL REPORT FOR SEPTEMBER 1994 - JANUARY 1996

Distribution authorized to U.S. Government agencies and their contractors,
Critical Technology; Jan 1996. Other requests for this document shall be
referred to: WL/FIGC, 2210 Eighth St, Suite 11, WPAFB OH 45433-7521

WARNING - This document contains technical data whose export is restricted by the Arms Export Control Act (Title 22, U.S.C., Sec 2751, et seq.) or the Export Administration Act of 1979, as amended, Title 50, U.S.C., App. 2401, et seq. Violations of these export laws are subject to severe criminal penalties. Disseminate in accordance with the provisions of DOD Dir. 5230.25. (Include this statement with any reproduced portions.)

DESTRUCTION NOTICE: Destroy by any method that will prevent disclosure of contents or reconstruction of the document.

FLIGHT DYNAMICS DIRECTORATE
WRIGHT LABORATORY
AIR FORCE MATERIEL COMMAND
WRIGHT-PATTERSON AIR FORCE BASE, OHIO 45433-7562

19960730 139

DTIC QUALITY INSPECTED 1

NOTICE

WHEN GOVERNMENT DRAWINGS, SPECIFICATIONS, OR OTHER DATA ARE USED FOR ANY PURPOSE OTHER THAN IN CONNECTION WITH A DEFINITE GOVERNMENT-RELATED PROCUREMENT, THE UNITED STATES GOVERNMENT INCURS NO RESPONSIBILITY OR ANY OBLIGATION WHATSOEVER. THE FACT THAT THE GOVERNMENT MAY HAVE FORMULATED OR IN ANY WAY SUPPLIED THE SAID DRAWINGS, SPECIFICATIONS, OR OTHER DATA, IS NOT TO BE REGARDED BY IMPLICATION, OR OTHERWISE IN ANY MANNER CONSTRUED, AS LICENSING THE HOLDER, OR ANY OTHER PERSON OR CORPORATION; OR AS CONVEYING ANY RIGHTS OR PERMISSION TO MANUFACTURE, USE, OR SELL ANY PATENTED INVENTION THAT MAY IN ANY WAY BE RELATED THERETO.

This technical report has been reviewed and is accepted for publication.



WILLIAM J. GILLARD
Project Engineer
Control Dynamics Branch



SIVA S. BANDA, Chief
Control Dynamics Branch
Flight Control Division



DAVID P. LEMASTER, Chief
Flight Control Division
Flight Dynamics Directorate

If your address has changed, if you wish to be removed from our mailing list, or if the addressee is no longer employed by your organization, please notify WL/FIGC, 2210 Eighth St. Suite 11, WPAFB OH 45433-7521 to help maintain a current mailing list.

Copies of this report should not be returned unless return is required by security considerations, contractual obligations, or notice on a specific document.

The following notice applies to any unclassified (including originally classified and now declassified) technical reports released to "qualified U.S. contractors" under the provisions of DoD Directive 5230.25, Withholding of Unclassified Technical Data From Public Disclosure.

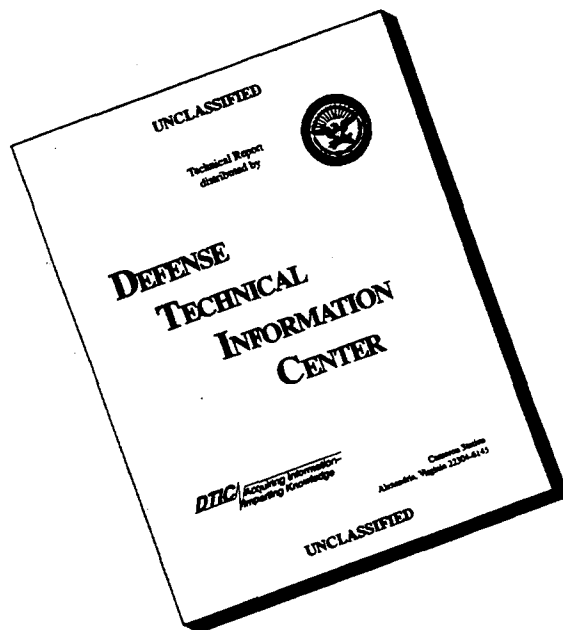
NOTICE TO ACCOMPANY THE DISSEMINATION OF EXPORT-CONTROLLED TECHNICAL DATA

1. Export of information contained herein, which includes, in some circumstances, release to foreign nationals within the United States, without first obtaining approval or license from the Department of State for items controlled by the International Traffic in Arms Regulations (ITAR), or the Department of Commerce for items controlled by the Export Administration Regulations (EAR), may constitute a violation of law.
2. Under 22 U.S.C. 2778 the penalty for unlawful export of items or information controlled under the ITAR is up to two years imprisonment, or a fine of \$100,000, or both. Under 50 U.S.C., Appendix 2410, the penalty for unlawful export of items or information controlled under the EAR is a fine of up to \$1,000,000, or five times the value of the exports, whichever is greater; or for an individual, imprisonment of up to 10 years, or a fine of up to \$250,000, or both.
3. In accordance with your certification that establishes you as a "qualified U.S. Contractor", unauthorized dissemination of this information is prohibited and may result in disqualification as a qualified U.S. contractor, and may be considered in determining your eligibility for future contracts with the Department of Defense.
4. The U.S. Government assumes no liability for direct patent infringement, or contributory patent infringement or misuse of technical data.
5. The U.S. Government does not warrant the adequacy, accuracy, currency, or completeness of the technical data.
6. The U.S. Government assumes no liability for loss, damage, or injury resulting from manufacture or use for any purpose of any product, article, system, or material involving reliance upon any or all technical data furnished in response to the request for technical data.
7. If the technical data furnished by the Government will be used for commercial manufacturing or other profit potential, a license for such use may be necessary. Any payments made in support of the request for data do not include or involve any license rights.
8. A copy of this notice shall be provided with any partial or complete reproduction of these data that are provided to qualified U.S. contractors.

D E S T R U C T I O N N O T I C E

For classified documents, follow the procedures in DoD 5200.22-M, Industrial Security Manual, Section II-19 or DoD 5200.1-R, Information Security Program Regulation, Chapter IX. For unclassified, limited documents, destroy by any method that will prevent disclosure of contents or reconstruction of the document.

DISCLAIMER NOTICE



THIS DOCUMENT IS BEST QUALITY AVAILABLE. THE COPY FURNISHED TO DTIC CONTAINED A SIGNIFICANT NUMBER OF PAGES WHICH DO NOT REPRODUCE LEGIBLY.

REPORT DOCUMENTATION PAGE			Form Approved OMB No. 0704-0188	
Public reporting burden for this collection of information is estimated to average 1 hour per response, including the time for reviewing instructions, searching existing data sources, gathering and maintaining the data needed, and completing and reviewing the collection of information. Send comments regarding this burden estimate or any other aspect of this collection of information, including suggestions for reducing this burden, to Washington Headquarters Services, Directorate for Information Operations and Reports, 1215 Jefferson Davis Highway, Suite 1204, Arlington, VA 22202-4302, and to the Office of Management and Budget, Paperwork Reduction Project (0704-0188), Washington, DC 20503.				
1. AGENCY USE ONLY (Leave blank)		2. REPORT DATE January 1996		3. REPORT TYPE AND DATES COVERED FINAL 09/30/94 - 01/01/96
4. TITLE AND SUBTITLE INNOVATIVE CONTROL EFFECTORS (ICE)			5. FUNDING NUMBERS C F33615-94-C-3610 PE 62201F PR 2403 TA 05 WU 9B	
6. AUTHOR(S) Kenneth M. Dorsett David R. Mehl				
7. PERFORMING ORGANIZATION NAME(S) AND ADDRESS(ES) Lockheed Martin Tactical Aircraft Systems P.O. Box 748 Fort Worth TX 76101-0748			8. PERFORMING ORGANIZATION REPORT NUMBER FZM-8394	
9. SPONSORING / MONITORING AGENCY NAME(S) AND ADDRESS(ES) Flight Dynamics Directorate Wright Laboratory Air Force Materiel Command Wright-Patterson AFB OH 45433-7562			10. SPONSORING / MONITORING AGENCY REPORT NUMBER WL-TR-96-3043	
11. SUPPLEMENTARY NOTES Export Restrictions Apply				
12a. DISTRIBUTION / AVAILABILITY STATEMENT Distribution authorized to U.S. Government agencies and their contractors; Critical Technology; Jan 1996. Other requests for this document shall be referred to WL/FIGC, 2210 Eighth St, Suite 11, Wright-Patterson OH 45433-7521			12b. DISTRIBUTION CODE C	
13. ABSTRACT (Maximum 200 words) This report describes a joint U.S. Air Force - U.S. Navy sponsored investigation of innovative aerodynamic control concepts for fighter aircraft without vertical tails. Land-based and carrier-based configurations were analyzed to determine the flying qualities, performance, and aircraft-level integration impacts of the innovative controls. Five control concepts were evaluated for their potential to provide sufficient lateral-directional control power to a highly maneuverable tailless fighter. They were: (1) all-moving wing tip (AMT); (2) spoiler-slot-deflector (SSD); (3) differential leading edge flaps (DLEF); (4) deployable rudder; (5) lower surface spoiler. After a preliminary screening, only the first three were pursued for further investigation. Detailed evaluations of the three selected controllers against baseline tailless fighter configurations employing "conventional" control concepts (e.g., spoilers, clamshells, etc.) included low-speed, high-speed, and high AOA flying qualities performance, structural weight and subsystem integration impacts, signature performance, carrier suitability, and range/transonic acceleration impacts. The AMT was evaluated as the best all-round control effector of those investigated. The SSD and DLEF were ranked 2nd and 3rd, respectively.				
14. SUBJECT TERMS Tailless Aircraft, Lateral-Directional Control Power, Flight Control Effectors, All Moving Wing Tips, Spoiler-Slot-Deflector, Differential Leading Edge Flaps, Deployable Rudder, Lower Surface Spoiler, Effector Integration			15. NUMBER OF PAGES 403	
			16. PRICE CODE	
17. SECURITY CLASSIFICATION OF REPORT UNCLASSIFIED	18. SECURITY CLASSIFICATION OF THIS PAGE UNCLASSIFIED	19. SECURITY CLASSIFICATION OF ABSTRACT UNCLASSIFIED	20. LIMITATION OF ABSTRACT SAR	

Summary

The Innovative Control Effectors (ICE) program was jointly sponsored by Wright Laboratory (WL/FIGC) and the Naval Air Warfare Center Aircraft Division (NAWCAD) to investigate innovative aerodynamic control concepts for fighter aircraft without vertical tails. Land-based and carrier-based configurations were analyzed to determine the flying qualities, performance, and airplane-level integration impacts of the innovative controls.

Five control concepts were evaluated for their potential to provide sufficient lateral-directional control power to a highly maneuverable tailless fighter. They were: (1) all-moving wing tip (AMT); (2) spoiler-slot-deflector (SSD); (3) differential leading edge flaps (DLEF); (4) deployable rudder (DRUD); (5) lower surface spoiler (LSP). The first three concepts were selected as having the greatest potential following a screening study.

Detailed evaluations of the three selected controllers against baseline tailless fighter configurations employing "conventional" control concepts (e.g., spoilers, clamshells, etc.) included low-speed, high-speed and high AOA flying qualities performance, structural weight and subsystem integration impacts, signature performance, carrier suitability, and range/transonic acceleration impacts. The AMT was evaluated as the best all-round control effector of those investigated. The SSD and DLEF ranked 2nd and 3rd, respectively. Land-based and carrier-based configurations employing the AMT for yaw control in place of more conventional control concepts realized a 700 lbs and 400 lbs weight savings, respectively. Furthermore, these configurations enjoyed a 16% and 21% range improvement over their respective baselines.

Radar cross-section (RCS) performance evaluations were completed using computational analysis tools. RCS models with undeflected and deflected control surfaces were analyzed. Configurations employing the AMT and SSD performed well considering no control deflections. The AMT configuration performed well compared to the baseline RCS model when the control surfaces were deflected; whereas the SSD configuration performed poorly. These evaluations did not include the effects of material treatments,

hinges, pivot trunions or other actuation details that will make integration for low-RCS challenging.

Future work should focus on: (1) structural modeling to evaluate the aeroelastic effects on AMT and SSD control effectiveness; (2) additional detailed RCS testing and analysis to evaluate the effects of actuation details on RCS performance as well as potential material treatment suites to maintain signature performance; and (3) low-speed, transonic and rotary balance wind tunnel testing to refine the aerodynamic database for the selected innovative control effectors.

Forward

The Innovative Control Effectors (ICE) program was sponsored jointly by Wright Laboratory FIGC at Wright Patterson AFB, Ohio and the Naval Air Warfare Center Aircraft Division (NAWCAD) located in Warminster, Pennsylvania. The USAF program manager and technical monitor was Mr. William Gillard. The Navy program manager and technical monitor was Mr. Steve Hynes. This work was performed under USAF contract number F33615-94-C-3610 between September 1994 and January 1996.

The Lockheed Martin Tactical Aircraft Systems (LMTAS) program manager was Mr. Kenneth M. Dorsett. Many people supplied their time and technical talents to this effort. The principle investigators are listed below:

- Stability & Control Analysis—Ken Dorsett, Patrick Forner, Alan Albright
- Control Law Design & Analysis—Naji Yakzan, John Bessolo, John Virnig
- Configuration Design—Gary Anderson, Brian Kiger, Mark Witte, Ron Stroud
- Signature Integration—Dave Mehl
- Aeromechanics—Bert Webb
- Flight Mechanics—Mike Yokell
- Mass Properties—Doug McMahon, Doug Sanders
- Structural Integration and Analysis—Bill Benner, Phil Perdan, Mike Henson, Carl Fink
- Hydraulic System Analysis—Darwin White, Ted Savard
- Technical Advisory Group—Russ Killingsworth, Fred Robertson, Spence Peters
- Engineering Administration—Bill Thias
- Editing and Technical Content—Chris Stewart

Table of Contents

<i>Summary</i>	<i>ii</i>
<i>Forward</i>	<i>iv</i>
<i>Table of Contents</i>	<i>v</i>
<i>List of Figures</i>	<i>viii</i>
<i>List of Tables</i>	<i>xxii</i>
<i>List of Symbols</i>	<i>xxiv</i>
1 Introduction	1
1.1 Background	2
1.2 Scope of the Study	4
1.3 The Need for Aerodynamic Yaw Power	5
1.4 Previous Research	7
1.5 ICE Study Approach	8
2 Control Power Analysis Methodology	11
2.1 CPR	11
2.2 CPA	16
2.3 Conceptual Design Process Using Control Power Analysis Tools	20
3 Vehicle/Effector Selection	21
3.1 Description of Control Effectors	23
4 Control Power Requirements and Baseline Evaluation	73
4.1 Maneuver Requirements	73
4.2 Flight Conditions	76
4.3 Configuration 101-Series Baseline Evaluation	77

4.4 Configuration 201-Series Baseline Evaluation	89
5 Initial Evaluation of Innovative Controls -- Derivative Configurations	113
6 Effector Performance Study	122
6.1 101-Series Maneuver Performance Evaluation	122
6.2 Control Power Analysis with Innovative Controls on 201-Series Configurations	148
7 Integration Study	162
7.1 Flight Control Actuator Requirements	162
7.2 Hydraulic System Requirements	174
7.3 Structural Integration	178
7.4 Detailed Structural Assessment of Selected Configurations	188
7.5 Weight Impacts	205
7.6 Up and Away Performance Impacts	212
7.7 Flight Control System Design Requirements	213
7.8 Transition of Innovative Controllers to Other Configurations	217
7.9 Signature Integration Studies	226
7.10 Carrier Suitability Impacts	241
7.11 Reliability, Maintainability and Supportability (RM&S) Assessment	242
7.12 External Stores Carriage Assessment	246
7.13 Control Summaries	247
8 Risk Reduction Plans	251
8.1 Plan for Phase II	252
8.2 Wind Tunnel Model Requirements	254
8.3 Wind Tunnel Test Plans	259

8.4 Post-Test Analysis & Documentation	264
9 Conclusions and Recommendations	266
10 References	270
11 APPENDIX A: Aerodynamic Data Sources	274
11.1 Wind Tunnel Test Data	274
11.2 Hinge Moment Data	276
11.3 Aeroelastic Effects	277
11.4 Dynamic Derivatives	279
11.5 Modifications to the 101-Series Pitching Moment Data	279
11.6 References	282
12 APPENDIX B: ADF Wind Tunnel Data Evaluation	284
12.1 ADF Repeatability	284
12.2 Test-to-Test Comparisons	286
12.3 Summary	297
12.4 References	298
13 APPENDIX C: Configuration 201 Aerodynamic Data Analysis	299
13.1 Longitudinal Data Analysis	301
13.2 Comparison of Wind Tunnel Data with HASC Predictions	310
13.3 Longitudinal Trim Analysis	315
13.4 Lateral-Directional Stability	319
13.5 Control Effectiveness	328
13.6 References	346
14 Appendix D: RCS Data	347

List of Figures

<i>Figure 1-1 High AOA Agility and Low Observability Combine to Force Technology into the Corners of the Envelope</i>	2
<i>Figure 1-2 Land-Based Baseline Configuration (101-Series)</i>	3
<i>Figure 1-3 Carrier-Based Baseline Configuration (201-Series)</i>	4
<i>Figure 1-4 Aerodynamic Control Power is More Effective Than TV Control Through a Large Portion of the Flight Envelope</i>	6
<i>Figure 1-5 ICE Study Approach</i>	10
<i>Figure 2-1 CPR is a Preliminary Design Simulation Tool</i>	11
<i>Figure 2-2 Pitch Flight Control System</i>	14
<i>Figure 2-3 Lateral-Axis Control System</i>	14
<i>Figure 2-4 Directional-Axis Control System</i>	15
<i>Figure 2-5 Lateral-Directional Mixer</i>	15
<i>Figure 2-6 Example CPA Results</i>	18
<i>Figure 2-7 Example CPA Control Power Boundary Data</i>	19
<i>Figure 2-8 Conceptual Design Process Using Control Power Analysis Tools</i>	20
<i>Figure 3-1 Configuration 101-Series -- USAF Baseline</i>	22
<i>Figure 3-2 Configuration 201-Series -- USN Baseline</i>	23
<i>Figure 3-3 Clamshell Control Effectiveness</i>	25
<i>Figure 3-4 Clamshell Effectiveness at Varying Hingeline Sweeps</i>	26
<i>Figure 3-5 Clamshell Effectiveness vs Deflection</i>	27
<i>Figure 3-6 Clamshell Effectiveness at Sideslip</i>	29
<i>Figure 3-7 Aft Swept Spoilers Provide Greater Yaw Capability</i>	31

<i>Figure 3-8 Spoiler Control Effectiveness for 65-deg Sweep Tailless Fighter</i>	32
<i>Figure 3-9 Windward Sideslip Degrades Spoiler Effectiveness</i>	33
<i>Figure 3-10 Spoiler Deflections Cause Adverse Interactions with Trailing Edge Flaps</i>	35
<i>Figure 3-11 AMT Control Effectiveness</i>	37
<i>Figure 3-12 AMT Yaw Effectiveness is Linear with Deflection</i>	39
<i>Figure 3-13 AMT Control Effectiveness is Relatively Unaffected by Sideslip</i>	41
<i>Figure 3-14 AMT Control Effectiveness to Hinge Moment Ratios are Much Greater than a Conventional Trailing Edge Flap</i>	42
<i>Figure 3-15 Differential LEF Effectiveness</i>	43
<i>Figure 3-16 Increased Suction on the LEF Contributes to the Yawing Moment</i>	44
<i>Figure 3-17 Inboard LEF Aerodynamic Interaction with Outboard LEF</i>	45
<i>Figure 3-18 DLEF Effectiveness vs Deflection</i>	46
<i>Figure 3-19 DLEF Effectiveness with Windward Sideslip</i>	48
<i>Figure 3-20 DLEF Effectiveness with Leeward Sideslip</i>	49
<i>Figure 3-21 Differential LEF Improve Directional Stability</i>	50
<i>Figure 3-22 DLEF Effectiveness is Degraded at Transonic Mach Numbers</i>	51
<i>Figure 3-23 Limiting DLEF to Positive Deflections on one Side Reduces the Yaw Control Power Available</i>	52
<i>Figure 3-24 The SSD Provides Greater Lateral-Directional Control Power to Higher AOA than Conventional Spoilers</i>	54
<i>Figure 3-25 The SSD Generates More Lateral-Directional Control Power than a Conventional Spoiler at Transonic Mach Numbers</i>	55
<i>Figure 3-26 The Spoiler and Deflector Can be Mechanically Linked to a Single Actuator Resulting in Lower Overall Hinge Moments</i>	56

<i>Figure 3-27 The SSD Improves the Linearity of Response with Deflection over a Conventional Spoiler</i>	57
<i>Figure 3-28 The SSD Degrades Elevon Control Effectiveness</i>	59
<i>Figure 3-29 The SSD Places a Higher Demand on Elevon Control Power to Trim out Nose-Up Control Interactions</i>	60
<i>Figure 3-30 The Deployable Rudder Generates Yawing Moment Through Side Forces and Axial Forces Acting on the Surface</i>	62
<i>Figure 3-31 DRUD Control Effectiveness</i>	63
<i>Figure 3-32 DRUD Effectiveness vs Deflection</i>	64
<i>Figure 3-33 Lower Surface DRUD Effectiveness</i>	65
<i>Figure 3-34 DRUD has Negligible Directional Stabilizing Tendencies</i>	66
<i>Figure 3-35 Windward Sideslip Adversely Affects DRUD Effectiveness at High AOA</i>	67
<i>Figure 3-36 LSP Control Effectiveness is a Strong Function of AOA</i>	69
<i>Figure 3-37 Longitudinal Effects due to LSP Deflections</i>	70
<i>Figure 3-38 Sideslip Effects on LSP</i>	71
<i>Figure 3-39 Interaction of LSP with Elevons</i>	72
<i>Figure 4-1: ICE Roll Performance Goals</i>	74
<i>Figure 4-2 ICE Flight Conditions</i>	77
<i>Figure 4-3 Configuration 101 Control Power Requirements</i>	78
<i>Figure 4-4 Planview of Configuration 101</i>	81
<i>Figure 4-5 Configuration 101 Control Power Available vs Required at 30 deg AOA</i>	82
<i>Figure 4-6 Configuration 101-Series Roll Performance Summary</i>	83
<i>Figure 4-7 Configuration 101-TV Planview</i>	84
<i>Figure 4-8 Yaw Vectoring Side Force Required to Match Conventional Rudder Power</i>	85

<i>Figure 4-9 Controls Usage for Maximum Roll Power</i>	87
<i>Figure 4-10 Configuration 101 and 101-TV Augmented Directional Stability Characteristics</i>	88
<i>Figure 4-11 Canards Analyzed on Configuration 201</i>	91
<i>Figure 4-12 The Canard was Scheduled to Maintain Adequate Control Margin at High AOA</i>	92
<i>Figure 4-13: Effect of Symmetric Aileron on Trim</i>	93
<i>Figure 4-14 LEF Deflections Improve Lateral-Directional Stability</i>	94
<i>Figure 4-15 Configuration 201 Trimmed Lift Data</i>	95
<i>Figure 4-16 Launch Time History at 10' Sink Speed</i>	96
<i>Figure 4-17 Pop-up Maneuver Time History</i>	98
<i>Figure 4-18 Waveoff Time History</i>	99
<i>Figure 4-19 Roll Performance Generates the Greatest Control Power Requirements at Power Approach Conditions</i>	100
<i>Figure 4-20 Thrust Vectoring Provides Excess Control Power for Launch Roll Performance</i>	101
<i>Figure 4-21 Configuration 201-Series Power Approach Control Power Requirements</i>	102
<i>Figure 4-22 Thrust Vectoring Provides Large Improvements in the Launch WOD Required for Level 1 Flying Qualities</i>	103
<i>Figure 4-23 Insufficient Yaw Power is Available to Coordinate the Roll Power on Configuration 201</i>	104
<i>Figure 4-24 Thrust Vectoring at Idle Power Provides Small Improvements to PA Roll Performance</i>	105
<i>Figure 4-25 Thrust Vectoring Provides no Trimmed Lift Benefits over the Baseline High Lift Configuration</i>	106

<i>Figure 4-26 Thrust Vectoring in Mil-Power Provides Great Improvements to Nose Wheel Liftoff Performance</i>	<i>108</i>
<i>Figure 4-27 Single Engine Controllability is More Critical for Configurations without TV</i>	<i>109</i>
<i>Figure 4-28 Yaw Control Deflections Significantly Impact SEROC Performance</i>	<i>110</i>
<i>Figure 4-29 Maximum Coordinated Roll Control Power</i>	<i>111</i>
<i>Figure 4-30 Augmented Directional Stability Characteristics</i>	<i>112</i>
<i>Figure 5-1 Six Innovative Control Suites were Defined for the Initial Screening</i>	<i>113</i>
<i>Figure 5-2 An Iterative Process was used to Yield Six Configurations with Similar Maneuver Capabilities</i>	<i>114</i>
<i>Figure 5-3 Configuration 101-1 Control Layout</i>	<i>115</i>
<i>Figure 5-4 Configuration 101-2 Control Layout</i>	<i>115</i>
<i>Figure 5-5 Configuration 101-3 Control Layout</i>	<i>116</i>
<i>Figure 5-6 Configuration 101-4 Control Layout</i>	<i>116</i>
<i>Figure 5-7 Configuration 101-5 Control Layout</i>	<i>117</i>
<i>Figure 5-8 Configuration 101-6 Control Layout</i>	<i>117</i>
<i>Figure 5-9 Roll Performance at Three Flight Conditions for Six Innovative Control Suites</i>	<i>118</i>
<i>Figure 5-10 Augmented Directional Stability with Aerodynamic Controls Only</i>	<i>119</i>
<i>Figure 5-11 Aerodynamic Nose-Down Pitch Capability at 30 deg AOA</i>	<i>119</i>
<i>Figure 5-12 Configuration Weight Changes Due to Varying Control Suite</i>	<i>120</i>
<i>Figure 5-13 Final Trade Study Ranking Results</i>	<i>121</i>
<i>Figure 6-1 AMT Control Effectiveness Trend with Mach Number</i>	<i>123</i>
<i>Figure 6-2 SSD Control Effectiveness Trend with Mach Number</i>	<i>124</i>

<i>Figure 6-3 101-Series Roll Performance Summary</i>	<i>125</i>
<i>Figure 6-4 High Speed Control Power Requirements vs Control Power Available</i>	<i>128</i>
<i>Figure 6-5 Configuration 101-1 High-Speed Step Sideslip Time History</i>	<i>129</i>
<i>Figure 6-6 Low-Speed Yaw Augmentation Capabilities</i>	<i>130</i>
<i>Figure 6-7 High AOA Roll Performance</i>	<i>131</i>
<i>Figure 6-8 Crosswind Landing Control Requirements</i>	<i>133</i>
<i>Figure 6-9 Geometry of Crosswind Landing in Crabbed Attitude</i>	<i>134</i>
<i>Figure 6-10 Static Analysis of Crosswind Landing Rollout</i>	<i>135</i>
<i>Figure 6-11 Crosswind Landing 2-Point Attitude Control Requirements</i>	<i>136</i>
<i>Figure 6-12 All Five Control Suites Can Achieve Level 1 Crosswind Capability</i>	<i>137</i>
<i>Figure 6-13 Innovative Control Power Trade Offs</i>	<i>140</i>
<i>Figure 6-14 Effect of Varying AMT Deflection Limits on Coordinated Roll Power Available</i>	<i>142</i>
<i>Figure 6-15 Effect of Varying AMT Deflection Limits on Lateral-Directional Augmentation</i>	<i>143</i>
<i>Figure 6-16 Effect of AMT Deflection Limits at High Speed</i>	<i>144</i>
<i>Figure 6-17 The SSD/Elevon Interaction Adversely Affects Control Power Available</i>	<i>145</i>
<i>Figure 6-18 Decoupling the SSD Improves Lateral-Directional Control Power Available</i>	<i>146</i>
<i>Figure 6-19 Greater Pitch Authority Increased Deflector Usage at All AOA</i>	<i>147</i>
<i>Figure 6-20 Increased Pitch Power Resulted in Greater Lateral-Directional Capability on Configuration 101-1</i>	<i>148</i>
<i>Figure 6-21 Configuration 201-Series Control Suites</i>	<i>149</i>
<i>Figure 6-22 Power Approach Roll Capabilities at Idle Power</i>	<i>151</i>
<i>Figure 6-23 Increased AMT Size Significantly Improved PA Roll Performance</i>	<i>151</i>

<i>Figure 6-24: Configuration 201-1</i>	<i>152</i>
<i>Figure 6-25 Configuration 201-3</i>	<i>153</i>
<i>Figure 6-26 Configuration 201-4</i>	<i>154</i>
<i>Figure 6-27 Control Deflections Required for Maximum Coordinated PA Roll</i>	<i>155</i>
<i>Figure 6-28 Variation of WOD Required for Level 1 FQ with Bring Back Weight at Trim Power and AOA</i>	<i>156</i>
<i>Figure 6-29 Increased Throttle Settings Provide Significant Improvements to PA Roll Performance on Configuration 201-1</i>	<i>157</i>
<i>Figure 6-30 High AOA Roll Coordinated Roll Control Power Available</i>	<i>158</i>
<i>Figure 6-31 Low-Speed Augmented Lateral-Directional Stability Characteristics</i>	<i>159</i>
<i>Figure 6-32 Augmented Directional Stability Characteristics using Max A/B TV</i>	<i>159</i>
<i>Figure 6-33 Roll Performance at 30 deg AOA</i>	<i>160</i>
<i>Figure 6-34 Aft cg Limits for 201-Series Configurations</i>	<i>161</i>
<i>Figure 7-1 Control Power Required vs Virtual Control Rate Limit</i>	<i>164</i>
<i>Figure 7-2 Control Envelopes were Used to Determine Maximum Control Deflection Requirements at High Speeds</i>	<i>167</i>
<i>Figure 7-3 All Moving Control Surface Actuator Sizing Diagram</i>	<i>169</i>
<i>Figure 7-4 Example Control Surface Criticality Matrix</i>	<i>171</i>
<i>Figure 7-5 Total Hydraulic Flow Requirements -- Each System</i>	<i>174</i>
<i>Figure 7-6 Hydraulic Pump Size Requirements</i>	<i>175</i>
<i>Figure 7-7 Total Flight Control Actuator Displacement -- Each System</i>	<i>177</i>
<i>Figure 7-8 Configuration 101 Internal Arrangement</i>	<i>181</i>
<i>Figure 7-9 Configuration 101-TV Internal Arrangement</i>	<i>182</i>
<i>Figure 7-10 Configuration 101-1 Internal Arrangement</i>	<i>183</i>

<i>Figure 7-11 Configuration 101-2 Internal Arrangement</i>	184
<i>Figure 7-12 Configuration 101-3 Internal Arrangement</i>	185
<i>Figure 7-13 Configuration 101-4 Internal Arrangement</i>	186
<i>Figure 7-14 Configuration 101-5 Internal Arrangement</i>	187
<i>Figure 7-15 Configuration 101-6 Internal Arrangement</i>	188
<i>Figure 7-16 Final Configuration 101-TV Internal Arrangement</i>	190
<i>Figure 7-17 Final Configuration 101-1 Internal Arrangement</i>	191
<i>Figure 7-18 Final Configuration 101-3 Internal Arrangement</i>	192
<i>Figure 7-19 Final Configuration 101-4 Internal Arrangement</i>	193
<i>Figure 7-20 Configuration 101-4 AMT Integration</i>	194
<i>Figure 7-21 Three SSD Actuation Alternatives</i>	195
<i>Figure 7-22 Scissors Link SSD Actuation</i>	196
<i>Figure 7-23 Linear Actuator Driven SSD</i>	197
<i>Figure 7-24 Rotary Actuator Driven SSD</i>	198
<i>Figure 7-25 Simplified Four-Bar SSD Linkage</i>	199
<i>Figure 7-26 Isometric View of F-16 Derivative Wing FEM</i>	200
<i>Figure 7-27 Planform View of Wing Skin Model with Cutout for SSD Control Surfaces</i>	201
<i>Figure 7-28 Substructure Required Near and Inside Cutouts for SSD Control Surfaces</i>	204
<i>Figure 7-29 Configuration 101-Series Weights Build-up</i>	207
<i>Figure 7-30 Configuration 201-Series Weights Build-up</i>	208
<i>Figure 7-31 Zero-Fuel Weight Variations</i>	209
<i>Figure 7-32 Internal Fuel Weight Variations</i>	210
<i>Figure 7-33 Control Surface Weight Comparisons</i>	211

<i>Figure 7-34 Performance Impacts due to Innovative Control Concepts</i>	213
<i>Figure 7-35 Control Law Architecture</i>	214
<i>Figure 7-36 Control Allocation Evaluation</i>	215
<i>Figure 7-37 Maximum Throughput Requirements</i>	216
<i>Figure 7-38 HASC Models were used to Compute F/A-18 and F-14 Aerodynamics</i>	219
<i>Figure 7-39 The Flying Wing Configuration Offers the Least Amount of Directional Instability at Low AOA</i>	220
<i>Figure 7-40 Lateral-Directional Control Requirements for Various Configuration Classes</i>	221
<i>Figure 7-41 Conventional Example: F/A-18</i>	223
<i>Figure 7-42 Swing Wing Example: F-14</i>	224
<i>Figure 7-43 Tailless Delta Example: F-16XL</i>	225
<i>Figure 7-44 Tailless F-16XL High AOA Roll Performance</i>	226
<i>Figure 7-45 Target 19 RCS Model</i>	228
<i>Figure 7-46 Line Drawings of the Four Gap Configurations Studied</i>	230
<i>Figure 7-47 VISAGE Results for Target 19 Baseline at 9.7 GHz, 0 deg Elevation</i>	231
<i>Figure 7-48 MESSAGE Results for Configuration 101-1/Target 19 at 9.7 GHz, 0 deg Elevation</i>	232
<i>Figure 7-49 Scalar Sum of MESSAGE and VISAGE Results for Configuration 101-1/Target 19 at 9.7 GHz, 0 deg Elevation</i>	232
<i>Figure 7-50 5.4 GHz Frontal Sector Comparison with No Control Deflections</i>	233
<i>Figure 7-51 9.7 GHz Frontal Sector Comparison with No Control Deflections</i>	234
<i>Figure 7-52 16 GHz Frontal Sector Comparison with No Control Deflections</i>	234
<i>Figure 7-53 Target 19 Configuration Models with Deflected Controls</i>	237

<i>Figure 7-54 Configuration 101-1/Target 19 with Deflected Controls at 9.7 GHz, 0 deg Elevation</i>	238
<i>Figure 7-55 5.4 GHz Frontal Sector Comparison with Deflected Controls</i>	238
<i>Figure 7-56 9.7 GHz Frontal Sector Comparison with Deflected Controls</i>	239
<i>Figure 7-57 16 GHz Frontal Sector Comparison with Deflected Controls</i>	239
<i>Figure 7-58 Configuration 201-TV Clearance Requirements during Catapult Launch</i>	241
<i>Figure 7-59 Inverse Relationship Between Reliability and System Complexity</i>	244
<i>Figure 7-60 External Stores Carriage Area</i>	247
<i>Figure 7-61 Control Effector Summary</i>	249
<i>Figure 7-62 Innovative Control Suite Summary</i>	250
<i>Figure 8-1 Phase II Plan</i>	253
<i>Figure 8-2 Configuration 101-Series ADF Model Planform</i>	256
<i>Figure 8-3 Configuration 201-Series ADF Model Planform</i>	256
<i>Figure 8-4 1/18th Scale LMTAS Tailless Fighter Wind Tunnel Model</i>	258
<i>Figure 11-1 LMTAS Tailless Fighter Model in ADF Wind Tunnel</i>	275
<i>Figure 11-2 1/18th Scale Tailless Fighter Model in SARL Wind Tunnel</i>	276
<i>Figure 11-3 Tailless Fighter Model Exhibited Undesirable Pitch Characteristics</i>	280
<i>Figure 11-4 The Pitch Instability was Sensitive to Leading Edge Radius</i>	280
<i>Figure 11-5 ADF Data were used to Adjust the Pitching Moment Curve</i>	281
<i>Figure 11-6 The Configuration is Pitch Trim Limited at 50 deg AOA</i>	282
<i>Figure 12-1 ADF Repeatability -- Lift Coefficient</i>	285
<i>Figure 12-2 ADF Repeatability -- Pitching Moment Data</i>	286
<i>Figure 12-3: Facility to Facility Lift Comparison</i>	288

<i>Figure 12-4 Facility to Facility Comparison -- Pitching Moment</i>	289
<i>Figure 12-5 Facility-to-Facility Comparison - Directional Stability</i>	290
<i>Figure 12-6 Test-to-Test Comparison - Lateral Stability</i>	290
<i>Figure 12-7 Facility-to-Facility Comparison - Sideslip Cuts at 0 deg AOA</i>	292
<i>Figure 12-8 Facility to Facility Comparison -- Sideslip Cuts at 10 deg AOA</i>	293
<i>Figure 12-9 Facility to Facility Comparison -- Sideslip Cuts at 20 deg AOA</i>	294
<i>Figure 12-10 Facility-to-Facility Comparison - Sideslip Cuts at 30 deg AOA</i>	295
<i>Figure 12-11 Test-to-Test Comparison - Nose-Down Control Power</i>	296
<i>Figure 13-1 Configuration 201-Series 1/40th Scale Wind Tunnel Model</i>	299
<i>Figure 13-2 The Inlet Flow Exited at the Bottom of the Model</i>	300
<i>Figure 13-3 Longitudinal Data with Varying Small Canard Deflection (LEF = 0 deg)</i>	302
<i>Figure 13-4 High AOA Longitudinal Results with Small Canard (LEF = 25 deg)</i>	303
<i>Figure 13-5 Large Canard Longitudinal Data (LEF = 25 deg)</i>	304
<i>Figure 13-6 Effect of Canard Size on Longitudinal Stability</i>	305
<i>Figure 13-7 25 deg LEF Deflections Linearize the Pitching Moment Data</i>	307
<i>Figure 13-8 Maximum Nose-Down Control Power (LEF = 25 deg)</i>	308
<i>Figure 13-9 The AMT Provides Additional Nose-Down Control Power at High AOA</i>	309
<i>Figure 13-10 Comparison of Longitudinal Data with HASC Predictions</i>	311
<i>Figure 13-11 HASC Correctly Predicted Low AOA Canard Control Effectiveness</i>	312
<i>Figure 13-12 The Empirical Increment Added to HASC Results to Account for the Chined Forebody was not Required</i>	314
<i>Figure 13-13 Canard/TEF Aerodynamic Interactions (LEF = 25 deg)</i>	316
<i>Figure 13-14 Canard Schedules for Takeoff and Power Approach</i>	317

<i>Figure 13-15 Untrimmed Longitudinal Data with Canard Scheduled (LEF/Aileron = 25/15 deg)</i>	318
<i>Figure 13-16 Drooping the Aileron Improves Trimmed Lift Values at PA Conditions</i>	319
<i>Figure 13-17 Canard-Off Lateral-Directional Stability (LEF = 0 deg)</i>	321
<i>Figure 13-18 Effect of Small Canard on Lateral-Directional Stability (LEF = 0 deg)</i>	322
<i>Figure 13-19 Effect of Small Canard on Lateral-Directional Stability (LEF = 25 deg)</i>	323
<i>Figure 13-20 Effect of Canard Deflection of Lateral-Directional Stability (LEF=0)</i>	325
<i>Figure 13-21 Effect of Large Canard Deflections on Lateral-Directional Stability (LEF = 25)</i>	326
<i>Figure 13-22 Lateral-Directional Stability (Canard/LEF = Scheduled/25 deg)</i>	327
<i>Figure 13-23 Pitch Flap Control Effectiveness</i>	329
<i>Figure 13-24 Left Elevon Control Effectiveness</i>	330
<i>Figure 13-25 Effect of a 10 deg Canard Deflection of Elevon Control Effectiveness</i>	332
<i>Figure 13-26 Left Aileron Control Effectiveness</i>	333
<i>Figure 13-27 Effect of Spoiler on Aileron Control Power</i>	335
<i>Figure 13-28 Effect of Canard Deflection on Aileron Control Power</i>	336
<i>Figure 13-29 AMT Interaction with Aileron Effectiveness</i>	338
<i>Figure 13-30 All-Moving Wing Tip Control Effectiveness</i>	340
<i>Figure 13-31 Effect of Canard Deflection on Spoiler Control Effectiveness</i>	342
<i>Figure 13-32 Effect of Spoiler Hingeline Sweep on Control Power</i>	344
<i>Figure 13-33 Effect of the Small Canard on Spoiler Control Power</i>	345
<i>Figure 14-1: RCS Gap Data; 5.4 GHz; 0 deg Elevation</i>	348
<i>Figure 14-2: RCS Gap Data; 9.7 GHz; 0 deg Elevation</i>	349

Figure 14-3: RCS Gap Data; 16 GHz; 0 deg Elevation	350
Figure 14-4: RCS Gap Data; 5.4 GHz; 10 deg Elevation	351
Figure 14-5: RCS Gap Data; 9.7 GHz; 10 deg Elevation	352
Figure 14-6: RCS Gap Data; 16 GHz; 10 deg Elevation	353
Figure 14-7: RCS Gap Data; 5.4 GHz; -10 deg Elevation	354
Figure 14-8: RCS Gap Data; 9.7 GHz; -10 deg Elevation	355
Figure 14-9: RCS Gap Data; 16 GHz; -10 deg Elevation	356
Figure 14-10: RCS Physical Optics Data; 5.4 GHz; 0 deg Elevation	357
Figure 14-11: RCS Physical Optics Data; 9.7 GHz; 0 deg Elevation	358
Figure 14-12: RCS Physical Optics Data; 16 GHz; 0 deg Elevation	359
Figure 14-13: RCS Physical Optics Data; 5.4 GHz; 10 deg Elevation	360
Figure 14-14: RCS Physical Optics Data; 9.7 GHz; 10 deg Elevation	361
Figure 14-15: RCS Physical Optics Data; 16 GHz; 10 deg Elevation	362
Figure 14-16: RCS Physical Optics Data; 5.4 GHz; -10 deg Elevation	363
Figure 14-17: RCS Physical Optics Data; 9.7 GHz; -10 deg Elevation	364
Figure 14-18: RCS Physical Optics Data; 16 GHz; -10 deg Elevation	365
Figure 14-19: Beam Sector Averages; 5.4 GHz; Gap Effects	366
Figure 14-20: Beam Sector Averages; 9.7 GHz; Gap Effects	366
Figure 14-21: Beam Sector Averages; 16 GHz; Gap Effects	367
Figure 14-22: Aft Sector Averages; 5.4 GHz; Gap Effects	368
Figure 14-23: Aft Sector Averages; 9.7 GHz; Gap Effects	368
Figure 14-24: Aft Sector Averages; 16 GHz; Gap Effects	369
Figure 14-25: Beam Sector Averages; 5.4 GHz; Deflected Controls Effects	370

<i>Figure 14-26: Beam Sector Averages; 9.7 GHz; Deflected Controls Effects</i>	<i>370</i>
<i>Figure 14-27: Beam Sector Averages; 16 GHz; Deflected Controls Effects</i>	<i>371</i>
<i>Figure 14-28: Aft Sector Averages; 5.4 GHz; Deflected Controls Effects</i>	<i>371</i>
<i>Figure 14-29: Aft Sector Averages; 9.7 GHz; Deflected Controls Effects</i>	<i>372</i>
<i>Figure 14-30: Aft Sector Averages; 16 GHz; Deflected Controls Effects</i>	<i>372</i>

List of Tables

<i>Table 3-1 Baseline Configuration Naming Convention</i>	21
<i>Table 3-2: Control Surface Deflection Conventions</i>	24
<i>Table 4-1 Preliminary Mass Properties Data for 101-Series Configurations</i>	79
<i>Table 4-2 Final Configuration 101 Control Surface Areas</i>	80
<i>Table 4-3 Final Configuration 101-TV Control Surface Sizes</i>	83
<i>Table 4-4 Configuration 201-Series Mass Properties Data</i>	90
<i>Table 4-5 Final Configuration 201 Control Surface Summary</i>	95
<i>Table 4-6 Configuration 201-Series Launch Performance Summary</i>	96
<i>Table 4-7 Configuration 201-Series Recovery Performance Summary</i>	97
<i>Table 4-8 CV Performance Sensitivities</i>	98
<i>Table 6-1 101-Series Aft cg Limits (% MAC)</i>	138
<i>Table 7-1 Control Surface Actuator Requirements</i>	166
<i>Table 7-2 Sizing Conditions for Maximum Hinge Moments</i>	168
<i>Table 7-3 Control Surface Actuator Redundancy</i>	173
<i>Table 7-4 Control Surface Actuator Requirements</i>	176
<i>Table 7-5 Summary of Weight Impacts to an F-16 Derivative Wing Structure as a Result of Adding SSD Control Surfaces</i>	203
<i>Table 7-6 Historical Aircraft Flight Control System Reliability</i>	243
<i>Table 7-7 ICE Configurations Predicted Reliability</i>	246
<i>Table 11-1 Wind Tunnel Test Summary</i>	274
<i>Table 11-2 Hinge Moment Data Sources</i>	277
<i>Table 11-3 Aeroelastic Data Sources</i>	278

Table 13-1 Configuration 201 Data Reduction Constants (Full Scale) _____300

Table 13-2 Effect of Canard on Aerodynamic Center Location _____301

Table 13-3 Deep Stall Aft CG Limit Capabilities (LEF = 25 deg; All TEF = 20 deg; \dot{q} Margin = -0.07 rad/sec²) _____310

List of Symbols

Symbol or Acronym	Definition	Units
A/C	Aircraft	---
a/g	Longitudinal Acceleration During Catapult Launch	g's
AC	Aerodynamic Center	% MAC
ADF	Aerodynamic Development Facility	---
AFTI	Advanced Fighter Technology Integration	---
AMT	All Moving Tip	---
AOA, α	Angle-of-Attack	deg
A _y	Lateral Acceleration	g's
b	Wing Span	ft
BAR	Birhle Applied Research, Inc.	---
Beta, β	Angle of Sideslip	deg
BL	Butt Line	inches
C _A	Axial Force Coefficient	---
CAP	Control Anticipation Parameter	rad/sec ² / g
cg	Center-of-Gravity	% MAC
C _h	Hinge Moment Coefficient	---
C _L	Lift Coefficient	---
C _l	Rolling Moment Coefficient	---
C _l '	Primed Stability Axis Roll Coefficient	---

C_{l_p}	Lateral Stability Derivative	1/deg
$C_{l_{\delta}}$	Roll Control Derivative	1/deg
C_m	Pitching Moment Coefficient	---
C_m^*	Minimum Nose-Down Control Power	---
C_n	Yawing Moment Coefficient	---
C_N	Normal Force Coefficient	---
C_n'	Primed Stability Axis Yaw Coefficient	---
$C_{n\beta}$	Directional Stability Derivative	1/deg
$C_{n\beta dyn}$	Directional Stability Departure Parameter	1/deg
$C_{n\delta}$	Yaw Control Derivative	1/deg
CPA	Control Power Available	---
CPAP	Composite Panel Analysis Package	---
CPR	Control Power Required	---
CV	Aircraft Carrier	---
$C_{x\delta}$	Partial Derivative $\frac{\partial C_x}{\partial \delta}$	1/deg
C_y	Side Force Coefficient	---
δ	Control Surface Deflection Angle	deg
DATCOM	USAF Digital DATCOM Program	---
DLEF	Differential Leading Edge Flap	---
DOF	Degrees-of-Freedom	---
DRUD	Deployable Rudder	---
ϕ	Bank Angle	deg

EM	Electro magnetic	---
EXCEL	Microsoft Spreadsheet Software	---
FCS	Flight Control System	---
FEM	Finite Element Model	---
FSLEMAC	Fuselage Station Leading Edge Mean Aero- dynamic Chord	inches
γ	Flight Path Angle	deg
GFE	Government Furnished Equipment	---
h	Altitude	ft
HASC	High Angle-of-Attack Stability & Control Analysis Code	---
HL	Hingeline	---
HM	Hinge Moment	in-lbs
IB	Inboard	---
ICE	Innovative Control Effectors	---
IRAD	Independent Research & Development	---
I_{xx}	Moment of Inertia About the X-Axis	slug-ft ²
I_{xz}	Cross-Product of Inertia About the X-Z Axis	slug-ft ²
I_{yy}	Moment of Inertia About the Y-Axis	slug-ft ²
I_{zz}	Moment of Inertia About the Z-Axis	slug-ft ²
JAST	Joint Advanced Strike Technology	---
KCAS	Knots Calibrated Airspeed	nm/hr
KTAS	Knots True Airspeed	nm/hr

L-D	Lateral-Directional	---
L/H	Left-Hand	---
$L'_{\delta a}$	Generalized Primed Stability Axis Dimensional Roll Control Derivative	1/sec ²
L_{AERO}	Aerodynamic Rolling Moment	ft-lbs
LAMP	Large Amplitude Multi-Purpose Vertical Wind Tunnel (Bar Germany Facility)	---
LaRC	NASA Langley Research Center	---
LEF	Leading Edge Flap	---
LMTAS	Lockheed Martin Tactical Aircraft Systems	---
LO	Low-Observable	---
LSP	Lower Surface Spoiler	---
M	Mach Number	---
M_{δ}	Dimensional Pitch Control Derivative	1/sec ²
MAC	Mean Aerodynamic Chord	inches
MATV	Multi-Axis Thrust Vectoring	---
MAX-A/B	Maximum Afterburner Power Setting	---
MFHBF	Mean Flight Hours Between Failure	---
MIL-Pwr	Maximum Dry Power Setting	---
MLG	Main Landing Gear	---
MOE	Measures of Effectiveness	---
MRC	Moment Reference Center	% MAC
MOM	Method-of-Moments	---

MSC/NASTRAN	Macneal-Schwendler, Corporation/NASA	---
	Structural Analysis	
$N'_{\delta r}$	Generalized Primed Stability Axis Dimensional Yaw Control Derivative	1/sec ²
N_{AERO}	Aerodynamic Yawing Moment	ft-lbs
N_L	Left MLG Normal Force	lbs
N_R	Right MLG Normal Force	lbs
N_z	Normal Acceleration	g's
OB	Outboard	---
OML	Outer ? Line	---
p	Roll Rate	deg/sec
PA	Power Approach	---
PDU	Power Drive Unit	---
PG1 - PG6	Virtual Pitch FCS Gains	---
PLA	Power Lever Setting	% Power
Θ	Pitch Angle	deg
q	Pitch Rate	deg/sec
QFD	Quality Function Deployment	---
r	Yaw Rate	deg/sec
R/H	Right-Hand	---
RCS	Radar Cross Section	---
RG1	Virtual Roll Mixing Gain	---

RG2 - RG4	Virtual Roll FCS Gains	---
R_N	Reynolds Number	---
R_{STK}	Lateral Stick Force	lbs
\dot{q}	Pitch Acceleration	rad/sec ²
\bar{q}	Dynamic Pressure	lbs/ft ²
S	Wing Reference Area	ft ²
SARL	Subsonic Aerodynamic Development Laboratory (WL Facility)	---
SEROC	Single Engine Rate-of-Climb	ft/min
SL	Sea Level	---
S_L	Left MLG Skidding Reaction Force	lbs
S_R	Right MLG Skidding Reaction Force	lbs
SSD	Spoiler-Slot-Deflector	---
τ_a	FCS Time Delay	sec
TED	Trailing Edge Down	---
TEF	Trailing Edge Flap	---
TEU	Trailing Edge Up	---
τ_r	Roll Mode Time Constant	sec
TV	Thrust Vectoring	---
t_x	Time-to-Bank; $x = \Delta\phi$	sec
V	Velocity	nm/hr
V_A	Launch Velocity Required for 10' Sink	KTAS
V_{CW}	Crosswind Velocity	KCAS

V_{ENGAGE}	Tail Hook/Arresting Wire Engagement Velocity	KTAS
V_{MC}	Single Engine Minimum Control Speed	KTAS
V_{NGU}	Nose-Gear Unstick Velocity	KCAS
V_{POPUP}	Velocity Required for Popup	KTAS
V_{STALL}	Stall Speed	KTAS
V_{WAVEOFF}	Waveoff Velocity	KTAS
W	Weight	lbs
ω_{dr}	Dutch Roll Frequency	rad/sec
WL	Wright Laboratory	---
WOD	Wind Over Deck	nm/hr
$WPAFB$	Wright Patterson Air Force Base	---
ω_{sp}	Short Period Frequency	rad/sec
x_{cg}	cg Location in X-Direction	inches
Y_{AERO}	Aerodynamic Side Force	lbs
$YG1$	Virtual Yaw Mixing Gain	---
$YG2 - YG6$	Virtual Yaw FCS Gains	---
Y_{PED}	Rudder Pedal Force	lbs
z_{cg}	cg Location in Z-Direction	inches
$\frac{1}{TA}$	Actuator Time Constant	1/sec
Ψ	Heading Angle	deg
2-D	Two-Dimensional	---

3-D	Three-Dimensional	---
ζ_{dr}	Dutch Roll Damping Ratio	---
ζ_{sp}	Short Period Damping Ratio	---

Subscripts

s, spoil	Spoiler
clam	Clamshell
e	Elevon
pf	Pitch Flap
a	Aileron
c	Canard
R, Rud	Deployable Rudder
TE	Trailing Edge
AUG	Augmented

1 Introduction

The recent application of low-signature technologies to high performance aircraft has led to new constraints in air vehicle design. Signature-related geometry considerations and higher standards for maneuverability are driving the need for new and innovative control concepts for tactical aircraft.

Constraints on aircraft configuration and controls are required to achieve reduced detection signature and increased survivability in the current air combat environment. Low radar cross section (RCS) design practices manifest themselves in the form of external shaping, elimination of vertical control surfaces, and alignment of control surface edges with external airframe edges. As a result, aircraft designed for low RCS require new control concepts to achieve the required maneuvering capability and tactical utility throughout the flight envelope.

Additionally, new benchmarks for fighter maneuverability have been demonstrated with the emergence of the YF-22, Su-27/Su-35 and the F-16 multi-axis thrust vectoring (MATV) demonstration. Piloted simulation studies have shown significant benefits to air-to-air combat using high angle-of-attack (AOA) or post-stall maneuvering¹. Trying to satisfy both low-signature and high agility requirements results in pushing the target design space into the far corner of the technology envelope (Figure 1-1).

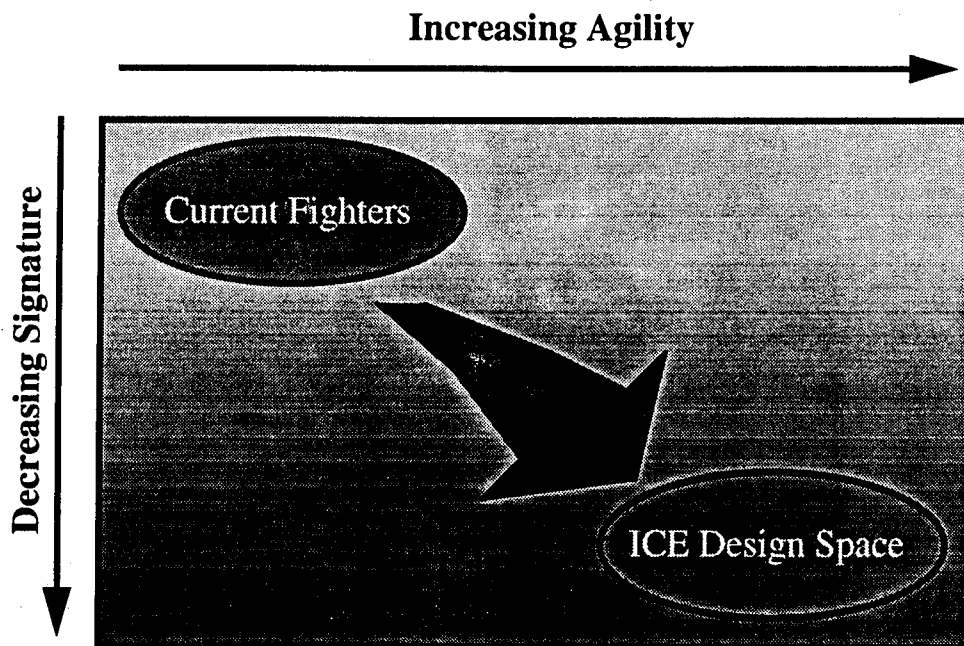


Figure 1-1 High AOA Agility and Low Observability Combine to Force Technology into the Corners of the Envelope

Configurations without vertical tails offer unique integration challenges driven by flight control and RCS concerns. Oftentimes, a control suite integrated into a tailless fighter configuration exhibits a high degree of coupling about all three axes (pitch, roll and yaw) and the controls interact aerodynamically to introduce complex nonlinearities into the problem of control allocation. It is also typical for tailless fighters to exhibit relaxed static stability in both pitch and yaw axes, requiring prioritization of control power to the appropriate axes to retain control under conditions when control rate and authority limits are reached. Unlike their predecessors, tailless fighters typically have highly coupled, interactive control suites that require unique approaches to control power integration.

1.1 Background

The innovative control effectors (ICE) program was conceived in 1993 to investigate the potential for new and innovative methods for stabilization and control of high performance, low all-aspect signature fighters. Sponsored by both Wright Laboratory (WL/FIGC) and the Naval Air Warfare Center (NAWCAD), Phase I of the ICE program involved an

18-month effort including: (1) selection of a baseline vehicle and innovative control concept(s); (2) investigation of the performance of each control effector; (3) evaluation of the integration impacts of each concept; (4) development of a risk reduction plan to implement the control concepts and (5) documentation of the study.

Two configuration concepts were defined as baseline vehicles. An all-wing tailless concept employing a 65-deg sweep delta wing was used as the land-based, or USAF configuration (Figure 1-2). A canard-delta planform with 42-deg leading edge sweep was chosen for the Navy baseline (Figure 1-3). Both vehicles are single-engine multi-role fighter aircraft incorporating internal or low-observable weapons-carriage measures for reduced RCS.

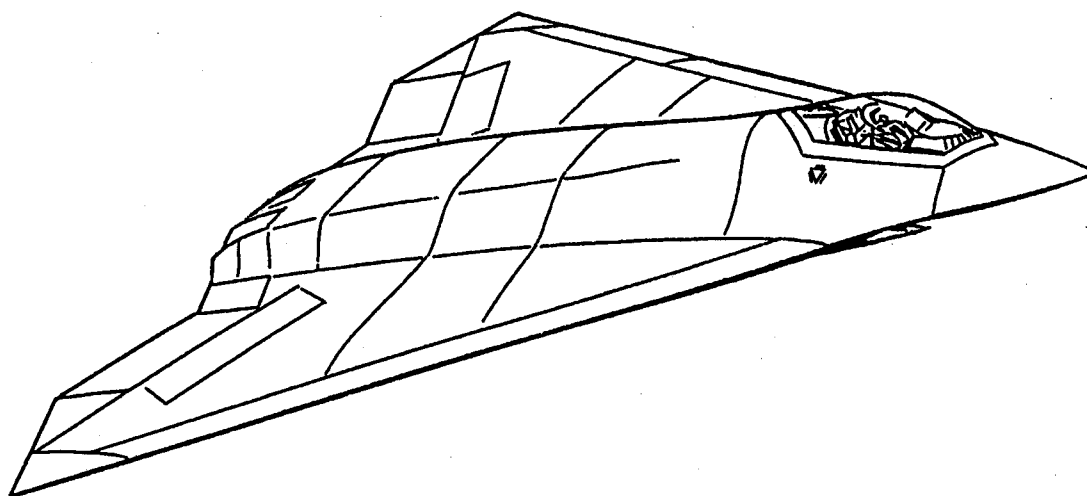


Figure 1-2 Land-Based Baseline Configuration (101-Series)

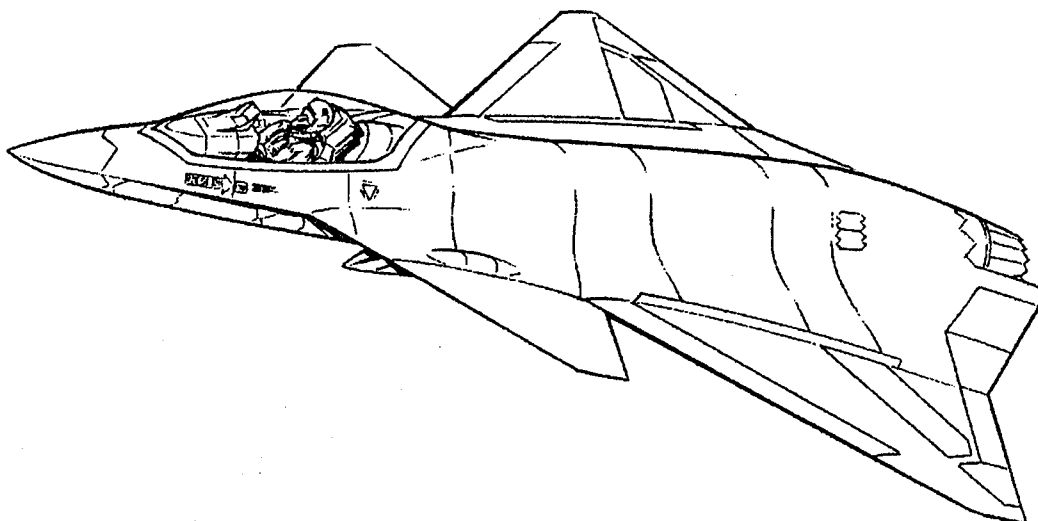


Figure 1-3 Carrier-Based Baseline Configuration (201-Series)

1.2 Scope of the Study

This study focuses on highly maneuverable fighter aircraft without vertical tails. Removal of the vertical tail has been touted as an advantage for the past several years^{2,3}. Not only are there potential beam signature improvements, but weight and drag reduction is possible as well. One of the objectives of the ICE program was to quantify the impact of applying innovative aerodynamic control technologies to tailless fighters.

The ICE study investigated promising aerodynamic lateral-directional control devices for integration into a representative flight vehicle. The condition(s) for critical control power requirements were identified, and the devices sized and integrated into various control suites to examine system level impacts including weight, maneuver performance, signature, hydraulic requirements, demands on the flight control system (FCS) design, and carrier (CV) suitability.

Another objective was to quantify the potential of aerodynamic controls for high AOA flying qualities. Vertical tailless fighters may rely on thrust vectoring (TV) control power to achieve high AOA maneuverability. Aerodynamic control power will still be required to supplement TV in other areas of the flight envelope, and provide recovery from high

AOA conditions should vectoring control be lost. Aerodynamic controls were traded with TV to determine the aerodynamic control capabilities and the weight impacts of sizing a control suite considering TV as a primary flight control (i.e., required for Level 1 flying qualities).

1.3 The Need for Aerodynamic Yaw Power

Yaw TV is one method of integrating yaw power into a tailless fighter. However, vectoring alone cannot provide the needed control moments throughout the entire flight envelope². Previous studies have investigated substitution of conventional rudder control with yaw TV²⁻⁴. Yaw vectoring is a very powerful controller at low-speeds; however, at moderate to high speeds, load limitations on the engine and fuselage structure result in nozzle deflection limits. Together with the reduced control moment at high dynamic pressures, the deflection limits result in very small control potential from vectoring at moderate to high speeds. An aerodynamic device is much more efficient at generating a control moment at high speed than vectored thrust.

Figure 1-4 illustrates the yaw power available (at zero angle-of-attack) as a function of Mach number from both a conventional centerline vertical tail/rudder and yaw TV for a number of altitudes. The rudder control effectiveness includes the effects of flexibility and hinge moment limiting at high speeds, while the vectoring effectiveness includes nozzle deflection limitations considering an off-axis load limitation of 4,000 lbs. The conventional rudder is superior to yaw vectoring over the majority of the flight envelope. The primary advantage that vectoring has over the rudder is its ability to provide large body axis control moments throughout the angle-of-attack (AOA) range whereas the rudder loses effectiveness at high AOA.

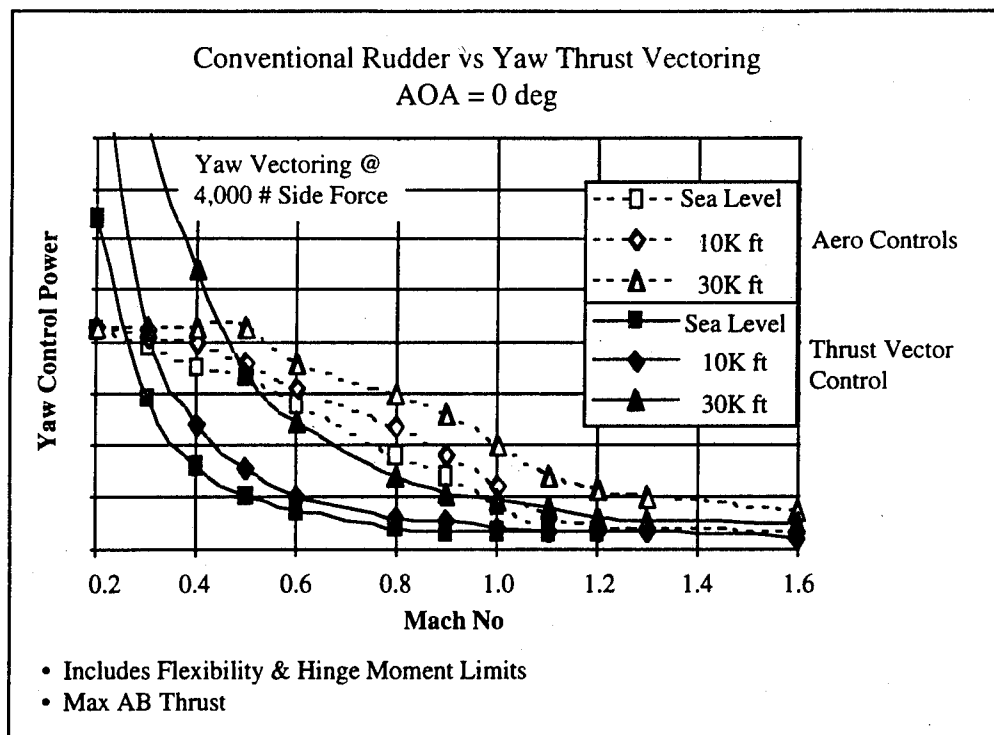


Figure 1-4 Aerodynamic Control Power is More Effective Than TV Control Through a Large Portion of the Flight Envelope

In addition to the high-speed limitations of TV, landing considerations require that the engine operate at low power settings, significantly reducing the control power available from yaw vectoring during approach. Reference 5 demonstrated a unique solution to the power approach problems inherent with TV by using an integrated throttle/thrust reversing control system to allow a high power setting during the approach so that thrust vectoring remained effective. Glide path was controlled by modulating the degree of thrust reversing. A similar system could be implemented using an integrated throttle/speedbrake system. The added drag of the speedbrake would allow higher power settings resulting in greater TV control moments than could be accomplished using conventional means.

Finally, engine or nozzle failure considerations for a single-engine tailless fighter provide an obvious need for aerodynamic yaw control devices. A vectoring failure at high AOA may result in an unrecoverable departure. At high speeds, an engine or nozzle failure on

a fighter relying solely on TV for stability could result in the catastrophic loss of the vehicle.

Considering all of the above, aerodynamic yaw control devices could be integrated along with TV into a tailless vehicle to provide good flying qualities throughout the flight envelope along with excellent high AOA maneuvering characteristics provided by TV. Typically, on fighter-class aircraft, the controls are sized by low-speed maneuvering considerations. The addition of TV as a primary flight control would allow the designer to size the aerodynamic controls for other conditions -- reducing the overall size and weight of the aerodynamic control suite and the attendant hydraulic power systems. The approach taken during the ICE study was not to replace the vertical tail with yaw thrust vectoring, but find a means of implementing yaw vectoring along with the aerodynamic control devices to determine the real-world impacts of tailless control suite design on vehicle integration.

1.4 Previous Research

The ICE study relied heavily on independent research and development (IRAD) studies conducted by Lockheed Martin Tactical Aircraft Systems (LMTAS) since 1991. An extensive aerodynamic database, representative of the land-based baseline vehicle, was compiled including low-speed, transonic and supersonic wind tunnel test entries. The low-speed wind tunnel data was collected at both the LMTAS Aerodynamic Development Facility (ADF) and during a cooperative test with WL at the Subsonic Aerodynamic Research Laboratory (SARL) at Wright-Patterson AFB. Cooperative transonic and supersonic test entries were also completed at the NASA Langley Research Center (LaRC) 8-foot and 4-foot Unitary wind tunnels, respectively (see Appendix A)^{6,7}.

A 1/18th scale high-speed wind tunnel model of the 65-deg sweep configuration was used during the cooperative tests with WL and NASA. A wide range of lateral-directional control concepts were investigated during these tests. During the LMTAS tailless fighter IRAD program, over forty individual control concepts were tested and screened down to a few of the more promising controls.

In addition to the IRAD wind tunnel testing, two software tools were developed in-house to facilitate the analysis of tailless aircraft. CPR, or Control Power Required is a 6-degree-of-freedom (DOF) simulation tool used for preliminary evaluation and sizing of control suites. CPA, or Control Power Available is a control power blending tool that computes the maximum control moments (or control envelopes) about the roll, pitch and yaw axes (see Section 2).

CPR can be used in conjunction with CPA to run simulations limited by the control envelope to determine the maneuver capabilities of an aircraft. The advantage of using this approach is that the control mixing strategy does not need to be known a-priori, and yet the effects of control nonlinearities and interaction can be accounted for. Furthermore, CPA provides the control system designer with insight into how the controls should best be used to provide maximum coordinated control moments.

The two tools, CPR and CPA, were used to evaluate the promising control concepts and determine viable control suites that could achieve pre-determined maneuver capabilities. The results of these IRAD efforts were used to move forward into the ICE study.

1.5 ICE Study Approach

Five of the more promising lateral-directional controls investigated during the LMTAS IRAD were used during the ICE study. They consisted of: (1) an all-moving wing tip; (2) differential leading edge flaps; (3) deployable rudder; (4) lower surface spoiler; (5) spoiler-slot-deflector. An innovative control was defined as a control not currently in use by a modern aircraft. This groundrule eliminated clamshells from contention, although they were evaluated on the baseline vehicles.

The five selected controls are not unique; in fact, a literature search will show that many have been around since before World War II! (The spoiler-slot-deflector was tested as early as 1941, and was incorporated on the North American XF-107 and RA-5 Vigilante for roll control.) However, no published study has ever evaluated these controls for use on a purely tailless fighter, or developed system level integration impacts for use in selecting the most favorable concepts for additional investigation.

Figure 1-5 shows a schematic of the ICE study approach. The baseline vehicles are those shown in Figures 1-2 and 1-3, above. The baseline vehicle control suites were sized to achieve pre-set roll performance goals (Section 3) using aerodynamic control power alone. In cases where the maneuver goals could not be achieved, limitations were identified. The control suites were then resized assuming the incorporation of a MATV system. Weight impacts were determined for each configuration. Six control suites were then sized to the same maneuver characteristics using the land-based configuration. Each control suite was evaluated and the three most favorable chosen for further evaluation. The most promising innovative control suites were integrated onto the carrier-based configuration and evaluated from a CV suitability standpoint. After final sizing, hydraulic system, weight, drag, signature and other integration impacts were determined for each control suite. Signature analysis was performed on a representative test body to keep results unclassified. Finally, a risk reduction plan was prepared to determine what additional test data are required to achieve a low level of technical risk prior to implementing these controls on a full-scale vehicle.

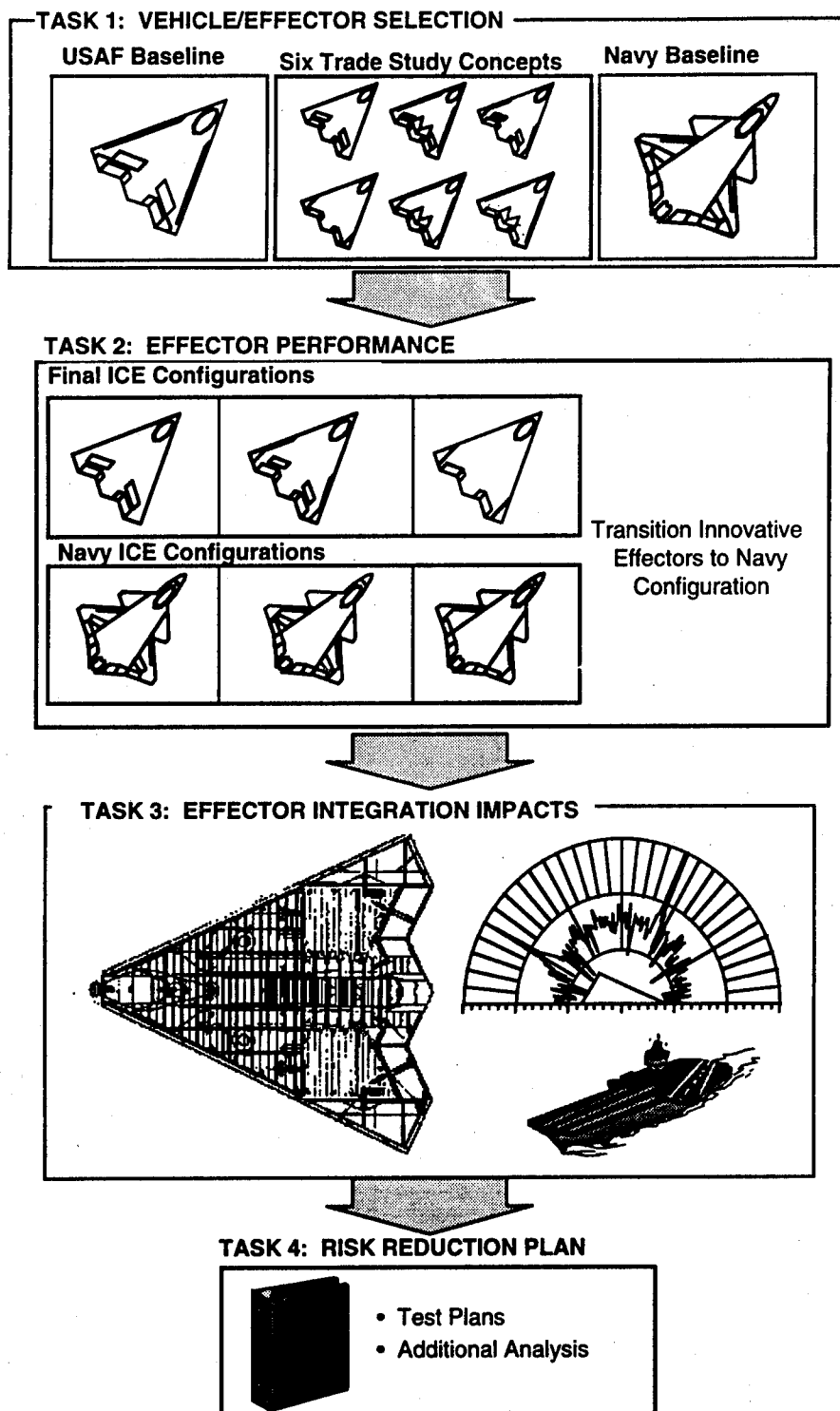


Figure 1-5 ICE Study Approach

2 Control Power Analysis Methodology

The two primary analysis tools used during the ICE program were CPR and CPA. These tools are used for preliminary evaluation of configuration maneuver capabilities and control suite sizing.

2.1 CPR

CPR is a 6-DOF simulation tool used to determine aircraft maneuver capabilities and required control moments for a wide range of configurations. It utilizes a generic feedback flight control system (FCS) with gains computed on-line at each time step based on bare airframe characteristics and desired closed-loop flying qualities parameters. The idea for CPR was born from work documented in references 8 and 9 (Figure 2-1).

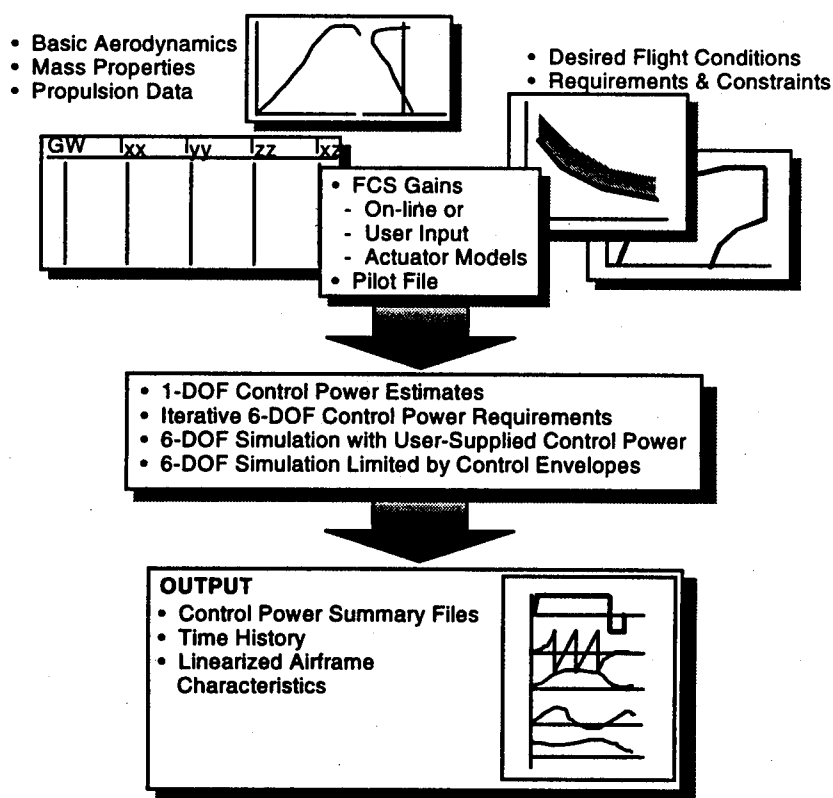


Figure 2-1 CPR is a Preliminary Design Simulation Tool

CPR has four modes of operation: (1) static control power requirements; (2) iterative control power requirements; (3) basic simulation; (4) simulation within CPA envelopes.

Option 1 computes total control moment requirements using the traditional control requirement approximations for roll, pitch and yaw⁹ (i.e., nose-down control for inertial coupling, roll power for given time-to-bank, etc.). Given the bare airframe characteristics (i.e., C_L , C_m , $C_{n\beta}$, etc. vs α), time-to-bank requirements and minimum nose-down pitch acceleration, the program computes the required control moments.

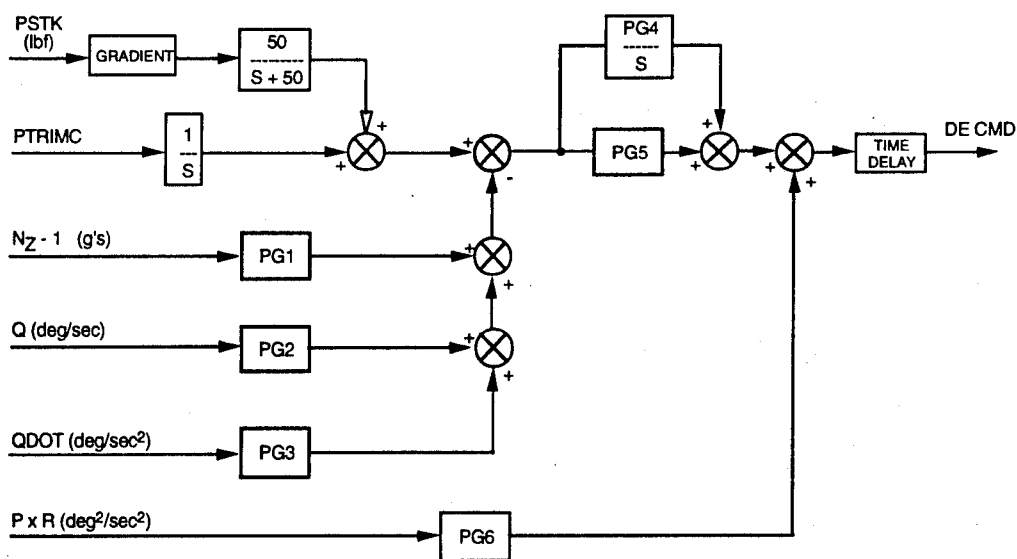
Option 2 runs a 6-DOF simulation of a roll maneuver treating the control power available as unknown, and using the bare airframe characteristics along with maneuver requirements and constraints (e.g., time-to-bank, minimum pitch acceleration, and maximum sideslip). Control power is successively iterated upon until the desired maneuver performance can be achieved within the specified constraints. Control requirements are output in a summary file. Time histories of each iteration are also provided. In this manner, the effects of coupling, bare airframe stability, and control system nonlinearities can be properly evaluated.

Option 3 is a 6-DOF simulation for which the user supplies all of the required aerodynamic data -- including control power. The database used for the simulation can be as simple or complex as the user desires. Typically, this option is used to evaluate fairly conventional configurations. A pilot input file is provided to fly arbitrary maneuvers.

Option 4 is similar to Option 3 except control power available is limited by CPA envelope files (see Section 2.2). This method is useful for evaluating highly coupled control suites having significant control interactions between surfaces and about multiple axes. It provides a method to analyze a tailless fighter configuration at the conceptual level without having to know the details of the control surface blending scheme. Again, a pilot input file allows the user to fly arbitrary maneuvers. Both Options 2 and 4 were used extensively during the ICE program to evaluate the control power available for each configuration.

The flight control system used in CPR is a generic feedback structure incorporating on-line gain computation during the simulation. Figures 2-2, 2-3, 2-4 and 2-5 illustrate the pitch, roll, yaw and lateral-directional mixing strategies for the CPR simulation.

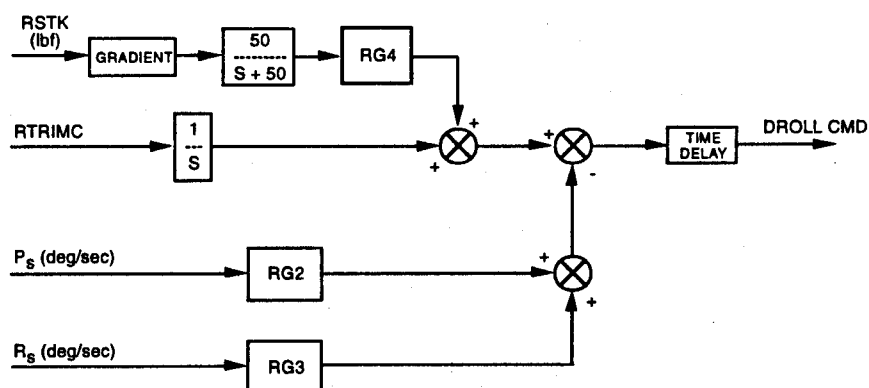
PITCH CONTROL LAWS - NZ COMMAND



Gains can be calculated internally or user-input.
(Reference AFWAL-TR-87-3018)

Figure 2-2 Pitch Flight Control System

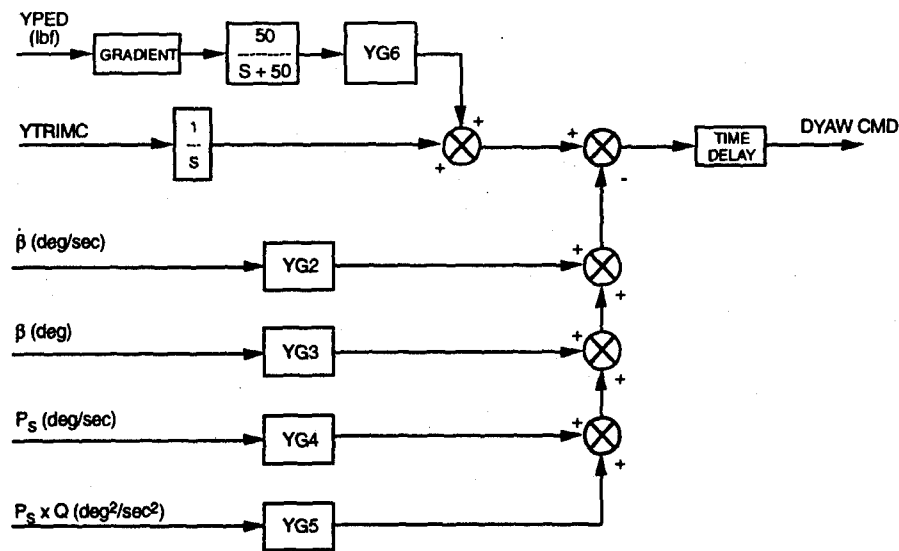
ROLL CONTROL LAWS - P COMMAND



Gains can be calculated internally or user-input.

Figure 2-3 Lateral-Axis Control System

YAW CONTROL LAWS - β COMMAND



Gains can be calculated internally or user-input.

Figure 2-4 Directional-Axis Control System

MIXER LOGIC

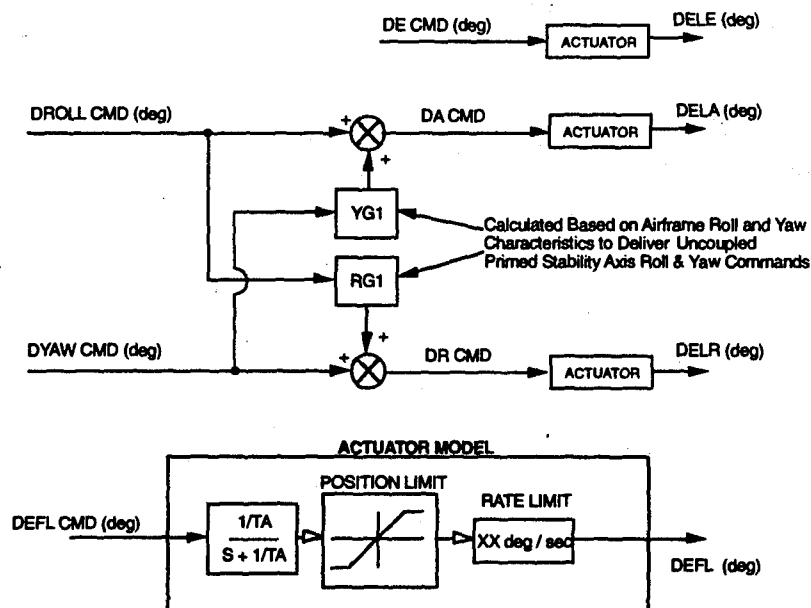


Figure 2-5 Lateral-Directional Mixer

The longitudinal FCS is an N_z command system consisting of feedbacks of normal acceleration and pitch rate to augment short period dynamics. A pitch acceleration term is fed

back to cancel the first order actuator pole. Body axis roll rate and yaw rate are fed back to offset inertial pitch coupling during rolling maneuvers. The longitudinal FCS is very similar to that described in Reference 8. By specifying the desired closed loop flying qualities (e.g., ω_{sp} or CAP and ζ_{sp}), the user can expect the longitudinal FCS to emulate the desired short-period dynamics so long as longitudinal controller rate and position limits are not saturated.

The lateral FCS is a stability axis roll rate command system that uses feedbacks of stability axis roll and yaw rates. The gains are computed such that the system achieves the desired user-specified close-loop roll mode time constant (τ_r) so long as the lateral control rate or position limits are not saturated.

The directional axis FCS consists of a sideslip command system utilizing feedbacks of sideslip, sideslip rate, roll rate and the product of roll rate and pitch rate to counter inertial coupling. The user specifies the desired closed-loop dutch roll frequency and damping along with the bare airframe characteristics to achieve the desired augmented system.

Lateral-directional mixing is accomplished with feedback gains YG1 and RG1. These gains are computed based on the roll-to-yaw characteristics of the lateral-directional controls. YG1 and RG1 are computed such that the lateral-directional flight control system generates decoupled primed stability axes rotational accelerations. First order models with actuator rate and position limiting are used to approximate each actuator.

2.2 CPA

CPA is an aerodynamic database search tool that determines the maximum and minimum control moment capability for a given control suite. Other methods using much more finesse can provide similar results (e.g., Reference 10); CPA takes the brute force approach using a global search method, but it provides the capability to evaluate nonlinear effects. An aerodynamic database is constructed using predictions or wind tunnel data. Control effectiveness for each surface can be a function of any parameter, including sideslip or

other control deflections. In this manner, the user can evaluate the effects of sideslip and control interactions on total control power available.

The user runs CPA after supplying the flight condition, the controls to be evaluated, their deflection ranges, and deflection breakpoints (e.g., sweep the elevon from -30 to 30 by 10 deg increments). The routine computes control moments for every possible combination of deflections specified. For configurations having a large number of control surfaces and deflection breakpoints, the total number of possible deflection combinations can become very large. By computing each combination of control deflections, the boundary of maximum control power available can be determined. The physical control surface deflections corresponding to each data point on the boundary are stored. Physical surface deflections give the control law designer insight into how the controls should be used to maximize control power potential. (For a tailless aircraft at high AOA, this is not a trivial problem.) The resulting output file includes a map of the control "envelope" (roll vs pitch vs yaw) at each flight condition. Results are typically presented in the primed stability axis system¹¹.

Figure 2-6 shows an example of CPA results. The top portion of the figure shows a contour map of roll versus yaw power at varying levels of pitch power for a single flight condition (AOA and Mach number). The lower portion shows the same data in 3-D with nose-up pitch power along the Z-Axis. Note the functionality of lateral-directional control power available at various levels of pitch control.

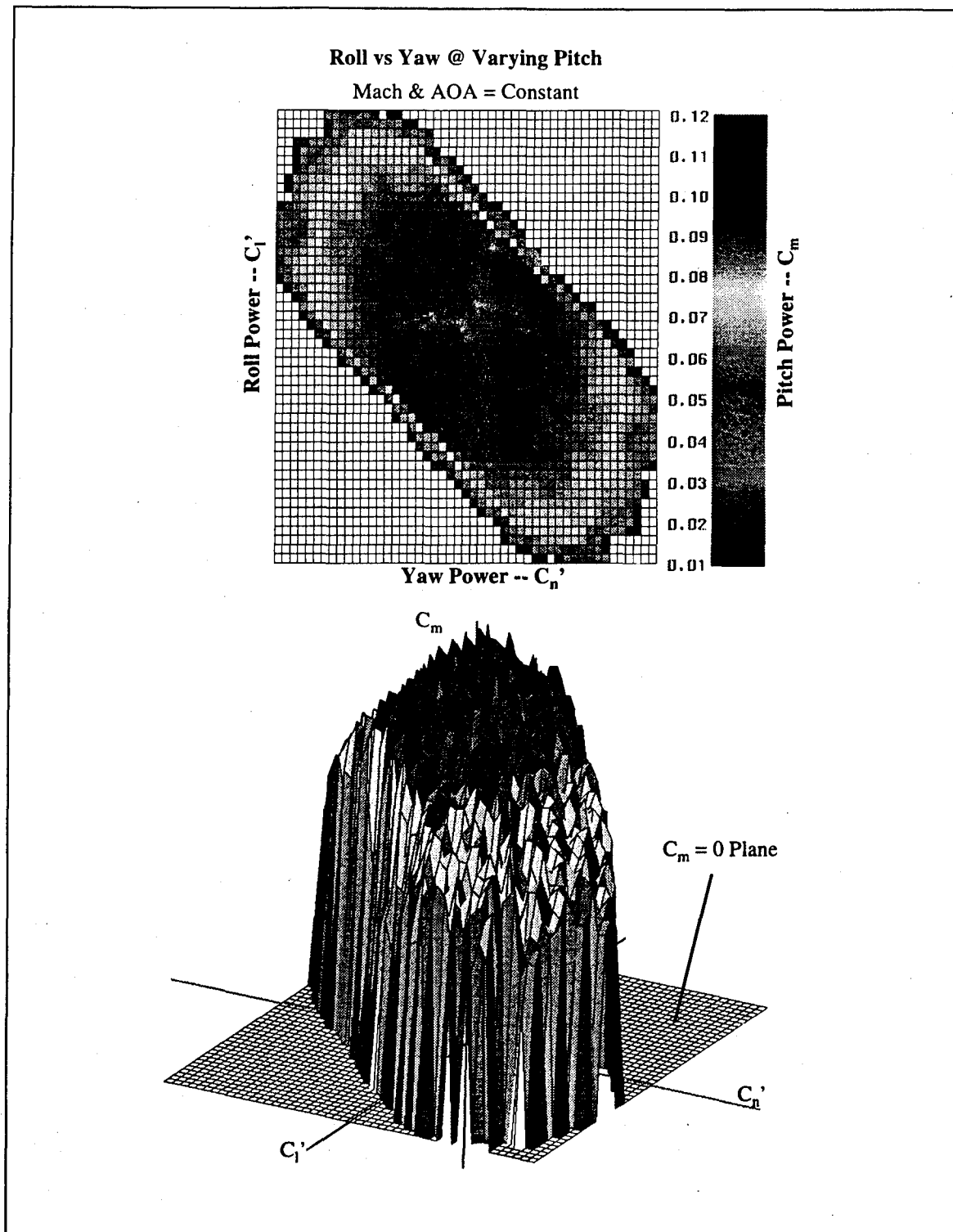


Figure 2-6 Example CPA Results

Figure 2-7 shows 2-D control power boundaries cut from a control envelope. From the resulting map, the analyst can find the maximum coordinated roll control power for varying levels of pitch control. Assuming some maximum level of sideslip along with the maximum trimmed yaw power, the maximum augmented directional stability can be determined including the effects of sideslip on the control surfaces used for augmentation. The analyst can also evaluate the roll/yaw/pitch control availability at various portions along the surface of the envelope. For a tailless aircraft employing control surfaces that generate moments about all three axes, control power available about any one axis is a function of the control usage about the remaining axes.

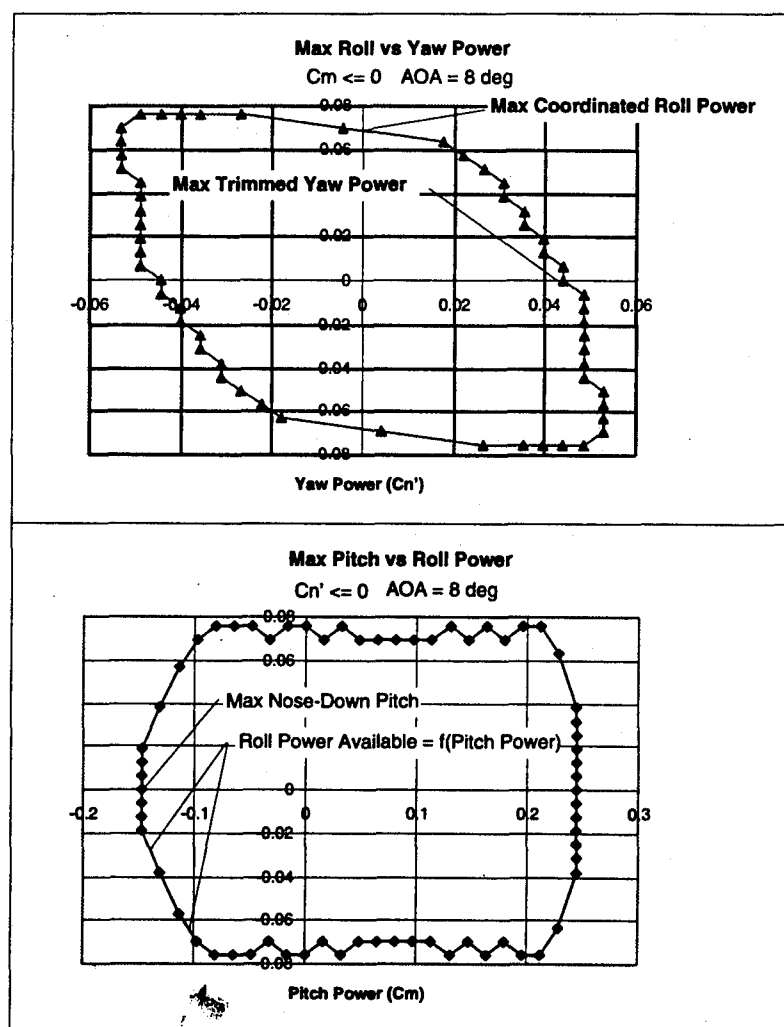


Figure 2-7 Example CPA Control Power Boundary Data

The real power of the control envelope is its use in simulation. By running CPR in option 4 (Section 2.1), the user can evaluate a tailless configuration's maneuver capability using the CPR simulation tool. Usually the control blending scheme is not known during the conceptual design stage. The control envelope concept gives the analyst the ability to quickly evaluate each candidate control suite, and optimize control surface sizes to meet flying qualities requirements.

2.3 Conceptual Design Process Using Control Power Analysis Tools

Figure 2-8 illustrates a typical process flow using CPR and CPA. This process was used during the ICE study to evaluate each proposed control suite. External constraints placed on a control suite such as maximum surface size (due to structural limitations), or deflection limits (e.g., ground contact during takeoff or landing) may result in a particular control suite not being able to meet maneuver requirements. These limitations must be considered during the control suite sizing process based on engineering judgment, close cooperation between technical specialties, and design iteration. Interdisciplinary coordination can ferret out unreasonable configurations.

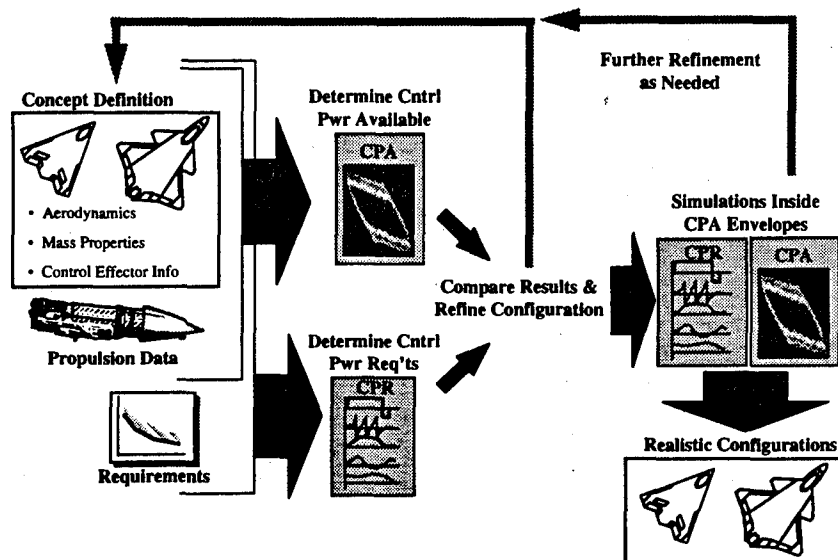


Figure 2-8 Conceptual Design Process Using Control Power Analysis Tools

3 Vehicle/Effector Selection

Two advanced multi-role strike fighter concepts were used as baselines for analysis of the innovative controls. The land-based design is a 65 deg sweep flying wing configuration embodying aggressive, all-aspect signature features, internal weapons carriage, and supersonic capability. The configuration was originally sized to meet an 1100 nm high-low-low-high USAF mission. This configuration and its derivatives will be referred to as the 101-series aircraft (Figure 3-1).

A configuration developed during preliminary Joint Advanced Strike Technology (JAST) studies was chosen for the Navy analysis due to its low-speed capabilities and representative features of a typical Navy aircraft (e.g., wing fold, launch and recovery provisions, fuselage keel structure, geometric constraints, etc.). The Navy configuration (201-series) was sized to meet high-medium-high and high-low-low-high mission profiles of 600 nm radius. It is a vertical-tailless canard-delta design with internal carriage of air-to-air missiles. The air-to-ground payload is carried on a conformal weapons pallet. Figure 3-2 shows a three view of the basic 201 configuration.

The baseline configurations were analyzed both with and without MATV. The analysis goals were to trade off aerodynamic controls with TV, resulting in a potential weight savings. Table 3-1 lists configuration callouts that will be used throughout this document.

Table 3-1 Baseline Configuration Naming Convention

Configuration	Application	Notes
101	Land-Based	Aero Controls Only
101-TV	Land-Based	Aero + MATV
201	Carrier-Based	Aero Controls Only
201-TV	Carrier-Based	Aero + MATV

Derivatives of each configuration have a dash-number following the series callout (e.g., 201-1, 201-3, etc.) The derivative configurations will be discussed in detail in a later section.

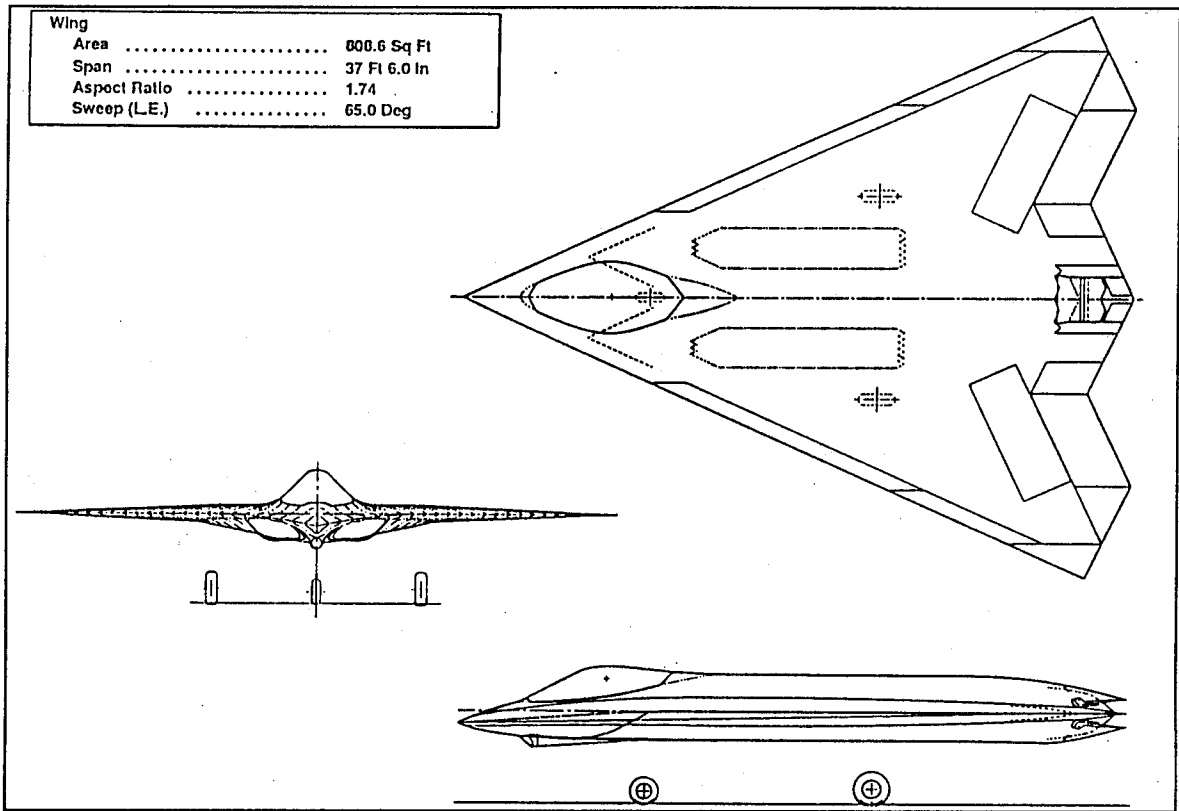


Figure 3-1 Configuration 101-Series -- USAF Baseline

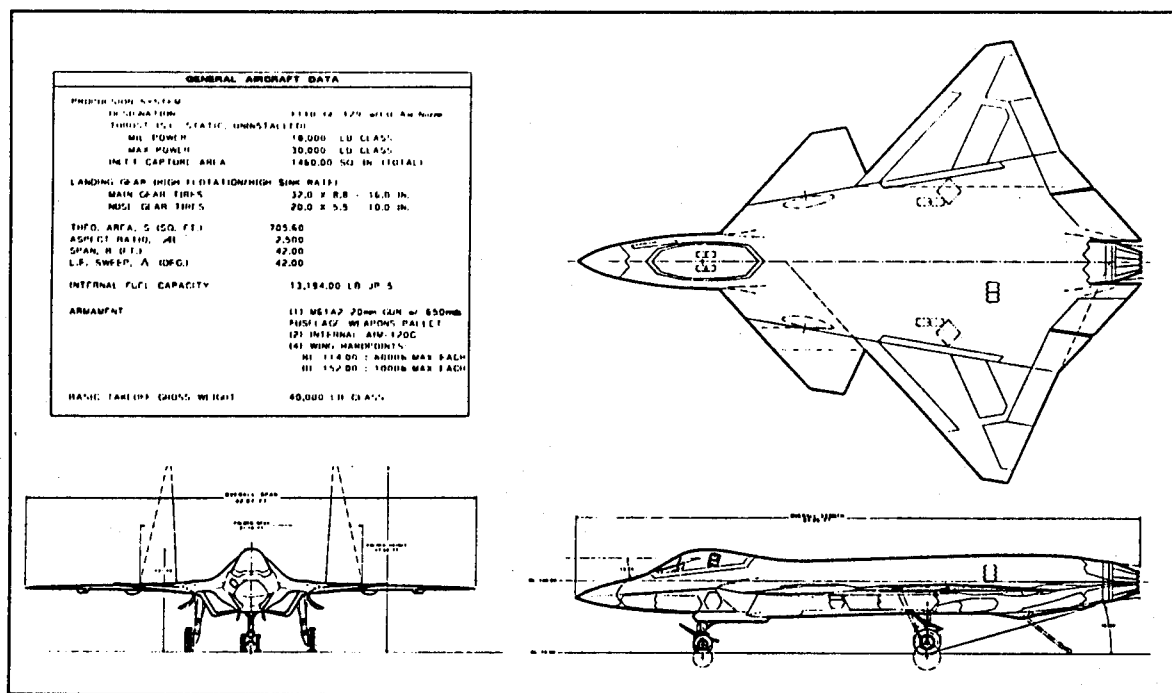


Figure 3-2 Configuration 201-Series -- USN Baseline

3.1 Description of Control Effectors

Five innovative control concepts were investigated during the ICE program. Innovative control concepts were defined as those controllers that are not currently used, or have not seen widespread use in the high performance aircraft arena but which have potential utility on a tailless LO fighter design. Goals for the control concepts included: (1) improved low signature characteristics over conventional controls; (2) improved high AOA effectiveness; (3) applicability to tailless fighters; (4) potential weight and drag reduction over conventional controls; (5) reduced hinge moment and reduced susceptibility to aeroelastic effects. The all moving wing tip (AMT), differential leading edge flap (DLEF), spoiler-slot deflector (SSD), deployable rudder (DRUD), and lower surface spoiler (LSP) were each evaluated for their lateral-directional control power. Table 3-2 describes the control deflection sign conventions used throughout this report.

Table 3-2: Control Surface Deflection Conventions

Control Surface	Direction for Positive Deflection
Canard (201)	TED
Trailing Edge Controls	TED
Spoiler	TEU
Deflector	LED
All Moving Tips	TED
Leading Edge Flaps	LED

Note: TED = Trailing Edge Down; TEU = Trailing Edge Up; LED = Leading Edge Down

This section describes aerodynamic characteristics of each innovative control effector in detail. However, a discussion of two conventional lateral-directional control concepts, clamshells and large spoilers, is first warranted to better illustrate the advantages of the selected innovative controls.

3.1.1 Clamshells

Clamshells, or drag rudders, have been used on a number of flying wing aircraft; most recently, the B-2 bomber^{12, 13}. Clamshells produce yawing moment through a drag force acting at the wing tip. Figure 3-3 shows typical clamshell effectiveness curves for a 65 deg sweep tailless fighter.

CLAMSHELL INCREMENTS
Body Axis; $M=0.3$; SARL Data

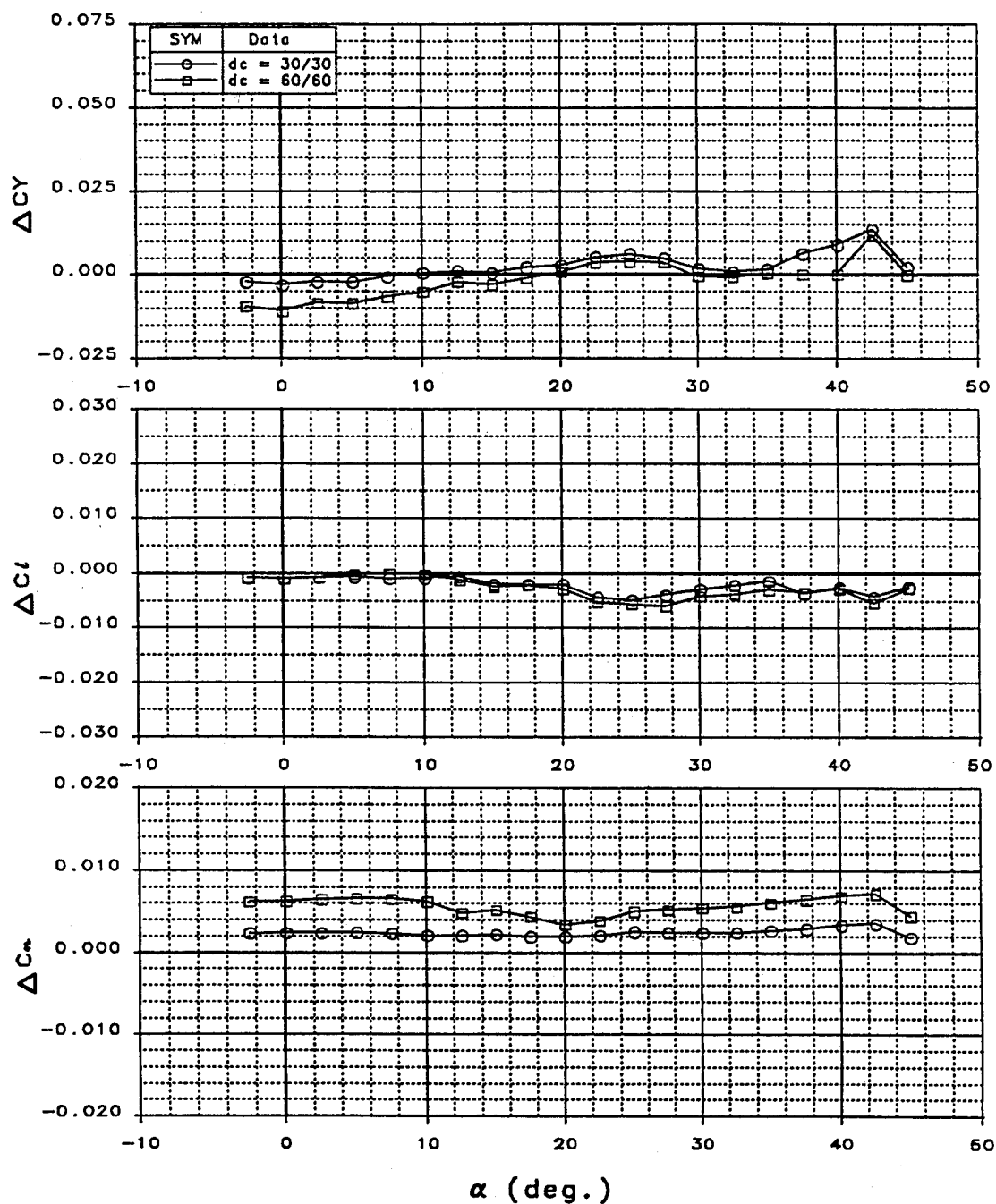


Figure 3-3 Clamshell Control Effectiveness

At high AOA, flow over the upper surface of the wing separates, and the top half of the clamshell loses effectiveness. This results in a loss of yaw effectiveness, and an unfavorable roll-yaw relationship. The lower surface retains its effectiveness at high AOA, and acts like a conventional aileron generating adverse roll and yaw.

Hingeline sweep is an important parameter in clamshell design. To maximize the effectiveness of controls located behind the aircraft center-of-gravity (cg), surfaces should have moderate aft sweep to increase the moment arm relative to the cg. Figure 3-4 shows yaw control effectiveness curves for various clamshell hingeline sweeps. Aft sweep beyond a certain point will reduce overall effectiveness because of reduced profile drag area presented to the local flow.

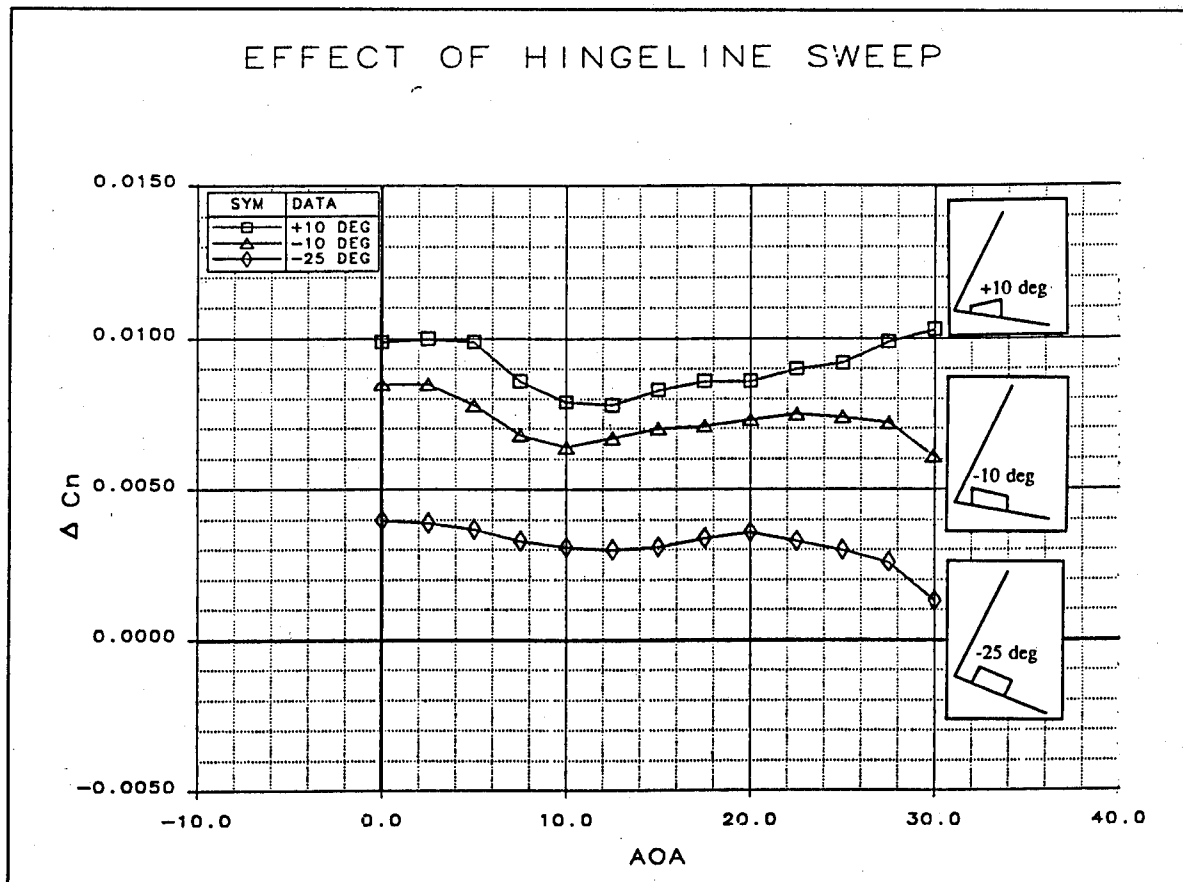


Figure 3-4 Clamshell Effectiveness at Varying Hingeline Sweeps

Clamshell yawing moments are generally linear with increasing deflection, even at high AOA. These surfaces generate sizable adverse rolling moments at high AOA; roll-to-yaw ratios exceed 1:1. (Figure 3-5).

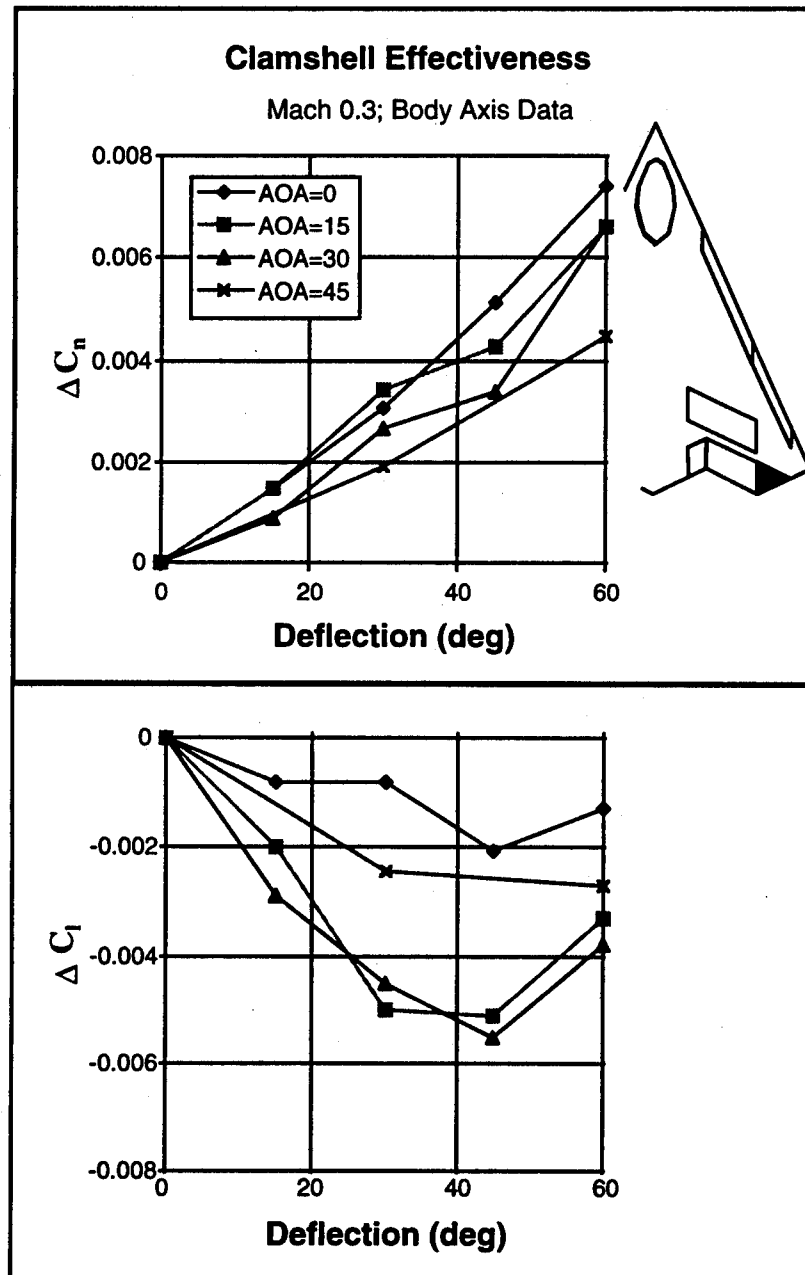


Figure 3-5 Clamshell Effectiveness vs Deflection

Effects of sideslip on clamshell effectiveness are shown in Figure 3-6. The data represent a right-side clamshell deflection; the positive sideslip data are representative of a distur-

bance for which a right-side deflection would be used to return to trimmed flight. The data shows little effect of sideslip on yaw control power -- a desirable quality. Windward clamshell deflection during sideslip increased adverse roll between 10 and 30 deg AOA. Deflecting the clamshell on the leeward wing resulted in an increase in yaw control power over the zero sideslip condition in the 10 to 30 deg AOA region; control power is degraded for AOA > 38 deg.

CLAMSHELL INCREMENTS WITH SIDESLIP

Body Axis; $M=0.3$; SARL Data

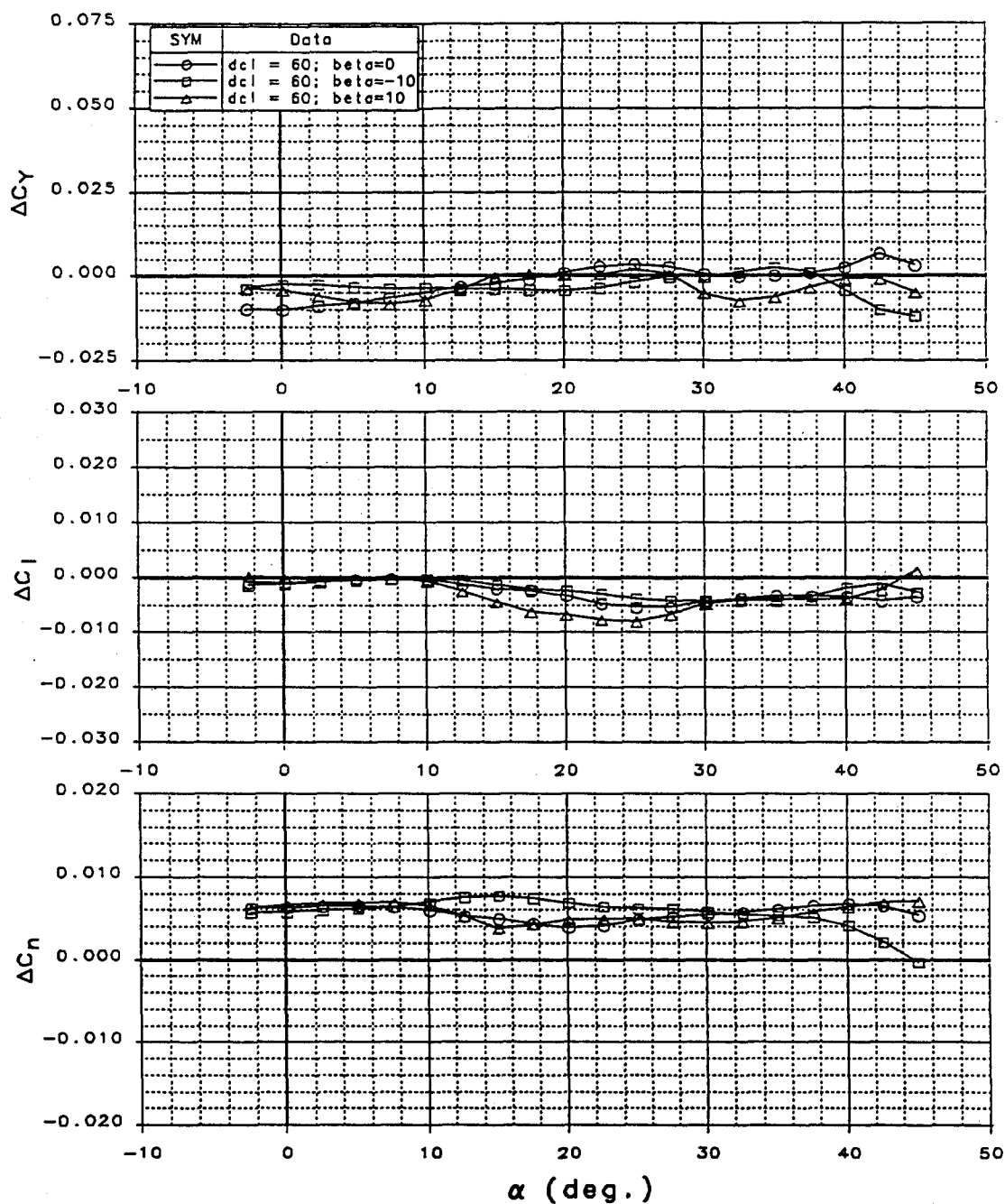


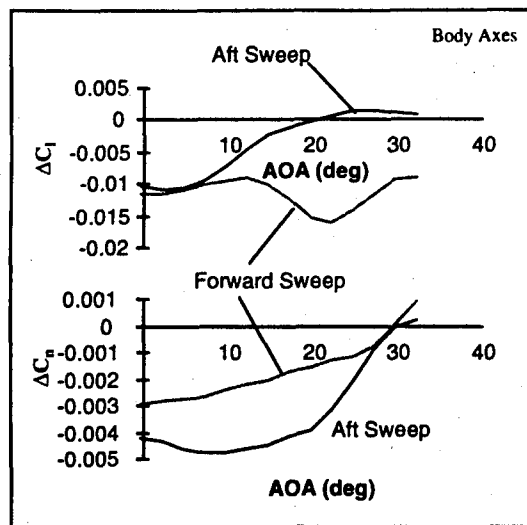
Figure 3-6 Clamshell Effectiveness at Sideslip

In summary, the clamshell provides good yaw control effectiveness up to high AOA; however, significant adverse rolling moments at high AOA reduce its usefulness on a fighter aircraft. Control power is generally linear with clamshell deflection. Its effectiveness is a direct function of moment arm to the cg, and therefore wingspan and hingeline orientation. Aft swept hingelines create a side force component when deflected, and increase the yaw control available. For the configuration tested, clamshell control power was fairly insensitive to windward sideslip angles. For typical fighter designs with short spans and thin wings, integration is difficult due to control surface area constraints coupled with structural integration challenges.

3.1.2 Spoiler

Integrated properly, large conventional spoilers can provide a great deal of lateral-directional control power to a tailless fighter. Spoilers are one of the few lateral controls that produce favorable roll-yaw characteristics. When integrated with a conventional elevon, blended spoiler-elevon deflections are useful for providing decoupled yaw and roll control power, and can function as speed brakes¹⁴. One drawback of spoilers is the lift loss created by the control during rolling maneuvers. This is especially detrimental during the power approach phase.

Like the clamshell, spoiler yaw effectiveness is a strong function of hingeline sweep. Aft swept hingelines generate a side force component when the spoiler is deflected, resulting in increased yaw power. Figure 3-7 shows spoiler data for two different hingeline sweeps on a tailless fighter. Forward swept spoiler hingelines result in better roll effectiveness, but poor yaw characteristics. Aft swept hingelines greatly improve the high AOA yaw characteristics at the expense of reduced roll effectiveness. Geometric constraints typically imposed by low signature design dictate that the spoiler edges be lined up with major airframe components, reducing the design space allowable for hingeline orientation. Figure 3-7 shows that even though roll effectiveness is greatly degraded, for the tailless configuration in question, the aft-swept spoiler results in greater overall coordinated roll control available.



Configuration 201 Blended
Control Envelope at 12 deg AOA

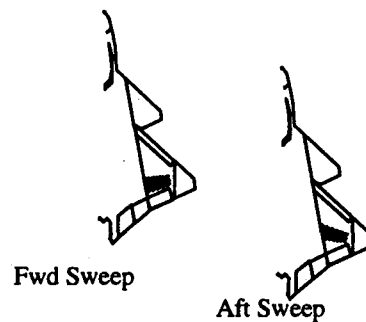
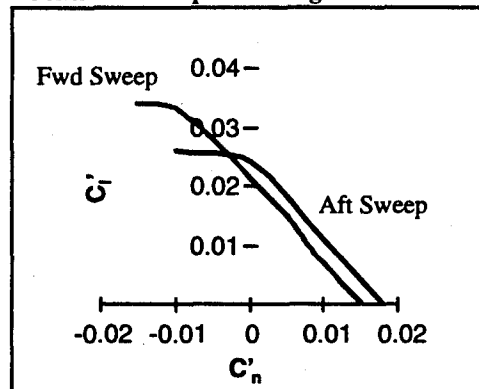


Figure 3-7 Aft Swept Spoilers Provide Greater Yaw Capability

The spoilers tested on the 65 deg sweep tailless fighter were effective through 40 deg AOA (Figure 3-8). The spoiler streamwise chord lengths were approximately 12% mean aerodynamic chord (MAC), and had an aft hingeline sweep of 25 deg.

Sideslip effects on spoiler control power are shown in Figure 3-9. The data represent a right-side spoiler deflection. The spoiler is on the windward side when sideslip is positive. At high AOA where maximum control power is required (often coupled with large sideslip), roll power is severely degraded by sideslip. Yaw power is improved by leeward sideslip, but degraded by windward sideslip.

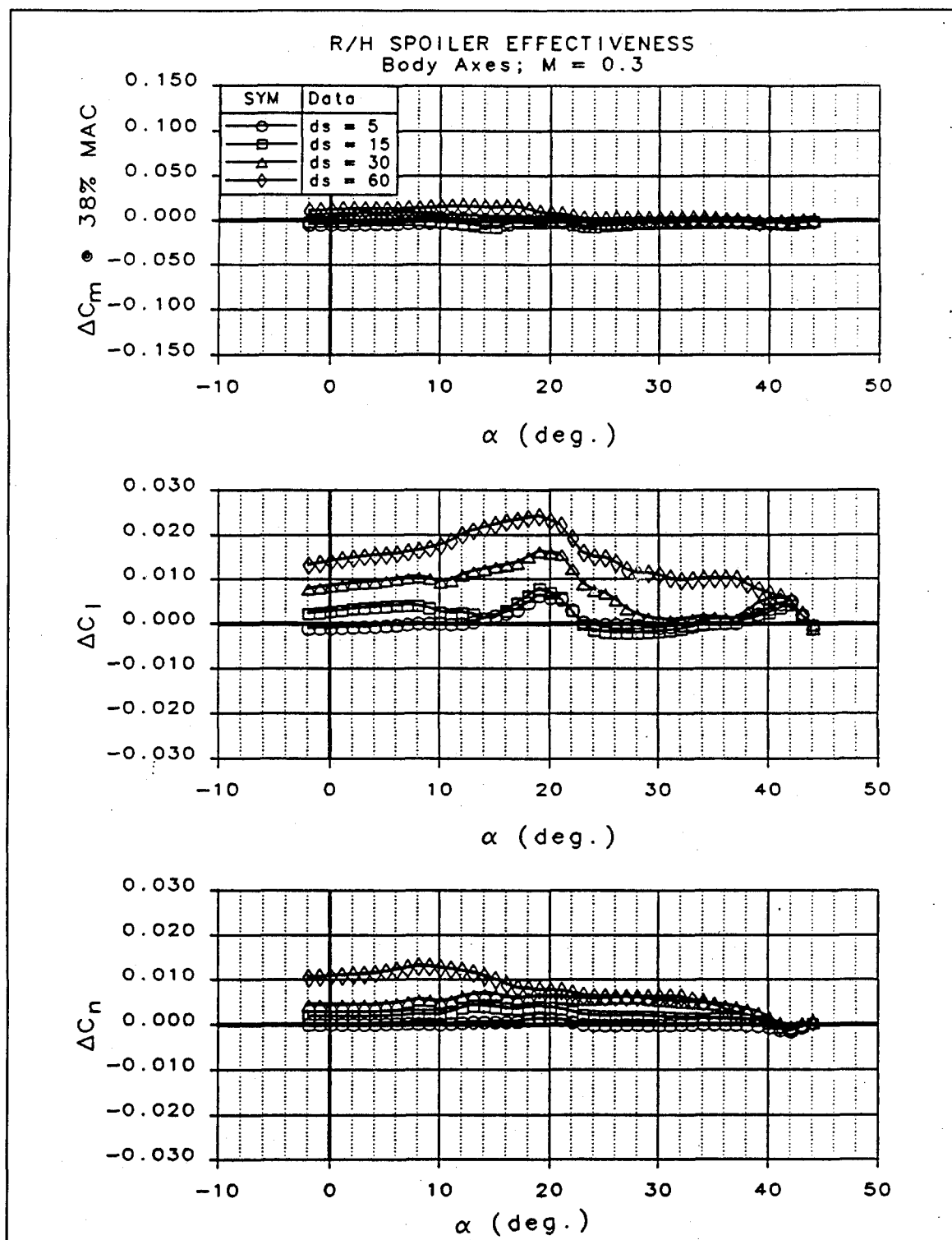


Figure 3-8 Spoiler Control Effectiveness for 65-deg Sweep Tailless Fighter

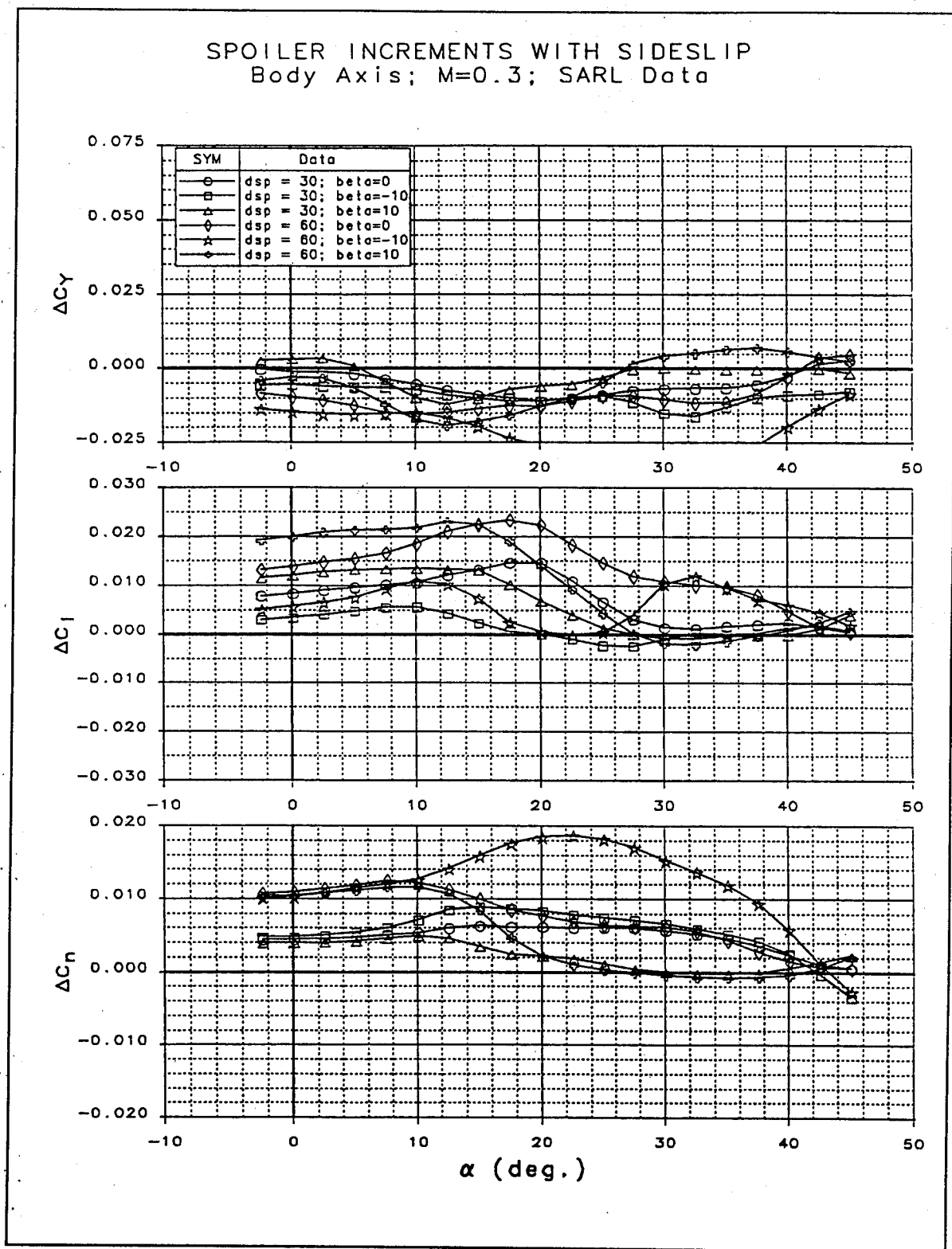


Figure 3-9 Windward Sideslip Degrades Spoiler Effectiveness

Drawbacks of spoilers are the associated loss in lift when deployed, and loss of effectiveness at high AOA and transonic speeds. Spoiler effectiveness reverses at small deflections and is generally nonlinear with deflection; however, the spoilers can be biased up at increasing AOA to help reduce the "deadband" at small deflections. An additional problem complicating spoiler integration is the effect that spoiler deflections have on trailing edge control surfaces. Figure 3-10 shows the effect of spoiler deflection on elevon control effectiveness. Finally, while effective at supersonic speeds, spoiler hinge moments are very high, and require large actuators for operation.

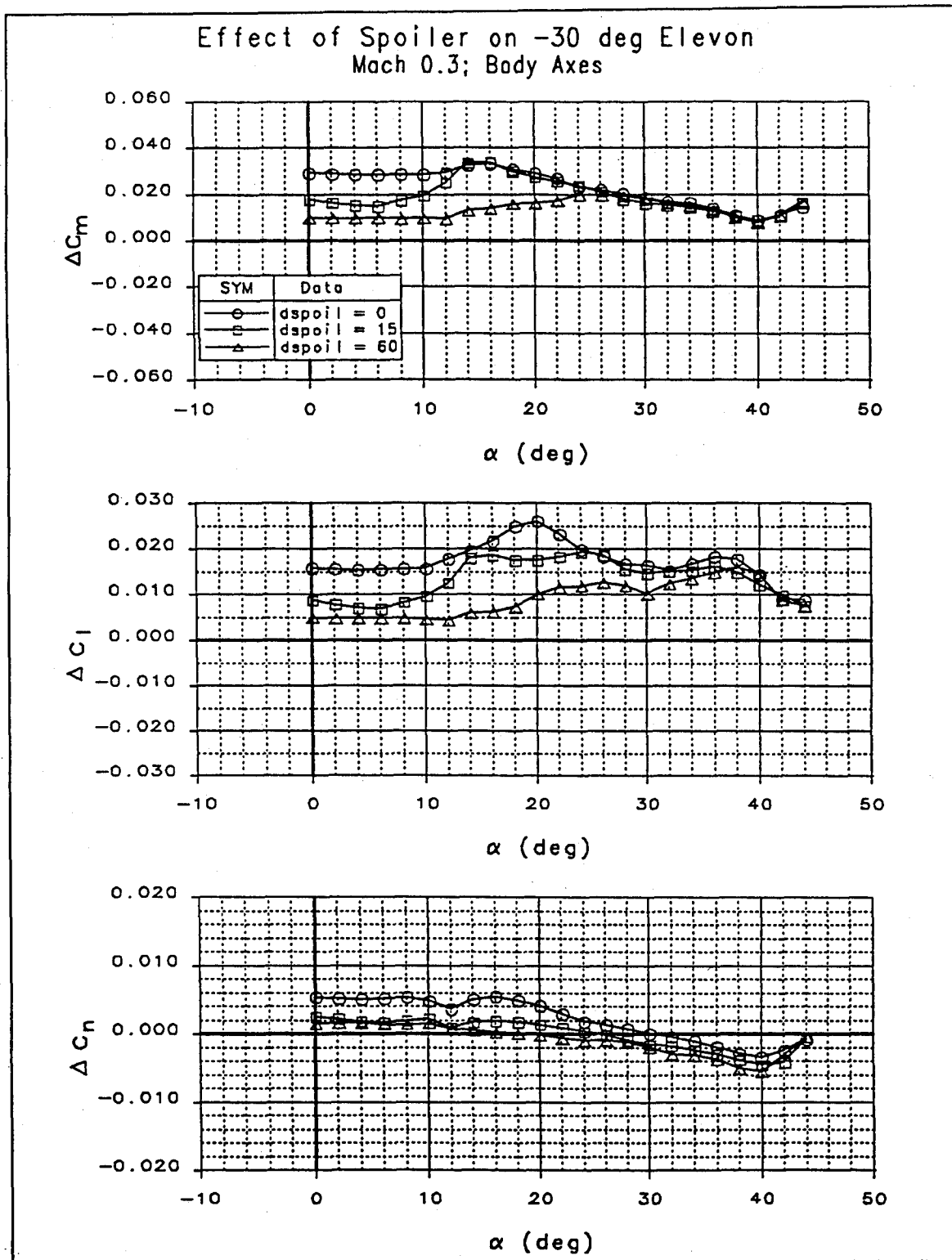


Figure 3-10 Spoiler Deflections Cause Adverse Interactions with Trailing Edge Flaps

3.1.3 All Moving Wing Tip

The AMT is not a new concept. The Horton brothers used an all moving wing tip control on the Horton H Va flying wing¹⁵. The AMT is described as an "all-moving elevator" in Reference 16; several examples are shown including the *Pterodactyl* flying wing and the more conventional *Short's Sherpa*. NACA tested a series of all moving tip control surfaces during the 1950's^{17, 18}. More recently, MBB wind tunnel tested a series of fighter configurations, one employing an all moving "wingeron", or all moving tip¹⁹. Both McDonnell Douglas and General Dynamics investigated very large all moving wing tips during the AFTI competition^{20, 21}. An early version of the F-16XL (SCAMP) configuration employed an all moving tip for roll control²². Finally, all moving wing tips were investigated on a generic tailless fighter model at the SARL low-speed wind tunnel at Wright Patterson Air Force Base, Ohio (WPAFB)²³.

Previous AMT studies have focused on the AMT for roll control, direct lift, and general lateral-directional control. The present investigation focuses on the AMT as a yaw control device. The AMT produces roll through conventional means -- e.g., change in local lift coefficients with deflection acting through a moment arm. Trailing edge down (TED) deflections create yaw control through increased profile and induced drag (similar to a clamshell). The advantage of the AMT over a clamshell is that it is easier to integrate into a thin wing section, simpler to actuate, and can be made larger than the clamshell and therefore more effective.

Past wind tunnel test experience has indicated that the all-moving tip is an excellent source of yaw control power. When deflected at large angles (up to 60 deg TED), the tip produces body axis yawing moments to very high AOA. Depending on AOA, rolling moments range from adverse (at low AOA) to favorable (high AOA). Figure 3-11 shows data collected for a representative tailless fighter configuration during small scale testing at the LMTAS 2' x 3' ADF tunnel.

ALL MOVING TIP INCREMENTS
 Body Axis; $M=0.13$; CONFIGURATION 201; ADF 9502

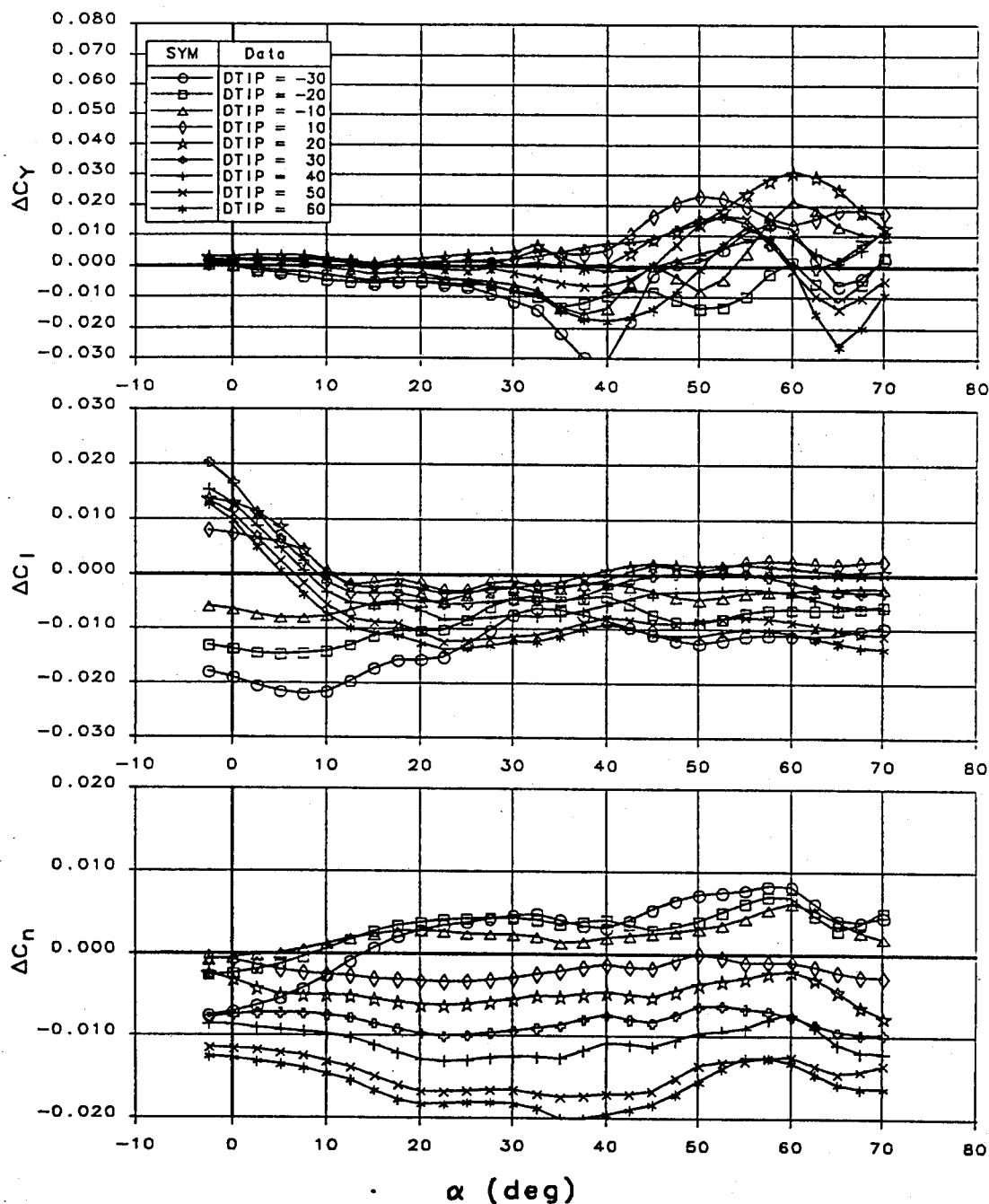


Figure 3-11 AMT Control Effectiveness

Analysis of Figure 3-11 shows that trailing edge up (TEU) deflections produce significant constant body axis rolling moments through 70 deg AOA. Associated yawing moments are favorable at low AOA, but become adverse above 10 deg AOA. TED deflections produce body axis yawing moments up to the highest AOA tested. At low AOA, rolling moments are adverse. However, at AOA greater than 10 deg, all TED deflections generate favorable roll-yaw relationships.

The AMT configuration tested did not produce significant pitching moments for TED deflections. This is dependent on wing geometry, and fore/aft location with respect to the cg. TEU deflections produced small nose up moments. Nose up control power generated by symmetric tip deflections may be useful for trim at elevated g's and high speeds where elevon hinge moments are high. By unloading some of the elevon deflection required for trim at high speed, elevon actuator size could be reduced (assuming that high speed trim sets the elevon hinge moment requirement).

Figure 3-12 shows the same data plotted for different deflections at three AOA. Overlaid on the plots are F-16 rudder control effectiveness data for comparison. The F-16 data were referenced to be representative of the wing area and span of the tailless fighter data. Note the linearity of the AMT's yaw effectiveness with deflection -- even at 45 deg AOA. As expected, the F-16 rudder data is very linear at low AOA with a 30 deg rudder deflection corresponding to an AMT deflection of about 50 deg (AOA = 10 deg). The F-16 rudder is ineffective above 40 deg AOA, becoming nonlinear at large deflections, while at high AOA, the AMT produces even greater yawing moments than at 10 deg AOA.

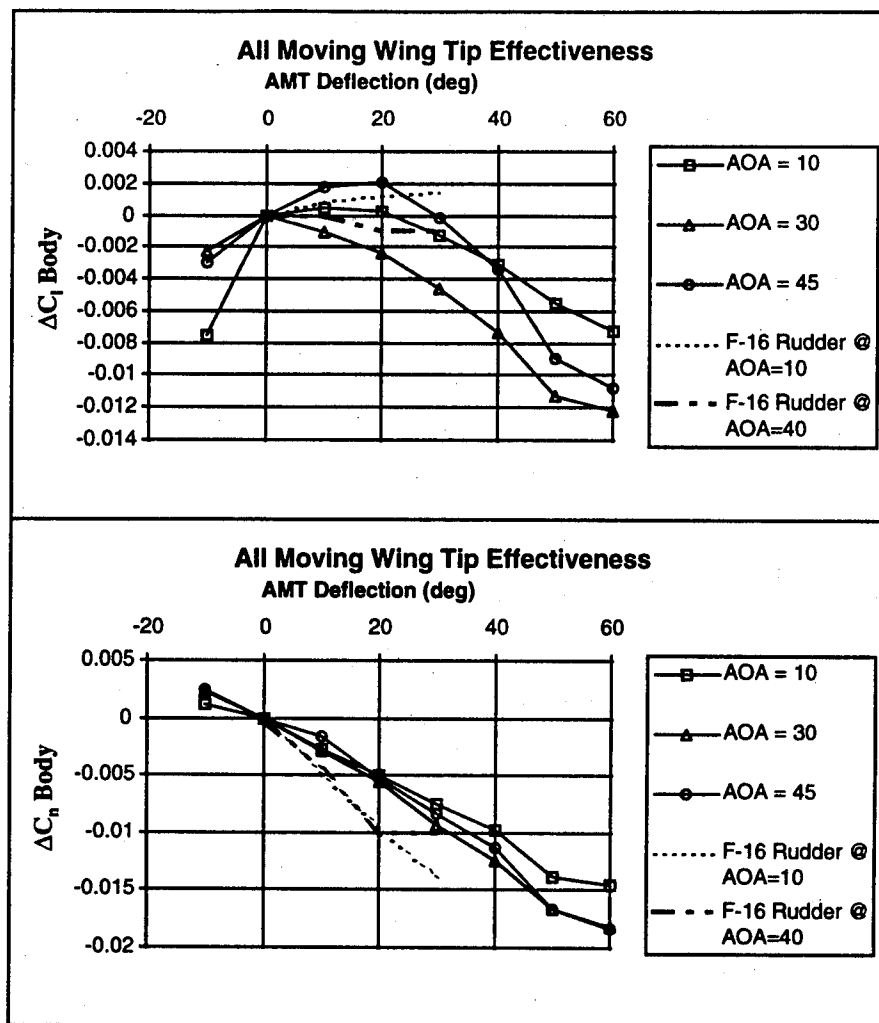


Figure 3-12 AMT Yaw Effectiveness is Linear with Deflection

Analysis of Figures 3-11 and 3-12 show that TED deflections are most useful for yaw control. TEU deflections provide good roll effectiveness up to high AOA. If the deflection can be constrained to be in only one direction (e.g., TED), the hingeline can be sealed to some degree for RCS purposes. This is discussed further in Section 6.1.7. Rolling moments are nonlinear at small deflections, but become favorable, and more linear at larger deflections.

The effect of sideslip on AMT yaw effectiveness is shown in Figure 3-13. Unfortunately, data with sideslip are only available up to 32.5 deg AOA. Based on the information available, the AMT behaves well when exposed to sideslip angles up to ± 10 deg. For comparative purposes, conventional rudder effectiveness can be a strong function of

sideslip at AOA near C_{Lmax} . While the F-16 rudder remains effective up to 40 deg AOA at zero sideslip, yaw control is lost at small sideslip angles and AOA > 30 deg; as a result yaw augmentation is impossible with rudder alone for AOA greater than 30 deg.

Figure 3-14, taken from Reference 24, shows the benefits of aerodynamic balance afforded by the AMT. The AMT is a much more efficient roll control device than conventional trailing edge controls at transonic speeds when hinge moment is taken into account.

Summarizing, the AMT is an excellent source of yaw control power up to very high AOA. Yaw control magnitudes at large deflections are on the order of that produced by an F-16 rudder. Adverse roll/yaw relationships occur at low AOA while favorable roll/yaw relationships are available at high AOA (TED deflections). Sideslip effects on AMT control effectiveness are satisfactory, and generally more favorable than for more conventional control concepts (e.g., clamshell, spoiler, rudder, etc.). The aerodynamic balance of the AMT arrangement results in relatively small high-speed hinge moments with excellent control effectiveness. If TEU deflections are allowed, the AMT can be used to offset some of the elevon pitch trim requirements at high-speed, potentially reducing elevon hinge moment requirements.

ALL MOVING TIP INCREMENTS WITH SIDESLIP
 Body Axis; $M=0.13$; CONFIGURATION 201; ADF 9502

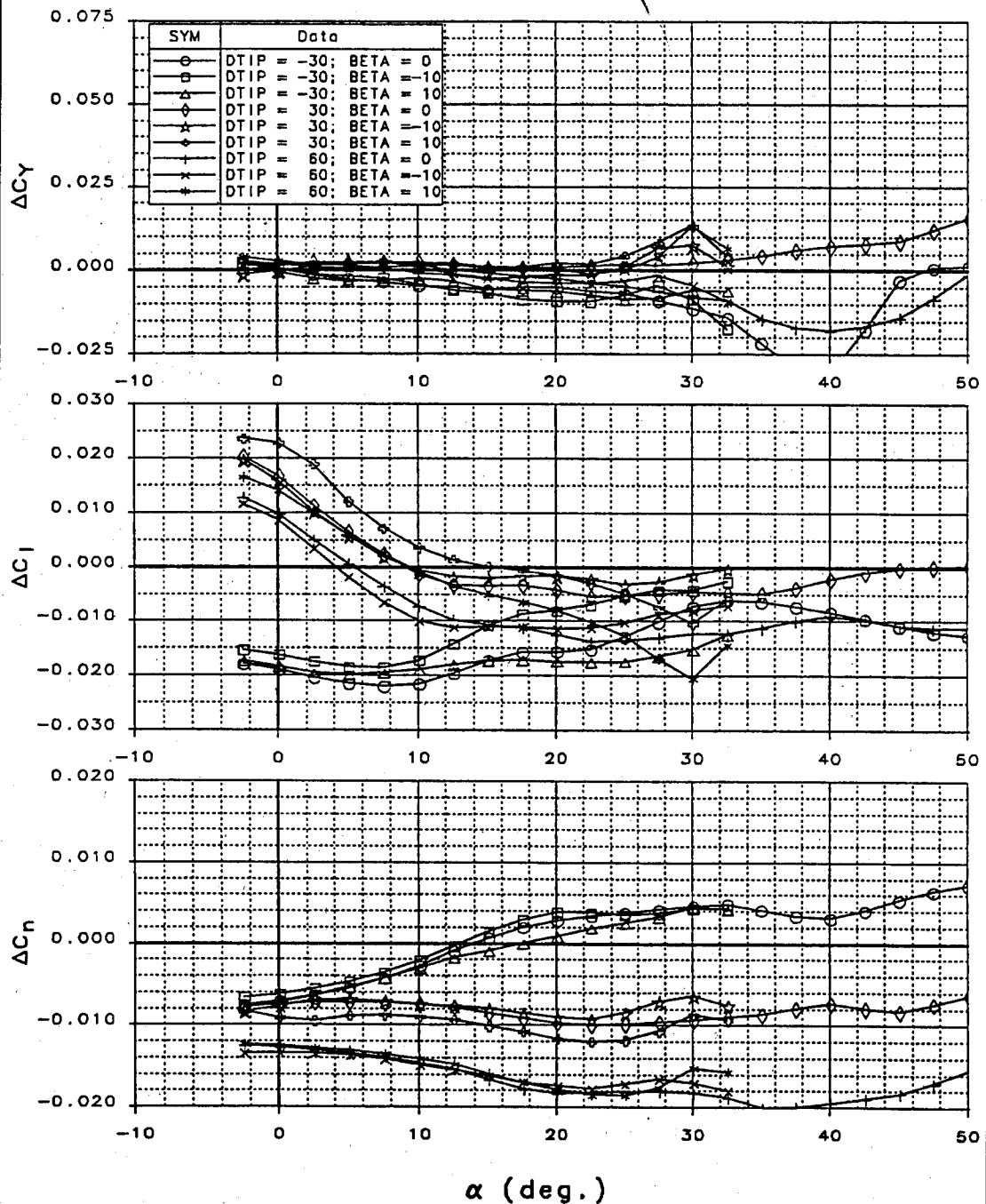


Figure 3-13 AMT Control Effectiveness is Relatively Unaffected by Sideslip

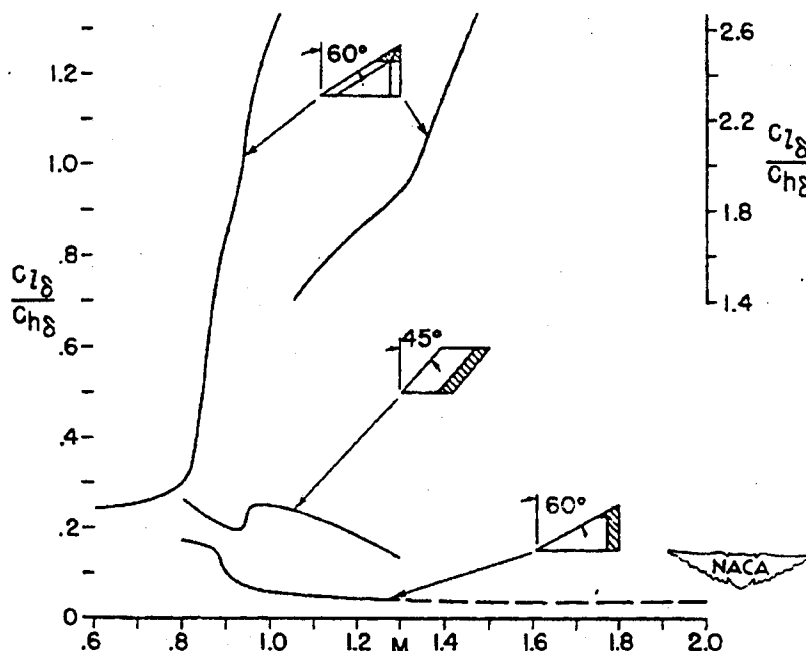


Figure 3-14 AMT Control Effectiveness to Hinge Moment Ratios are Much Greater than a Conventional Trailing Edge Flap

3.1.4 Differential Leading Edge Flaps

Differential leading edge flap (DLEF) deflections provide lateral-directional control power at high AOA by reorienting the leading edge vortex system. As a result, their application is a function of leading edge sweep, leading edge radius and operating AOA. The F-22 will use DLEF to augment roll performance in the 13 deg - 26 deg AOA region²⁶. The F-16XL used DLEF for anti-spin control and spin recovery²⁷. DLEF was investigated as a means to augment lateral-directional stability in the 27-35 deg AOA range during the F-16 Agile Falcon program²⁸.

Figure 3-15 shows control power available from various deflections of the right-hand outboard leading edge flap (LEF) on the 65 deg sweep tailless fighter. Analysis of this

figure shows that useable control power is available between approximately 15 deg and 40 deg AOA. Flow visualization studies indicated that downward deflections of the LEF appeared to strengthen the leading edge vortex on the deflected side.

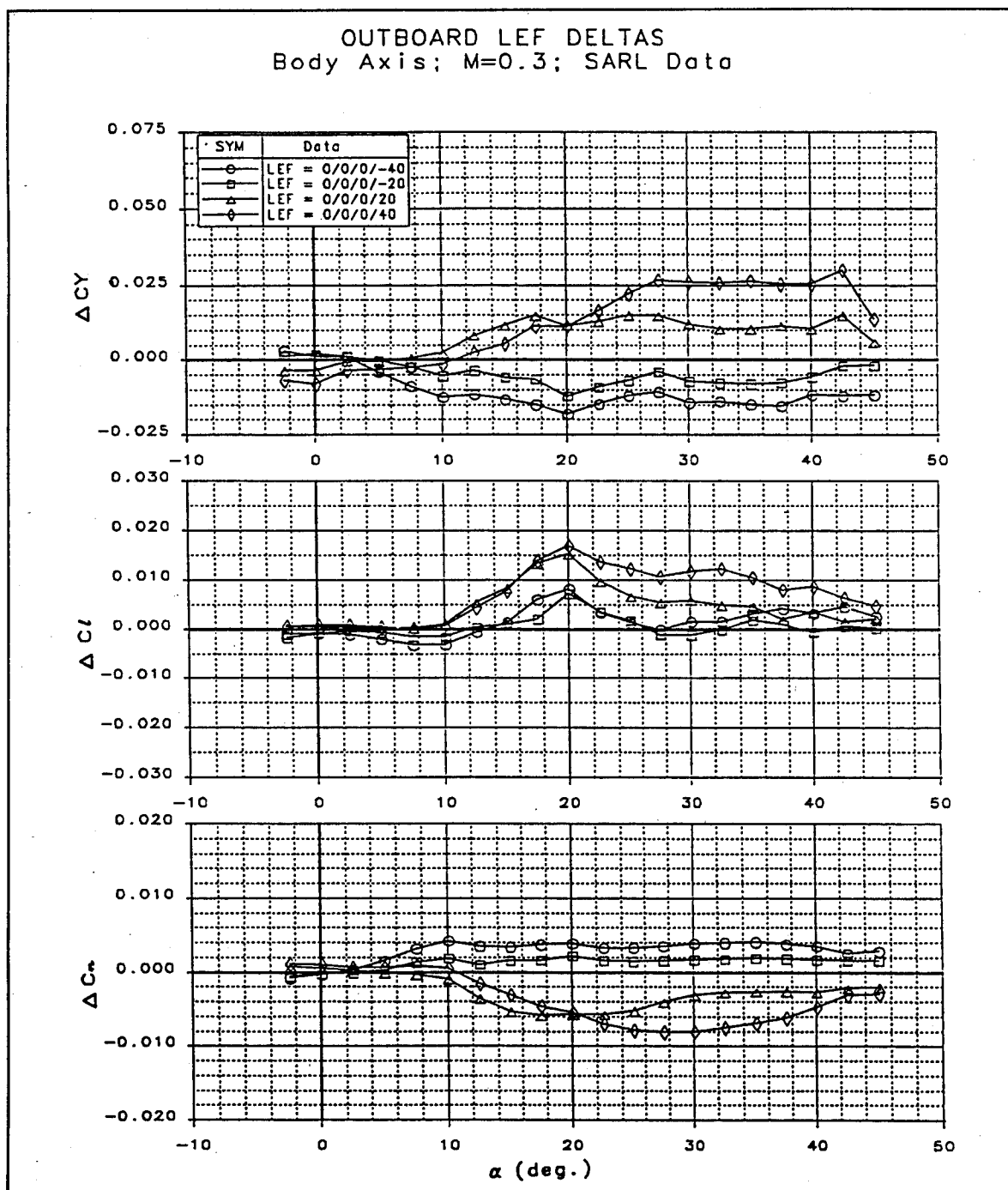


Figure 3-15 Differential LEF Effectiveness

Analysis of the axial force data shows an increase in leading edge suction on the downward-deflected flap, contributing to the body axis yawing moment. Likewise, negative flap deflections (leading edge up) trap a vortex behind the flap and increase the axial force on the deflected side resulting in a yawing moment in the opposite direction (Figure 3-16).

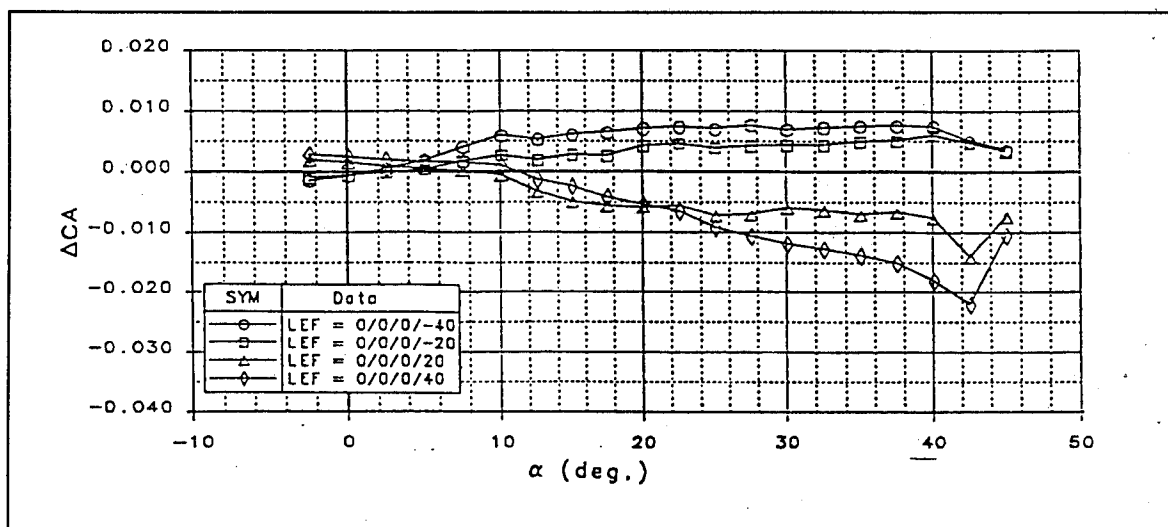


Figure 3-16 Increased Suction on the LEF Contributes to the Yawing Moment

Significant aerodynamic interactions were observed when a LEF was deflected inboard of the differential flap. Comparison of Figure 3-17 with Figure 3-15 shows that in general, outboard flap deflections in the presence of a 40 deg inboard flap deflection resulted in less yaw effectiveness. Other flap deflections may give different results.

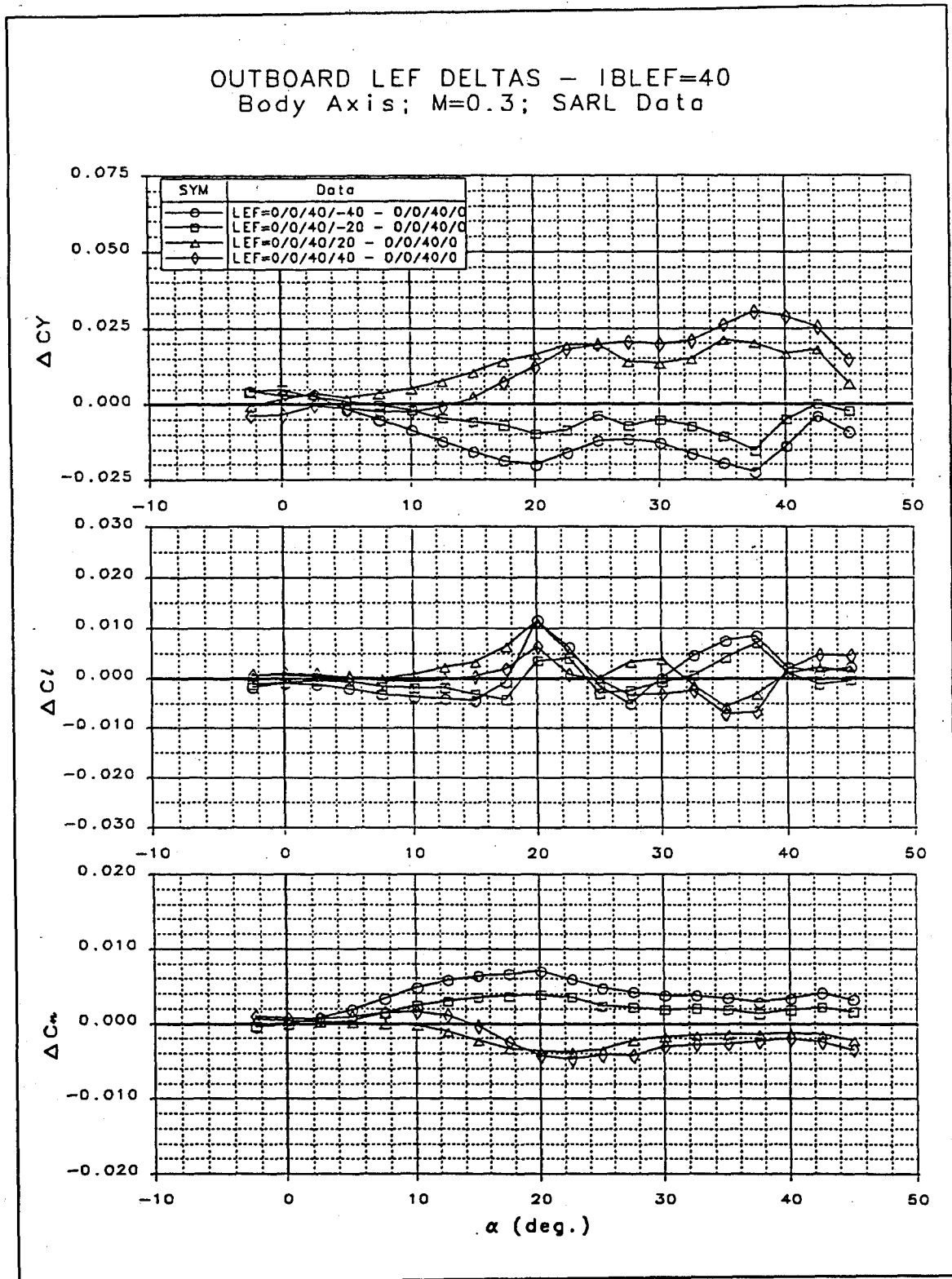


Figure 3-17 Inboard LEF Aerodynamic Interaction with Outboard LEF

Figure 3-18 shows differential flap effectiveness versus deflection. The data are presented for three AOA both with and without an interacting inboard LEF deflection. Analysis of this figure illustrates how the inboard flap degrades the outboard flap effectiveness at 15 and 30 deg AOA. At 45 deg AOA, effectiveness is essentially unchanged by the inboard deflection. One can also see the nonlinear nature of the controller both in roll and yaw. (DLEF is used on the F-22 as a "bang-bang" yaw controller due to large nonlinearities with deflection.) At high AOA, positive deflections (leading edge down) create more control power than negative deflections.

Differential LEF Data -- Body Axes; Mach 0.3

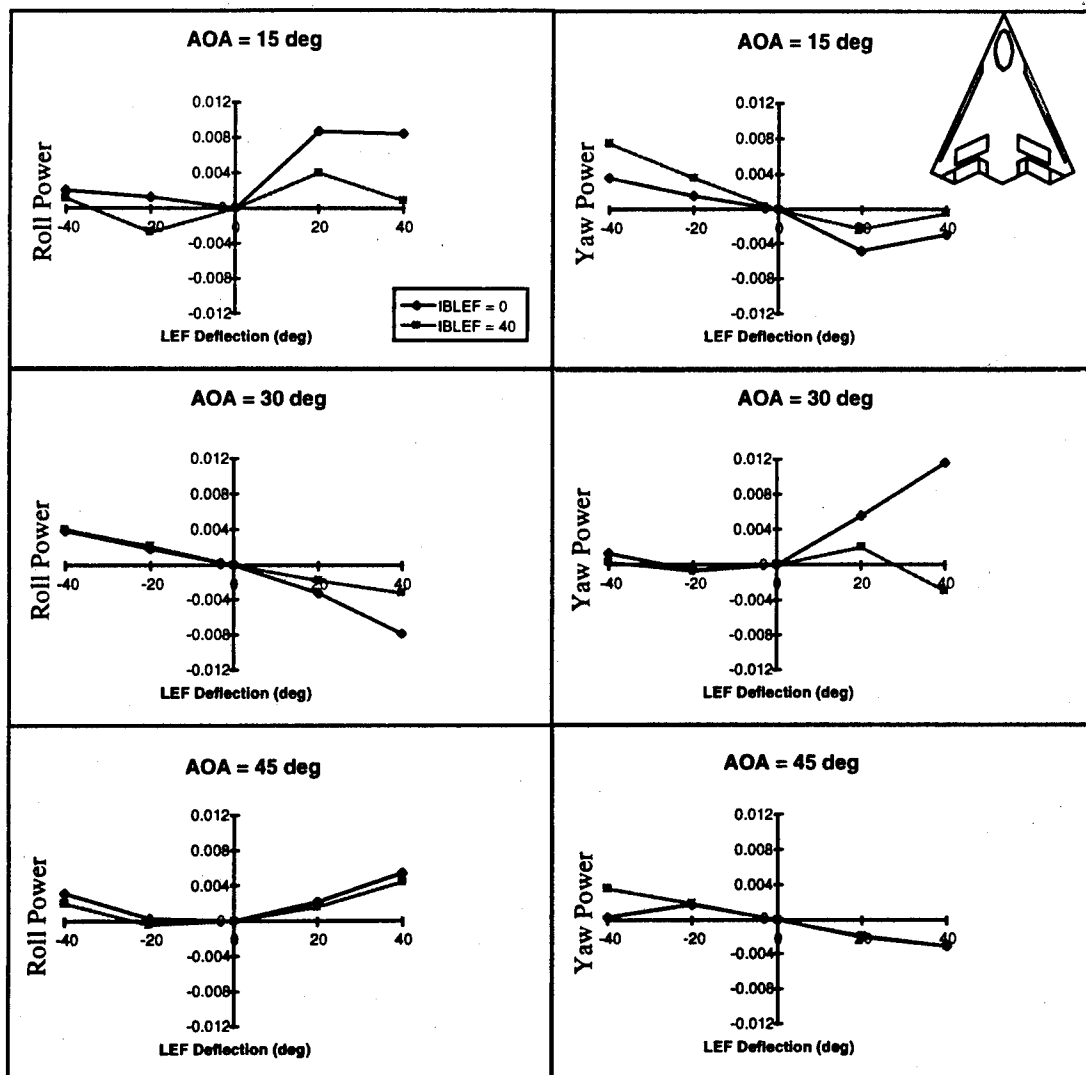


Figure 3-18 DLEF Effectiveness vs Deflection

Figures 3-19 and 3-20 show the stabilizing influence of DLEF at ± 10 deg of sideslip, respectively. Both sets of data represent right side flap deflections. In Figure 3-19, sideslip is $+10$ deg; therefore, the flaps are on the windward side. Conversely, in Figure 3-20, sideslip is -10 deg and the flaps are on the leeward side. All data are in body axes.

Analysis of Figure 3-19 shows that positive DLEF deflections on the windward side provide a stabilizing influence in roll between 20 and 34 deg AOA. Unfortunately, they have a destabilizing influence on yaw above 12 deg AOA. Furthermore, positive deflections create nose-up pitching moments above 25 deg AOA. Negative DLEF deflections on the windward side have the opposite effect. In Figure 3-20, one sees that positive DLEF deflections on the leeward side provide stabilizing influences in both roll and yaw at AOA greater than 8 deg. Negative deflections on the leeward side result in destabilizing tendencies.

Figure 3-21 shows the combined effect of DLEF and sideslip on stability axis yawing moment. The curves show that positive DLEF deflection on the leeward side and negative deflections on the windward side improved directional stability (the cross-over to instability went from 24 deg to 28 deg). Furthermore, the magnitude of instability in the region between 30 and 45 deg AOA was reduced. This is important for a tailless fighter design. Reduction of the unstable lateral-directional moments in the stall region using DLEF will reduce the demand on other yaw control surfaces for stabilization. Neutral to stable lateral-directional characteristics are acceptable at lower AOA where sufficient yaw control power can successfully augment the dynamics.

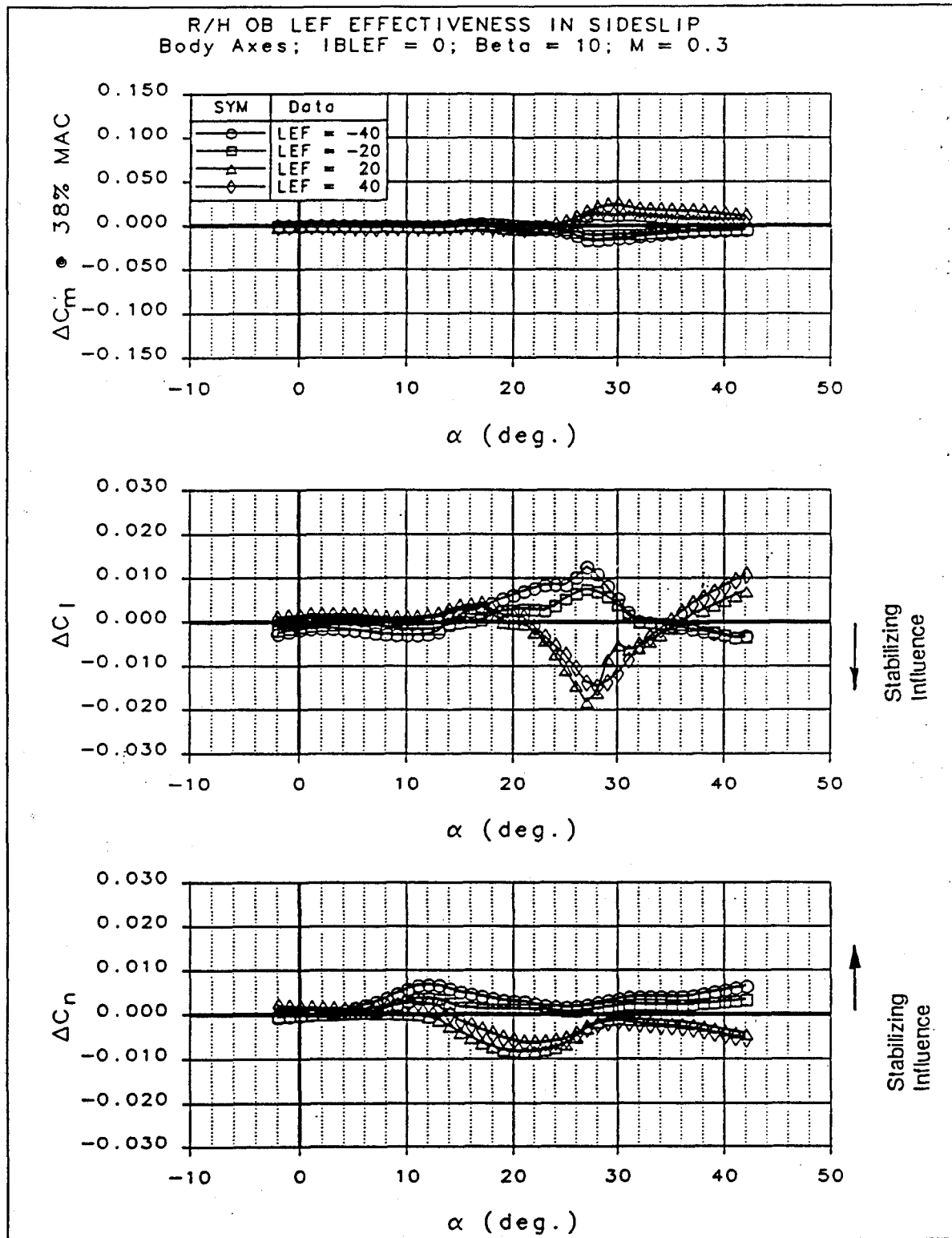


Figure 3-19 DLEF Effectiveness with Windward Sideslip

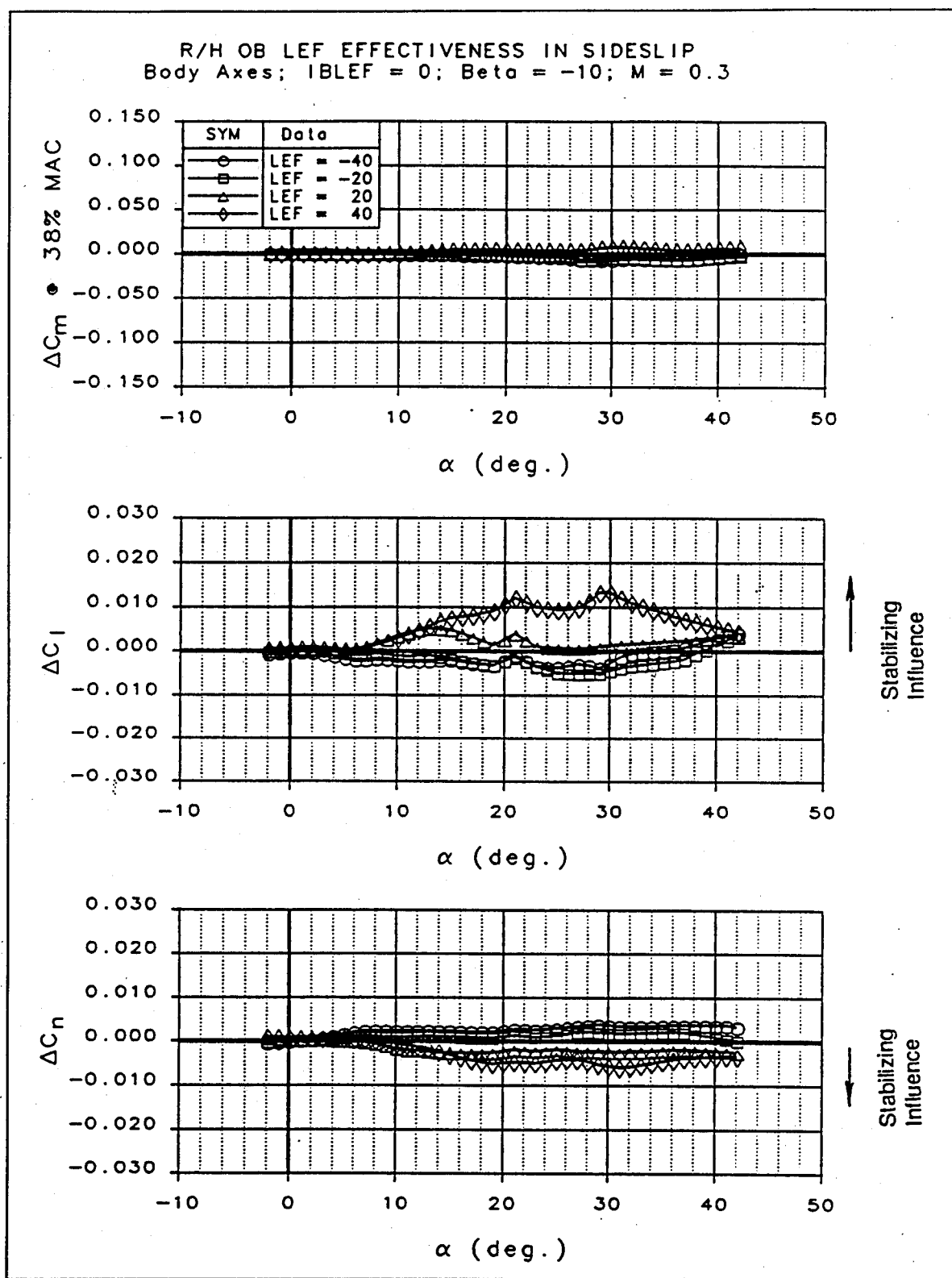


Figure 3-20 DLEF Effectiveness with Leeward Sideslip

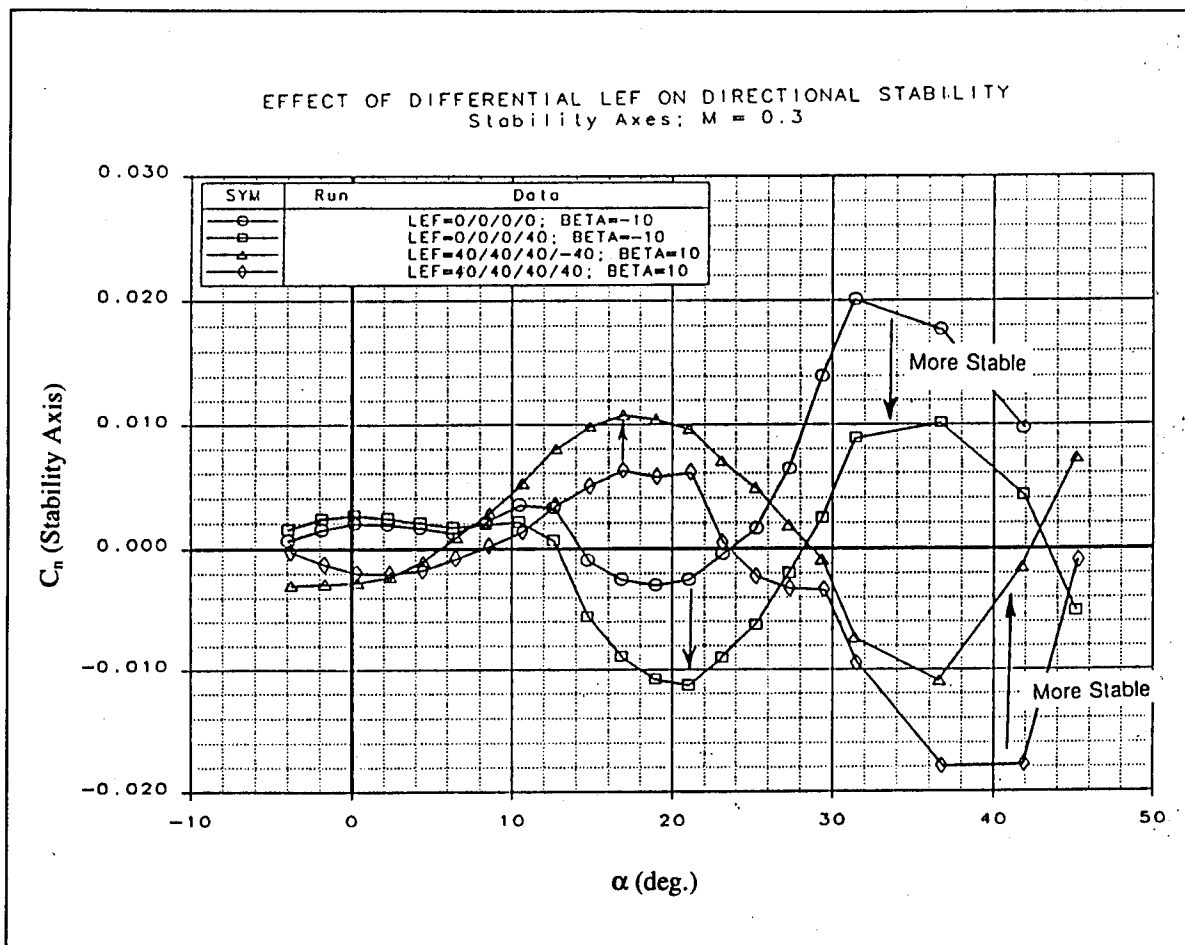


Figure 3-21 Differential LEF Improve Directional Stability

DLEF retains control effectiveness at higher Mach numbers (Figure 3-22). However, its usefulness at high AOA is considerably degraded above Mach 0.6. Typically, aeroelastic effects on LEF improve the controls effectiveness (i.e., flex-to-rigid ratios are greater than one). This may offset the decreased rigid control effectiveness at high-Mach, elevated-g conditions.

Negative DLEF deflections will be difficult to actuate and seal. Blade seals are required on control surfaces to improve aerodynamic efficiency and RCS. A negative deflection requirement makes seal integration improbable, resulting in poor RCS performance. Figure 3-23 compares the control power available due to downward deflections versus differential deflections (positive and negative on opposing sides). Study of Figure 3-23 shows that the addition of a negative deflection provides some control effectiveness be-

low 10 deg AOA. The 0/40 deflection case has only about two-thirds the yaw control power as the -40/40 deflection. Control power reductions resulting from limiting LEF control deflections to the positive direction are not insignificant.

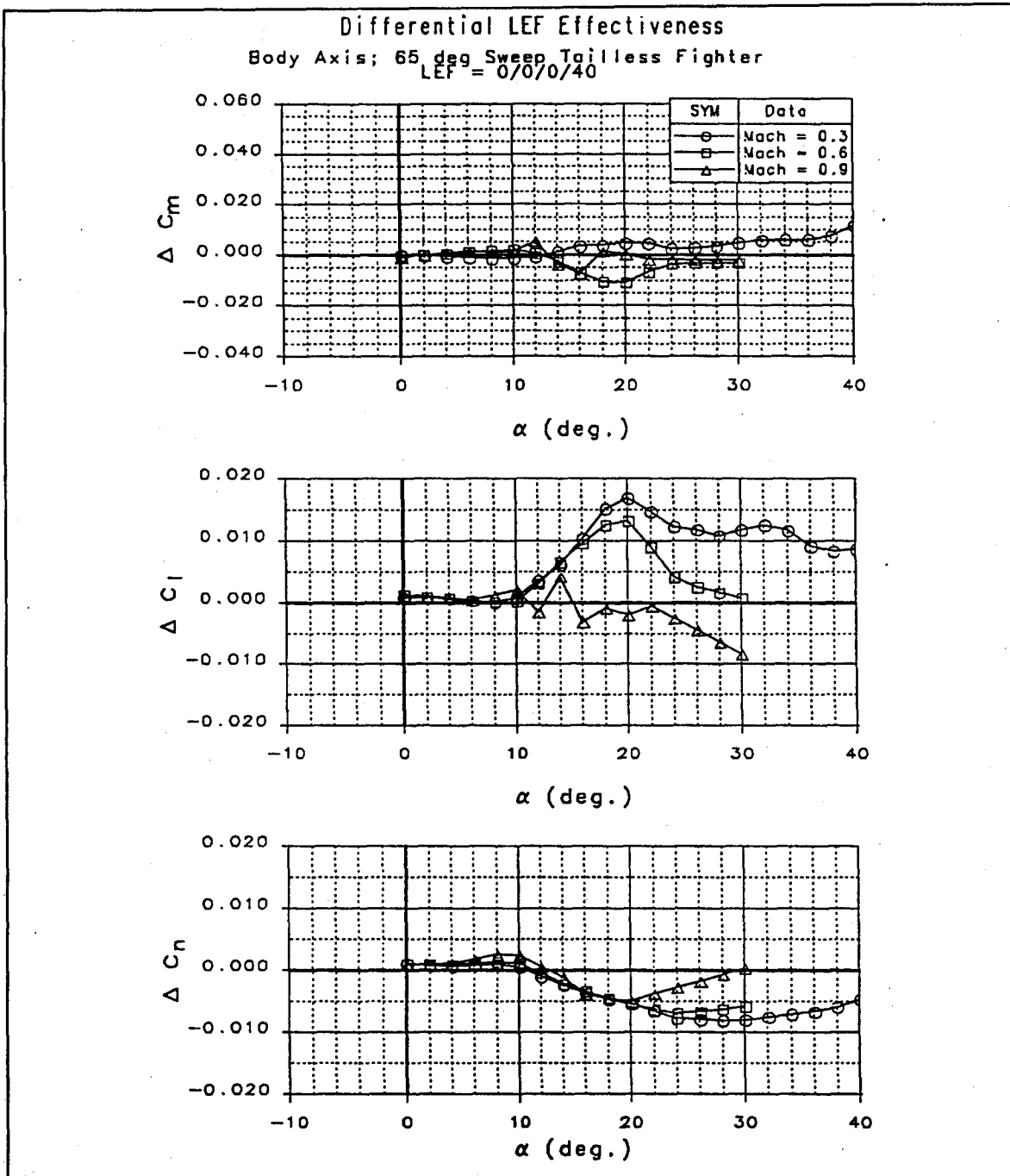


Figure 3-22 DLEF Effectiveness is Degraded at Transonic Mach Numbers

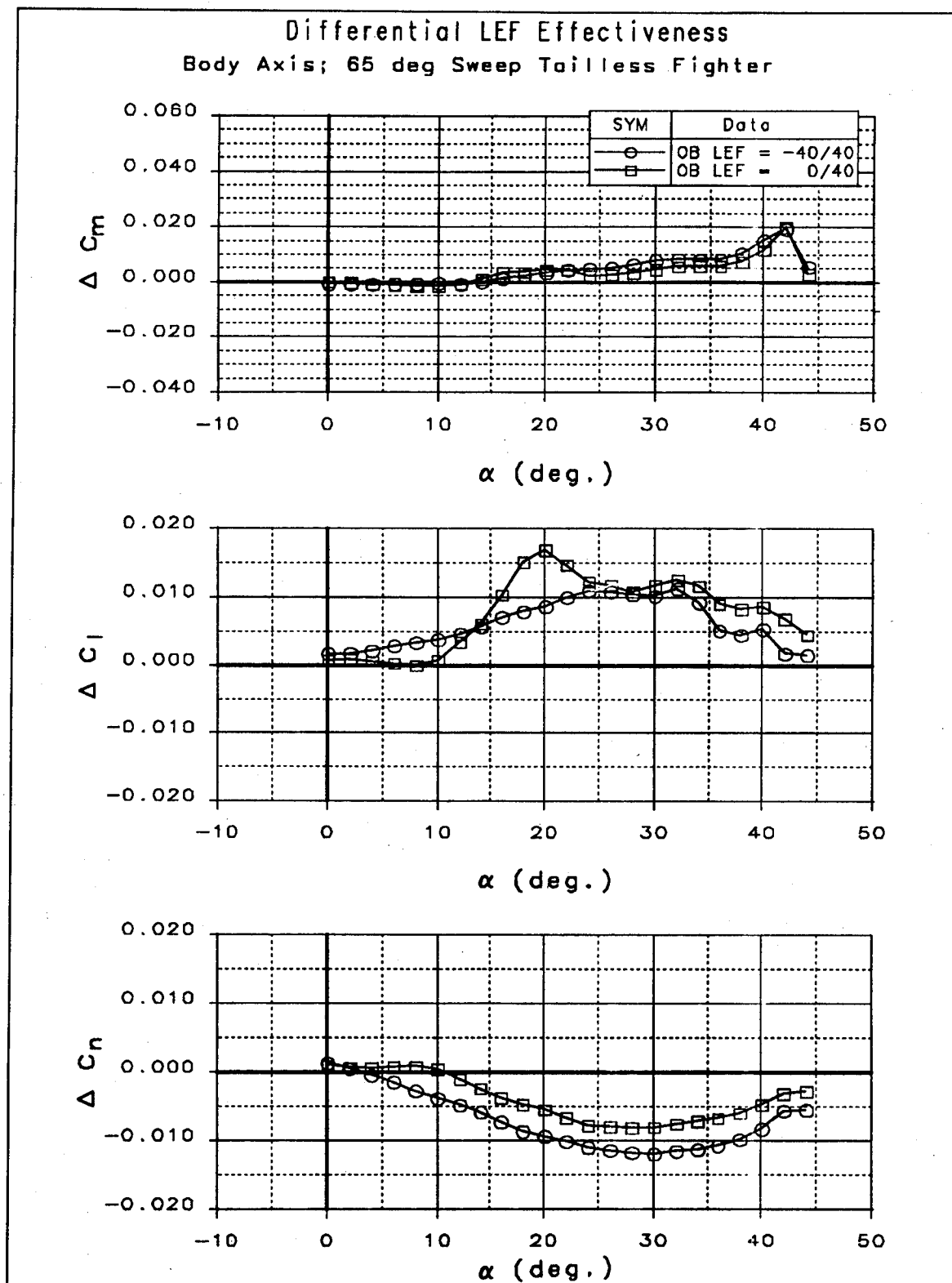


Figure 3-23 Limiting DLEF to Positive Deflections on one Side Reduces the Yaw Control Power Available

Modern LEF drive units consist of a power drive unit (PDU), and several rotary gear boxes located along a torque shaft. The gear boxes reduce the very high rotational rates generated by the PDU to a low rate-of-travel. In this manner, very high stiffness at the LEF can be achieved. The torque multiplication inherent in the system allows small hydraulic motors to meet the high hinge moment requirements of a LEF. Typical state-of-the-art LEF drive systems operate at 30 deg/sec with a 30 Hz bandwidth. This rate is marginally high enough to augment lateral-directional dynamics at low speeds. Higher rate limits and large leading edge up deflections will affect the PDU design, and may result in lower overall hinge moment capability at high speeds.

To summarize, DLEF provides significant lateral-directional control moments at moderate to high AOA. DLEF generates stabilizing tendencies in lateral-directional stability in regions where conventional yaw controls lose effectiveness. Control effectiveness is nonlinear in both roll and yaw depending on AOA, and will require scheduling of flight control gains to be useful -- implementation as a "bang-bang" type of control may be simplest. Control effectiveness is retained at higher Mach numbers; although it is not as effective at high AOA as for low Mach conditions. There is a significant benefit in yaw control power to deflect the opposing LEF upward to large angles. Actuator and RCS integration issues will probably limit deflections to leading edge down angles only. This control is most useful for power approach and low-speed high AOA flight conditions for stability augmentation and roll coordination.

3.1.5 Spoiler-Slot Deflector

The SSD is one of the older "innovative" concepts investigated. Deflector concepts were investigated as early as 1941 with the goal of improving high AOA characteristics of lateral control devices²⁹. With the advent of hydraulically boosted control surfaces and high speed flight, interest again peaked in the 1950's for reduced hinge moment control devices that retained good effectiveness at transonic speeds and high AOA. Various slot deflector arrangements were tested by NACA throughout the 1950's³⁰⁻³³. A number of

high-speed aircraft have been designed using SSD arrangements including the XF-107 and the RA-5 Vigilante^{34, 35}. Boeing's SST proposal used SSD for lateral control³⁶.

A properly designed SSD arrangement has better high AOA and transonic lateral-directional control effectiveness over a conventional spoiler (Figures 3-24 and 3-25). Furthermore, the SSD arrangement is less affected by high-speed flexibility effects compared to a conventional aileron. The deflector can be mechanically linked to the upper-surface spoiler, resulting in lower total hinge moment over a flap-type spoiler configuration (Figure 3-26). A significant savings in actuator and subsystem weight can be realized compared to a conventional spoiler.

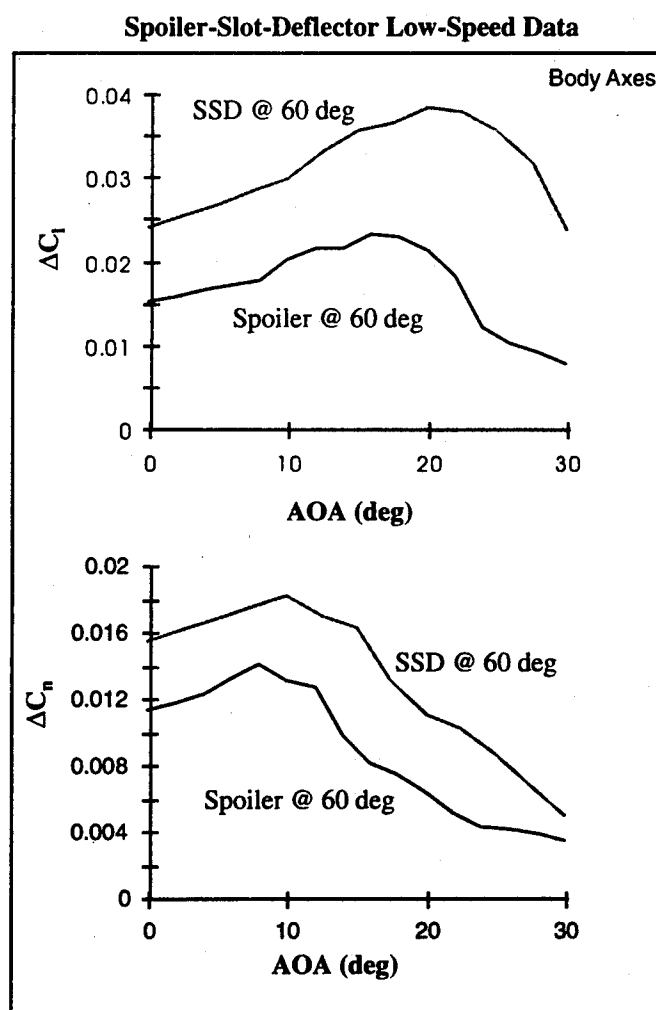


Figure 3-24 The SSD Provides Greater Lateral-Directional Control Power to Higher AOA than Conventional Spoilers

SSD High-Speed Roll Effectiveness

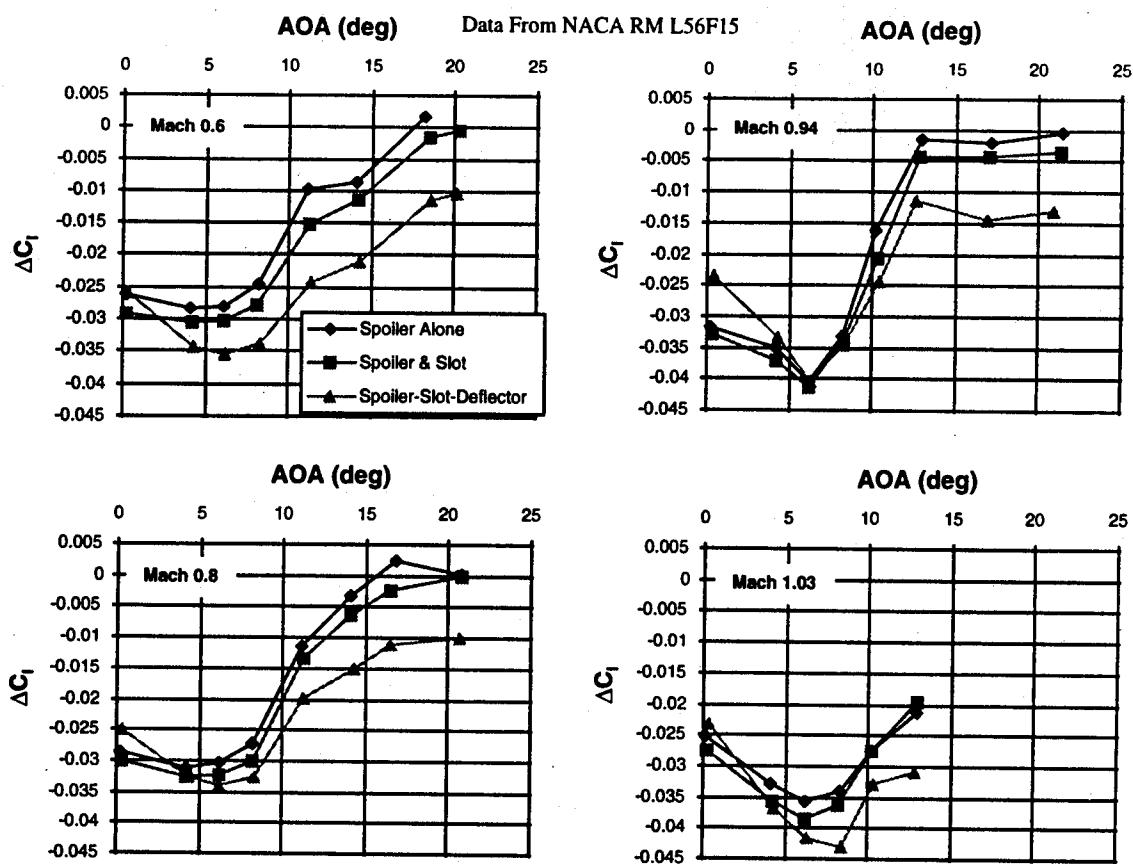


Figure 3-25 The SSD Generates More Lateral-Directional Control Power than a Conventional Spoiler at Transonic Mach Numbers

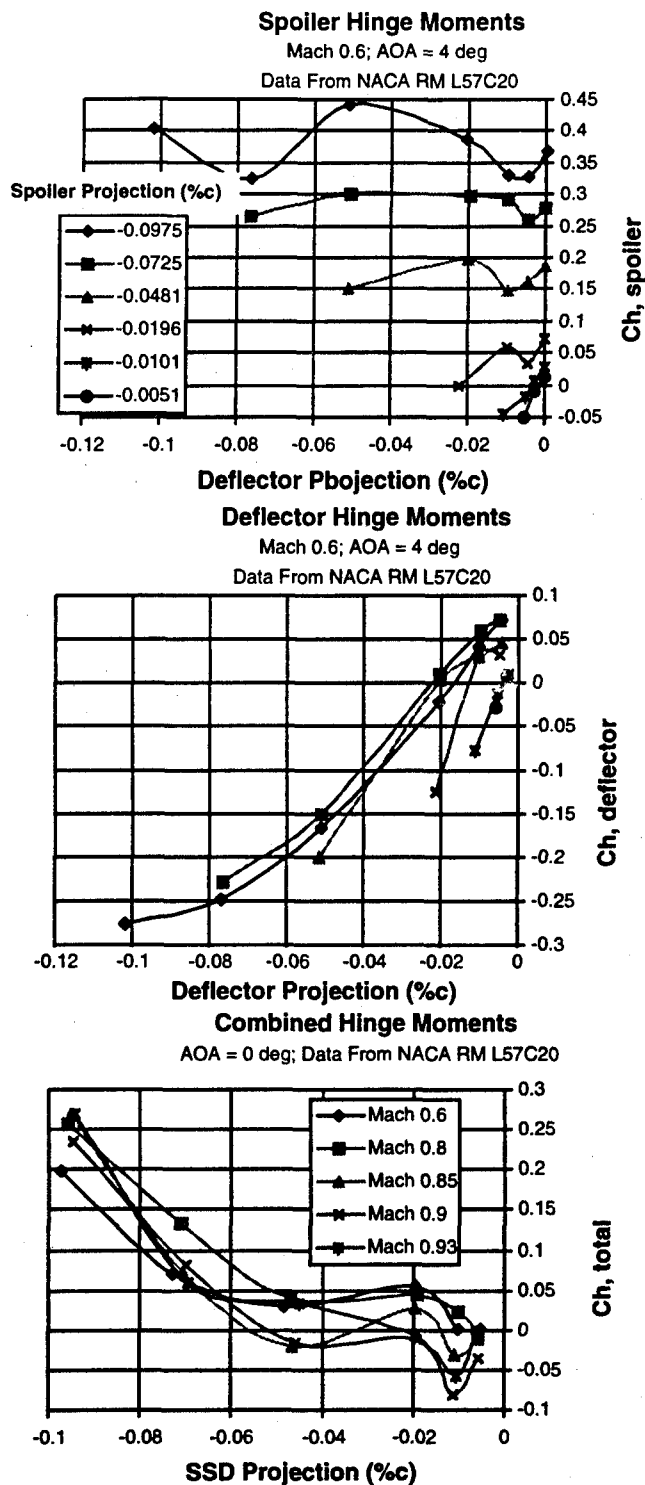


Figure 3-26 The Spoiler and Deflector Can be Mechanically Linked to a Single Actuator Resulting in Lower Overall Hinge Moments

In addition to the benefits already demonstrated, the SSD improves the linearity of control moment versus deflection compared to a conventional spoiler. At 30 deg AOA, the control reversal observed in the spoiler data is eliminated (Figure 3-27).

Spoiler & SSD Effectiveness vs Deflection; Low-Speed; Body Axes

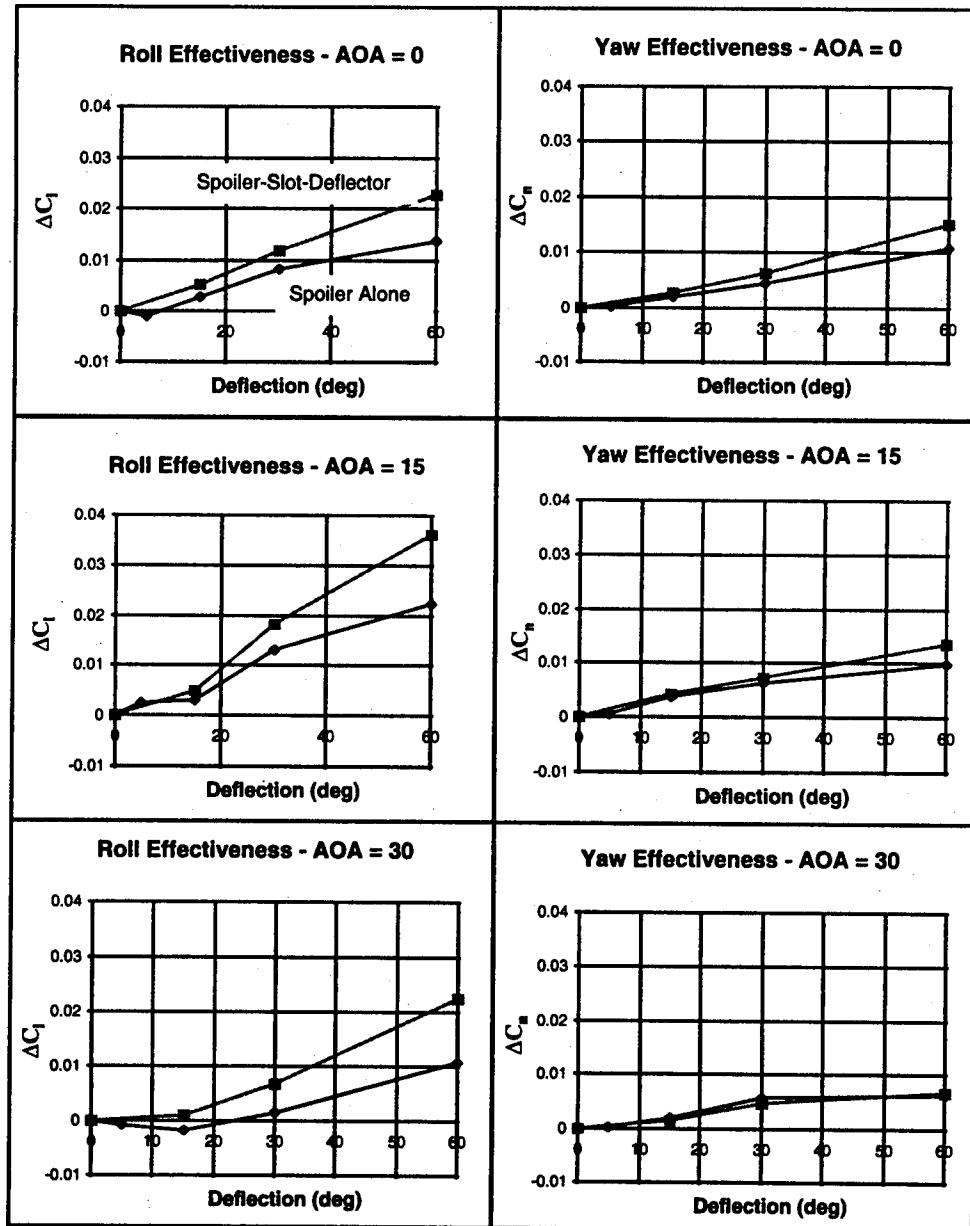


Figure 3-27 The SSD Improves the Linearity of Response with Deflection over a Conventional Spoiler

Unfortunately, the SSD concept can severely degrade trailing edge flap effectiveness when deployed. Figure 3-28, taken from ADF wind tunnel data, shows the effects of SSD deflection on elevon effectiveness when the elevon is hinged directly behind the SSD. Figure 3-29 illustrates the pitch-up created by SSD deflections. The data are compared with pitch-up created by a conventional spoiler. The elevon deflection requirements to trim out the interaction are also tabulated. The large elevon deflections required attest to the reduction in elevon effectiveness caused by the SSD. At 15 deg AOA, the pitch-up cannot be trimmed by the elevons alone. The second set of trim deflections represent elevon deflections required if small pitch flaps are deflected 30 deg TED. Two conclusions can be drawn from this analysis: (1) small surfaces with pitch priority that are unencumbered by adverse aerodynamic interactions are invaluable for aircraft employing SSD concepts; (2) the SSD greatly increases the demand on the elevon required for trim over a conventional spoiler -- both due to increased overall pitch-up and reduced elevon effectiveness.

The SSD arrangement requires cutting holes in both the upper and lower wing skins (as opposed to just the upper skin for a spoiler). This in conjunction with the required "hole" through the wing makes the SSD system difficult to integrate structurally; however, the weight may be offset by the reduced actuation and subsystem requirements when compared to a spoiler.

Effect of SSD on Elevon Effectiveness
Low-Speed ADF Data; Body Axes

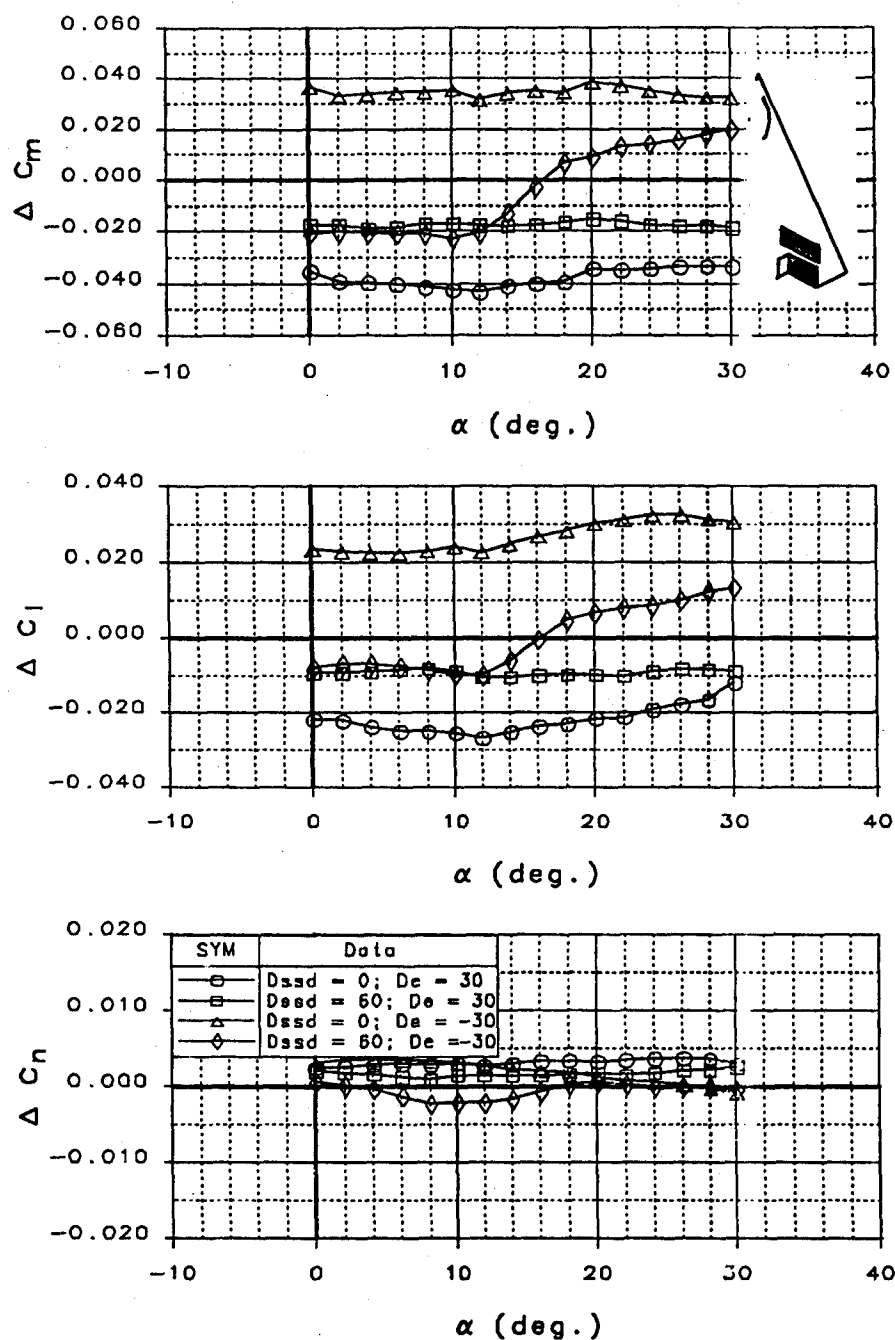
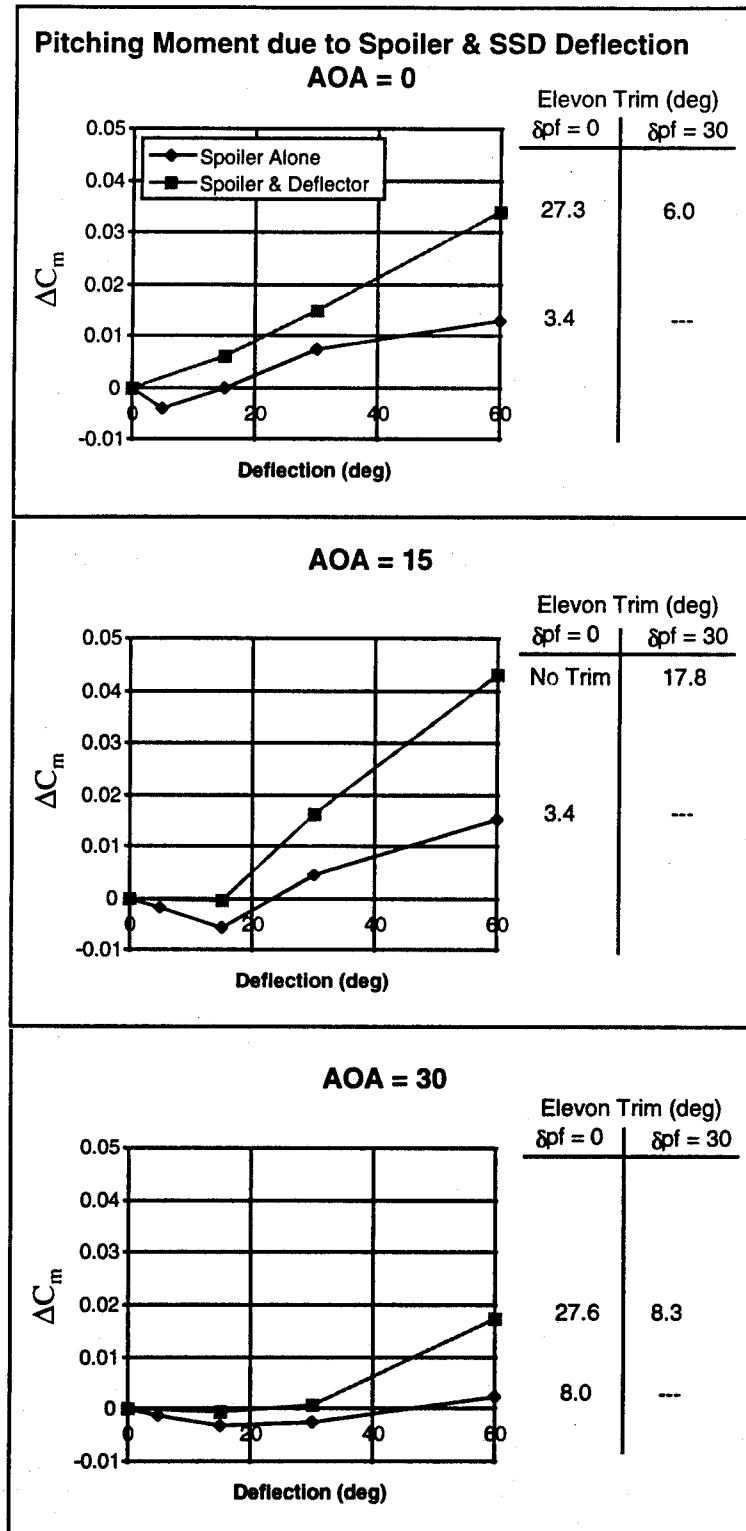


Figure 3-28 The SSD Degrades Elevon Control Effectiveness



**Figure 3-29 The SSD Places a Higher Demand on Elevon Control Power to Trim out
Nose-Up Control Interactions**

In summary, the SSD concept is a valuable control arrangement for tailless aircraft that can result in lower actuator (and therefore hydraulic) requirements, improved high AOA and transonic effectiveness, and improved control linearity over a conventional spoiler arrangement. The drawbacks of the system should be offset by reduced subsystem requirements, and properly designed pitch control surfaces.

3.1.6 Deployable Rudder

Reference 2 described several deployable yaw control devices similar in operation to the deployable rudder described here. It seems a natural engineering decision to study a deployable vertical tail on an all-wing aircraft. Presumably, the deployable rudder would primarily be used during low-speed flight conditions (e.g., takeoff and landing, high AOA flight, etc.).

The DRUD analyzed for the ICE program was developed in 1991 during small-scale testing in the ADF tunnel at LMTAS. An "optimized" version was tested on the 1/18th scale tailless fighter model at subsonic through supersonic speeds^{6,7}. The DRUD was designed to produce decoupled yawing moments at low to moderate AOA. The hingeline is skewed so that as the tail is deployed, it has an angle-of-incidence with the local flow. A yawing moment is generated by the resulting side force. The axial force resulting from the surface's deployment also adds to the yawing moment due to the offset location of the controller from the centerline (Figure 3-30).

Figure 3-31 shows the yaw control power available from the DRUD. Due to the short-coupled nature of the flying wing configuration, magnitudes were small for the size of surface tested. Small favorable rolling moments are associated with DRUD deflections at low to moderate AOA. Yaw effectiveness is maintained up to 40 deg AOA. Figure 3-32 illustrates the linearity of the surface with deflection. As expected, some deadband is apparent at small deflections

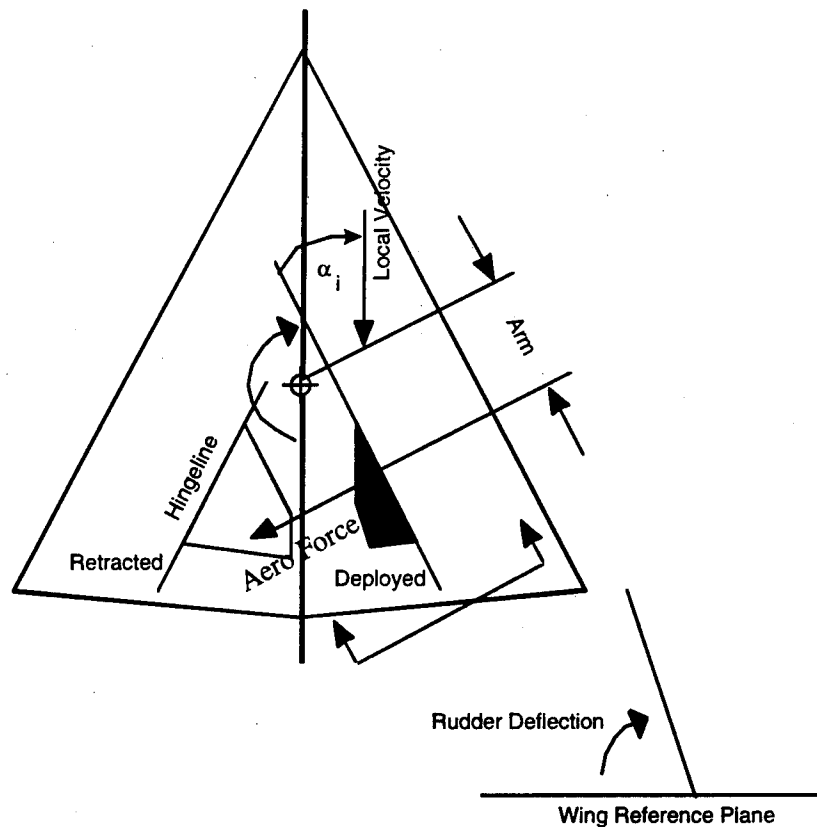


Figure 3-30 The Deployable Rudder Generates Yawing Moment Through Side Forces and Axial Forces Acting on the Surface

Control effectiveness at high AOA was found to be very sensitive to location on the wing. Proximity of the DRUD to the leading edge vortex and its burst point had adverse effects on high AOA yaw control power. An aft inboard location was found to be optimal. It maximized the moment arm with the cg, and minimized interactions with the leading edge vortex. A lower surface rudder location was tested as well (Figure 3-33). Control effectiveness of the upper surface rudder was better in the 12 deg to 30 deg AOA region for the same size surface and moment arm. There are indications (and it seems feasible) in the limited amount of data that the lower surface rudder may provide better high AOA effectiveness; although this remains to be tested. A lower surface rudder location would have a negative impact on ground clearance; it probably would have limited use during power approach conditions.

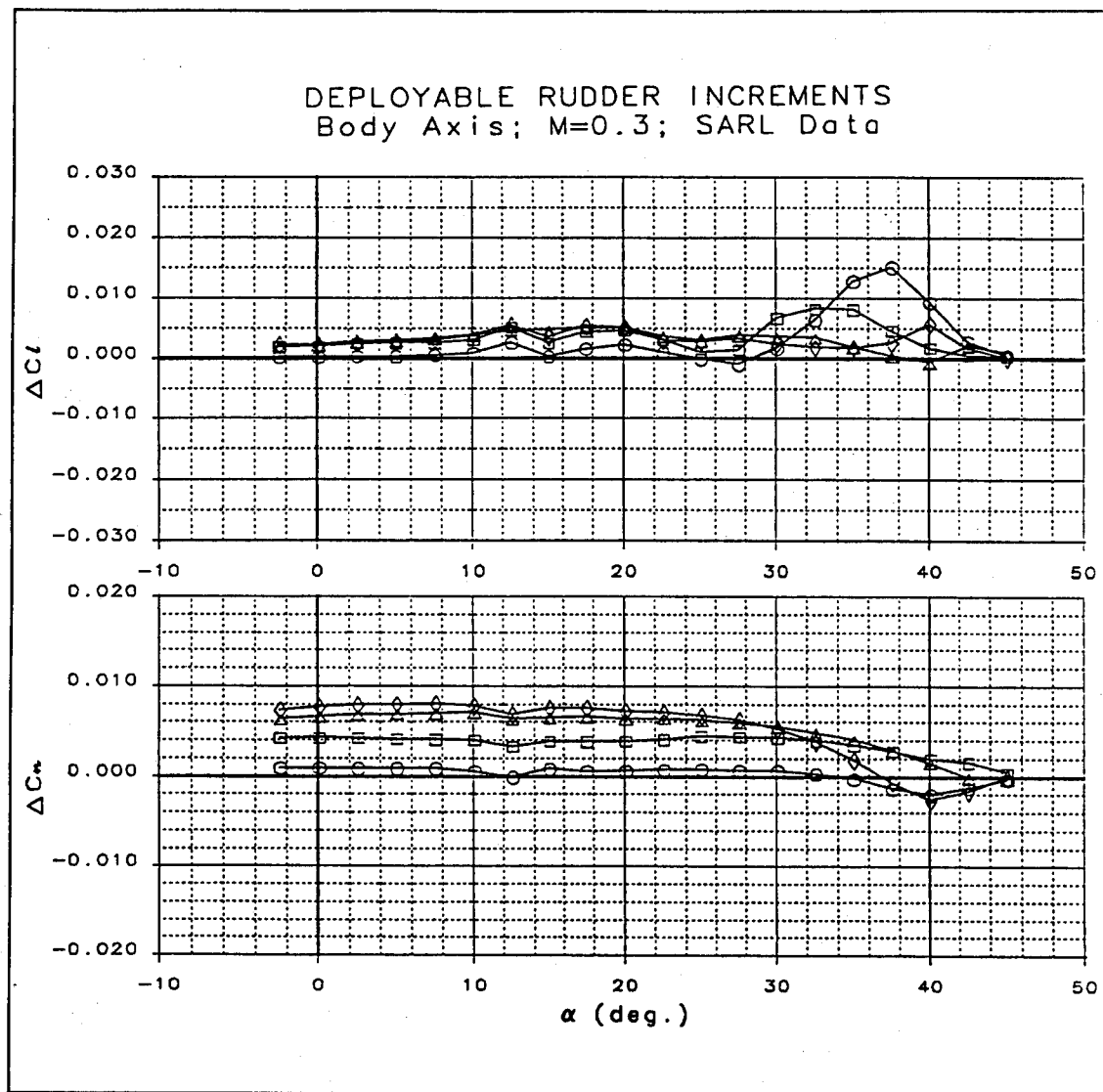


Figure 3-31 DRUD Control Effectiveness

Deployable Rudder Effectiveness vs Deflection; Mach 0.3; Body Axes

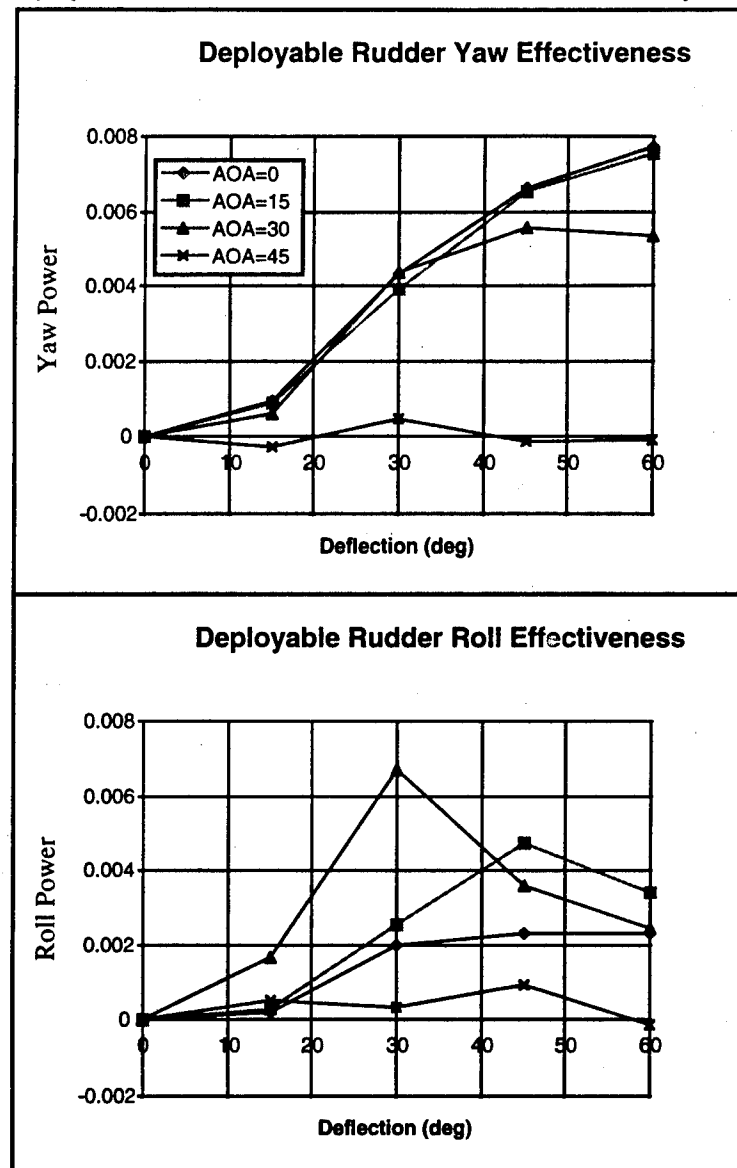


Figure 3-32 DRUD Effectiveness vs Deflection

Figure 3-34 indicates that symmetric deployable rudder deflections do not appreciably affect bare airframe directional stability. This was seen as one of the potential benefits of the surface, but because of the short moment arm to the cg and the inboard cant of the rudders, the stabilizing tendencies are negligible. At high AOA, symmetric deflections result in worse overall stability than the bare airframe.

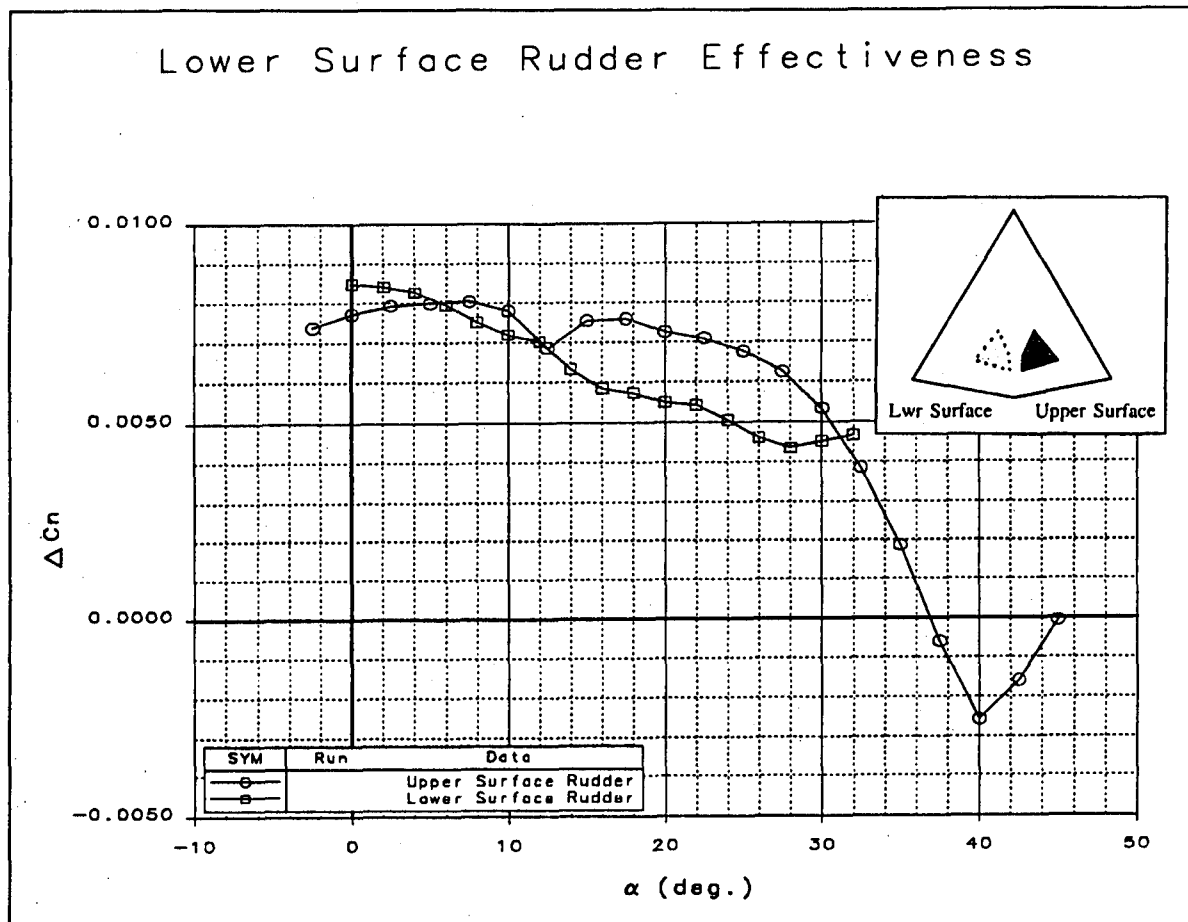


Figure 3-33 Lower Surface DRUD Effectiveness

Effects of sideslip on rudder control power are shown in Figure 3-35. At low to moderate AOA, windward sideslip has essentially no effect on yaw control power. For AOA > 20, rudder deflections on the windward side suddenly lose control effectiveness -- a highly undesirable trait. Leeward side deflections have less control power than the zero sideslip case.

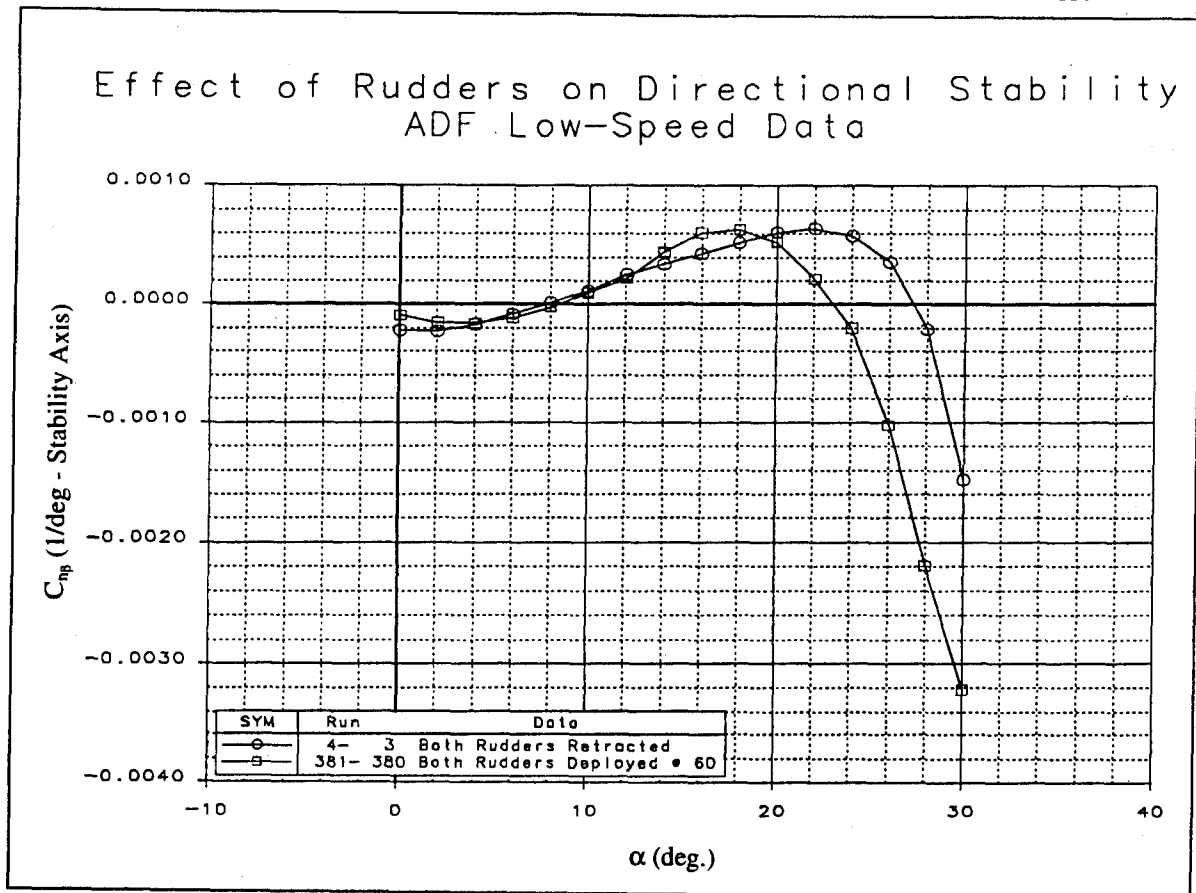


Figure 3-34 DRUD has Negligible Directional Stabilizing Tendencies

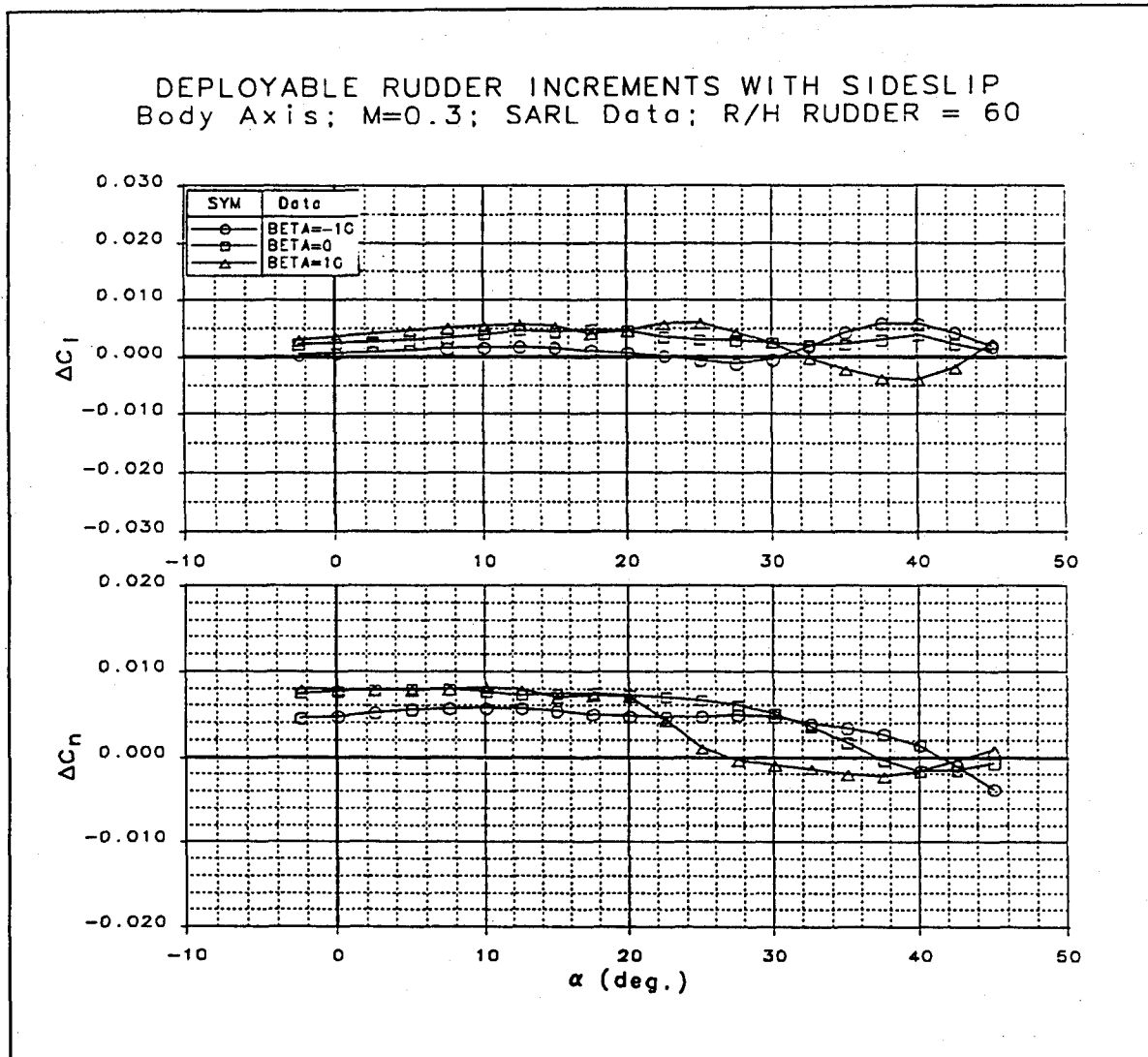


Figure 3-35 Windward Sideslip Adversely Affects DRUD Effectiveness at High AOA

3.1.7 Lower Surface Spoiler

Lower surface flaps have found a variety of applications, and are not exactly "innovative"^{20, 29}. The lower surface spoiler was investigated for the ICE program as a means of improving high AOA lateral-directional control power.

LSP generate rolling moment at low AOA by an increase in the local wing camber on the lower surface -- much like a trailing edge flap. Body axis yaw is adverse at low AOA due to the increase in profile and induced drag on the wing with deflected LSP.

Figure 3-36 shows lateral-directional control effectiveness from a small-scale test for a variety of deflections. Rolling moment changes sign at 10 deg AOA, becoming twice the value of the low AOA magnitude. Except in the critical region between 10 and 20 deg AOA, the magnitude is predictable with increasing deflection -- albeit nonlinear. Yawing moment is small in magnitude but favorable at high AOA.

Figure 3-37 shows the longitudinal increments due to LSP deflection. The positive normal force accompanied by the nose-down pitch at low AOA reflects the increase in camber created by the flap deflection. The near simultaneous change in sign of pitching moment, rolling moment and normal force increments indicates that at high AOA, a strong region of suction exists behind the LSP, acting on the trailing edge of the wing. This would account for the change in characteristics of the force and moment data. The nose-up pitch generated by this control at high AOA increases the demand on pitch control surfaces to maintain control during rolling maneuvers.

Sideslip data with LSP deflections were collected during a low-speed test at the SARL facility. Figure 3-38 shows adverse effects due to sideslip on roll control power for a 15 deg LSP deflection at high AOA. Effects on yaw are favorable at high AOA for windward sideslip.

LSP deflections adversely affect trailing edge surface effectiveness (Figure 3-39). TED elevon deflections are essentially unaffected above 22 deg AOA. However, only 15 deg LSP deflection data are available. Larger LSP deflections will probably impact elevon roll and pitch effectiveness at high AOA. Coupled with the nose-up pitch generated by deflecting the device, this characteristic will require large nose-down pitch deflections just to maintain trim -- let alone overcome inertial pitch coupling during high AOA rolls.

The predictable nature and large body axis rolling moments at high AOA initially made the LSP attractive as a high AOA control device. Its structural integration drawbacks are similar to conventional spoilers. At high speeds, hinge moments would be high. The cutout in the lower wing skin necessitates beefed-up spar structure around the void. Lack of control effectiveness between 10 and 20 deg AOA negate the usefulness of this surface

for takeoff and landing. At high AOA, adverse interactions with trailing edge control surfaces will result in high pitch requirements during rolls.

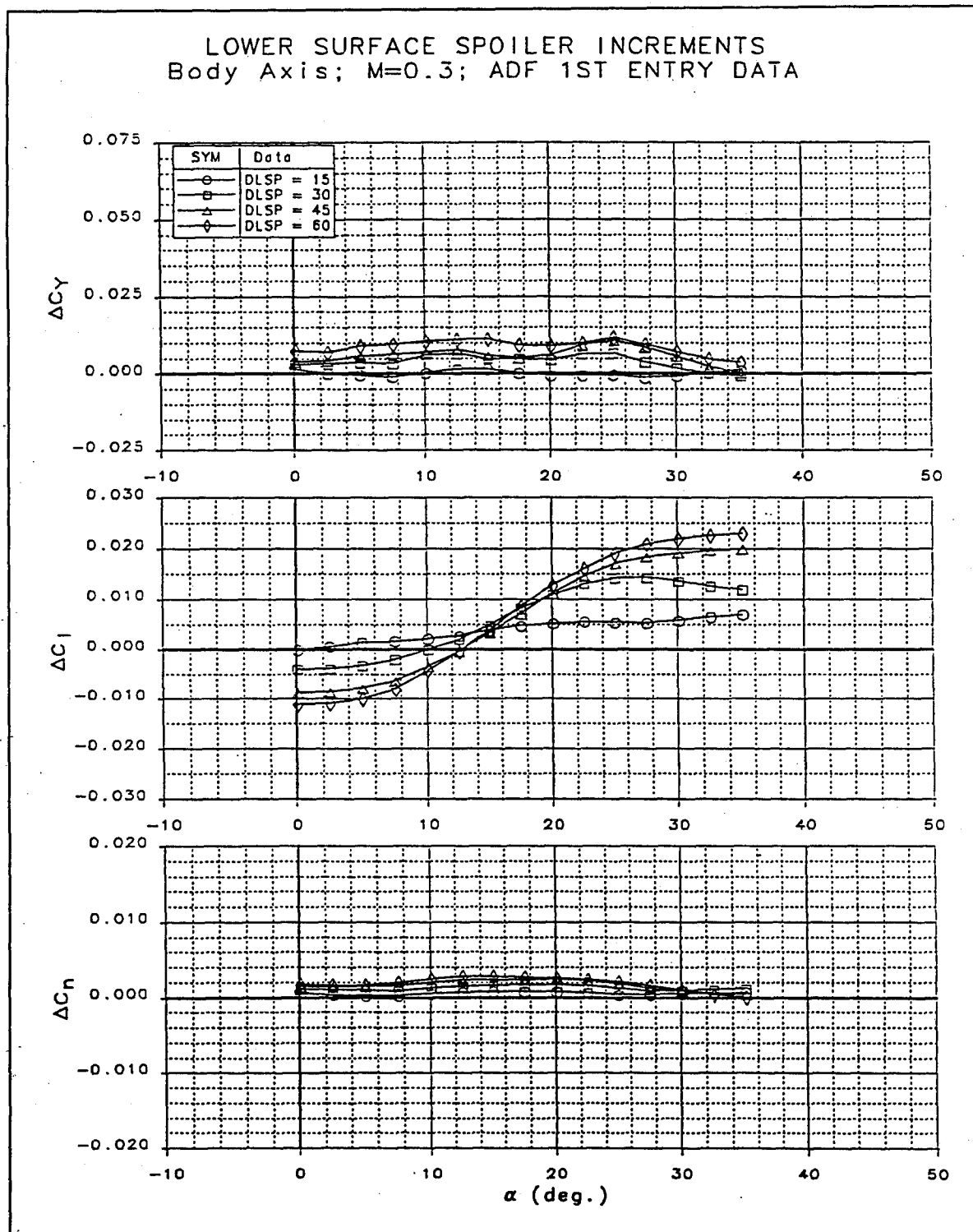


Figure 3-36 LSP Control Effectiveness is a Strong Function of AOA

LOWER SURFACE SPOILER INCREMENTS
Body Axis; $M=0.3$; ADF 1ST ENTRY DATA

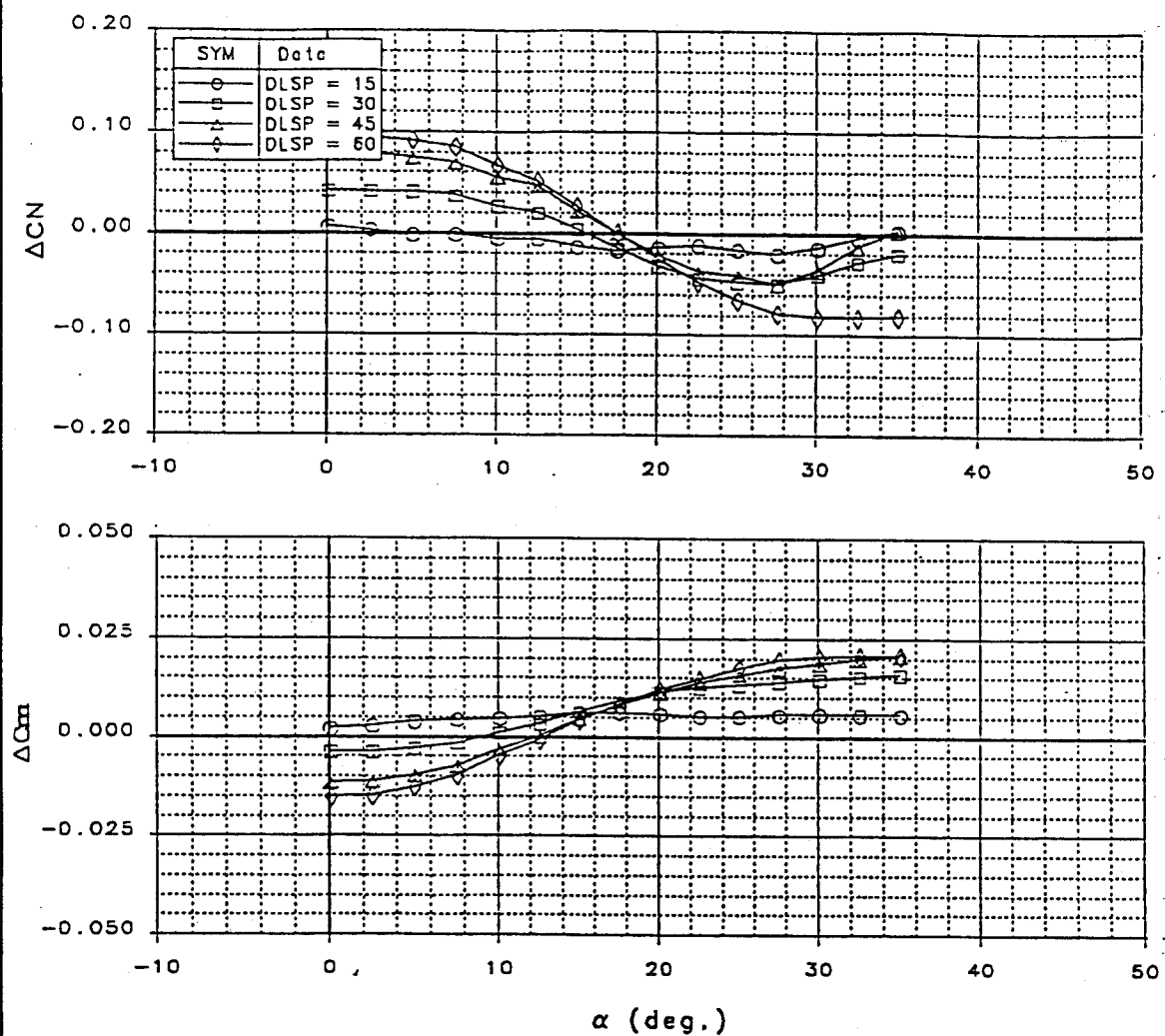


Figure 3-37 Longitudinal Effects due to LSP Deflections

LOWER SURFACE SPOILER INCREMENTS
Body Axis; $M=0.3$; SARL Data; R/H SPOILER = 15

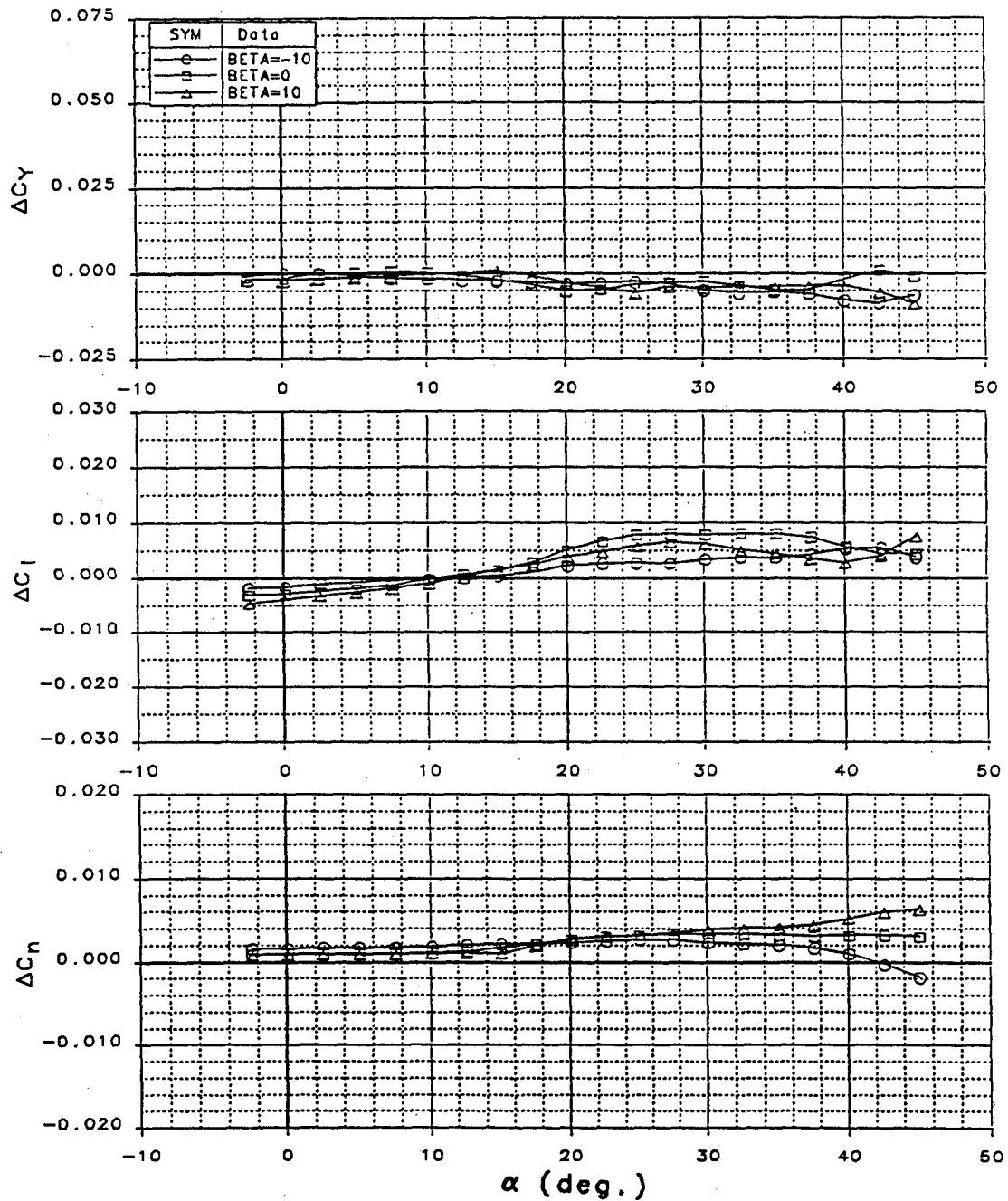


Figure 3-38 Sideslip Effects on LSP

LOWER SURFACE SPOILER INTERACTION ON ELEVON
Body Axis; $M=0.3$; SARL Data

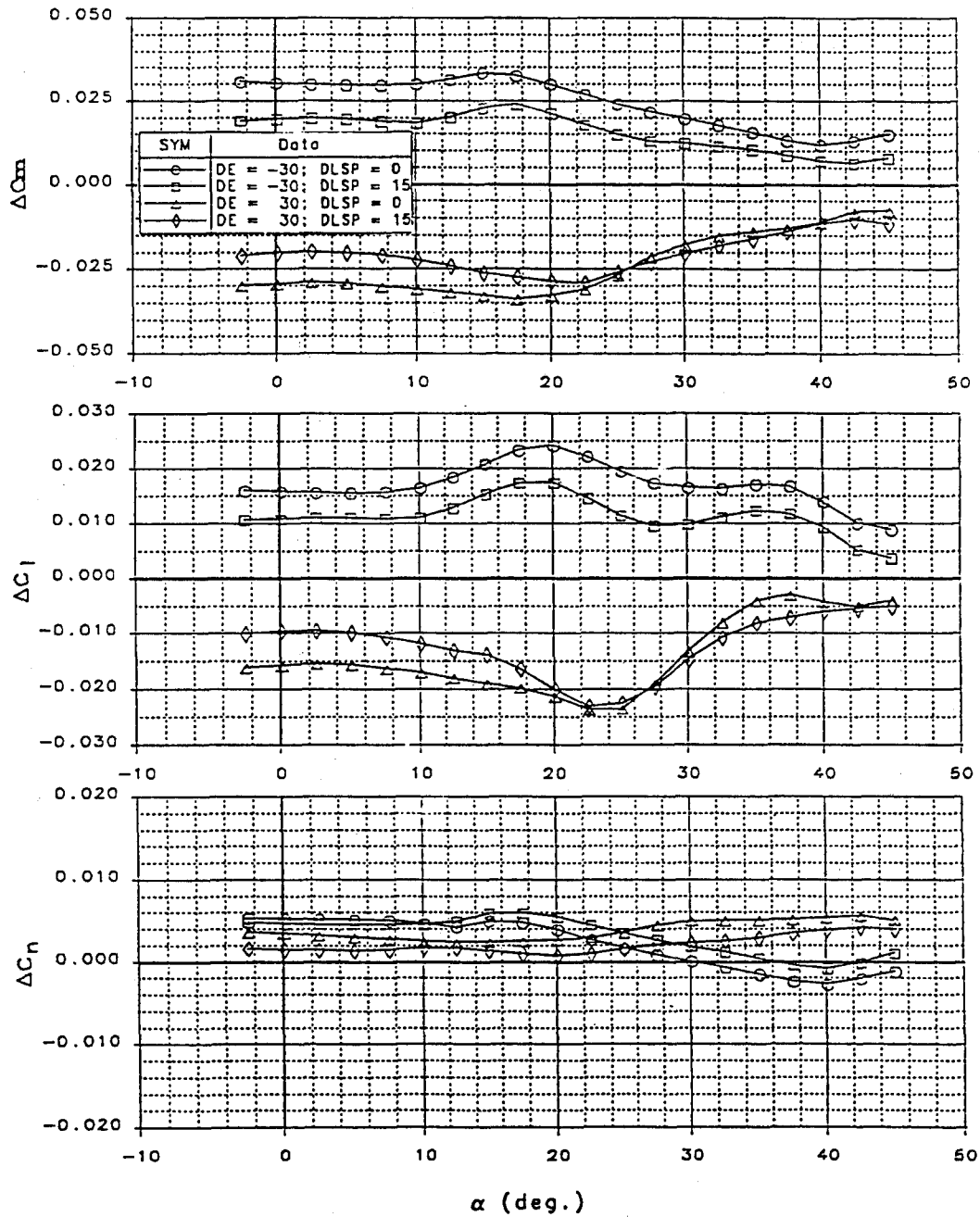


Figure 3-39 Interaction of LSP with Elevons

4 Control Power Requirements and Baseline Evaluation

Key maneuver goals were defined for the ICE study in the form of high AOA roll performance capabilities, Level 1 flying qualities in the low to moderate AOA range, and carrier suitability considerations. Control power requirements were estimated for each configuration series (101 and 201). This section describes the control power requirement studies, and the subsequent evaluation of each baseline configuration.

Two "baselines" were evaluated for each configuration series -- one with pitch and yaw thrust vectoring and one without. Aerodynamic control power was traded versus propulsion control power. The benefits and liabilities of thrust vectoring were evaluated and described in this section and in Section 7.

4.1 Maneuver Requirements

The following maneuver performance goals were specified for both the land-based and carrier-based configurations

- Level 1 flying qualities at low AOA as defined in MIL-STD-1797 and MIL-F-8785C.
- Minimum nose-down pitch acceleration of -0.07 rad/sec^2 with aerodynamic controls only during symmetric maneuvering. . (Note that the nose-down pitch acceleration requirements are referenced to a dynamic pressure of 40 psf.)
- Minimum nose-down pitch acceleration of -0.25 rad/sec^2 with aerodynamic and propulsion controls during symmetric maneuvering.
- Minimum nose-down pitch acceleration of -0.07 rad/sec^2 with both aerodynamic and propulsion controls while meeting roll specifications.
- Bank angle change of 90 deg in 2.0 sec at 30 deg AOA, 4.0 sec at 45 deg AOA, and 6.0 sec at 60 deg AOA.

- Maintain sideslip less than 6 deg during high AOA rolls.

Figure 4-1 shows the ICE high AOA roll performance goals compared to several current fighter aircraft. For this comparison, the 1-DOF roll equation was used to convert ICE time-to-bank requirements into steady state stability axis roll rate. One can see from the figure that the ICE roll performance requirements are consistent with the high AOA capabilities of future fighters (e.g., YF-22).

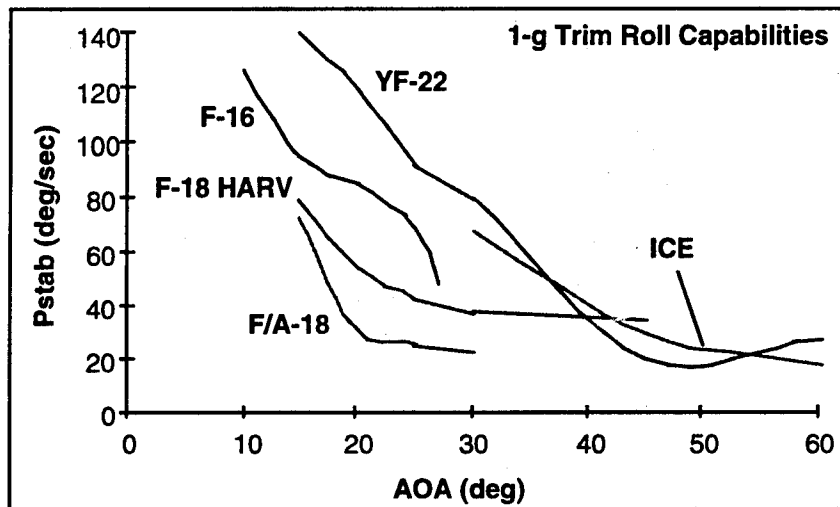


Figure 4-1: ICE Roll Performance Goals

In addition to the above, the carrier-based configurations had to meet all aerodynamic requirements imposed by CV suitability design constraints. CV suitability criteria are typically referenced to airspeeds required for the configuration to achieve the design criteria. Wind over deck (WOD) is a critical design parameter that must be minimized for a good CV suitable aircraft. WOD is essentially the difference between the airspeed required of the aircraft, and the catapult endspeed or arresting cable engagement speed. Carrier suitability performance criteria were evaluated using tropical day conditions. Catapult endspeeds and arresting cable engagement speeds are determined by the carrier's machinery capability to impart or absorb energy³⁷. Catapult and arresting gear performance data are contained in Reference 38.

Airspeed criteria during catapult launch can be set by one or more of the following:

- Longitudinal acceleration of at least 1.24 knots/sec^2 .
- Center-of-gravity sink after launch not to exceed 10 feet.
- Pitch rate not to exceed 12 deg/sec nose-up or 2.5 deg/sec nose down.
- Pitch rotation not requiring more than 90% of $C_{L\text{max}}$.
- Level 1 flying qualities.
- Crosswind capability greater than 15 knots at 90 deg.
- Single engine rate of climb $> 200 \text{ ft/min}$.
- Minimum control speed for single engine flight.
- Launch performance analyses were done at a mission weight representative of full fuel plus ordnance. The design WOD goal for this analysis was zero knots.
- Recovery speed criteria include airspeeds required to achieve:
- Level 1 flying qualities at V_{PA} with the exception of time-to-bank 30 deg in 1.0 sec instead of 1.1 sec as defined in MIL-F-8785C.
- Over-the-nose vision requirements during approach -- pilot must see the stern waterline when intercepting a 4 deg glideslope at 600 ft altitude.
- Glidepath correction maneuver -- 50 ft glidepath change in 5 sec at a fixed thrust setting using only one-half of the additional available lift.
- Approach speed greater than $1.1V_{\text{stall}}$.
- Longitudinal acceleration during waveoff of 3 knots/sec^2 within 2.5 sec after initiation of go-around.
- Engine response -- not considered during this study.
- Assuming a twin engine concept, acceptable single engine controllability (V_{mc}) and SEROC $> 500 \text{ fpm}$. ($V_{mc} < V_{pa} - 5 \text{ knots}$)

For recovery analysis, wind over deck is defined as $WOD = 1.05V_{PA} - V_{engage}$. The recovery WOD goal for this study was zero knots at a 5K lbs bring back weight. Analysis was done using bring back weights of 0, 5K, and 10K lbs.

Obviously, for a single engine concept, the SEROC and V_{mc} criteria defined above do not apply. However, for this study, a second engine was assumed to determine control requirements for single engine flight. The goal of this analysis was to evaluate the innovative controls independently of the configuration type to determine their applicability to other configuration concepts -- including twin engine fighters.

4.2 Flight Conditions

Figure 4-2 illustrates the flight conditions for which control power requirements were investigated. Flight conditions were chosen at the boundaries of the flight envelope to ensure each configuration would have sufficient control power to meet flying qualities requirements at any condition.

For consistency and comparison purposes, high AOA roll performance control power requirements were computed at a calibrated airspeed of 108 knots, corresponding to a dynamic pressure of 40 psf. Maximum airspeed was defined as 800 KCAS, corresponding to Mach 1.2 at sea level. Thrust settings used for evaluating configurations that include thrust vectoring are shown below:

- MAX A/B : all high AOA conditions except 20 deg AOA/300 KCAS
- MIL Power : 20 deg AOA/300 KCAS
- Idle and trim power: power approach conditions

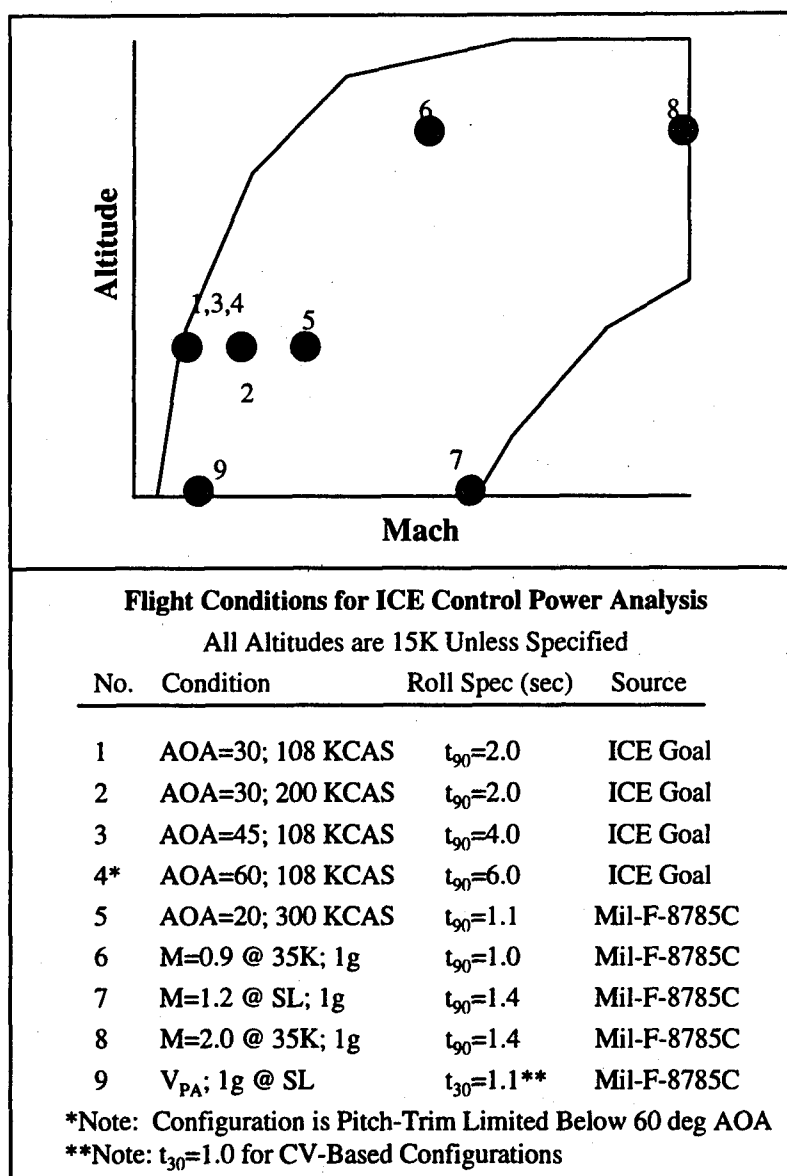


Figure 4-2 ICE Flight Conditions

4.3 Configuration 101-Series Baseline Evaluation

The following sections describe the control power requirements and maneuver performance evaluation of the land-based baseline configurations.

4.3.1 Configuration 101-Series Control Power Requirements

The simulation tool CPR was used to compute control power requirements at each flight condition. Control power requirements are shown in Figure 4-3 for the 101-Series configuration.

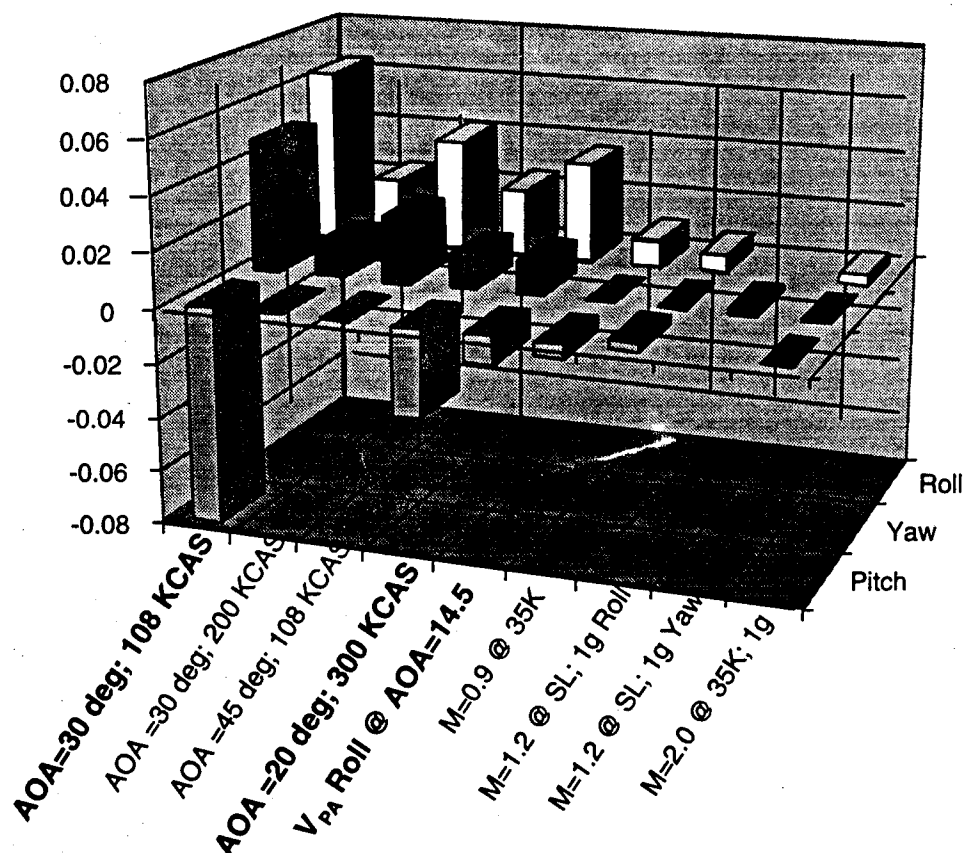


Figure 4-3 Configuration 101 Control Power Requirements

The 30 deg AOA roll at 108 KCAS requires the highest absolute control power. At this flight condition, TV provides large control moments. Because of the dependence of TV control power on flight condition and power setting, other flight conditions may also be critical. For instance, the power approach condition requires a low power setting, and therefore control power from vectoring may be insufficient. At the 20 deg AOA/300 KCAS case, dynamic pressure is relatively high, and the control power available analysis was done with the throttle at mil-power (see above). As will be shown later, these three conditions ended up sizing the control suites for the 101-series airplanes. The maximum

dynamic pressure condition (Mach 1.2/sea level) set hinge moment requirements for the actuators.

4.3.2 Maneuver Performance Evaluation

All 101-series configurations were evaluated by computing control power envelopes at the nine flight conditions of interest. CPR simulations were run inside the envelopes to determine maximum maneuver performance. Nose-down pitch acceleration requirements were met by defining aft cg limits where pitch acceleration could still be achieved. Table 4-1 shows the mass properties used during the maneuver performance evaluation. Weight differences between Configurations 101 and 101-TV are attributable to the thrust vectoring system. These mass properties represent the preliminary values used during control sizing studies, and do not reflect final weight estimates made after sizing. Note too that the cg locations were set at 38.84 % MAC for both configurations for the initial evaluation. Aft limits are discussed in Section 6.1.5.

Table 4-1 Preliminary Mass Properties Data for 101-Series Configurations

Configuration 101

Parameter	Value
Weight (lbs)	32,372
cg (%MAC)	38.84
I_{xx} (sl-ft ²)	36,794
I_{yy} (sl-ft ²)	75,103
I_{zz} (sl-ft ²)	109,384
I_{xz} (sl-ft ²)	-542

Configuration 101-TV

Weight (lbs)	32,750
cg (%MAC)	38.84
I_{xx} (sl-ft ²)	35,479
I_{yy} (sl-ft ²)	78,451
I_{zz} (sl-ft ²)	110,627
I_{xz} (sl-ft ²)	-525

4.3.3 Configuration 101 (Aerodynamic Controls Only)

The goal for this portion of the study was to determine the maximum maneuver capability of this configuration with aerodynamic controls alone, and then trade off aerodynamic control power using TV (Section 4.3.4). Throughout this study, control surfaces were sized up and down by applying control volume ratios to the lateral-directional control effectiveness. Table 4-2 lists the controls incorporated into the final Configuration 101. Figure 4-4 shows a planview layout of Configuration 101.

Table 4-2 Final Configuration 101 Control Surface Areas

Controller	Usage	Deflection Limit (deg)	Area (ft ²)
Pitch Flap	Pitch	+/-30 (Sym Only)	7.77
Elevon	Pitch/Roll/Yaw	+/- 30	22.77
IB Spoiler	Roll/Yaw	0/60	15.71
OB Spoiler	Roll/Yaw	0/60	15.71
Clamshell	Yaw	0/60 (upr & lwr)	12.41
IB LEF	Pitch/L-D Stab	0/40 (sym)	14.35
OB LEF	Pitch/L-D Stab	0/40 (sym)	11.11

Notes: (1) Surface areas represent single side surfaces only

(2) Clamshell area for upper surface only

The LEF were split into inboard and outboard segments for structural reasons, but move together as maneuver flaps to provide improved high AOA directional stability and nose-down control power. Past experience with the high-sweep (65 deg) delta wing studied here indicated that scheduling the LEF with flight condition did not appreciably improve the drag polar over what was achievable using a fixed camber design.

The clamshell retains good yaw effectiveness at high speed. However, large hinge moments limit its potential. The clamshell actuator was sized to provide full deflection capability up to 300 KCAS. Combined spoiler-elevon deflections were relied upon to provide high-speed yaw control power -- resulting in very large spoiler actuators. The spoiler was split into an inboard and outboard section to supply directional control redundancy.

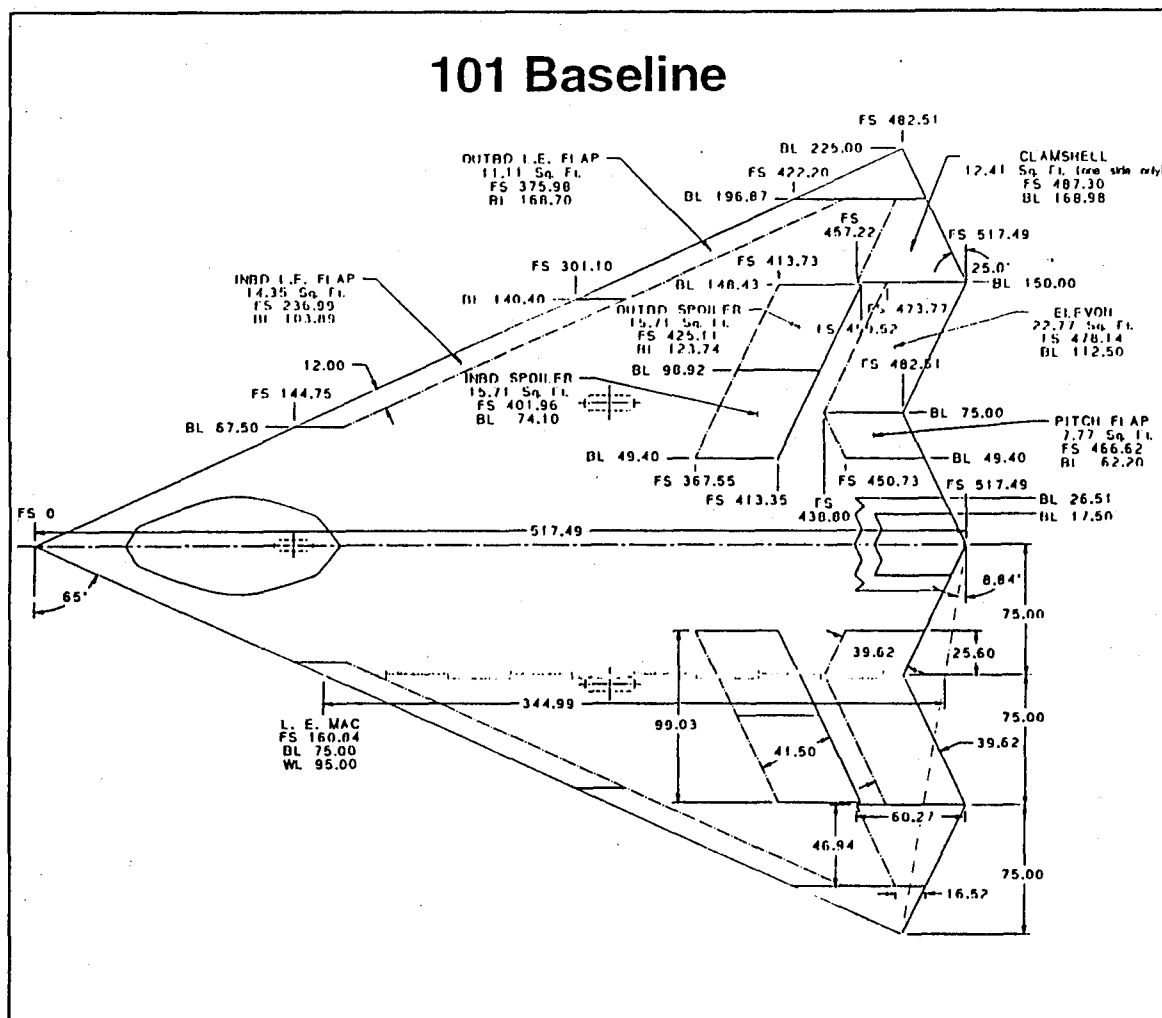


Figure 4-4 Planview of Configuration 101

Configuration 101 was limited by yaw control power. The clamshell, although effective for its size, could not be made large enough to provide sufficient yaw power at high AOA to achieve the roll performance goals. Spoiler size was increased in an attempt to improve high AOA roll performance; however, the structural weight penalties did not justify the small improvement in roll coordination.

Figure 4-5 shows a portion of a CPA control envelope at 30 deg AOA. This diagram represents the maximum roll and yaw control power available while trimmed in pitch. The control requirements to achieve the desired 90 deg bank in 2.0 sec are overlaid. The point where the Configuration 101 envelope crosses the Y-Axis is the maximum coordinated roll control power available for this condition. It is readily apparent that Configuration

101 fell far short of the high AOA roll criteria. Note the 101-TV CPA curve (discussed in Section 4.3.4).

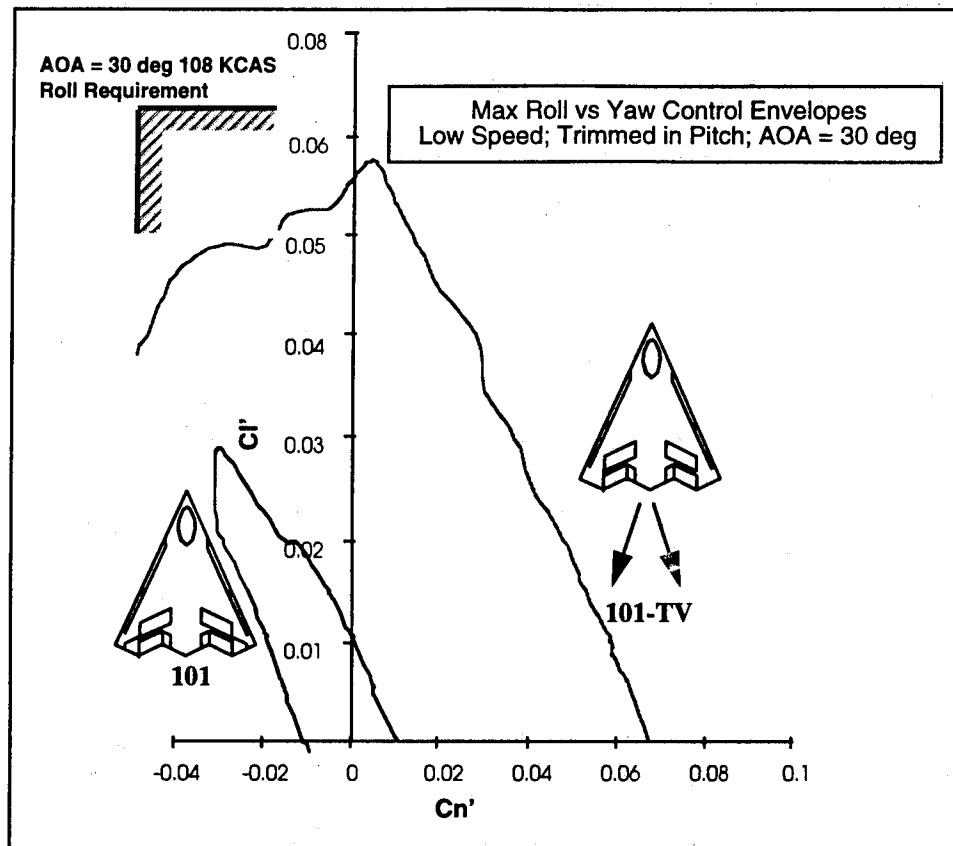


Figure 4-5 Configuration 101 Control Power Available vs Required at 30 deg AOA

Figure 4-6 summarizes roll performance for Configuration 101. The maneuver goals are shown alongside the actual capabilities. Although the high AOA roll performance goals could not be achieved, the configuration has considerable capability considering it has no TV or vertical surfaces. Other than the high AOA cases, critical maneuvers were the power approach roll, and the 20 deg AOA/300 KCAS condition. High-speed roll performance capabilities were adequate.

Note that this evaluation did not include the effects of flexibility on the airframe. Therefore the high-Mach roll performance prediction is probably optimistic. Hinge moment limitations were considered.

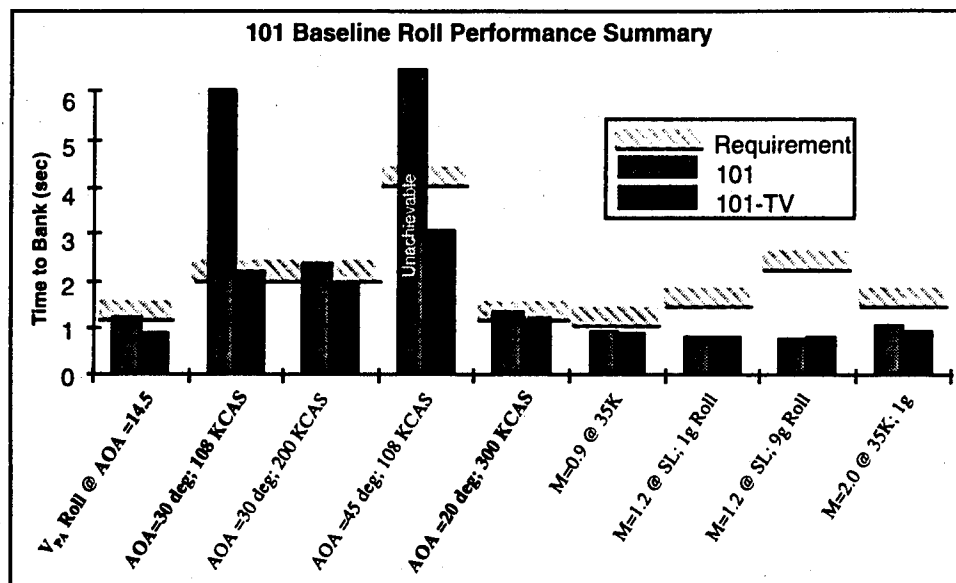


Figure 4-6 Configuration 101-Series Roll Performance Summary

Approach roll performance was evaluated at the 1-g trim speed for 14.5 deg AOA. The approach AOA was limited by tipback angle. Level 1 power approach roll capability could not be achieved at this condition. Configuration 101 thus requires a higher approach speed than that corresponding to 14.5 deg AOA to achieve Level 1 roll performance.

4.3.4 Configuration 101-TV

Configuration 101-TV roll performance was evaluated using the same methods and assumptions presented above. Table 4-3 summarizes the final control suite for 101-TV. Figure 4-7 shows a planview layout of this configuration.

Table 4-3 Final Configuration 101-TV Control Surface Sizes

Controller	Usage	Deflection Limit (deg)	Area (ft ²)
MATV	Pitch/Yaw	+/-15	---
Pitch Flap	Pitch	+/-30 (Sym Only)	7.77
Elevon	Pitch/Roll/Yaw	+/- 30	22.77
IB Spoiler	Roll/Yaw	0/60	15.71
OB Spoiler	Roll/Yaw	0/60	15.71
IB LEF	Pitch/L-D Stab	0/40 (sym)	14.35
OB LEF	Pitch/L-D Stab	0/40 (sym)	11.11

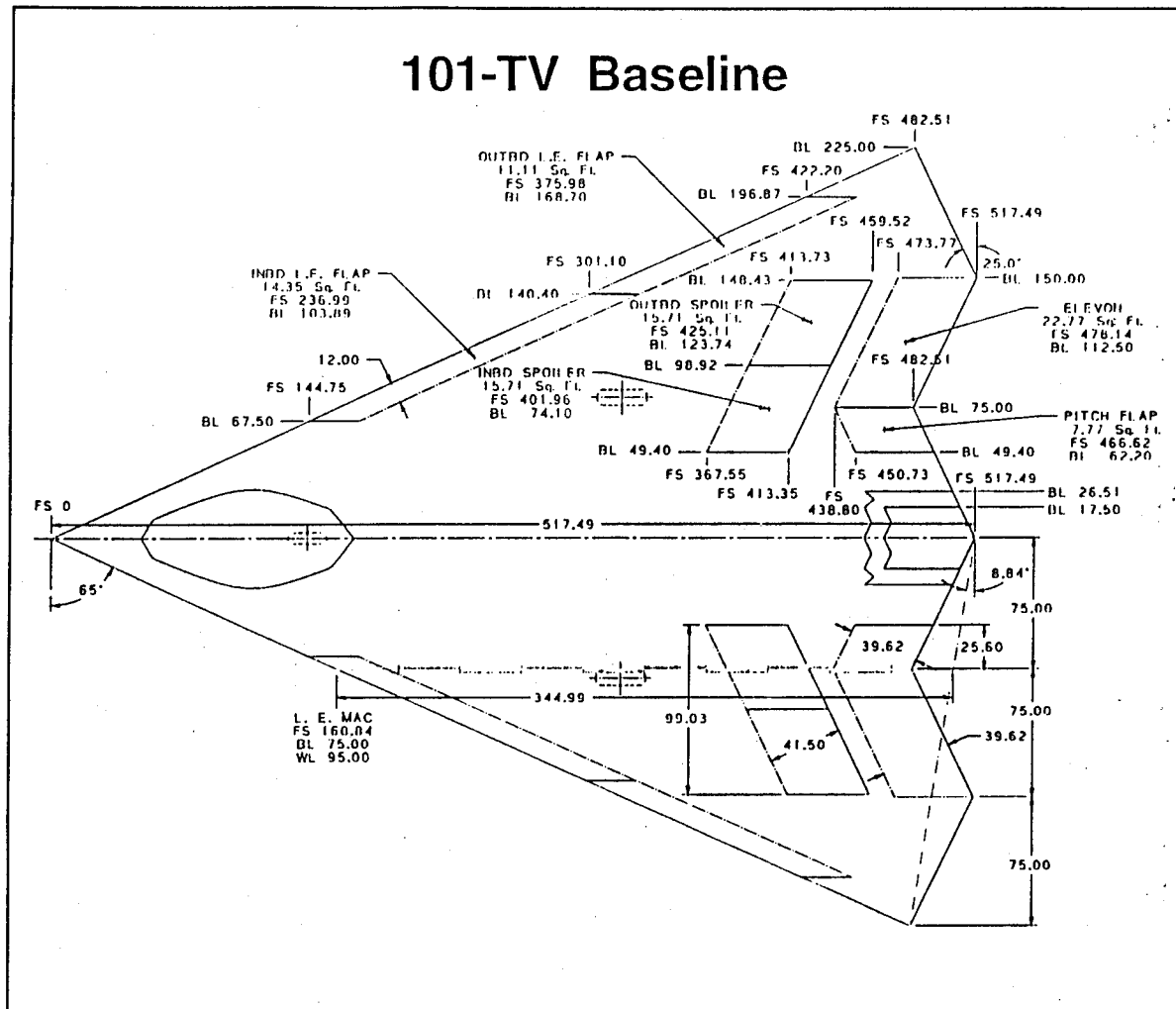


Figure 4-7 Configuration 101-TV Planview

Thrust Vectoring Model

Thrust vectoring was modeled using an F110-GE-129 propulsion deck. The propulsion data file included ram drag and gross thrust as a function of Mach, altitude, and power setting. The thrust and ram drag vectors were applied at the appropriate locations on the flight vehicle. Together with nozzle deflection assumptions, pitch and yaw control moments were computed at the various flight conditions.

Axi-symmetric engine-mounted TV nozzles are typically deflection limited by mechanical constraints at low speeds and power settings, and off-axis side load limits at high

speeds and thrust settings. Typical applications (i.e., F-16 MATV) have an off-axis load limit of 4,000- 6,000 lbs and mechanical deflection limits of 15 - 20 deg. At high speeds, the nozzle is deflection-limited to maintain acceptable side-loads and minimize structural weight penalties.

Figure 4-8 shows the yaw vector side force required of a vectoring nozzle to generate the same yawing moment as a conventional centerline vertical tail and rudder. One can see that the 4,000 lbs nozzle load limit would result in smaller TV control moments than a conventional vertical tail at high speeds as was shown in Figure 1-4 comparing rudder and TV control power.

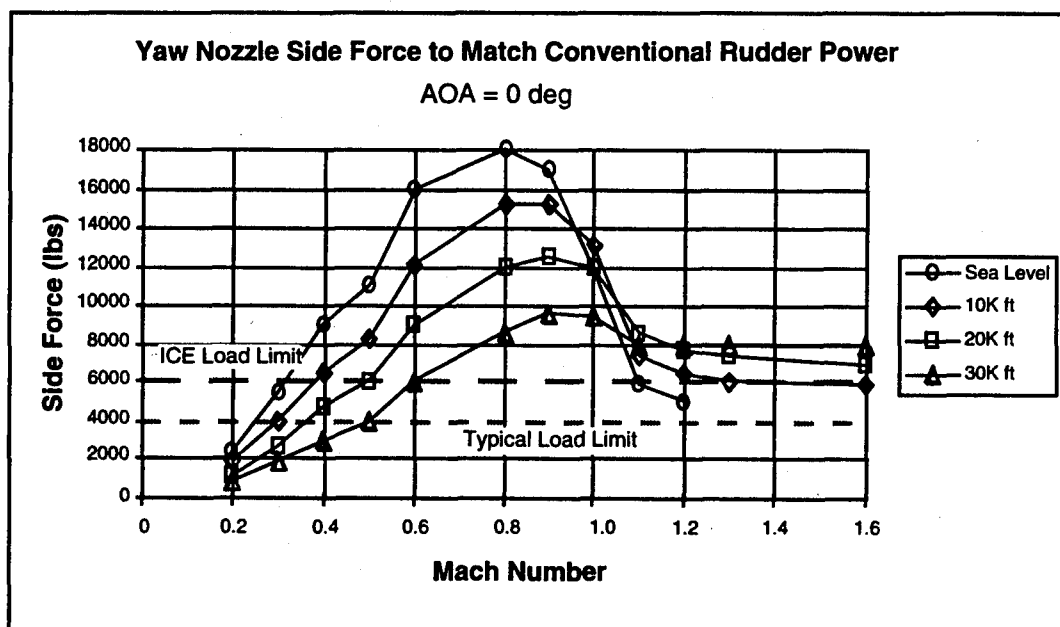


Figure 4-8 Yaw Vectoring Side Force Required to Match Conventional Rudder Power

For the purposes of this study, engine side load limits were set at 6,000 lbs to improve high-speed yaw vectoring effectiveness. Nozzle deflection limits were set at +/-15 deg for both pitch and yaw. An additional 100 lbs was added to the thrust vectoring nozzle weight increment to account for the increase in structure needed for the higher side load limit. A low-observable (LO) multi-axis nozzle concept was the chosen thrust vectoring system. These parameters were left unchanged throughout the study. Except for the en-

engine-out analysis on Configuration 201 (see below), the same engine and nozzle combination were assumed for both Configuration 101 and 201-series analysis.

Control Suite Sizing

Incorporation of vectoring onto the 101-series airplane allowed the clamshell to be deleted. Also, not apparent in the control surface data, is the reduction in size of the outboard spoiler actuator. For Configuration 101, both spoiler segments were required at high speed to provide adequate dutch roll augmentation. Yaw vectoring, along with the inboard spoiler segment can achieve acceptable dutch roll characteristics at high speed. The result is a significant weight savings due to replacement of the large outboard spoiler actuators with a single smaller actuator. (See actuator and structural integration in Section 7.) The outboard spoiler actuator was sized for full deflection capability up to 300 KCAS to provide lateral-directional control at elevated-g.

A portion of a 30 deg AOA/108 KCAS control envelope was shown in Figure 4-5 for Configuration 101-TV. Thrust vectoring effects were computed at maximum power for this flight condition. Comparison of the blended control power available and the attendant control power requirements show that Configuration 101-TV comes very close to achieving the goal of 90 deg bank angle change in 2.0 seconds. With increased vectoring deflections beyond the assumed ± 15 deg limits, the roll performance goal should be achievable.

Figure 4-9 shows the control deflections required to achieve the maximum coordinated roll power illustrated in Figure 4-5. Note that incorporation of thrust vectoring on Configuration 101-TV provides sufficient coordinating yaw power to overcome elevon adverse roll. As a result, the elevons are used for roll power on 101-TV, whereas they were used symmetrically on Configuration 101 at the 30 deg AOA condition.

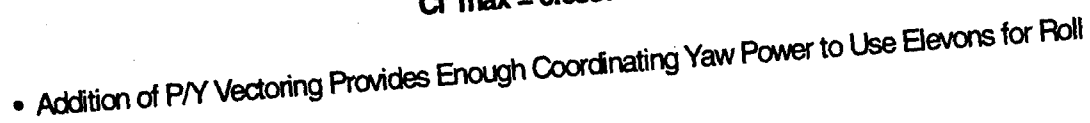
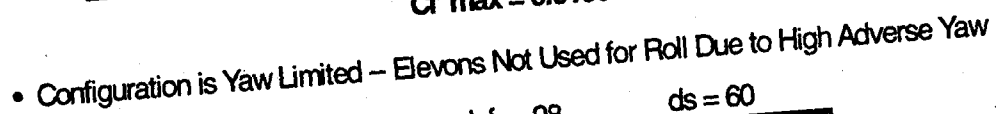


Figure 4-9 Controls Usage for Maximum Roll Power

Roll performance results were summarized above (Figure 4-6). Configuration 101-TV achieved all of the roll performance goals with the exception of the 30 deg AOA at 108 KCAS and 20 deg AOA at 300 KCAS (these were very close to meeting the goals). The 300 KCAS condition was evaluated at MIL power. In MAX A/B, 101-TV can achieve the 20 deg AOA/300 KCAS roll performance requirement. Note too that the power approach roll performance requirement is met. Recall that the Configuration 101 approach speed was set by roll performance. Thrust vectoring allows the approach speed to be reduced such that it is now set by the tipback AOA limit.

High AOA Lateral-Directional Capability

Maximum augmented lateral-directional stability characteristics are shown in Figure 4-10. The parameter used in this analysis is $C_{n\beta_{dyn Aug}}$, defined in Equation 139, 40.

$$C_{n_{\beta \text{dyn Aug}}} = \left[C'_{n_{\beta}} \cos \alpha - \left(\frac{I_{zz}}{I_{xx}} \right) C'_{l_{\beta}} \sin \alpha \right]_{\text{Body}} + \left[\frac{C'_{n_{\text{MAX}}}}{\beta} \right]_{\text{Stability}} \quad (1)$$

The first bracketed term in equation (1) is recognizable as the expression for $C_{n_{\beta \text{dyn}}}$. The second term represents control power for controls deflected to provide $C'_{n_{\text{MAX}}}$, trimmed in pitch and roll. The user selects the maximum sideslip to augment by specifying β . Equation (1) can be rewritten

$$C_{n_{\beta \text{dyn Aug}}} = \left[C'_{n_{\beta}} \right]_{\text{Stability}} + \left[\frac{C'_{n_{\text{MAX}}}}{\beta} \right]_{\text{Stability}} \quad (2)$$

This calculation is implemented in CPA. Where data are available, the effect of sideslip on the controls is included in the calculation.

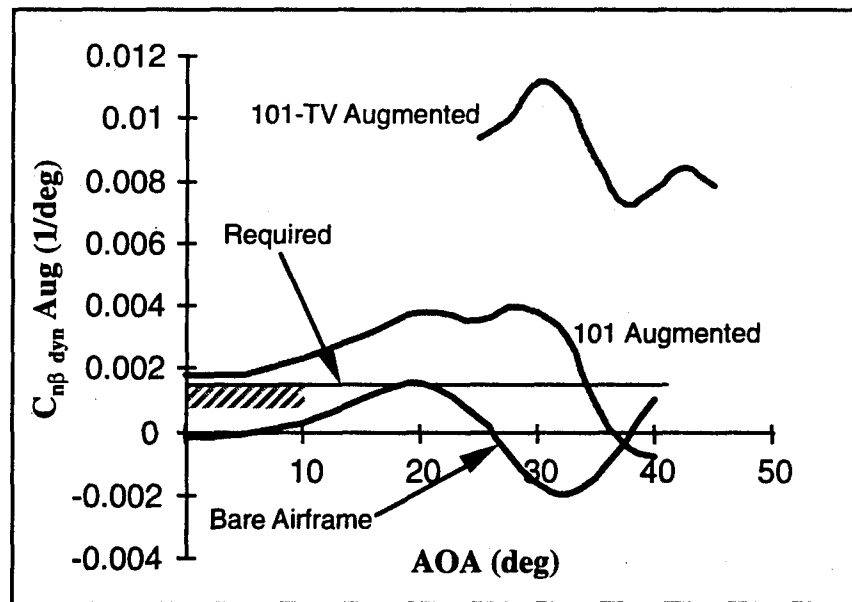


Figure 4-10 Configuration 101 and 101-TV Augmented Directional Stability Characteristics

The curves shown in Figure 4-10 represent the maximum lateral-directional augmentation capability at 10 deg of sideslip. The boundary is the amount of $C_{n_{\beta} \text{stab}}$ required to maintain dutch roll frequency greater than 1.0 rad/sec (Level 1, MIL-F-8785C) at a dynamic pressure of 40 psf. Instability is defined when $C_{n_{\beta \text{dyn Aug}}}$ becomes negative. The bare airframe curve shows that the basic configuration is slightly unstable at low AOA,

becoming stable at moderate AOA, and unstable again between 25 deg and 38 deg AOA. Configuration 101 has sufficient yaw power to maintain Level 1 frequencies up to 35 deg AOA, and becomes unstable at 36 deg AOA. This indicates an approximate AOA limit for Configuration 101 of 35 deg (other factors may set the practical AOA limit -- i.e., rotational damping characteristics, etc.). Roll performance analysis indicated that lateral-directional maneuvering is restricted to AOA < 30 deg due to highly adverse roll-yaw relationships in the high AOA control envelopes. Configuration 101-TV can achieve unlimited AOA performance based on this analysis. A large control margin is apparent between the required curve for Level 1 dutch roll, and the capability of 101-TV. Configuration 101-TV is pitch-trim limited above 45 deg AOA.

4.4 Configuration 201-Series Baseline Evaluation

Configuration 201 control suites were sized by power approach condition flying qualities. At approach conditions, power setting is low, and thrust vectoring control components are relatively small. Aerodynamic control surfaces must make up the difference to achieve the required control power.

The roll performance analyses were carried out at a number of loadings. Recovery WOD sensitivity to weight was determined by analyzing three bring back weights -- 0, 5K, and 10K lbs. Launch analysis was conducted at the mission takeoff weight of 44,437 lbs. Inertias for all 201-series airplanes were calculated using empirical preliminary design techniques.

For initial control sizing, the cg was assumed to be located at 20% MAC. Aft limit capabilities are discussed in Section 6.2.3. Table 4-4 lists mass properties data for 201-series configurations.

Table 4-4 Configuration 201-Series Mass Properties Data*Configuration 201*

Condition	Weight (lbs)	cg (% MAC)	I _{xx} (sl-ft ²)	I _{yy} (sl-ft ²)	I _{zz} (sl-ft ²)
Launch	44,437	20.0	49,067	100,506	152,580
0K BB	28,497	20.0	31,437	64,393	97,757
5K BB	33,497	20.0	36,592	75,692	114,909
10K BB	38,497	20.0	42,468	86,990	132,062

Configuration 201-TV

Launch	45,287	20.0	50,005	102,428	155,499
0K BB	29,347	20.0	32,347	66,314	100,673
5K BB	34,347	20.0	37,925	77,685	117,935
10K BB	39,347	20.0	43,446	88,994	135,103

4.4.1 Aerodynamic Assessment of Configuration 201

Aerodynamic data for the 201-series analysis were obtained from LMTAS ADF test entries 9502 and 9505, described in Appendix C. Data sources are listed below:

- Basic configuration data from ADF 9502/9505 (5-component data only)
- Drag data predicted using preliminary design methods
- Control effectiveness (except clamshell data) from ADF 9502/9505
- Clamshell control effectiveness from LMTAS tailless fighter wind tunnel data
- Dynamic derivatives from HASC (High Angle-of-Attack Stability and Control) predictions

A 63 ft² and a 90.5 ft² canard were evaluated to determine the size best suited for good trimmed lift capabilities. A sketch of the two canards is shown in Figure 4-11. Also shown is the advantage that the large canard provides at power approach conditions. The large canard, while not providing any significant lift increment by itself, allows the trailing edge flaps to be deflected more TED, resulting in a trimmed lift benefit. The large canard was used for the remainder of the study.

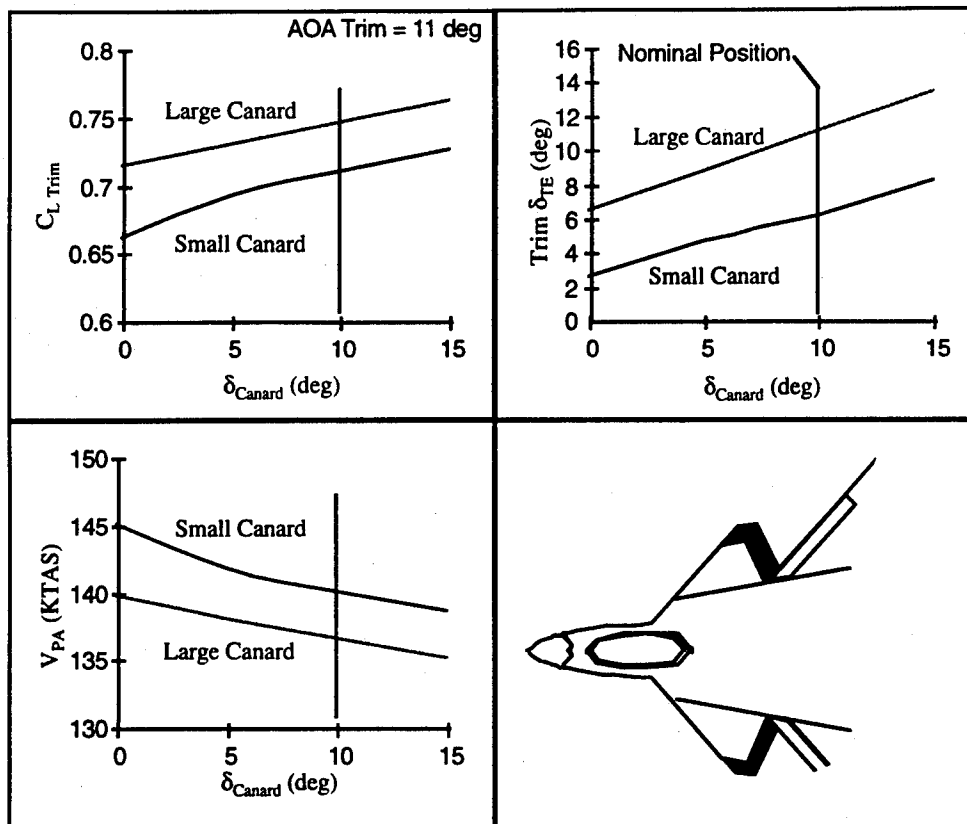


Figure 4-11 Canards Analyzed on Configuration 201

The canard was scheduled so that adequate trailing edge surface control margin could be maintained for roll control and to arrest nose-up inertial coupling moments during rolls. Figure 4-12 shows the canard schedule required to keep trailing edge surface deflections from exceeding 15 deg TED, leaving a control margin of 15 deg on each the aileron, elevon and pitch flap.

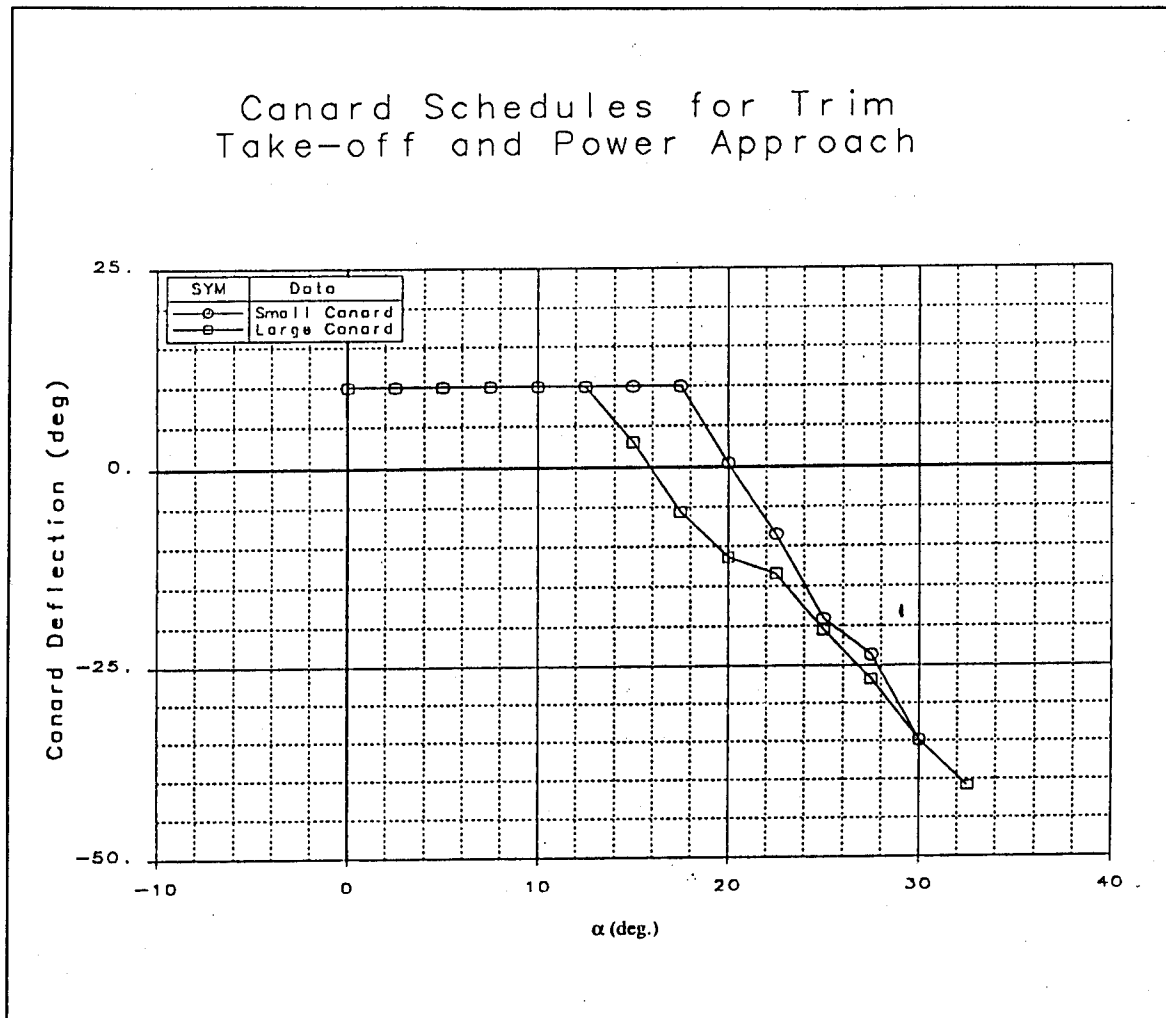


Figure 4-12 The Canard was Scheduled to Maintain Adequate Control Margin at High AOA

For this type of configuration in the high lift condition, the canard is typically scheduled slightly LE up at the approach AOA. The trailing edge surfaces are used to trim the airplane with TED deflections, resulting in a net positive lift increment.

Several trailing edge deflection combinations can be used to generate a trim solution. The best high lift trim solution is desired for the power approach condition. To maximize lift, the surface that provides the greatest lift per unit deflection ($C_{L\delta}$) along with the minimum pitching moment ($C_{m\delta}$) should be fixed (i.e., drooped). The remaining surface(s) are used for trim. The designer can then maximize the positive lift benefit of all

the trailing edge surfaces. Intuition leads to the conclusion that the aileron, having the shortest moment arm to the cg, would be the best surface to fix at a drooped position.

Figure 4-13 shows the effect of fixed aileron deflections on trim. Increasing TED aileron deflection provides increased trim normal force for a fixed canard setting. Furthermore, trailing edge deflection (pitch flap and elevon moving 1:1) required to trim is reduced, providing increased control margin at the approach AOA of 11.2 deg. While 30 deg of aileron droop provides the highest trimmed lift (note that the elevon and pitch flap are slightly TEU for trim at the approach AOA), it also saturates both ailerons; when rolling, one aileron must move from 30 deg TED to 30 deg TEU -- 60 deg of deflection. As a result, very fast aileron actuators would be required to provide sufficient low-speed roll mode augmentation.

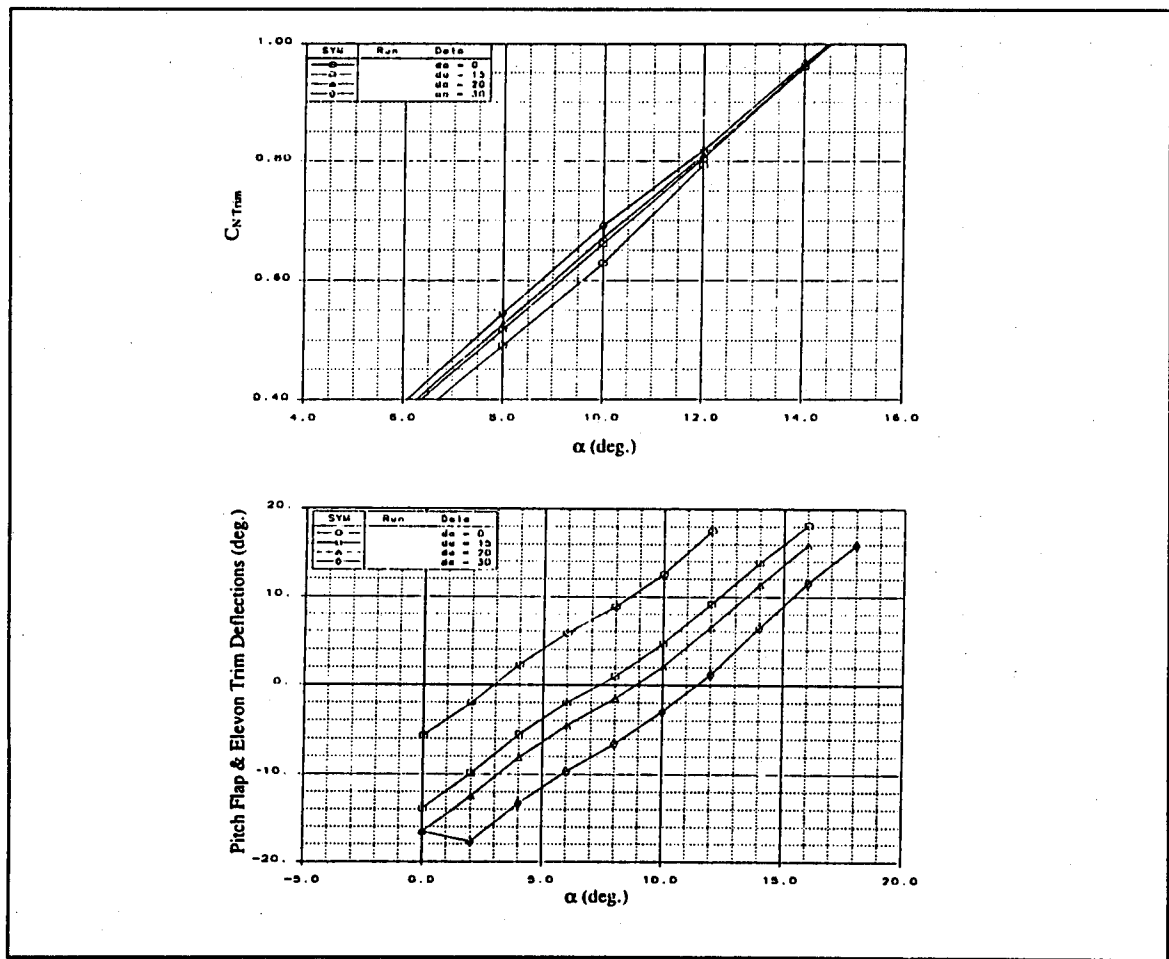


Figure 4-13: Effect of Symmetric Aileron on Trim

Based on the above analysis, the surfaces were set up such that at low speeds, the canard was fixed at 10 deg TED. The pitch flaps and elevons were used together for trim, and the aileron was fixed at 15 deg TED for improved high lift and elevon/pitch flap control margin.

The LEF improved C_{LMAX} , linearized the pitching moment and greatly improved lateral-directional stability above 15 deg AOA. The LEF was deflected 25 deg down at high AOA to improve bare airframe lateral-directional stability (Figure 4-14).

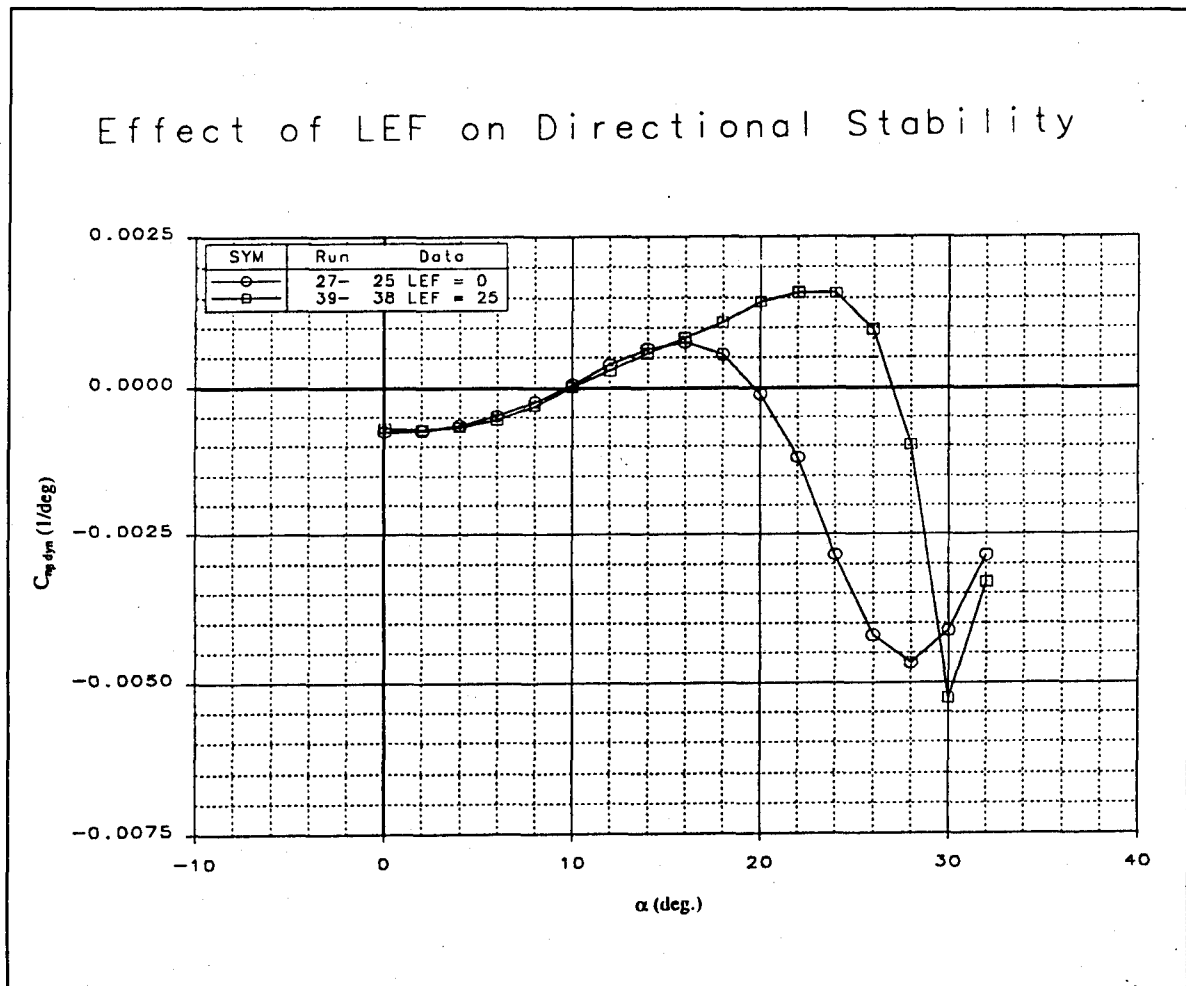


Figure 4-14 LEF Deflections Improve Lateral-Directional Stability

Figure 4-15 shows trimmed lift data for the resulting configuration. The data represent scheduled canard deflections with the aileron drooped 15 deg. Pitch flaps and elevons are

used as the trimming surfaces. Table 4-5 summarizes the control surfaces on Configuration 201.

Table 4-5 Final Configuration 201 Control Surface Summary

Controller	Usage	Deflection Limits (deg)	Area (ft ²)
Canard	Pitch/High Lift	10/-60	43.92
Pitch Flap	Pitch/High Lift	+/-30 (Sym)	15.48
Elevon	Pitch/Roll/High Lift	+/-30	13.43
Aileron	Pitch/Roll/Yaw/High Lift	+/-30	14.48
Spoiler	Roll/Yaw	0/60	18.81
Clamshell	Yaw	0/60 (each)	13.35
LEF	L-D Stability	0/25 (Sym)	16.91

Note: (1) Surface areas represent single side surfaces only.

(2) Clamshell area for one surface only (e.g., upper)

Configuration 201-Series with Large Canard

Canard/Aileron = Sched/15

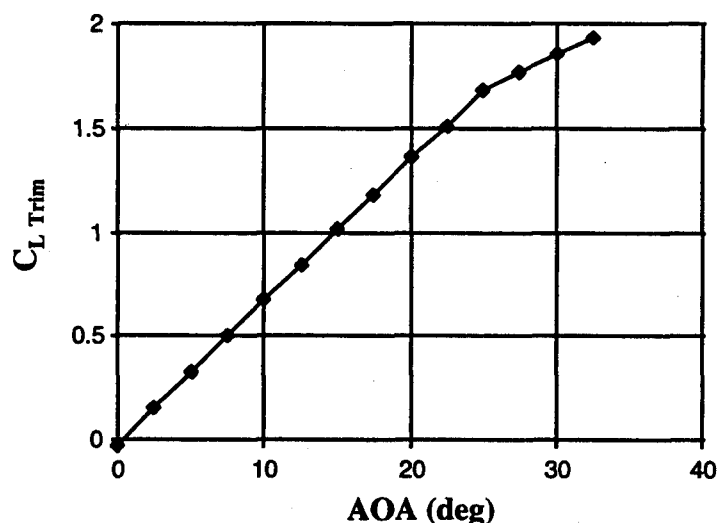


Figure 4-15 Configuration 201 Trimmed Lift Data

4.4.2 Carrier Suitability Performance Summary

Both 2-DOF and 3-DOF performance analysis tools were used to analyze the launch, recovery and waveoff performance of Configuration 201. Launch and arresting gear machinery were assumed to be a C13-1 catapult and Mk7 Mod 3 arresting gear on CV71

(USS Roosevelt), respectively. A summary of the configuration's launch performance is shown in Table 4-6.

Table 4-6 Configuration 201-Series Launch Performance Summary

Parameter	Threshold	Value
Launch Weight (lbs)	---	44,437
Deadload Endspped (C13-1) (KTAS)	---	167.0
Endspeed Increment from Thrust (KTAS)	---	4.1
Total Catapult Endspped (KTAS)	---	171.1
Launch Speed for 10' Sink (KTAS)	---	158.0
Design WOD (KTAS)	<0	-13.1
Operational WOD (KTAS)	---	1.9
a/g (Velocity Required)	>0.065	0.266
SEROC (Velocity Required + 10 KTAS) (fpm)	>200	500
SEROC (Design WOD=0 KTAS) (fpm)	---	825

Note: Performance based on target AOA = 16 deg

Not counting flying qualities, Configuration 201 has a design launch WOD of -13.1 KTAS set by the 10' sink requirement. Figure 4-16 shows a representative time history of a launch.

**Launch Performance at CG = 20%
VA = 160.7 KTAS, Sink = 10 ft
Time History Chart #1**

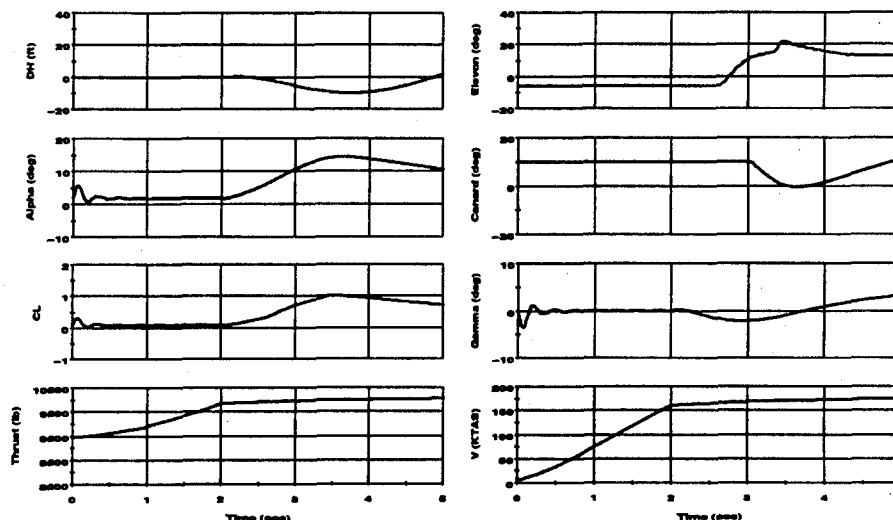


Figure 4-16 Launch Time History at 10' Sink Speed

Table 4-7 summarizes recovery performance capabilities at a bring back weight of 5K lbs. Not including flying qualities, V_{PA} is set by the vision limit. Vision limit AOA is 11.2 deg for this configuration resulting in an approach speed of 137.1 KTAS, or a design WOD of -1.1 KTAS.

Table 4-7 Configuration 201-Series Recovery Performance Summary

Parameter	Threshold	Value
Carrier Landing Performance Weight (lbs)	---	33,497
Engaging Speed (MK7 Mod 3) (KTAS)	---	145.0
Candidate V_{PA} Speeds (KTAS):	---	---
Vision	---	137.1
Popup	---	111.5
Power-on Stall	---	91.1
Level Acceleration ¹	---	---
Level 1 Flying Qualities	---	Varies w/ Config.
Small Transient Accel/Decel ²	---	---
V_{PA} (KTAS)	---	137.1
WOD = $1.05V_{PA} - V_{ENGAGE}$ (KTAS)	<0	-1.1
SEROC ($1.05V_{PA}$) (fpm)	>500	1500

Notes: (1) Not computed (depends on engine transients). Not usually a design driver.

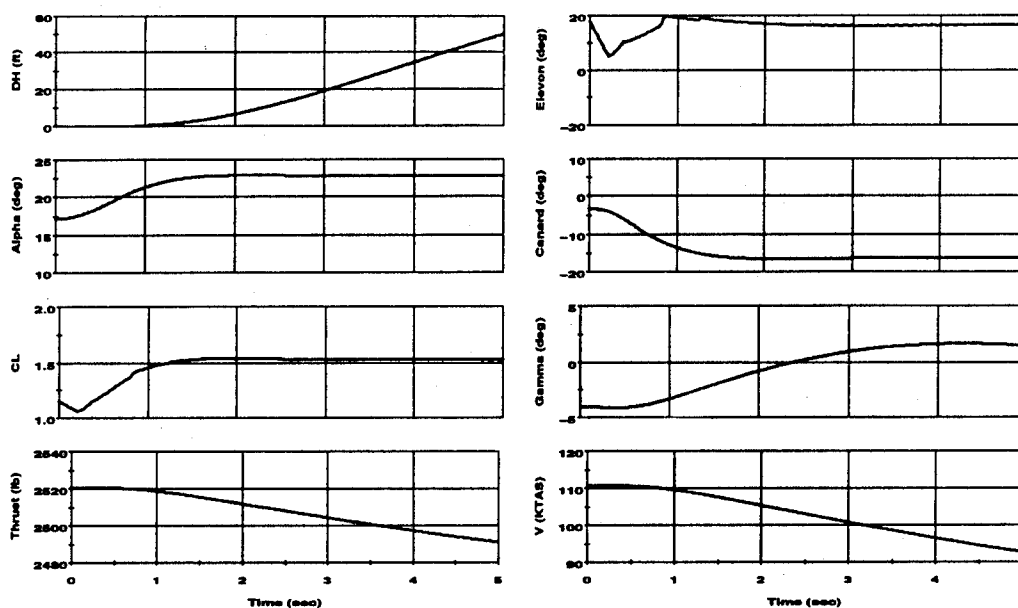
(2) Computed as a check at V_{PA} . Decel may be a concern.

There is a wide margin between the speed for the 50' pop-up and the vision limit. This is driven by the high C_{Lmax} value, and indicates that the LEF are not required to achieve acceptable pop-up performance. The LEF could be traded off for reduced bare airframe lateral-directional stability as long as sufficient high AOA yaw control power is available. Figure 4-17 shows a time history of the pop-up maneuver.

Table 4-8 lists CV performance sensitivities for the configuration. Launch speed for 10' sink over bow is strongly influenced by the initial flight path angle when the airplane leaves the end of the flight deck. This in turn is a strong function of nose landing gear dynamics. (A landing gear model representative of this class of configuration was assumed during the analysis.) This result is typical, and shows the importance of careful detailed design of the landing gear. Not surprisingly, recovery performance is most influenced by vision limit AOA. Note too that pop-up performance is not strongly influenced by maximum pop-up AOA. Together with the good pop-up performance, this sen-

sitivity again indicates that the LEF could be traded off and/or an AOA limit could be imposed during power approach with acceptable pop-up performance penalties.

Popup Performance at CG = 20%
Vpopup = 110.8 KTAS, Altitude Change = 50 ft
Time History Chart



Innovative Control Effectors (ICE)

Figure 4-17 Pop-up Maneuver Time History

Table 4-8 CV Performance Sensitivities

Launch

Parameter	Value	Units
γ_0	2.6	KTAS/0.1 deg
Weight	3.5	KTAS/1000 lbs
cg	-1.7	KTAS/% MAC

Recovery

Parameter	Value	Units	Applicability
Maximum AOA	-0.9	KTAS/deg	Pop-up
Vision AOA	-6.2	KTAS/deg	---
Weight	2.1	KTAS/1000 lbs	---
cg	-1.4	KTAS/% MAC	Vision
cg	-1.2	KTAS/% MAC	Pop-up
Δh	-33.3	ft	Waveoff

Figure 4-18 shows a waveoff time history. Altitude loss during the waveoff was 33 ft.

Waveoff Performance at CG = 20%
V_{waveoff} = 137.6 KTAS, Sink = 33.3 ft
Time History Chart

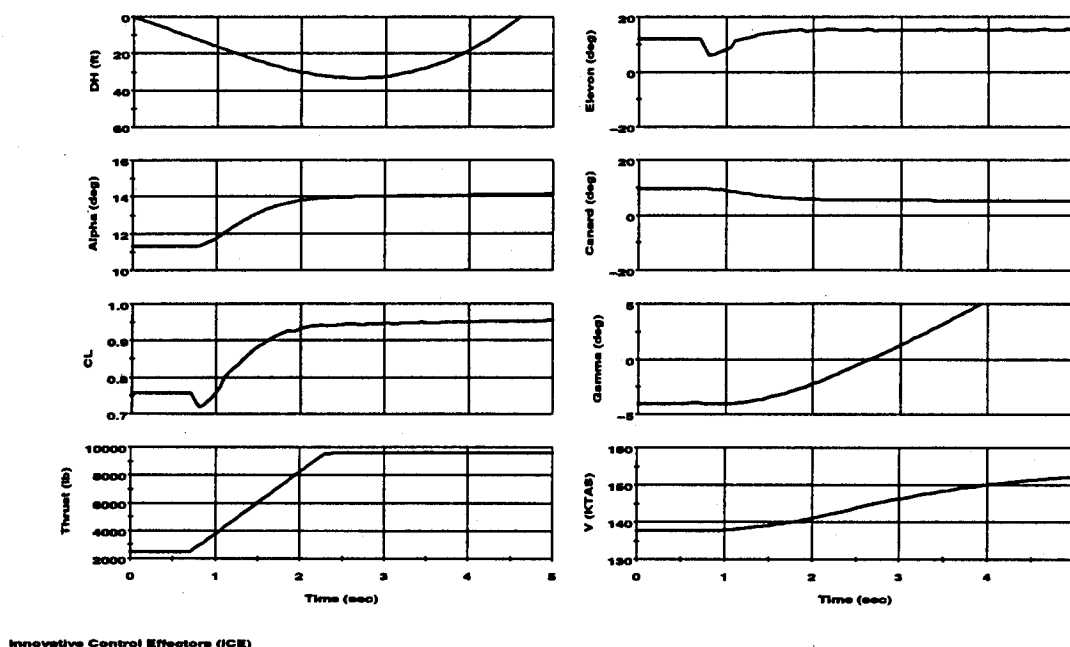


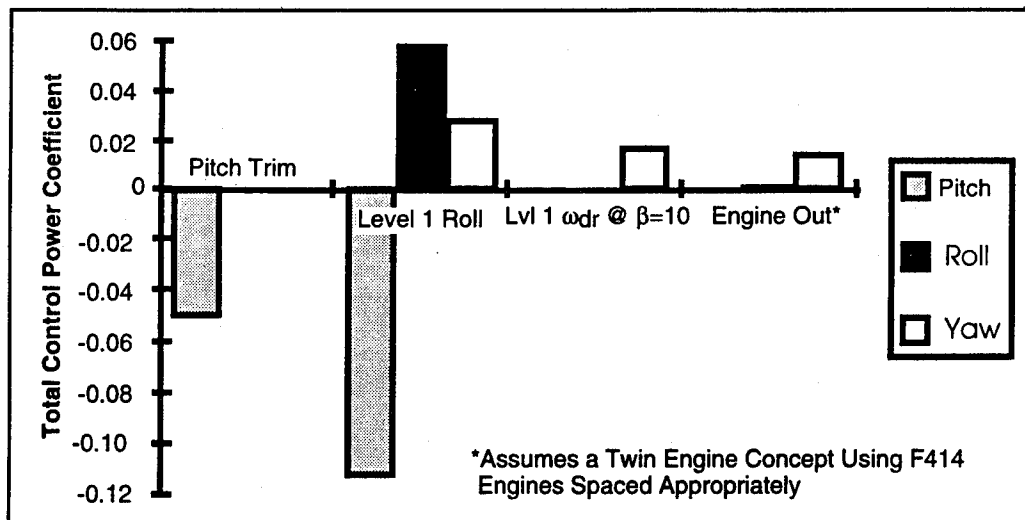
Figure 4-18 Waveoff Time History

4.4.3 Control Power Requirements for Configuration 201

Control power requirements for 201-series configurations concentrated on launch and approach roll performance. Usually, the critical maneuver that sizes the aerodynamic control surfaces on a CV suitable tailless fighter is power approach roll. Two examples are provided below for illustration.

First, the control requirements for various cases are presented in Figure 4-19 for the 201 configuration at the PA condition: pitch trim; Level 1 roll performance; Level 1 dutch roll frequency at 10 deg of sideslip; and engine out. (Note that although the 201 configuration is a single engine aircraft, a twin engine concept was assumed for the engine out analysis. Two F414 powerplants, each spaced 20 inches off of the aircraft centerline, were assumed. Engine spacing is consistent with the F/A-18 E/F using the same powerplant.) It

is readily apparent that the control power magnitudes for Level 1 roll performance are the most severe for each axis.



Example Requirements at Vision Limit Approach Speed and 10K Bring Back Weight

Figure 4-19 Roll Performance Generates the Greatest Control Power Requirements at Power Approach Conditions

The second example shows the control power available versus required during launch (Figure 4-20). This analysis used the catapult endspeed, including thrust increments, for a C13-0 catapult on CV67 (USS Kennedy). Two cases are shown: one with no vectoring; the second with TV in mil-power. The power approach time-to-bank requirement was modified by the ratio $I_{xx}(\text{Max TO})/I_{xx}(\text{VPA})$. The figure shows that excess control capability exists to meet the launch condition roll requirement with MIL-Power TV. TV nozzles were incorporated on all of the 201 innovative control configurations to achieve the high AOA roll performance goals.

The control power requirements for varying bring back weights and airspeeds are given in Figure 4-21. The diagrams show the total pitch and incremental roll and yaw control power required to achieve Level 1 roll performance as a function of WOD for varying AOA and bring back weight. These requirements are for time-to-bank 30 deg in 1.0 sec, constraining sideslip within 6 deg, and maintaining a nose-down pitch acceleration capa-

bility of at least -0.07 rad/sec^2 . The results are relatively insensitive to bring back weight (i.e., changing inertias), but are primarily a function of trim airspeed or AOA.

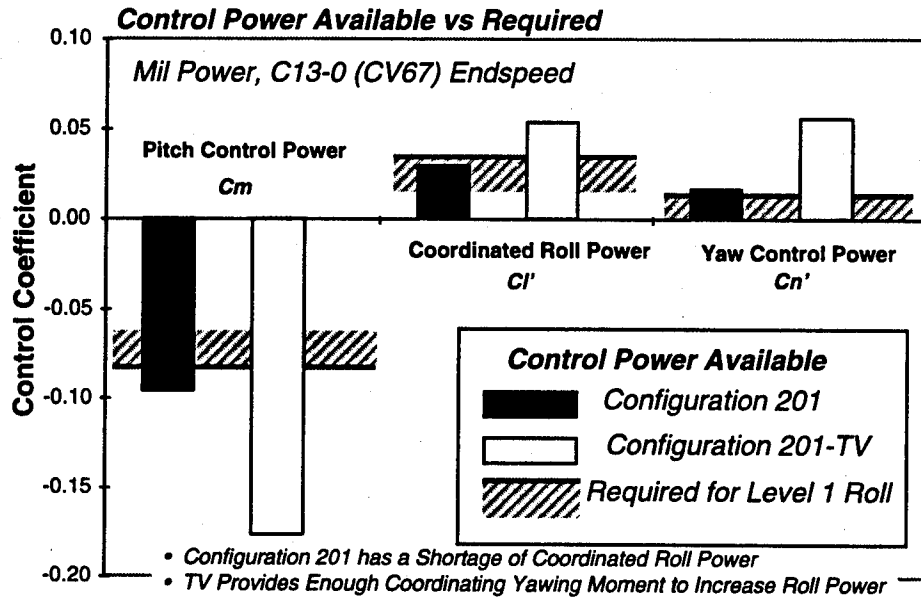


Figure 4-20 Thrust Vectoring Provides Excess Control Power for Launch Roll Performance

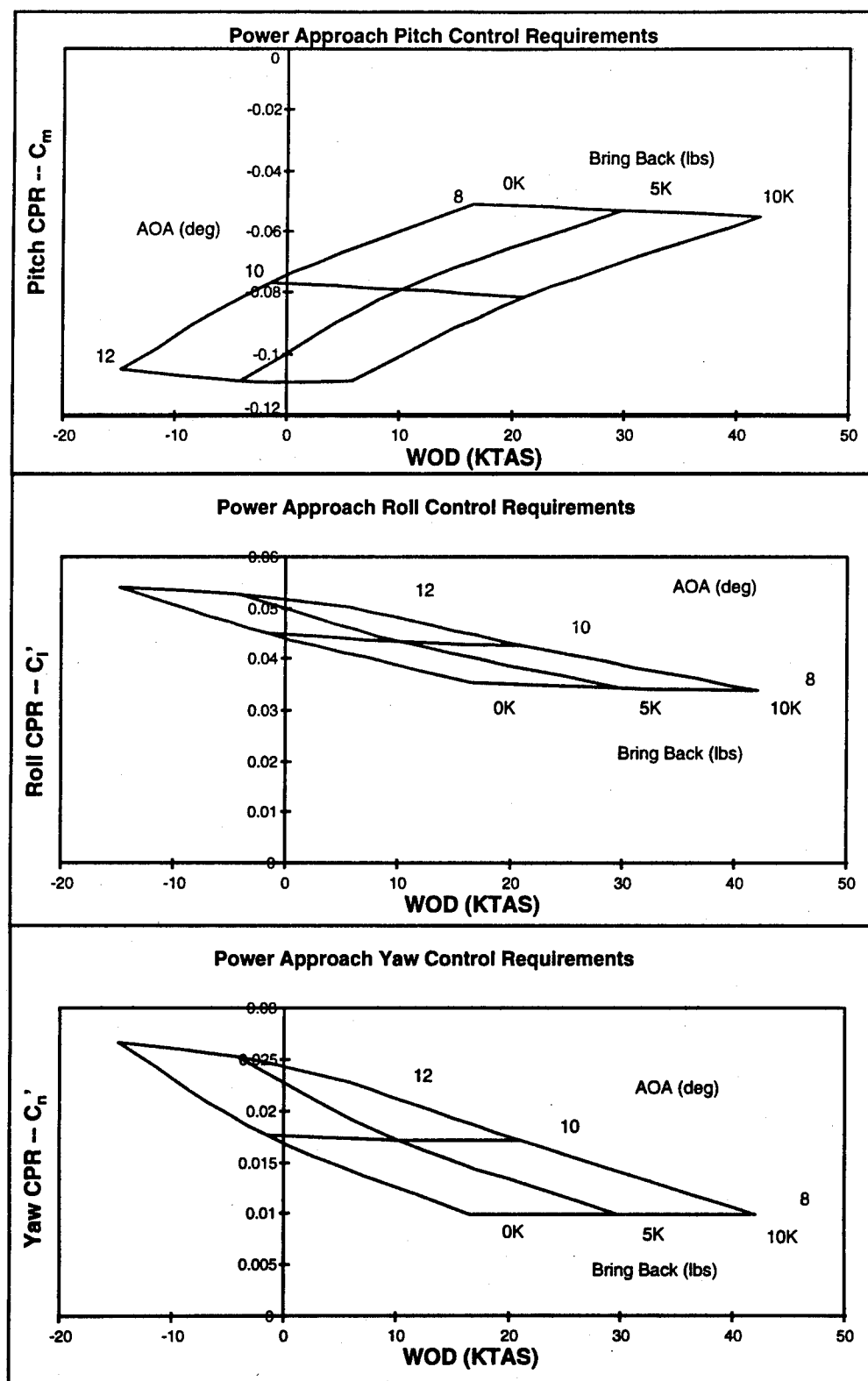


Figure 4-21 Configuration 201-Series Power Approach Control Power Requirements

4.4.4 Launch and Power Approach Roll Performance Assessment

The previous section illustrated that power approach roll performance would set the control surface sizes for this configuration. Without thrust vectoring, launch roll performance is also a concern (i.e., Configuration 201). Figure 4-22 shows the WOD required to achieve Level 1 roll performance during launch. Curves are shown for both C13-0 and C13-1 catapults. Recall that excess capability exists to meet the WOD required for 10' sink off of the bow (-13 KTAS with the C13-1 catapult). Figure 4-22 illustrates that the configuration without thrust vectoring would have its WOD set by Level 1 roll performance (-10 KTAS). The addition of thrust vectoring improves the launch WOD required for Level 1 flying qualities by approximately 30 KTAS; the WOD for the configuration with thrust vectoring would be set by 10' sink off the bow speed.

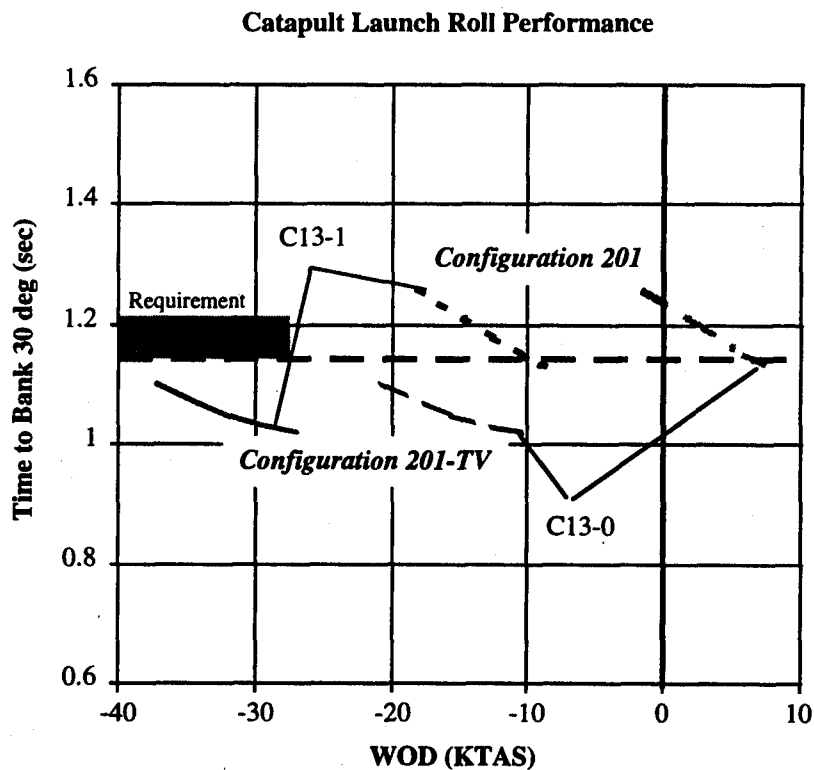


Figure 4-22 Thrust Vectoring Provides Large Improvements in the Launch WOD Required for Level 1 Flying Qualities

Figure 4-23 shows the control power required to meet Level 1 roll performance versus the control power available at the vision limit AOA for Configuration 201 (5K lbs bring back weight). It is apparent from the figure that the configuration lacks sufficient coordinating yaw power to meet the roll requirement. If sufficient yaw power were provided to coordinate all of the available roll power, the configuration would be able to achieve the Level 1 bank angle requirement.

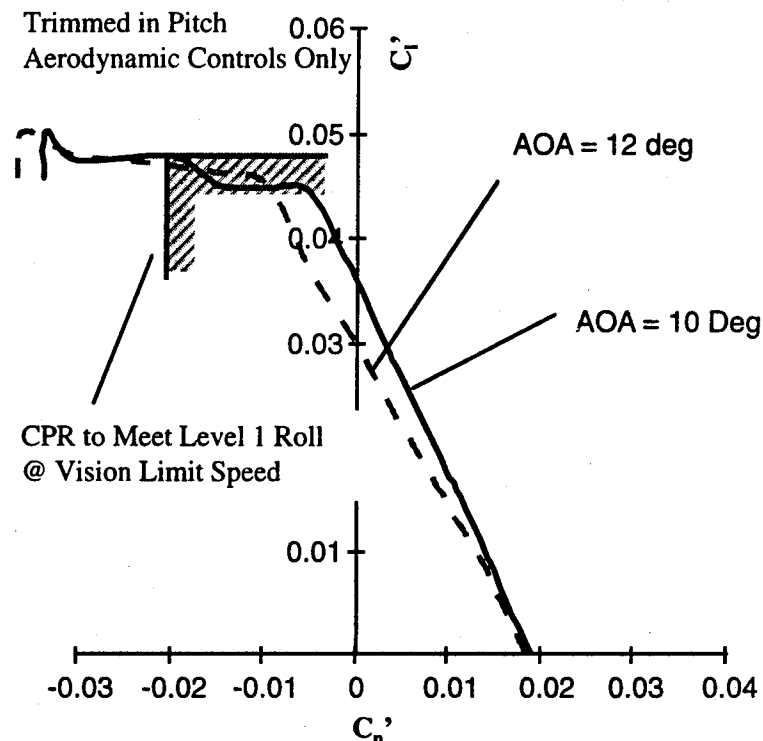


Figure 4-23 Insufficient Yaw Power is Available to Coordinate the Roll Power on Configuration 201

4.4.5 Effect of Thrust Vectoring on Power Approach Roll Performance

Thrust vectoring has the potential of providing coordinating yawing moments for Configuration 201. However, when the throttle setting is at idle power during PA (i.e., small TV control potential), yaw coordination is the most demanding. This analysis shows the effect of idle power TV on PA roll performance.

Figure 4-24 shows a summary of simulation results run within control envelopes for Configuration 201 with and without MATV (201-TV). Lines of constant AOA and bring

back weight are plotted on a bank angle at one second versus WOD diagram. The resulting chart shows that roll performance is relatively insensitive to bring back weight at a constant AOA, but drops off sharply with increasing AOA or reduction in WOD. Comparing the solid lines with the dashed shows that while thrust vectoring offers an improvement in PA roll performance, Level 1 flying qualities still cannot be achieved at zero WOD. At a given bring back weight, idle power TV offers a 1 to 2 knot improvement in recovery WOD.

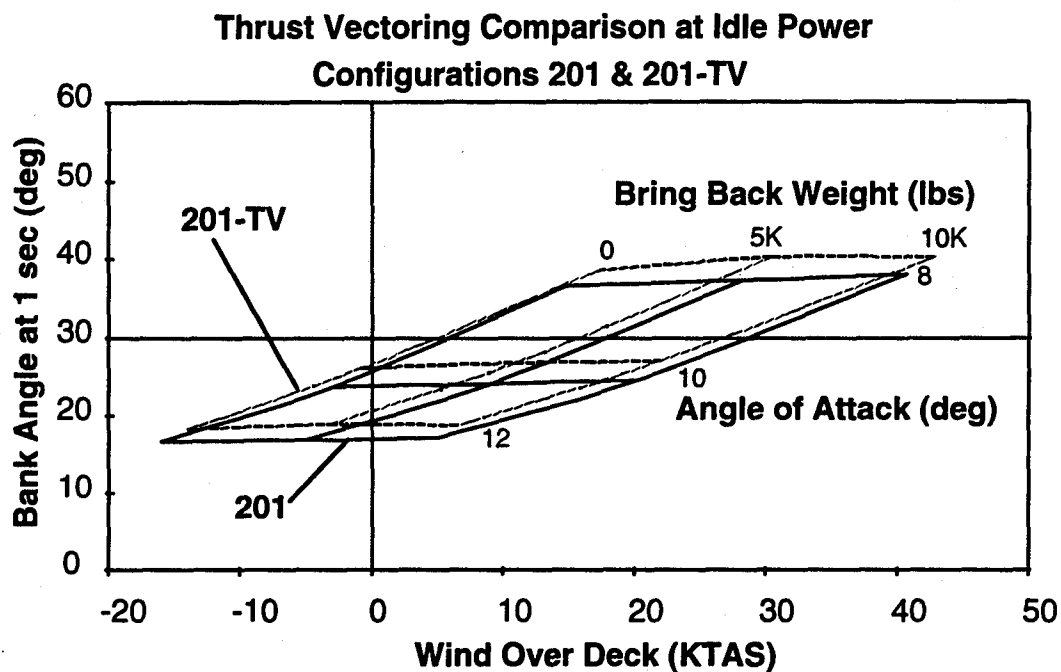


Figure 4-24 Thrust Vectoring at Idle Power Provides Small Improvements to PA Roll Performance

If the flight and throttle control systems were integrated to control glidepath using a speedbrake or thrust reversing system, the throttle could be fixed at a minimum value to provide sufficient yawing moments for roll coordination during landing. Reference 5 describes such a system using thrust reversing to maintain low speeds at high throttle settings. Section 6 of this report describes the potential recovery roll performance improvements that could be realized assuming such a system. The impact of Innovative Controls on WOD is also discussed in Section 6.

4.4.6 Thrust Vectoring Impact on Trimmed Lift

An assessment of the potential that thrust vectoring has to improve trimmed lift was made using Configuration 201-TV. Figure 4-25 compares the trimmed normal force for each trim strategy with the baseline trim (see above) at 11 deg AOA. The canard was fixed at 10 deg in each case. Also shown are the trailing edge elevon, pitch flap and nozzle deflections required for trim. The resulting trim coefficients were normalized to the baseline level with the baseline defined as 1.0. None of the alternate trim strategies exceed the baseline level.

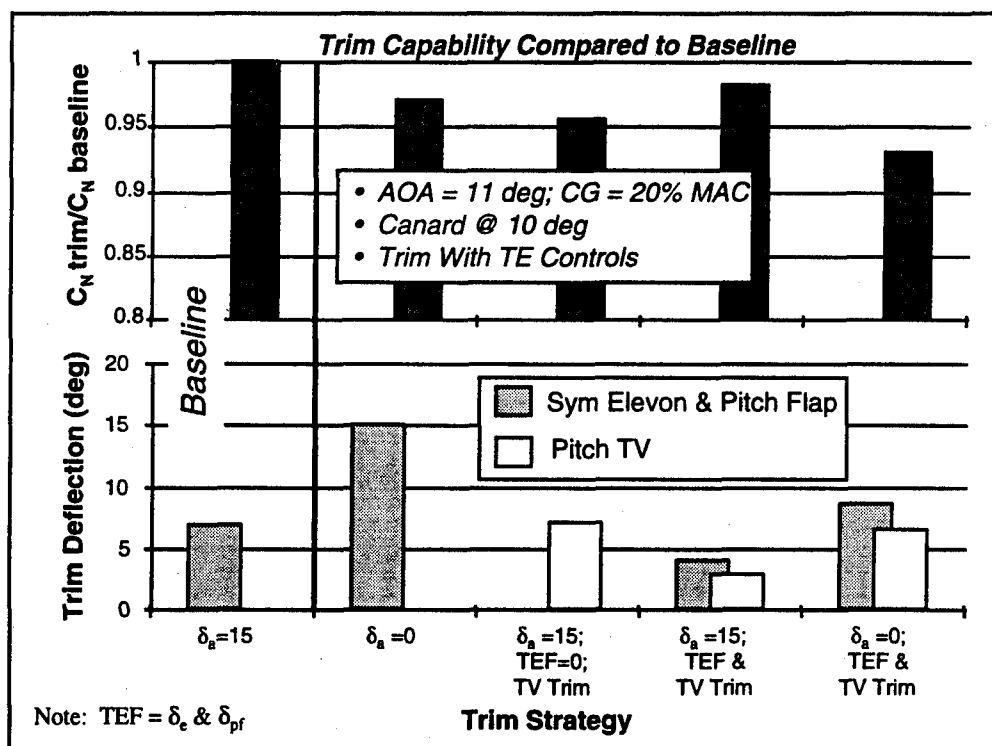


Figure 4-25 Thrust Vectoring Provides no Trimmed Lift Benefits over the Baseline High Lift Configuration

The results of Figure 4-25 are configuration dependent. On Configuration 201-TV, the thrust and aerodynamic controls being used for trim are located in about the same place longitudinally. Therefore, their lift and pitching moment effectiveness are similar resulting in no net benefit trading one for the other. For the canard-delta arrangement to utilize more trailing edge trim power, either the canard deflection or size must be increased. For

this configuration, increasing the canard deflection beyond 10 deg did not appreciably increase the nose-up pitching moment (and therefore the required trailing edge trim deflections). During this study, canard size was increased to load up the trailing edge flaps at the approach AOA. More wind tunnel testing with different canard geometries may offer an improved configuration.

The trim capability of thrust vectoring is a function of power setting. Trim throttle settings were used in the above analysis. To increase the power setting, a speedbrake or thrust reversing system must be implemented to control glidepath; furthermore, the speedbrake design must not adversely affect trimmed lift. Fortunately, such a system would offer synergistic improvements to PA roll performance (see discussion in Section 4.4.5).

4.4.7 Thrust Vectoring Impact on Nose Wheel Lift Off Performance

The carpet plot in Figure 4-26 shows the effect of pitch vectoring on nose wheel lift off. The analysis was done at a weight of 44,000 lbs and cg location of 18% MAC. No ground effects were included in the aerodynamic data. The plot shows nose gear unstick velocity at various canard and aileron settings. The elevon and pitch flaps were set full nose up. Canard deflection has little impact on unstick performance, but nose up pitch from the aileron significantly improves performance. Without vectoring, Configuration 201 performs quite well, easily achieving the requirement of α_{LO} at $0.9V_{LO}$ with significant control margin left over -- even at a cg location of 18% MAC. This indicates that the forward cg limit for unstick speed is forward of the 18% MAC analyzed. The addition of pitch vectoring in mil-power greatly reduced nose gear unstick speed and the dependence on aerodynamic control deflections. With vectoring, a realistic forward cg limit would probably not be set by nose gear unstick, but by other considerations such as nose gear load limits or other FCS considerations.

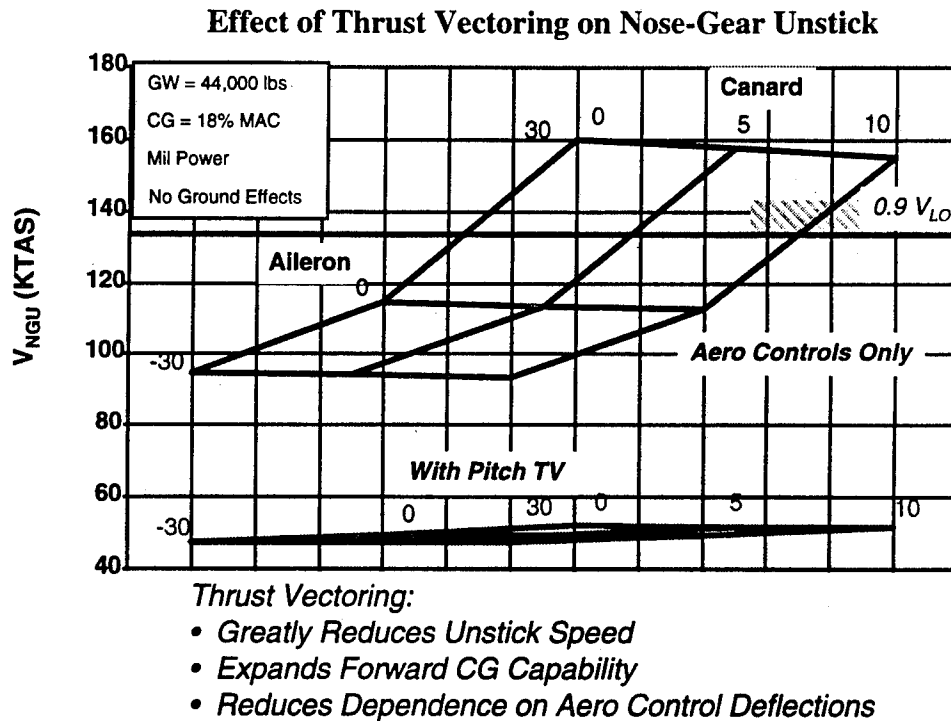


Figure 4-26 Thrust Vectoring in Mil-Power Provides Great Improvements to Nose Wheel Liftoff Performance

4.4.8 Effect of Control Deflections on SEROC

Usually, yaw control power for a tailless fighter is generated using devices that create differential drag. For a twin engine design, a significant amount of yaw power is required to offset the yawing moment created when an engine fails. The drag produced by a tailless fighter's yaw controls is detrimental to single engine rate-of-climb (SEROC) performance. This analysis was carried out to determine the impact that drag producing controls have on SEROC performance for twin engine fighters.

For this analysis, it was assumed that the configuration was powered by two F404 engines located 20" off centerline. Sea level tropical day thrust data were used. For configurations that employ thrust vectoring, it was assumed that vectoring control was available from the operating engine. Since the aerodynamic data for the 201-Series configuration was collected using a 5-component balance, no drag increments were available for

the controls. Therefore, control surface drag increments were scaled from similar controls tested on the 65 deg sweep flying wing configuration.

Based on the above assumptions, Figure 4-27 shows that single engine controllability is more critical for a configuration without thrust vectoring. In the figure, total yaw power available at 1-g is plotted versus true airspeed. The yaw control requirement at MIL-Pwr and MAX-A/B are overlaid on the plot. Even in MIL-power, the thrust vectored configurations have a substantial single engine control margin over the non-vectored Configuration 201. On vectored configurations, TV on the remaining engine provides excess yaw authority, thereby minimizing required aerodynamic control deflections and the resulting drag. The aerodynamic-only control configuration (201) was chosen for the SEROC analysis.

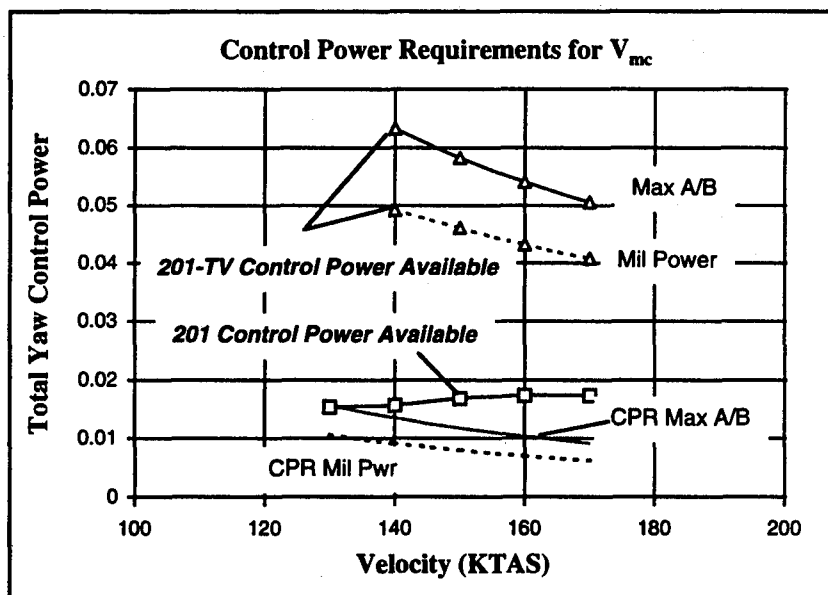


Figure 4-27 Single Engine Controllability is More Critical for Configurations without TV

The minimum control speed for a twin-engine version of Configuration 201 is 130 KTAS. A small yaw control margin is available at the vision limit speed of 138 KTAS. Since all of the yaw power for this configuration comes from differential drag-producing controls (i.e., clamshell, spoiler, etc.), the drag effects during single engine flight will be significant.

Figure 4-28 shows the effect of control-induced drag on launch and recovery SEROC performance. Launch SEROC was found to be more critical than recovery due to higher gross weight. Incorporation of the control drag increments increased the velocity required to achieve the 200 fpm rate-of-climb requirement by approximately 9 KTAS in mil-power. The 171 knot endspeed of the C13-1 catapult provides a SEROC of nearly 500 fpm at launch. In MAX-A/B, the launch requirement is easily achieved. Recovery SEROC was not a limiting factor, even when considering the control-induced drag effects.

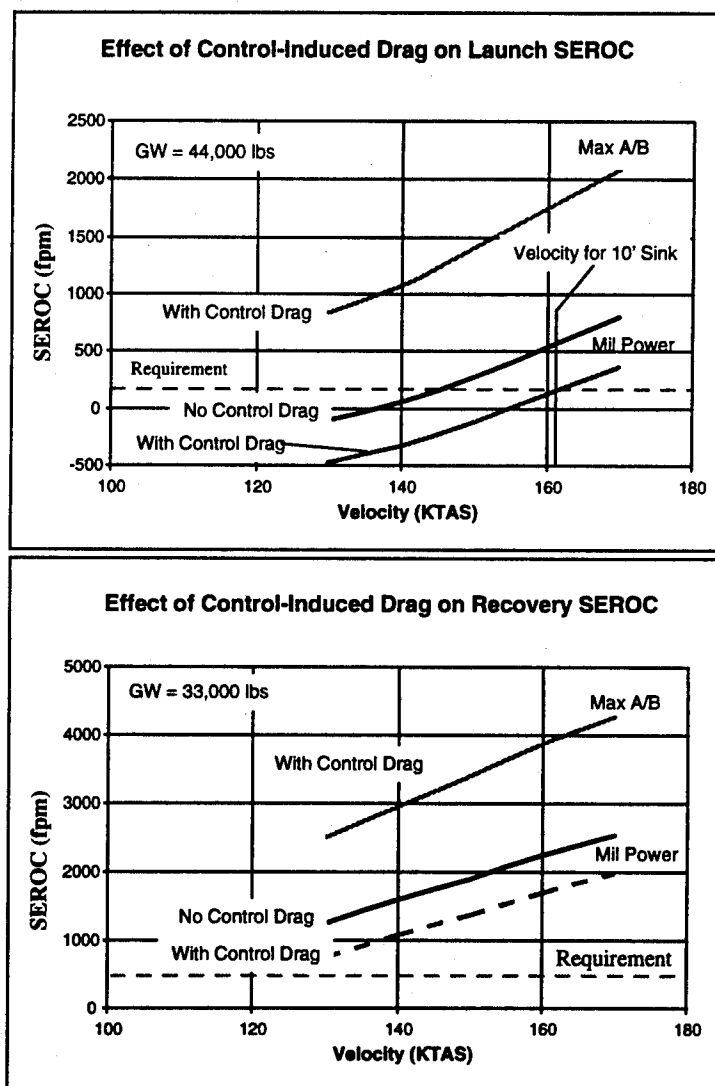


Figure 4-28 Yaw Control Deflections Significantly Impact SEROC Performance

4.4.9 High AOA Capabilities

Figure 4-29 shows coordinated and trimmed, primed stability axis roll power versus AOA for Configurations 201 and 201-TV. Thrust vectoring control moments were applied at 150 KCAS. Without vectoring, Configuration 201 coordinated roll control power drops off significantly at high AOA. Part of the reason for this is the poor spoiler performance for this configuration (see Appendix C).

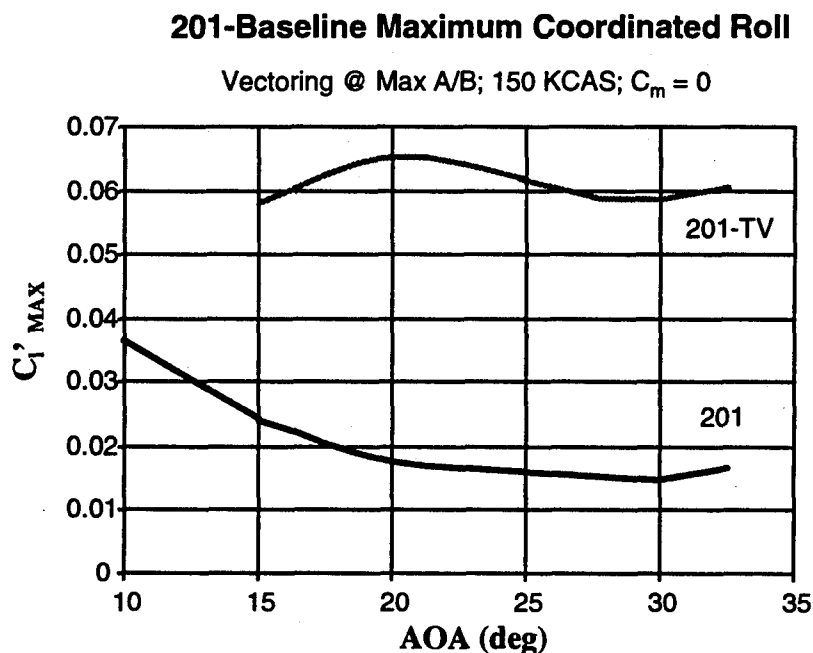
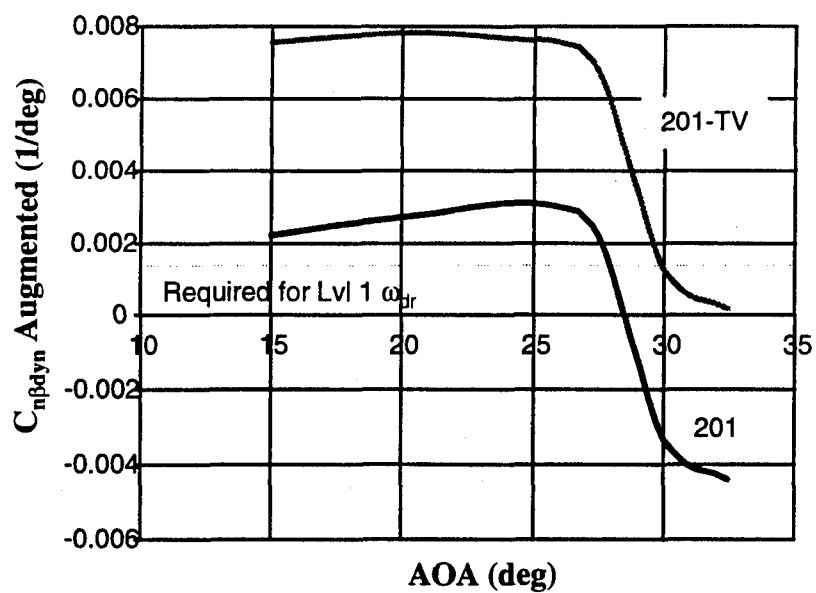


Figure 4-29 Maximum Coordinated Roll Control Power

Augmented directional stability is shown in Figure 4-30. Without thrust vectoring, the configuration can maintain sufficient augmented directional stability up to 27 deg AOA. With MAX-A/B thrust vectoring the augmented directional stability drops below the desired level at 30 deg AOA. This configuration exhibits a large lateral-directional instability above 30 deg AOA that demands significant lateral-directional control power to augment. Unfortunately, no sideslip data were available for AOA's greater than 32.5 deg.

201-Baseline Augmented Lateral-Directional Stability

Max Sideslip = 10 deg

**Figure 4-30 Augmented Directional Stability Characteristics**

5 Initial Evaluation of Innovative Controls -- Derivative Configurations

Six control suites were defined to fit within a design space bounded by signature characteristics, high AOA capability, and structural design. Configurations 101-1 through 101-6 include combinations of the five innovative control concepts discussed in Section 3 (Figure 5-1).

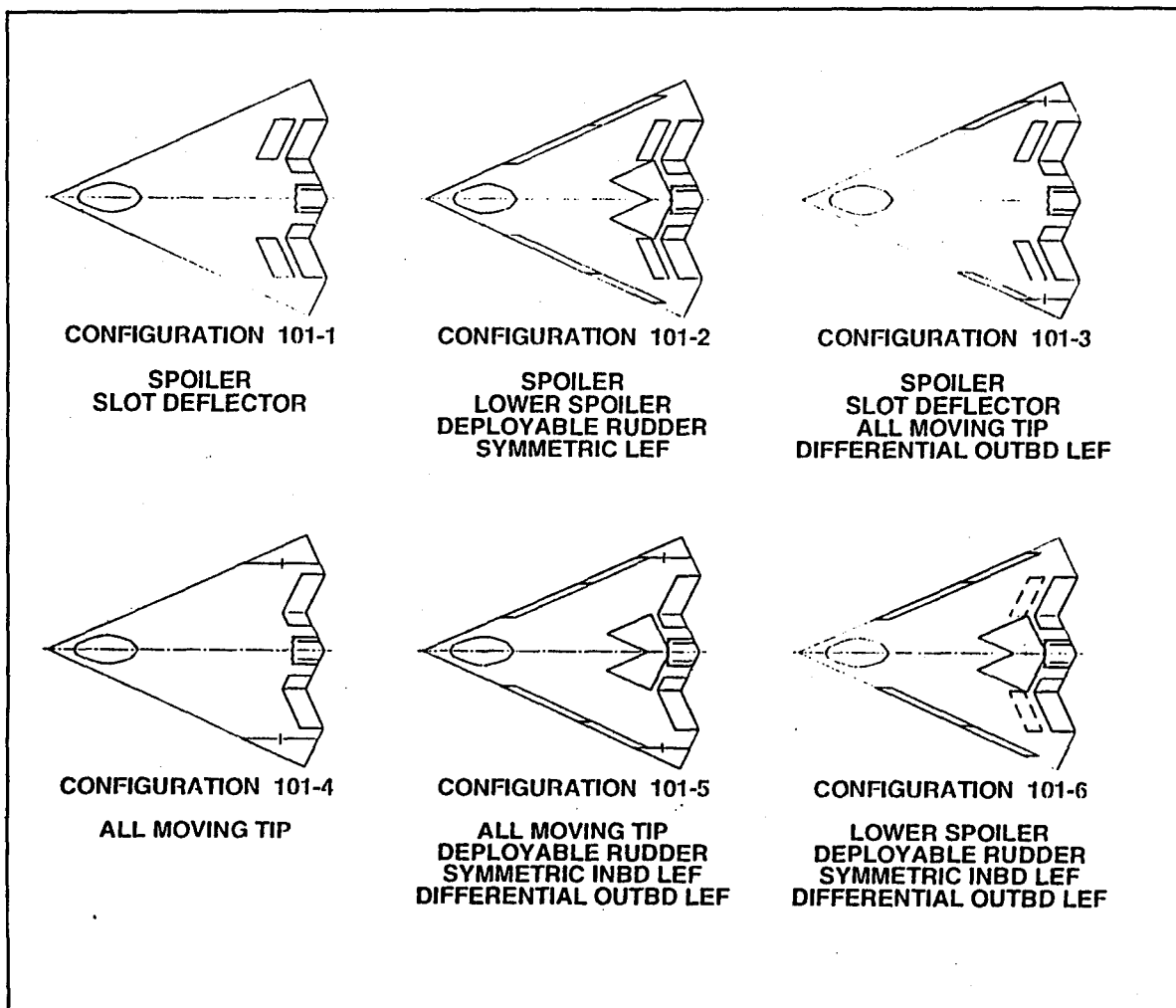


Figure 5-1 Six Innovative Control Suites were Defined for the Initial Screening

Analysis of Configurations 101 and 101-TV showed that MATV would be required to achieve the high AOA roll performance goals defined in Section 3 (i.e., aerodynamic control power alone could not achieve the high AOA agility goals). Therefore, MATV

nozzles were implemented on all six trade study configurations. Aerodynamic controls were sized using the three critical conditions for control power requirements defined above; power approach, 30 deg AOA at 108 KCAS -- MAX-A/B, and 20 deg AOA at 300 KCAS -- MIL-Pwr. After appropriate control suite sizes were determined, the resulting configurations were weighed (Figure 5-2). In this manner, the six configurations would have similar maneuver performance capabilities at the three design flight conditions. The control suites are shown in Figures 5-3 through 5-8.

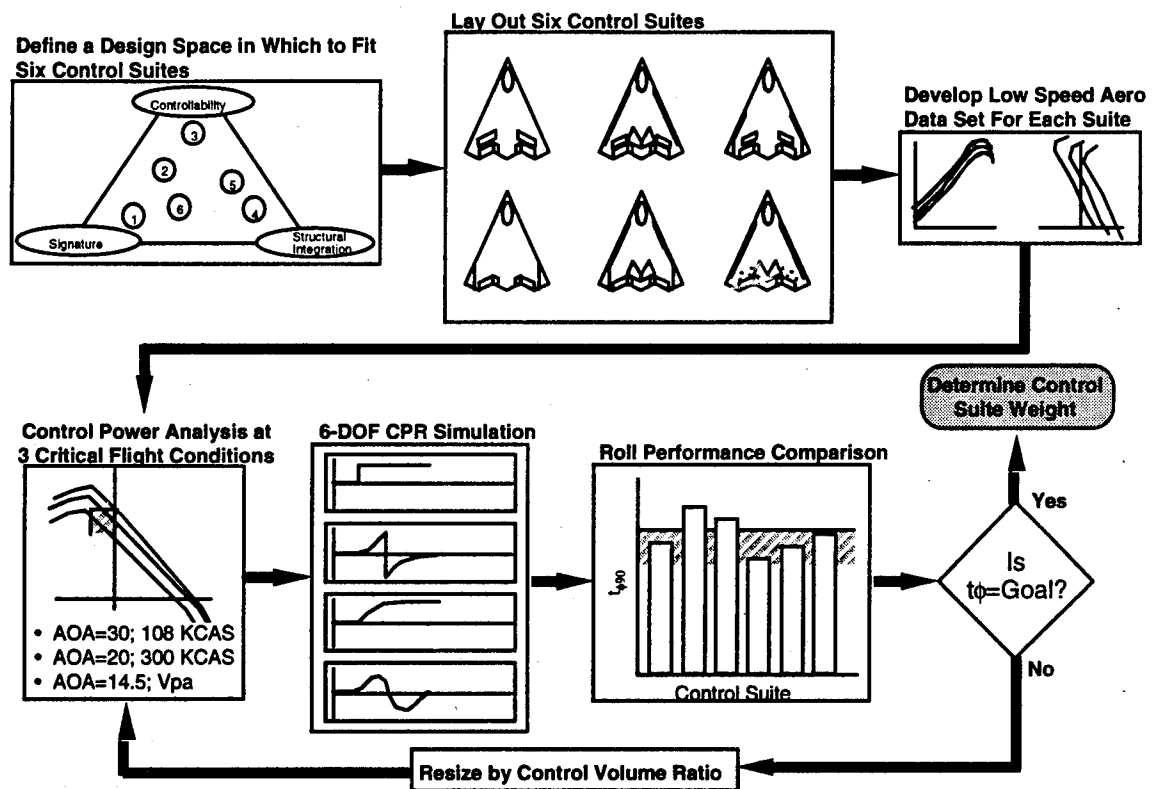


Figure 5-2 An Iterative Process was used to Yield Six Configurations with Similar Maneuver Capabilities

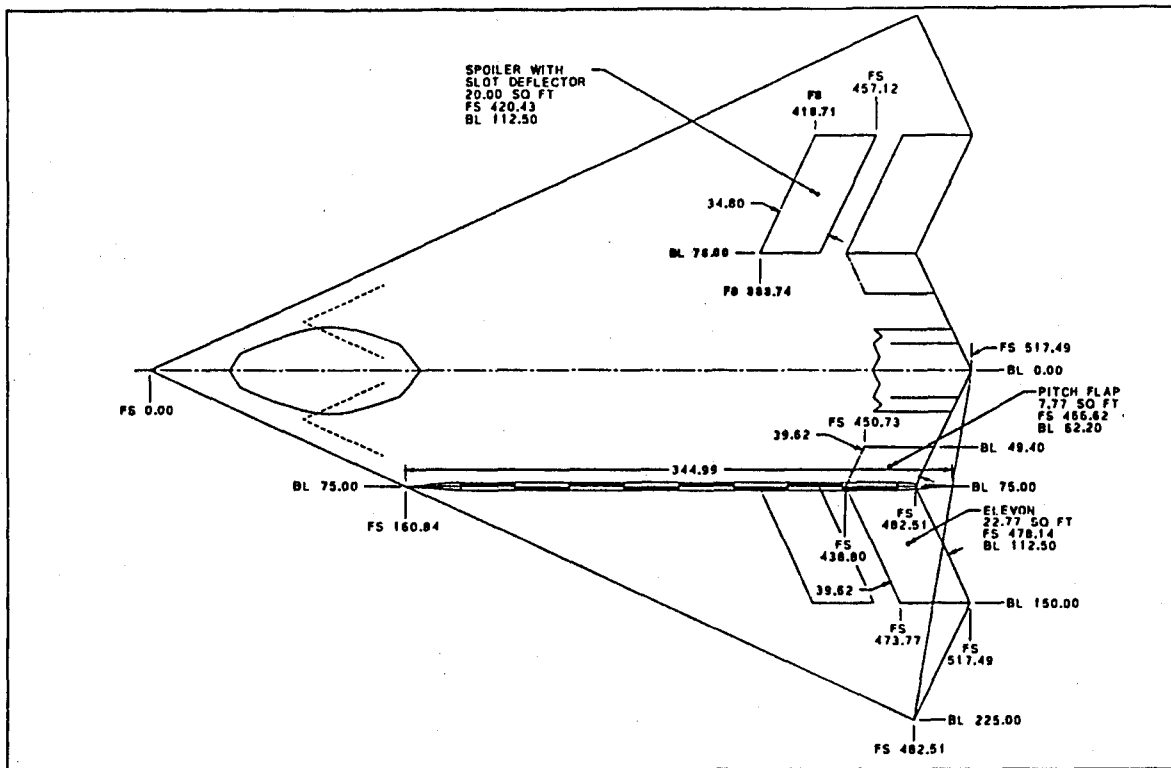


Figure 5-3 Configuration 101-1 Control Layout

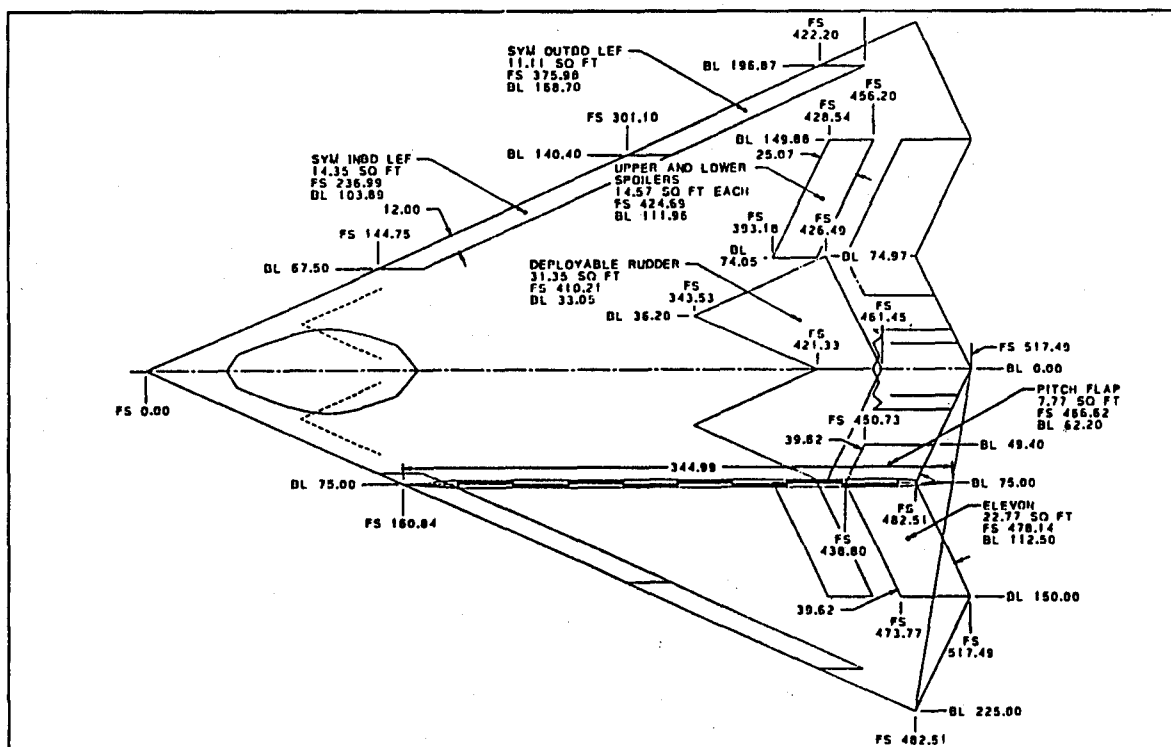


Figure 5-4 Configuration 101-2 Control Layout

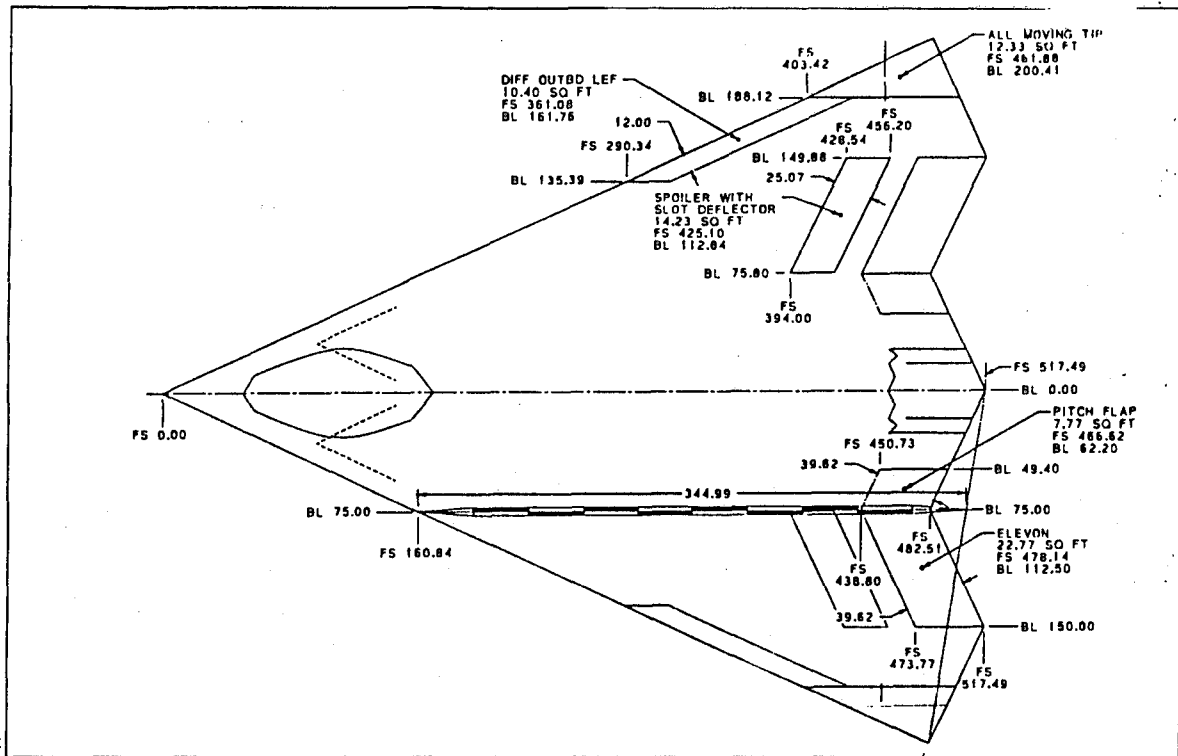


Figure 5-5 Configuration 101-3 Control Layout

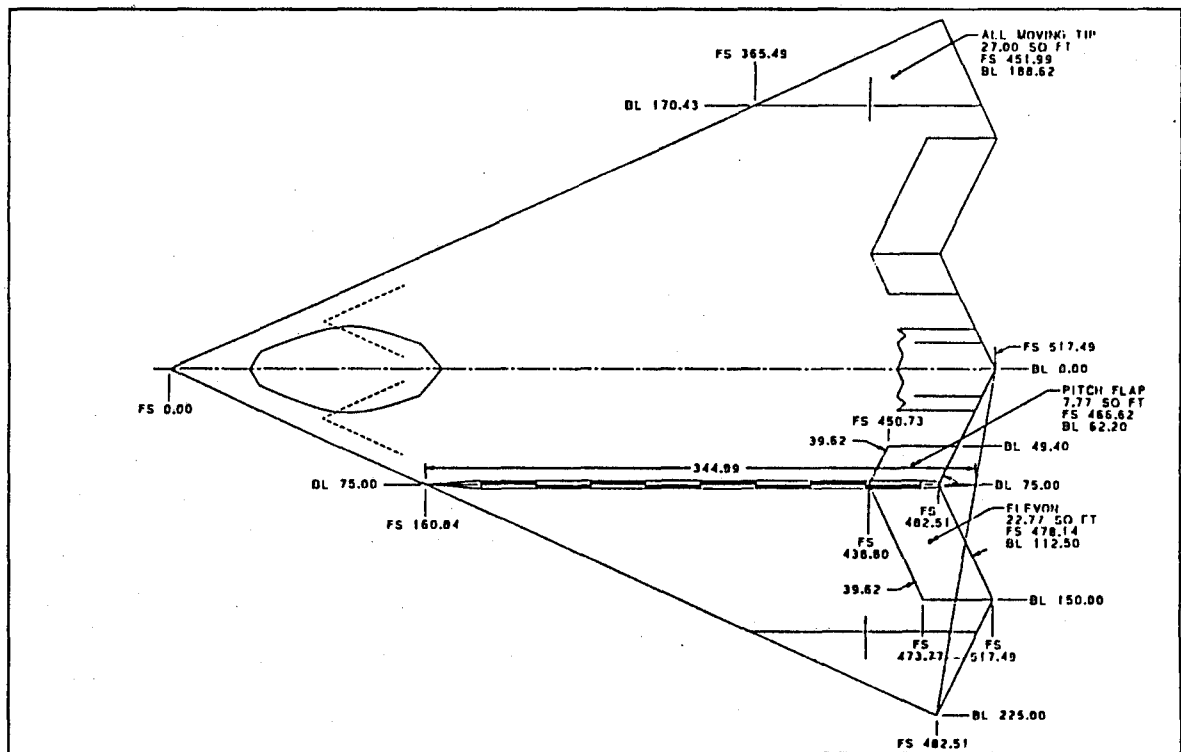


Figure 5-6 Configuration 101-4 Control Layout

117

Once the control suites were properly sized, high AOA departure criteria with vectoring off, control suite weights, and a relative evaluation of the vehicle's signature performance were made. The best three control suites were selected for further evaluation (Section 6).

Roll performance at the three critical flight conditions is shown for each configuration in Figure 5-9. Each control suite was sized to have roughly the same roll capabilities at the critical conditions.

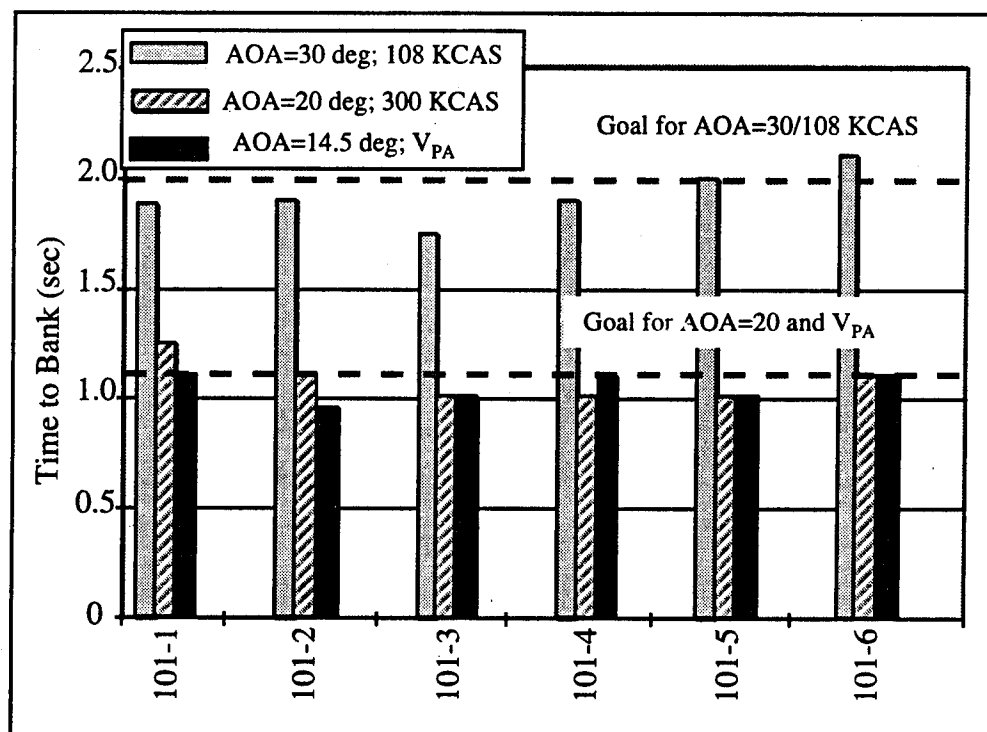


Figure 5-9 Roll Performance at Three Flight Conditions for Six Innovative Control Suites

To provide a fair assessment of the aerodynamic lateral-directional control potential of each configuration, $C_{n\beta_{dyn}} Aug$ was compared for all configurations without thrust vectoring. Vectoring-off, augmented lateral-directional stability for each configuration is shown in Figure 5-10. Also shown in the accompanying bar chart is the minimum level of $C_{n\beta_{dyn}} Aug$ for each configuration. Configurations with the AMT (101-3, 101-4, and 101-5) have the best high AOA lateral-directional performance. Configurations 101-3 and 101-4 are never unstable for sideslips up to 10 deg. Configuration 101-4 maintains

Level 1 dutch roll frequencies at all AOA. Configuration 101-1 would be the most limited configuration without thrust vectoring. All six configurations can maintain Level 1 dutch roll frequencies up to 23 deg AOA.

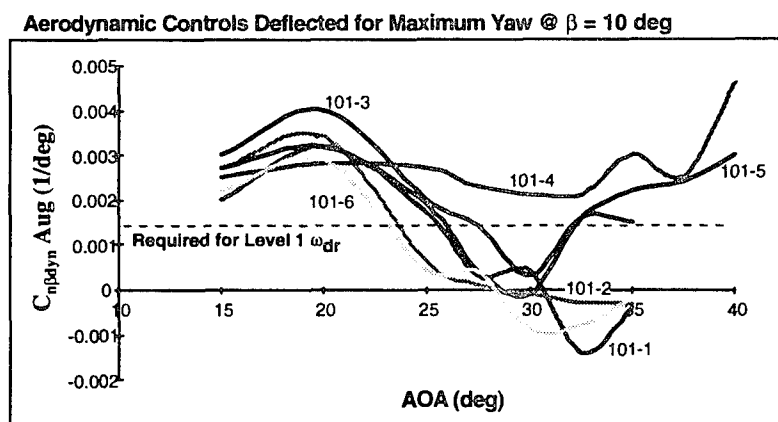


Figure 5-10 Augmented Directional Stability with Aerodynamic Controls Only

Nose-down pitch capability at 30 deg AOA was determined for each control suite, and is shown graphically in Figure 5-11. These results are presented as pitch accelerations to include the estimated changes in pitch inertia (I_{yy}) between configurations. Also, some of the configurations employ inboard LEF, resulting in greater nose-down pitching moments at 30 deg AOA. Configurations with greater nose-down capability would have more aft cg limit capability for a given level of pitch acceleration.

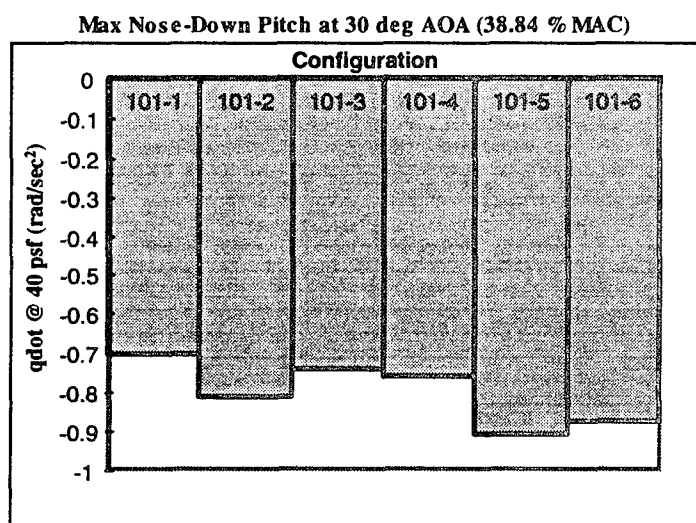


Figure 5-11 Aerodynamic Nose-Down Pitch Capability at 30 deg AOA

Weight comparisons with Configuration 101-TV are shown in Figure 5-12. Changes in weight range from an 800 lbs penalty (101-2) to a 600 lbs savings (101-4). Configurations employing the deployable rudder tended to be heavier.

Trade Study Weight Summary

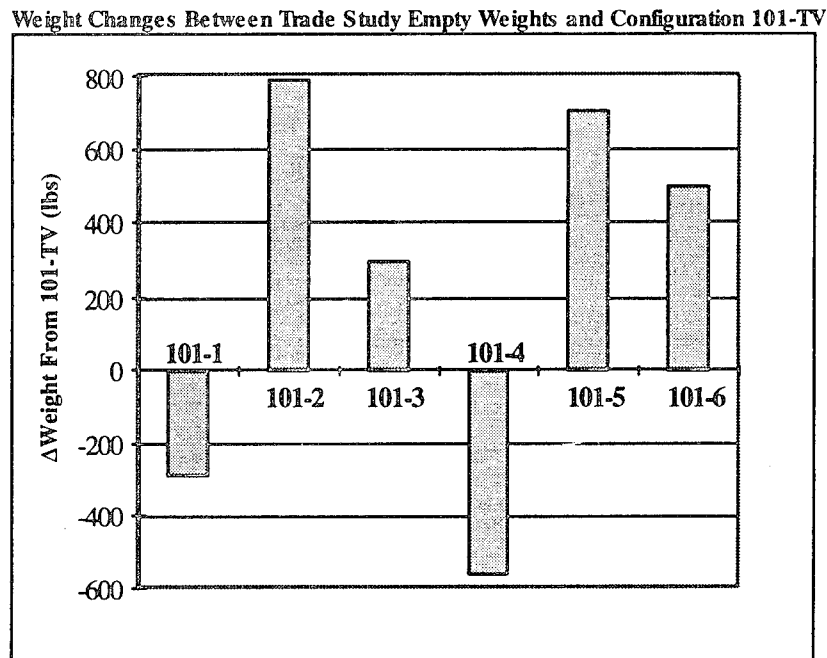


Figure 5-12 Configuration Weight Changes Due to Varying Control Suite

The configurations were ranked from one to six depending on a qualitative signature assessment. Configuration 101-1 was ranked the best due to the lack of leading edge controls. Configurations with the AMT ranked lower due to the difficulties associated with signature integration. Furthermore, it was thought that the titanium trunion and pivot shaft required for the tip would be difficult to hide with radar absorbent materials.

Each configuration was ranked ordinally in the following categories: (1) weight impact; (2) pitch capability at 30 deg AOA; (3) yaw augmentation without vectoring; (4) signature. Qualitative weightings were given each category, and the scores totaled. The top three control suites were Configurations 101-1, 101-3 and 101-4 (Figure 5-13). Perhaps not surprisingly these three configurations lay at the "corners" of the original design space depicted in Figure 5-1.

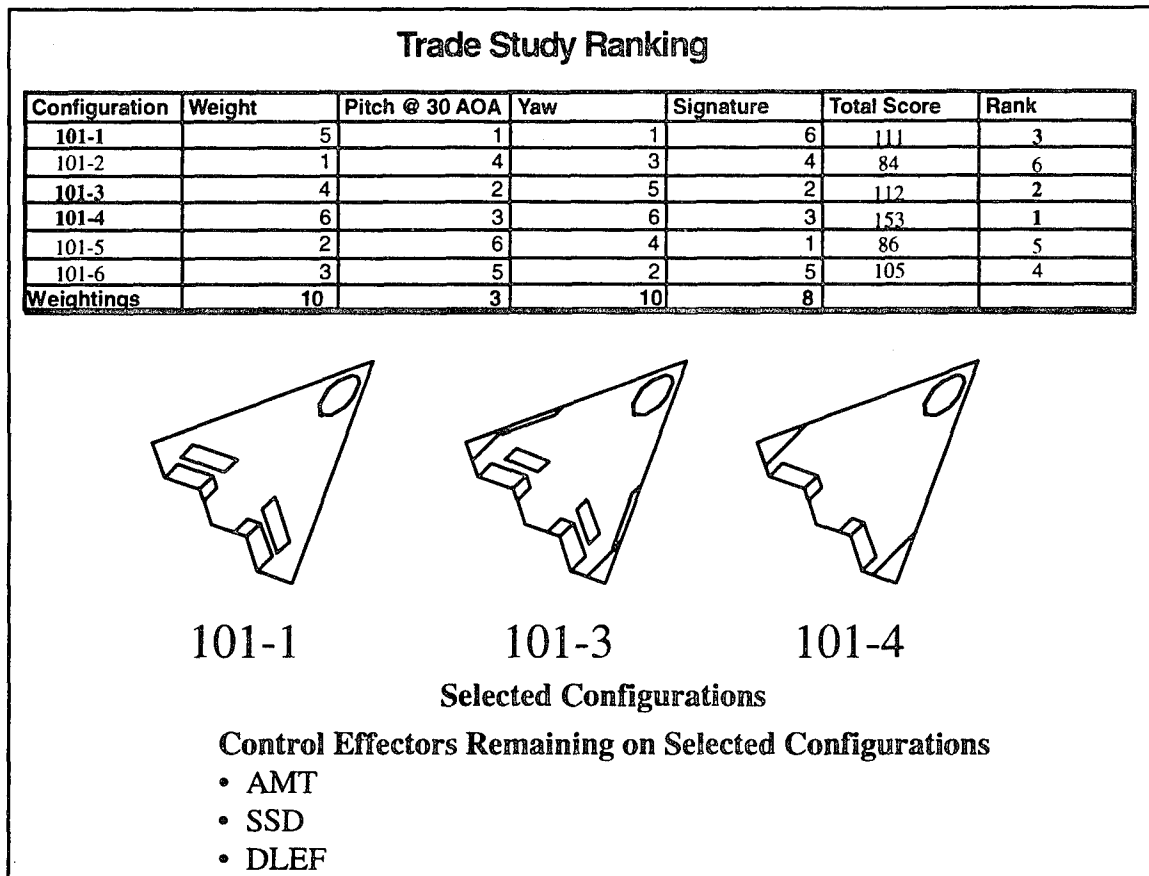


Figure 5-13 Final Trade Study Ranking Results

It was decided, based on the above analyses, to conduct further work with the AMT, SSD and DLEF. The deployable rudder and lower spoiler were dropped from the study matrix. The three remaining controllers were integrated into the carrier-based configuration; more detailed analysis was conducted on the remaining three land-based airplanes.

6 Effector Performance Study

The effector performance study consisted of roll performance evaluations conducted on the remaining three 101-series configurations and evaluation of the AMT, DLEF and SSD on the 201-series airplanes, resulting in Configurations 201-1, 201-3 and 201-4. Off-design conditions, including high-speed and crosswind landing capabilities were also analyzed. Control power available versus deflection limit trade-offs were made on each innovative controller.

6.1 101-Series Maneuver Performance Evaluation

Aerodynamic data were developed for each innovative controller and applied to the 101-series high-speed simulation data set. Low-speed data were available from LMTAS IRAD testing of all three innovative controls. Lateral-directional stability, longitudinal characteristics, and conventional surface control effectiveness were already available at transonic and supersonic Mach numbers as a result of IRAD wind tunnel testing. Little additional development work was required during the ICE program to expand the low-speed database for 101-series configurations. However, no high-speed wind tunnel testing had been done with the AMT or SSD during the LMTAS IRAD.

6.1.1 High-Speed Dataset Development

Fortunately, a great deal of information on AMT and SSD high-speed control effectiveness and hinge moment characteristics were found in NACA research memorandums. DLEF control effectiveness data were taken from IRAD wind tunnel test results conducted on the 65 deg sweep configuration.

AMT and SSD control effectiveness predictions were made for high speed conditions by applying Mach trends developed from the NACA papers to the available low speed data. Control effectiveness was scaled up or down using control volume ratios.

Figure 6-1 shows that AMT control effectiveness is scaleable using control volume ratios. SSD yaw control power (Figure 6-2) is also easily scaled with control volume ratio due to

its dependence on profile drag, and therefore projected area. However, SSD roll effectiveness is related to the control-induced flow separation over the wing, and is dependent on planform. SSD roll predictions were made by applying the LMTAS IRAD fighter spoiler effectiveness Mach trends to the low-speed SSD effectiveness available from small scale IRAD testing. It is apparent from the data in Figure 6-2 that this is probably a conservative estimate.

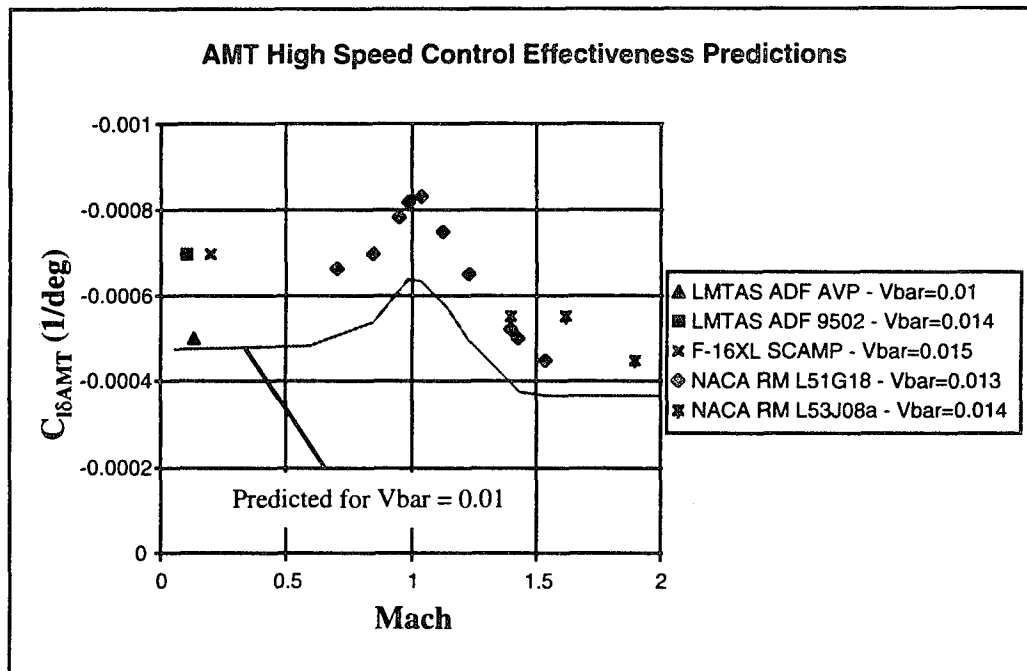


Figure 6-1 AMT Control Effectiveness Trend with Mach Number

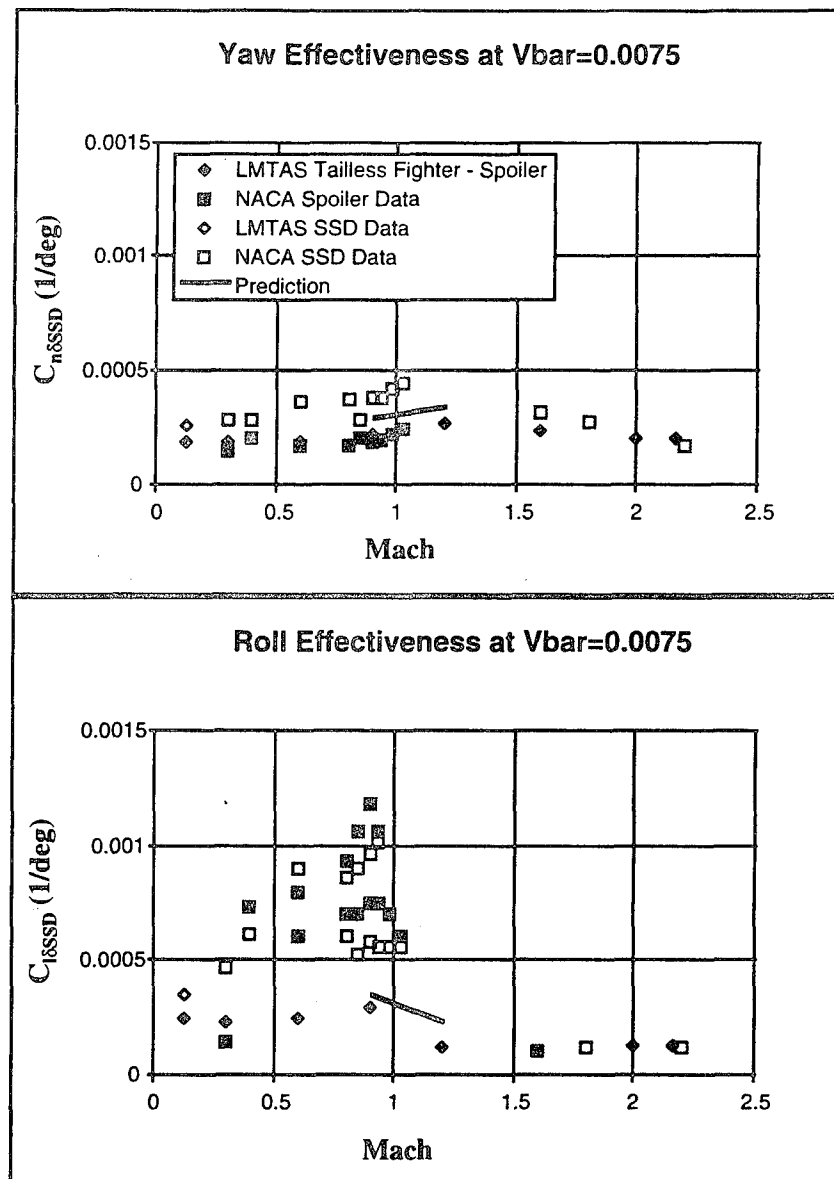


Figure 6-2 SSD Control Effectiveness Trend with Mach Number

Control surface hinge moment data were gathered for similar controllers and/or similar configurations, and referenced to control surface area and local chord. Likewise, airframe flexibility effects were estimated by applying aeroelastic flex-to-rigid ratios from F-16XL, and other similar tailless delta configurations. Appendix A details the data sources used during the study. The resulting hinge moment and flexibility effects are approximate. These data were required to add realism to the flying qualities assessments and provide inputs into the actuator sizing efforts. High-speed flight conditions were investi-

gated to define hinge moment capabilities needed to maintain Level 1 flying qualities throughout the flight envelope. This analysis is discussed in greater detail in Section 7.

6.1.2 Full Envelope Control Power Analysis

Control power envelopes were computed for each configuration at the flight conditions defined in Section 4. Roll performance capabilities were determined by running CPR simulations inside the resulting control envelopes. Figure 6-3 summarizes the roll capabilities of each configuration. Configuration 101-TV is shown as well for comparative purposes.

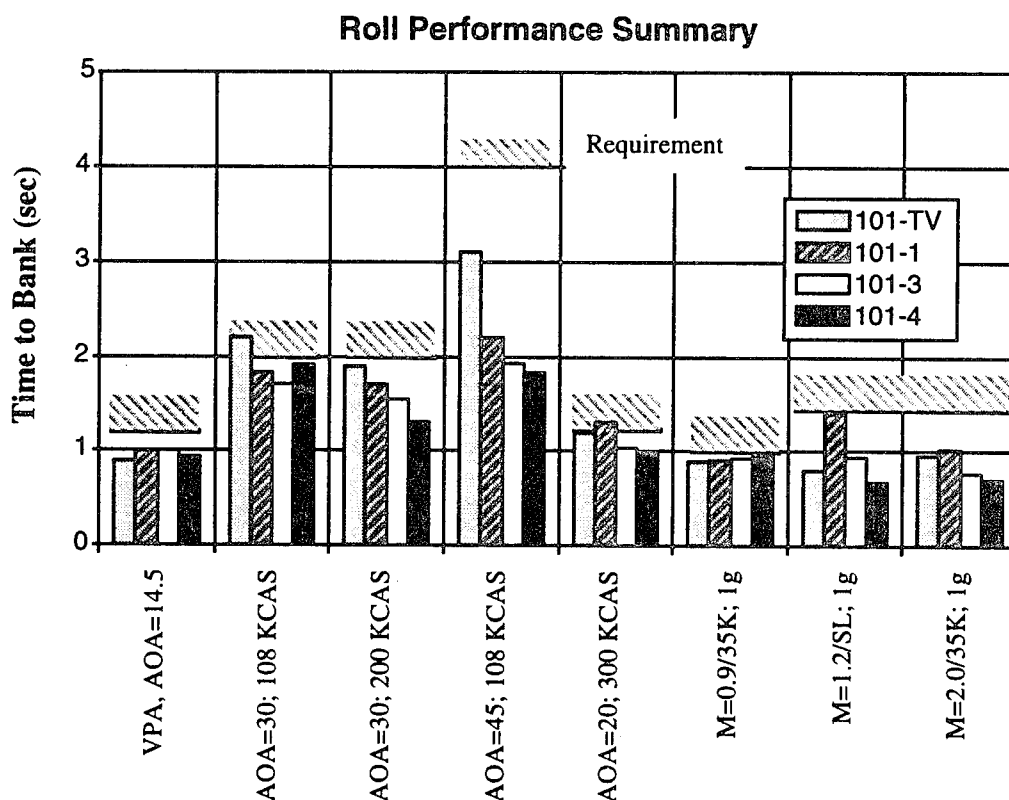


Figure 6-3 101-Series Roll Performance Summary

Configurations 101-1, -3, and -4 exceed Configuration 101-TV's 30 deg and 45 deg AOA roll capabilities. At 20 deg AOA and 300 KCAS, Configuration 101-1 did not meet the roll requirement, and did not perform as well as the other configurations. This is due to the lack of aerodynamic yaw power on this configuration, and the reduced effectiveness

of thrust vectoring at high dynamic pressure flight conditions (recall that this condition was analyzed in mil-power); MAX-A/B thrust would have provided sufficient control moment to meet the requirement. Note that 101-1 is the poorest performing configuration at the Mach 1.2/sea level and Mach 2.0/35K flight conditions for the same reasons; although, roll performance requirements are met for both cases.

High speed control power capabilities are usually limited not by absolute control power, but by flexibility and hinge moment limits. The maximum airspeed goal for this configuration was 800 KCAS, or Mach 1.2 at sea level. This condition drives hinge moment requirements, and therefore actuator and hydraulic system size. Flexibility effects reduce control surface effectiveness, and in some cases, may result in control reversal. Stiffness requirements for a control surface will drive structural weight, and for an all-moving surface, size the actuator.

Actuators for conventional control surfaces such as elevons or pitch flaps, are typically sized by roll requirements and/or pitch trim. For a tailless fighter with neutral lateral-directional stability, yaw control power is critical for high-speed flight. Unfortunately, yaw thrust vectoring is not very effective at high speed conditions due to the dependence of TV control power on dynamic pressure, and structural limitations on nozzle deflections at high speeds. Additionally, if a tailless fighter were to rely solely on propulsion control for yaw augmentation, engine failure at high speed would probably result in loss of the aircraft due to sudden loss of control. As a result, to operate at high speeds, this class of tailless fighters must rely on both propulsive and aerodynamic controls, with aerodynamic control power providing at least Level 2 flying qualities to handle TV failure cases.

Configurations 101 and 101-TV used segmented spoilers along with the elevons to provide aerodynamic yaw power; however, the hinge moment requirements for even small spoilers were such that the hydraulic power requirements are not feasible (Section 7). All three derivative configurations use lateral-directional controls with relatively small hinge moments. For instance, Configuration 101-1 uses the SSD for yaw control similar to 101 and 101-TV, but with much smaller hinge moment requirements. Configurations 101-3 and 101-4 use the SSD and/or the AMT for high speed yaw control.

Figure 6-4 shows control envelopes for each configuration both with and without vectoring control power at Mach 1.2/sea level. The control power requirements for Levels 1 and 2 roll are overlaid on the plots along with the control power required to augment a 5 deg sideslip command at this flight condition. All three configurations have sufficient control power available with aerodynamic controls to meet the control power requirements. Figure 6-5 shows a time history of a commanded 5 deg sideslip at Mach 1.2/sea level completed using Configuration 101-1. Control saturation is avoided, and the configuration retains Level 1 flying qualities.

Mach 1.2 @ Sea Level

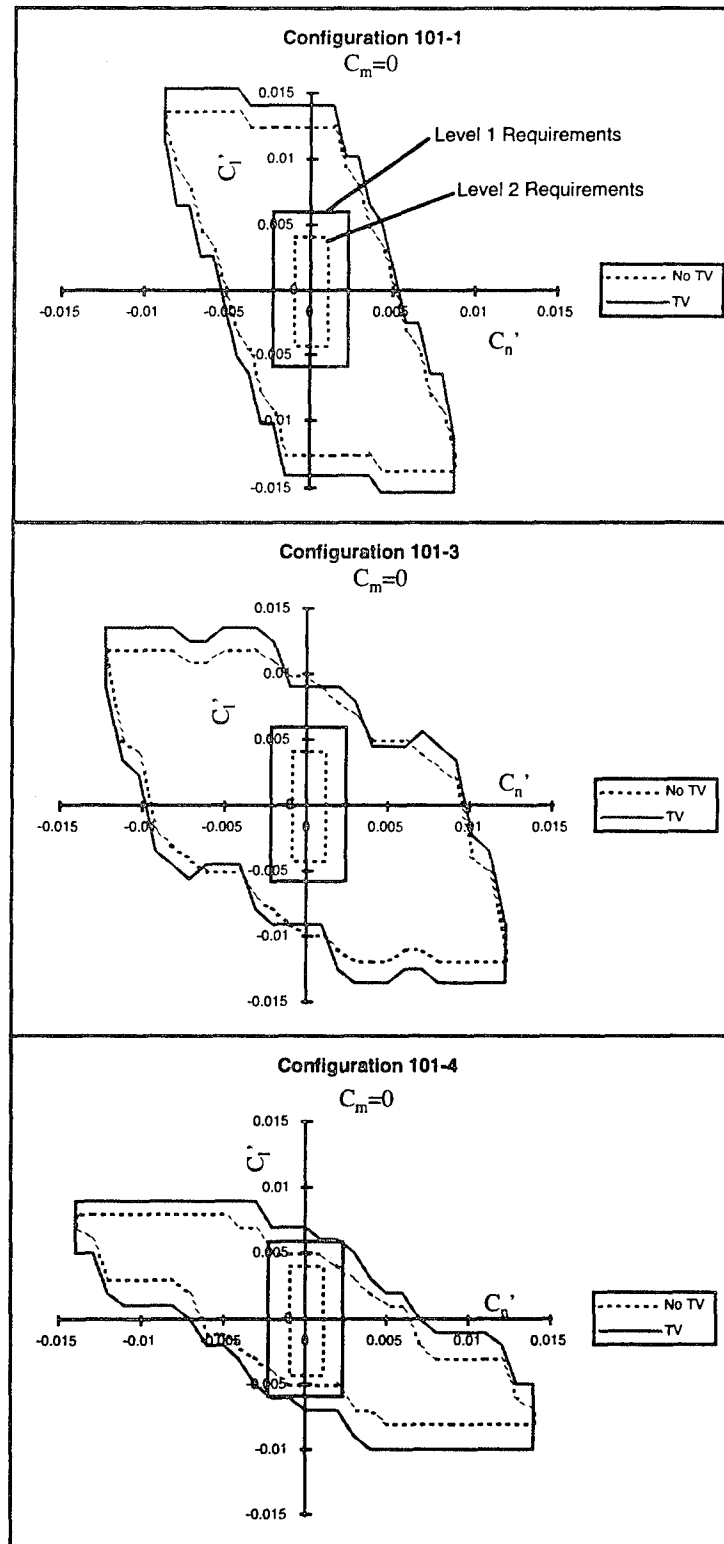


Figure 6-4 High Speed Control Power Requirements vs Control Power Available

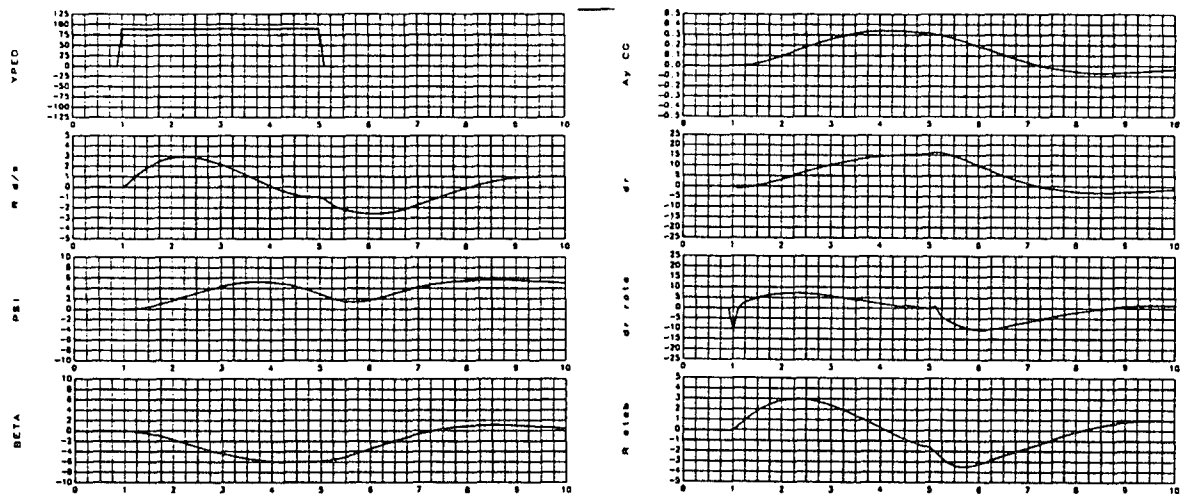


Figure 6-5 Configuration 101-1 High-Speed Step Sideslip Time History

6.1.3 High AOA Capabilities

Low-speed lateral-directional augmentation without thrust vectoring is shown in Figure 6-6. Once again, Configuration 101-4 performs the best at high AOA. This analysis includes the effects of sideslip on the SSD, AMT and DLEF control power. The results show that Configurations 101-3 and 101-4 can maintain Level 1 dutch roll frequencies throughout the AOA range at low-speeds with aerodynamic control power alone.

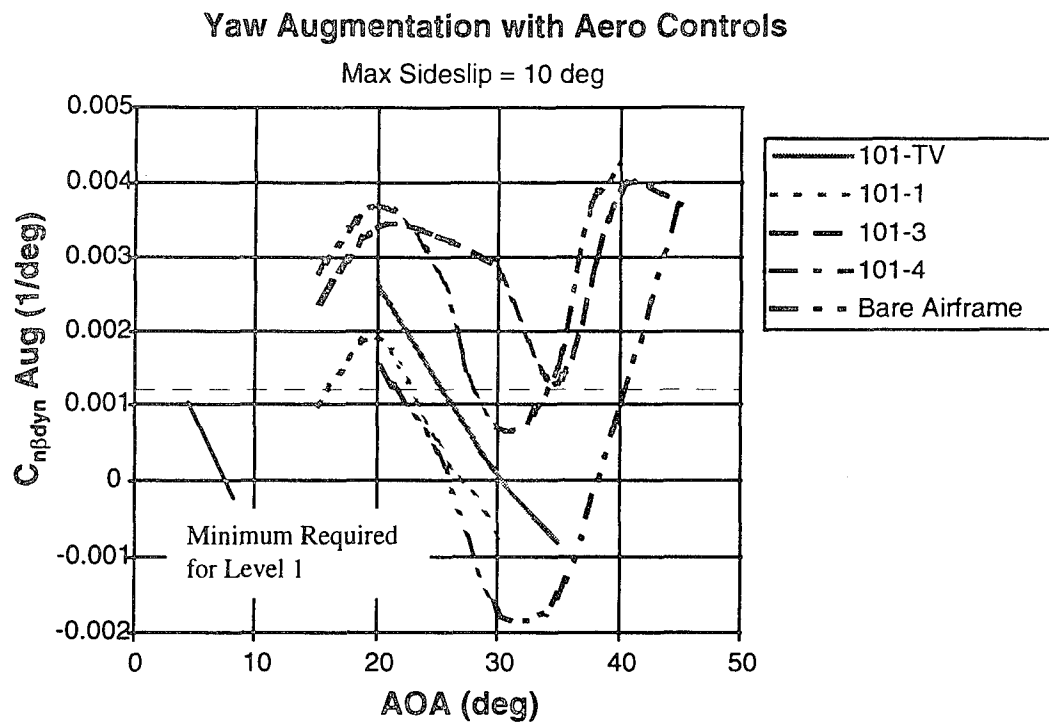


Figure 6-6 Low-Speed Yaw Augmentation Capabilities

Figure 6-7 demonstrates high AOA roll performance capabilities both with and without TV. All three configurations exhibit good roll performance using thrust vectoring in MAX-A/B. Configuration 101-4 exhibits unlimited AOA capabilities, and significant high AOA roll capabilities using aerodynamic control power alone.

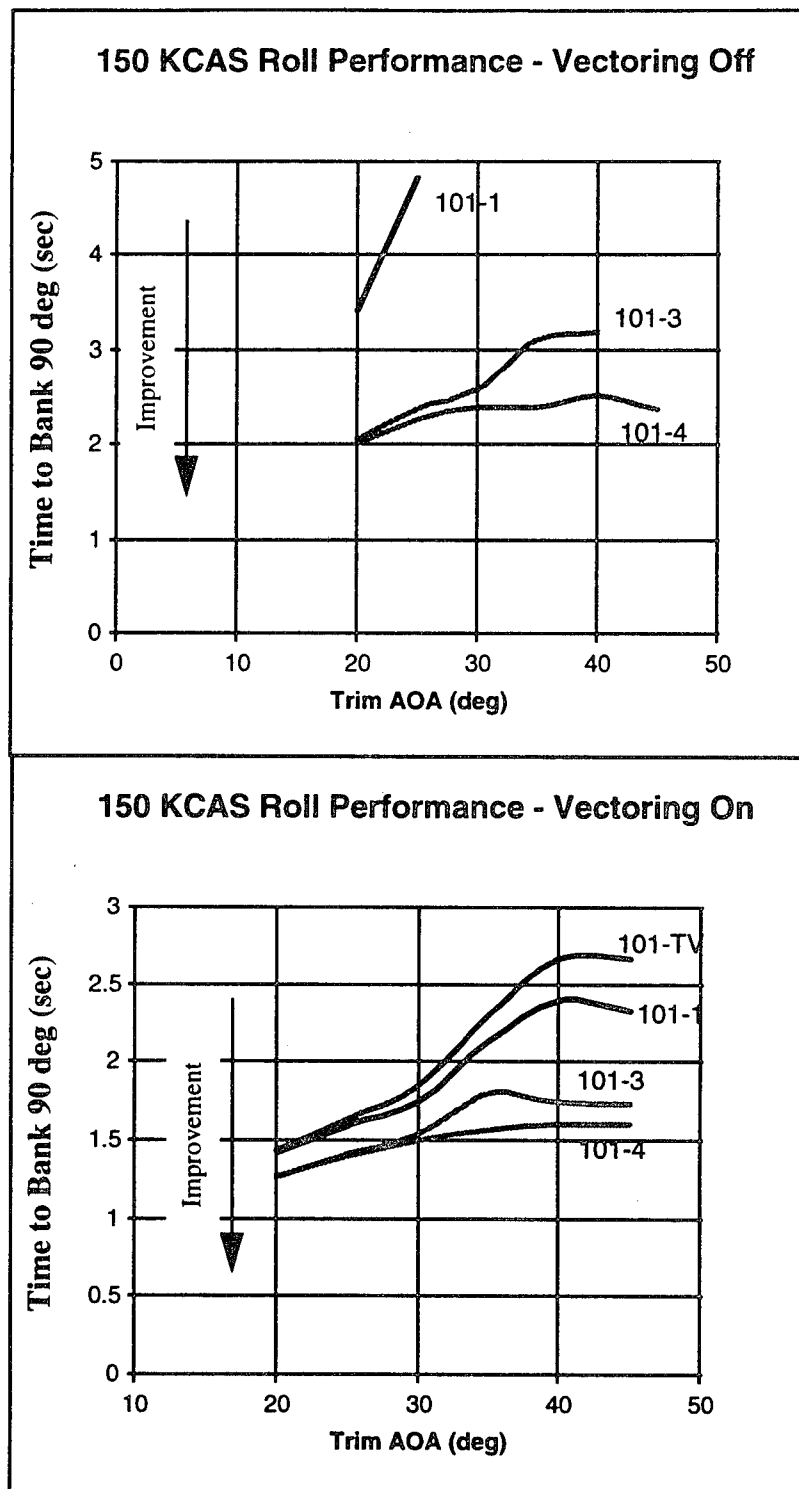


Figure 6-7 High AOA Roll Performance

6.1.4 Crosswind Landing Performance

MIL-F-8785C defines Level 1 crosswind requirements for Class IV aircraft as 30 knots at 90 deg. Level 2 and 3 requirements are 20 knots and 10 knots, respectively. An additional restriction is that no more than 75% of the available roll control power should be used to trim out a 10 deg sideslip angle at approach airspeeds. These requirements assume that the pilot is using a steady sideslip to counter crosswinds during the approach. A static crosswind landing analysis shows that the 101-series configurations can meet the 30 knot crosswind requirement. Configuration 101 is included in this analysis to illustrate performance without TV control power. Except for Configuration 101, all of the configurations meet the 10 deg sideslip requirement using less than 75% of the available roll control power (Figure 6-8). Configuration 101 requires 80% of its available roll power to offset lateral-stability and coordinate the yaw control interactions.

Typically, fighters use a crabbed approach method where the aircraft velocity vector is pointed into the wind to maintain the desired ground track. Upon touchdown, loads on the main landing gear "de-rotate" the aircraft to point down the runway centerline. A two-point landing attitude is maintained to aero-brake the aircraft until safe wheel brake speeds can be reached (approximately 100 knots for the F-16). Figure 6-9 illustrates the geometry of the problem.

During the time that the aircraft is in the two-point attitude, at airspeeds greater than safe braking speeds, aerodynamic controls must be relied upon to maintain directional control, and counter the tendency of dihedral effect ($C_{l\beta}$) to roll the airplane over. After ground speed has slowed, differential braking can be used in lieu of aerodynamic control power for directional authority.

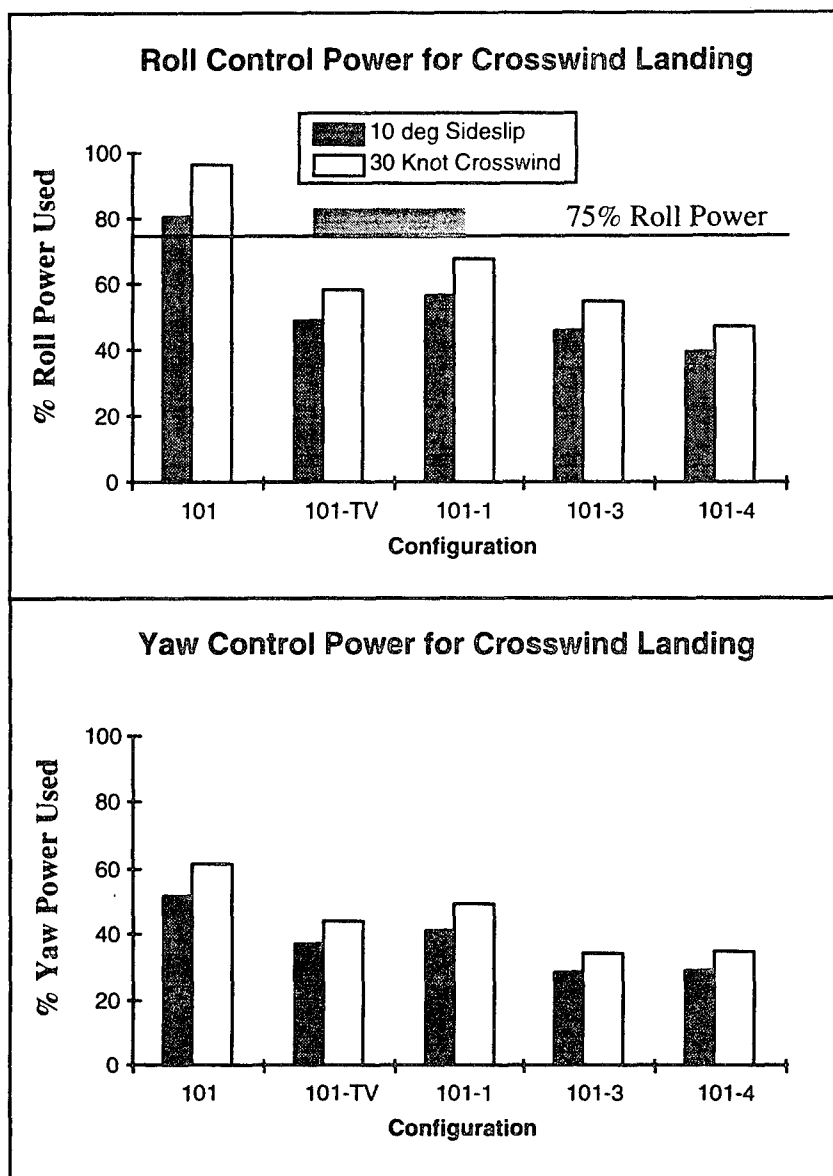


Figure 6-8 Crosswind Landing Control Requirements

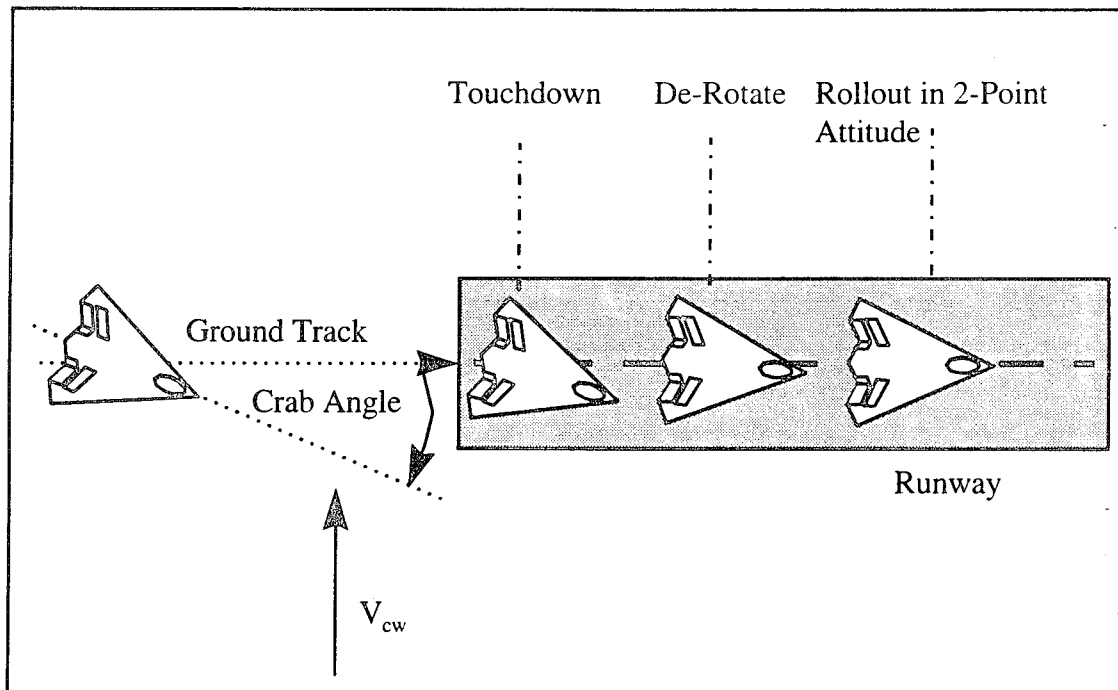


Figure 6-9 Geometry of Crosswind Landing in Crabbed Attitude

Several areas contribute to the control power required during the ground roll portion of a crosswind landing. Directional control is affected by the relative sideslip acting on directional stability, and any adverse yawing moments generated by lateral controls. In the two-point attitude, this is resisted by the skidding forces on the main gear, and in the three-point attitude, the nose gear. Lateral control is primarily affected by $C_{l\beta}$ tending to roll the airplane away from the wind direction. Additional rolling moments can be caused by yaw control inputs. The rolling tendency is resisted by the downwind main landing gear normal force. Finally, side forces generated through $C_{Y\beta}$ tend to skid the airplane laterally across the runway. The skidding reaction forces on the main landing gear add to the couple already created by the dihedral effect.

Three unique factors affect tailless fighters with highly swept wings during crosswinds: (1) high-sweep delta wings typically have greater dihedral effect at elevated AOA (i.e., two-point aero-brake attitude); (2) bare airframe directional stability is weak resulting in smaller yaw control requirements than conventional aircraft; (3) aerodynamic side-forces are very small, reducing the skid tendency.

A static analysis was programmed on an EXCEL spreadsheet. The two-point aero-brake attitude was assumed most critical because of the reliance upon aerodynamic control power during the transition to the three point attitude, and the high $C_{l\beta}$ at elevated AOA. Summing moments about the downwind main landing gear tire for the tip-over condition ($N_R = 0$), one can eliminate the moment generated by lateral skidding (Figure 6-10). Because $C_{Y\beta}$ is small for a tailless fighter, the moment produced about the tire by aerodynamic side force is neglected. Summing vertical forces, one finds that airspeed can be solved in terms of percent main gear load (gear normal forces and remaining lift must exactly cancel weight). As airspeed is reduced, relative sideslip angle increases assuming a constant crosswind velocity. Assuming no coupling of the equations through control interaction (this is taken care of in the CPA analysis), the lateral-directional control requirements are then just a function of bare airframe stability, airspeed and weight.

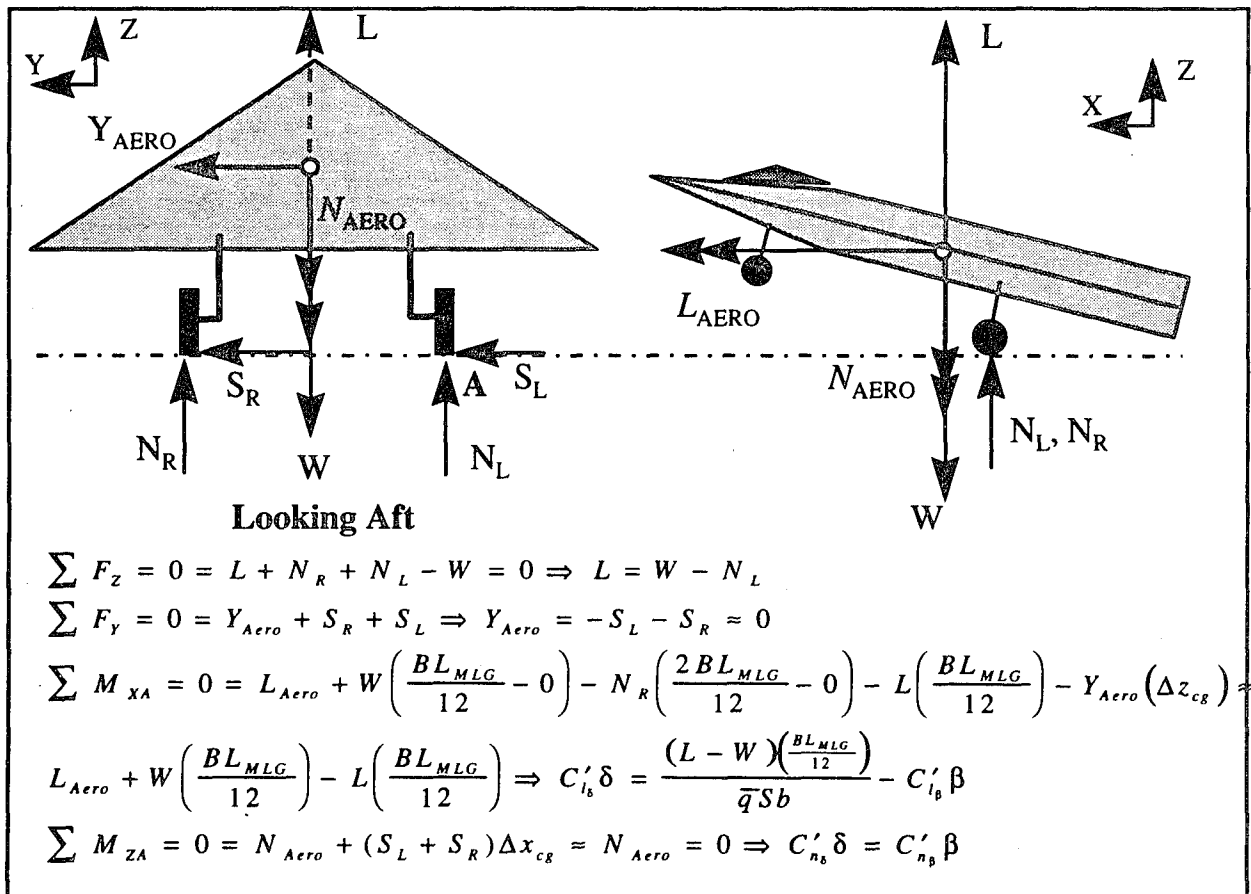


Figure 6-10 Static Analysis of Crosswind Landing Rollout

A sample of the results are plotted vs airspeed in Figure 6-11. DATCOM was used to estimate ground effects on the lift coefficients. Negative rolling moments can be ignored; this result simply means that weight has overcome the aerodynamic rolling moment produced by sideslip, and the main landing gear are firmly on the ground. Yawing moment requirements are nearly constant with changing airspeed (for fixed crosswind velocity) because sideslip is ever increasing as airspeed is reduced; therefore, the required yawing moment remains relatively constant with reduction in velocity. Aerodynamic directional control requirements can be supplemented and eventually replaced by differential braking once velocity has dropped below 100 knots.

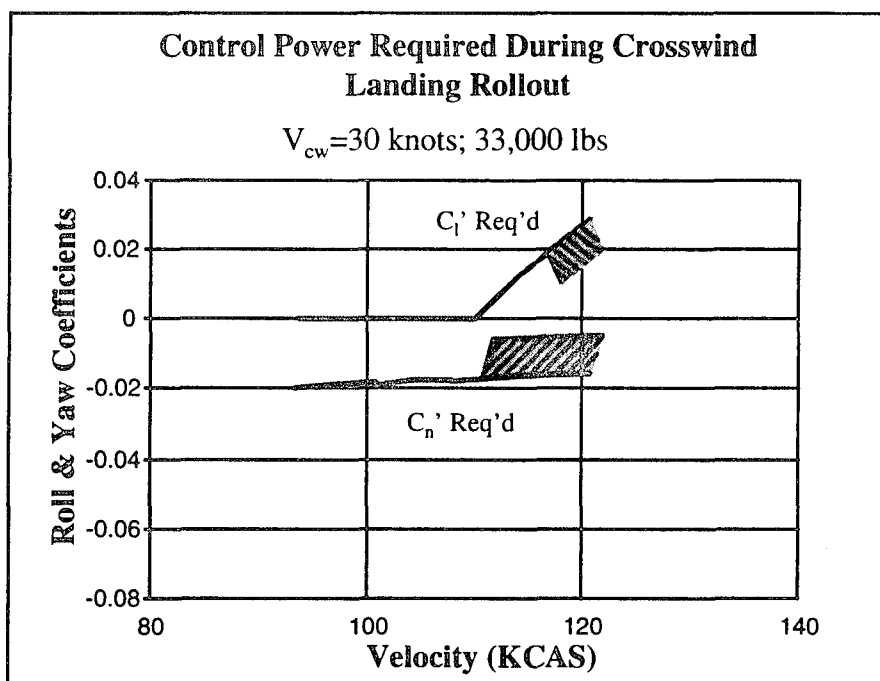


Figure 6-11 Crosswind Landing 2-Point Attitude Control Requirements

The maximum roll and yaw requirements during the groundroll portion of a crosswind landing were overlaid on control power envelopes computed for each configuration in the two-point aero-brake attitude (no ground effects were included in this portion of the analysis). Results are shown in Figure 6-12. As long as the requirement line lies within the control envelope, a set of control deflections exist that will provide sufficient roll and yaw control to offset the demands imposed by crosswind. The figure shows that all five

configurations can achieve at least a 30 knot (Level 1) crosswind capability. Configuration 101-1 is marginal at the 30 knot requirement.

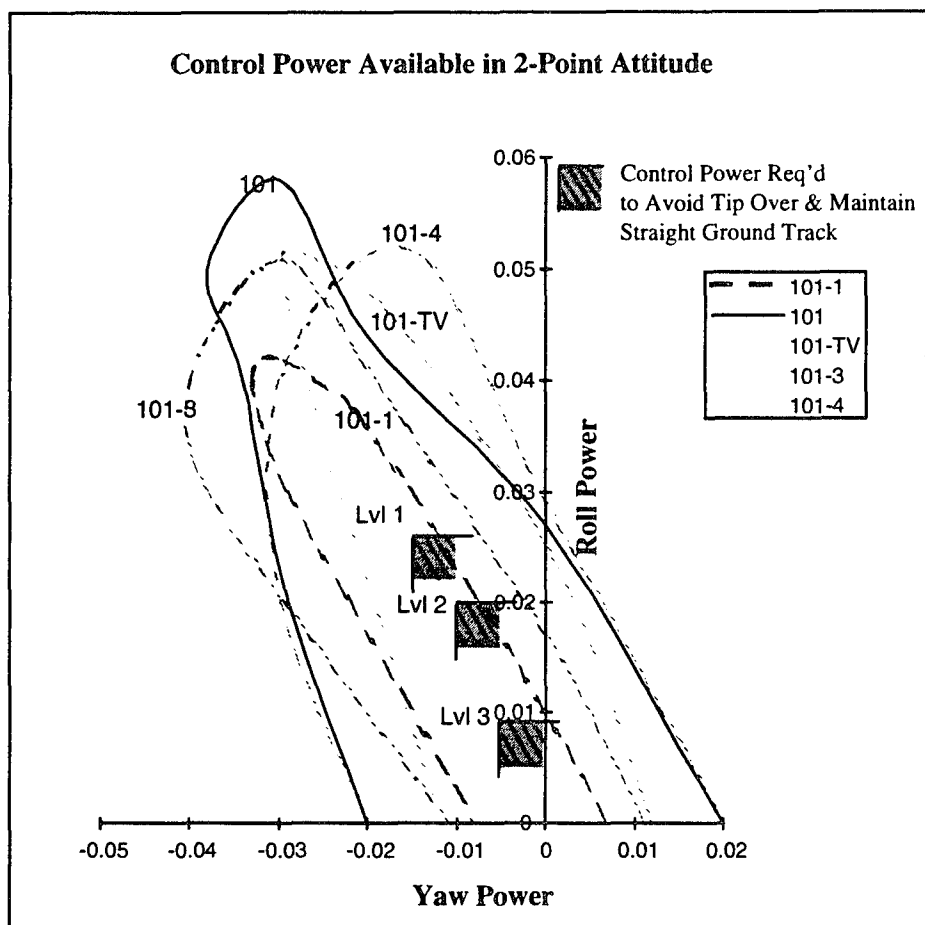


Figure 6-12 All Five Control Suites Can Achieve Level 1 Crosswind Capability

6.1.5 Center-of-Gravity Limits

Aft cg limits were computed for each configuration using the nose-down control margins for symmetric and rolling maneuvers defined in the maneuver requirements section. Aft limits set by roll coupling were analyzed using the maximum stability axis roll rates achieved at the high AOA conditions. Table 6-1 shows the aft limit for each condition.

Table 6-1 101-Series Aft cg Limits (% MAC)

Condition	101	101-TV	101-1	101-3	101-4
Symmetric Maneuver - $\dot{q} < -0.07$ Aero Cntrl Only	41.45	41.45	41.45	42.45	42.47
Symmetric Maneuver - $\dot{q} < -0.25$ Aero & Prop Cntrl	---	56.04	56.04	58.63	58.69
$t_{90}=2.0$ sec @ 30 deg AOA; $\dot{q} < -0.07$ Aero & Prop Cntrl	---	46.22	46.22	46.37	46.55
$t_{90}=4.0$ sec @ 45 deg AOA; $\dot{q} < -0.07$ Aero & Prop Cntrl	---	57.97	57.97	58.16	58.41
$t_{90}=1.1$ sec @ 20 deg AOA; $\dot{q} < -0.07$ Aero & Prop Cntrl	42.34	45.24	45.24	45.65	45.90
Aft cg Limit	41.45	41.45	41.45	42.45	42.47

The symmetric nose-down margin required with aerodynamic controls set the aft limits for each control suite concept. Configuration 101 could not come close to achieving the high AOA roll performance goals. Therefore, Configuration 101 was not evaluated from a roll coupling standpoint at these conditions. Note that the two configurations employing the AMT have aft limits approximately 1% MAC aft of the other configurations. The AMT generates small nose-down pitching moments; however, they are nonlinear with deflection. The slight differences between Configuration 101-3 and 101-4 aft limits are attributable to the different AMT sizes for each configuration.

The 101-series class of configurations should be balanced neutrally stable in pitch. A nominal cg location of approximately 39% MAC provides neutral stability at low-speeds resulting in a 2.5% to 3.5% MAC or 8.5" to 12" cg margin (depending on control suite) to the aft limit. The F-16XL, a similar class configuration, had a 7.4" margin between nominal and aft cg. Assuming that the configuration could be nominally balanced at 39% MAC, the aft limits listed above are acceptable.

The forward cg limits were determined using a nose-wheel lift off routine programmed on an EXCEL spreadsheet. The cg was varied until the rotation requirement at $0.9V_{\min}$ could no longer be achieved. All of the forward limits lay around 30% MAC. This limit is not unique to tailless fighters, but is simply a function of the pitch control power available to rotate the nose. No TV control power was included in this analysis.

6.1.6 Control Power Trade-Offs

Since Configuration 101-3 includes each of the innovative control concepts (DLEF, AMT and SSD), it was used to determine the relative merits of each controller to the overall configuration's capabilities. The capabilities provided by each of the controls was studied by turning off each effector one at a time, and computing the resulting control power envelopes.

Figure 6-13 shows the maximum coordinated roll power and yaw augmentation versus AOA with aerodynamic controls alone. The four curves represent the basic 101-3 configuration, 101-3 without the SSD, 101-3 without an AMT, and 101-3 without the DLEF. It is apparent that the AMT has the greatest impact on configuration roll capabilities. At 15 deg AOA, $C_{l'_{max}}$ was reduced by over 40% due to removing the AMT. The basic 101-3 has significant coordinated roll control power up to 40 deg AOA. Eliminating the AMT would result in a severe reduction in capabilities at high AOA.

Removing the SSD reduced coordinated roll power by a small amount up to 30 deg AOA. Unfortunately, no wind tunnel data were available for the SSD for AOA > 32.5 deg; no analysis was done at higher AOA with the SSD. Finally, eliminating DLEF reduced roll power by 11% at 15 deg AOA. Significant reductions in roll power were observed through 35 deg AOA.

Similar conclusions are drawn by analyzing the yaw augmentation plot. Maximum lateral-directional augmentation capabilities are severely curtailed by removing the AMT from 101-3. With the tip, 101-3 has unlimited AOA potential. Without it, the configuration loses lateral-directional stability above 28 deg AOA. Removal of the DLEF had almost as great an impact on lateral-directional augmentation. In this case, directional stability was lost above 31 deg AOA. The SSD has the smallest impact on stability. Although, a significant reduction is apparent in the 20 deg to 30 deg AOA range. Once again, no data were available above 32.5 deg AOA; the controller may retain some effectiveness at higher AOA.

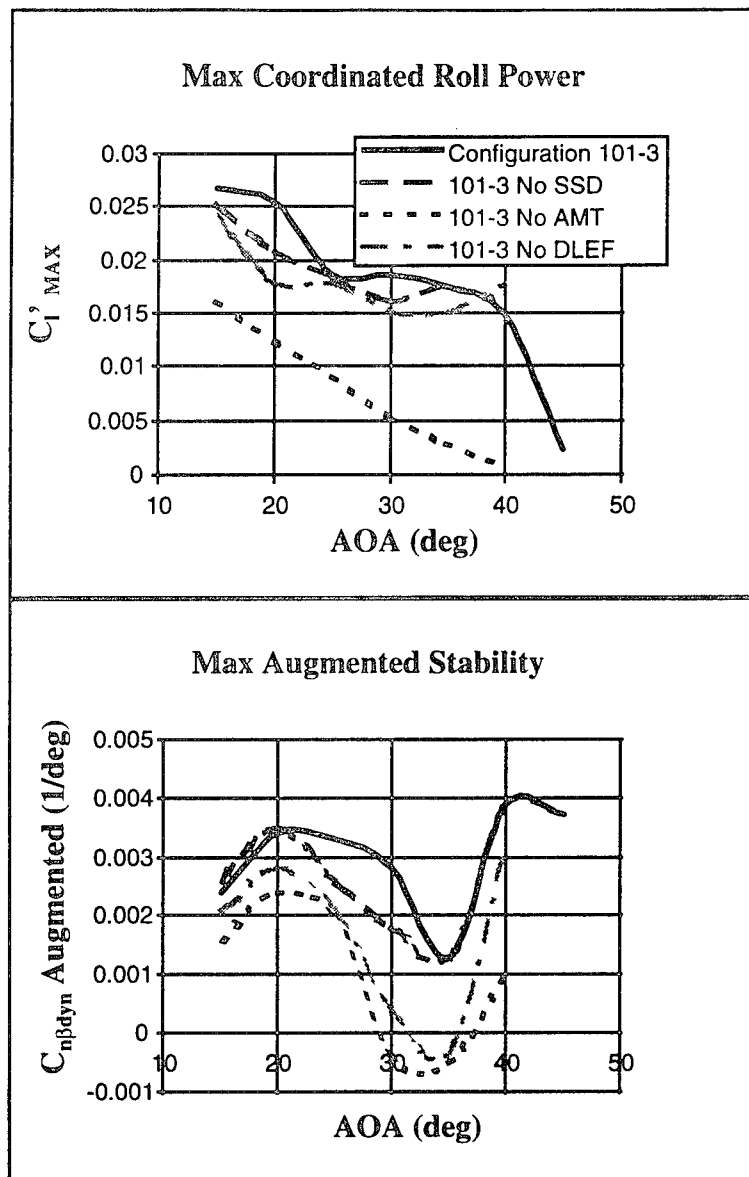


Figure 6-13 Innovative Control Power Trade Offs

6.1.7 AMT Deflection Limits

Analysis of all of the previous results show the AMT to have a clear advantage over the other controls in high AOA lateral-directional control effectiveness. This section discusses the effects that various AMT deflection limits have on control power available. Configuration 101-4 was used exclusively for this analysis using aerodynamic controls only.

Section 3 showed that AMT yaw control power was linear with deflection (up to 60 deg max) through very high AOA. In some cases, restricted deflections of the surface may be required (e.g., during take-off and landing or high speed flight). Actuator throw could be reduced, and control linkages minimized if the deflection were more constrained. Additionally, if the controller could be limited to deflect in only one direction, some amount of hingeline sealing could be integrated to reduce the impact that the AMT has on signature.

Figure 6-14 illustrates the maximum coordinated roll control power available on Configuration 101-4 for varying tip deflection limits. Through most of the AOA range, negative tip deflection limits do not appreciably change the coordinated roll power available. The lower portion of the figure shows the tip deflections required to generate the maximum coordinated roll power. The example shown was for a right roll, or positive roll power. At zero deg AOA, the tip was used as a roll device (i.e., left tip TED). At increased AOA's the tip was used for roll coordination with the right tip saturated TED. This characteristic is due to the adverse roll/yaw relationship at low AOA; recall that at high AOA, the roll/yaw relationship is more favorable. TED-only tip deflection limits can be used without appreciably affecting the coordinated roll power.

Figure 6-15 shows the lateral-directional augmentation capability (trimmed in pitch and roll at 10 deg of sideslip) and the corresponding AMT usage for various tip deflection limits. In each case, the right tip is saturated TED at low AOA, with small deflections of the left tip used along with the other controls to help balance the rolling moment. For the cases with both TEU and TED motion, CPA used the left tip for additional roll trim power at higher AOA. There is a slight decrease in the level of $C_{n\beta_{dyn Aug}}$ in the 20 to 32 deg AOA range for the case with the AMT constrained to TED motion (i.e., the left tip is unavailable for roll trim). Note that in each case the right tip is not used to maximum deflection in the 20 - 40 deg AOA range due to the reduction in trim roll power available from the other control surfaces. In all cases, the configuration retains positive lateral-directional augmentation capability out to 10 deg of sideslip at all AOA with aerodynamic control power alone. Furthermore, restricting the tip to TED motion can be accomplished without adversely affecting control power available.

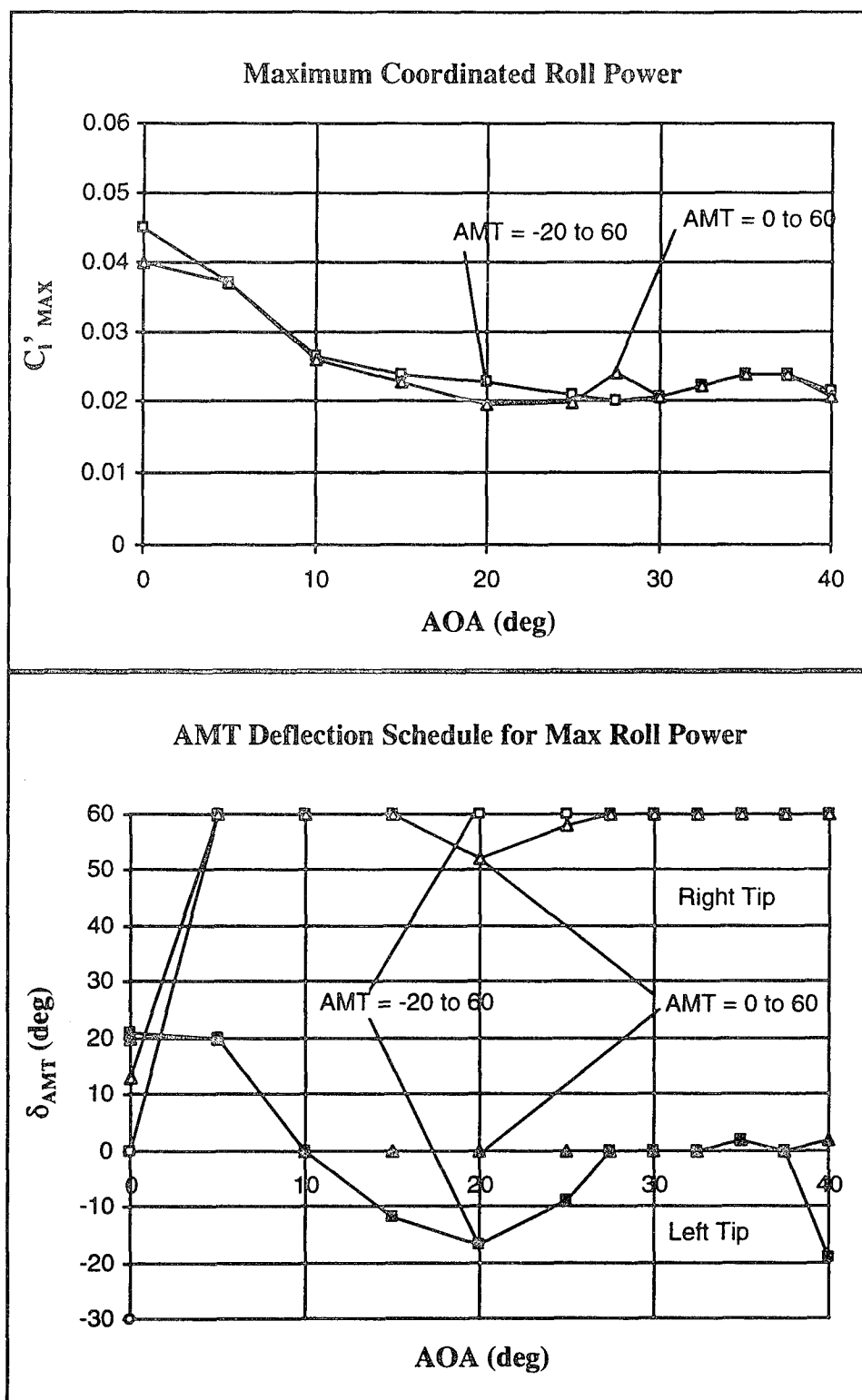


Figure 6-14 Effect of Varying AMT Deflection Limits on Coordinated Roll Power Available

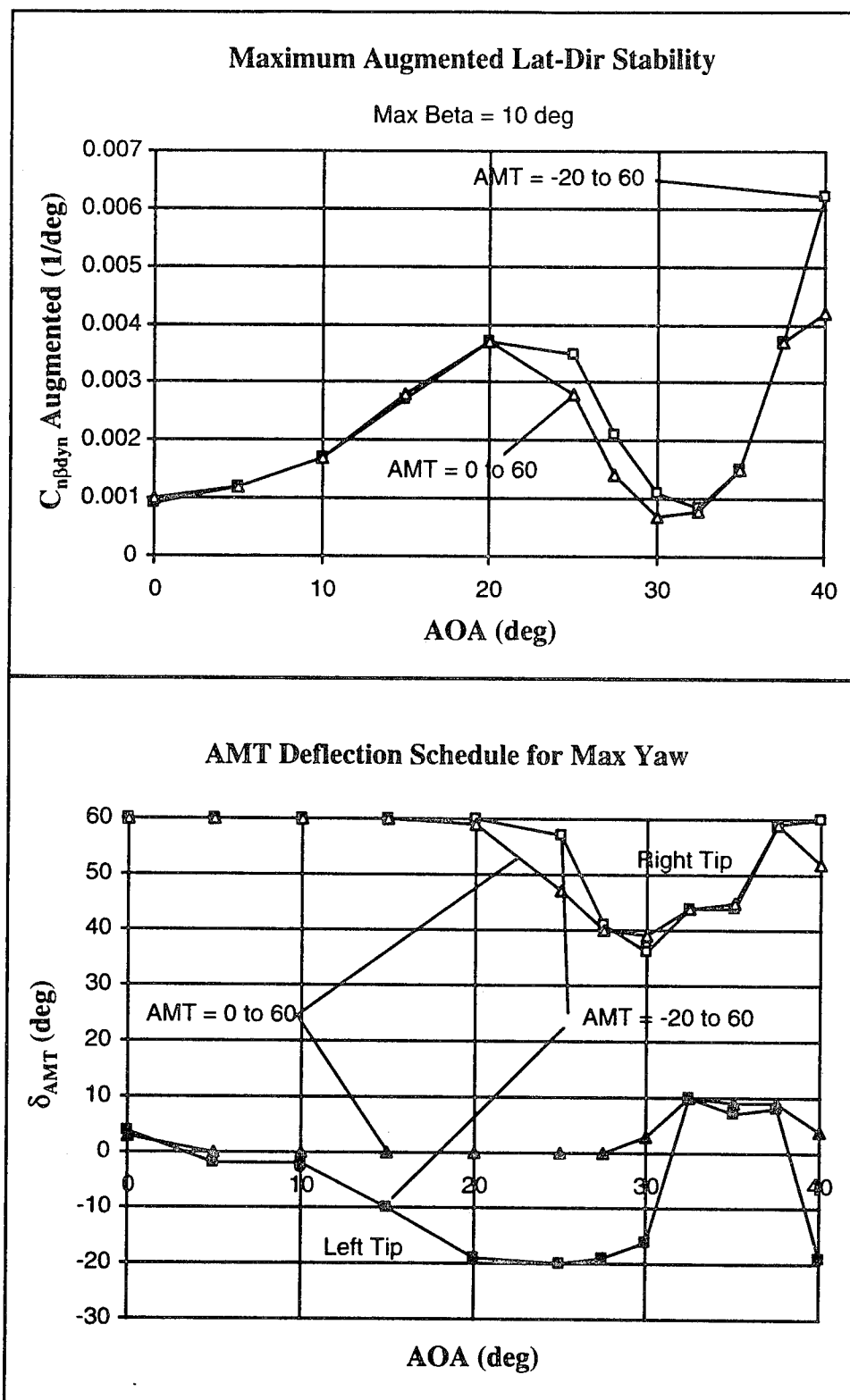


Figure 6-15 Effect of Varying AMT Deflection Limits on Lateral-Directional Augmentation

Finally, Figure 6-16 illustrates the effect of limiting the AMT to positive deflections at high speed. Hinge moment limits and flexibility estimates are included in these results. While the TED deflection-limited tip has a smaller control envelope, the control requirements at high-speed are still achievable. For the remainder of this study, it was decided to limit AMT deflections between 0 deg and 60 deg. These deflection limits result in sufficient control power across the flight envelope, and have the potential for signature-reducing techniques to be integrated with the control surface.

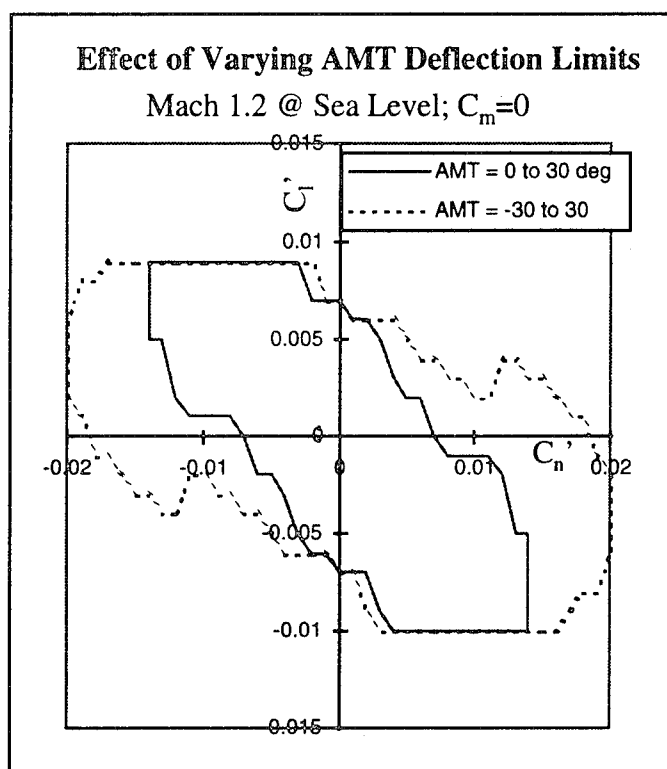


Figure 6-16 Effect of AMT Deflection Limits at High Speed

6.1.8 Effect of SSD Aerodynamic Interactions

SSD deflections have a significant impact on the elevon control characteristics (Figure 3-28 in Section 3) through aerodynamic interactions. CPA analysis indicated that Configuration 101-1 had poor yaw control capability at low AOA when thrust vectoring was turned off. Further analysis indicated that decoupling the SSD resulted in significant improvements in lateral-directional control power, indicating that the SSD/elevon interaction was the culprit.

Unfortunately, such a solution would negate one of the primary benefits of the SSD. To realize the benefits of reduced hinge moment and hydraulic system power, the spoiler and deflector in the SSD system must be mechanically linked, allowing the system to be driven by one actuator. The aerodynamic loads on the individual surfaces result in a balance of hinge moments, and smaller actuator requirements than a conventional flap-type spoiler.

Figure 6-17 shows the difference in low-speed lateral-directional control capability (trimmed in pitch) when the SSD/elevon interaction is included or ignored. Both coordinated roll power and augmented directional stability suffer due to the SSD/elevon interaction.

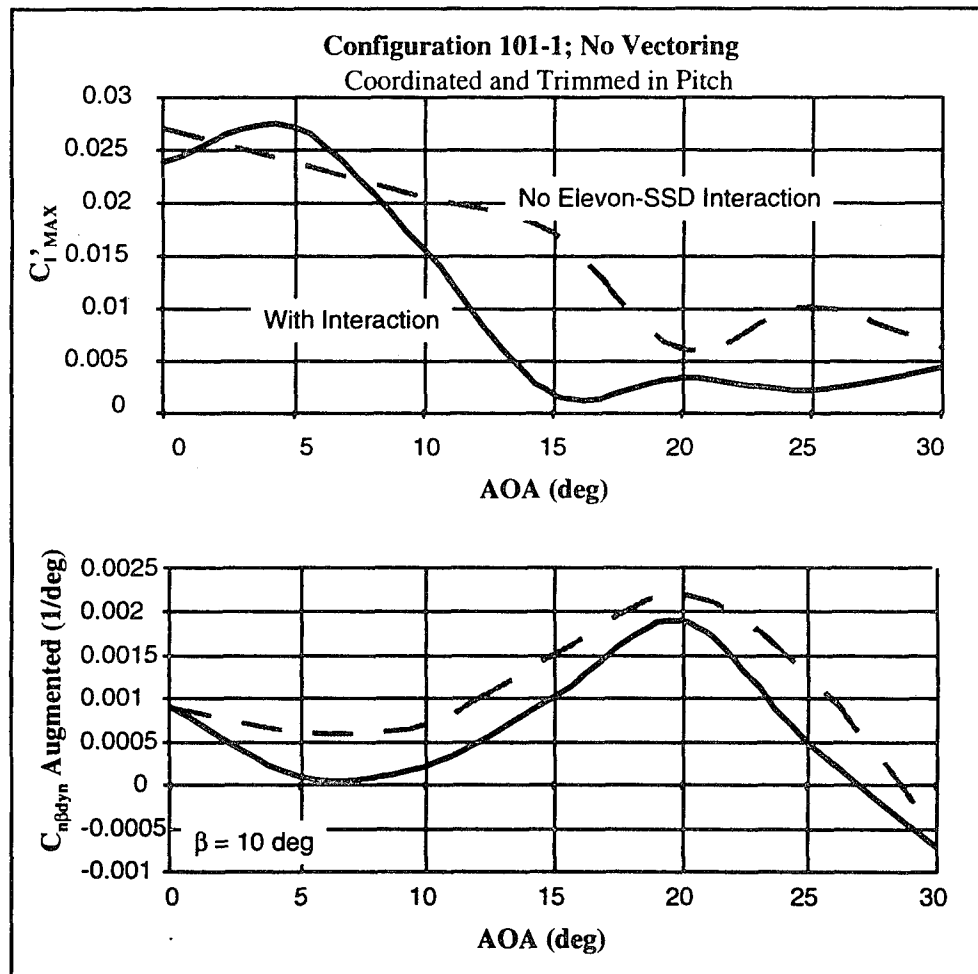


Figure 6-17 The SSD/Elevon Interaction Adversely Affects Control Power Available

By decoupling the SSD, CPA envelope results showed improved lateral-directional control capability (Figure 6-18).

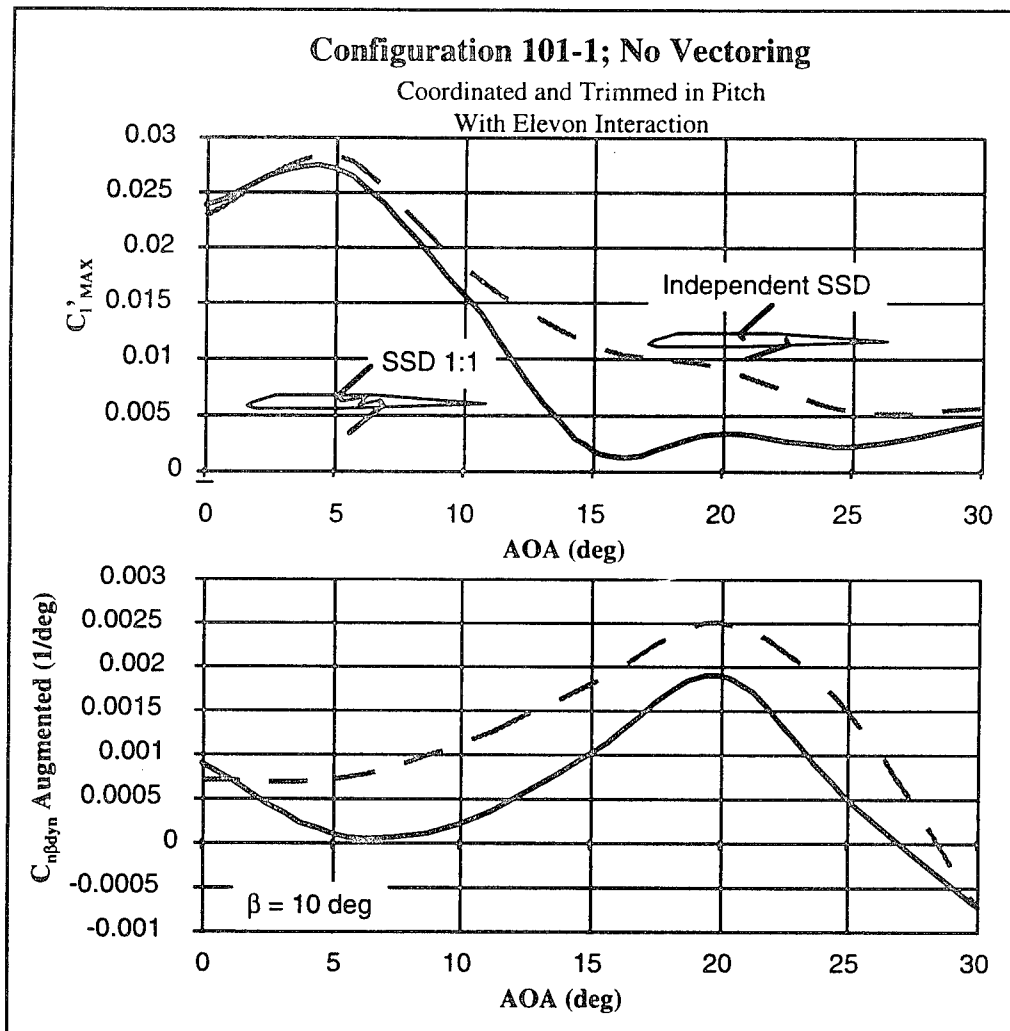


Figure 6-18 Decoupling the SSD Improves Lateral-Directional Control Power Available

Further analysis into the computed results showed that the CPA data supported not using the deflector at high AOA, and used less than half the available deflector power at low AOA. The adverse effect that the deflector has on the elevon was found to be the cause. Significant improvements in deflector usage were achieved by increasing the pitch flap power (e.g., twice the pitch flap area). Figure 6-19 shows the impact on deflector usage due to increased pitch power.

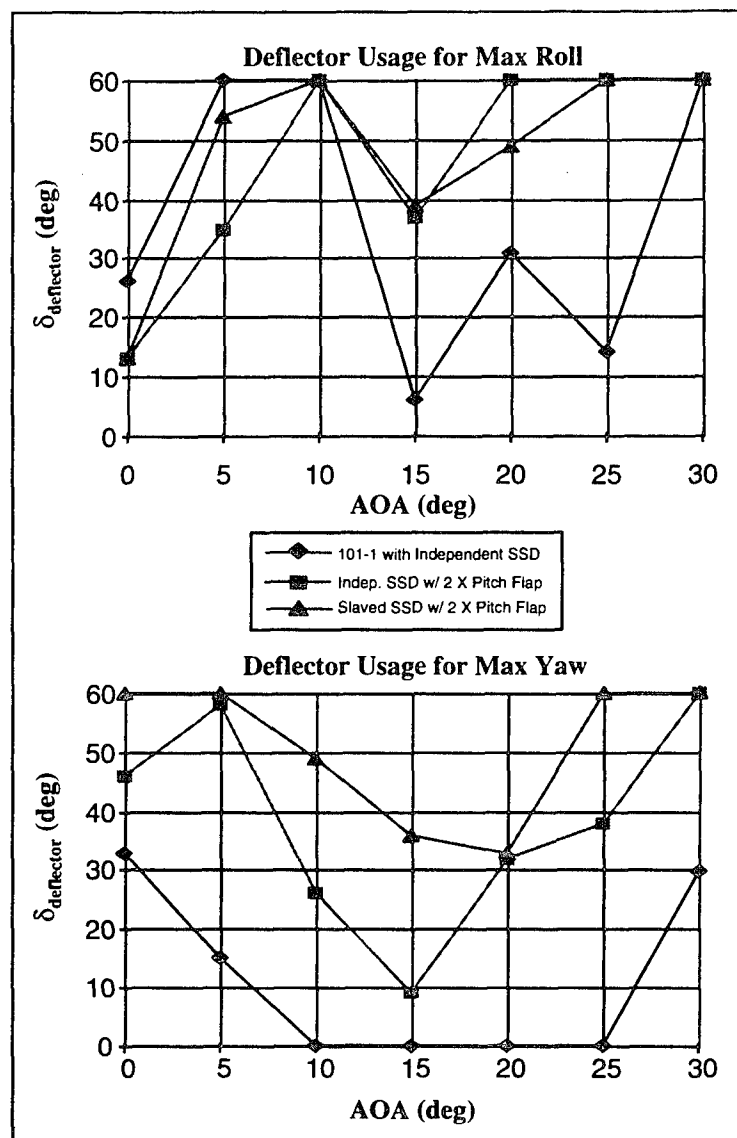


Figure 6-19 Greater Pitch Authority Increased Deflector Usage at All AOA

The pitch flap is located inboard of the elevon, and while no SSD/pitch flap interaction data were available, it is assumed that the interaction will be much less severe than for the elevon. Figure 6-20 shows the effect on lateral-directional control capability with increased-area pitch flaps compared to the original configuration. The compromise of having to increase the available pitch control power results in better lateral-directional capability while still retaining the low hinge moment features of the SSD control concept.

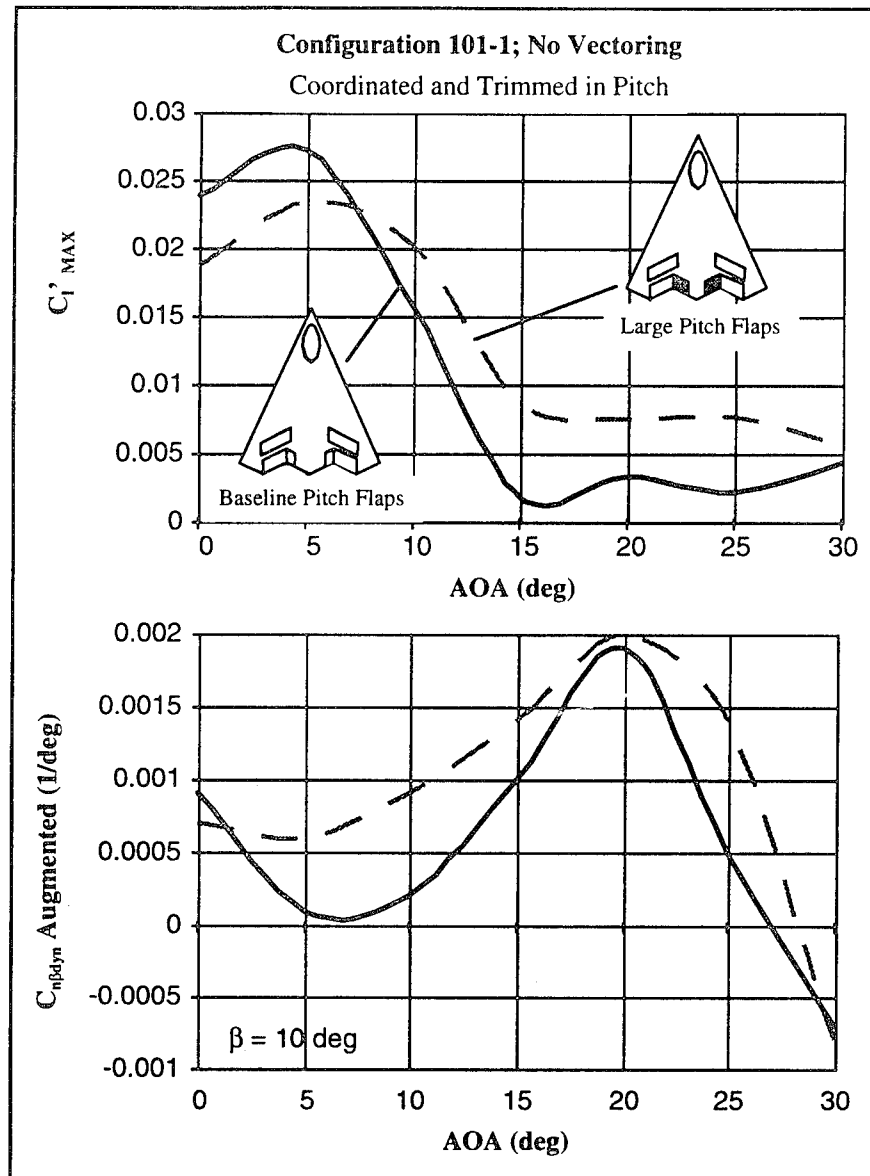


Figure 6-20 Increased Pitch Power Resulted in Greater Lateral-Directional Capability on Configuration 101-1

6.2 Control Power Analysis with Innovative Controls on 201-Series Configurations

The three favored innovative control suites selected in Section 5 were transitioned to the 201-series configuration, resulting in Configurations 201-1, 201-3 and 201-4. Figure 6-21 shows the evolution of each control suite on the 201-Series configurations. Controls are shaded in light gray. Gray surfaces represent the control concepts modified to achieve each configuration.

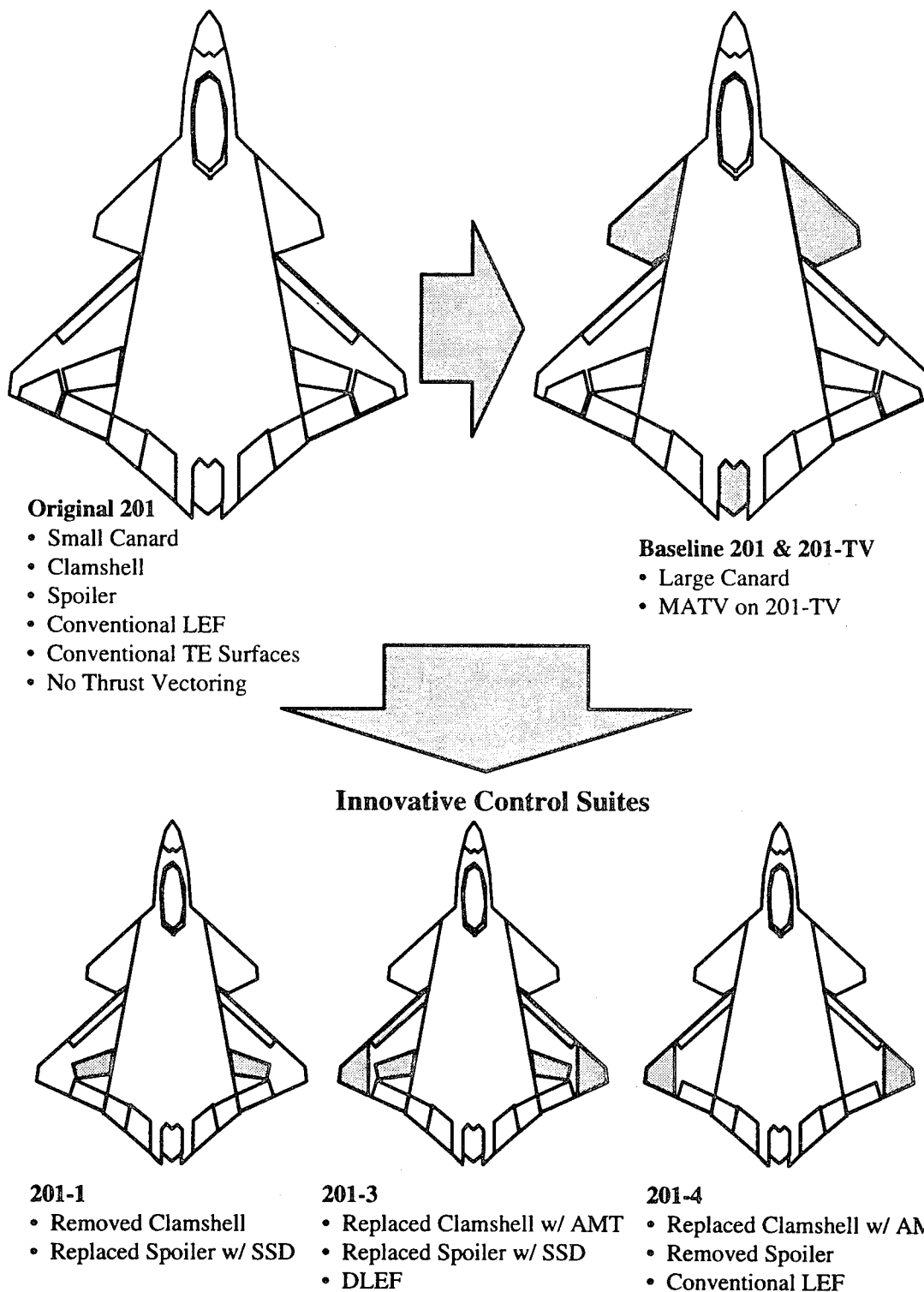


Figure 6-21 Configuration 201-Series Control Suites

Each innovative control suite included pitch and yaw thrust vectoring to achieve the high AOA roll performance goals. The same engine/nozzle combination with a 15 deg deflection limit and 6,000 lbs off-axis load limit were assumed throughout the analysis.

6.2.1 Power Approach Roll Performance

Power approach roll performance was analyzed for each concept. Recall that PA roll performance was found to be the critical lateral-directional control power sizing condition in Section 4.4.3. Each configuration was analyzed with the throttle set at both trim and idle power. The objective of this analysis was to identify control suite(s) that could achieve Level 1 flying qualities at or below the vision limit speed (zero WOD with 5K lbs bring back).

Idle Power PA Roll Performance

Figure 6-22 shows the idle power PA roll performance at various AOA and bring back weights compared with Configuration 201-TV. Configuration 201-3 is the only control suite capable of achieving Level 1 roll performance in idle power at the vision limit AOA of 11.2 deg. Configuration 201-1 requires the greatest WOD to meet Level 1 objectives. Configuration 201-4 has similar performance as 201-TV.

Configuration 201-4 provided 21 deg of bank angle change in 1 sec at the vision limit AOA; similar to the baseline configuration. In this case, the AMT alone provided sufficient coordinating yaw power to replace both the clamshell and spoiler on 201-TV. In addition, the AMT provides better high AOA yaw control capability than either the clamshell or the spoiler.

The original analysis on 201-4 was done with an AMT the same size as the one on 201-3. A second iteration was completed with a 25% increase in the AMT size. The aileron and LEF span were reduced slightly to accommodate the larger tip. Improvements in PA roll performance were significant. WOD requirements for Level 1 flying qualities at 5K bring back weights were reduced by approximately 10 knots. Results are shown in Figure 6-23.

At the vision limit AOA, bank angle at 1 sec was improved from 21 deg to 25 deg which is still short of the 30 deg bank requirement.

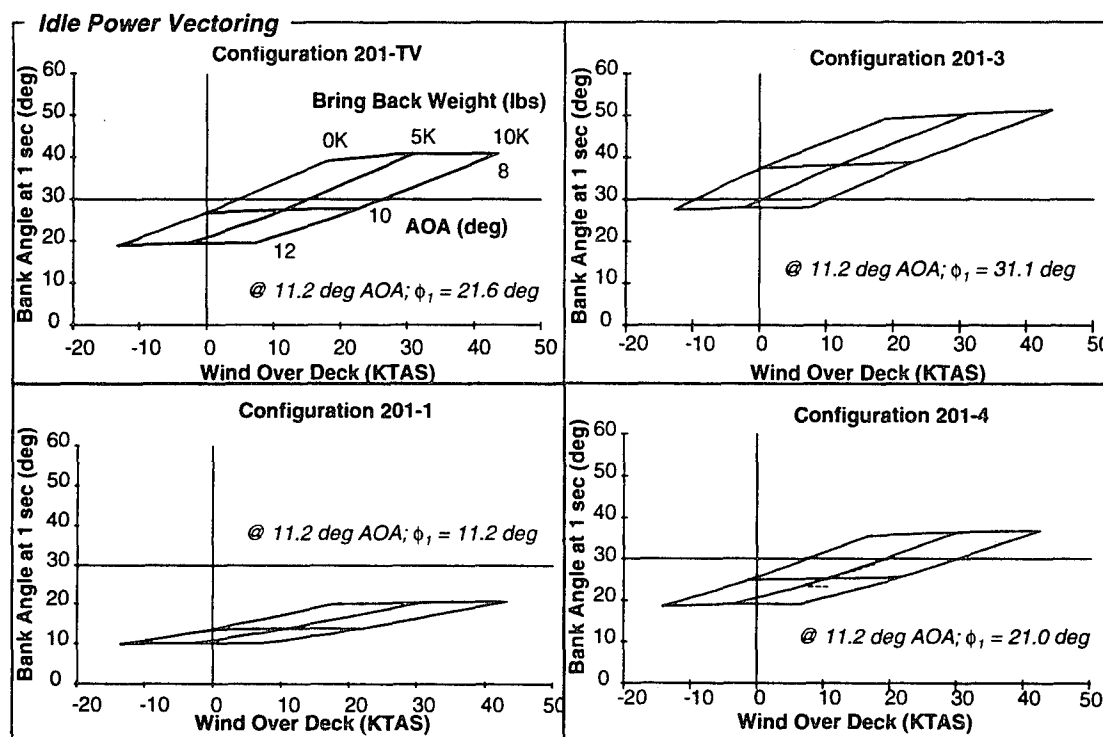


Figure 6-22 Power Approach Roll Capabilities at Idle Power

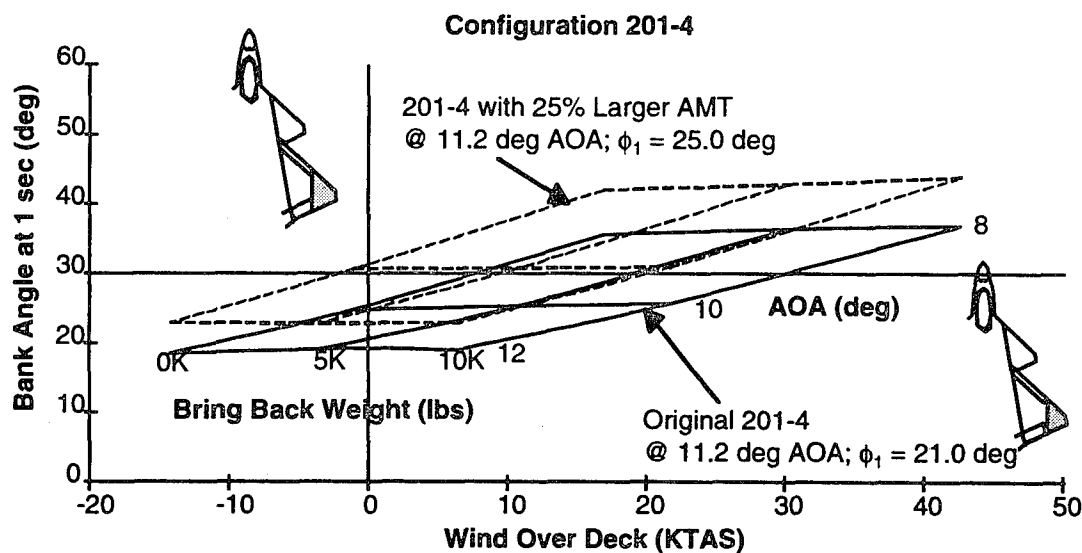


Figure 6-23 Increased AMT Size Significantly Improved PA Roll Performance

Planviews of the final three innovative control suite concepts are shown in Figures 6-24 through 6-26. The drawing in Figure 6-26 incorporates the increased-size AMT. To increase the tip size further would significantly reduce the aileron's size, thereby reducing high-lift and roll effectiveness.

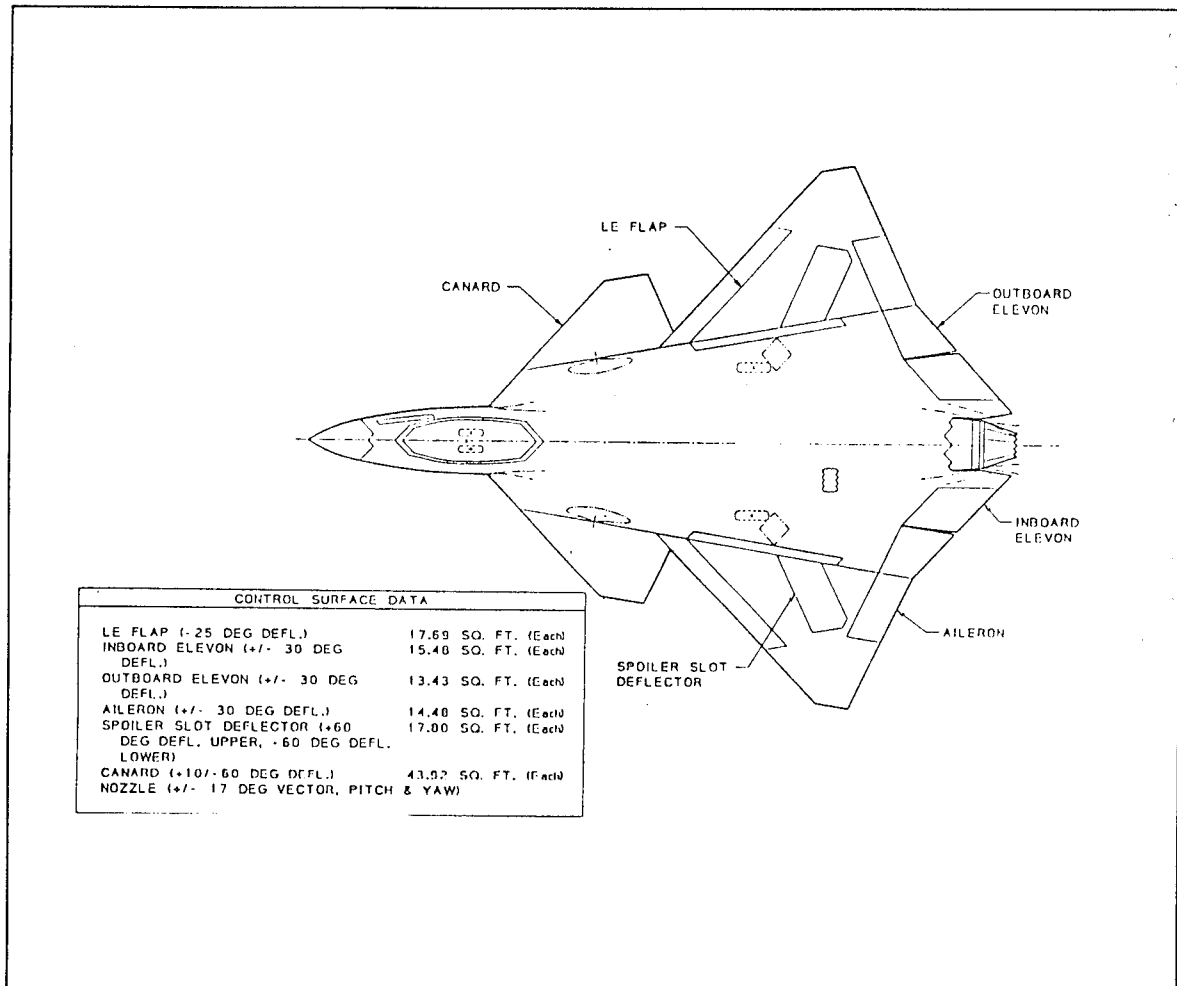


Figure 6-24: Configuration 201-1

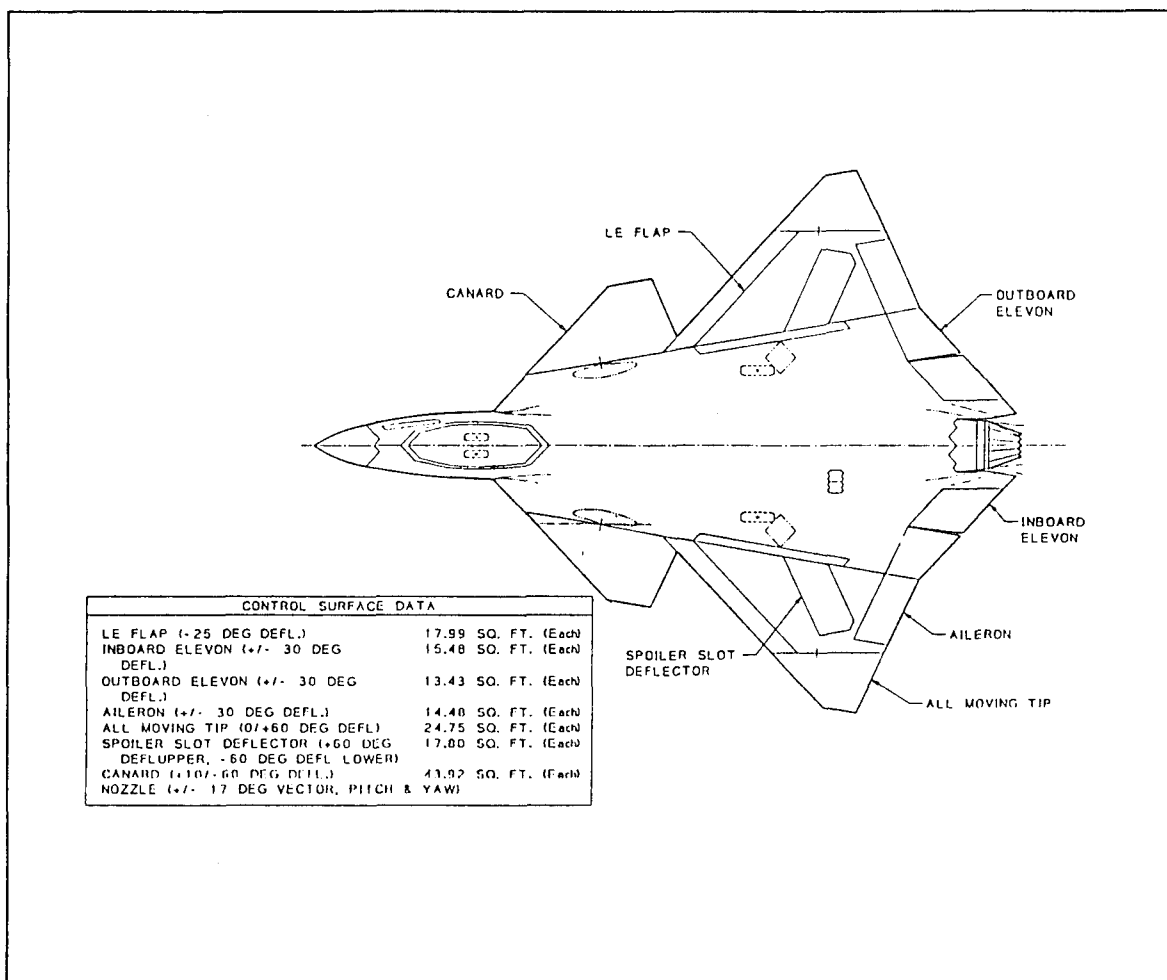


Figure 6-25 Configuration 201-3

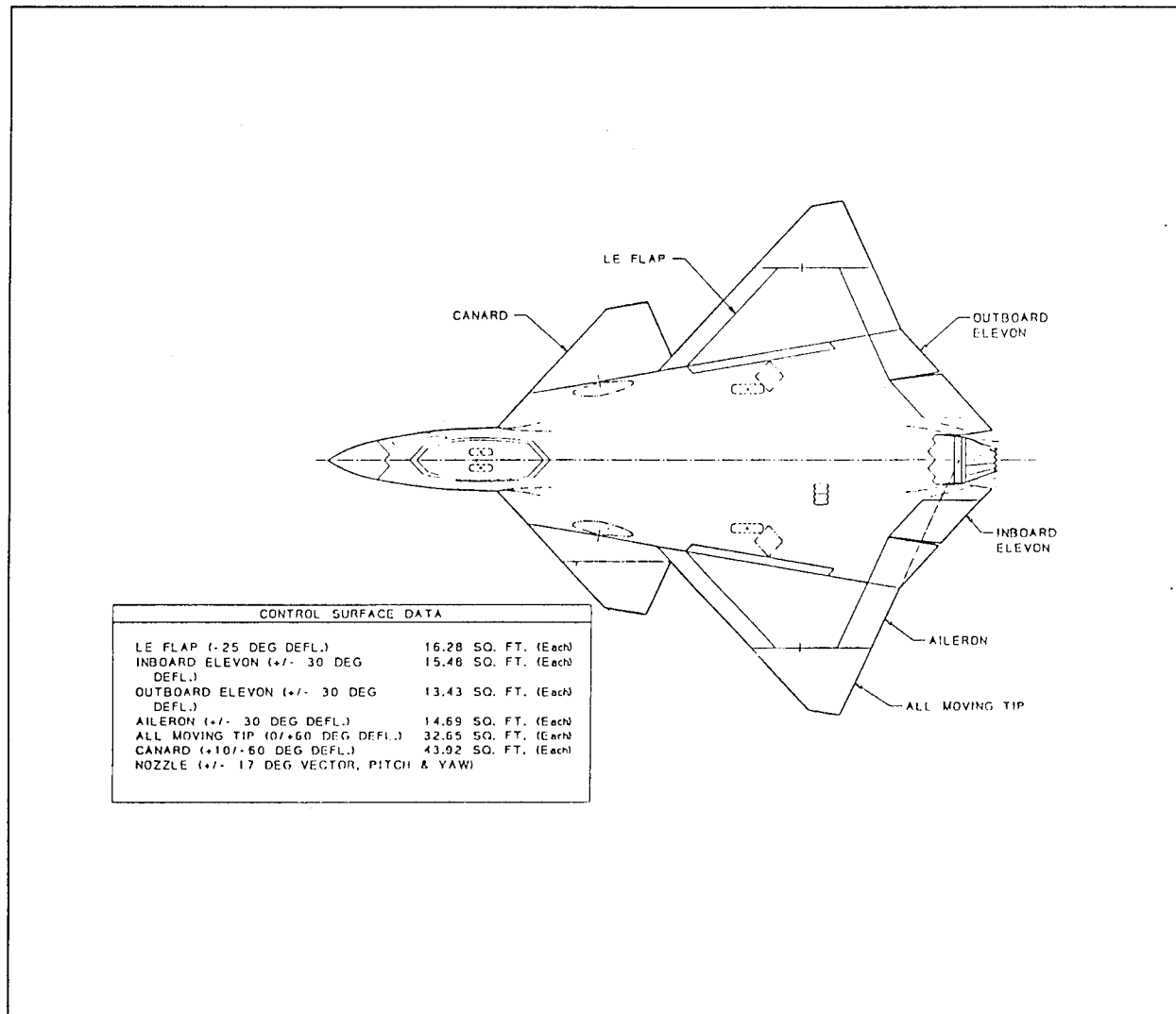


Figure 6-26 Configuration 201-4

Figure 6-27 illustrates the control deflections required to generate a maximum coordinated right roll at the power approach condition in idle power (i.e., $C_l' = \max$; $C_n' = 0$; $C_m = 0$). Note that the AMT is always used TED on the wing in the direction of the roll. For all of these cases the yaw control power available from the AMT was used for roll coordination. Note that the trailing edge controls are not saturated differentially (e.g., for maximum roll power). None of these configurations have sufficient yaw power to coordinate all of the roll power available from the trailing edge controls at this condition.

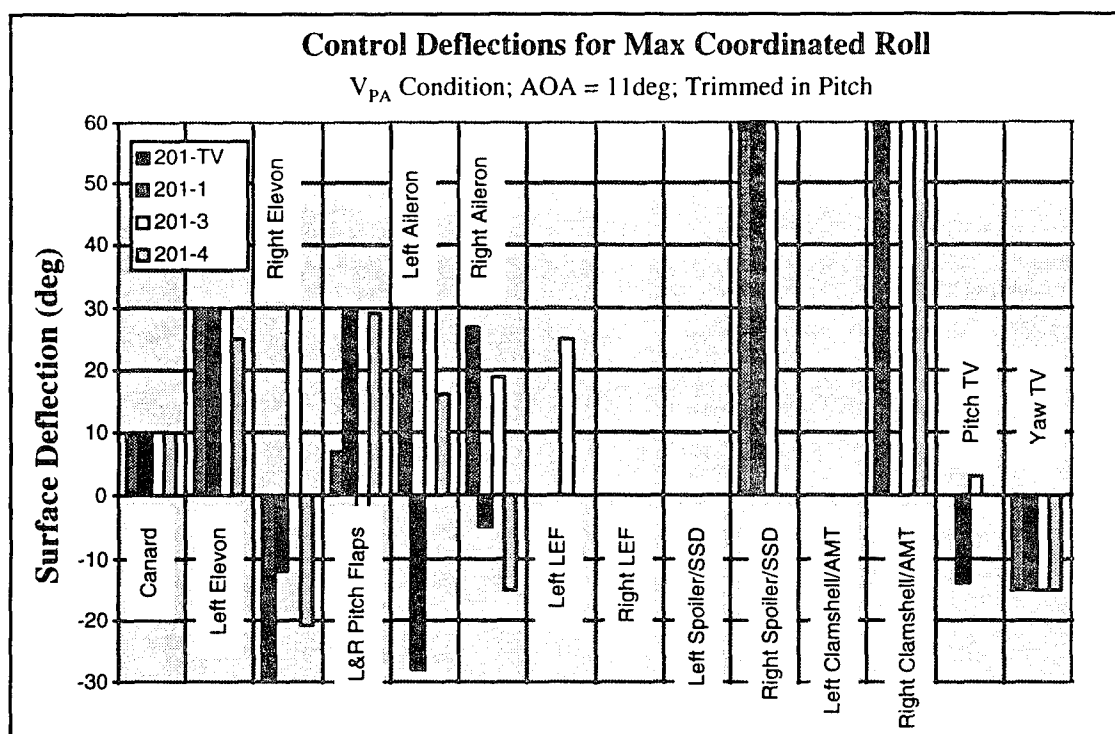


Figure 6-27 Control Deflections Required for Maximum Coordinated PA Roll

Effects of Increased Throttle Setting on PA Roll Performance

Thrust vectoring has the potential to provide the needed yaw control moments for roll coordination during PA. An integrated throttle and speedbrake controller would be required for glide path control during the approach. For example, if the pilot needed to retard the throttle when high on the glideslope, speedbrakes would extend to increase drag, resulting in an increased rate-of-descent. The throttle would stay fixed at some minimum value required to provide sufficient control moments for Level 1 flying qualities. The speedbrake would need to be sized to make up the difference (trading drag for thrust) for adequate flight path control. Furthermore, the design would require a significant change in the speedbrake control and actuation system potentially requiring dual hydraulics to the surface and positive feedback to the FCS to provide control-loop closure.

Control power envelopes were computed with the throttle set at the power required for trim, resulting in a thrust increase from approximately 500 lbs at idle to 5500 lbs. (These values vary somewhat depending on the 1-g trim speed.) The WOD required for Level 1

flying qualities was determined at 5K and 10K bring back weights. The results are shown in Figure 6-28 at trim power and AOA. These results do not consider other CV suitability limitations such as vision limit or pop-up. They simply define the WOD requirements for Level 1 flying qualities.

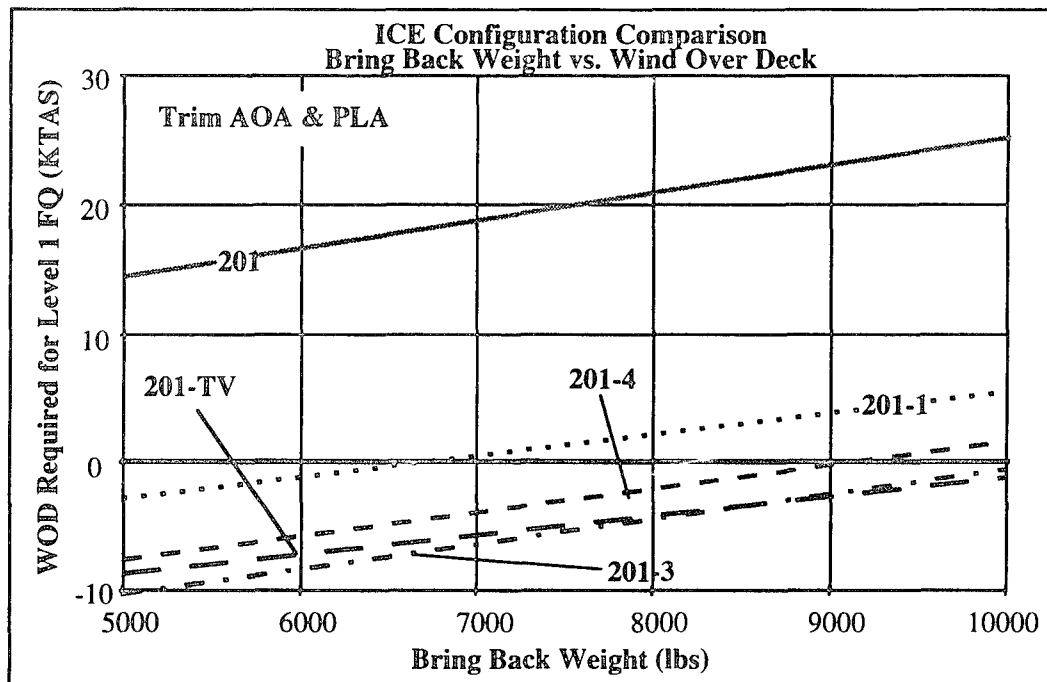


Figure 6-28 Variation of WOD Required for Level 1 FQ with Bring Back Weight at Trim Power and AOA

Compared with the results of Figures 4-24 and 6-22, Figure 6-28 shows that increased power settings significantly improve roll performance at the PA condition because of greater coordinating yaw power from TV. Even Configuration 201-1 (the poorest performing innovative control configuration) can meet Level 1 roll performance at zero WOD and 6,700 lbs of bring back. The results shown for Configuration 201-4 included the original "small" AMT. The unvectored Configuration 201 is shown for comparative purposes.

A roll performance versus WOD diagram was prepared for Configuration 201-1 at the trim throttle setting and compared with the original plot at idle power (Figure 6-29). There is a significant reduction in the WOD required for Level 1 roll performance by

simply increasing the throttle from idle to trim power. The SSD arrangement on this configuration could be used to double as speedbrakes for glidepath control. Likewise, the spoilers and clamshells on Configuration 201-TV could serve the same purpose. The AMT may also be able to perform the speedbrake function on Configuration 201-4.

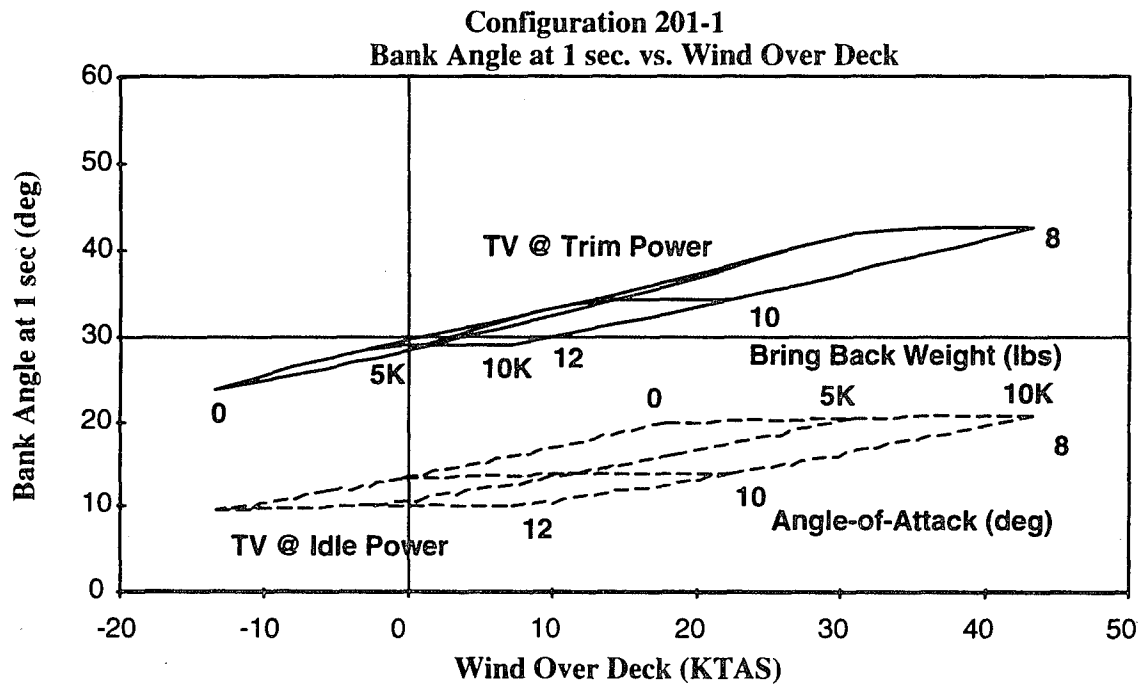


Figure 6-29 Increased Throttle Settings Provide Significant Improvements to PA Roll Performance on Configuration 201-1

6.2.2 High AOA Capabilities

Coordinated roll control power was evaluated at 150 KCAS at high AOA with thrust vectoring in MAX-A/B. Figure 6-30 shows the coordinated roll power for the thrust vectored configurations. Configurations 201-3 and 201-4 have the greatest roll capabilities and Configuration 201-1 the least. These results are similar to the 101-series configurations.

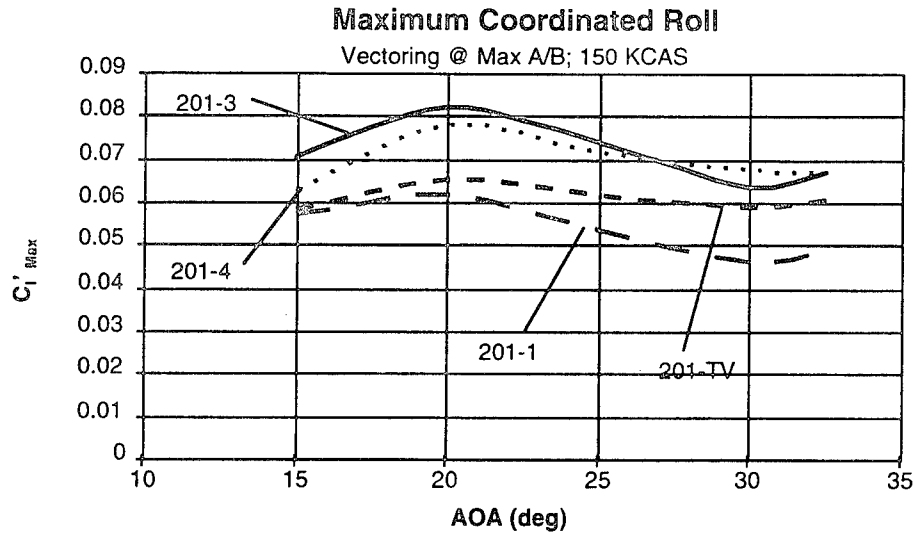


Figure 6-30 High AOA Roll Coordinated Roll Control Power Available

Figure 6-31 shows the augmented lateral-directional stability characteristics of the 201-series configurations at a maximum sideslip angle of 10 deg. All of the curves are shown with 25 deg LEF deflections except 201-3 which uses differential LEF for additional yaw control power; the canards were fixed at -30 deg. No sideslip data were available for canard deflections less than -30 deg; other deflections may considerably affect the bare airframe lateral-directional stability. The bare airframe exhibits a severe lateral-directional instability above 30 deg AOA (see Appendix C). None of the configurations have sufficient control power with aerodynamic controls alone to overcome the instability. Configuration 201-3 has the greatest augmentation capability and 201-1 the least.

Augmented directional stability at 30 deg and 32.5 deg AOA is shown in Figure 6-32 using both aerodynamic and MAX-A/B TV control power. Configurations 201-3 and 201-4 can meet the augmentation requirements using both aerodynamic and propulsion controls. Configuration 201-TV and 201-1 cannot achieve satisfactory levels of augmentation. Greater TV deflections than 15 deg should provide the required yawing moments for these two configurations.

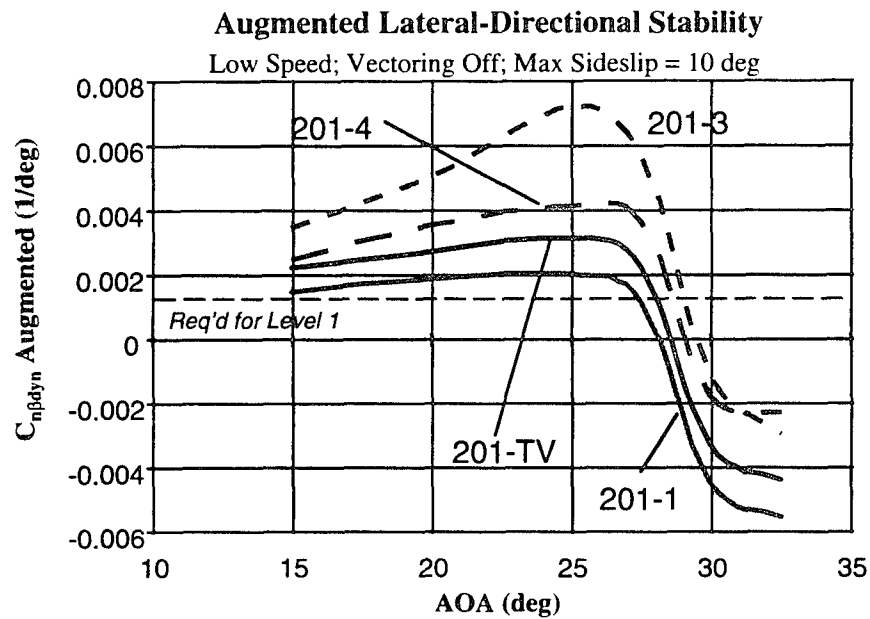


Figure 6-31 Low-Speed Augmented Lateral-Directional Stability Characteristics

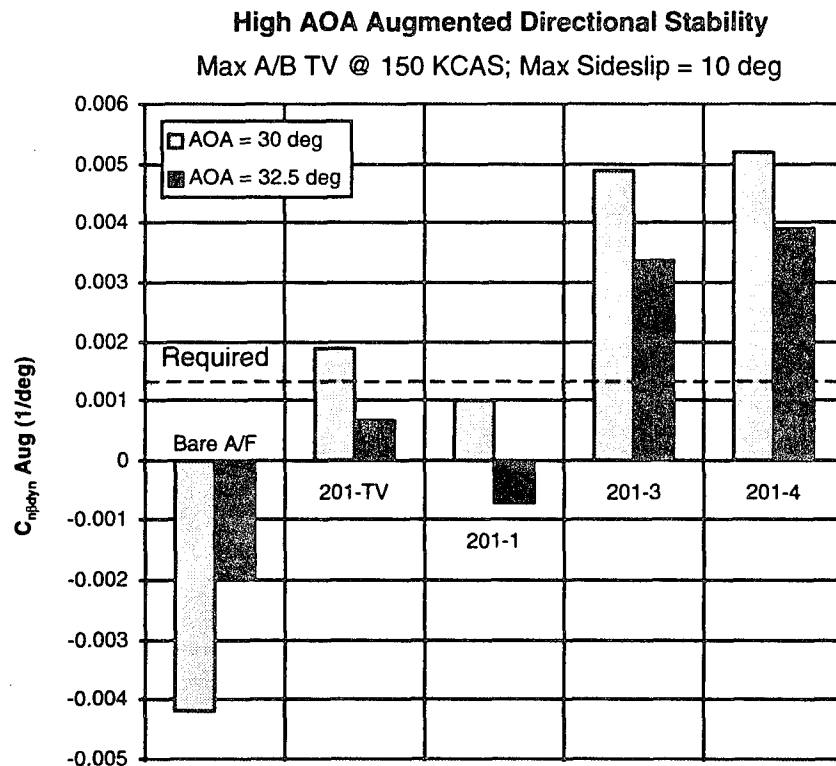


Figure 6-32 Augmented Directional Stability Characteristics using Max A/B TV

The relatively poor lateral-directional augmentation characteristics with aerodynamic controls is not an indictment of the innovative control concepts, but the high degree of instability that the bare airframe exhibits. Additional configuration refinement may improve the bare airframe lateral-directional stability at high AOA.

Figure 6-33 shows the 30 deg AOA roll performance capabilities at 108 KCAS. The configurations with thrust vectoring are all close to the goal of 90 deg bank angle change in 2.0 seconds. Configurations 201-3 and 201-4 are the best performers principally due to the high AOA yaw control power available from the AMT.

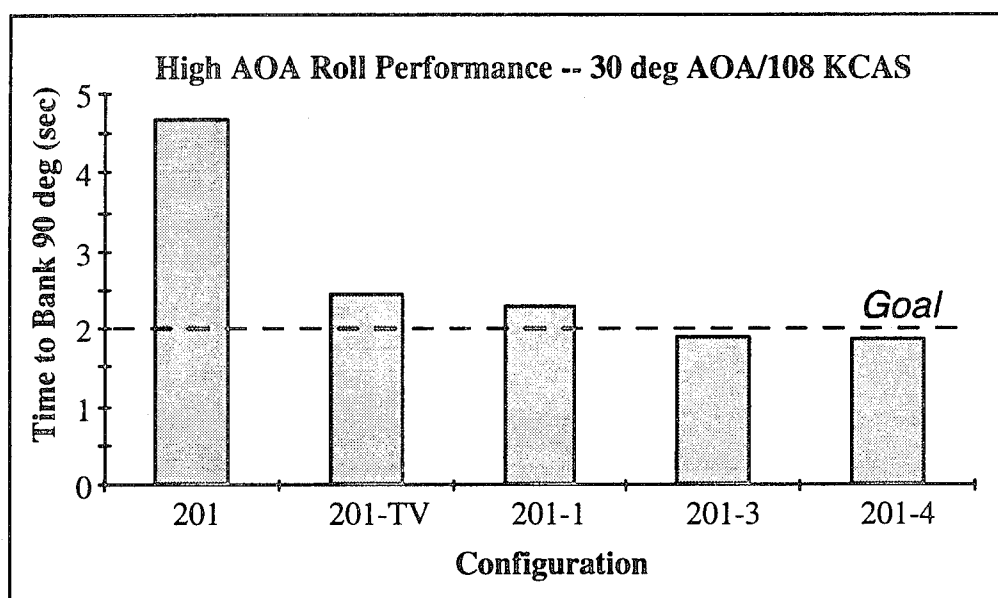


Figure 6-33 Roll Performance at 30 deg AOA

6.2.3 Operational cg Ranges

The operational cg limits were determined by finding the most forward cg where the nose-wheel lift off requirements could be met, and checking aft cg limits for symmetric nose-down pitch acceleration and the ability to counter inertial coupling during rolls. The forward cg limits were discussed in Section 4.4.7. Recall that with thrust vectoring, the forward cg limits would not be set by nose-wheel lift off, but by other criteria such as FCS considerations or nose-gear load limits. Even with aerodynamic controls alone, Configuration 201 easily achieved the $0.9V_{LO}$ requirement at a cg of 18% MAC. Addi-

tional nose-up control margin existed for further forward cg movement. (See Figure 4-26.)

Aft cg limits were determined by applying the nose-down criteria described in Section 4. Figure 6-34 shows the aft limit variation with steady state roll rate for the 201-series configurations. The most critical aft limit criteria on these configurations is the -0.07 rad/sec^2 control margin requirement with aerodynamic controls at the condition for minimum nose-down pitch control power (C_m^*). The roll rates generated at high AOA are not high enough to supplant this condition as the most critical aft limit. (The inertial roll coupling results include a -0.07 rad/sec^2 pitch control margin.) Finally, the symmetric nose-down pitch acceleration requirement of -0.25 rad/sec^2 using both aerodynamic and propulsion controls is the least critical condition. Considering all of the conditions shown on the diagram, the most critical aft cg limit is 22.24 % MAC, set by the symmetric maneuvering requirement with aerodynamic controls alone. Configurations with AMT have an additional 0.36% MAC aft cg limit capability using the AMT for nose-down control.

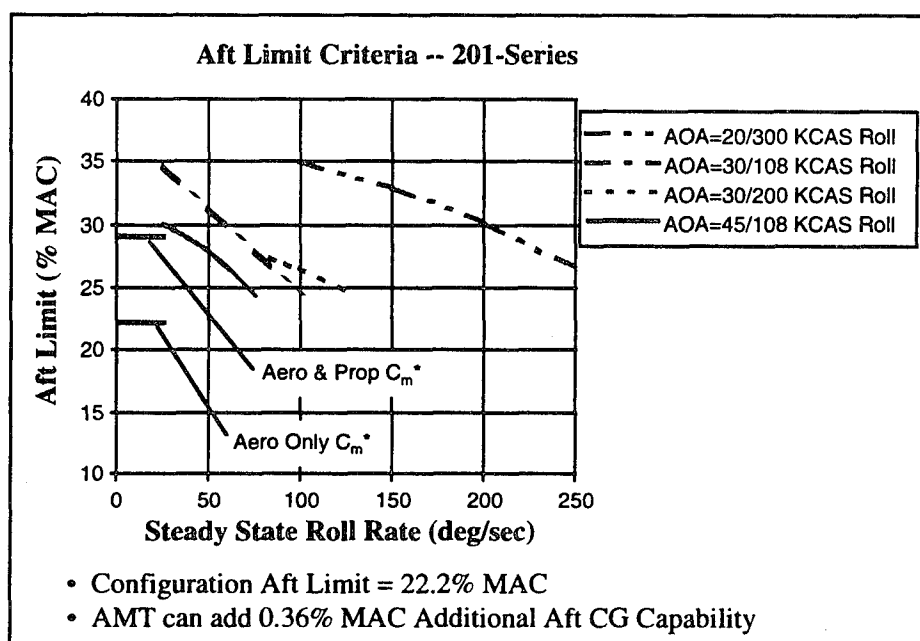


Figure 6-34 Aft cg Limits for 201-Series Configurations

7 Integration Study

Control integration impacts were evaluated by developing structural arrangements, subsystem requirements, and making maneuver assessments of the baseline vehicles. Preliminary analyses on six control suites employing innovative control concepts were completed. Three of these concepts were selected to be analyzed in detail (Sections 5.0 and 6.0). The following section describes results of the integration study, where subsystem, structural, aerodynamic, signature and weight impacts were determined for the three configurations, and compared with the baseline. (The structural integration discussion includes an evaluation of all five innovative control concepts on the original six land-based derivative configurations.)

7.1 Flight Control Actuator Requirements

Actuation requirements for each configuration were determined from hinge moment and rate limit information developed during the control sizing studies. Hinge moment data from similar configurations and/or control concepts were scaled to be representative of the concepts employed on the study aircraft. Flexibility effects were included based on F-16XL and other F-16 derivative experience. Rate limit requirements were determined using the CPR software tool.

7.1.1 Actuator Rate Limit Requirements

Control surface rate limits are a function of the control power available, and the desired augmented flying qualities. The CPR software uses a flight control approach that deflects virtual controls (i.e., pitch, roll and yaw controllers).

To completely validate rate limit requirements for a highly coupled control suite requires 6-DOF simulation analysis with control blending logic in place. However, during the conceptual design stages, the control blending design is unknown, and simplifying assumptions must be made. The approach taken here, using CPR and CPA results, assumes

linear "virtual" control effectiveness with deflection. The manner in which the controls are best used was determined by analyzing CPA envelope results.

Control power requirements at representative virtual roll surface rate limits for a high AOA roll maneuver are presented in Figure 7-1. Rate limits are presented in deg/sec, but can be thought of as "rate of control power". From the figure, a roll controller rate limit of 75 deg/sec appears to provide a good trade-off between control power required, and an acceptable rate limit. Figure 7-1 also shows that control power requirements are insensitive to yaw virtual surface and pitch virtual surface rate limits for the same maneuver.

Rate limit requirements for pitch control surfaces are a function of augmented short period frequency, and control power available. For a g-command flight control system, control anticipation parameter (CAP) can be related to pitch control effectiveness, and control surface rate using

$$\text{CAP} = (M_{\delta} \tau_a) (\delta_{rl}/\Delta n_z) (1 \text{ rad}/57.3 \text{ deg}) \quad (4)$$

where τ_a is the total equivalent system time delay in the pitch axis.

Rate limit requirements are usually set at low-speed conditions where available control power is relatively small. For 101-series configurations at a typical power approach condition, M_{δ} is -4.33 1/sec^2 . Assuming a maximum time delay of 0.07 sec and a design CAP of 0.5, then $\delta_{rl \text{ req'd}}/\Delta n_z = 94.5 \text{ deg/sec/g}$. For a 0.5g incremental command (a reasonable value for a low-speed condition), the pitch control rate limit is 47 deg/sec required to achieve the desired flying qualities. For the 101-series tailless configuration, the only decoupled pitch control surface is the pitch flap. All other control surfaces are used in other axes. Therefore, the 75 deg/sec rate limit (for a 30 deg position limit) required to complete the roll maneuver (Figure 7-1) takes precedence over the pitch control rate limit for the elevon; the pitch flap rate limit can be set based on the above analysis.

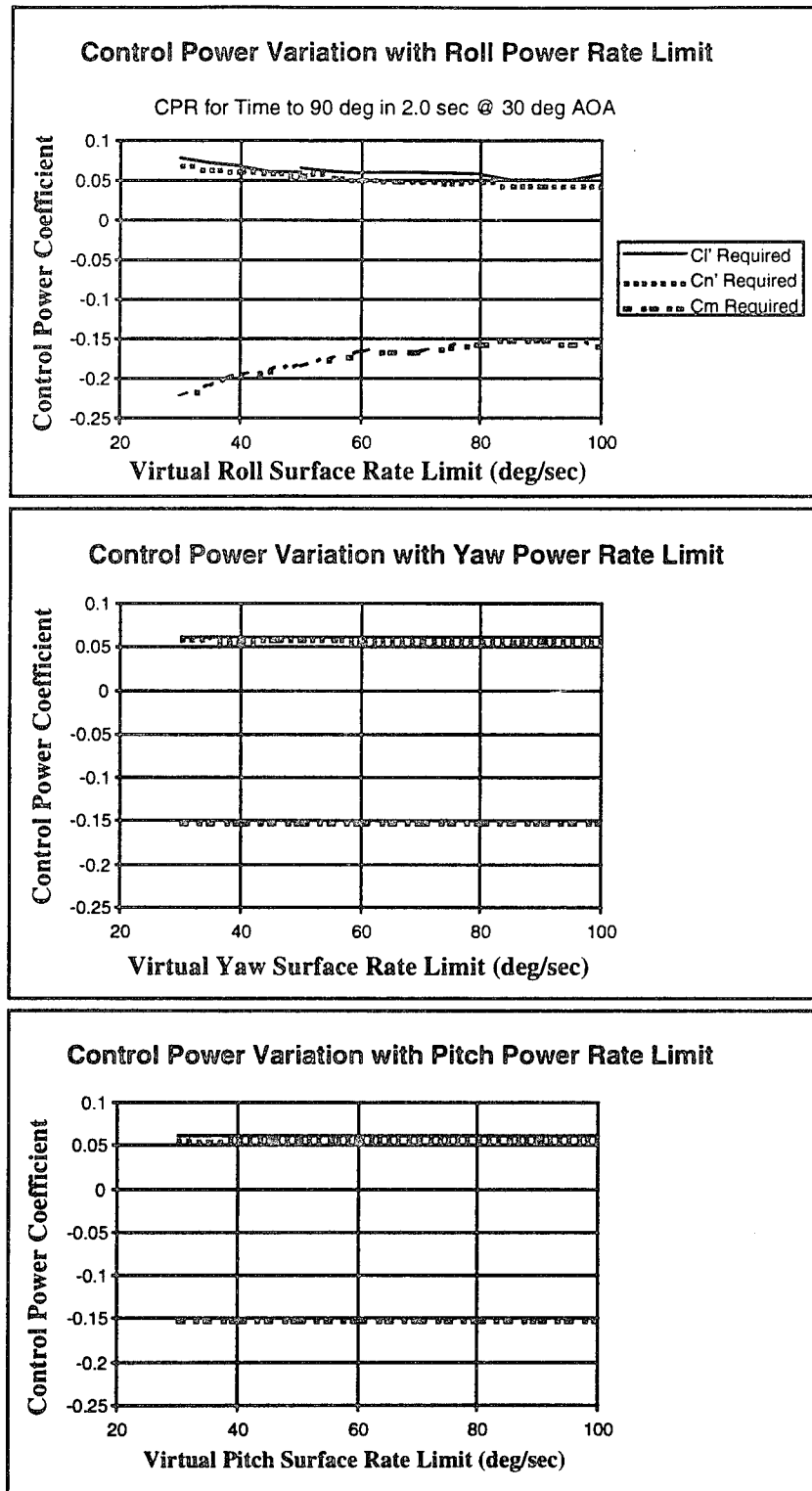


Figure 7-1 Control Power Required vs Virtual Control Rate Limit

The control power requirements discussed in Section 4 were determined using virtual surface rate limits of 75 deg/sec on the controls. Virtual surface position limits of +/-30 deg were assumed as well. For physical controls having to move through deflections other than 30 deg, the rate limit can be approximated by ratioing the physical deflection limit to the virtual deflection limit. For example, if a spoiler is required to move through 60 deg, its required physical rate limit can be estimated from

$$\delta_{RLsp} = \delta_{RLvirtual} (\delta_{sp \text{ limit}} / \delta_{virtual \text{ limit}}) = 75 \times (60/30) = 150 \text{ deg/sec}$$

This rate limit will enable the spoiler to reach its maximum control potential in the same amount of time as the virtual control surface in CPR.

Likewise, elevon rates would presumably be set at the virtual surface rate limit of 75 deg/sec because they only move through +/-30 deg; however, for a maximum performance rolling reversal, the elevons can be against their stops in one direction, and then be required to move at maximum rate until against their stops in the opposite direction (60 deg of throw). Since the elevons are used together with the spoilers or SSD's to provide yaw as well as roll on all but one of the configurations, the timing of the elevon/spoiler control relationship is critical. The elevons must move as quickly as the spoilers to avoid adverse coupling during aggressive rolling maneuvers. For Configuration 101-4, this is not the case. The AMT is used as a decoupled yaw control. Since the elevons are relieved from the job of having to provide yaw control as a function of spoiler deflection, their rate limit requirements can be relaxed back to the 75 deg/sec limit.

Using the above methods and assumptions, control surface rate limits were determined for each of the configurations. Table 7-1 summarizes hinge moment and rate limit requirements for each.

Table 7-1 Control Surface Actuator Requirements*Configuration 101*

Control Surface	Position Limits (deg)	Rate Limit (deg/sec)	HM (K in-lbs)
Elevon	+/-30	150	300
Pitch Flap	+/-30	50	100
IB Spoiler	0/60	150	652
OB Spoiler	0/60	150	652
Clamshell	0/60 (upr & lwr)	150	127
LEF	0/40	30	400

Configuration 101-TV

Elevon	+/-30	150	300
Pitch Flap	+/-30	50	100
IB Spoiler	0/60	150	652
OB Spoiler	0/60	150	133
MATV	+/-15	60	---
LEF	0/40	30	400

Configuration 101-1

Elevon	+/-30	150	300
Pitch Flap	+/-30	50	100
IB SSD	0/60	150	93
OB SSD	0/60	150	41
MATV	+/-15	60	---

Configuration 101-3

Elevon	+/-30	150	300
Pitch Flap	+/-30	50	100
SSD	0/60	150	39
AMT	0/60	150	30
MATV	+/-15	60	---
OB DLEF	0/40	40	124

Configuration 101-4

Elevon	+/-30	150	300
Pitch Flap	+/-30	50	100
AMT	0/60	150	149
MATV	+/-15	60	---

Note: TV rate limit is based on current technology systems.

7.1.2 Hinge Moment Limits

CPR was used to determine control power requirements to achieve levels 1 and 2 flying qualities at high speed. The surface deflections required to provide sufficient control power to meet the flying qualities requirements were determined by running CPA at various deflection limits until a control envelope of sufficient size was generated (Figure 7-2). Maximum hinge moments were computed based on the maximum deflections required at the critical flight conditions. Control suites were designed to provide Level 1 flying qualities at Mach 1.2/sea level. Some of the yaw controls were needed only at low-speeds (e.g., clamshell on Configuration 101). In this case, the actuators were sized to provide full deflection capability at 300 KCAS for elevated-g roll coordination. A summary of the conditions that set the various deflection limits for each configuration is provided below (Table 7-2).

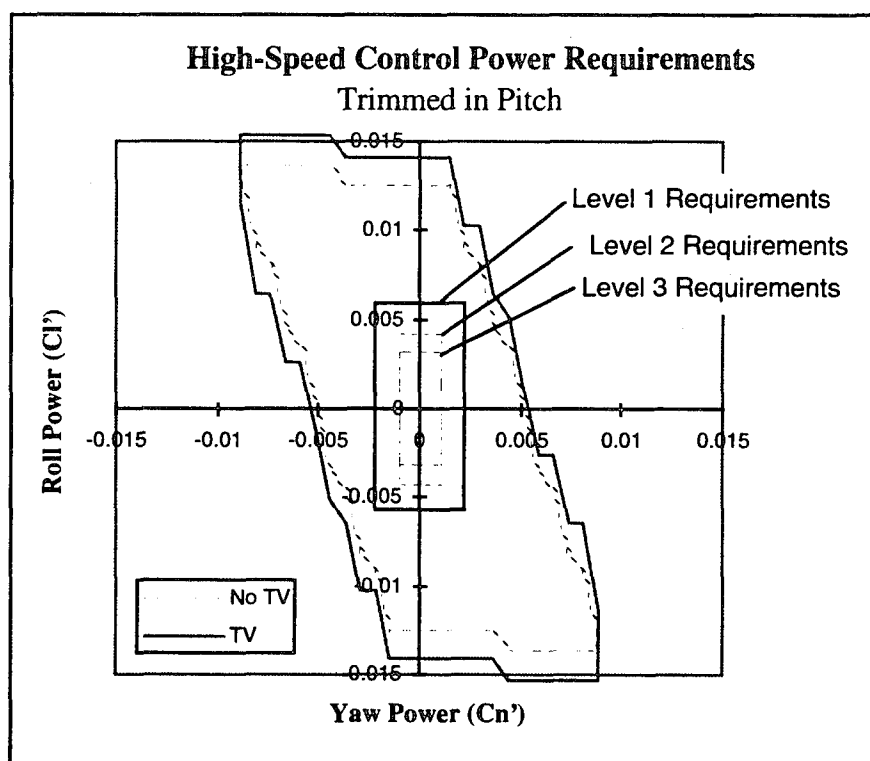


Figure 7-2 Control Envelopes were Used to Determine Maximum Control Deflection Requirements at High Speeds

Table 7-2 Sizing Conditions for Maximum Hinge Moments*Configuration 101*

Control Surface	Flight Condition	Maneuver
Elevon	Mach 1.2/SL	Level 1 Roll
Pitch Flap	Mach 1.2/SL	9-g Trim
IB Spoiler	Mach 1.2/SL	Level 2 Yaw
OB Spoiler	Mach 1.2/SL	Level 1 Yaw
Clamshell	300 KCAS	Roll
LEF	Mach 1.2/SL	Elevated-g Turn

Configuration 101-TV

Elevon	Mach 1.2/SL	Level 1 Roll
Pitch Flap	Mach 1.2/SL	9-g Trim
IB Spoiler	Mach 1.2/SL	Level 2 Yaw
OB Spoiler	300 KCAS	Roll
LEF	Mach 1.2/SL	Elevated-g Turn

Configuration 101-1

Elevon	Mach 1.2/SL	Level 1 Roll
Pitch Flap	Mach 1.2/SL	9-g Trim
IB SSD	Mach 1.2/SL	Level 2 Yaw
OB SSD	300 KCAS	Roll

Configuration 101-3

Elevon	Mach 1.2/SL	Level 1 Roll
Pitch Flap	Mach 1.2/SL	9-g Trim
SSD	Mach 1.2/SL	Level 2 Yaw
AMT	Mach 1.2/SL	Level 1 Roll/Yaw
OB DLEF	Mach 1.2/SL	Sym Deflection

Configuration 101-4

Elevon	Mach 1.2/SL	Level 1 Roll
Pitch Flap	300 KCAS	9-g Trim
AMT	Mach 1.2/SL	Level 1 Roll/Yaw

LEF drive units were sized for high speed, elevated-g conditions to provide capability for symmetric scheduling. The hinge moment required to keep the LEF from moving at maximum speed is actually greater than that shown in Table 7-1. The drive system was

sized to provide deflection capability for wing cambering during a maximum effort turn at high speed. At high speed 1-g cruise conditions, the drive system is allowed to stall because flap movement is not required -- the holding power of the drive system is typically much greater than the power required to drive the flaps.

The AMT actuators were sized for stiffness to resist flutter. This is generally the case for any all-moving surface. A finite element structural model would be required to evaluate actuator stiffness requirements. Such a model is not usually available during the conceptual design stage, and assumptions based on historical data must be made. An empirical design chart was prepared by compiling control surface and actuator data for a number of high performance aircraft (Figure 7-3). This chart assumes that stiffness sized each of the actuators. Most of the data came from horizontal tail data -- however, a few data points were available from AMT and all-moving vertical tail configurations. To use this chart for actuator sizing, it is assumed that stiffness, and not hinge moment requirements will size the actuator; and is therefore primarily useful for all-moving control surfaces. The AMT actuators were sized in this manner.

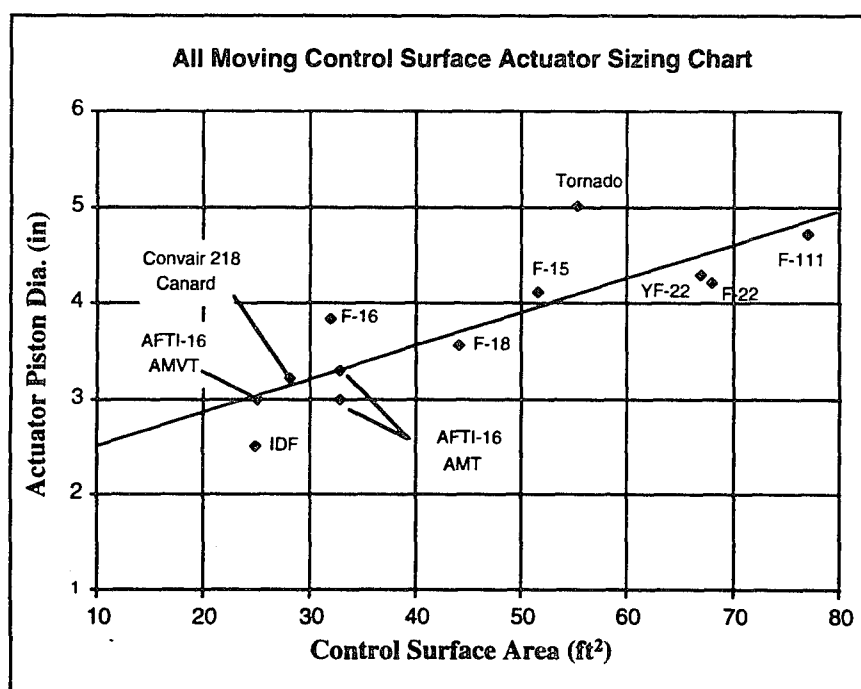


Figure 7-3 All Moving Control Surface Actuator Sizing Diagram

7.1.3 Control Redundancy

In order to assess the actuator and hydraulic requirements for each control suite, it is first necessary to establish how critical single and dual control surface failures are.

The most accurate method to accomplish this would be to run a nonlinear, 6-DOF simulation with reconfiguration control laws to evaluate the impact of each set of failures. If reconfiguration control laws are unavailable, a control power envelope method can be used to reallocate the available control power. This second method involves running a predetermined maneuver in a 6-DOF simulation, and then overlaying the control power required for the maneuver with the control power available from each failed configuration (similar to the maximum deflection determination described above). When the requirements exceed the availability, the next lower flying qualities level is applied. If it is not possible to achieve Level 2 with a single failure or Level 3 with a dual failure, then the situation is deemed critical. A third, preliminary method for analyzing control surface criticality has been developed for the conceptual design phase.

The third method involves assigning a rank to each control surface, and then combining the rankings to form an overall control failure matrix. Since control law development may be relatively immature in the preliminary design phase, engineering judgment is used to determine the relative criticality of each surface.

Rankings are based on a scale of 0 to 3 with 0 being not very critical (e.g., maneuvering flaps) and 3 being most critical (horizontal tails or rudders). Once a ranking has been assigned to each surface, the single surface criticality can be assessed using the following scale:

- 0 - 2: Level 1
- 3 - 4: Level 2
- 5 - 6: Level 3
- 7: Uncontrollable

Using this scale will yield no worse than a Level 2 rating for any single surface failure. This is where engineering judgment comes into play again. If a critical surface will potentially yield a Level 3 or worse response, the rating should be changed to reflect this result. Similarly, a Level 1 surface may be moved to a Level 2 rating.

Obviously, this ranking system is not indispensable when analyzing single surface failures; it merely provides a means of quantifying criticality. The real value of the procedure is apparent when considering two surfaces failed at once. By setting up a matrix (Figure 7-4) of dual failures and then combining surface rankings, an initial assessment of dual surface criticality can be attained. One additional aspect is added to the dual surface analysis; if both surfaces are on the same side of the airplane, the combined rank is increased by one to reflect the increased lateral-directional control requirements. The resulting rank is again applied to the flying qualities scale to yield the achievable flying qualities level.

Example: Mach 1.2 @ Sea Level
Flying Qualities Level

D	1	D	2	D	3	D	4	D	5	D	6	D	6B	D	6OB	D	10	D	20	D	16OB	D	16B	D	15	D	14	D	13	D	12	D	11
X	1	2	1	X	2	X		1	2	X		2	X		2	X		2	2	2	2	1	D	2		2	2	2	2	1	D	2	
	X	3	2	X	3	X		1	2	X		2	X		2	X		2	2	2	2	2	D	3		2	2	2	2	2	D	3	
		X	3	X	3	X		2	3	X		3	X		3	X		3	3	3	3	3	D	4		3	3	3	3	1	D	4	
			X	X	3	X		2	3	X		3	X		3	X		3	3	3	3	3	D	5		X	X	X	X	X	D	5	
				X	X	X		X	X	X		X	X		X	X		X	X	X	X	X	D	6B		X	X	X	X	X	D	6B	
					X	X		2	L	X		3	X		3	X		3	3	3	3	3	D	6OB		X	X	X	X	X	D	6OB	
						X		X	X	X		X	X		X	X		X	X	X	X	X	D	10		X	X	X	X	X	D	10	
								X	X	X		X	X		X	X		X	X	X	X	X	D	16OB		X	X	X	X	X	D	16OB	
									X	X		X	X		X	X		X	X	X	X	X	D	16B		X	X	X	X	X	D	16B	
										X		X	X		X	X		X	X	X	X	X	D	15		X	X	X	X	X	D	15	
												X	X		X	X		X	X	X	X	X	D	14		X	X	X	X	X	D	14	
													X		X	X		X	X	X	X	X	D	13		X	X	X	X	X	D	13	
															X	X		X	X	X	X	X	D	12		X	X	X	X	X	D	12	
																		X	X	X	X	X	D	11		X	X	X	X	X	D	11	

1 = Level 1

2 = Level 2

3 = Level 3

L = Loss-of-Control

X = Not Applicable

1 = Level 1
2 = Level 2
3 = Level 3
L = Loss-of-Control
X = Not Applicable

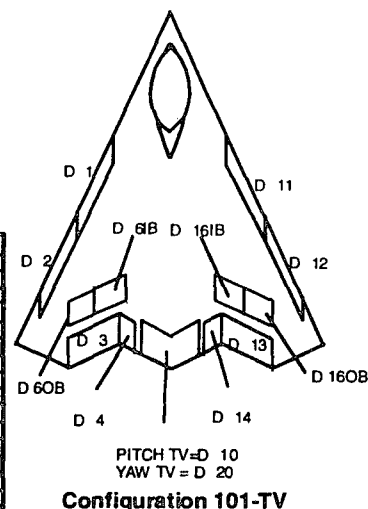


Figure 7-4 Example Control Surface Criticality Matrix

This method was used along with the control envelopes and simulation method discussed above to determine critical control surface failure combinations. First, each configuration was analyzed using the qualitative ranking method. Questionable results were checked using the control power tools CPR and CPA, and the ranking adjusted if needed. In this way, the matrix was scoped down to a few critical cases on which to perform control

power analysis. These methods can be used to evaluate both hard-over or fail-safe control surface conditions. For this analysis, only fail-safe (i.e., actuator failure resulting in damped by-pass) conditions were evaluated.

The final results desired from this study were (1) which control surfaces would require dual hydraulics and actuation, and (2) which could be simplex. These results were provided to the hydraulic system designer to better estimate hydraulic power requirements. Table 7-3 provides results of the control redundancy study.

Table 7-3 Control Surface Actuator Redundancy*Configuration 101*

Control Surface	Required Actuation Redundancy (per Surface)
Elevon	Dual
Pitch Flap	Simplex
IB Spoiler	Dual
OB Spoiler	Simplex
Clamshell	Simplex
LEF	Simplex

Configuration 101-TV

Elevon	Dual
Pitch Flap	Simplex
IB Spoiler	Dual
OB Spoiler	Simplex
LEF	Simplex
MATV	Dual

Configuration 101-1

Elevon	Dual
Pitch Flap	Simplex
IB SSD	Dual
OB SSD	Simplex
MATV	Dual

Configuration 101-3

Elevon	Dual
Pitch Flap	Simplex
SSD	Simplex
AMT	Dual
OB DLEF	Simplex
MATV	Dual

Configuration 101-4

Elevon	Dual
Pitch Flap	Simplex
AMT	Dual
MATV	Dual

7.2 Hydraulic System Requirements

Hydraulic flow rate requirements were determined using the information presented in Tables 7-1 and 7-3. This analysis was completed for the land-based configurations only. The hydraulic and actuator requirements were scaled to determine subsystem weights for the carrier-based configurations.

Thrust vectoring hydraulic requirements were derived from engine/nozzle manufacturer data, and were assumed to be shared equally between the two aircraft-mounted hydraulic systems. Aircraft hydraulic power was assumed to be provided by two 4,000 psi systems. Hydraulic system interfaces with the control surfaces were selected based on power distribution only, with no consideration given to failure effects.

Figure 7-5 shows the resulting hydraulic flow requirements. The systems were sized based on a maximum dynamic pressure condition at 300 KCAS (Mach 1.2/sea level). Obviously, some of the flow requirements are totally unrealistic; a realizable system would require flight envelope restrictions due to hinge moment limitations.

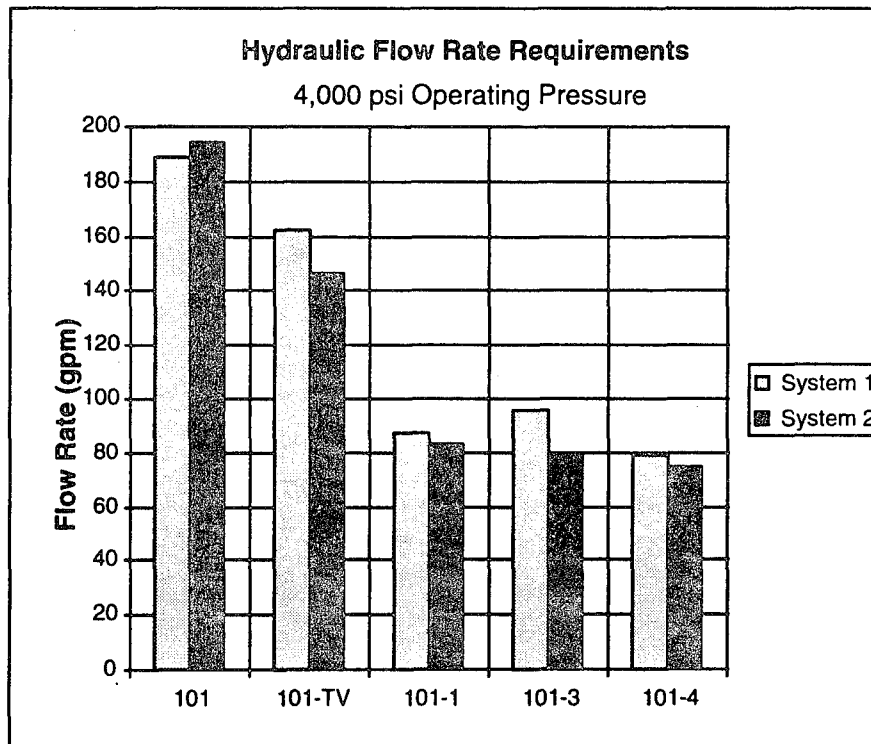


Figure 7-5 Total Hydraulic Flow Requirements -- Each System

All of the flow requirements are relatively high considering that this is a single-engine configuration -- not an unexpected result for a tailless fighter. Configurations 101 and 101-TV flow requirements are very large for this class of aircraft. The high flow rates are driven by the large spoiler hinge moments, which were in turn driven by yaw stabilization at the maximum speed condition. The SSD and AMT provide yaw effectiveness with an aerodynamically balanced surface, and therefore have lower hinge moment requirements - - resulting in an achievable hydraulic system design.

Hydraulic pumps were sized for each configuration based on a maximum possible demand situation (i.e., max pitch, max roll with yaw compensation, etc). Figure 7-6 shows the resulting pump sizes. For comparative purposes, the F-16 uses (2) 42 gpm pumps and the F-22 uses (4) 72 gpm pumps.

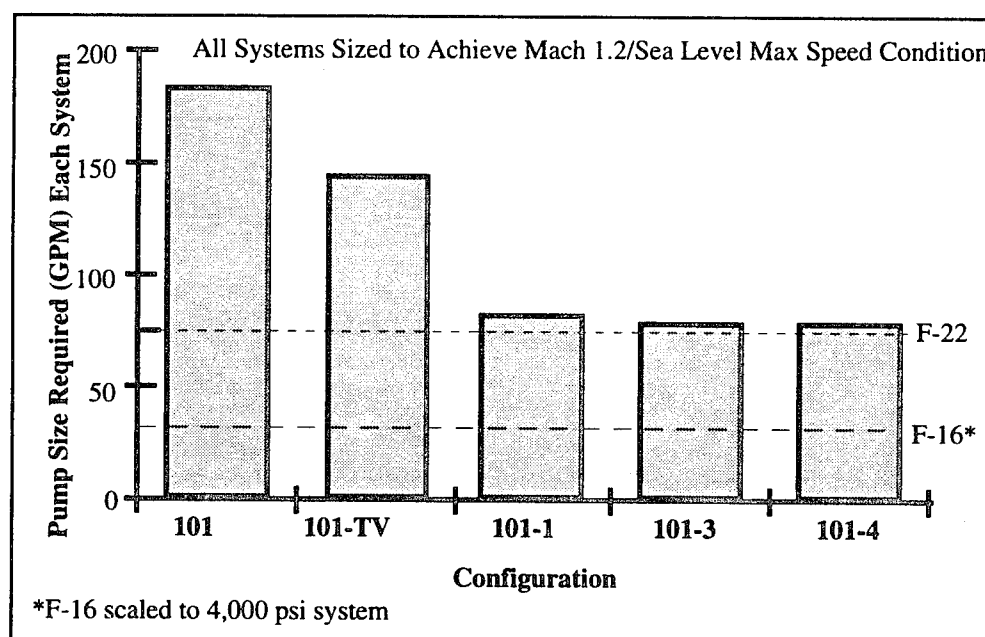


Figure 7-6 Hydraulic Pump Size Requirements

Actuators were sized by assuming horn lengths for each control surface and using the hinge moment requirements defined in Table 7-1. Table 7-4 shows actuator sizes for the aerodynamic surfaces on each configuration. Rotary power drive units (PDU) are used for the LEF actuation system, and are not called out in the table. Thrust vectoring actuators are part of the nozzle system architecture specified by the engine manufacturer.

*Table 7-4 Control Surface Actuator Requirements**Configuration 101*

Control Surface	System 1 Displacement (in ³)	System 2 Displacement (in ³)	Stroke (in.)	Rod Diameter (in)	Piston Diameter (in)
Elevon	78.5	78.5	6.0	1.50	3.50
Pitch Flap	---	52.4	4.0	1.25	3.15
IB Spoiler	170.7	170.7	6.0	1.75	4.98
OB Spoiler	170.7	170.7	6.0	1.75	4.98
Clamshell	---	66.5	4.0	2.00	3.82
LEF	Rotary PDU	---	---	---	---

Configuration 101-TV

Elevon	78.5	78.5	6.0	1.50	3.50
Pitch Flap	52.4	---	4.0	1.25	3.15
IB Spoiler	170.7	170.7	6.0	1.75	4.98
OB Spoiler	---	69.6	5.0	1.25	3.56
LEF	Rotary PDU	---	---	---	---

Configuration 101-1

Elevon	78.5	78.5	6.0	1.50	3.50
Pitch Flap	52.4	---	4.0	1.25	3.15
IB SSD	24.2	24.2	4.0	1.25	2.33
OB SSD	---	21.4	3.0	1.00	2.35

Configuration 101-3

Elevon	78.5	78.5	6.0	1.50	3.50
Pitch Flap	52.4	---	4.0	1.25	3.15
AMT	7.9	7.9	2.5	1.00	1.88
SSD	---	20.3	3.0	1.00	2.30
OB DLEF	Rotary PDU	---	---	---	---

Configuration 101-4

Elevon	99.1	99.1	6.0	1.75	3.96
Pitch Flap	18.9	---	3.0	1.00	2.24
AMT	39.1	39.1	5.0	1.25	3.14

Figure 7-7 shows the total flight control system actuator displacement requirements for each configuration. Utility system actuators (i.e., landing gear, weapons bay, etc.) are neglected. Replacement of the spoilers with AMT or SSD for high-speed yaw control sig-

nificantly reduced the overall hydraulic requirements of the study configurations. For comparative purposes, the total F-16 flight control actuator displacement is 108 in³ for each hydraulic system.

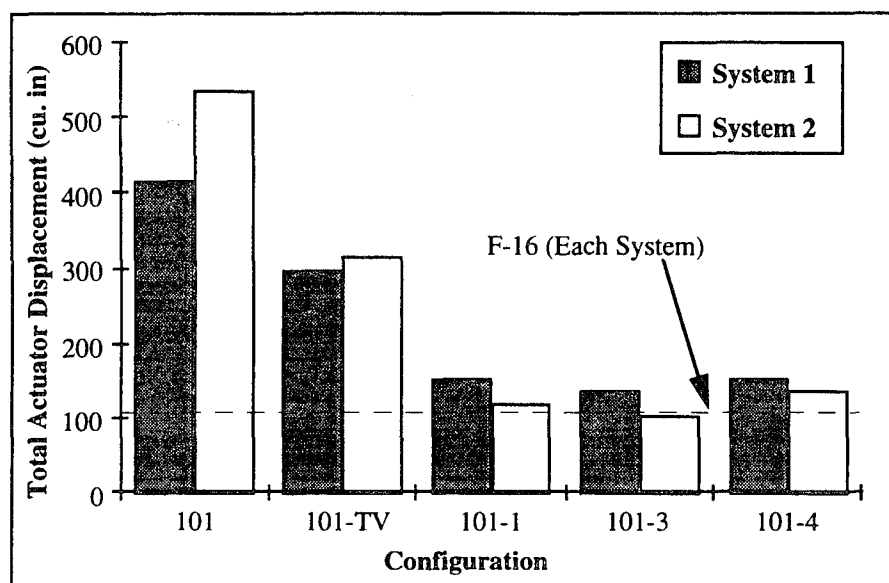


Figure 7-7 Total Flight Control Actuator Displacement -- Each System

Summary of Hydraulic System Requirements Study

1. Configuration 101 flows and component sizes are very large. Providing this level of hydraulic power in an aircraft of this size would be difficult due to volume and extraction requirements. Significant weight penalty is also associated with this configuration. The configuration was modified to achieve a better flow rate balance between the two systems by making the outboard spoilers dual-redundant; however, the power level requirement could not be reduced.
2. Configuration 101-TV flows and component sizes are less than those of 101; although, they are still relatively large and have significant volume, power extraction and weight penalties.
3. Configurations 101-1, 101-3 and 101-4 have similar flows and component sizes. Although larger than those of contemporary aircraft, they present fewer penalties and challenges than the foregoing baseline configurations.

7.3 Structural Integration

The following are general comments regarding structural integration of the various innovative control concepts. All five control concepts (i.e., AMT, DRUD, LSP, DLEF, SSD) are described for completeness.

7.3.1 *Differential Leading Edge Flaps*

Advantages:

- (1) With reasonable deflections (e.g., -5 deg to +30 deg), DLEF are easy to integrate into the wing structure, as the LEF and rotary hinges are outside the wing box.
- (2) Rotary hinges provide a stiff attachment for the LEF.

Disadvantages:

- (1) Large deflections make for complicated seals along the hingeline. A secondary door/seal arrangement that moves out of the way will probably be required.
- (2) Rotary hinges, because of their gear ratios, tend to be slow moving.
- (3) As the wing bends under load, the spanwise deflection of the LEF produces a natural tendency to bind. Splitting the LEF into multiple pieces helps alleviate this problem.
- (4) End caps are required for RCS purposes making integration difficult.

7.3.2 *All Moving Wing Tip*

Advantages:

- (1) Easy to build.
- (2) Simple Mechanism.

Disadvantages:

- (1) Flutter is a concern with any all-moving surface.
- (2) AMT is hung out on the end of the wing. What is the weight penalty of making the wing stiff enough?

- (3) Structural and RCS integration of the trunion and actuation system is difficult in the thin section of the tip.

7.3.3 Spoilers & Spoiler-Slot Deflectors

Advantages:

- (1) Actuators can be mounted within the spoiler cavity using the spoiler itself as the actuator access cover; thereby simplifying the wing skin design.
- (2) Slot deflectors can be mechanically linked to the spoilers to reduce the total hinge moment of the system.

Disadvantages:

- (1) The spoiler cavity cuts out a large area of the wing box resulting in inefficient load carriage by the wing skins.
- (2) Slot deflectors cut a hole through both the upper and lower wing skins.

7.3.4 Deployable Rudder

Advantages:

- (1) If built into the fuselage structure, the hole cut through the skin will have less impact than a similar hole cut through a wing skin. This is because fuselage loads are typically carried by bulkheads and longerons; wing loads are carried by the skins.
- (2) Using the deployable rudder as a large fuselage access cover could reduce the number of smaller exposed covers, simplifying the fuselage skin design.

Disadvantages:

- (1) Current fuselage contour will force the rudder to be shaped like a potato chip. It is difficult to construct a stiff curvy part.
- (2) Large gooseneck hinges will be required.
- (3) Acoustic effects in the cavity under the surface may create additional design challenges.

Considering these technical challenges, preliminary structural arrangements for the eight original control configurations are shown in Figures 7-8 through 7-15 (i.e., 101, 101-TV, and 101-1 through 101-6). Fuel boundaries are shown as hashed lines. Double-walled structural members detail where major skin panels are joined.

As a result of the weapons and landing gear bay locations, the forward-half of the airplane is built essentially like a fuselage. The only wing-like structure is aft of the main landing gear, and outboard of the wing attach fittings. Since the controls primarily impact the wing structure and fuselage aft of the main landing gear bulkhead, this structure was studied in detail.

These preliminary structural arrangements were used for the screening study described in Section 5. After the three favored innovative control suites were selected, the structural design was refined, and control surface integration addressed in greater detail. Comments pertaining to the initial integration analysis are detailed below.

7.3.5 Configuration 101

The spoilers and clamshells created the majority of the structural problems for this configuration. The size of the spoilers and their actuators required an aft beam between the spoilers and elevons to carry wing loads around the spoiler cut-outs. The spoiler hinge moment requirements create the need for parallel actuators to fit within the wing contour.

As designed, the clamshell will be very difficult to integrate. The wing is extremely thin in this area, and may require thickening to integrate the clamshell. Fuel boundaries around the clamshell and spoiler are complicated.

The elevon actuator eliminates any direct load paths inboard from the clamshell area. The continuation of the rear spar from the clamshell region will likely terminate at the outboard elevon support structure. That, coupled with the reduced area wing box due to the spoiler, could make the clamshell and outboard portion of the LEF ineffective due to aeroelasticity.

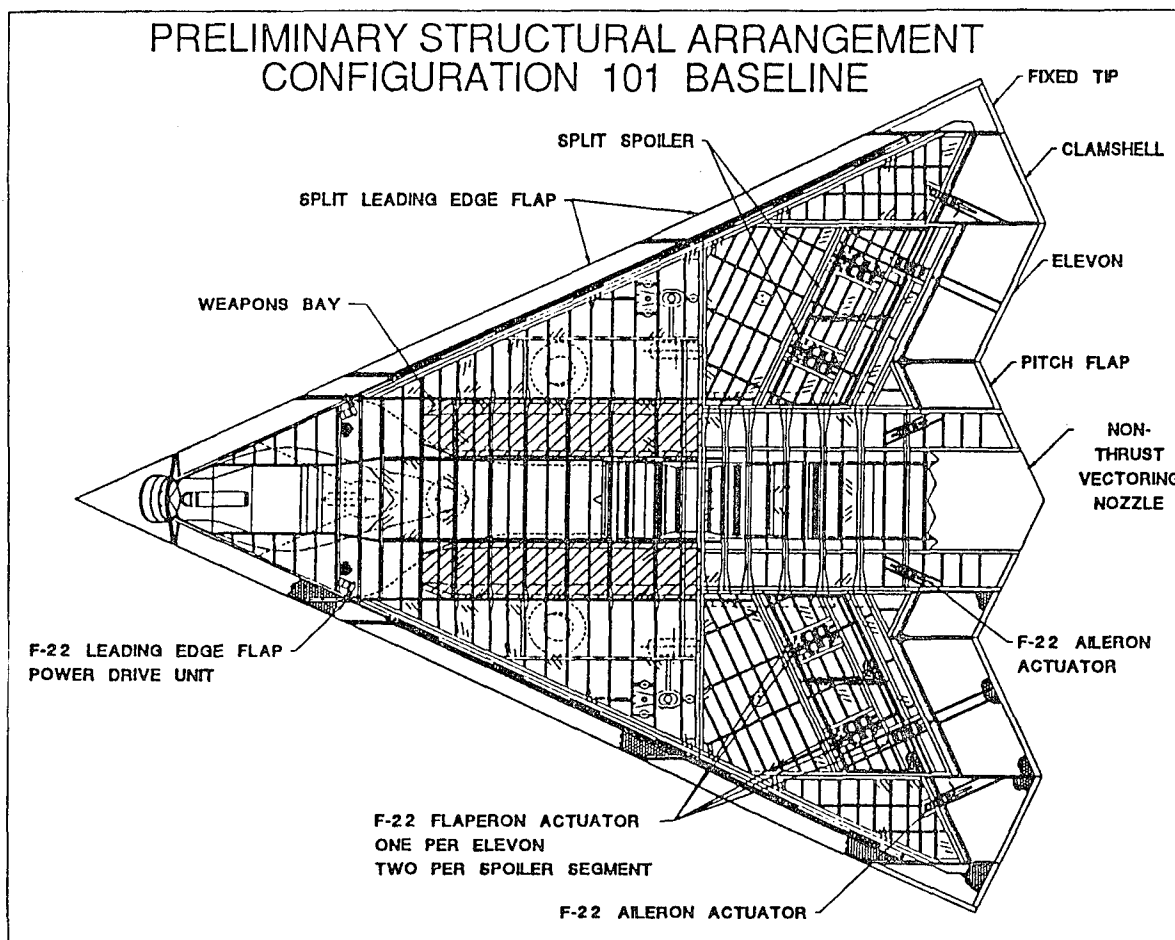


Figure 7-8 Configuration 101 Internal Arrangement

7.3.6 Configuration 101-TV

Deletion of the clamshell greatly simplified the wing-tip structure. Reduction of the outboard spoiler hinge moment requirements simplified the actuator integration as well. The inboard spoiler is located in a relatively thick portion of the wing, and large actuators can be accommodated more easily. The upper wing skin cut-outs required by the spoilers still complicates the load paths in the wing box. Fuel sealing is complicated around the spoiler cutouts.

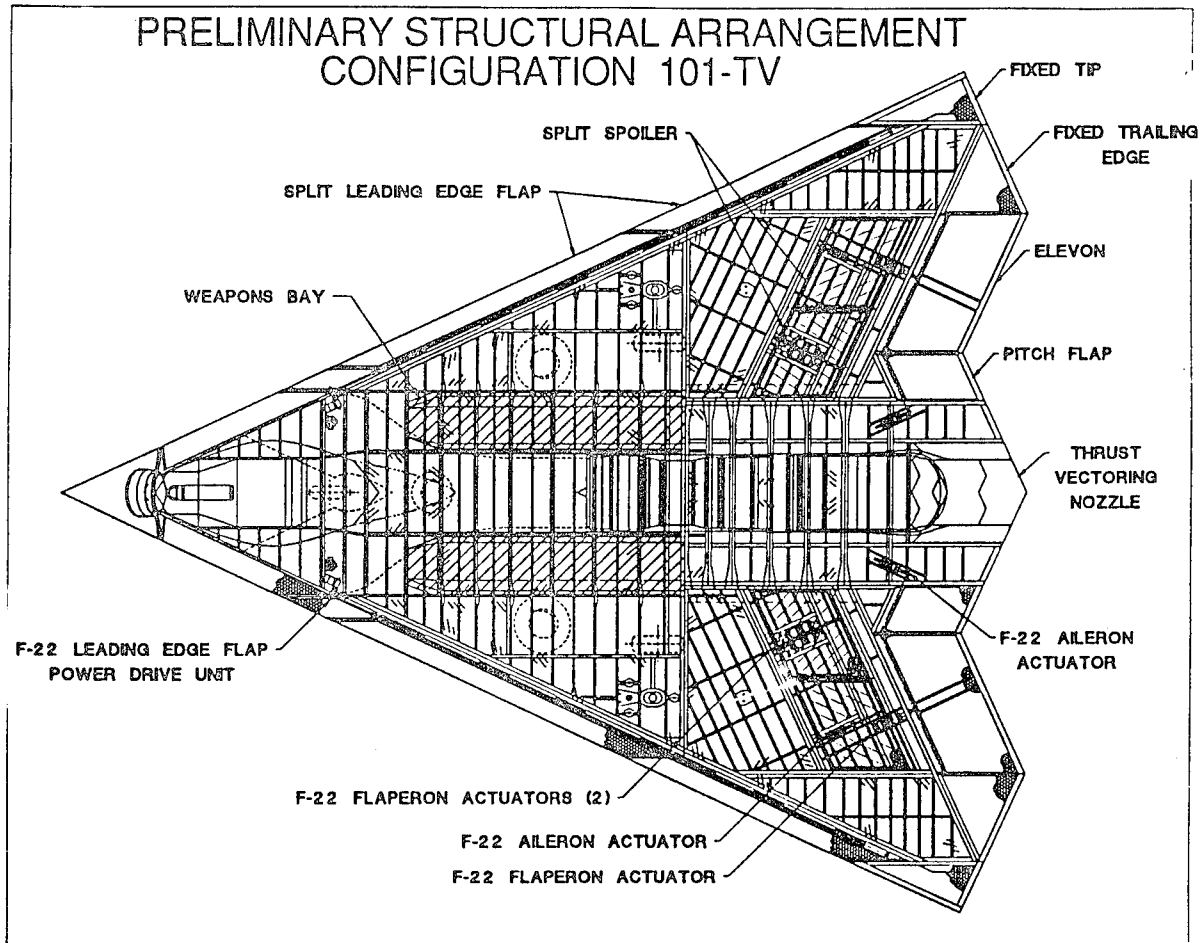


Figure 7-9 Configuration 101-TV Internal Arrangement

7.3.7 Configuration 101-1

Removal of the LEF and its drive mechanism simplifies the leading edge structure. The smaller SSD arrangement provides more room for the aft-spar between the SSD and elevon; however, the hole cut in the lower wing skin will create additional weight penalties.

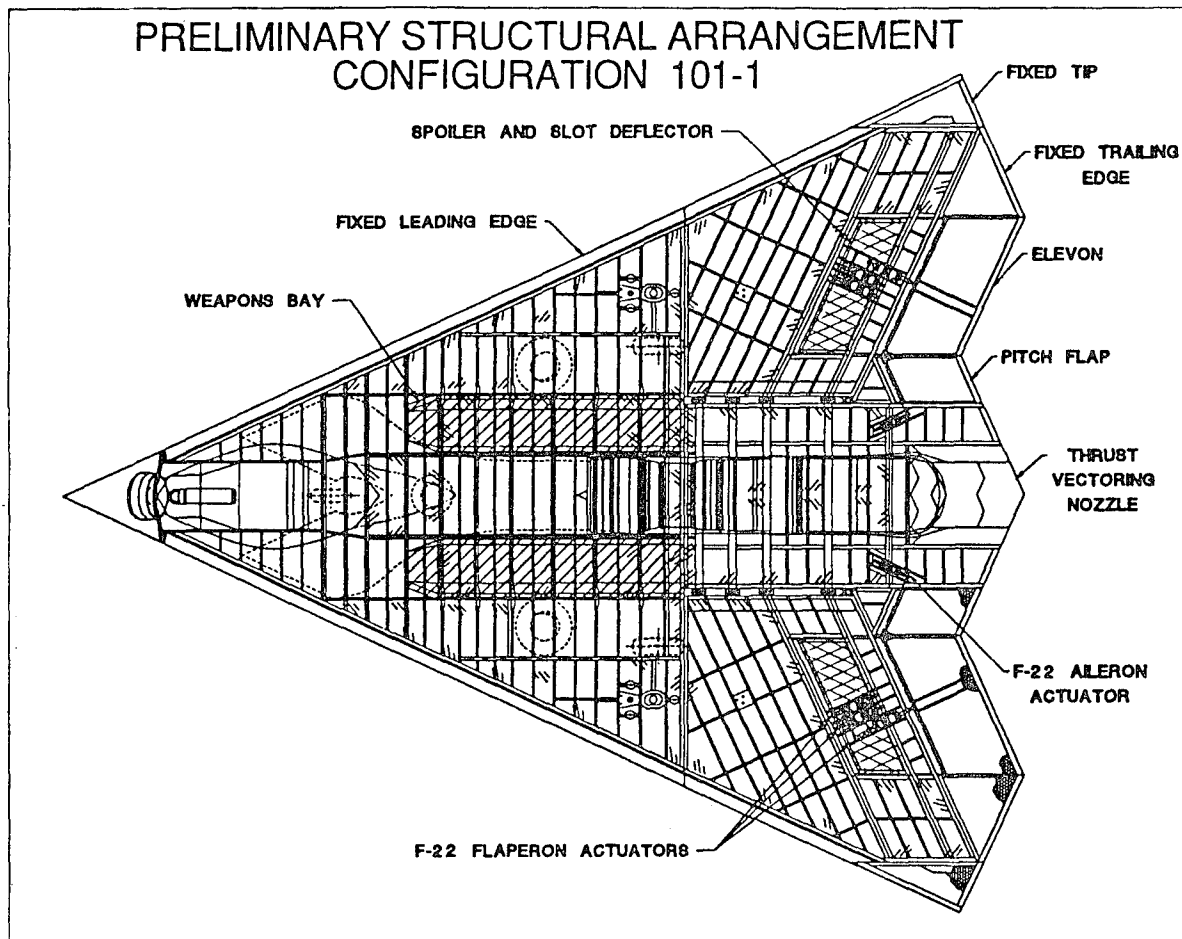


Figure 7-10 Configuration 101-1 Internal Arrangement

7.3.8 Configuration 101-2

The fuselage structure was extended out into the wing to carry the deployable rudder. This also minimizes the impact of the large hole cut out by the rudder. Shear fittings replaced the tension fittings at the wing attach points due to the reduced local wing thickness and the proximity of the rudder. Shear fittings require tighter wing tooling tolerances making the wing more difficult and costly to build.

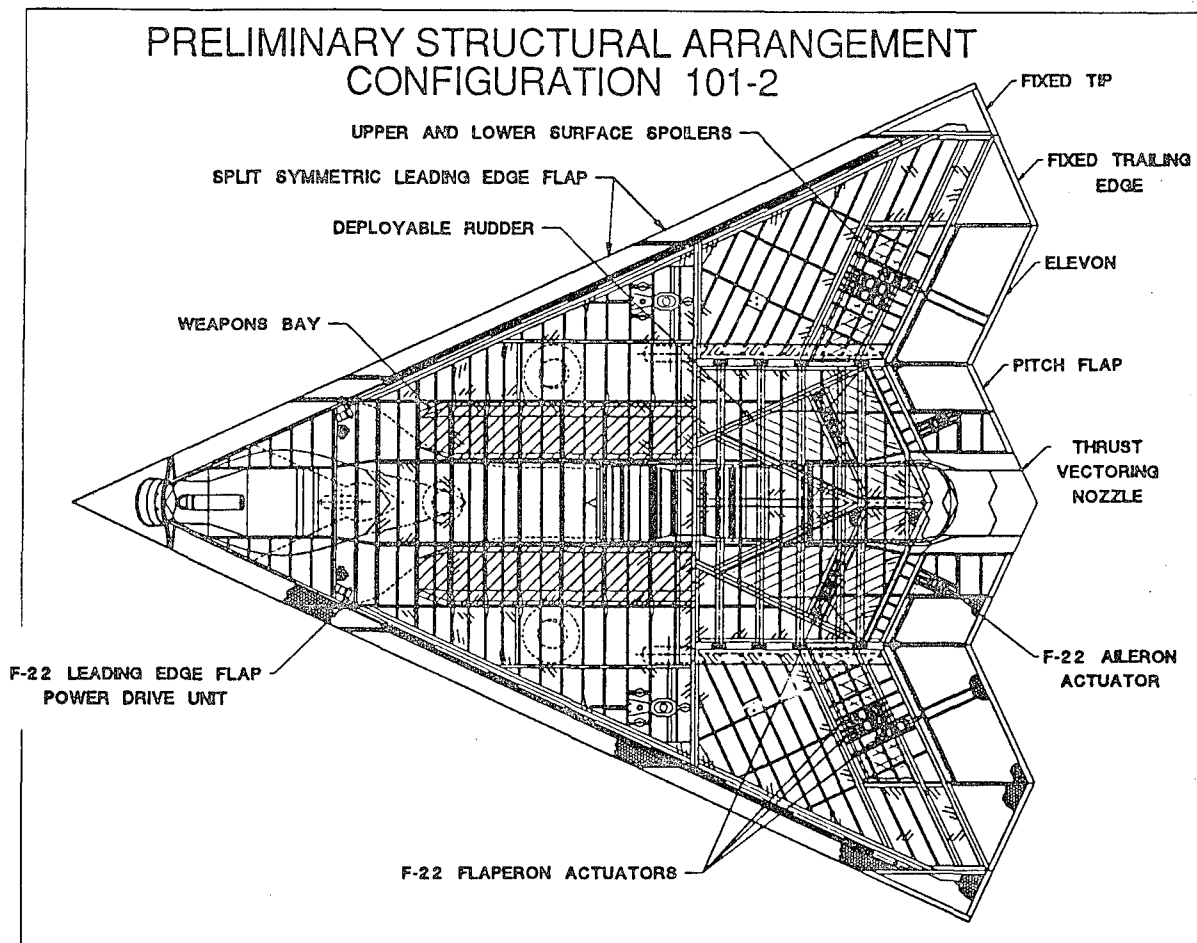


Figure 7-11 Configuration 101-2 Internal Arrangement

7.3.9 Configuration 101-3

The AMT, SSD and outboard LEF clutter the outboard wing panel structure and make fuel sealing difficult. It may not be possible to carry fuel in the outboard sections of the wing anyway. The stiffness required of the AMT will be challenging considering the SSD and LEF arrangements. Two PDU's are required to drive the differential LEF system.

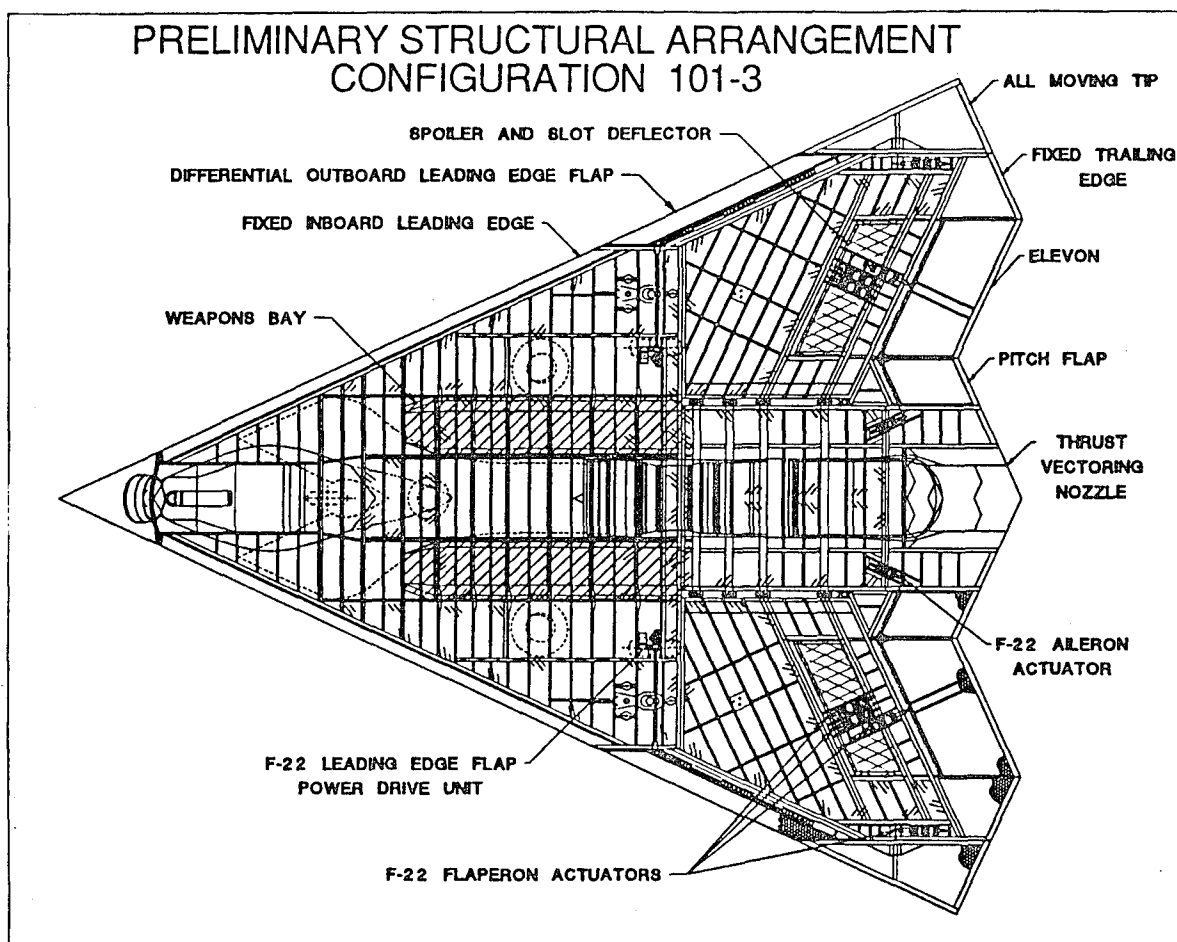


Figure 7-12 Configuration 101-3 Internal Arrangement

7.3.10 Configuration 101-4

Removal of the spoilers and LEF makes fuel sealing and wing box construction very straight-forward. The large tip will require a large pivot trunion -- comparable to a horizontal tail. The difficulty lies in that this "tail" attaches to very thin wing structure. A large fairing or local wing thickness change will be required to cover the trunion and actuator.

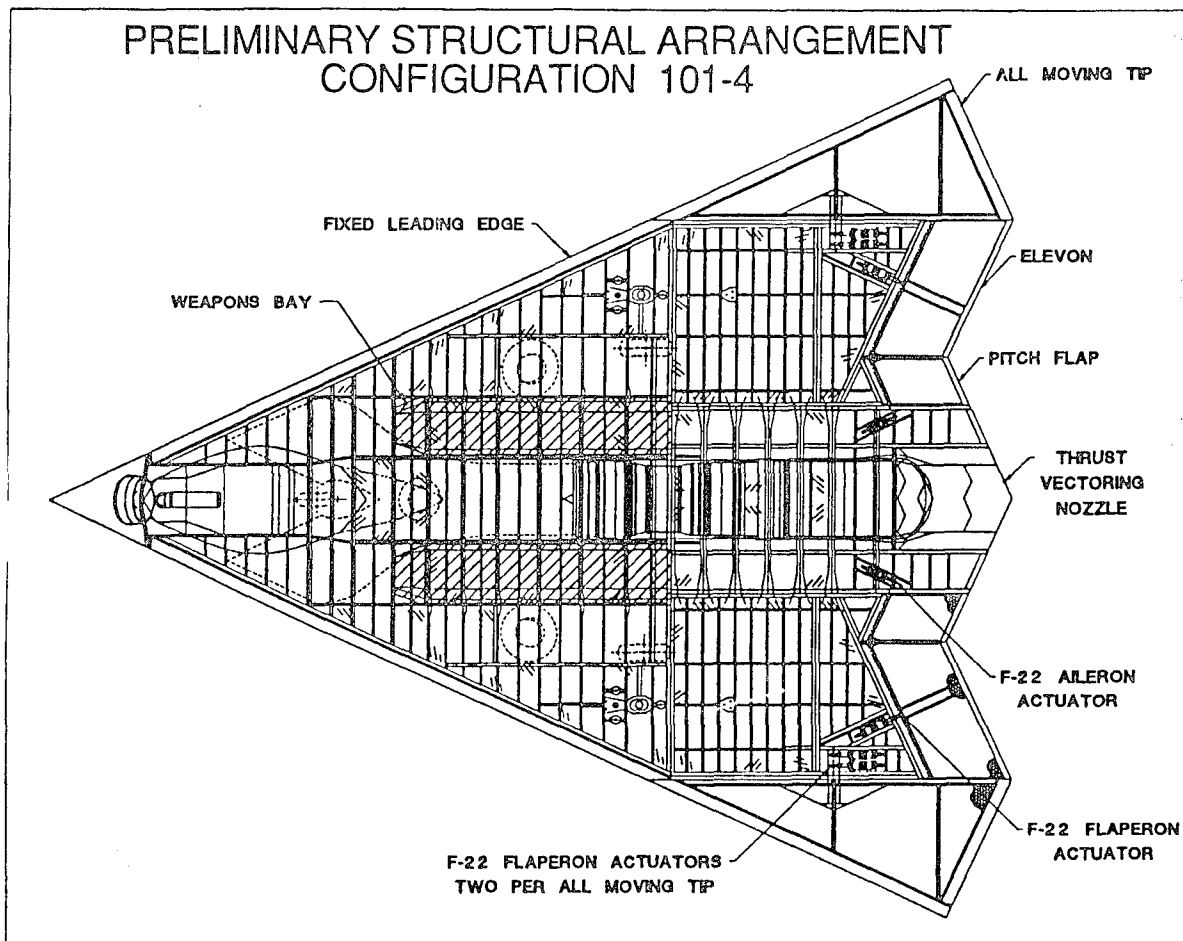


Figure 7-13 Configuration 101-4 Internal Arrangement

7.3.11 Configuration 101-5

Concerns are similar to 101-2. The differential outboard LEF requires two additional PDU's located inboard, similar to 101-3. The deletion of the spoilers and/or SSD's from this configuration simplify the wing box. Shear fittings are again required to accommodate the deployable rudder.

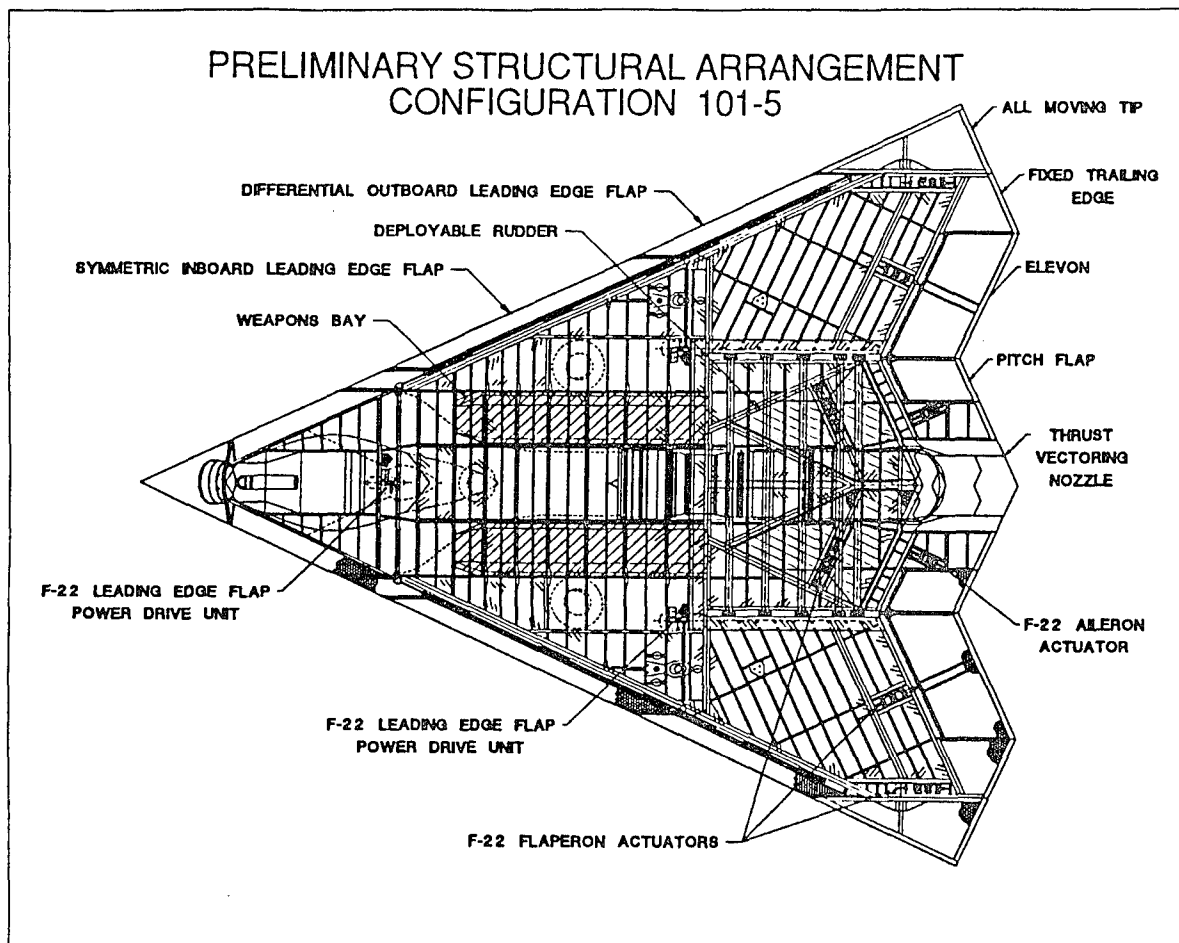


Figure 7-14 Configuration 101-5 Internal Arrangement

7.3.12 Configuration 101-6

The removal of the upper surface spoiler provides a whole wing skin through which to carry wing loads; however, the lower surface spoiler requires a significant cut-out in the lower skin. Deployable rudder integration is the same as 101-2 and 101-5, only the rudders are larger. The differential LEF integration is the same as 101-3 and 101-5.

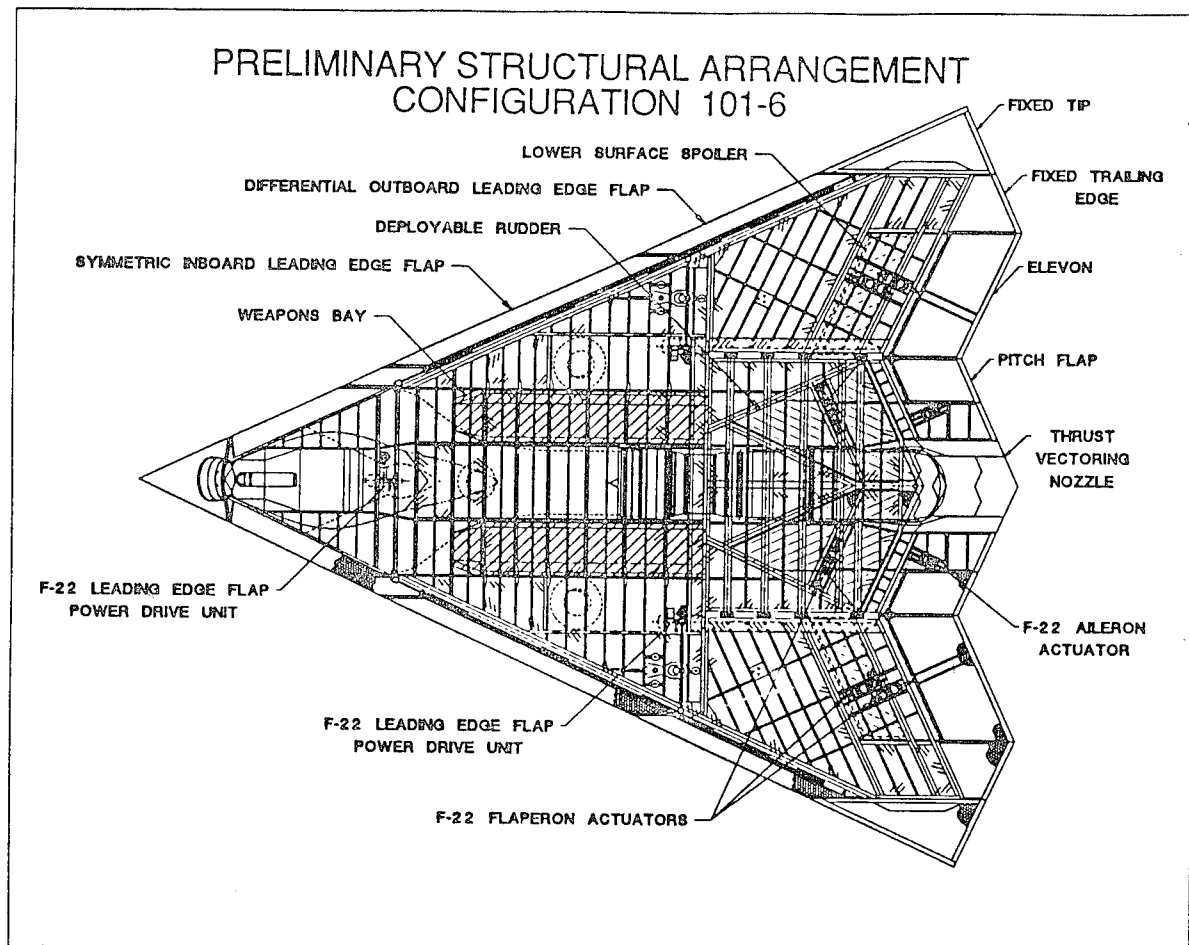


Figure 7-15 Configuration 101-6 Internal Arrangement

7.4 Detailed Structural Assessment of Selected Configurations

After selection of the favored configurations, structural and actuator integration was studied in greater detail for configurations 101-TV, 101-1, 101-3 and 101-4. The following discussion describes changes made to the structural layouts during this phase.

7.4.1 General Arrangement Comments

After studying the original layouts, it was observed that the back-up structure (hardbacks) for the actuators were too close to the actuators themselves. Clearance was provided around the actuator for hydraulic tube routing. Initially, none of the actuator valves were shown. Valves can be located directly on the actuator, or remotely depending on space constraints.

To improve pitch flap stiffness, the pitch flap actuator was moved outboard such that it actuated directly on the pitch flap spar. The current pitch flap actuator is a conventional installation lying within the wing contour; no fairing is required.

The elevon hinge moments are of such magnitude that significant backup structure will be required. On all of the configurations except 101-4, the actuator was shifted from its previous location (under the spoiler) inboard to improve stiffness, and provide greater structural depth for elevon actuator loads. The final solution was to locate the elevon actuator externally to avoid cutting wing skins and spars. It is a conventional installation within a large fairing.

On all configurations, an axisymmetric LO vectoring nozzle was included in place of the 2-D nozzle arrangement shown in the original drawings. This was done primarily to save weight. No attempt was made to improve the integration of the nozzle with the aft fuselage. As a result, the aft fuselage/nozzle interface appears rough. Additional work could improve the nozzle interface, but was beyond the scope required to generate the needed aerodynamic control integration impacts.

Note that all of the current internal arrangements show shear fittings for the wing attachment. With the absence of the deployable rudder, conventional tension fittings could have been used as well.

The only other major change was to move the main landing gear aft to improve ground clearance during takeoff and landing and improve the load distribution between the nose-gear and main gear.

7.4.2 Final Structural Assessment

The following discussions pertain to specific changes made to Configurations 101-TV, 101-1, 101-3 and 101-4.

Configuration 101-TV

A transverse scissors linkage replaced the original spoiler actuator arrangement to avoid disturbing the spars underneath the spoiler. The actuators and linkage lie between the

spars, preserving the understructure. Four wing attach points tie the wing to the fuselage. Note that the fuselage bulkhead adjacent to the inboard spoiler actuator does not have an attachment fitting. The spoiler arrangement negated the usefulness of the fitting. See Figure 7-16.

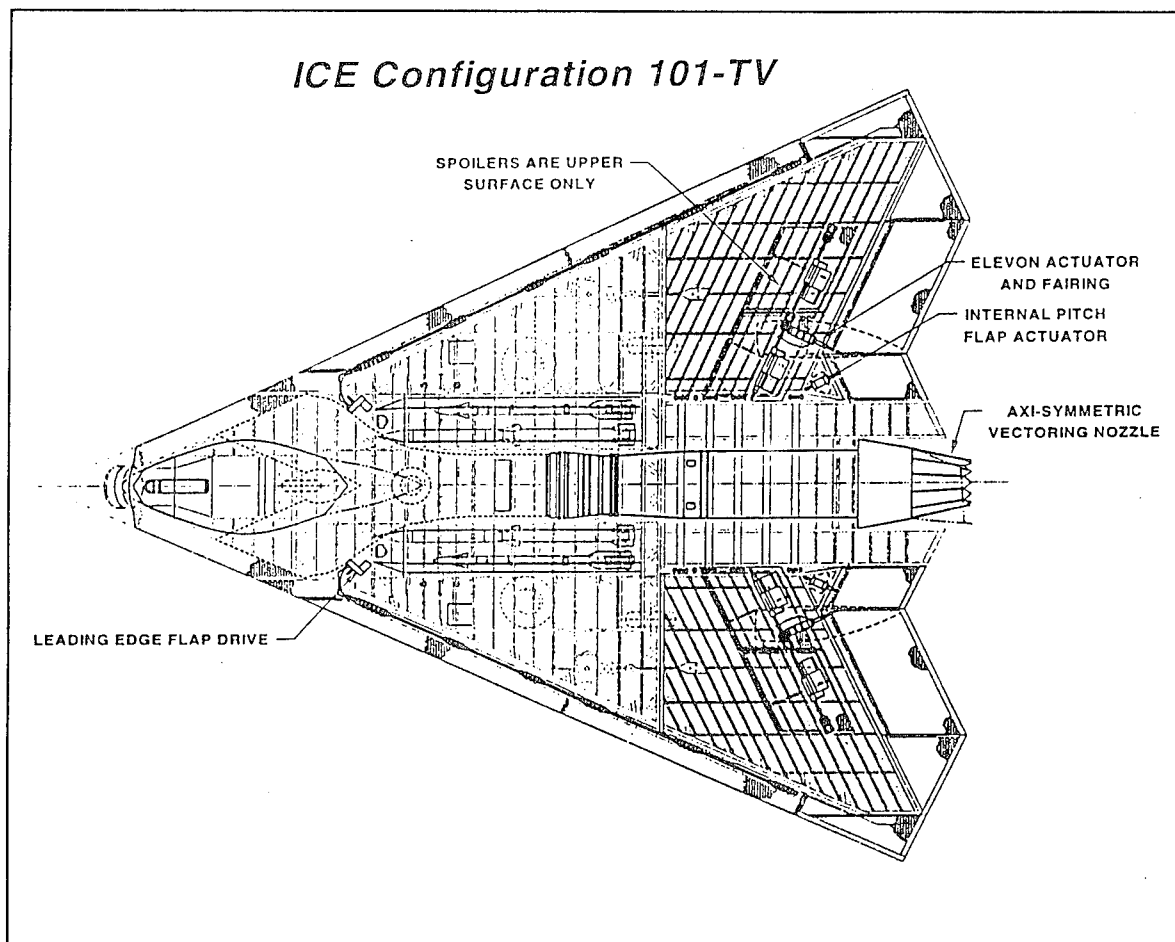


Figure 7-16 Final Configuration 101-TV Internal Arrangement

Configuration 101-1

The SSD's were shifted outboard to provide clearance for the elevon actuator and fairing. Four SSD actuation concepts were investigated as part of the ICE study (see below). The concept shown in this configuration uses a PDU and associated rotary actuator gear boxes. Unfortunately, such a design cuts through all of the wing spars in this region, and contributes to significant blockage within the slot. The effects of partial slot blockage on

SSD performance are unknown. Note that five wing attachment fittings are included with this arrangement. See Figure 7-17.

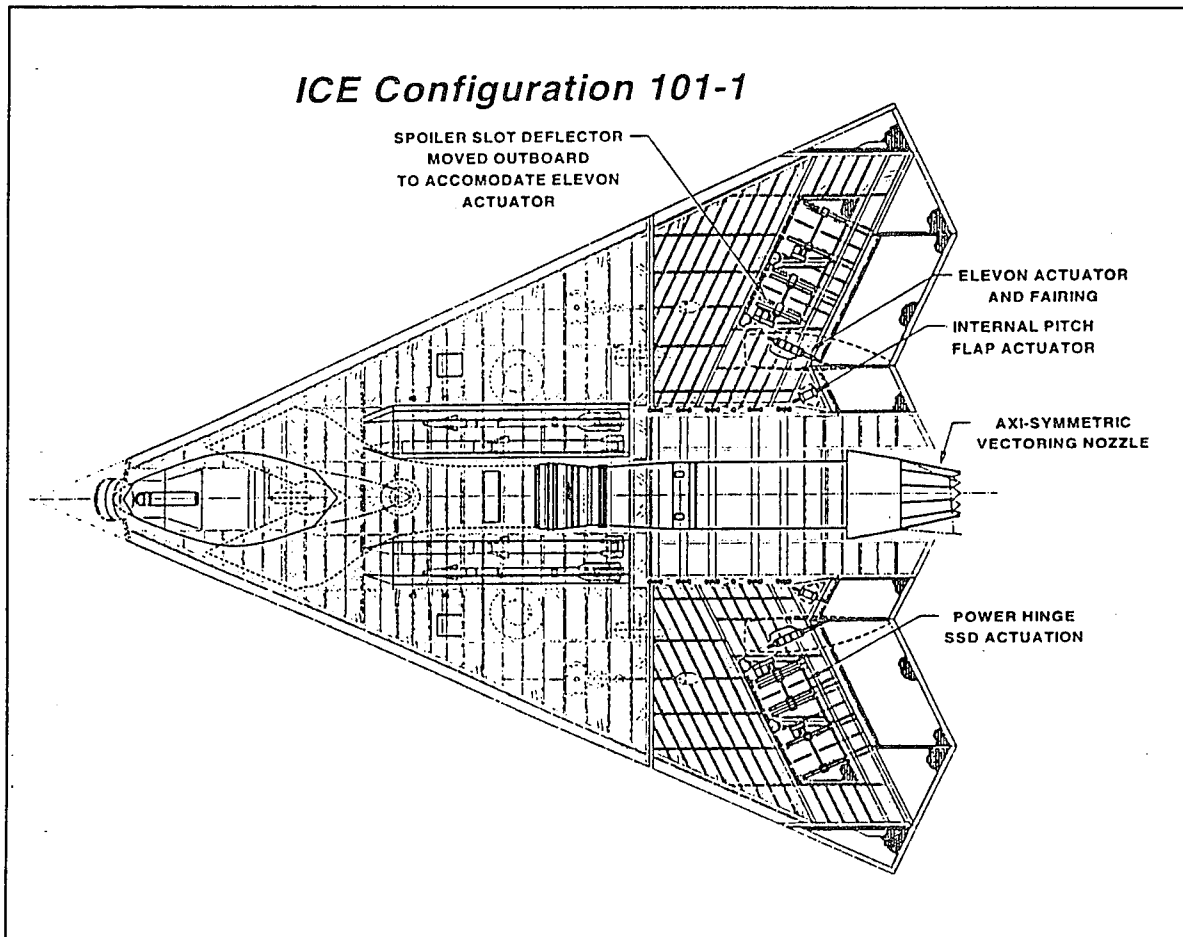


Figure 7-17 Final Configuration 101-1 Internal Arrangement

Configuration 101-3

The SSD's were shifted outboard similar to Configuration 101-1. Note the SSD size difference between this configuration and 101-1. The actuation system shown uses a scissors arrangement similar to the spoiler actuation system described for 101-TV and detailed below (Section 7.4.3). This arrangement preserves the wing spars running through the SSD region by placing the actuator and linkages between spar bays. The AMT actuator is mounted externally in a fairing. The DLEF PDU's were moved outboard, closer to the LEF than the original design. Five shear fittings provide the wing/fuselage interface. See Figure 7-18.

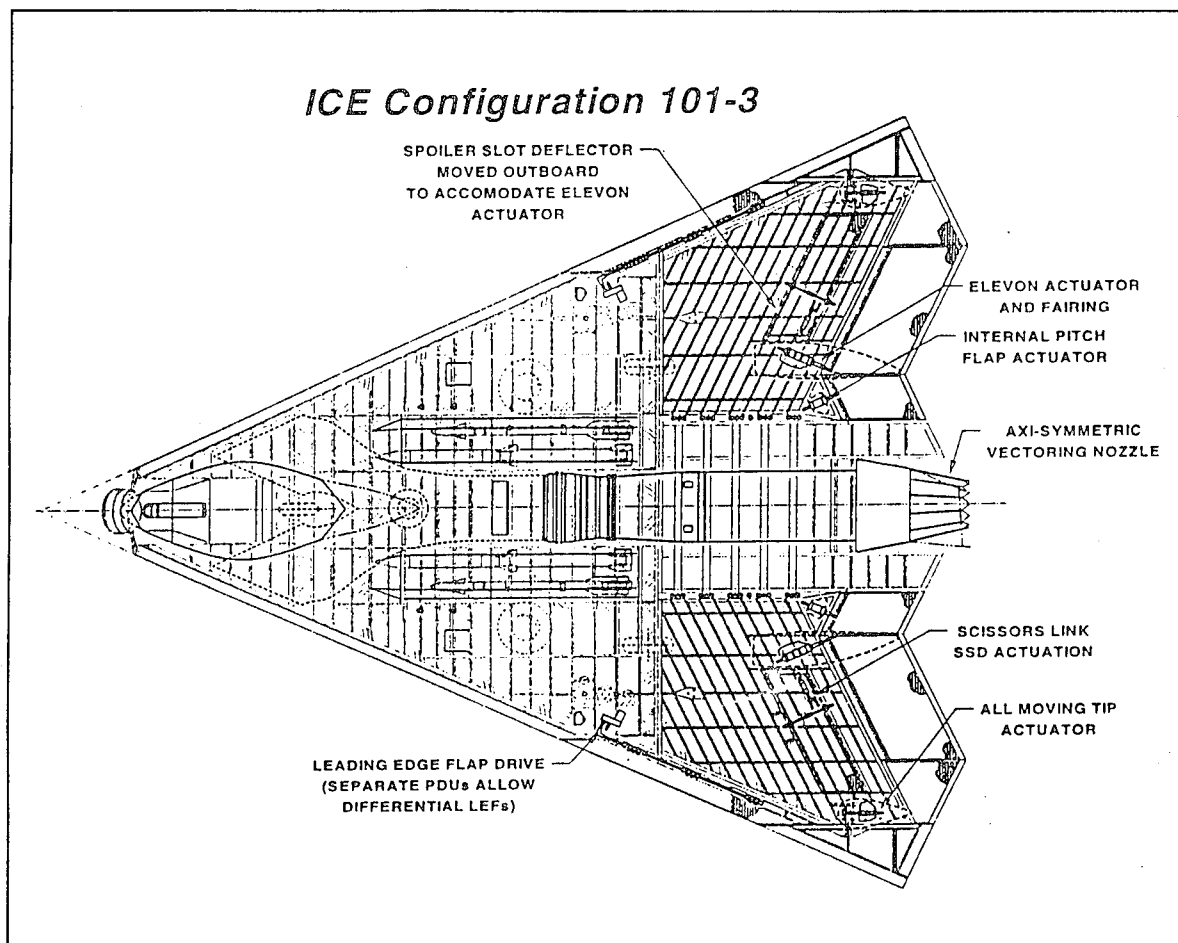


Figure 7-18 Final Configuration 101-3 Internal Arrangement

Configuration 101-4

The elevon actuator was moved outboard to lie close to the AMT actuator. It was thought that a single large fairing could cover both actuators. Later analysis indicated that an inboard location of the elevon actuator would be preferable because of the impact of the large fairing on the configuration's area curve, and the resulting transonic drag impact. The inboard actuator location also provides a stiffer elevon installation. See Figure 7-19.

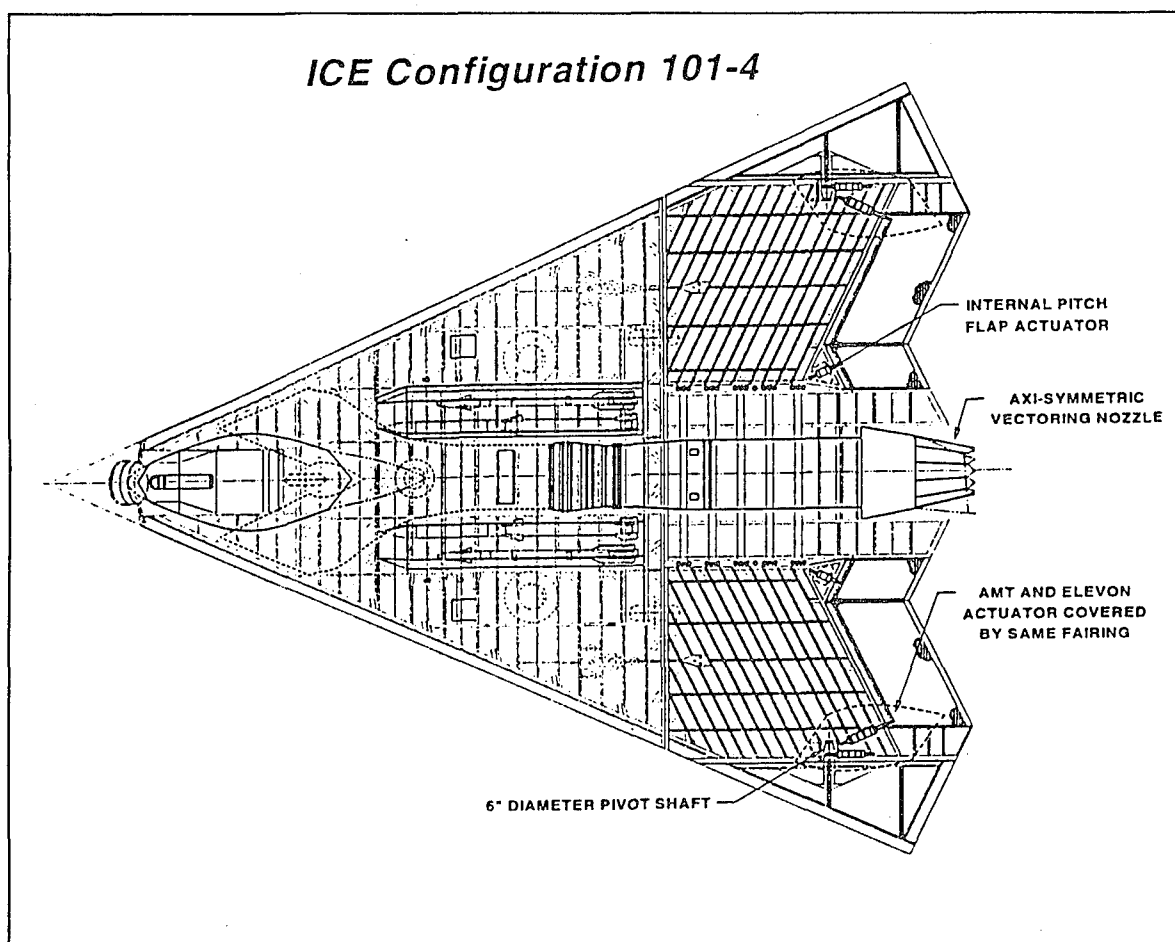


Figure 7-19 Final Configuration 101-4 Internal Arrangement

The AMT pivot trunion was sized based on loads predicted using a preliminary design analysis code. Not surprisingly, the loads are comparable to those found on a horizontal tail. The primary difference is that there is less structural depth available for the pivot shaft integration than for a typical horizontal tail. A 6 inch Titanium shaft was designed to carry the AMT loads into the wing (Figure 7-20).

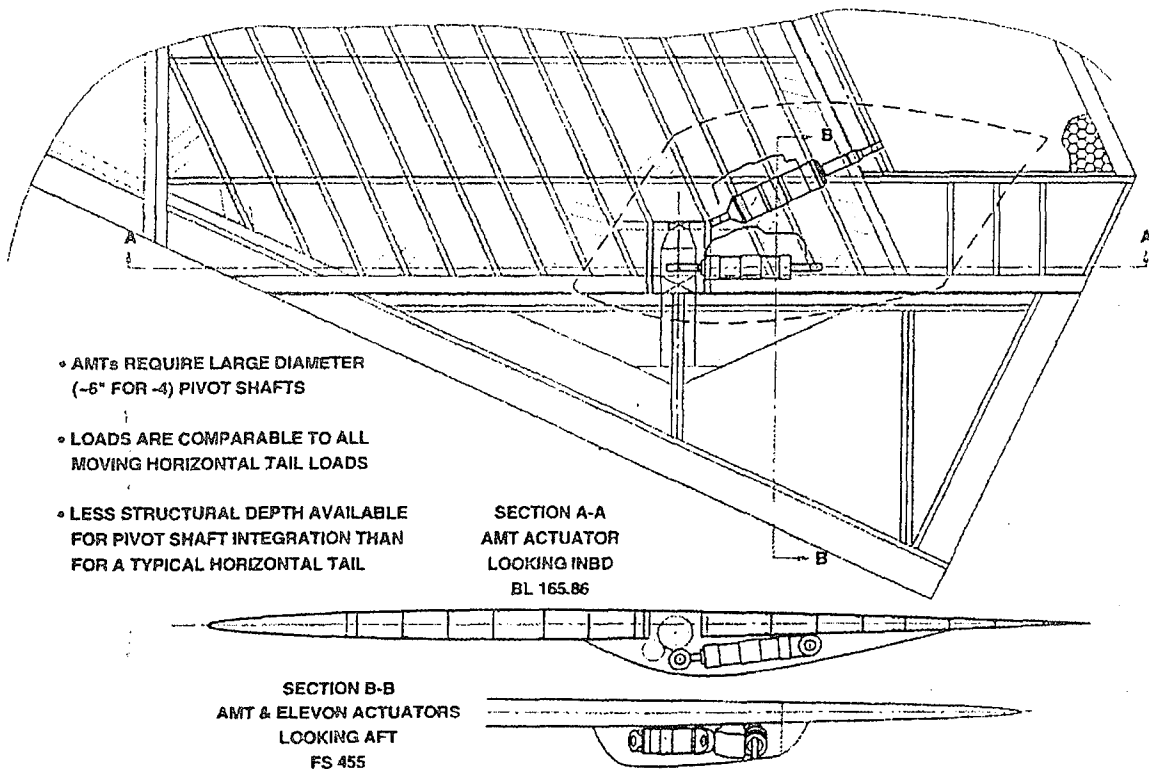


Figure 7-20 Configuration 101-4 AMT Integration

7.4.3 SSD Actuation Concepts

Three concepts for SSD actuation were investigated as a part of the ICE study. A fourth concept was discovered when the spoiler-slot-deflectors on the XF-107 were examined at the United States Air Force Museum in Dayton, Ohio.

Figure 7-21 shows the three basic concepts developed during the course of the ICE research. The first uses a scissors link actuation with a 4-bar interconnect between the spoiler and the deflector. Next, the same linkage is used with a linear actuator. Finally, a PDU with rotary actuator drives was investigated. The first and third concepts were shown above in Configurations 101-3 and 101-1, respectively. Each concept is described in greater detail, below.

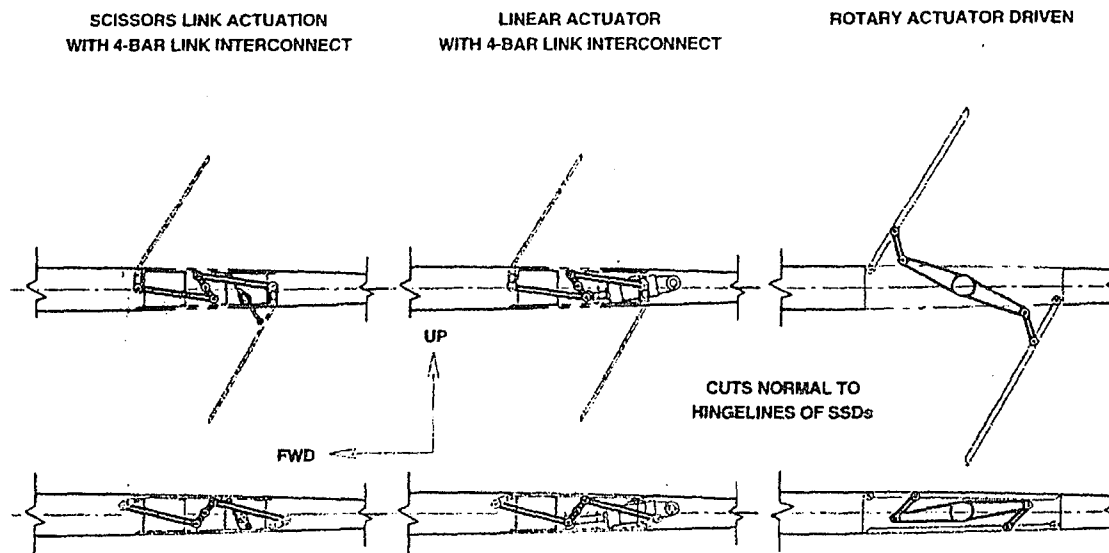


Figure 7-21 Three SSD Actuation Alternatives

The scissors link actuation was developed to avoid disturbing any of the wing substructure. It was assumed that the partial blockage of the slot by structure and actuator would have negligible impacts on the SSD performance. Further testing is warranted to determine if this is the case. Figure 7-22 shows details of the scissors link concept.

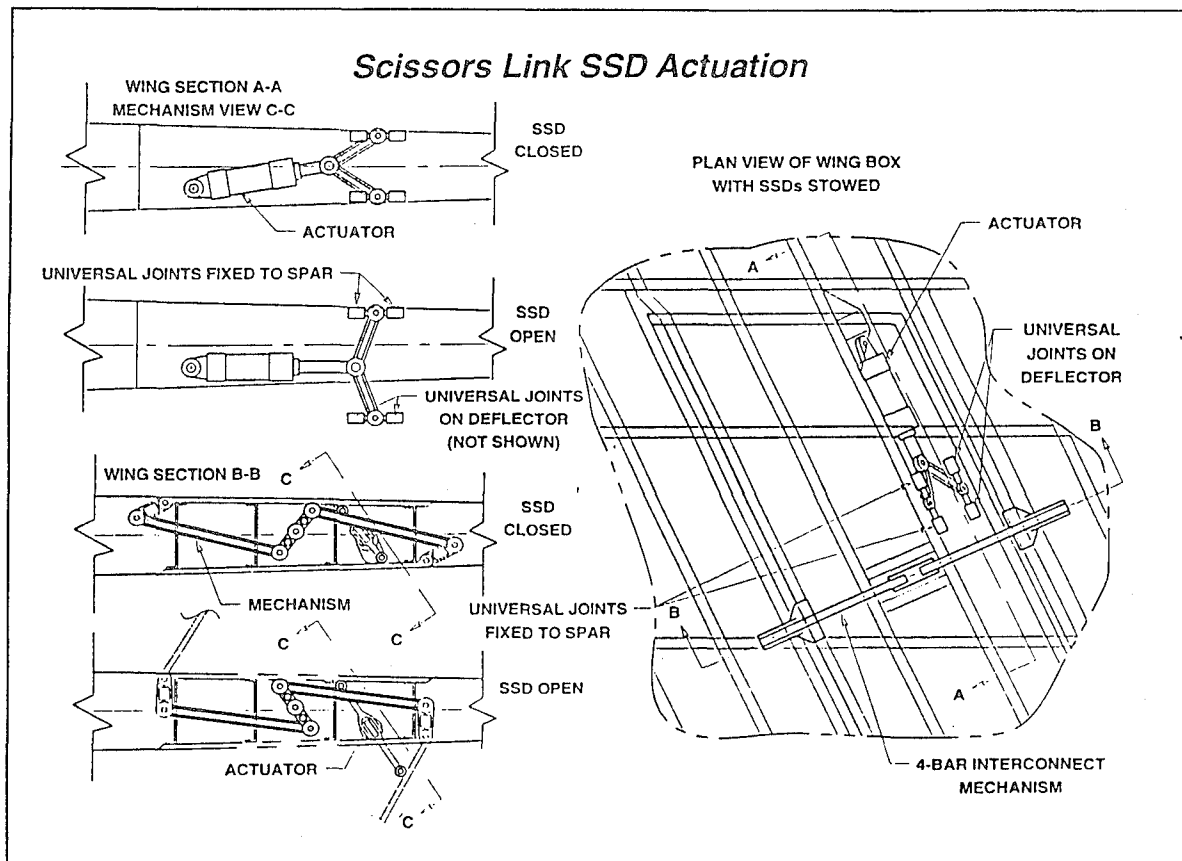


Figure 7-22 Scissors Link SSD Actuation

The actuator is placed parallel to and between the wing spars. Universal joints are fixed at each end of the scissors linkage, with one end attached to rigid spar structure, and the other to the deflector. As the actuator extends, the scissors are driven apart, opening the deflector. The spoiler is connected to the deflector through four-bar linkages, and moves together with the deflector.

The advantages of such an arrangement are: (1) the spar caps need not be cut, although holes must be provided through the spar webs to feed the linkages; (2) the scissors provide additional mechanical advantage to the system, resulting in a very small actuator requirement. Disadvantages include: (1) high loads in the linkages and at the universal joint fittings; (2) the scissors system is susceptible to out-of-plane deflections resulting in binding.

Figure 7-23 shows the same four-bar linkage system driven by a linear actuator. This system has the advantage over the previous one in that out-of-plane stability is not a concern. A larger actuator is required because the scissors are not available to provide mechanical advantage; furthermore, the large actuator pierces the aft spar shear web resulting in lost structural efficiency. This concept is somewhat of a brute force approach. High loads in the linkages and at the surface attach points are still a concern. Both four-bar systems would result in some "wrapping up" of the control surface at high dynamic pressure conditions (i.e., the actuated edge would deflect more than the free end resulting in reduced control effectiveness).

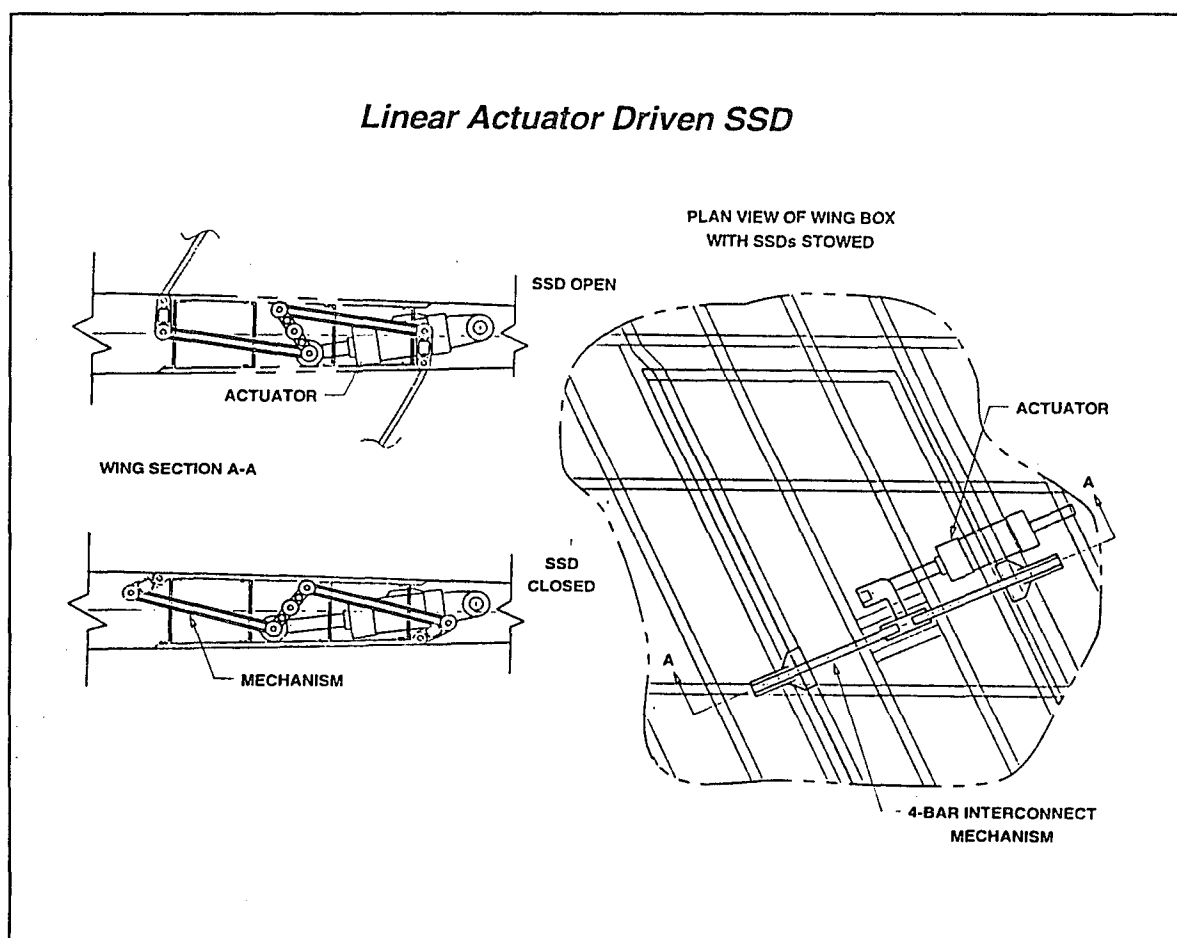


Figure 7-23 Linear Actuator Driven SSD

The rotary actuator driven SSD is shown in Figure 7-24. Unfortunately, this concept requires cutting through all of the spar understructure. This system is very straightforward

in its operation. The rotary drive system is connected directly to the pivot shaft. Large ear pieces drive four-bar links to open the deflector and spoiler. One advantage that it has over the two previous concepts is that multiple actuators can easily be integrated resulting in a stiffer control surface arrangement (i.e., the surface will not suffer as much "wrap up" as with the other concepts).

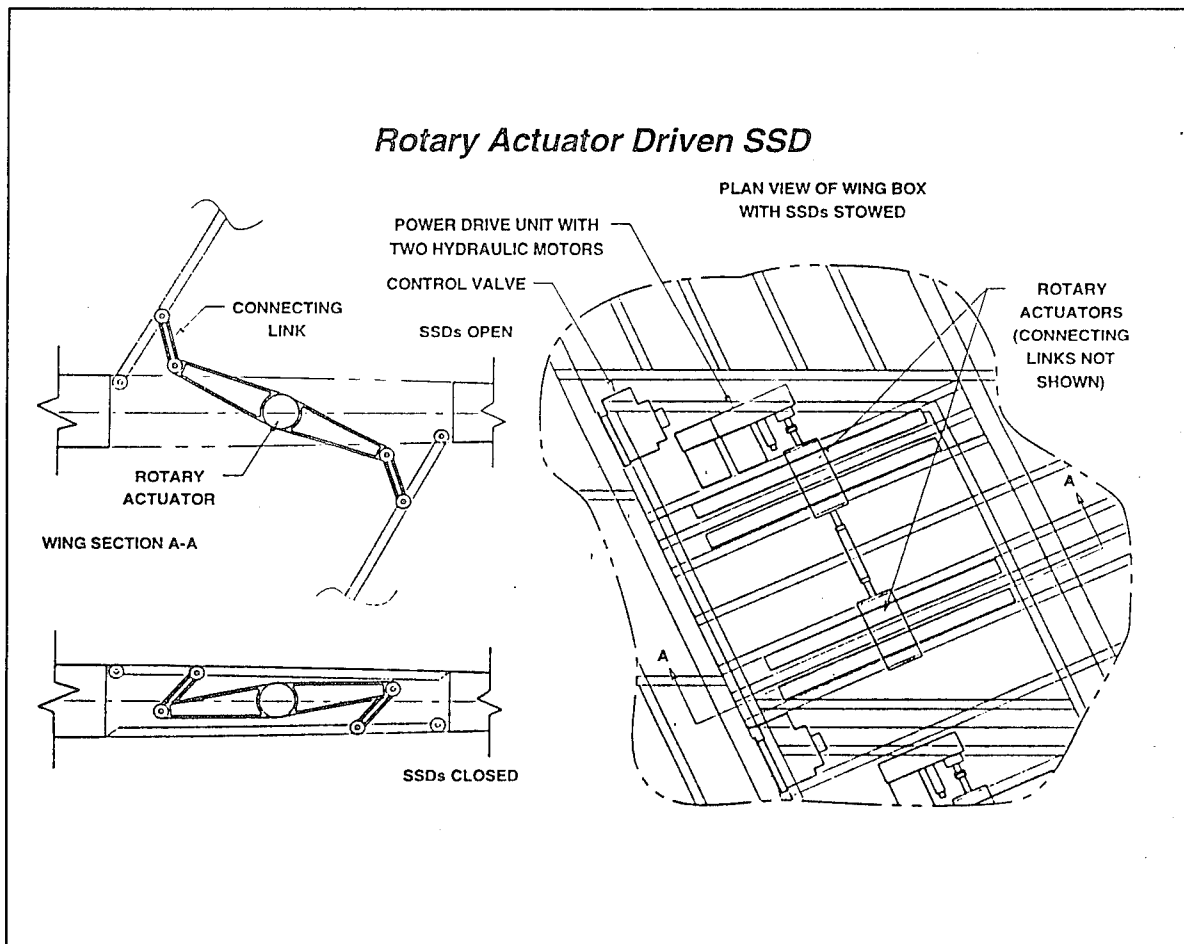


Figure 7-24 Rotary Actuator Driven SSD

Two concerns with this arrangement are actuator rate and bandwidth. Fortunately, the pivot shaft does not have to rotate through a very large arc to provide the needed 60 deg of control surface deflection -- only about 22 deg, resulting in a 2.7:1 ratio for actuator throw to surface deflection. Given a desired 150 deg/sec surface rate limit, the actuator need only move at 56 deg/sec.

Perhaps the most elegant SSD linkage system was discovered upon examination of the XF-107 at the USAF museum (Figure 7-25). This system eliminates one complete four-bar linkage of the system shown in Figure 7-23. The deflector is mounted on a gooseneck-style hinge, and swings away from the wing as the control surface opens. A linear actuator (not shown) can be attached to one ear of the spoiler or deflector to drive the system. One potential disadvantage is that the deflector must be made smaller than the spoiler to accommodate the gooseneck hinge. However, this is probably not a big concern. This arrangement requires that no understructure pass through the SSD cavity to provide clearance for the gooseneck deflector hinge. The XF-107 and RA-5 Vigilante used multiple SSD segments separated by structural ribs. Each segment was actuated by a separate actuator and 4-bar gooseneck linkage.

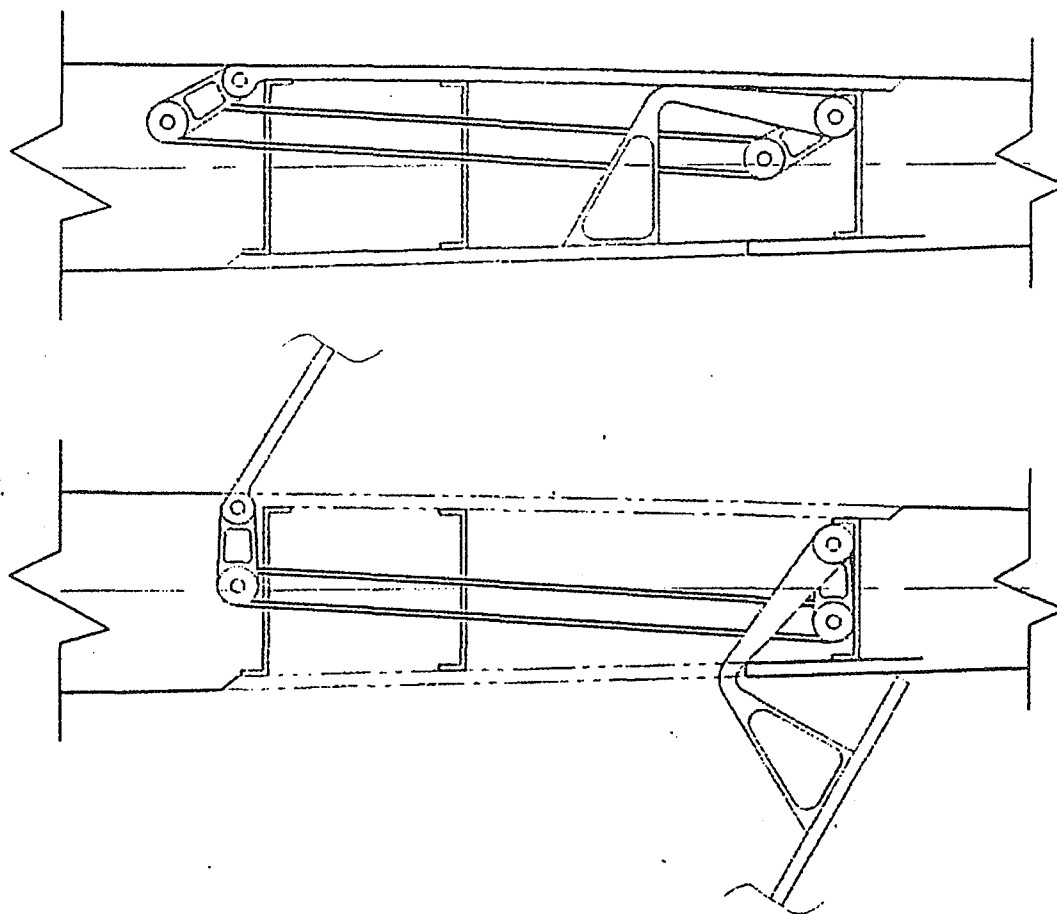


Figure 7-25 Simplified Four-Bar SSD Linkage

7.4.4 Finite Element Analysis of SSD Concept

An airframe finite element model (FEM) of an F-16 derivative wing was used to simulate the influence of SSD control surfaces on the structural behavior of the wing. The objective of this task was to study the changes in structural weight accompanied by modifying a delta wing aircraft to accommodate SSD control surfaces within the wing structure. Additionally, the analysis was undertaken to get a feel for the substructure requirements within the SSD slot. A 1/2-symmetry F-16 derivative FEM, shown in Figure 7-26, served as the starting point for the analysis.

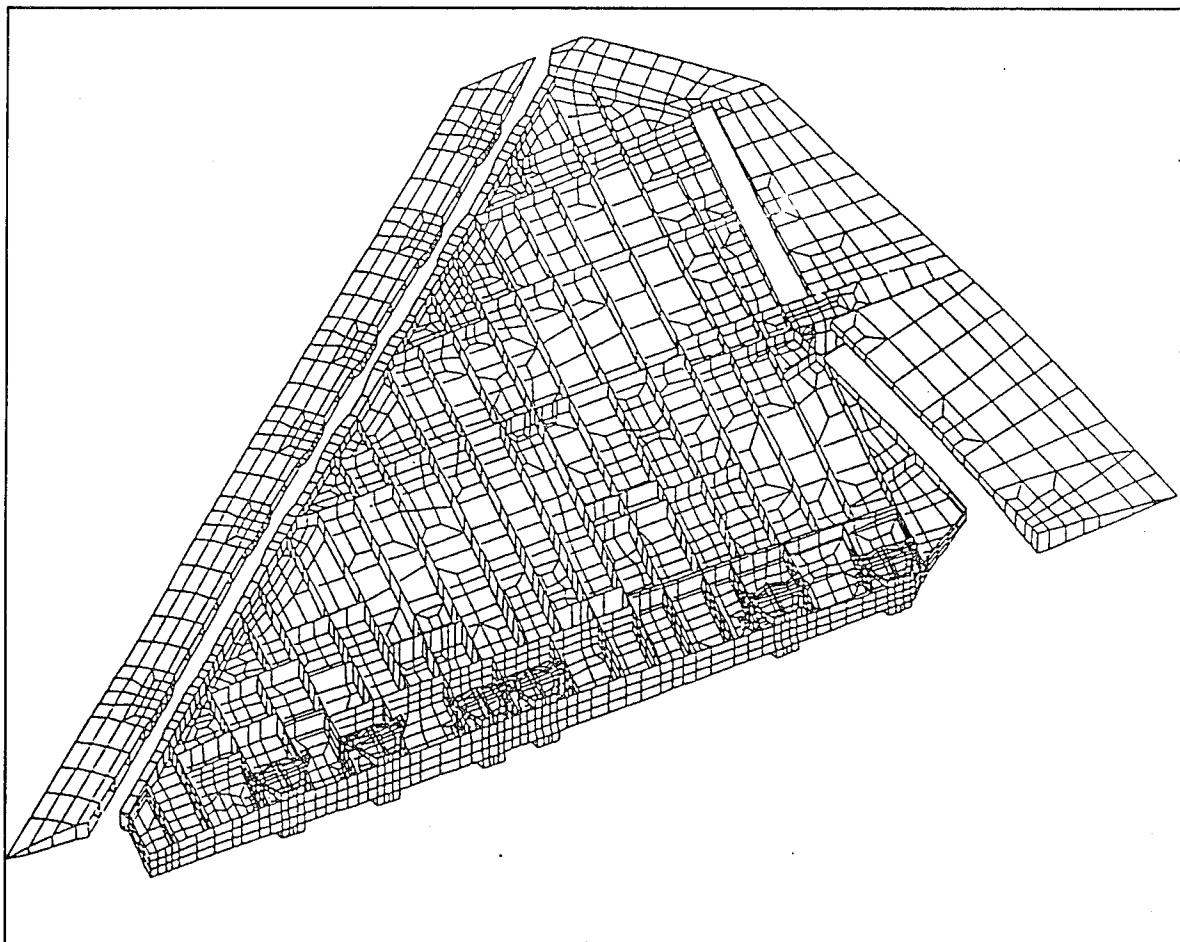


Figure 7-26 Isometric View of F-16 Derivative Wing FEM

Since the SSD control surfaces cannot sustain primary in-plane wing skin loads, elements from the upper and lower wing skins were removed from the baseline model to produce the cutout shown in Figure 7-27. Air loads from the deleted skin elements were re-dis-

tributed to the forward and aft spars. Seven critical load conditions were selected to re-analyze the modified FEM and to calculate new margins of safety for the wing structure.

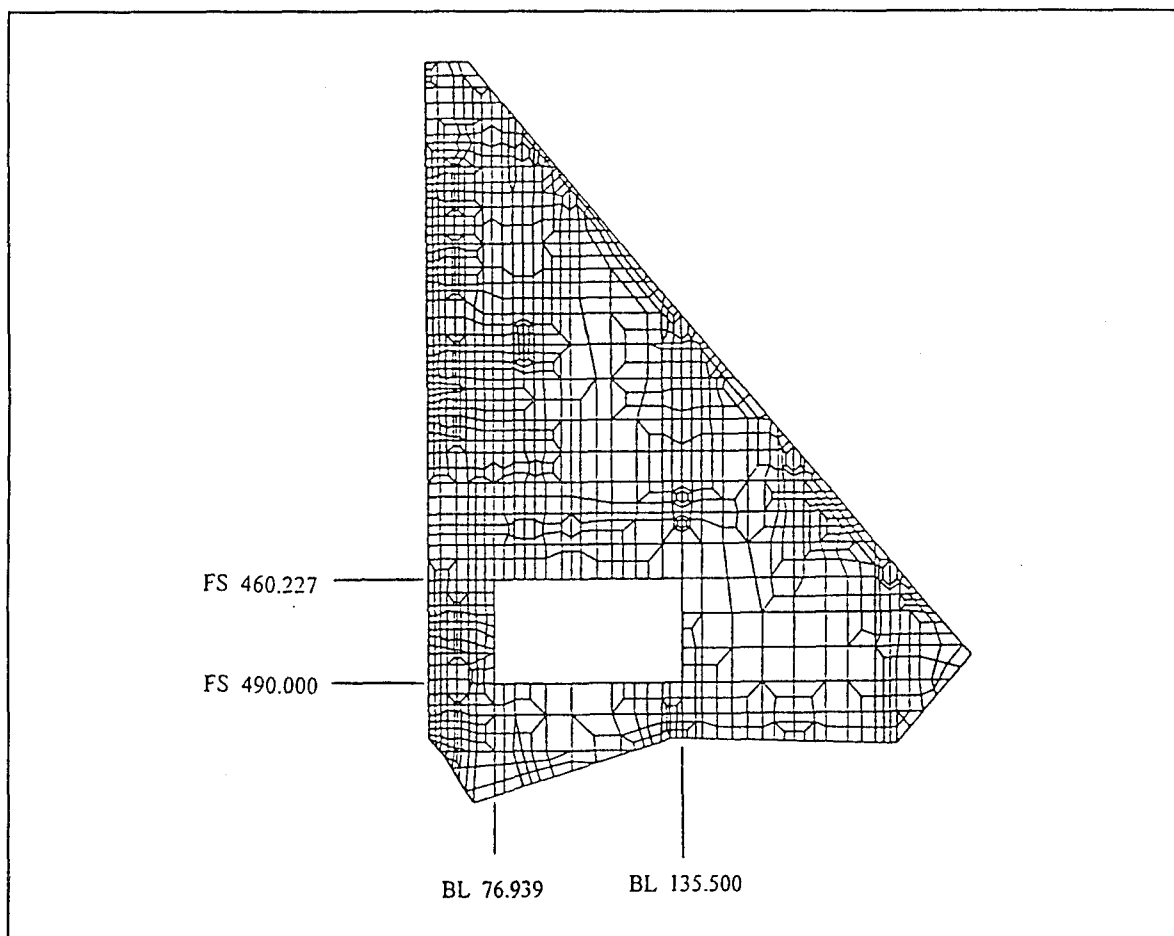


Figure 7-27 Planform View of Wing Skin Model with Cutout for SSD Control Surfaces

MSC/NASTRAN was used to analyze the airframe model. NASTRAN results were used to perform CPAP (Composite Panel Analysis Package) analyses of the composite wing skin panels. CPAP used the internal load results from the FEM analysis to perform margin of safety calculations for panel response to fuel pressure loads and panel buckling. Similar calculations for panel strength were performed outside of CPAP using the strains calculated from NASTRAN. Portions of the wing skin and substructure were re-sized in order to produce positive margins of safety. Weight increments were calculated based upon re-sized structure, using the FEM to calculate weight changes.

Model Assumptions

Several assumptions were made to perform the analysis. These assumptions are outlined below:

1. The wing has a delta planform
2. The wing structure is comprised of aeroelastically tailored graphite/epoxy composite skins and aluminum sub-structure.
3. Finite element analyses were based upon a coarse-grid F-16 derivative airframe model.
4. Presence of the SSD control surface was modeled as a rectangular cutout from the wing skins (30.0" x 58.6" = 12.21 ft²).
5. Substructure within the cutout was allowed to remain continuous.
6. Analysis and resizing of the FEM address only the unactuated control system.
7. Changes in the aerodynamic control and effectiveness of the modified wing were ignored.
8. Seven critical load conditions were used for the analysis, including:
 - M = 1.6 @ 25K balanced symmetric pull-up
 - M = 0.95 @ sea level, rolling pullout
 - M = 1.45 @ 20K, unbalanced symmetric pull-up
 - M = 1.1 @ 5K, unbalanced symmetric pull-up
 - M = 1.6 @ 25K, unbalanced symmetric pull-up
 - M = 1.6 @ 25K, balanced symmetric pull-up
 - M = 0.9 @ sea level, rolling pullout

The simplifying assumptions used in the analysis place restrictions on application of the results. No attempts were made to include masses, inertias, stiffness or internal loads that would be representative of the installed control system hardware. These factors would increase the structural weight of the wing. Also, due to the location of the control surface

cutouts, aileron flexibility will be significantly affected. The cutouts are positioned at a point in the wing skins where large torsional stiffness is required to produce effective aileron control. The control surfaces create a discontinuity in the load path at this location and thereby affect aileron stiffness.

Results

Results from the study include a summary of the weight impacts to the wing structure. Weights were calculated based upon the FEM and are shown in Table 7-5.

Table 7-5 Summary of Weight Impacts to an F-16 Derivative Wing Structure as a Result of Adding SSD Control Surfaces

FEM Description	FEM Weight (lbs/aircraft)	Δ FEM Weight (lbs)
Baseline	10,935.4	---
Baseline w/ Cutouts	10,799.4	-136.0
Resized Wing Skins (1st Iteration)	10,874.4	+75.0
Resized Wing Skins (2nd Iteration)	10,895.6	+21.2
Resize Substructure	10,897.8	+2.2
Total Wt Change	---	+98.4

Note Cutout weight of the skins (-136 lbs) was ignored in the total.

Based on the lessons learned during analysis of the F-16 derivative wing, a preliminary requirement for the structure surrounding the slot was developed. The cutouts for the SSD control surfaces should be broken into three equal segments, parallel to the long direction, and separated by a minimum of two primary rib members (see Figure 7-28). Boundary ribs must also be present. Boundary spars must be located on the two long-side edges of each cutout. The rib and spar members will perform several functions. The ribs must allow installation of the control surface actuation hardware and will act as a hard-back structure to react actuator and air loads for the three control surface pairs. The ribs must also carry air loads from the TEF structure to the surrounding wing structure. Boundary spars must be present to transfer air loads from the wing past the cutouts to the wing attachment structure. These same spars will also be used to react actuation loads

and to install actuation hardware and control surface hinges. An intermediate spar may also be necessary to satisfy panel stability of wing strength requirements.

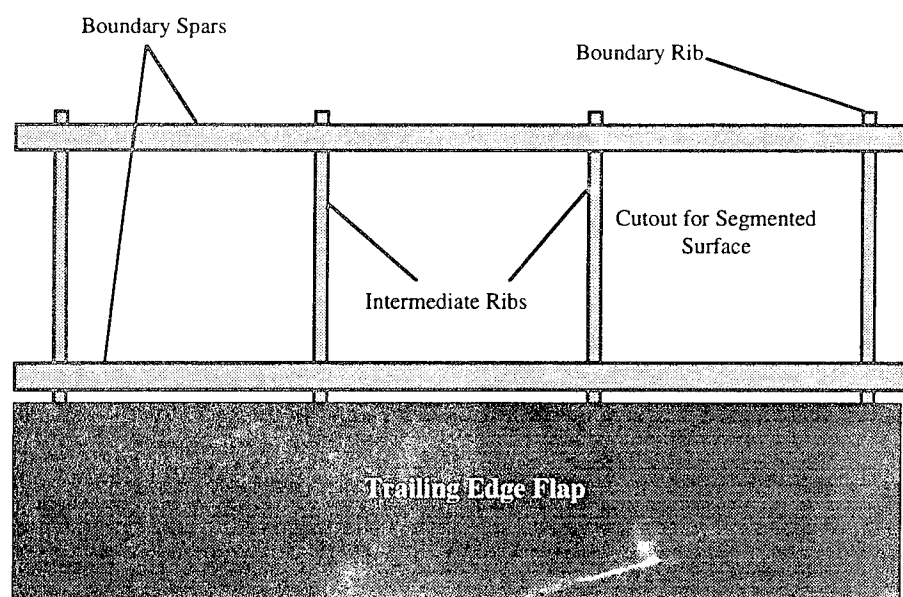


Figure 7-28 Substructure Required Near and Inside Cutouts for SSD Control Surfaces

Cross-section dimensions for the ribs and boundary spars would be dictated by their internal loads and compatibility with the surrounding wing structure. All of these members will likely have flanges and webs and could be channel or I-sections. Typical flange widths are 1.0 to 3.0 inches and typical thicknesses are 0.1 to 0.3 inches. Definition of these details would require additional analysis.

Summary and Conclusions

An F-16 derivative FEM was exercised to study the potential structural weight impacts caused by modifying the wing structure to accommodate SSD controls in the wing. The presence of these control surfaces were simulated by introducing a 30 in x 58.6 in cutout into both the upper and lower wing skins. Portions of the wing skins and substructure were re-sized to account for negative margins of safety that resulted from the introduction of the cutouts. It was concluded that modifications needed to accommodate control sur-

faces within the wing structure would increase the structural weight of the wings by about 100 lbs per aircraft.

The results of this study can be applied to other wing planforms using the following equation:

$$\Delta W_{SSD} = 0.351(S_{planform}) \quad (5)$$

This weight penalty only includes the weight associated with increases to the wing skin and substructure of the wing as a result of introducing the SSD cutouts. It does not account for the control surfaces themselves or the actuation hardware. The structural weight penalty associated with the cutouts was found to compare favorably with the structural penalty assessed during the configuration weights analysis (Section 6.5).

The weight of the control surfaces, system hardware and related internal loads were not modeled. Internal loads, lumped and distributed masses, actuator reaction points and related structural stiffness would be produced from the installed control surfaces and actuation system. These loads and stiffness would require an additional sizing increment to the FEM. Aerodynamic effectiveness of the wing must also be re-evaluated with the installed surfaces. It is likely that many of these factors would lead to additional changes in the structural weight and possibly flight performance. Some of the weight impacts can be reduced by making provisions for the SSD control surfaces early in the preliminary design process.

7.5 Weight Impacts

The following subsections summarize the weight impacts of integrating the various control concepts. Both configuration-level and individual control surface weights are discussed.

7.5.1 Configuration Level Weights

Figures 7-29 and 7-30 include the weight build-ups for the 101 and 201-series configurations, respectively. The two configurations include slightly different systems and equip-

ment. For instance, 201-series airplanes include an integrated energy management system while 101-series airplanes do not; furthermore, the 201-series has an entirely different weapons carriage concept than the 101-series configurations. Finally, the 201-series airplanes include Navy-specific weight penalties such as dual-keel structure, landing gear, tail hook, etc. As a result, care should be taken when making comparisons between 101-series and 201-series configuration weights data. Direct comparisons between the individual configurations within a series (e.g., 101) can be made.

Primary weight differences between the individual 101-series configurations can be found in the wing structure, thrust vectoring system, flight controls, hydraulic systems, and internal fuel weights. Small additional differences can be found in the unusable fuel and avionics weights.

Differences between the 201-series configuration weights are found in the wing structure, thrust vectoring system, flight controls, hydraulic systems, avionics, and internal fuel weights.

Figure 7-31 illustrates the differences between the zero-fuel weights for each configuration. Weight differences are taken from the 101-TV and 201-TV configuration baselines. It is interesting to note that except for the -4 (large AMT and no spoilers) configurations, the weight difference trends are not the same for the USAF and Navy configurations. This is due to the carrier-based emphasis on power approach performance and control-suite integration with high lift devices.

Weight Buildup -- Configuration 101-Series

	ICE 101	ICE 101-TV	ICE 101-1	ICE 101-3	ICE 101-4
Structure	11741	11649	11828	11847	11567
Wing	5721	5629	5808	5827	5547
Fuselage	4027	4027	4027	4027	4027
Landing Gear	1499	1499	1499	1499	1499
Engine Section	76	76	76	76	76
Air Induction	418	418	418	418	418
Propulsion	4894	5398	5398	5398	5398
Engine (F110-GE-129)	3940	3940	3940	3940	3940
- Simplex TV	0	354	354	354	354
- Dual Hyd	0	50	50	50	50
- Coatings	100	100	100	100	100
- Nozz Thrust Delta	0	100	100	100	100
AMAD (incl Oil)	141	141	141	141	141
Engine Cntrls	21	21	21	21	21
Fuel System	692	692	692	692	692
Systems & Equipment	6105	5846	5230	5355	5189
Flight Controls	1332	1098	610	713	566
APU/EPU	315	315	315	315	315
Instruments	6	6	6	6	6
Hydraulics & Pneumatics	609	534	406	428	409
Electrical System	823	823	823	823	823
Avionics	1683	1733	1733	1733	1733
Armament	450	450	450	450	450
Furnishings & Equipment	338	338	338	338	338
Air Conditioning	499	499	499	499	499
Load & Handling	50	50	50	50	50
Weight Empty	22740	22893	22456	22600	22154
Op & Basic Wt Items	1095	1096	1116	1111	1133
Crew	215	215	215	215	215
Unusable Fuel	300	301	321	316	338
Eng Oil & Res. Fluids	80	80	80	80	80
AVEL (2)	240	240	240	240	240
AIM-9 Launcher (2)	196	196	196	196	196
Chaff/Flare	48	48	48	48	48
Misc	16	16	16	16	16
Operating Weight	23835	23989	23572	23711	23287
Payload	1066	1066	1066	1066	1066
AIM-120 (2)	676	676	676	676	676
AIM-9L (2)	390	390	390	390	390
Zero Fuel Weight	24901	25055	24638	24777	24353
Internal Fuel	15001	15036	16034	15775	16887
Takeoff Gross Weight	39902	40091	40672	40552	41240

Figure 7-29 Configuration 101-Series Weights Build-up

Weight Buildup -- Configuration 201-Series

	ICE 201	ICE 201-TV	ICE 201-1	ICE 201-3	ICE 201-4
Structure	15016	15016	15184	15419	14947
Wing	5009	5009	5177	5412	4940
Canard	565	565	565	565	565
Fuselage	7207	7207	7207	7207	7207
Landing Gear	1786	1786	1786	1786	1786
Engine Section	83	83	83	83	83
Air Induction	366	366	366	366	366
Propulsion	4919	5423	5423	5423	5423
Engine (F110-GE-129)	3940	3940	3940	3940	3940
- Simplex TV	0	354	354	354	354
- Dual Hyd	0	50	50	50	50
- Coatings	100	100	100	100	100
- Nozz Thrust Delta	0	100	100	100	100
AMAD (incl Oil)	141	141	141	141	141
Engine Cntrls	14	14	14	14	14
Fuel System	724	724	724	724	724
Systems & Equipment	6690	6740	6495	6533	6367
Flight Controls	1676	1676	1477	1493	1374
APU/EPU	0	0	0	0	0
Instruments	50	50	50	50	50
Hydraulics & Pneumatics	713	713	667	689	642
Electrical System	823	823	823	823	823
Avionics	1673	1723	1723	1723	1723
Armament	214	214	214	214	214
Furnishings & Equipment	441	441	441	441	441
Air Conditioning	0	0	0	0	0
Integrated Energy Mgmt Sys	1100	1100	1100	1100	1100
Weight Empty	26625	27179	27102	27375	26737
Op & Basic Wt Items	2483	2483	2472	2472	2507
Crew	215	215	215	215	215
Unusable Fuel	233	233	222	222	257
Eng Oil & Res. Fluids	80	80	80	80	80
AVEL (2)	240	240	240	240	240
MAXSER Ejector (4)	320	320	320	320	320
Countermeasures	150	150	150	150	150
Internal Weapons Pallet	1215	1215	1215	1215	1215
Misc	30	30	30	30	30
Operating Weight	29108	29662	29574	29847	29244
Payload	2596	2596	2596	2596	2596
AIM-120 (2)	676	676	676	676	676
TMD (2)	1920	1920	1920	1920	1920
Zero Fuel Weight	31704	32258	32170	32443	31840
Internal Fuel	13194	13194	12542	12542	14551
Takeoff Gross Weight	44898	45452	44712	44985	46391

Figure 7-30 Configuration 201-Series Weights Build-up

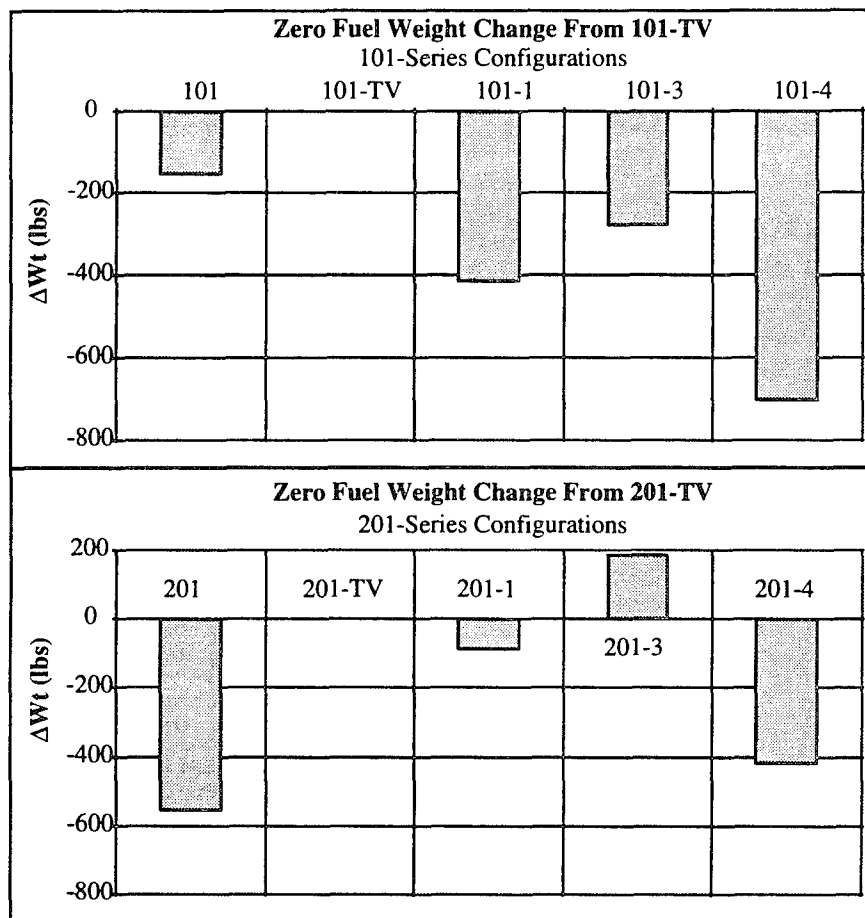


Figure 7-31 Zero-Fuel Weight Variations

Figure 7-32 shows the internal fuel weight variations between the configurations. Once again, except for the -4 configurations, the trends for the 101-series airplanes are not the same as the 201-series airplanes. This is primarily due to the different planforms and structural integration of the controls. The weight savings and internal fuel improvements afforded by the -4 airplanes is due to deletion of the spoiler control surfaces.

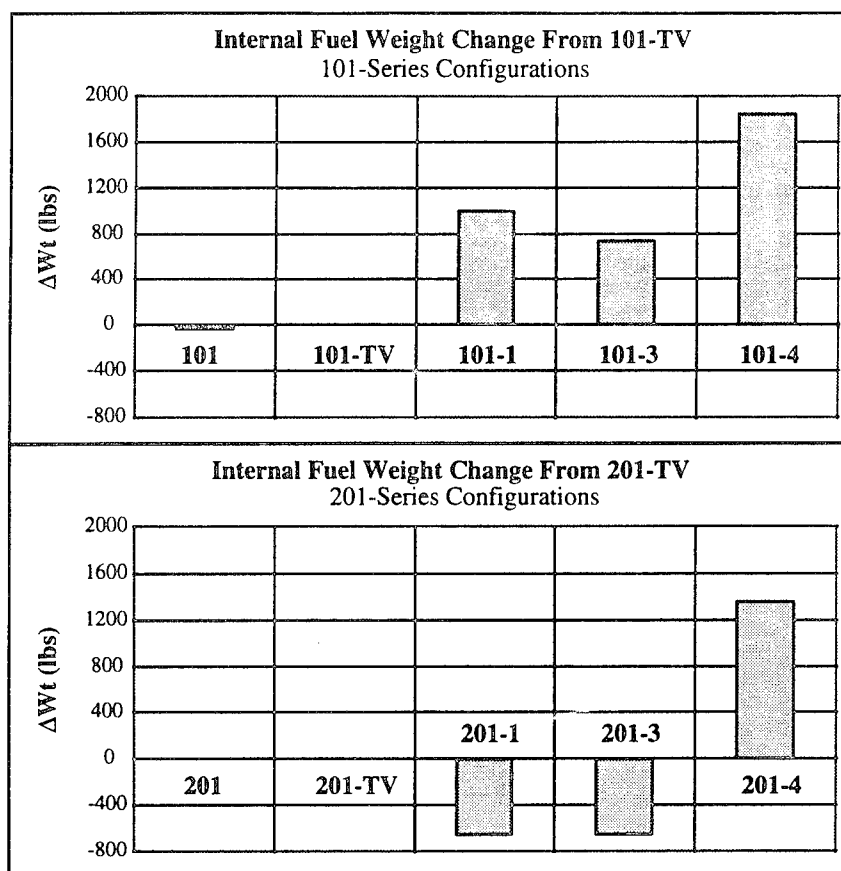


Figure 7-32 Internal Fuel Weight Variations

7.5.2 Individual Control Surface Weight Comparisons

Weight comparisons for each control surface are shown in Figure 7-33 for each configuration series; both total weights and normalized weights (lbs/ft²) are shown. These data include the actuator weights. Note that the 201-series normalized weights are generally greater than the 101-series weights due to the higher load demands consistent with the CV environment. The all-moving surfaces (canard and AMT) are generally lighter on a per square ft basis, but have higher total weights than the other surfaces. The heaviest controls on a normalized basis are the SSD and clamshells. The total additional weight for adding multi-axis thrust vectoring to the engine is included for comparison purposes (504 lbs). The thrust vectoring weights include provisions for dual hydraulics to the nozzle actuators (50 lbs) and an additional 100 lbs for increased off-axis loads. The thrust

vectoring weight impact is considered conservative, and could be as small as 350 lbs - 400 lbs.

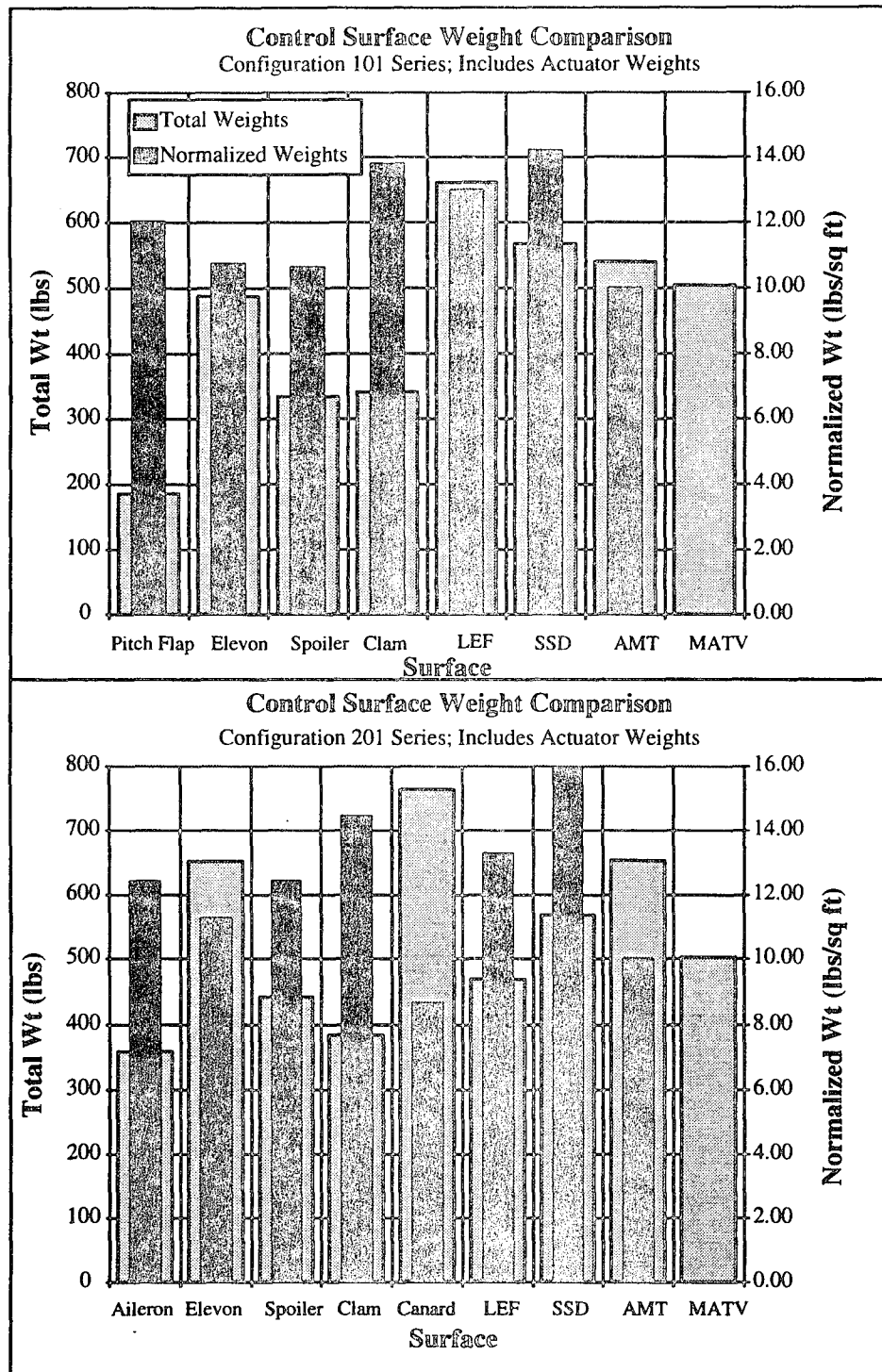


Figure 7-33 Control Surface Weight Comparisons

7.6 Up and Away Performance Impacts

Two approaches can be used to quantify the performance impacts of innovative controls. The net change in performance can be quantified using a sensitivity analysis, or the vehicle can be resized to maintain a constant performance metric. The first method was used during the ICE study.

Traditional performance impacts were estimated by determining the sensitivity of the 101-series configuration to transonic drag, dry weight and fuel weight changes. As a first approximation to performance changes, the sensitivities were applied to both 101 and 201-series configurations; results are given in terms of percent-change. Figure 7-34 summarizes the results for both configuration series.

Changes in fuel weight had the greatest effect on range with dry weight and drag having secondary impacts. Configurations 101-4 and 201-4 had significant range improvements (16% and 20%, respectively) due to elimination of the spoilers from the wing box; thereby providing greater fuel volume. Additional weight and cost savings could be realized by resizing the configurations to maintain the desired range.

Transonic drag primarily affected the acceleration times; weight changes had a small impact. The large AMT actuator fairings on the -3 and -4 configurations had a significant impact on the acceleration performance. The AMT actuator fairings on the 201 configurations affected the peak of the area curve, whereas the fairings on the 101 configurations mainly affected the aft-slope portion of the area curve. As a result, acceleration times were more adversely affected on the 201 configurations. Turn performance effects due to weight and drag changes were relatively small (< 1 deg/sec).

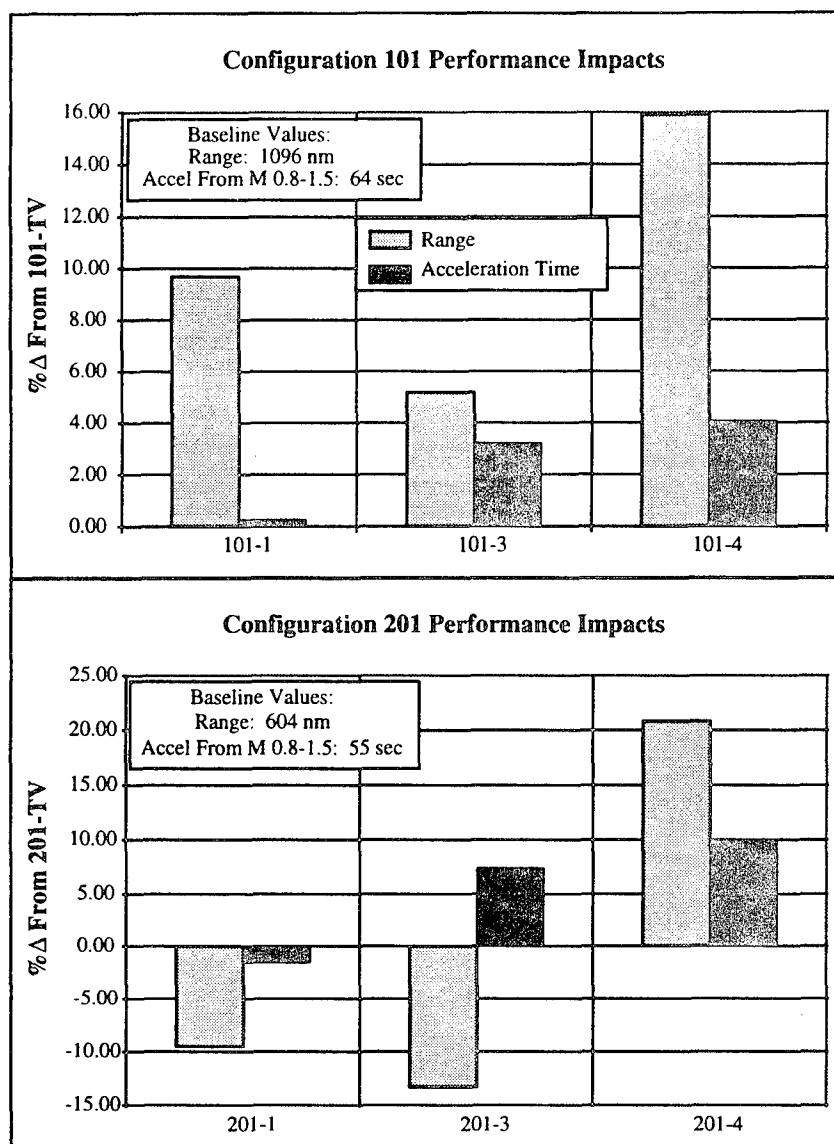


Figure 7-34 Performance Impacts due to Innovative Control Concepts

7.7 Flight Control System Design Requirements

In general, tailless fighters will require more complex flight control systems than conventional configurations. Tailless fighters employ large control suites effective in multiple axes. Significant control coupling, nonlinearities and uncertainties exist in the control effectiveness data. Finally, static stability is relaxed both in pitch and yaw. Conventional fighters typically employ relatively few controls that are decoupled (e.g., a rudder deflection primarily produces a yawing moment); furthermore, while relaxed stability is usually

desired in the pitch axis for performance benefits, directional instabilities must be tolerated to achieve survivability improvements. For tailless applications the control effectors must be properly blended to achieve the maximum control power and maintain acceptable flying qualities under any condition including saturation and effector failures.

The control law architecture for an air vehicle can be approached by partitioning the control allocation tasks from the basic control law feedback functions (Figure 7-35). The control redundancy/deficiency problem then can be solved using a weighted pseudo-inverse method with redistribution capability⁴¹.

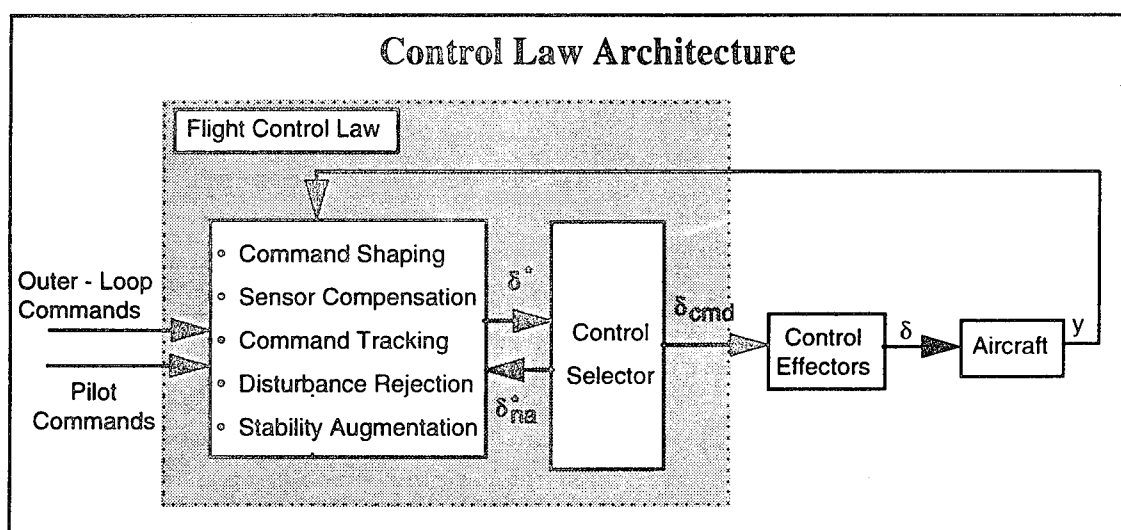


Figure 7-35 Control Law Architecture

Control power is allocated such that the most effective controls for a particular axis are prioritized, with secondary controls being used as necessary. As effectors saturate (rate or position limit), control power is redistributed to other effectors to make up the short-fall. Additionally, a control prioritization scheme can be implemented through a weighting matrix to prioritize control power to important control axes. For instance, pitch power might be prioritized over roll power, etc. This scheme will provide performance optimization and redistribution when there is a control redundancy, and axis prioritization when there is a control deficiency.

A study was made to determine the control allocation demands placed on the flight control system by the various ICE control suites. This analysis was performed for the land-

based configurations only; however, the trends and conclusions are applicable to the carrier-based configurations. Figure 7-36 summarizes an assessment of the ICE series 101 configuration control allocation evaluation.

ICE CONTROL ALLOCATION EVALUATION RESULTS

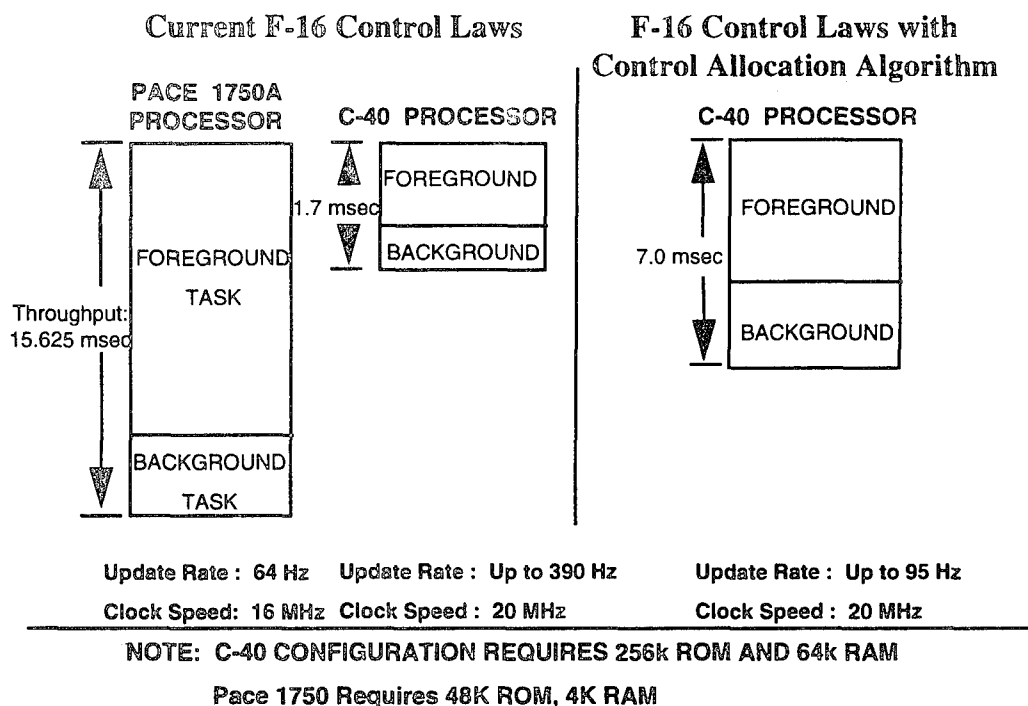
ICE AIRCRAFT CONFIGURATION	Total Number of Control Effectors	Relative Level of Aerodynamic Interaction Among Control Effectors	Relative Level of Aerodynamic Coupling of Controls Into Pitch, Roll, and Yaw Axes	Impact On Algorithm Computation Effort	Impact On Algorithm Data Storage
101TV	Very High (14)	Very High (Inboard and Outboard LEF's and Spoilers on Elevons and Pitch Flaps)	Very High	Very High	Very High
101-1	Moderate (10)	Moderate (SSD on Elevons and Pitch Flaps)	High	High	Moderate
101-3	High (12)	High (Outboard LEF's and SSD on Elevons and Pitch Flaps)	High	High	High
101-4	Moderate (8)	Low	Moderate	Moderate	Low

Figure 7-36 Control Allocation Evaluation

Qualitative ratings were given the various control suites to determine the computational and data storage requirements for the various control suites. Configuration 101-4 was evaluated as the least challenging configuration to implement. Configuration 101-TV was evaluated as the most difficult.

A calculation of the most demanding control allocation throughput requirement was made using Configuration 101-TV. It was assumed that the foreground task (i.e., command shaping, stabilization feedbacks, filters, etc.) would be similar to current F-16 control laws. The primary difference would be the more demanding control allocation task using the weighted pseudo-inverse method described above.

Figure 7-37 shows a comparison of the throughput requirements for the current F-16 control law using the Pace 1750A processor with the requirements for an F-16 control law and Configuration 101-TV control allocation. The other configurations will require less than 101-TV because they are not as complex.



CONTROL ALLOCATION THROUGHPUT REQUIREMENT

Figure 7-37 Maximum Throughput Requirements

The left side of Figure 7-37 shows that the Pace chip requires 15.625 ms to run the current F-16 digital flight controls with an update rate of 64 Hz and clock speed of 16 MHz. (An update rate slightly less than 64 Hz is considered a lower bound for fighter-type flight control software.) This update rate shows that the current Pace 1750A chip has little room for growth with the baseline F-16 control algorithms. The next bar shows the same F-16 control laws running on a 32-BIT Texas Instruments C-40 processor at an update rate of 390 Hz. The throughput using this chip is only 1.7 ms. The update rate of 390 Hz shows significant growth capability using this chip before the 64 Hz update rate is reached. Finally, the right-most bar shows the throughput for the F-16 control laws with the Configuration 101-TV pseudo-inverse control allocation algorithm on the C-40 proc-

essor. Even with the much greater complexity created by the tailless configuration, a throughput of 7.0 ms is achieved at an update rate of 95 Hz; a growth margin still exists before the 64 Hz update rate is reached. Note that the C-40 chip requires 256K ROM and 64K of RAM compared to the Pace 1750 requirement of 48K ROM and 4K RAM.

In summary, control allocation methodology provides a means to effectively employ the multiple control effectors associated with tailless configurations. The weighted pseudo-inverse allocation algorithm adds more complexity to the flight control laws as compared to conventional configurations employing control mixers (e.g., F-16). The methodology utilizes sophisticated on-line matrix manipulation software. Segments of the algorithm may require several iterations within each update of the flight control laws. These demands require faster processors than the current 16-bit Pace chips used in F-16-class control laws. Additional data storage and CPU memory are required in the flight control computers for the ICE configurations due to multi-axis control effectiveness, nonlinearities and aerodynamic interactions. The increased computational demands can be met by utilizing the 32 BIT Texas Instruments C-40 family of processors.

7.8 Transition of Innovative Controllers to Other Configurations

Each of the three innovative control concepts evaluated in detail during the ICE study (AMT, SSD and DLEF) were evaluated for their potential to replace the vertical tail(s) on current conventional configurations. Six classes of fighter configurations were identified:

- Conventional (F-16, F-15, F/A-18)
- Swing-Wing (F-14, F-111)
- 3-Surface (F-15 ACTIVE)
- Tailless Delta (F-16XL, F-117, Mirage 2000)
- Canard-Delta (Configuration 201, Viggen, Rafale)
- Flying Wing (Configuration 101, A-12)

The applicability of the innovative controls to each configuration class (except the 3-surface) was evaluated. The effectiveness was already demonstrated on the flying wing (101-series) and canard-delta (201-series) configurations. A cursory analysis to alternative configurations was conducted using the F/A-18, F-14 and F-16XL representing a conventional, swing wing and tailless delta class, respectively.

The yaw controls were sized to meet power approach roll performance requirements with the vertical tail off. The preliminary design analysis code, HASC, was used to obtain aerodynamic predictions for the F/A-18 and F-14. The F-16XL simulation database was used for the tailless delta analysis. Representative HASC models are shown in Figure 7-38.

Figure 7-39 shows the bare airframe directional stability characteristics with the vertical tail off for each configuration. The parameter N_{β}/q is used to account for the differences in wing geometry and inertia between the five configurations. The F-18, F-14 and F-16XL all have very similar tail-off directional characteristics at low AOA. The flying wing is the least unstable. This is not surprising given the small amount of side area forward of the cg on the flying wing configuration. At higher AOA (up to 20 - 25 deg), swept-wing configurations are typically slightly stable with the vertical tail off due to the dihedral effect inherent with high wing sweeps.

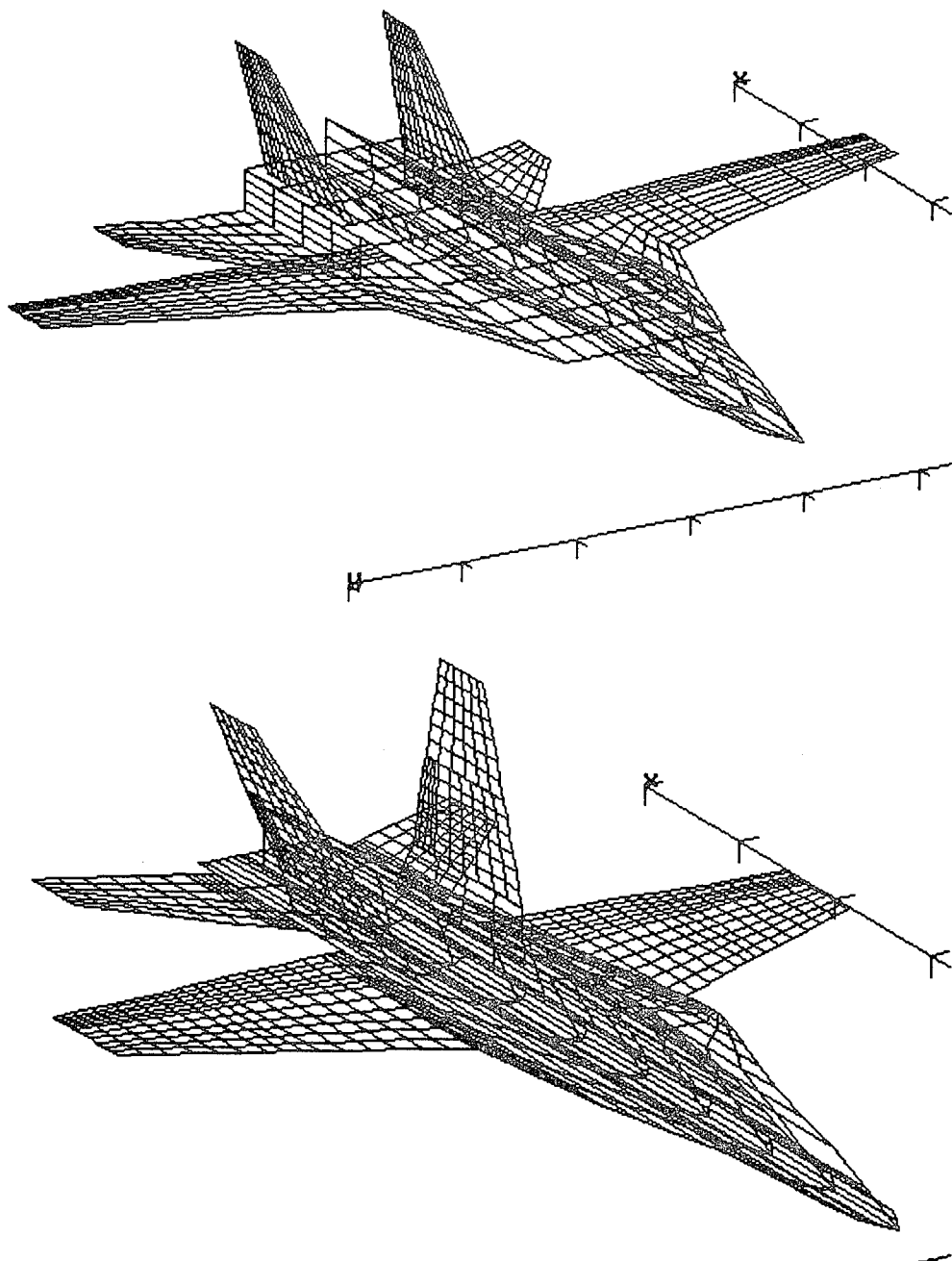


Figure 7-38 HASC Models were used to Compute F/A-18 and F-14 Aerodynamics

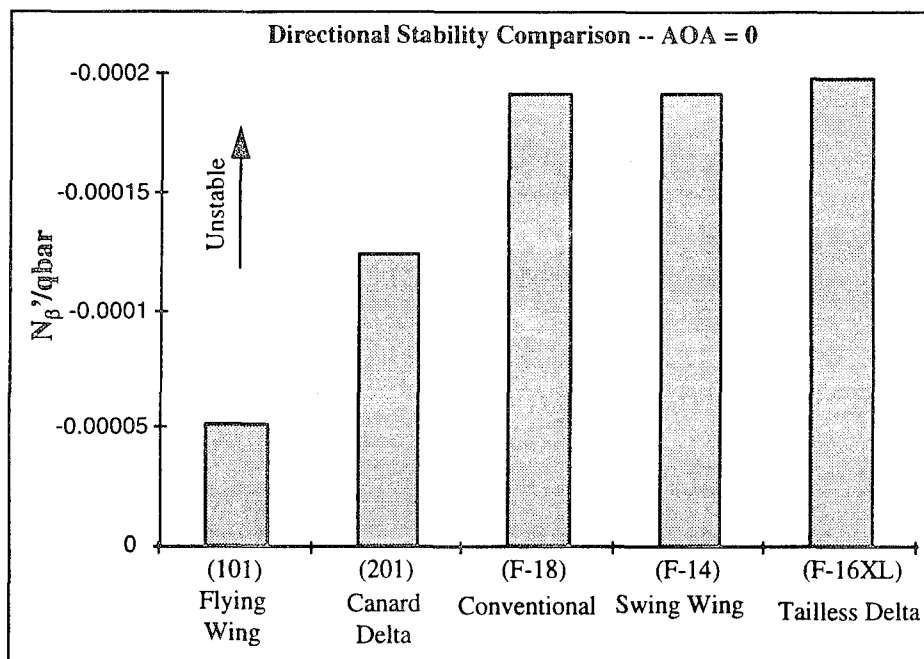
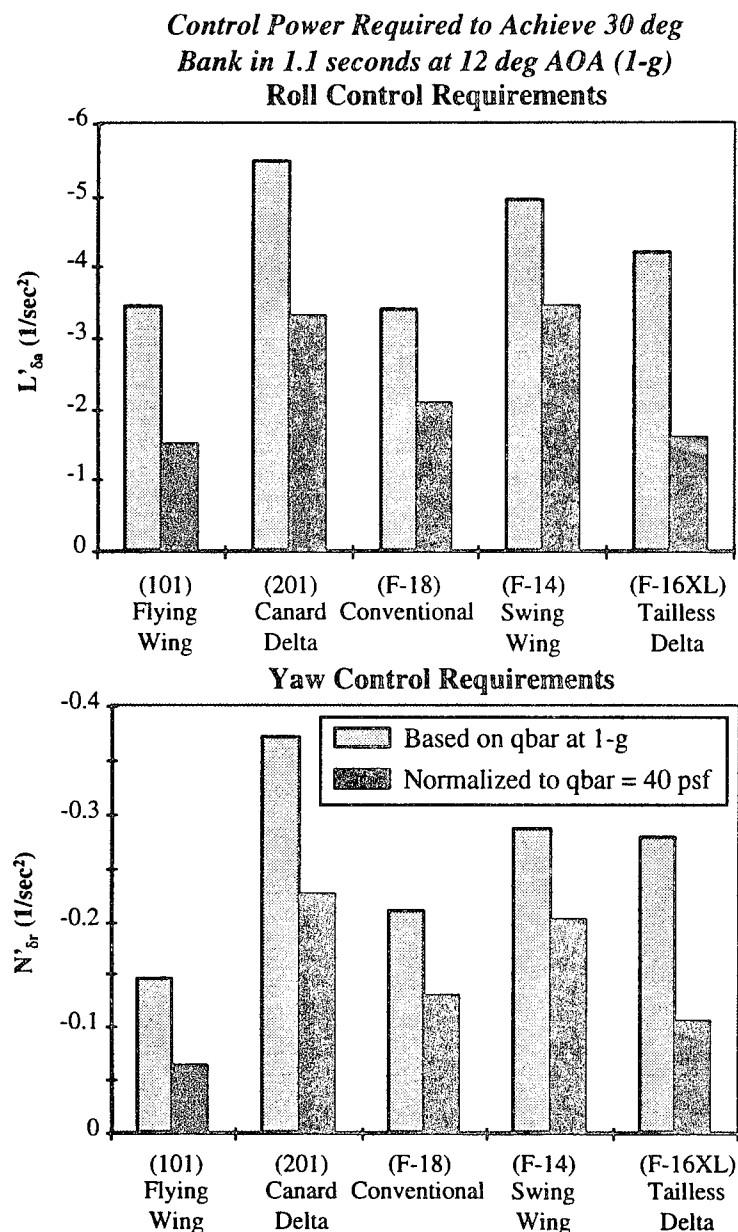


Figure 7-39 The Flying Wing Configuration Offers the Least Amount of Directional Instability at Low AOA

Lateral-directional control power requirements were determined for each configuration at 12 deg AOA -- consistent with a power approach condition. (Note: the F-14 control power requirements were determined for the forward wing sweep position.) Figure 7-40 shows roll and yaw control power required to accomplish a bank angle change of 30 deg in 1.1 sec. Sideslip was specified to be less than 6 deg during the roll. Dimensional derivatives are shown in the primed axis system to account for configuration geometry and inertial differences. Because of wing loading and high-lift system differences, 1-g trim airspeeds at 12 deg AOA varied between configurations. The dimensional derivatives were normalized using the 1-g trim dynamic pressure for each configuration. Normalizing the results with dynamic pressure provides a better comparison of the control power requirements.



**Figure 7-40 Lateral-Directional Control Requirements for Various Configuration
Classes**

The flying wing and tailless delta examples required the least roll and yaw control power for the maneuver of interest. The conventional configuration (F/A-18) was a close third. The canard-delta and swing-wing configurations required the greatest control power relative to the other configurations.

A first-order sizing process was used to estimate the AMT and SSD control surface sizes required to supply the needed yaw power in place of the vertical tails on the configurations of interest. Figures 7-41 through 7-43 show sketches of the controls on an F/A-18, F-14 and F-16XL, respectively.

The AMT is the only control effector in the matrix that could legitimately replace the vertical tails and rudder on the F/A-18 (Figure 7-41). The leading edge sweep is too low for DLEF to provide useful control moments at approach AOA. The relatively short span and large yaw-to-roll inertia ratio of this configuration ($I_z/I_x \cong 6$) create the need for a drag-producing surface with large area. An SSD sized to meet the requirement would completely destroy the structural integrity of the wing. Note that the AMT and SSD sizes shown in the figure are those required to by themselves replace the function of the vertical tails and rudder. A combination of both an SSD and AMT would result in smaller surfaces, but would still probably not be structurally feasible on the F/A-18.

The AMT prohibits integration of an aileron. On the F/A-18, the aileron is a primary roll control device and is also used for high lift during launch and approach. The configuration illustrated has insufficient roll power due to the lack of an aileron. A significant increase in wing span would provide room for an aileron, and allow a smaller AMT (due to increased moment arm).

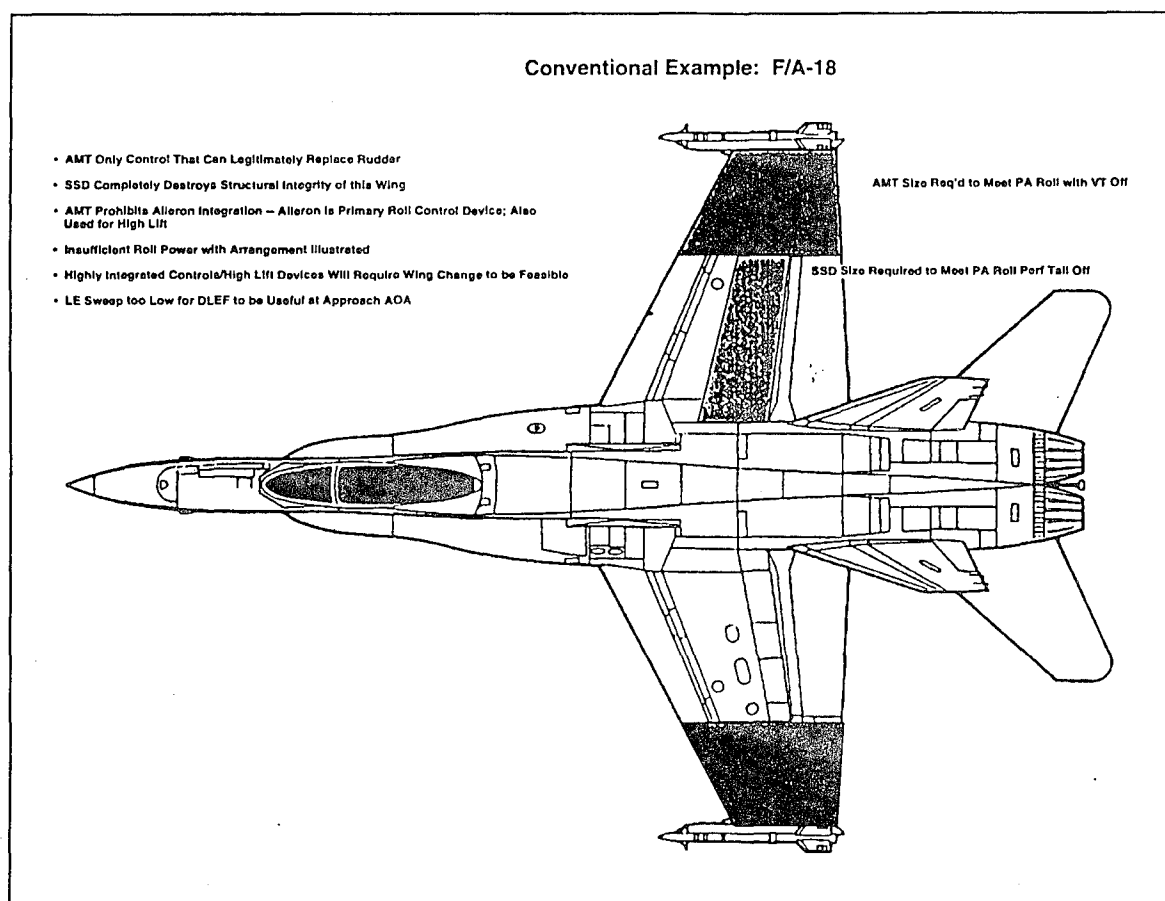


Figure 7-41 Conventional Example: F/A-18

Figure 7-42 shows the AMT size required to replace the vertical tails on the F-14. The AMT shown is completely unfeasible on this wing planform. The yaw control requirement is again driven by a large I_{zz}/I_{xx} ratio. Furthermore, it would be impossible to integrate spoilers and high lift devices with such a large AMT. DLEF would not be useful at the low sweep angles required for PA, but would provide meaningful lateral-directional control moments in aft sweep and high AOA. An SSD may improve roll and yaw power at low to moderate sweeps; they may not be very effective at the aft sweep position because of the high degree of spanwise flow. Insufficient SSD chord would be available (due to the narrow wing chord) to replace the function of the vertical tails. For swing-wing configurations, deployable controls (i.e., clamshell, spoilers, AMT) make more sense at low AOA while DLEF could be used in aft-sweep at high AOA.

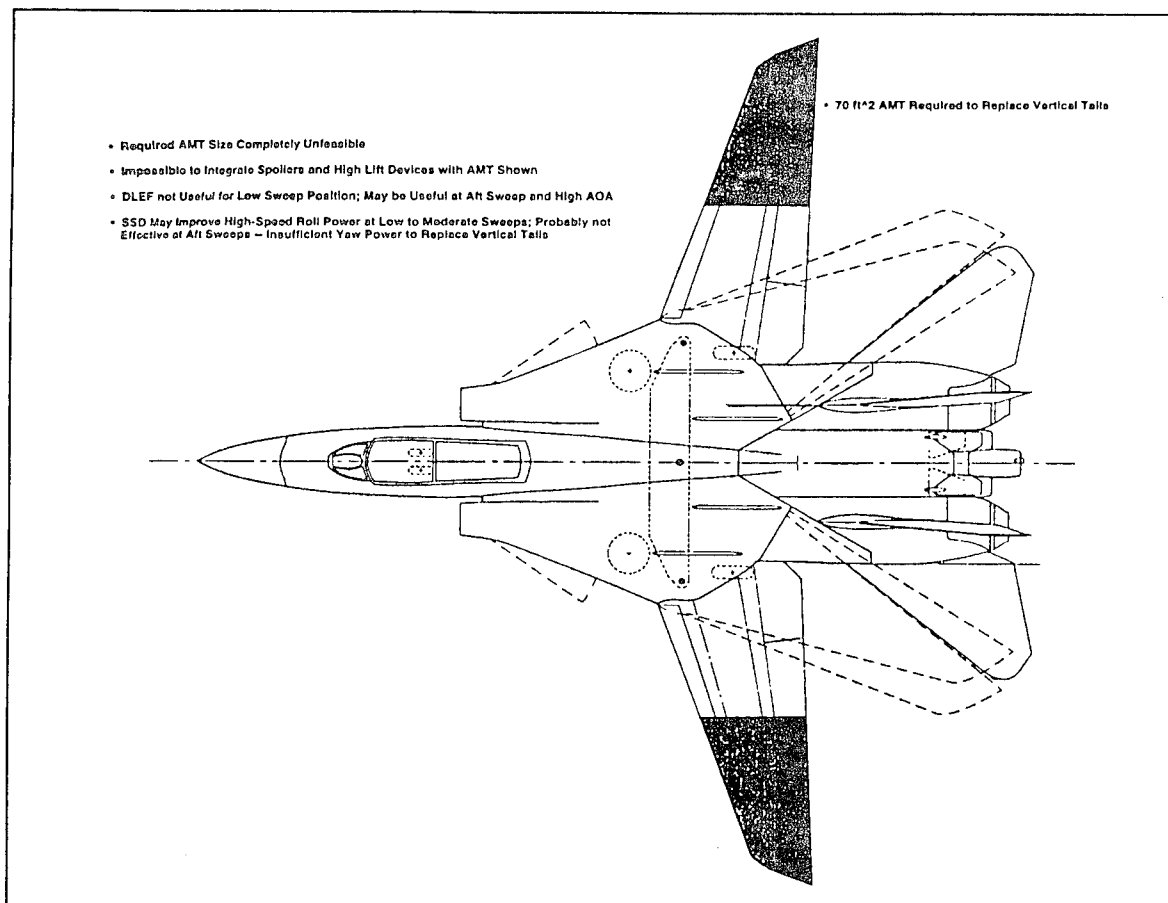


Figure 7-42 Swing Wing Example: F-14

Figure 7-43 shows two examples of control integration on the F-16XL. The high sweep, broad-chord planform lends itself well to tailless control suite integration because sufficient structural box is available to carry the wing loads. Furthermore, control integration is not constrained by low-speed CV suitability requirements. The control surfaces do not have to compete with trailing edge flaps for space on the wing. AMT control integration requires either extending the span (holding the existing trailing edge controls the same) or squeezing the elevons and ailerons to make the tip fit. Pitch control requirements may size the trailing edge controls making an alternate planform more attractive. The SSD is not very feasible on this planform due to the relatively short yaw moment arm. The second example shows the addition of DLEF on the high-sweep portion of the wing. The DLEF can provide significant lateral-directional control power at high AOA, and are effective at approach AOA because of the high sweep angle.

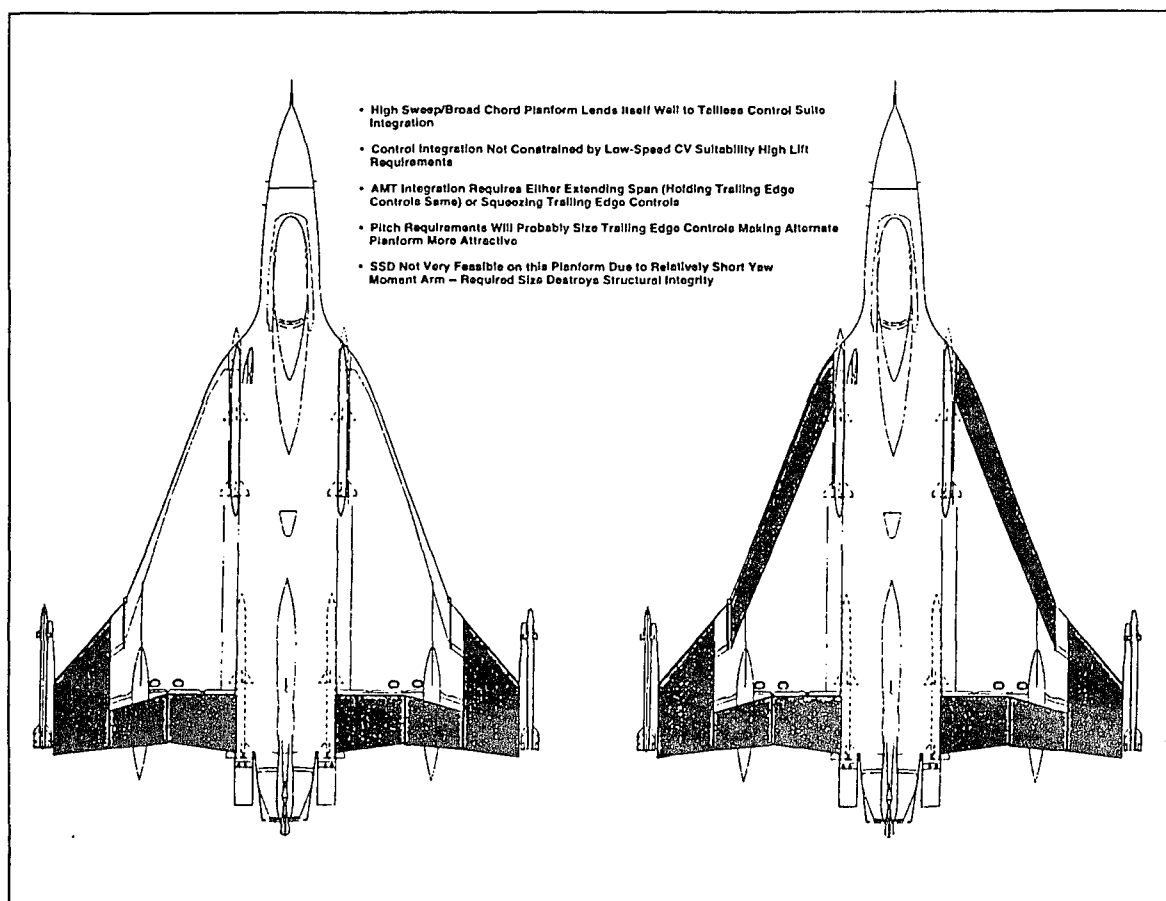


Figure 7-43 Tailless Delta Example: F-16XL

The HASC vortex lattice code and wind tunnel results from other configurations were used to estimate the effectiveness of DLEF on the inboard portion of the F-16XL wing. Figure 7-44 shows high AOA roll performance estimates for the F-16XL with the two tailless control suites. All CPR simulation results include sideslip feedback -- a feature that the original F-16XL did not incorporate in its FCS. The results show that the configuration with both the AMT and DLEF can roll as well or better than the baseline F-16XL up to 30 deg AOA.

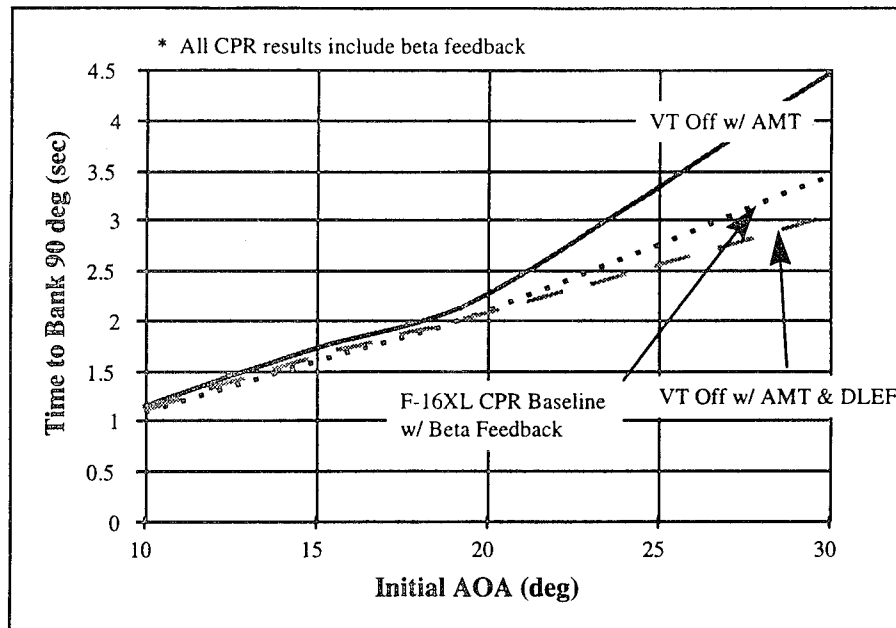


Figure 7-44 Tailless F-16XL High AOA Roll Performance

The flying wing and tailless delta arrangements are best suited for a vertical tailless design from a control power requirement standpoint. The canard-delta (201) and swing-wing arrangements exhibited high control power requirements compared to the other tailless configurations. The flying wing configuration offered the least amount of instability at low AOA due to the lack of a forebody. Integration of the ICE control concepts are planform dependent; high sweep, broad chord planforms are well suited for the ICE study control effectors. Many of the integration considerations are similar for the F-16XL, 101, and 201-series configurations. The competition between high lift devices and yaw controls make tailless control suite integration on carrier-based fighters challenging. The AMT and DLEF can replace the function of the vertical tail on the F-16XL; good high AOA roll capabilities can be expected even without TV. Finally, high-sweep flying wing planforms share a synergistic design space between low control power requirements and relatively simple tailless control suite integration.

7.9 Signature Integration Studies

The impact of aircraft control surfaces on the signature of LO designs poses a formidable set of challenges to the airframe designer. The problems encountered share some common

elements with skin features such as gaps and cracks, but with the additional complication of control surface movement in flight. Planform gap alignment, minimization of gap dimensions and reduction of surface contour changes are design choices employed for both gaps and control surfaces. Unfortunately, treatments such as filler and tape, useful in the treatment of fixed panel gaps, are inappropriate in the treatment of control surface gaps. Furthermore, planform alignment, which is valuable in signature control, affects control surface effectiveness. Deflected control surfaces, with the resulting exposure of edges and abrupt outer mold line (OML) contour changes bring another dimension to the signature problem.

The design trades for minimizing control effector contributions are multi-dimensional. Signature reduction methodology for components such as gap, hinge, or louvers involve tradeoffs of field repairability, access to interior equipment, reliability, and manufacturing cost. Before these issues are addressed, however, the designer must make a more fundamental choice. Control effectors have an inherent signature contribution that depends on design geometry. Their arrangement must be chosen before treatment details are considered. This choice is a preliminary design decision with significant effects in both signature and aerodynamic performance. Signature and performance goals have to be known in advance. The choice is a compromise between conflicting requirements: the signature advantages afforded by one particular arrangement may or may not be strong enough to override an aerodynamic advantage of another.

A fair comparison of control effector arrangements requires consistent ground rules. It is assumed here that regardless of the arrangement, the installed devices have "standard" aircraft tolerances and are untreated. For example, control surface gaps are taken to be 0.2" x 0.2" and perfectly conducting. Absolute signature contributions could be reduced by placing parasitic magnetic RAM around gaps, reducing gap widths and using gap seals. For the purpose of comparison, however, untreated gaps are employed.

The large number of parameters precludes exploration of all arrangements on all planforms. The four design configurations chosen (101-TV, 101-1, 101-3 and 101-4) are a meaningful set. The signature impacts of corresponding control effector suites were com-

pared to reveal any rule of thumb dependencies such as an increasing signature as a function of the total number of gaps or total gap length. More significant perhaps is the insight into the value of reducing the required surface deflections through sizing and placement.

7.9.1 Methodology

The LMTAS Target 19 RCS model was utilized as the basic planform to analyze the chosen control effectors' signature. It has been extensively studied both analytically and through radar range measurement. Hence, its scattering characteristics are familiar. Finally, Target 19 is a LO planform -- almost any change made to its OML will be immediately apparent in its radar signature. Figure 7-45 is a reproduction of the Target 19 facet model used in this study.

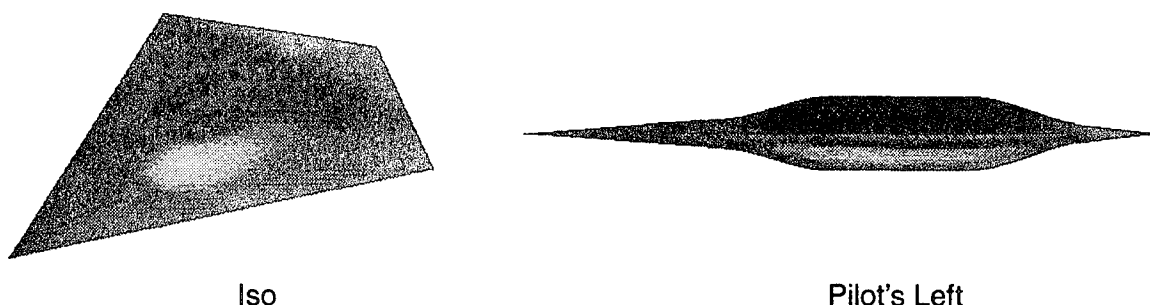


Figure 7-45 Target 19 RCS Model

Target 19 has a thick center body that houses the rotator assembly for radar range tests. This made it necessary to locate the spoilers and SSD's so that they did not occupy space on the center body.

Two in-house analysis codes, VISAGE (Visual Investigation of Scattering in an Advanced Graphics Environment) and MESSAGE (Multiple Element Surface Scatterer and Gaps Evaluation), were used to assess signature for the Target 19 planform and four configurations. VISAGE calculates multifrequency radar cross section for large, complex, metallic models using the theory of physical optics. MESSAGE uses coherent summation to evaluate the effects of all modeled surface scatterers on a three dimensional surface. Individual gap contributions employed by MESSAGE are derived from 2-D method-of-

moment (MOM) predictions verified by testing. These MOM results are modified using physical optics theory to handle off-normal impingement angles.

7.9.2 Undeployed Effectors

Surface edges, gaps, seams, ridges and curvature gradients adversely impact radar signature because they present electrical discontinuities to the incident electromagnetic (EM) field. These discontinuities scatter energy, thereby increasing the probability of detection by enemy radar. Undeployed control effectors are an unavoidable source of many or all of these energy scattering features, so it is important to minimize their signature impact through basic design considerations. This study assumed that abrupt changes in OML surface curvature due to control effectors can be avoided (this may or may not be true for the all-moving wing tip actuator fairing). Furthermore, the four configurations studied do not include hinges, seams or ridges. Therefore, the focus of this study is gaps.

The dominant mode of scattering on a surface depends on the EM field's angle of incidence with respect to surface normal of the planform. If the electric component's angle of incidence is less than about 60° with respect to normal, then specular, or optics-like scattering dominates the scatter. At greater angles (approaching grazing incidence), the incident electric field tends to generate a surface wave whose direction of propagation is parallel to the direction of incidence. This surface wave will scatter when any surface discontinuity is encountered, shedding energy. At near grazing incidence, almost all scattering is of this type. Target 19 is designed so that low observation elevations present a gently curving surface whose normal is at a large angle with respect to the incident EM field, so edge and surface wave scattering dominate radar scatter.

MESSAGE was used to determine the effects of gaps in the four configurations under consideration. In this case, the effector gaps were modeled as 0.2 x 0.2 inch rectangular troughs in the surface of Target 19, and both gaps and model were assumed to be perfectly electrically conducting (PEC). While MESSAGE calculates the scattered EM field for the case of vertically and horizontally polarized incident radiation, this study considers only the results of the vertically polarized electric field. This is because the surface of

Target 19 is primarily "horizontal" so vertical polarization will produce a surface wave. (See previous paragraph: In cases where the polarization is referenced to the local horizontal of the radar site, horizontal polarization refers to the emitted electric field component being parallel to the ground. Vertical polarization refers to the electric field component being perpendicular to the ground).

Line drawings (top view) of the four gap configurations of this study are presented in Figure 7-46.

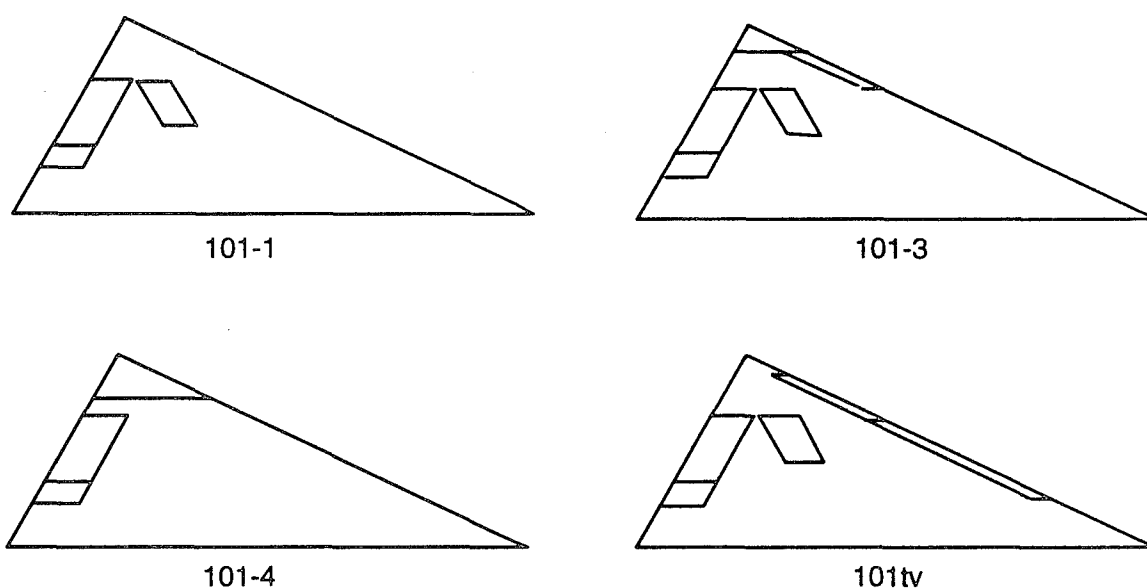


Figure 7-46 Line Drawings of the Four Gap Configurations Studied

MESSAGE data were added to the VISAGE baseline Target 19 data for each configuration, so that planform features (edges and OML) could be included in the analysis. Figure 7-47 shows the VISAGE baseline data for Target 19 at 9.7 GHz and 0° elevation. The planform edges are depicted in the center of the plot, and dashed arrows have been added to indicate the primary direction of scattering for those edges (note the data spikes pointed to by the arrows). Data is displayed in the 0° to -180° sector for brevity and for direct comparison to the deployed effectors of the following section.

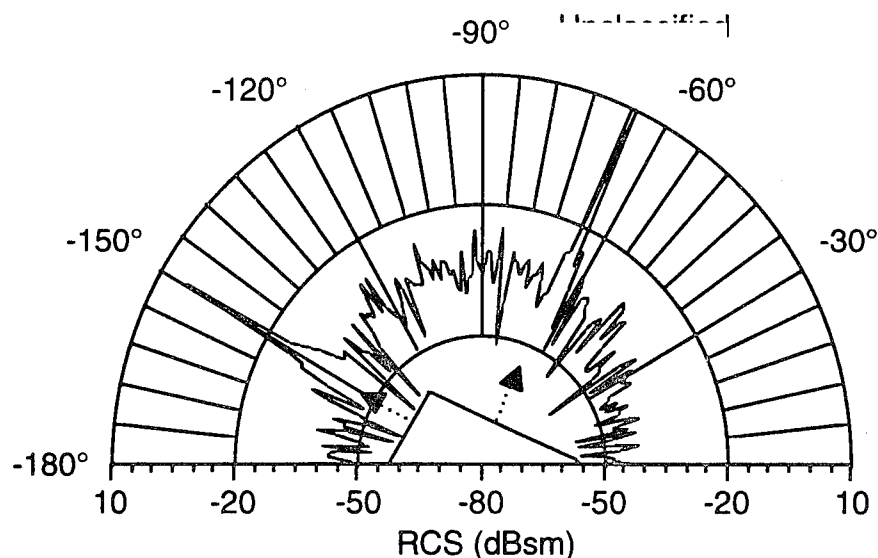


Figure 7-47 VISAGE Results for Target 19 Baseline at 9.7 GHz, 0 deg Elevation

Figure 7-48 is a plot of MESSAGE data for gaps representing Configuration 101-1 on the Target 19 planform. Note that these results only represent the contribution of the gaps -- not the RCS returns from the rest of the target; hence the lack of data in the 0 to -20 deg azimuth range. Arrows have been added to indicate the primary direction of gap scattering. Note that the data spikes are not as localized as those of Figure 7-47, and there are more of them. The scatter at any given angle is the phasor (coherent) sum of scatter from all gap segments. The gaps lie on a 3-D surface (i.e., the OML) and there are multiple gap segments; each gap segment contributes in amplitude and phase to the scattered EM field. A gap segment is a length of gap that has no interruption by another gap -- or other scattering feature -- intersecting it. For example, Configuration 101-1 shown in Figure 7-48 has 9 gap segments. Note that this figure only shows the incremental effects of the gaps, hence the lack of the planform outline in the center of the plot.

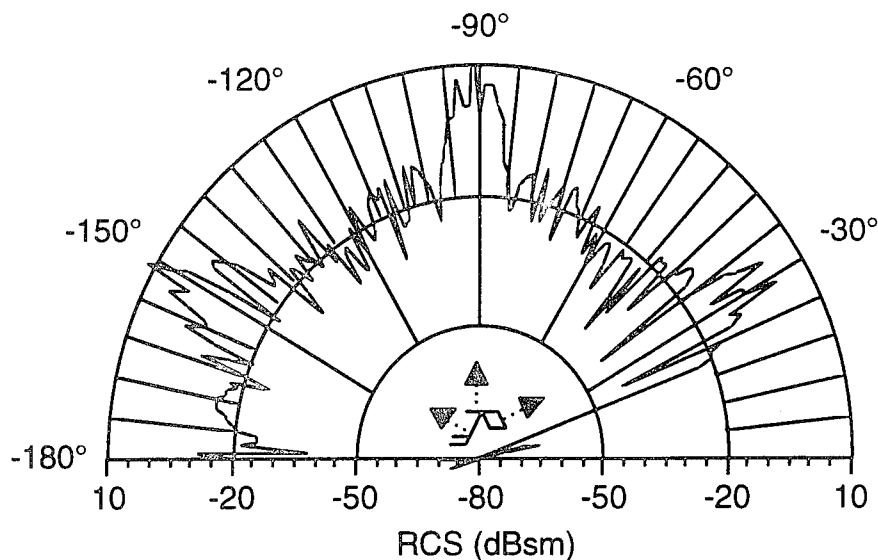


Figure 7-48 MESSAGE Results for Configuration 101-1/Target 19 at 9.7 GHz, 0 deg Elevation

Figure 7-49 shows the scalar summation of the VISAGE data of Figure 7-47 with the MESSAGE data of Figure 7-48. The data of Figure 7-49 is an approximation to the effects of gaps on the 101-1/Target 19 planform. The four configurations were analyzed by coherently summing the MESSAGE gaps results with the bare-target VISAGE data.

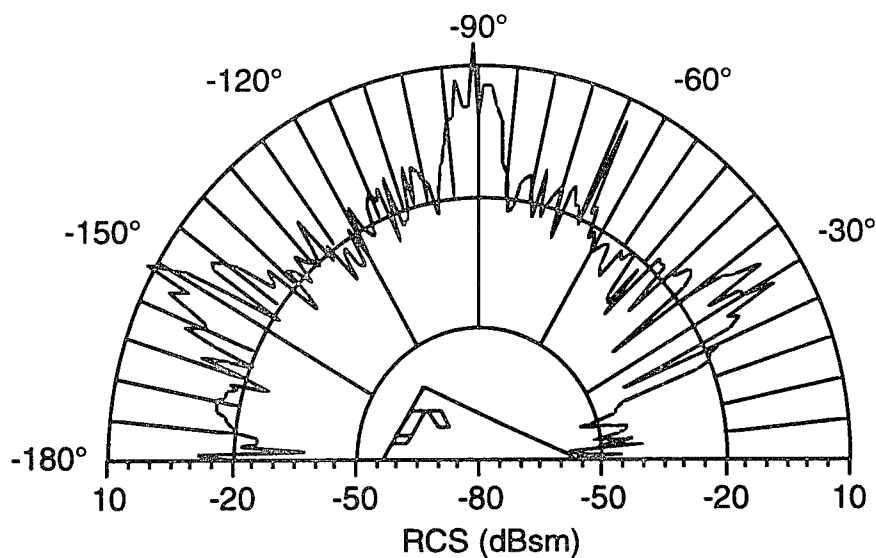


Figure 7-49 Scalar Sum of MESSAGE and VISAGE Results for Configuration 101-1/Target 19 at 9.7 GHz, 0 deg Elevation

A comparison of Figures 7-47 and 7-49 shows that gaps increase radar scatter, the effects being most prominent in the sectors perpendicular to gap length. For example, Figure 7-47 exhibits much less scatter around -30° of azimuth than Figure 7-49. Scatter in this sector arises from gaps (and gap-gap interactions) that lie along -120° (the gaps perpendicular to the right-most arrow in Figure 7-48). Similarly, increased scatter is seen around -90° and -150° of azimuth. These effects are often "quantified" in a sector average (or sector median) figure-of-merit for important azimuthal sectors. A common and important figure of merit is the frontal, or $\pm 60^\circ$ sector average. Frontal sector averages (0° to -60° in this case) were calculated for the four configurations of this study at 5.4, 9.7 and 16 GHz, and at 0° and $\pm 10^\circ$ elevations.

Figures 7-50 through 7-52 illustrate the differences in frontal sector averages for the indicated study parameters. Note that more negative values offer better RCS performance. The bar marked "planform" represents the baseline Target 19 VISAGE results with no control surfaces.

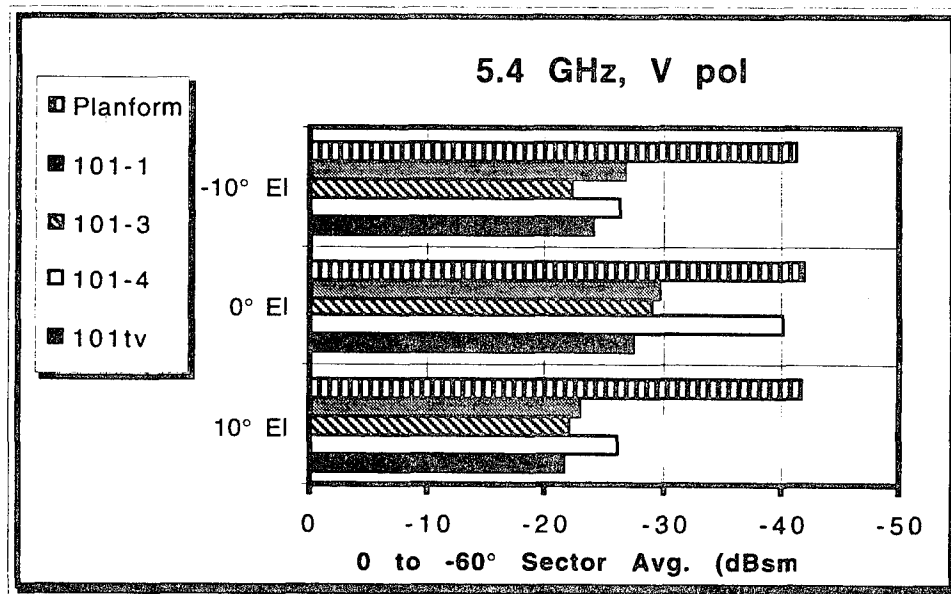


Figure 7-50 5.4 GHz Frontal Sector Comparison with No Control Deflections

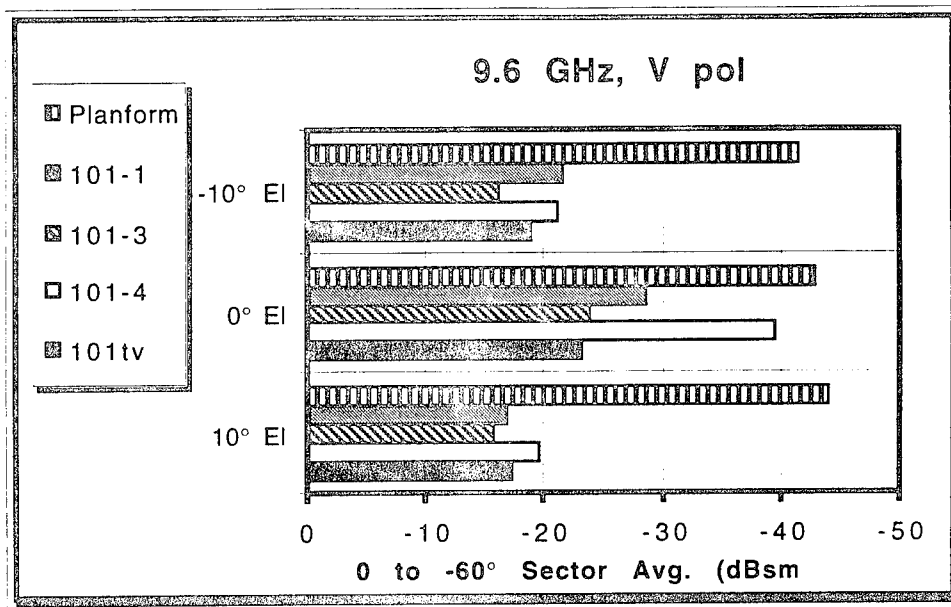


Figure 7-51 9.7 GHz Frontal Sector Comparison with No Control Deflections

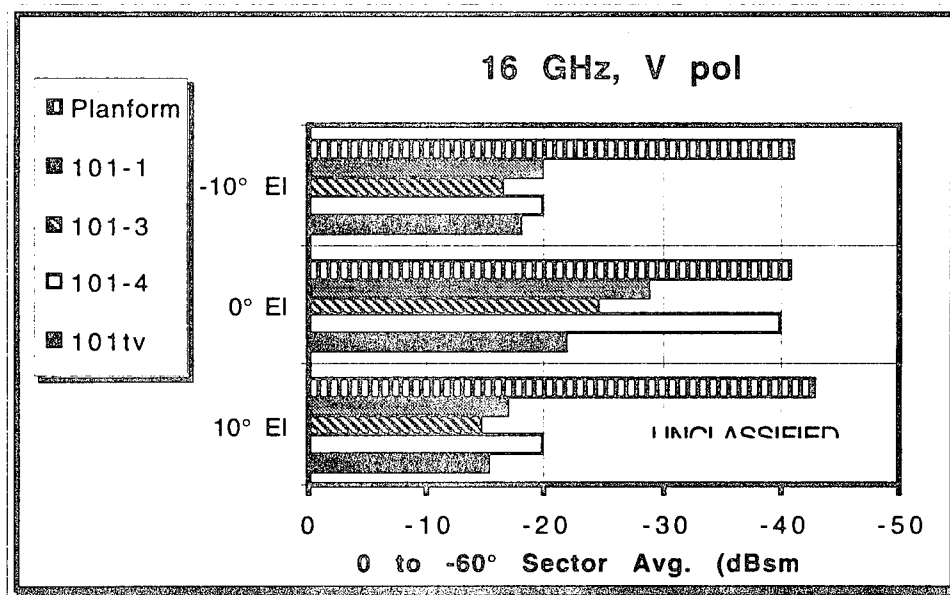


Figure 7-52 16 GHz Frontal Sector Comparison with No Control Deflections

Figures 7-50 through 7-52 make it clear that Configuration 101-4 yields the most desirable frontal sector average, with Configuration 101-1 coming in a distant second. Configuration 101-4 has the least number of gaps that are “perpendicular” to the studied sector (that is, gap segments that run along -120°), so most of the contribution in this sector

will be due to the Target 19 planform. Configuration 101-1 follows in desirability because it has the next fewest number of gaps perpendicular to this sector. Decreasing the number of gap segments perpendicular to a sector will improve signature in that sector. There are two ways to reduce the number of gap segments: eliminate gap segments completely (ideal), or combine gap segments into longer contiguous gap segments. The latter method will narrow the scatter distribution.

Figures 7-50 through 7-52 also show the effect of elevation angle on scatter. As observation angle of the transmit/receive radar varies, scatterers that were formerly shadowed by other surface features come into view. Or, scatterers that were formerly visible may become obscured by surface features. For example, Configuration 101-1 has a lower signature at -10° than at 10° elevation because the spoiler deflector gaps are less "visible" at that point. Also, Configuration 101-1 has a lower signature at 0° than at $\pm 10^\circ$ elevations because surface curvature of the Target 19 planform shadows gap segments at 0° .

7.9.3 Deployed Effectors

The previous section on undeployed effectors made note of the fact that the dominant mode of scattering from a surface feature is a function of the angle of incidence with respect to that feature. Specular scattering is the ray optics case of angle of reflection equal to angle of incidence, and generally this mode of scattering dominates for incident angles less than about 60° with respect to normal. For a flat plate, there is only one specular direction. For a curved surface, there is an infinite number of specular directions. The specular direction of concern for most tactical radars is that in which the direction of scattering is back toward the direction of incidence (backscatter). This yields the largest radar return of any scattering mechanism. In addition, physical optics theory predicts that some backscatter is present at angles removed from normal incidence. As the angle of incidence increases, backscatter falls off at a rate dependent on wavelength and effector dimensions. Large panel size and high frequencies tend to make the backscatter spike sharper, that is, confined to the surface normal direction. The deployment of an OML control effector, may therefore contribute to radar scatter in some sector even though the incidence is not along the surface normal.

When an OML effector is deployed, new scatterers appear and previous scatterers change. Gaps widen or become cavities. Surface contours change and new features are presented to the radar (edges, bottom surfaces, etc.). Scattering effects associated with these changes will involve both physical optic and surface wave mechanisms. Full analysis of these effects is beyond the scope of this study. Indeed, a rigorous treatment involving method-of-moment or finite-difference techniques is not currently possible given the model size, frequencies of interest, and state-of-the-art computer resources.

Given the computational restraints, this study focused on physical optics effects for deployed effectors on the four configurations. Also, infinite combinations of physical deflections for each configuration's effectors were eliminated from consideration by assuming maximum deflections required to augment flying qualities during LO ingress at Mach 0.9/25K when subjected to moderate random turbulence levels. The maximum deflection of any effector under these conditions was less than 5° .

To further ease model design work and computation, models representing only the pilot's left-hand-side of the planforms were created and analyzed. Surface currents are not represented in the physical optics method, so there is little loss of information in doing so. The deflections for each effector were the maximum needed to maintain stability under the conditions described above.. These models with deployed effectors are reproduced in Figure 7-53.

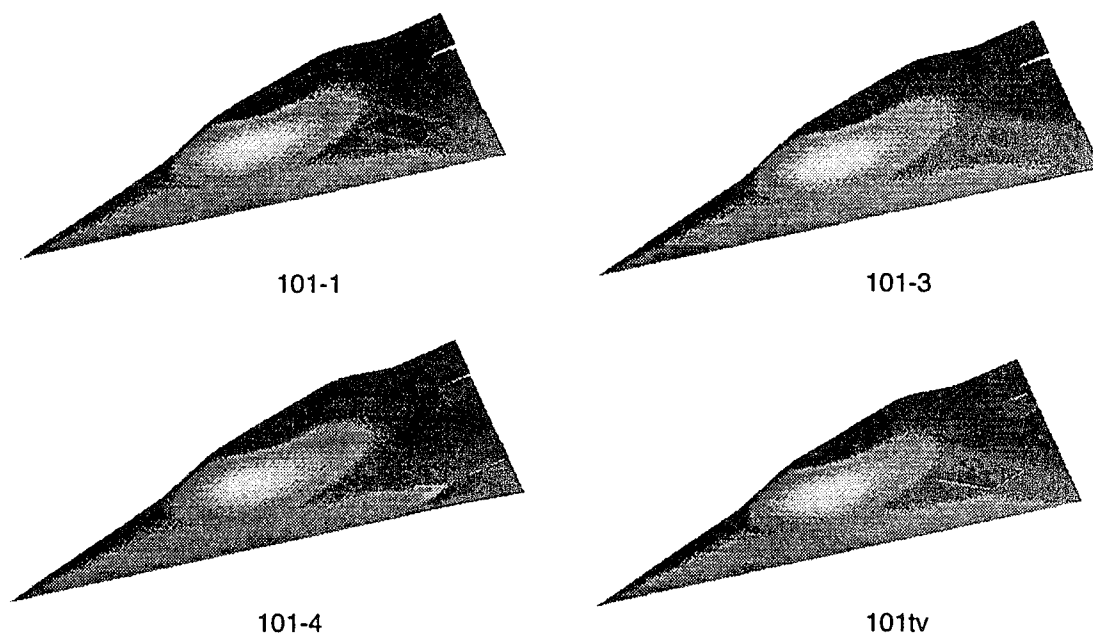


Figure 7-53 Target 19 Configuration Models with Deflected Controls

The scattered EM field for each configuration was calculated by VISAGE. Since deflections were rather small, differences between the models and Target 19 planform are not extremely pronounced, except in the case of newly exposed edges whose spike is visible at -90° azimuth. Figure 7-54 shows the VISAGE data for configuration 101-1 at 0° elevation and 9.7 GHz.

Figure 7-47 of the previous section is a polar plot of VISAGE data at 9.7 GHz and 0° elevation for the Target 19 planform (no effectors). Direct comparison of Figures 7-54 and 7-47 reveals the change in radar backscatter arising from deflected effectors on the planform. As mentioned above, a large spike at -90° due to the appearance of deflector edges is evident in Figure 7-54. A smaller spike due to the slight deflection of the spoiler appears at -30° . The slight deflection of the trailing edge flap serves to "break" the back edge line and hence slightly decrease the size of the spike at -150° . However, it does this at the expense of creating another spike at about -138° and increasing the overall scatter in the -120° to -180° sector.

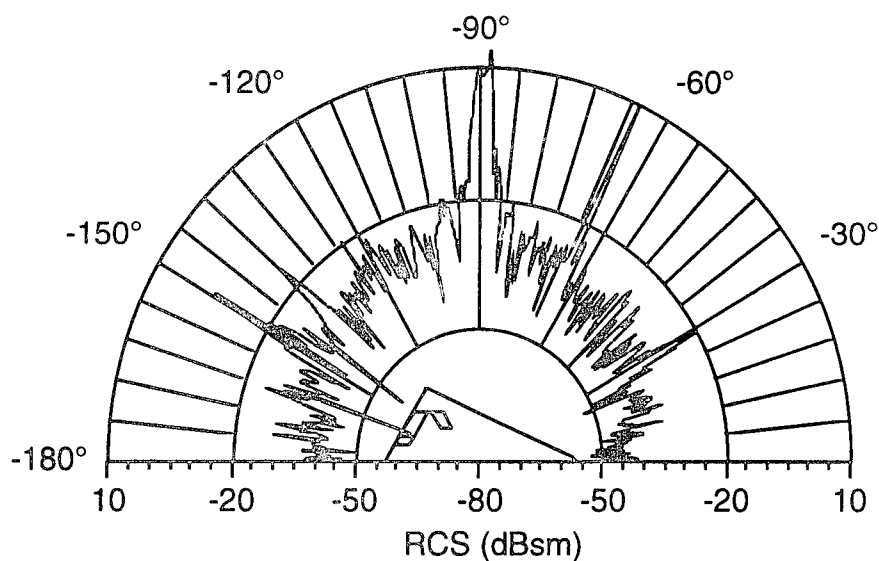


Figure 7-54 Configuration 101-1/Target 19 with Deflected Controls at 9.7 GHz, 0 deg Elevation

Frontal sector (0° to -60° azimuth) averages were computed for each of the four configurations with deployed effectors, and the results are shown for indicated parameters in Figures 7-55 through 7-57.

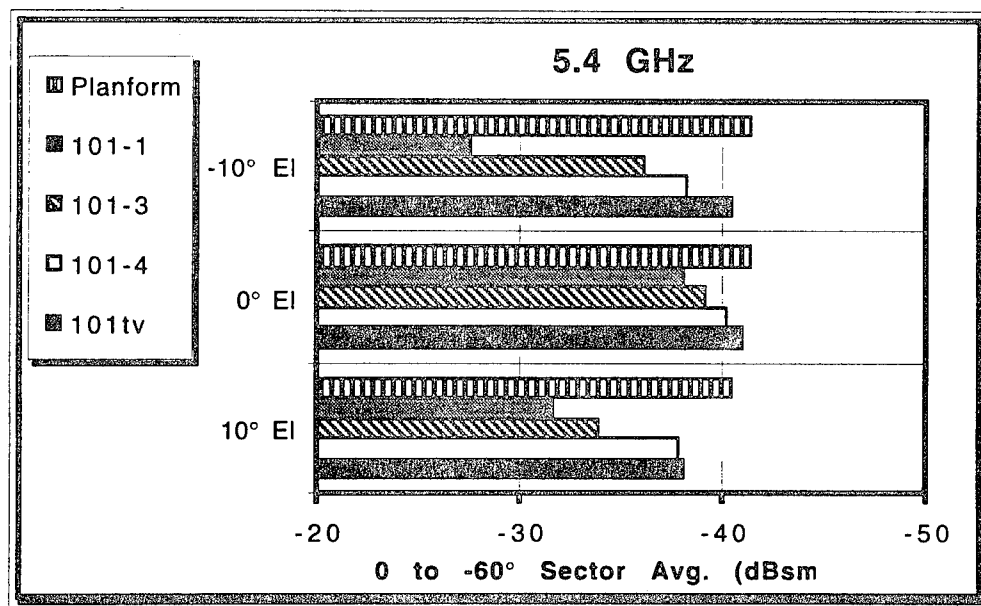


Figure 7-55 5.4 GHz Frontal Sector Comparison with Deflected Controls

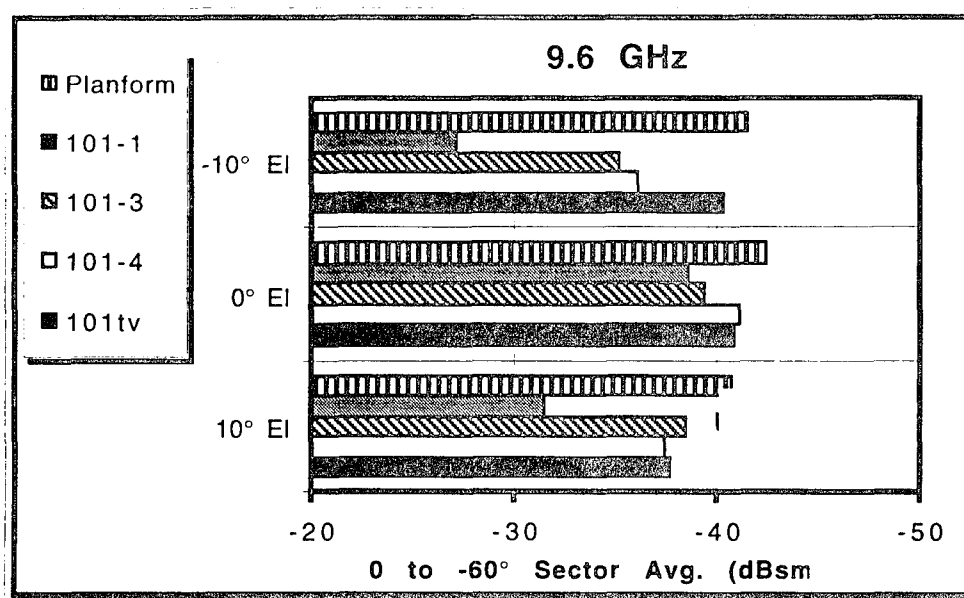


Figure 7-56 9.7 GHz Frontal Sector Comparison with Deflected Controls

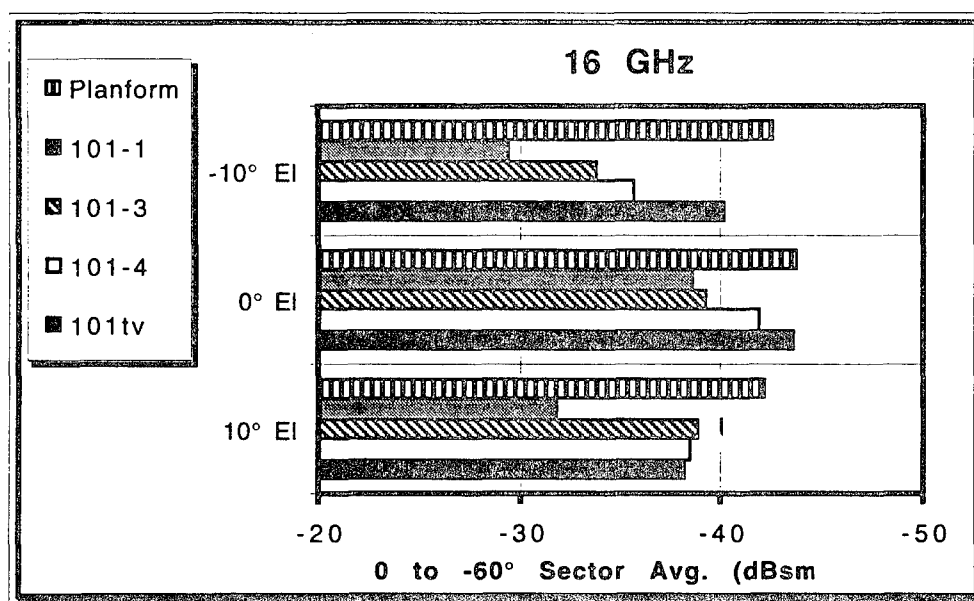


Figure 7-57 16 GHz Frontal Sector Comparison with Deflected Controls

Overall, it appears that Configuration 101-TV yields the best signature performance in the frontal sector for the given deflections, followed very closely by 101-4. In most cases, there is a slightly larger penalty from rotating the all-moving tip of 101-4 than from deflecting the spoiler of 101-TV. At 10° elevation 101-4 starts to gain advantage because the all-moving tip is pivoted TED. However, at -10° elevation 101-TV gains advantage

for the same reason. That 101-1 fares worst in this comparison is not surprising; the slot deflector presents two surfaces (top and bottom spoilers) that will greatly impact the frontal sector.

7.9.4 Summary and Conclusions

The primary design rule for a LO planform is straightforward: the planform should not have surface or edge scatter within the primary threat sector. Even if this is accomplished, spike flashes will occur in another sector. The designer of control effectors can do the following to mitigate the unavoidable fact that there will be spikes in some sector: planform align any spike-producing feature and make it as long as possible. This will have two desirable effects on radar scatter: it will narrow the distribution and place distribution centroids all in the same spatial direction.

The following conclusions are drawn from the 0 deg to -60 deg frontal sector average data presented above. The results of the MESSAGE gap analysis (undeflected controls) showed Configuration 101-4/Target 19 to have the best RCS performance with Configuration 101-1 coming in a distant second. Analysis with the control surfaces deflected consistent with the magnitudes required to augment flying qualities during an LO ingress indicated Configuration 101-TV performed the best with Configuration 101-4 second. Configuration 101-1 performed poorly due to the leading edges of the SSD being exposed to the radar in the frontal sector.

The models used in this analysis assumed a solid metal target with no treatments. No control surface details like hinges, internal cavity structure or pivot trunions were modeled. Analysis of these details would require high-order computational analysis and/or pole model testing. Analysis of the test configuration with treatments would require higher security classification than that considered during the ICE program. These results are provided as a guide to determine which control suites offer the most promising low-RCS performance when considering treatment suites. Details like internal structure within the SSD cavity, or the AMT pivot trunion will have a significant impact on the RCS performance and the integration of these controls.

This study focused on radar signature impacts of effectors without regard to other requirements. The designer that develops a clean sheet configuration that is "correct" from the standpoint of this study must be aware that on an LO planform any cavity, OML feature, duct, etc., is a signature issue. Almost any unanticipated -- or for that matter, anticipated -- external modification to a well designed LO configuration will be detrimental to signature. For instance, adding an actuator bump or fairing to an OML becomes an issue on LO planforms.

7.10 Carrier Suitability Impacts

Wing tip yaw controls like the AMT and clamshells require large deflections to be effective. The large surface sizes coupled with an aft location makes deck strike a problem for carrier-based aircraft. Control surface limiting by the FCS with gear and flaps down is one way to get around the problem. Unfortunately, yaw control power, and therefore roll performance would suffer. This would be especially critical for any of the 201-series configurations in the PA phase. Figure 7-58 shows an example of the clearance requirements during catapult launch for Configuration 201-TV. It is apparent from the figure that the deflected clamshell will interfere with objects on the deck. Similar problems would be experienced by the AMT.

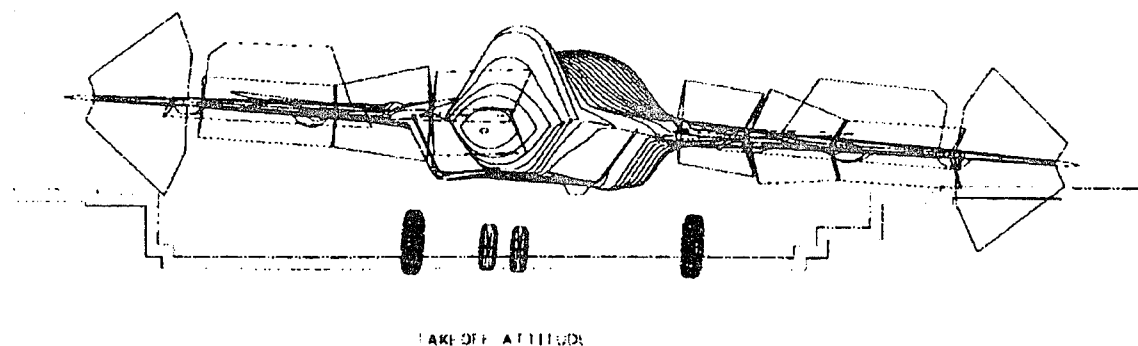


Figure 7-58 Configuration 201-TV Clearance Requirements during Catapult Launch

The current SSD location should not pose any deck-strike problems; however the control may pose a hazard to personnel working beneath the aircraft.

The wing fold location creates structural integration difficulties for both the SSD and spoiler. The current design limits potential spoiler or SSD locations. An outboard wing fold may improve spoiler/SSD integration resulting in a weight savings with the penalty of an increase in spot factor.

7.11 Reliability, Maintainability and Supportability (RM&S) Assessment

The purpose of this study is to assess the RM&S impacts of a variety of control surfaces for an advanced fighter design with no vertical tail or rudder. Configuration 101, a tailless delta flying wing, was established as a baseline earlier in the study with thrust vectoring. This baseline then had 3 variations selected for further analysis for a USAF aircraft. A USN variant with a canard-delta wing configuration was also studied with similar variations on the different baseline.

7.11.1 Approach

A top level comparative systems approach was chosen to attempt to quantify the expected logistics reliability levels of the ICE configurations. The reliability performance measured for a variety of previous USAF and USN aircraft flight control systems are recorded in Table 7-6. The parameter used is Mean Flight Hours Between Failures (MFHBF) which has a similar definition between both USAF and USN. Although some differences exist between the data collection systems, the intent is to measure verified "inherent" failures which are not caused by operator, induced by environment or falsely removed. MFHBF is also sometimes referred to as "logistics" reliability due to its primary use of measuring maintenance actions and replacements. A subset of these failures will actually affect a mission and these are termed "critical" failures and usually lead to a mission abort or deviation.

Table 7-6 Historical Aircraft Flight Control System Reliability

Aircraft	Control Effectors	Total Number of Control Effectors*	Flight Controls MFHBF**	% of Total Aircraft MFHBF
F-16C Block 50	plain trailing edge flaperon, leading edge flap all-moving differential horizontal tails, single rudder, dual speedbrakes, dual ventral fins	7	62.0	6.2
A-10A	Inbd LE slats, clamshell ailerons/speedbrake ("decelerons"), 2 section Fowler flaps, 2 section elevator, twin rudders	13	45.8	8.8
F-5E	single slot trailing edge flaps, ailerons outboard, plain leading edge flaps, all moving horizontal tails, rudder, two airbrakes under fuselage	10	41.5	9.5
F-15C	inner trailing edge plain flap, outer aileron, all-moving differential horizontal tails, twin rudders, airbrake upper fuselage	9	30.8	6.6
F-4E	plain trailing edge flaps, ailerons outboard (only down deflection), one spoiler on each wing, two section leading edge slats, all moving horizontal tail, rudder	13	13.1	8.4
F-105	LEFs, 5 section spoilers, Fowler flaps, ailerons, all moving horizontal tail, rudder, 4 segment speedbrake	20	8.1	12.0
AV-8B	aileron, plain flaps, airbrake, all moving horizontal tail, rudder, thrust vectoring(rotating nozzles), 4 reaction air jets for hover	9 (reaction jets not counted)	23.3	9.1
F/A-18C	2 section LEFs, inner trailing edge plain flap, outer aileron, all-moving differential horizontal tails, twin rudders, airbrake between tails	11	17.7	10.7
A-4M	2 section speedbrake, ailerons, split flaps, LE slats, spoilers, elevators on variable incidence stabilizers, rudder	12	12.0	10.4
A-6E	2 section LE slats, 2 section Fowler flaps, 2 segment spoilers, clamshell speedbrakes on each wingtip, all moving horizontal tail, rudder	16	7.5	8.3
A-7E	2 section LEFs, single slot flaps, ailerons, all moving horizontal tail, rudder, ventral speedbrake	12	7.2	11.6
F-14A	three section trailing edge single slotted flap over full span, two section leading edge slat over full span, four spoilers on each wing, all-moving differential horizontal tails, twin rudders, dual ventral fins, upper & lower speedbrakes	25	6.2	10.8

* Speedbrakes counted as 1 regardless of number of segments

** Flight Controls system includes actuators, surfaces and electronics

7.11.2 Results

As seen in Figure 7-59 the flight control system reliability generally decreases as more control effectors with the associated actuators, linkages, connections, etc. are added. This simple inverse relationship was used to predict the ICE configurations for USAF and USN variants. The F-16C was used as the baseline for the USAF versions, and the F/A-18C was the USN baseline. The values are shown in Table 7-7.

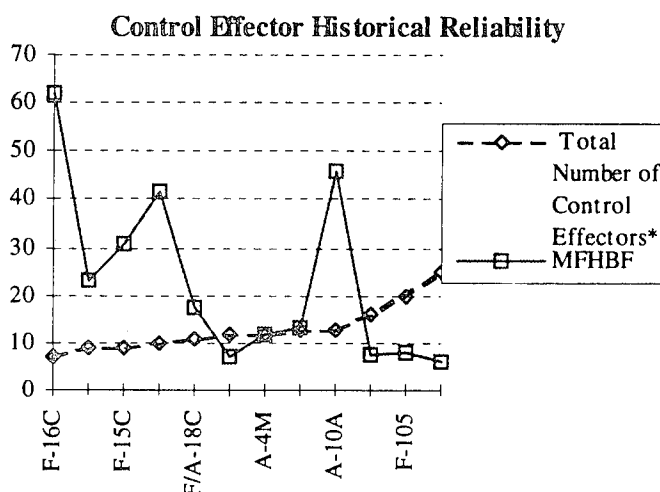


Figure 7-59 Inverse Relationship Between Reliability and System Complexity

7.11.3 Comments and Conclusions:

The predicted reliabilities shown in Table 7-7 are within the context of the baseline historical aircraft and do not reflect predicted improvements. A next generation aircraft will feature increased reliability and maintainability in the areas of actuators and electronics. Reliability improvements can be expected for most components in the range of 10% to 20% due to process and design improvements⁴³. Maintainability improvements can be expected in the increased diagnostics capability embedded in next generation actuators⁴⁴. Additional improvements (compared to existing aircraft) may be realized with careful architecture design, optimization of redundancies (quad vs. triplex, analog vs. digital backup, etc.) and an overall simple and robust design. Due to the limited scope of the ICE study, these influences were not fully explored but may provide total R&M perform-

ance increases of up to 50%, possibly more, even with increased numbers of control effectors.

Additional qualitative comments:

- Having such a large number of control effectors improves mission reliability by providing redundancy, assuming the flight control electronics can detect the failures and reconfigure the remaining surfaces as necessary.
- A larger number of actuators and hinge points will reduce the logistics reliability due to parts count, however this impact can be minimized through good mechanical design focusing on seals, minimizing slipper doors, robust surfaces and dealing with aerosonic fatigue.
- The ICE configurations add significantly to the number of effectors compared to previous fighter/attack aircraft, but the mechanical portions do not contribute significantly to the system reliability. The electronics (computer, air data, gyros and actuator controls) are the main drivers.
- Maintenance times will still be improved compared to the historical aircraft due to elimination of cables and reduction in mechanical connections. It is assumed that improved diagnostics and rigging features of the F-22 actuators will be utilized within an Integrated Diagnostics environment to provide fault filtering and health monitoring.

Table 7-7 ICE Configurations Predicted Reliability

Configuration	Control Effectors Description	Total Number of Control Effectors*	Predicted MFHBF
101 Baseline	Differential Inbd & Outbd LEF, Inbd & Outbd Spoilers, Pitch Flaps, Elevons, Clamshells	12	36.2
101 - TV	Differential Inbd & Outbd LEF, Inbd & Outbd Spoilers, Pitch Flaps, Elevons, Delete Clamshells, Thrust Vectoring	14	31.0
101 - 1	Inbd & Outbd Spoiler/Slot Deflectors(SSDs), Pitch Flaps, Elevons, Thrust Vectoring	10	43.4
101 - 3	Differential Outbd LEF, 1 Segment Spoiler/Slot Deflector(SSD), Pitch Flaps, Elevons, All Moving Tips (AMT), Thrust Vectoring	12	36.2
101 - 4	Pitch Flaps, Elevons, All Moving Tips (AMT), Thrust Vectoring	8	54.3
201 Baseline	Canards, Differential LEFs, Spoilers, Clamshells, Ailerons, Inbd & Outbd Elevons	14	13.9
201 - TV	Canards, Differential LEFs, Spoilers, Clamshells, Ailerons, Inbd & Outbd Elevons, Thrust Vectoring	16	12.2
201 - 1	Canards, Differential LEFs, Spoiler/Slot Deflector (SSD), Ailerons, Inbd & Outbd Elevons, Thrust Vectoring	14	13.9
201 - 3	Canards, Differential LEFs, Spoiler/Slot Deflector (SSD), Ailerons, Inbd & Outbd Elevons, All Moving Tips (AMT), Thrust Vectoring	16	12.2
201 - 4	Canards, Differential LEFs, Ailerons, Inbd & Outbd Elevons, All Moving Tips (AMT), Thrust Vectoring	14	13.9

* Assuming Thrust Vectoring counts as 2 - Pitch and Yaw

7.12 External Stores Carriage Assessment

Although these configurations were designed with internal weapons bays for RCS reasons, it may be desirable to carry external stores on missions where RCS requirements are not so stringent.

A rough assessment of the external stores carriage ability on four of the land-based configurations was made based on the wing area available for hardpoints (Figure 7-60). The

results will be similar for the carrier-based configurations. The area available is a fixed distance outboard of the main landing gear on the wing, and was normalized with the area available on Configuration 101 defined as 1.0. Configuration 101-TV has the greatest area available for underwing stores due to the absence of any tip control devices (area = 1.12). Not surprisingly, Configuration 101-3 has the least area available (0.82). A proposed MRF wing is shown for comparison (area = 1.2); and illustrates the configuration dependency of these results.

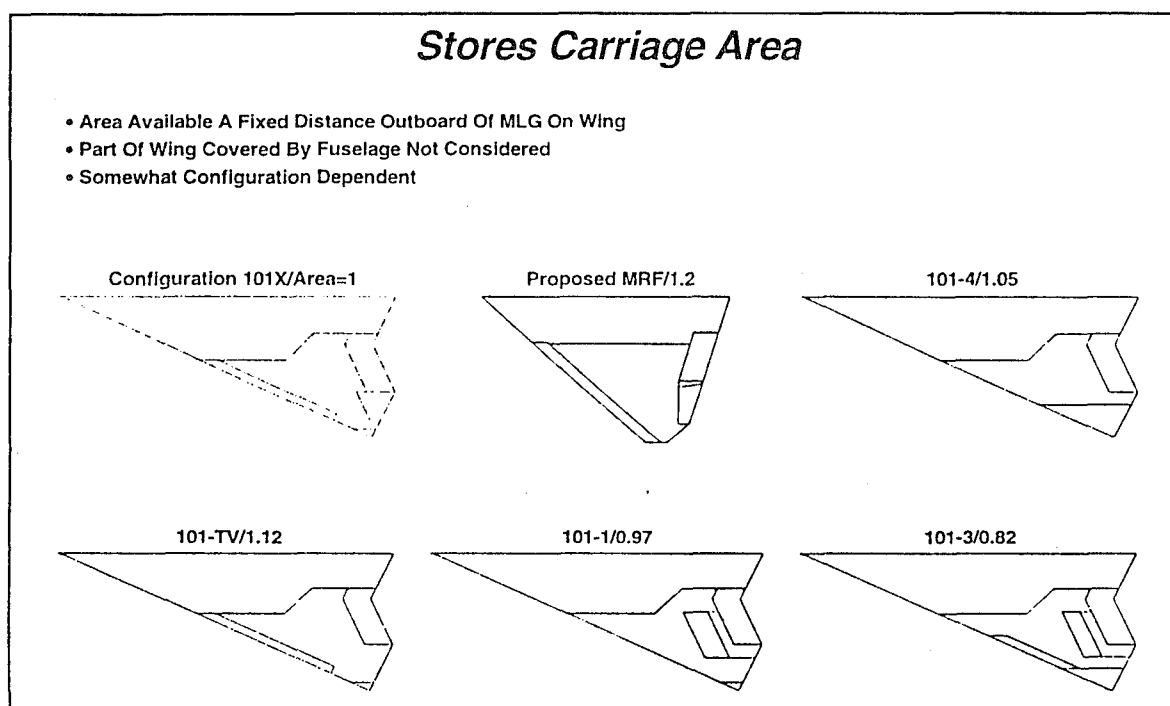


Figure 7-60 External Stores Carriage Area

Additionally, it is doubtful that configurations employing the SSD (101-1 and 101-3) could carry large stores forward of the control effector without disrupting SSD control effectiveness. Obviously, the area behind the SSD is off limits to stores.

7.13 Control Summaries

The integration impacts due to each control effector were compiled and ranked using a quality-function-deployment (QFD) approach. QFD is a method which can compare various methods with competing demands (measures of effectiveness or MOE).

Weightings are associated with each MOE based on customer desires. Scoring consists of giving each method or technology (in this case controller or control suite) a raw score (0, 3, 6 or 9) for each MOE category, multiplying by the appropriate weighting, and adding the results for each technology. Final rankings are determined by comparing the total weighted scores. Scores and rankings were based on the 0, 3, 6, or 9 scale with the hope that the final total scores would be widely separated, giving a clear final ranking.

QFD helps to illustrate the high payoff items based on the customer desires. QFD was used to provide structure to the overall ranking process, improve visibility into the system drivers and focus the customer desires. QFD is not a substitute for quantifiable engineering analysis. In this case, it was used to qualitatively rank the various control concepts and control suites based on quantitative engineering analysis.

7.13.1 Control Effector Summary

A summary of the control effector rankings is provided in Figure 7-61. The weighting and scoring scale are shown in the figure. Scores were applied based on previous quantitative results obtained during the ICE study. Transitionability (Trans) and CV suitability are included in the MOE categories. In this figure, CV suitability accounts for operations on-board the carrier (i.e., deck strike, deck handling, risk to personnel, etc.) and not carrier flying qualities. Effects on CV flying qualities are addressed at the configuration level in the next section. The innovative control effectors were compared with each other and with the more conventional controls (i.e., spoiler and clamshell) and thrust vectoring. The all moving wing tip and thrust vectoring scored highest within this matrix. The lower spoiler, deployable rudder and clamshell were ranked the lowest.

Control Effector Summary

Effector	Cntrl Pwr AOA < 20	Cntrl Pwr 20>AOA>30	Cntrl Pwr AOA > 30	Effect in Beta	Linear w/ Defl	Interact w/ TEF	Weight	Fwd Sector RCS	Aft Sector RCS	Beam RCS	Hyd Reqmts	Trans	CV Suit.	Total Score	Rank
All Moving Tip	9	9	9	9	9	9	6	3	3	3	9	6	6	639	1
Spoiler-Slot Deflector	9	6	0	6	9	0	3	6	6	6	9	3	6	504	4
Diff LEF	0	6	9	9	3	9	3	3	6	3	9	0	9	522	3
Deployable Rudder	9	3	0	3	6	6	3	3	3	3	3	3	9	396	7
Lwr Spoiler	6	3	0	3	3	3	6	6	6	6	3	6	6	396	7
Conv Spoiler	9	3	0	6	6	3	6	6	6	6	3	6	9	486	5
Clamshell	9	6	3	3	6	9	3	3	3	3	6	6	6	468	6
Thrust Vectoring	3	6	9	9	9	9	6	3	3	6	9	9	3	549	2
Weighting Factors	9	9	6	6	6	6	9	9	6	3	9	3	9	XXX	XXX

Weightings:

- 0 Not Important
- 3 Minor Importance
- 6 Moderate Importance
- 9 Very Important

Scores

- 0 Unacceptable
- 3 Poor
- 6 Good
- 9 Excellent

Figure 7-61 Control Effector Summary

7.13.2 Control Suite Summary

A summary of each innovative control suite was compiled in a manner similar to the control effector summary (Figure 7-62). Some of the categories are similar, but were applied at the airplane level for the entire suite of control effectors. This comparison is more a "control suite" ranking than a control effector ranking. The 101-series and 201-series configurations were broken up and ranked separately because of the 201 emphasis on carrier operations. Weight, range and acceleration changes were scored based on comparisons to baseline values. An improvement resulted in a positive score while a degradation resulted in a negative score. The other categories were scored based on relative value (unacceptable, poor, fair and excellent). The RM&S scores were based on comparisons of each configurations MFHBF predictions with the F-16C (USAF configurations) and F/A-18C (USN configurations).

Configuration Summary -- 101 Series

Configuration	Roll Perf AOA > 20	FQ w/o TV	Range Change	Weight Change	RCS	FCS Complex	Accel Change	Recov WOD	Launch WOD	Hyd System	RMS	Total Score	Rank
101	3	6	0	3	3	3	-3	0	0	0	3	144	4
101-TV	6	3	0	0	6	3	0	0	0	0	3	144	4
101-1	6	3	6	6	6	6	0	0	0	6	6	315	2
101-3	9	6	3	6	3	3	-3	0	0	6	3	270	3
101-4	9	9	9	6	6	9	-3	0	0	6	6	405	1
Weighting Factors	6	9	9	9	9	6	3	0	0	6	9	XXX	XXX

Configuration Summary -- 201 Series

Configuration	Roll Perf AOA > 20	FQ w/o TV	Range Change	Weight Change	RCS	FCS Complex	Accel Change	Recov WOD FQ	Launch WOD FQ	Hyd System	RMS	Total Score	Rank
201	3	6	0	9	3	3	0	0	0	0	6	234	5
201-TV	6	3	0	0	6	3	0	3	9	0	3	252	3
201-1	6	3	-6	3	6	3	0	3	9	6	6	288	2
201-3	9	6	-6	-3	3	3	-3	9	9	3	3	252	3
201-4	9	9	9	6	6	6	-6	6	9	6	6	531	1
Weighting Factors	6	9	9	9	9	6	3	9	9	6	9	XXX	XXX

Weightings:

- 0 Not Important
- 3 Minor Importance
- 6 Moderate Importance
- 9 Very Important

Scores

	Weight/Range/Accel	Others
-9	Large Degradation	
-6	Moderate Degradation	
-3	Small Degradation	
0	No Change	Unacceptable
3	Small Improvement	Poor
6	Moderate Improvement	Fair
9	Large Improvement	Excellent

Figure 7-62 Innovative Control Suite Summary

The 101-4 and 201-4 configurations clearly ranked the highest. The -1 and -3 derivative configurations ranked 2nd and 3rd for both the 101-series and 201-series airplanes. The baseline land-based configurations both ranked low with the thrust vectored airplane scoring higher than the baseline with aerodynamic controls only. Configuration 201-TV tied with Configuration 201-3 for 3rd place in the 201-series ranking matrix.

8 Risk Reduction Plans

Three promising control concepts were investigated in detail during Phase I of the ICE study -- the all-moving wing tip, spoiler-slot deflector and differential LEF. The following section summarizes the technical risks associated with integrating these controls on a full-scale aircraft. Also discussed are plans to conduct Phase II of the ICE effort in order to reduce some of these risks. Phase II will involve wind tunnel testing of the selected control concepts, integrating the new data into the Phase I control databases and additional analysis using the updated databases.

The following areas were identified as requiring further definition through testing and additional analysis. Some of these areas are considered objectives for Phase II of the ICE program while others should be addressed in follow-on efforts.

1. Evaluate the aeroelastic effects on AMT and SSD control effectiveness. This will require detailed finite element structural modeling to calculate the flexibility effects on the AMT and SSD aerodynamics, followed by simulation analysis to quantify the impacts on high-speed flying qualities.
2. Evaluate in detail the effects of hinges, internal cavity structure and pivot trunions on the RCS characteristics of the SSD and AMT. The potential RCS reductions available with various treatment suites should be investigated as well. This will at least require high order computational modeling and possibly pole model testing.
3. Refine the transonic AMT and SSD control effectiveness data.
4. Determine the effect that AMT hingeline orientation has on control effectiveness. Hingelines oriented other than streamwise to the flow may reduce the negative RCS impacts of the AMT.
5. Determine the effect that control surface geometry (e.g., location, size, slot geometry) has on SSD effectiveness. Structural design considerations may impact the effectiveness of the control surface.

6. Further define the SSD interaction with trailing control power at various deflections and Mach numbers. The design should be optimized to minimize the aerodynamic interactions between the controls or determine control surface requirements that will mitigate the adverse interactions.
7. Evaluate the rotational and large sideslip effects on available control power at high AOA. This has implications on departure and spin recovery.
8. Enhance the 201-series aerodynamic database and refine the analysis of this configuration series.
9. Expand the DLEF database including additional control deflections and interactions with other control surfaces.

Objectives 4 through 9 will be addressed by Phase II of the ICE program. Objective 3 is offered as an option to Phase II. The first objective, dealing with the aeroelastic effects on control power, is not currently funded, but needs to be addressed to minimize the structural design risk of incorporating these control surfaces. The second item (additional RCS analysis) is beyond the scope and security classification level of current Phase II planning.

8.1 Plan for Phase II

Phase II will consist of three major design, test and analysis tasks, plus a fourth task covering documentation and interim briefings. Figure 8-1 shows an outline of the Phase II ICE plan. The major tasks that will make up Phase II consist of: (1) Wind Tunnel Model Design and Construction; (2) Wind Tunnel Testing; (3) Post-Test Analysis; and (4) Documentation.

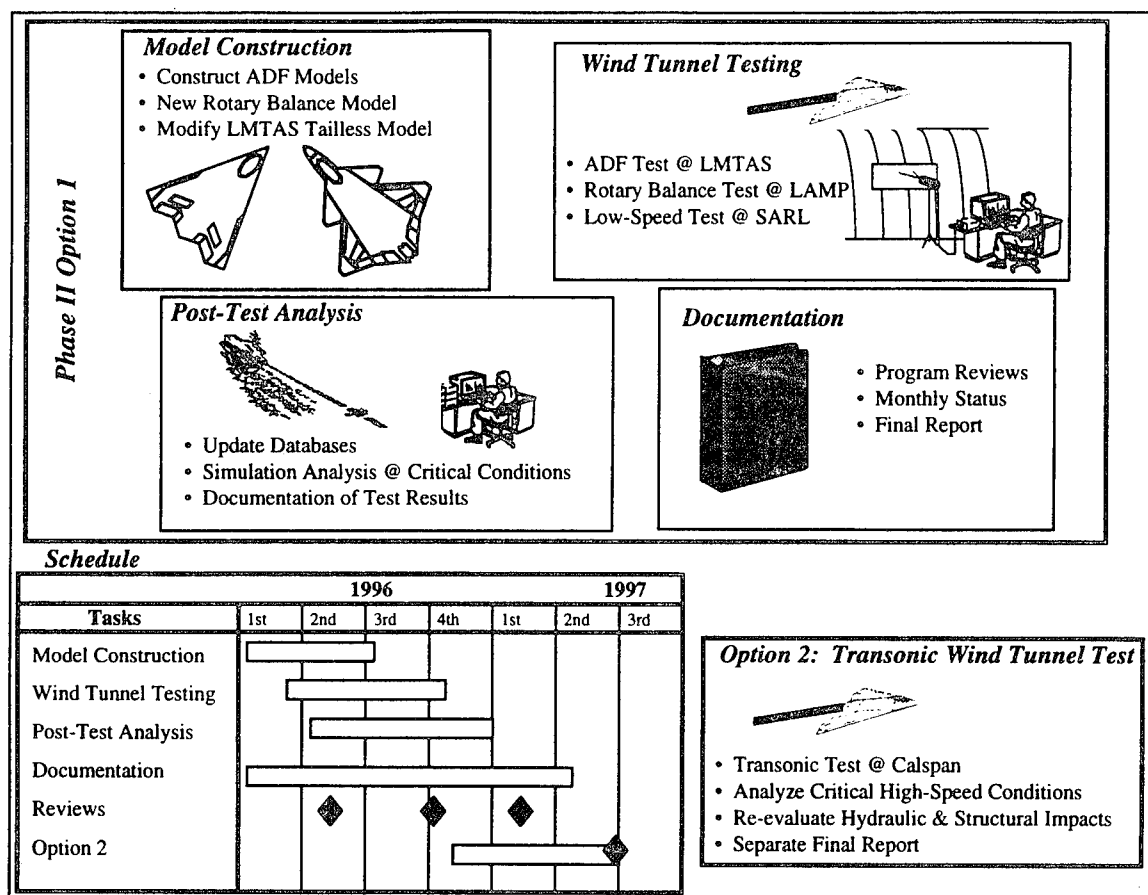


Figure 8-1 Phase II Plan

The first task will consist of model design and construction. Four wind tunnel models are planned for use during Phase II; three tests with an optional fourth are planned as well. Two 1/40th scale modular models will be designed and constructed for use in the LMTAS 2'x3' ADF low-speed wind tunnel; one of the models will be constructed by modifying the existing 1/40th scale Configuration 201 model tested during Phase I. An approximately 1/14th scale rotary balance model will be designed and constructed by Birhle Applied Research (BAR) for testing in the Large Amplitude Multipurpose (LAMP) wind tunnel facility in Neuberg, Germany. The rotary balance model will be modular such that it can be converted between the land-based 101-series configuration and the carrier-based 201-series canard-delta. Finally, the existing LMTAS high-speed tailless fighter wind tunnel model (representative of the 101-series configurations) will be modified to incorporate all-moving wing tips and spoiler-slot-deflectors. This model will

be tested in the SARL facility at WPAFB. The tailless fighter model and model parts will be designed for use in high-speed wind tunnels (i.e., Calspan 8'). This model will represent the USAF 101-series configuration only.

Post-test analysis tasks will consist of plotting and documenting the wind tunnel test results and incorporating the appropriate data into the existing simulation databases for both the 101 and 201-series configurations. High AOA and power approach flying qualities will be revisited using the new, updated databases in a 6-DOF simulation. Comparisons with the original Phase I predictions will be made as applicable.

Three interim reviews and a kickoff meeting will be held at sites alternating between Wright Laboratories, NAWCAD (Patuxent River, MD) and LMTAS. A final report will document the wind tunnel tests and analysis results. All wind tunnel model hardware generated under the contract will be delivered to Wright Laboratories and NAWCAD.

A fourth wind tunnel test is planned as an option using the LMTAS high-speed tailless fighter model. The test will be conducted at the Calspan-8' transonic tunnel with the purpose of collecting additional AMT, SSD and DLEF control effectiveness data throughout the transonic Mach range. A separate report will be prepared including the results and post-test analysis from this test if the transonic test option is exercised.

8.2 Wind Tunnel Model Requirements

Four wind tunnel models are required to complete the planned Phase II effort. Two 1/40th scale ADF models, a 1/14th scale rotary balance model and a modification to the existing 1/18th scale LMTAS tailless fighter model are required to fulfill the Phase II test objectives.

8.2.1 ADF Wind Tunnel Models

Two small-scale ADF models will be designed and constructed by the LMTAS model shop. ADF models are typically constructed of plywood, aluminum and plastic; stereo-lithography techniques are often used to construct complicated pieces like the fuselage.

For fighter-size configurations, 1/40th scale models work well in the 2'x3' ADF test section.

The 101-series model will be constructed from scratch. The 201-series model will be a modification of the Navy tailless fighter model tested during Phase I of the ICE contract (see Appendix C). Control surfaces will consist of:

Configuration 101-Series:

- Elevons (2-deflections and zero)
- Pitch Flap (2-deflections and zero)
- Spoiler-slot-deflector (one size, 3-deflections at three locations)
- All-moving wing tip (adjustable deflections, three variations of size and/or hingeline sweep)
- Leading edge flaps (2-deflections and zero)

Configuration 201-Series:

- Canard (adjustable deflections)
- Elevons (4-deflections and zero)
- Ailerons (4-deflections and zero)
- Pitch Flap (4-deflections and zero)
- Spoiler-slot-deflector (one size, 3-deflections at three locations)
- All-moving wing tip (adjustable deflections, three variations of size and/or hingeline sweep)
- Leading edge flaps (2-deflections and zero)

Figures 8-2 and 8-3 show planviews of the proposed ADF models.

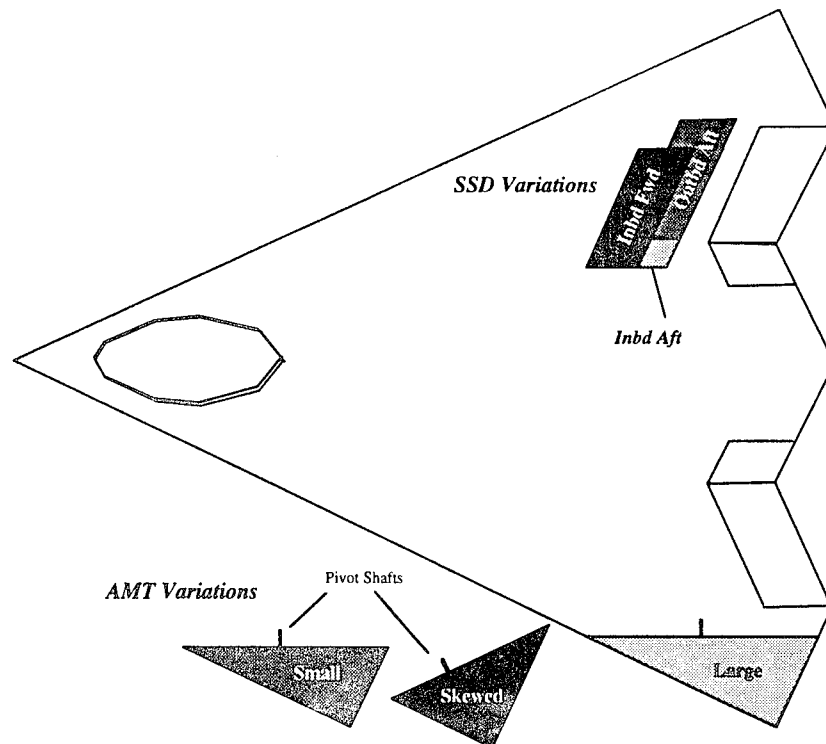


Figure 8-2 Configuration 101-Series ADF Model Planform

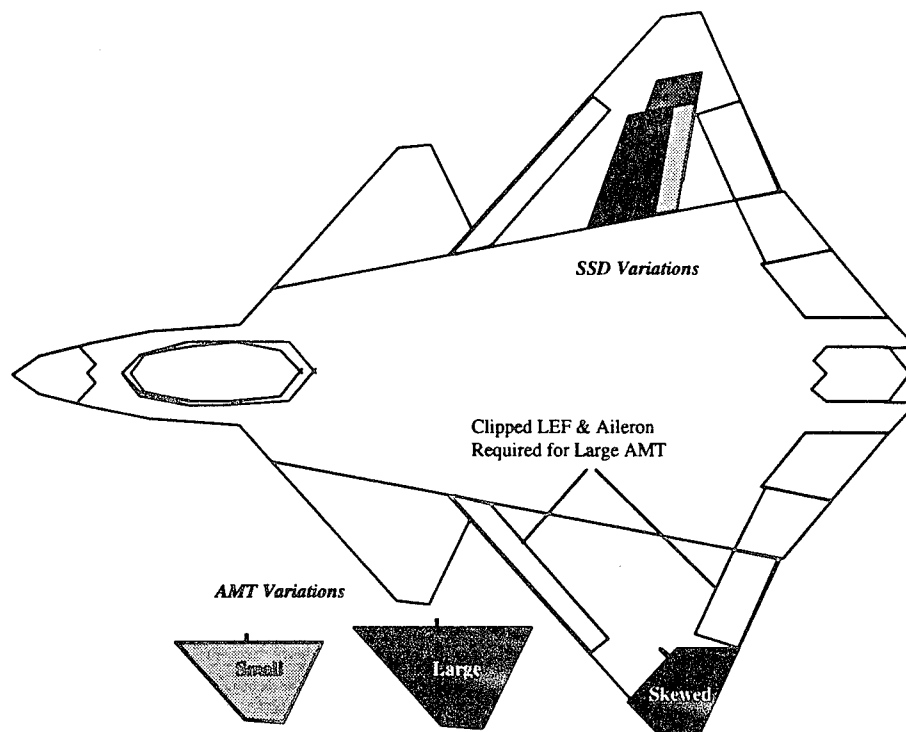


Figure 8-3 Configuration 201-Series ADF Model Planform

8.2.2 Rotary Balance Wind Tunnel Model

Birhle Applied Research will construct a rotary balance wind tunnel model representing both the 101 and 201-series configurations. The model will use common parts whenever possible. Control surface configurations that performed well during the ADF test will be integrated into this model.

Rotary balance models are typically constructed of wood and fiberglass and have approximately 2 ft -3 ft wingspans. A modular wind tunnel model representing both ICE configurations would be about 1/14th scale.

This model and associated control surfaces will have sufficient detail to investigate rotational and large sideslip effects on the configurations at high AOA. The primary emphasis of the test will be to investigate departure resistance, spin modes and the control effectors best suited for recovery.

8.2.3 Modifications to the 1/18th Scale High Speed Model

The 1/18th scale LMTAS tailless fighter model is a 65 deg flying wing configuration similar to the 101-series configurations (Figure 8-4). It is constructed of stainless steel, and has been tested at the SARL 7'x10' low-speed wind tunnel, the NASA LaRC 8' transonic tunnel, and the NASA LaRC 4' Unitary supersonic wind tunnel.

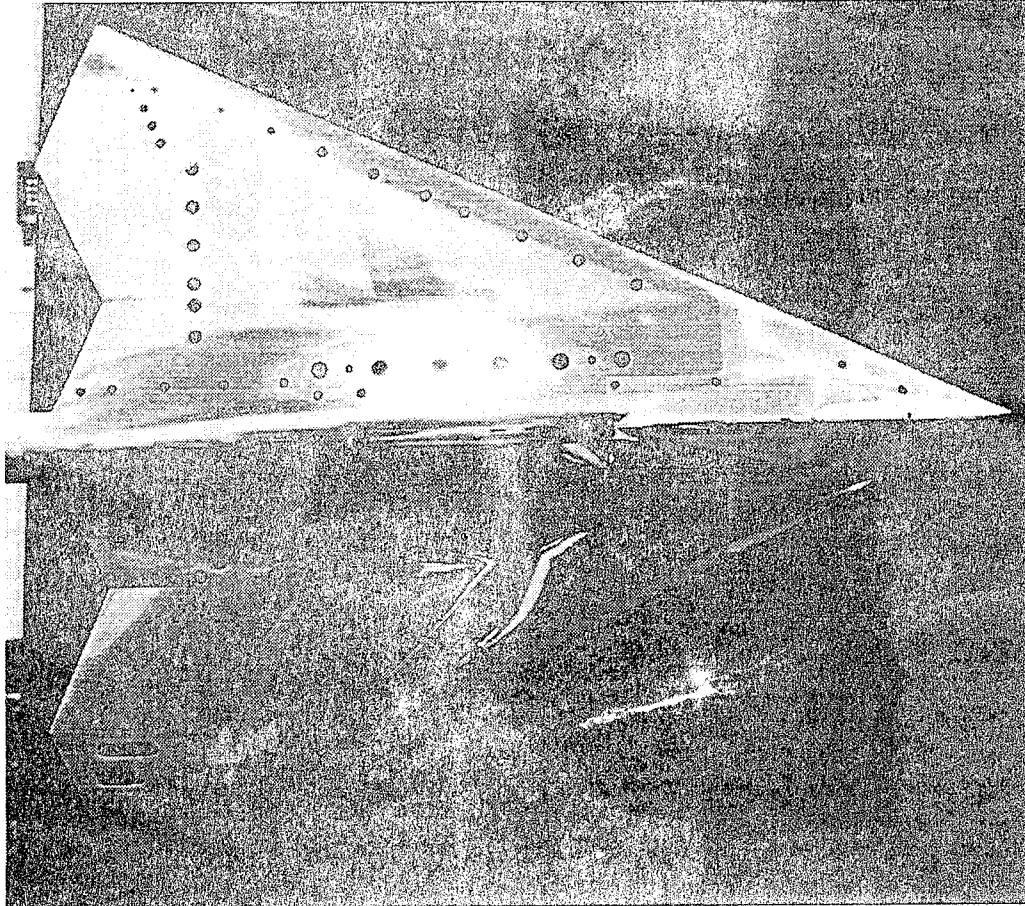


Figure 8-4 1/18th Scale LMTAS Tailless Fighter Wind Tunnel Model

Planned modifications to the model during Phase II of the ICE program include:

- A new left-hand wing to accommodate an AMT and SSD.
- Integration of an AMT on the new wing. Two AMT variations will be constructed with four deflections each.
- Integration of the SSD into the new wing. Three deflections each of the spoiler and deflector will be available. Two spanwise and two chordwise SSD locations will be available as well as two sizes of SSD. Three variations of inserts representing internal structure will be constructed for placement within the slot of the SSD. Rectangular covers will be provided to fill the holes created when testing alternate SSD locations or geometries.

- Three additional LEF deflections will be constructed for integration on the new wing with the AMT.
- New elevons (5-deflections) and pitch flaps (3-deflections) will be constructed to facilitate integration of the SSD and AMT on the new wing.

All model parts will be designed to be compatible with transonic wind tunnel testing.

8.3 Wind Tunnel Test Plans

The following subsections outline the objectives and plans for each of the three Phase II wind tunnel tests and the optional transonic test.

8.3.1 Small-Scale Testing

The small-scale test will take place in the LMTAS 2'x3' ADF wind tunnel. The wind tunnel is an open circuit atmospheric tunnel with a rectangular test section. A digitally controlled motor-drive system can position the model anywhere within 0 to 35 deg of pitch and +/-20 deg of yaw. A 15 deg sector is available to extend the pitch range to 50 deg while maintaining yaw capability. Furthermore, the model can be positioned wings vertical, and pitched between +/-90 deg. Tests are typically conducted at a dynamic pressure of 18 psf.

Two primary objectives of this test will be to investigate the effects of AMT and SSD geometry on control effectiveness and to expand the Configuration 201-series database. The most promising geometries will be incorporated into the other two wind tunnel models for additional investigation during the higher-fidelity tests. SSD interactions with trailing edge controls will be tested to determine an SSD/trailing edge geometry that minimizes the adverse aerodynamic interaction between the control surfaces. Both the 101-series and 201-series configurations will be tested to investigate the specific control power integration and control surface geometry impacts on each aircraft.

One-hundred-twenty hours of testing are planned; approximately 600 runs can be expected assuming current operating efficiencies. Test time and tunnel operation will be

provided by the contractor. Tunnel operating conditions will be a dynamic pressure of 18 psf ($R_N = 0.8 \times 10^6$ 1/ft), maximum AOA of 70 deg, and maximum sideslip angles of +/- 20 deg. A preliminary list of test configurations is included below.

Configuration 201-Series

- Canard effects with sideslip and canard/LEF interactions
- Trailing edge control effectiveness (pitch flap, elevon, and aileron) at -30, -10, 10 and 30 deg
- Three SSD geometries (including sideslip effects) and associated interactions with canard, LEF and aileron
- Three AMT geometries including sideslip effects and interactions with the aileron
- DLEF effectiveness with sideslip and interaction with the canard at various settings

Configuration 101-Series

- Three SSD geometries with associated effectiveness in sideslip and interactions with the elevon
- Three AMT geometries including sideslip effects

The bulk of the small scale test will be concentrated on the carrier-based configuration to expand the current Configuration 201-series simulation dataset. Sufficient low-speed data are already available for the 101 configuration; the purpose of additional testing with this configuration will be to evaluate SSD and AMT geometries.

8.3.2 Rotary Balance Testing

A rotary balance test will be conducted at the LAMP vertical wind tunnel operated by BAR in Neuberg, Germany. Test time and tunnel operation support will be provided by BAR, funded by the Phase II contract. This test will investigate departure characteristics of the two ICE configurations. The effects of rotation, large sideslip angles, and dynamic

oscillations on control power will be investigated. At least two AMT and SSD geometries will be tested along with the other baseline control surfaces on both the land-based and carrier-based configurations. The anticipated test conditions are listed below:

Rotary Balance Test Conditions

- Freestream Velocity: 27 ft/sec
- Reynolds Number: 0.16×10^6 1/ft
- AOA Range: 0 - 90 deg
- Sideslip Range: +/- 30 deg
- Non-Dimensional Rotation Range ($\Omega b/2V$): -0.3 - 0.3
- Forced Oscillation Reduced Frequencies --

$qc/2V$: 0.005 - 0.01

$pb/2V$ & $rb/2V$: 0.005 - 0.05

8.3.3 SARL Wind Tunnel Test

The low-speed wind tunnel test will be conducted in the SARL 7'x10' open-circuit wind tunnel at WPAFB. The 1/18th scale LMTAS tailless fighter model will be used for this test. No accompanying carrier-based configuration is anticipated. The purpose of this test will be to refine the AMT and SSD control effectiveness and interaction database to a higher fidelity than is possible in the ADF tunnel. AMT and SSD concepts found to be favorable during the ADF test will be investigated at a higher fidelity (larger model scale, higher R_N , etc.). Furthermore, additional DLEF deflections will be tested than were available during the Phase I analysis. Anticipated test conditions are listed below:

SARL Wind Tunnel Test Conditions:

- Mach No: 0.3
- R_N : 2.0×10^6 1/ft

- Maximum AOA: 45 deg
- Sideslip Range: +/-30 deg

The length of the test will be 100 occupancy hours. Approximately 300 runs are anticipated during this amount of test time. Test time and wind tunnel operation support will be Government Furnished Equipment (GFE). The anticipated test configurations are included below:

Preliminary SARL test Configurations (101-Series)

- Basic data including elevon and pitch flap effectiveness
- Spanwise and chordwise variation of SSD location (three locations each, including sideslip effects)
- SSD size variation (two sizes including sideslip effects and interactions with the elevon and pitch flaps)
- Effects of simulated structure within the SSD slot
- Two AMT geometries (including sideslip effects and interaction with the elevon)
- LEF interaction with the AMT and SSD
- DLEF effectiveness at varying deflections (including sideslip effects)

8.3.4 Optional Transonic Testing

A transonic wind tunnel test is proposed as an option for Phase II. Transonic wind tunnel data are required to validate the control effectiveness predictions made during Phase I of the ICE program. (Recall that trends from NACA tests of similar configurations were applied to the AMT and SSD control effectiveness to estimate transonic effects during Phase I.) Accurate transonic control effectiveness data are required to estimate the impact on flying qualities, actuator requirements and flight envelope limitations.

The objective of this test will be to accurately determine the transonic effects on SSD, AMT and DLEF control effectiveness for the 101-series configurations. Results will be compared with the original predictions made during Phase I of the ICE program. If the option is exercised, the test will be conducted at the Calspan 8' transonic wind tunnel. Test time and tunnel operation will be GFE. An 80 occupancy hour test entry is planned (approximately 460 runs with 60 configurations). Anticipated test conditions are listed below:

Anticipated Transonic Wind Tunnel Test Conditions

- Mach No: 0.6, 0.8, 0.85, 0.9, 0.95, 1.05, 1.1, 1.2
- R_N : 2.0×10^6 1/ft
- Maximum AOA: 25 deg (function of Mach)
- Sideslip Range: +/-10 deg (function of Mach)

The 1/18th scale LMTAS tailless fighter model with the modifications described in Section 8.2.3 will be used during the test. No Navy configuration testing is anticipated. The control surface geometries investigated at the SARL tunnel will be tested at transonic speeds to determine if adequate control power is available throughout the flight envelope. The focus of the test will be on the most favorable control surface geometries found during the SARL and rotary balance tests. Anticipated test configurations are summarized below.

Summary of Transonic Test Model Configurations

- Basic data including elevon and pitch flap effectiveness
- SSD effectiveness and interaction with the elevon and pitch flaps
- Effects of simulated structure in the SSD slot
- AMT effectiveness and interaction with the elevon

8.4 Post-Test Analysis & Documentation

Post test analysis will consist of documenting each wind tunnel test with data reports describing the test conditions, configurations, pertinent data, conclusions and recommendations. The simulation databases will be revised based on the new data. The control power tools CPR and CPA will be used to re-analyze the configuration with the new data. The critical low-speed and power approach flight conditions analyzed during Phase I will be the focus of this effort.

8.4.1 Data Reporting and Test Documentation

After each wind tunnel test, a report summarizing the test conditions, model, data reduction procedures, pertinent results and conclusions will be prepared. The reports will also contain comparisons of the new data with previous data used during Phase I of the ICE study. Each report will ultimately be integrated into the final Phase II documentation for a complete record of the Phase II effort.

8.4.2 Revisions to the Simulation Dataset

The simulation datasets for both the 101 and 201-series configurations will be updated using combinations of ADF, rotary balance and SARL wind tunnel data. The 101 dataset will primarily use SARL and rotary balance data while the 201 dataset will consist of ADF and rotary balance data. If control power trends are determined to be similar for both configurations, trends from the SARL data (101 configuration only) may be used in the 201 dataset as appropriate.

8.4.3 Simulation Analysis

Control power envelopes will be computed using the CPA software and the updated simulation datasets. Simulations will be run within the control power envelopes using the software tool CPR. The critical low-speed flight conditions determined during Phase I will be re-analyzed (i.e., power approach, 30 deg AOA at 108 KCAS/15K and 20 deg AOA at 300 KCAS/15K). All six innovative control configurations will be evaluated:

101-1; 101-3; 101-4; 202-1; 201-3; 201-4. Simulation results will be compared with the original Phase I CPR/CPA analysis.

8.4.4 Optional Analysis with Transonic Test Data

If the high-speed test option is exercised, additional analysis will be conducted using the transonic wind tunnel data. A data report, similar to those described in Section 8.4.1 will be prepared to summarize the results of the test. The Configuration 101-series high-speed simulation dataset will be updated using the new data, and control power envelopes computed at critical high-speed conditions (i.e., Mach 1.2 at sea Level 1-g, Mach 0.9 at 30K 1-g, 300 KCAS at 30K elevated-g). Simulation analysis using CPR will be accomplished to validate the original Phase I results. The three USAF innovative control configurations will be analyzed (101-1, 101-3 and 101-4). Finally, an assessment of the impact that the revised transonic predictions have on the hydraulic and structural analysis performed during Phase I will be made along with any necessary modifications to the designs. The entire analysis will be documented in a final report delivered as a separate volume to the primary Phase II report.

9 Conclusions and Recommendations

Phase I of the ICE program evaluated six innovative lateral-directional control concepts: the all-moving tip; differential LEF; spoiler-slot-deflector; deployable rudder; and lower surface spoiler. Three concepts, the AMT, SSD and DLEF, were found to have the greatest potential during initial evaluations. These controls were evaluated in detail on both a land-based and carrier-based fighter configuration. The controls were sized to achieve specific high AOA roll capabilities on the land-based and configuration and Level 1 flying qualities during power approach for the carrier-based aircraft.

A summary of the conclusions is provided below:

1. The most effective control effectors of the six studied were the AMT, SSD, and DLEF. The AMT was the highest payoff control effector from an aircraft-level standpoint. The AMT alone provided sufficient coordinating yaw control power to replace both the spoiler and clamshell on both land-based carrier-based configurations.
2. The AMT would result in the greatest aircraft-level cost savings over the baseline vehicles due to (1) reduced empty weight, (2) increased range or reduced aircraft size for a given range, and (3) reduced FCS complexity.
3. Due to the RCS integration challenges inherent with the AMT (i.e., gap in the leading edge, actuator trunion, actuator fairing, etc.) the SSD may be easier to integrate from an RCS perspective. RCS integration concerns associated with the SSD include treatment of the front edge of the deflector and the treatment of structure within the SSD cavity. The SSD may be more attractive than the AMT if high AOA capabilities are not deemed as critical as low RCS. Multi-axis thrust vectoring can supplement the SSD for adequate high AOA maneuver performance.
4. DLEF are only useful in the moderate to high AOA region of the envelope. As a result, they did not score as well when considering full-envelope employment. The AMT can provide greater yaw power at high AOA and still provide control throughout the flight envelope, obviating the need for dedicated DLEF. If the configuration already employs an LEF for wing cambering, differential usage can be integrated to improve high AOA capabilities.

5. The Innovative Controls studied here are at best suited for application to flying wing or tailless delta configurations. Application to other configurations (e.g. conventional, swing wing, etc.) is possible if accomplished during the earliest design stages to minimize the integration impacts.

The high AOA roll capabilities (i.e., $t_{90} = 2.0$ sec @ 30 deg AOA; $t_{90} = 4.0$ sec @ 45 deg AOA;) were achievable using multi-axis thrust vectoring. None of the configurations could achieve these roll performance capabilities with aerodynamic control power alone -- although the configurations employing the AMT and/or DLEF (Configurations 101-3 and 101-4) could achieve significant high AOA roll capabilities without using propulsion control power.

Evaluation of the carrier-based configuration demonstrated that Level 1 roll performance during power approach demanded the most of the lateral-directional controls. Power settings for thrust vectoring control during this flight phase were evaluated at off, idle and trim power.

The baseline canard-delta arrangement (defined as 201-series) had sufficient roll power to meet the specification; however, yaw control power was insufficient to coordinate all of the available roll power at the approach condition. As a result, the configuration could not achieve Level 1 roll performance at the design bring back weight of 5,000 lbs and zero wind-over-deck. Application of trim power thrust vectoring provided sufficient coordinating yaw control to meet the Level 1 roll requirement (Configuration 201-TV). Configuration 201-3 (AMT, DLEF and SSD) could achieve Level 1 roll capabilities using only idle power vectoring. Configuration 201-4, employing only the AMT (i.e., no spoiler), achieved 25 deg of bank in 1 sec @ idle thrust (equivalent to 30 deg of bank angle change in 1.1 sec -- consistent with MIL-F-8785C) at the desired WOD. In this case, the AMT alone more than made up for the spoiler and clamshell the baseline, resulting in an overall weight savings.

Integration of the AMT on the land-based configuration (101-4) resulted in an empty weight savings of 700 lbs over a baseline configuration employing spoilers for roll and yaw control. The resulting configuration had a 16% increase in the design mission range over the baseline due primarily to increased wing fuel volume. A 4% degradation in transonic acceleration time was noted due to the drag impacts of the large AMT actuator fairings.

The control suite integrated into Configuration 201-4 resulted in the greatest weight savings for the carrier-based configuration. The empty weight was reduced by 400 lbs over the baseline configuration. Together with the fuel volume increase due to deletion of the spoiler, the design mission range was improved over 20%. The large actuator fairings required by the AMT resulted in a 10% degradation in transonic acceleration performance.

The 101-4 control suite integrated with Target 19 had the best overall RCS performance considering both deflected (VISAGE analysis) and undeflected (MESSAGE gaps analysis) cases. The 101-1 control suite also performed well with no control deflections, but poorly when the controls were deflected. Configuration 101-TV performed the best when considering deflected controls and poorly in the gaps analysis -- primarily due to the LEF. The models did not consider actuation details that may significantly affect the RCS results.

The best overall control effector considering control power (both low and high AOA), potential weight savings, FCS requirements, RCS, and hydraulic requirements was the all moving wing tip. The highest ranking control suites were Configurations 101-4 and 201-4 -- employing the AMT. Configurations 101-1 and 201-1 (no AMT, SSD in place of spoiler) ranked a distant second in both configuration series. These configurations were most dependent on thrust vectoring to achieve acceptable flying qualities -- however, integration of the SSD was deemed easier from an RCS perspective than integration of the AMT.

Recommendations

1. Conduct rotary balance testing to determine rotational and dynamic effects on the controls. Evaluate the control power available for departure and spin recovery and the propensity for departures and spins.
2. Acquire transonic wind tunnel data for both the AMT and SSD to validate the predictions made during Phase I of the ICE effort.
3. Determine the best SSD orientation and geometry that maximizes lateral-directional control power with minimal impact on trailing edge control effectiveness.
4. Determine the impact that blockage (e.g., internal structure) within the slot of the SSD has on control effector performance.

5. Develop simple aeroelastic models including the AMT and SSD to evaluate high-speed flexibility effects on control power.
6. Evaluate the effects that the AMT actuation system details and structure within the SSD cavity have on RCS performance. Investigate the potential of material treatments to further improve RCS performance of these controls.

10 References

1. Doane, P.M., et al, "Multi System Integrated Control (MuSIC) Program", WRDC-TR-90-6001, Wright Research and Development Center, WPAFB, OH, June 1990.
2. O'Neil, P. J., et al, "Aero Configuration/Weapons Fighter Technology (ACWFT) -- Summary Technical Report", WL-TR-95-3002, WPAFB, OH, December 1994.
3. Bessolo, John, Henderson, J., "MuSIC Control Technology Design Trades -- Alternate Yaw Control Study", Chart Briefing to Wright Laboratories, General Dynamics Fort Worth Division, 1990.
4. Dorsett, K.M., Marquardt, R. F., "Agility Configuration Impact Study", FZM-8252-10, Final Report to NASA LaRC, August 1994.
5. Smith, Kenneth L., "Design Methods for Integrated Control Systems", AFWAL-TR-86-2103, December 1986.
6. Dorsett, K.M., "Low-Speed Wind Tunnel Data Analysis of a 1/18th Scale Tailless Fighter", Lockheed Fort Worth Company Proprietary Research Report, ERR-FW-4323, December 1994.
7. Peters, S.E., "Wind Tunnel Data Analysis of an Advanced Concept Fighter Aircraft", Lockheed Fort Worth Company Proprietary Report, SCTR 95-003, April 1995.
8. Beaufriere, H.L., et al, "Control Power Requirements for Statically Unstable Aircraft", AFWAL-TR-87-3018, June 1987.
9. Thomas, R.W., "Analysis of Aircraft Stability and Control Design Methods", AFWAL-TR-84-3038, May 1984.
10. Durham, W.C., "Constrained Control Allocation", Journal of Guidance, Control and Dynamics, Vol. 16, No. 4, July-August 1993.
11. McRuer, D., Ashkenas, I., Graham, D., Aircraft Dynamics and Automatic Control, Princeton University Press, Princeton, NJ, 1973, p. 257.
12. Grellmann, H., "B-2 Aerodynamic Design", AIAA 90-1802, February 1990.

13. Donlan, C.J., "An Interim Report on the Stability and Control of Tailless Airplanes", NACA Report No. 796, August 1944.
14. Wyatt, R.D., "LFWC Flight Control Experience with Tailless Aircraft", Lockheed Fort Worth Company Proprietary presentation to Naval Air Systems Command, September 1994.
15. Dabrowski, H.P., The Horten Flying Wing in World War II, Schiffer Military History, West Chester, PA, 1991, pp 1-5.
16. Nickel, K., Wohlfahrt, M., Tailless Aircraft in Theory and Practice, AIAA, Washington, DC, 1994, pp 255-260.
17. Lord, D.R., Czarnecki, K.R., "Recent Information on Flap and Tip Controls", NACA RM L53I17a, November 1953.
18. Martz, C.W., et al, "Rocket Model Investigation to Determine the Force and Hinge-Moment Characteristics of a Half-Delta Tip Control on a 59 deg Sweptback Delta Wing Between Mach Numbers of 0.55 and 1.43", NACA RM L52H06, October 1952.
19. John, H., Krauss, W., "High Angle of Attack Characteristics of Different Fighter Configurations", AGARD CP no. 247, Paper no. 2, October 1978.
20. Simon, J.M., "Control Concepts for a Vertical Tailless Fighter", AIAA 93-4000, 1993.
21. Lydick, L.N., et al, AFTI Predesign and Preliminary Development of DFCS and HAC, AFFDL-TR-79-3016, Vol I, Part B, May 1978.
22. Wray, W.O., "Wind Tunnel Data Report 1/15-Scale SCAMP Force Model General Dynamic Low Speed Tunnel Test GDLST 729-0", General Dynamics Technical Report no. FZT-334, May 1978.
23. Baldwin, A.W., Adamczak, D.W., "Experimental Evaluation of Aerodynamic Control Devices for Control of Tailless Fighter Aircraft", WL-TM-92-318, April 1992.
24. Stone, D.G., "Comparisons of the Effectiveness and Hinge Moments of All-Movable Delta and Flap-Type Controls on Various Wings", NACA RM L51C22, April 1951.
25. Anon., Unpublished SCAMP flexibility data.

26. Private communication with Paul James, Lockheed Martin F-22 Flight Controls Engineer, May 1995.
27. Ralston, J., "Rotary Balance Data for an Angle-of-Attack Range of 8 Degrees to 90 Degrees and Estimated Spin Modes for the F-16XL Configuration", Bihrl Applied Research Report BAR 81-1, February 1981.
28. Franks, J.M., *F-16 Agile Falcon/MLU Final Report*, vol. 1, 90PR064, General Dynamics Fort Worth Division, December 1989.
29. Wenzinger, C.J., Rogallo, F.M., "Wind-Tunnel Investigation of Spoiler Deflector, and Slot Lateral-Control Devices on Wings with Full-Span Split and Slotted Flaps", NACA Report No. 706, 1941.
30. Watson, J.M., "Low-Speed Lateral-Control Investigation of a Flap-Type Spoiler Aileron with and Without a Deflector and Slot on a 6-Percent Thick, Tapered, 45 deg Sweptback Wing", NACA RM L52G10, September 1952.
31. Vogler, R.D., "Wind Tunnel Investigation at High Subsonic Speeds of a Spoiler-Slot-Deflector Combination on an NACA 65A006 Wing with Quarter Chord Line Swept Back 32.6 deg", NACA RM L53D17, 1953.
32. Hammond, A.D., Brown, A.E., "Results of an Investigation at High Subsonic Speeds to Determine Lateral-Control and Hinge-Moment Characteristics of a Spoiler-Slot-Deflector Configuration on a 35 deg Sweptback Wing", NACA RM L57C20, June 1957.
33. Lord, D.R., Moring, R., "Aerodynamic Characteristics of a Spoiler-Slot-Deflector Control on a 45 deg Sweptback Wing at Mach Numbers of 1.61 and 2.01", NACA RM L57E16a, July 1957.
34. Gnos, A.V., Kurkowski, R.L., "Static Longitudinal and Lateral Stability and Control Characteristics of a Model of a Swept-Wing Fighter-Bomber-Type Airplane with a Top Inlet at Mach Numbers from 1.6 to 2.35", NACA RM A57K20, March 1958.
35. Anon., *An Aerodynamic Stability and Control Data Summary for Several Selected Military Aircraft, Vol. 1: Conventional Aircraft*, U.S. Naval Air Development Center, Report No. NADC-AM-7106, September 1971.

36. Kehrer, W.T., "Flight Control and Configuration Design Considerations for Highly Maneuverable Aircraft", AGARD-CP-262, Paper no. 5, May 1979.
37. Senn, C.P., "Evaluating Fixed Wing Aircraft in the Aircraft Carrier Environment", Strike Aircraft Test Directorate, Naval Air Test Center, Pax River, MD, 1992.
38. Zirkel, John, et al, Aircraft Carrier Reference Data Manual, NAEC-MISC-06900, Naval Air Warfare Center Aircraft Division, Lakehurst, NJ, January 1994.
40. Pelikan, R.J., "F/A-18 High Angle of Attack Departure Resistant Criteria for Control Law Development", AIAA Paper 83-2126, August 1983.
41. Johnston, D.E., Heffley, R.K., "Investigation of High AOA Flying Qualities Criteria and Design Guidelines", AFWAL-TR-81-3108, December 1981.
42. Virnig, J.C., Bodden, D.S., "Multivariable Control Allocation and Control Law Conditioning when Control Effectors Limit", AIAA paper no 94-3609, August 1994.
43. Reliability Toolkit: Commercial Practices Edition, Reliability Analysis Center, Rome Laboratory 1995
44. "Smart Actuation for Flight Control Systems", Geminder, Harvey J., Aerospace Engineering November 1995.

11 APPENDIX A: Aerodynamic Data Sources

A wide range of sources were consulted during execution of the ICE contract. Most of the aerodynamic data came from tests funded by a multi-year LMTAS IRAD project. Hinge moment data were extracted from a number of sources, including F-16, F-16XL, F-111 substantiation reports, and NACA research memorandums. Aeroelastic effects came primarily from F-16XL and other F-16 derivative configurations.

11.1 Wind Tunnel Test Data

The majority of the aerodynamic data used during this contract came from six wind tunnel test entries on three different configurations. Table 11-1 summarizes each wind tunnel test.

Table 11-1 Wind Tunnel Test Summary

Facility	A/C Configuration	No. Model Configurations	Mach Range	Date
LMTAS ADF	65 deg Sweep Delta Wing	366	0.1	Jan 1991
LMTAS ADF	LMTAS Tailless Fighter	95	0.1	Mar 1991
NASA 8'	LMTAS Tailless Fighter	57	0.6 - 1.2	Feb 1992
4' Unitary	LMTAS Tailless Fighter	67	1.6 - 2.16	Apr 1992
SARL	LMTAS Tailless Fighter	119	0.3	May 1994
LMTAS ADF	ICE 201-Series	89	0.1	Jan 1995

A variety of controls were tested on the 101-series configuration during the ADF tests including elevons, ailerons, pitch flaps, spoilers, clamshells, inboard and outboard LEF, SSD, AMT, deployable rudders, deployable strake extensions, lower surface flaps, and leading edge spoilers (Figure 11-1). A number of trailing edge geometries were tested as well. The ADF tunnel employs small-scale models, and is used for configuration screening studies. Appendix B discusses data accuracy from this tunnel.

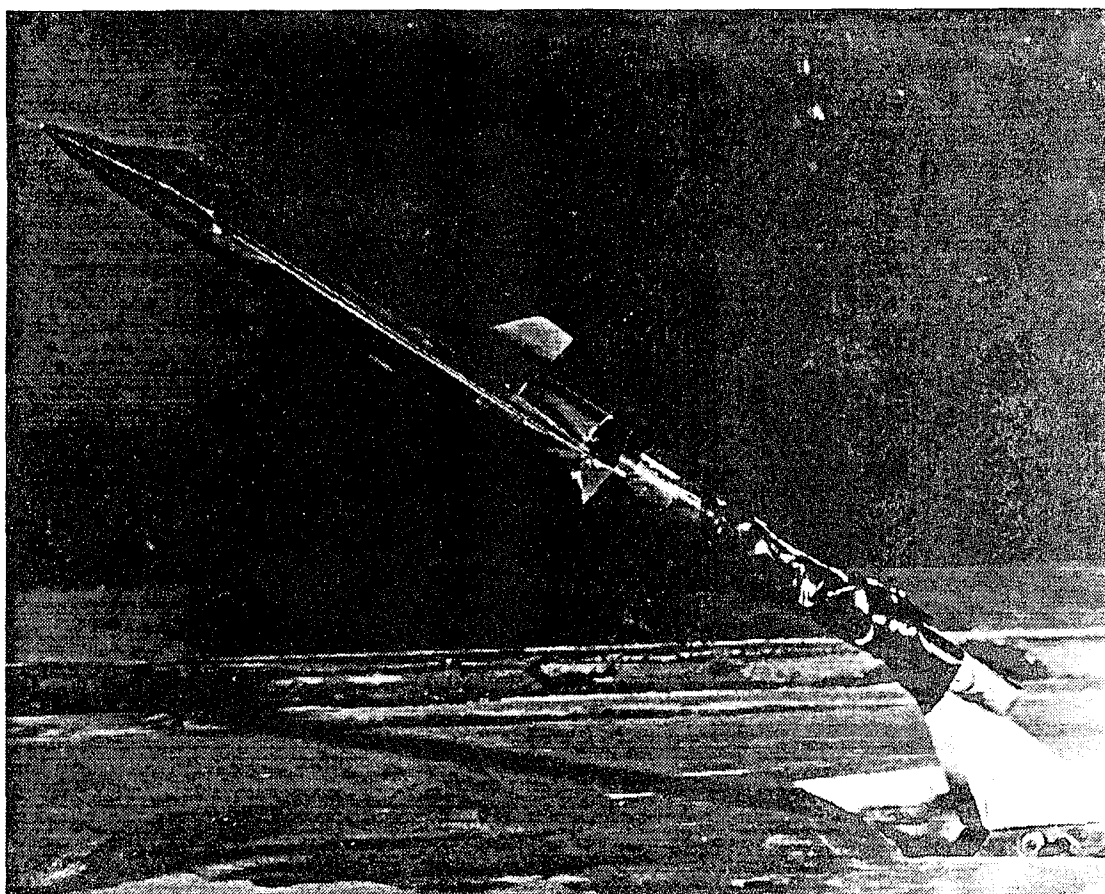


Figure 11-1 LMTAS Tailless Fighter Model in ADF Wind Tunnel

The transonic, supersonic and low-speed tests were conducted using a 1/18th scale model of the LMTAS tailless fighter. This model had faired-over inlets and a fuselage/canopy design representative of those shown in this report (Figure 11-2). A great deal of control interactions were investigated during the low-speed test at SARL.

The 201 configuration was tested during the course of the ICE contract (see Figure 13-1 in Appendix C). Runs consisted of basic configuration build-ups, longitudinal and lateral-directional characteristics, and determination of control effectiveness for the canard, trailing edge surfaces, spoiler, AMT, and LEF. A small amount of control interaction data were collected including spoiler/aileron, canard/spoiler, and AMT/aileron. Sideslip effects on the canard, LEF and AMT were investigated as well. A summary of these data is presented in Appendix C.

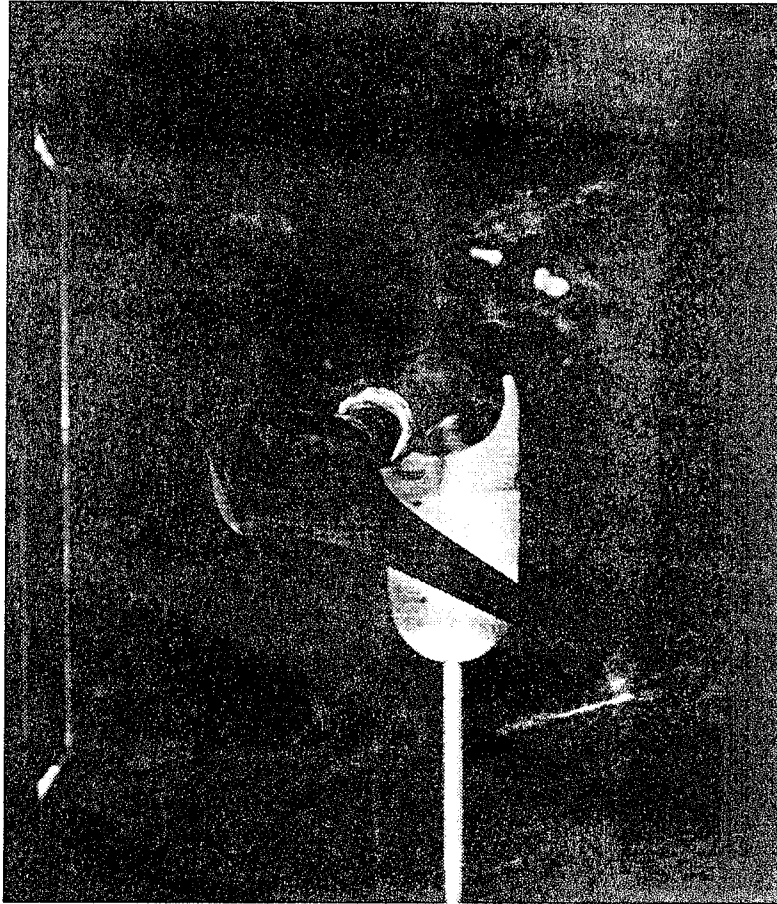


Figure 11-2 1/18th Scale Tailless Fighter Model in SARL Wind Tunnel

11.2 Hinge Moment Data

Hinge moment predictions were made using data representative of similar configurations and/or control surfaces. Hinge moments were non-dimensionalized by dynamic pressure, control surface area, and control surface chord (normal to the hingeline). Aeroelastic effects on hinge moments were included where available. Due to configuration dependence, these hinge moment data are approximate at best; past preliminary design studies utilizing this estimation method have yielded acceptable results when compared with actual wind tunnel data. These data were used to analyze all of the 101-series configurations. No hinge moment analysis was included for the 201-series aircraft. Any errors resulting from inaccuracies in the data are inherent in all of the configuration analyses. The

trends, comparisons and conclusions drawn from the analyses are still applicable. Table 11-2 summarizes the data sources for hinge moment information.

Table 11-2 Hinge Moment Data Sources

Control Surface	Mach Range	Altitude Effects?	Source
Elevon	Low-Speed to Supersonic	Yes	F-16XL Elevon ^{A1}
LEF	Low-Speed to Supersonic	Yes	F-16/F-16XL ^{A1,A2}
Pitch Flap	Low-Speed to Supersonic	Yes	F-16XL Elevon ^{A1}
Clamshell	Low-Speed to Supersonic	No	Potential Flow Theory with F-111 Spoiler & Speedbrake Trends ^{A3}
Spoiler	Low-Speed to Supersonic	No	NACA RM ^{A4, A5}
SSD	Low-Speed to Supersonic	No	NACA RM ^{A4, A5}
AMT	Low-Speed to Supersonic	No	NACA RM ^{A6}

11.3 Aeroelastic Effects

Airframe flexibility characteristics are some of the more difficult parameters to define, even for well defined configurations. Flexibility and hinge moment data are required to define actuator sizes. For this analysis, an effort was made to approximate the aeroelastic effects on the 101-series airframe using flexibility data from similar planforms and control configurations.

Aeroelastic effects (function of Mach and altitude) were applied to the basic longitudinal data and control surfaces. The data are applied as flex-to-rigid ratios and offsets to the rigid aerodynamic data. Aeroelastic effects on longitudinal stability are calculated using

$$C_{N\text{basic}} = C_{N0} + \Delta C_{N\text{oflex}} + (C_N(\alpha) - C_{N0}) (R_{CN})$$

$$C_{m\text{basic}} = C_{m0} + \Delta C_{m\text{oflex}} + (C_m(\alpha) - C_{m0}) (R_{Cm}) - (C_N(\alpha) - C_{N0}) (\Delta a_{c\text{flex}}) (R_{CN})$$

where R_{Cx} are the flexibility ratios, and the deltas to C_{No} , C_{mo} , and aerodynamic center were developed from a linear, flexible aerodynamic model of an F-16 tailless derivative configuration.

Table A-3 lists the sources for flexibility data. Unfortunately, only very crude flexibility estimates were available for the SSD, spoiler, and AMT.

Table 11-3 Aeroelastic Data Sources

Component	Source
Longitudinal Stability	F-16 Tailless Derivative Predictions
Lateral-Directional Stability	None
Dynamic Derivatives	None
Elevon Effectiveness	F-16XL Predictions
Pitch Flap Effectiveness	F-16XL Elevon Predictions
Spoiler Effectiveness	Reference A7
SSD Effectiveness	Reference A7
AMT Effectiveness	F-16XL SCAMP AMT Predictions
LEF Effectiveness	None
Clamshell Effectiveness	None

As seen from the table, some of the aerodynamic data had no aeroelastic effects applied. Static lateral-directional stability values for this class of aircraft are small. Flexibility effects are generally attributable to the vertical tail and thus aircraft without a vertical tail have small flexibility effects on lateral-directional stability. No flexibility effects were found in current literature for dynamic derivatives. Spoiler and SSD aeroelastic data came from a plot shown in Reference A7 for an SSD on a supersonic transport configuration with a high-sweep delta wing. It was assumed that flexibility effects would be similar for both a spoiler and SSD. LEF flexibility primarily effects longitudinal stability. It was not deemed critical. DLEF were only evaluated at conditions where flexibility effects are negligible (i.e., low-speed, high AOA). The clamshell controller was only used on Configuration 101 at low-speeds. Aeroelastic effects were not considered important for this surface.

11.4 Dynamic Derivatives

Dynamic derivatives used for the 101-series analysis were computed using the program DYNAMIC^{A8}. DYNAMIC allows the user to insert static wind tunnel results to improve the dynamic derivative predictions. LMTAS Tailless Fighter data were used where applicable.

The vortex lattice-based routine HASC95 was used to predict the dynamic derivatives for the ICE 201-series canard delta configuration^{A9}.

11.5 Modifications to the 101-Series Pitching Moment Data

Wind tunnel data for the 1/18th scale tailless fighter model showed a sharp, unstable pitching moment break at moderate AOA (Figure 11-3). Early testing with a 65 deg delta wing in the ADF tunnel indicated that pitch stability was sensitive to leading edge radius and wing-forebody integration (Figure 11-4).

With government concurrence, it was decided to modify the basic pitching moment curve for the 101-series configuration to keep the ICE results from being driven by the configuration-specific pitch instability. The justification for this modification was based on the feeling that with additional configuration refinement, the pitch instability problem could be solved. Since the objectives of the ICE program did not include development of a specific configuration, the modification was considered acceptable.

ADF data from a test of a 65 deg sweep delta wing were used to modify the SARL data. The ADF data were referenced to the proper wing area and MAC and adjusted to match the C_{mo} obtained from the SARL data (Figure 11-5).

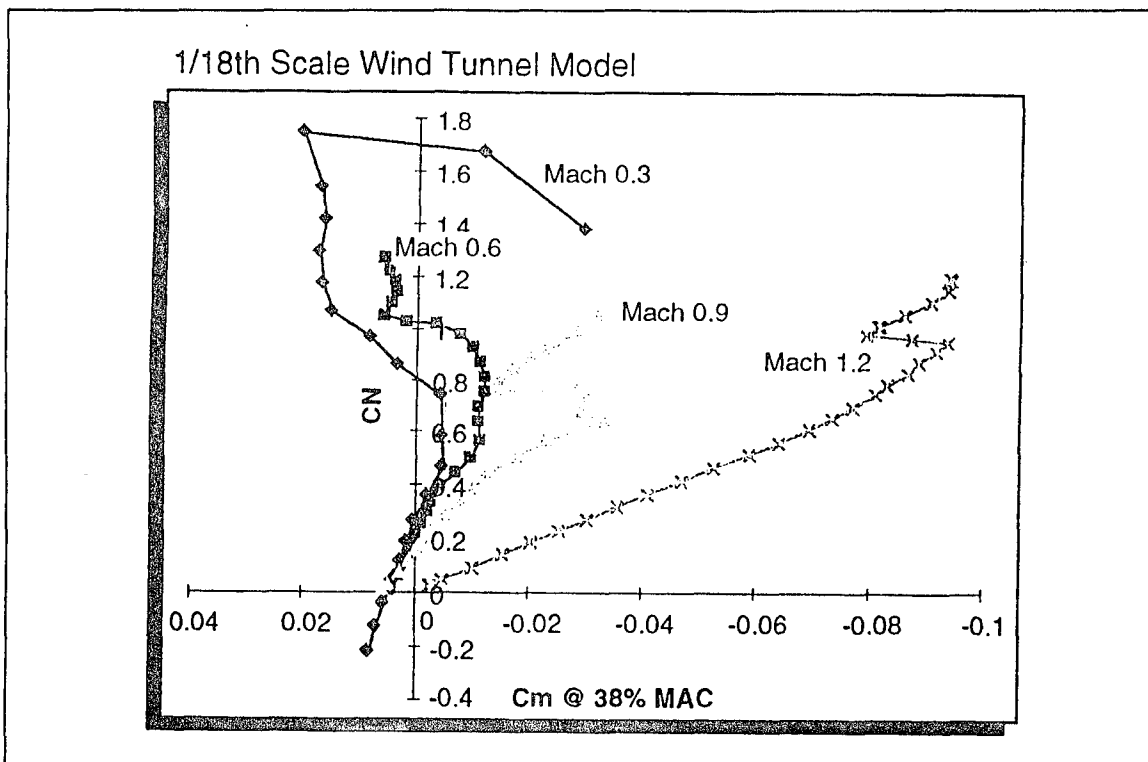


Figure 11-3 Tailless Fighter Model Exhibited Undesirable Pitch Characteristics

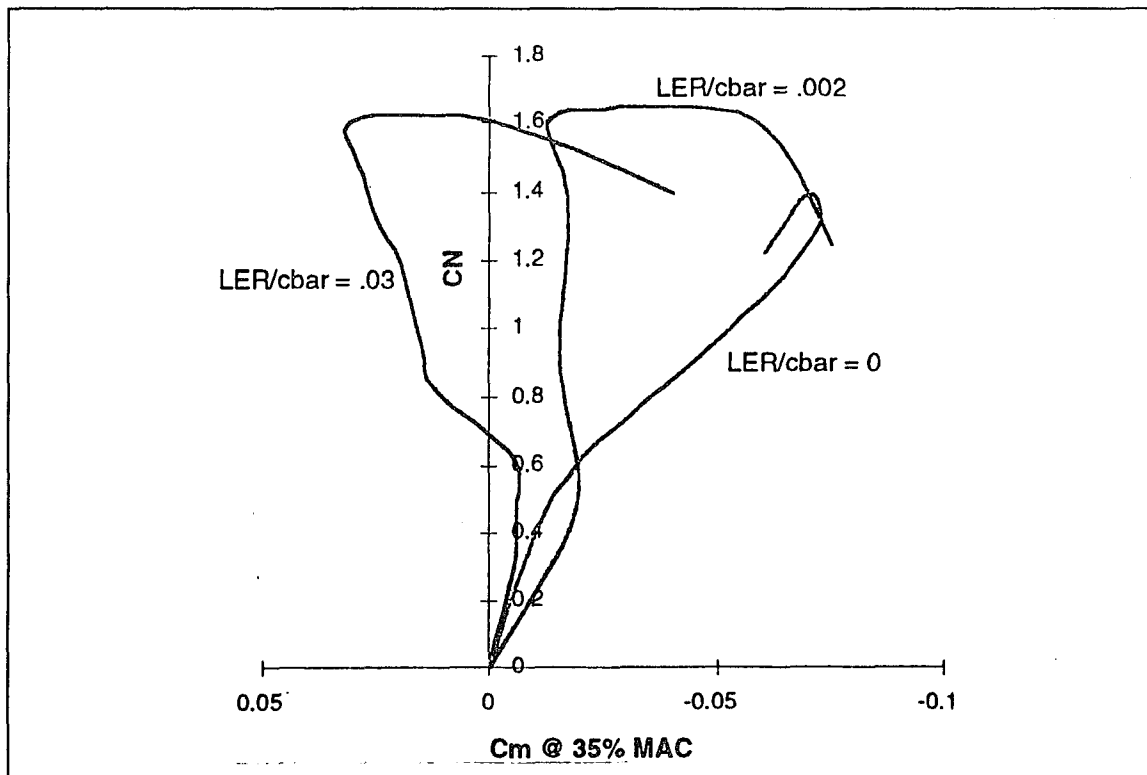


Figure 11-4 The Pitch Instability was Sensitive to Leading Edge Radius

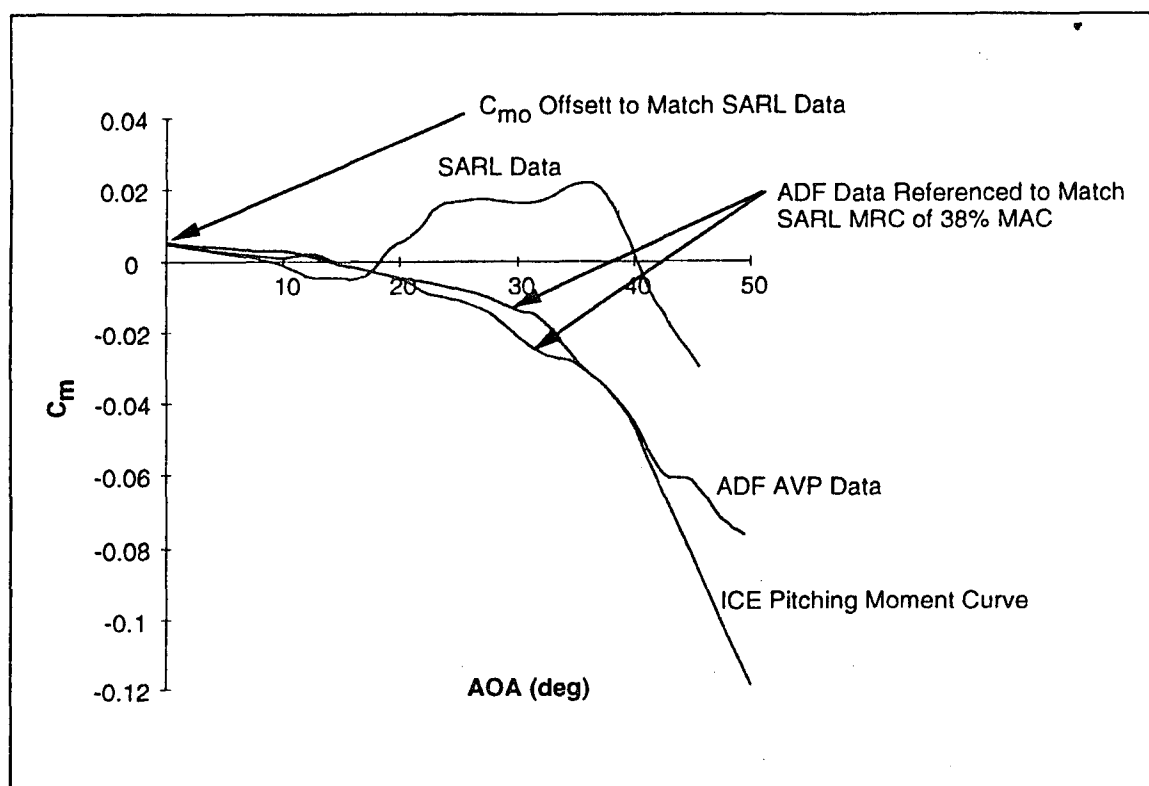


Figure 11-5 ADF Data were used to Adjust the Pitching Moment Curve

The resulting pitch control curves are shown in Figure 11-6. The stable break in the basic pitching moment curve results in the configuration being pitch trim limited at 50 deg AOA ($c_g = 38\%$ MAC) using maximum both aerodynamic and MAX-A/B propulsion control power.

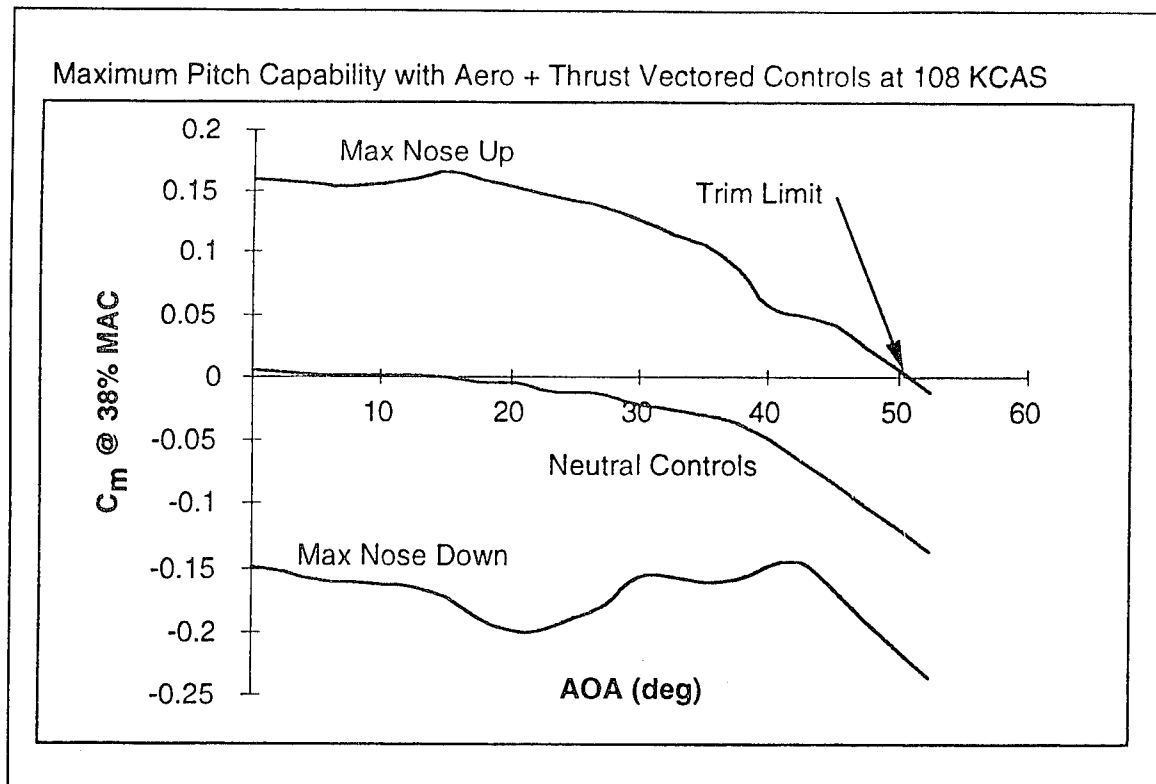


Figure 11-6 The Configuration is Pitch Trim Limited at 50 deg AOA

11.6 References

- A1. von Bose, D.R., Tierney, P.K., Wilson, J.W., F-16XL Stability & Control Data Substantiation Report, General Dynamics Fort Worth Division, 400PR050, May 1982.
- A2. F-16 Block 15 Stability & Control Substantiation Report, General Dynamics Fort Worth Division Report 16PR1949, September 1981.
- A3. Revised Preliminary Stability and Control Aerodynamic Data for the F-111 Airplane, General Dynamics Fort Worth Division Report FZM-12-951, December 1964.
- A4. Hammond, A.D., Brown, A.E., "Results of an Investigation at High Subsonic Speeds to Determine Lateral-Control and Hinge-Moment Characteristics of a Spoiler-Slot-Deflector Configuration on a 35 deg Sweptback Wing", NACA RM L57C20, June 1957.

- A5. Lord, D.R., Moring, R., "Aerodynamic Characteristics of a Spoiler-Slot-Deflector Control on a 45 deg Sweptback Wing at Mach Numbers of 1.61 and 2.01", NACA RM L57E16a, July 1957.
- A6. Martz, C.W., et al, "Rocket Model Investigation to Determine the Force and Hinge-Moment Characteristics of a Half-Delta Tip Control on a 59 deg Sweptback Delta Wing Between Mach Numbers of 0.55 and 1.43", NACA RM L52H06, October 1952.
- A7. Kehrer, W.T., "Flight Control and Configuration Design Considerations for Highly Maneuverable Aircraft", AGARD-CP-262, Paper no. 5, May 1979.
- A8. Thomas, R.W., "Analysis of Aircraft Stability and Control Design Methods, Vol. III, Functional Description and Users Manual for Program Dynamic", AFWAL-TR-84-3038, Vol III, May 1984.
- A9. Albright, A.E., Dixon, C.J., Hegedus, M.C., "Modification of Conceptual Design Aerodynamic Prediction Method HASC95 with VTXCHN", Draft Report to NASA Langley Research Center, November 1995.

12 APPENDIX B: ADF Wind Tunnel Data Evaluation

This appendix contains comparisons of force and moment results from the LMTAS ADF wind tunnel to results from other wind tunnel facilities. The section also contains repeatability comparisons for the ADF wind tunnel. F-16 wind tunnel test results were used for the comparisons.

12.1 ADF Repeatability

Repeatability comparisons for the ADF tunnel are provided below.

The first two plots contain longitudinal coefficients. The data from six runs are compared in the plots. Five of the runs are taken from the ADF 9519 test and one is taken from the ADF 9524 test. Two of the runs from the ADF 9519 test are high angle-of-attack pitch sweeps. The model must be rotated 90 degrees in the tunnel in order to reach the higher AOA's; therefore, the models are oriented differently for the high-AOA pitch sweeps than for the low-AOA pitch sweeps.

Figure 12-1 contains lift coefficient versus angle-of-attack. For each of the six runs, the models were configured with a 25 deg LEF deflection, with no other control surfaces deflected. Runs made with the model rotated wings vertical tend to give higher C_L values at $AOA > 10$ deg. The discrepancies are more evident at higher AOA values (25° to 35°). Note that all results from the ADF tunnel contain no blockage or other corrections.

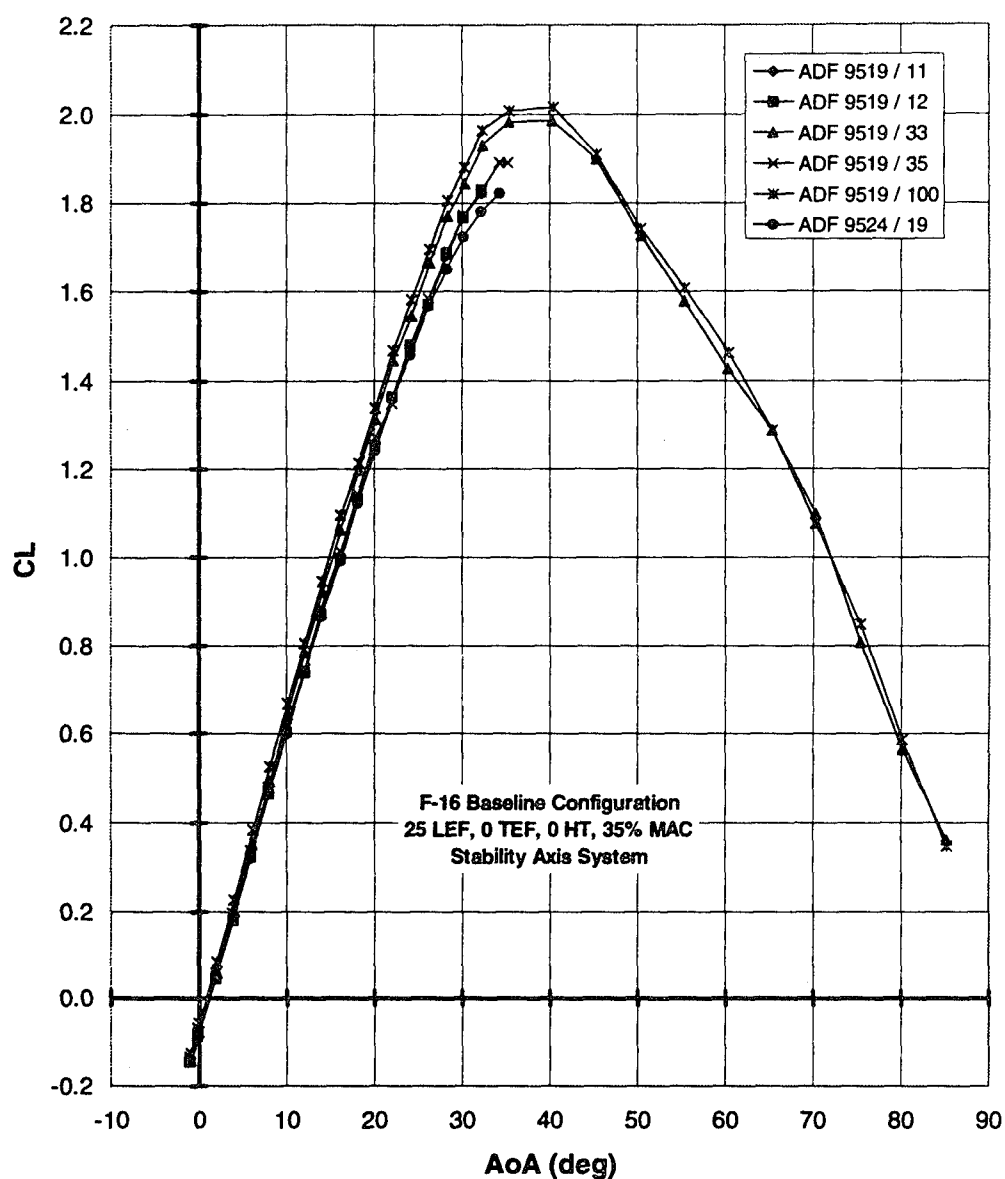


Figure 12-1 ADF Repeatability -- Lift Coefficient

There are also discrepancies between the ADF 9519 and ADF 9524 results at AOA > 25 deg. The 9524 C_L values are slightly lower than the 9519 values. The 9519 wings horizontal sweeps match well for all three runs.

Figure 12-2 contains pitching moment versus AOA for the same six runs. There are small discrepancies between the wings horizontal and wings vertical data. Significant discrepancies are apparent between the two wings vertical runs.

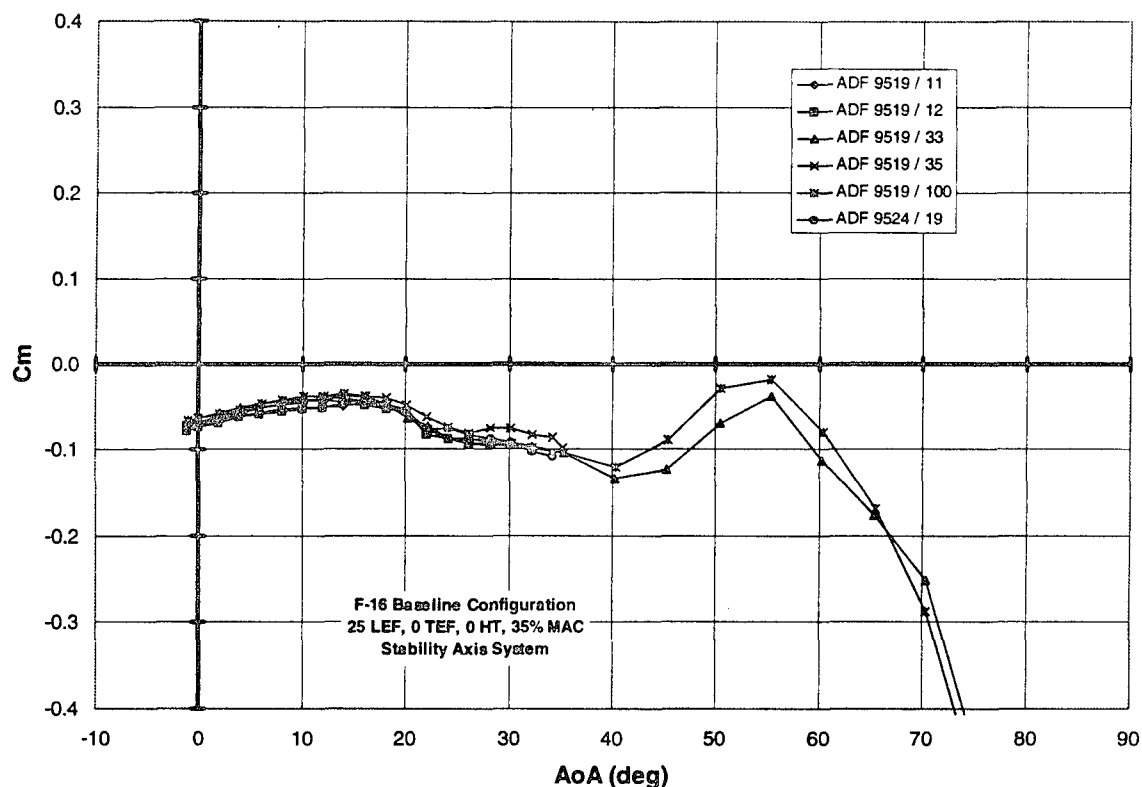


Figure 12-2 ADF Repeatability -- Pitching Moment Data

12.2 Test-to-Test Comparisons

Comparisons of LMTAS ADF wind tunnel results and test results from other wind tunnel facilities are provided below. These comparisons are provided for longitudinal coefficients, lateral-directional sideslip derivatives, and control power.

12.2.1 Longitudinal

Variations in lift data are shown in Figure 12-3. Figure 12-4 illustrates pitching moment variations for the same runs. The plots have results from six different wind tunnel tests at five facilities. The first run on each plot is from the LMTAS ADF 9519 test (diamonds). The ADF test used a 1/40 scale F-16 model. The ADF wind tunnel test section is 1/3 scale model of the Microcraft wind tunnel in San Diego, California (formerly the General Dynamics Low Speed Wind Tunnel – GDLST). Thus a 1/40th scale model in ADF is equivalent to a 1/13th scale model at GDLST. The second run on each plot is from the

GDLST 8905 test, which used a 1/9 scale F-16 model. The third run is from the GDLST 8525 test, which used a 1/15 scale F-16 model. The fourth run on each plot is from the LASC 1251 test. This test used a 1/7 scale F-16 model with minor forebody modifications. The fifth and sixth runs are included only in the pitching moment comparison plots. The fifth run is taken from the NASA LaRC 30' X 60' wind tunnel, which used a 15% scale F-16 model, and the sixth run is from a BAR test in the NASA LaRC vertical spin tunnel using a 1/9 scale F-16 model.

The results shown in this section were for a 25 deg LEF deflection with no other control surfaces deflected. All data shown are in the stability axis coordinate system and referenced to 35% MAC.

Figure 12-3 shows that the ADF tunnel yields slightly lower lift coefficients for $AOA < 22$ deg. The max C_L values of the ADF tunnel match well with the GDLST tests. Most of the difference in the data appears to be due to C_{L0} . Correcting the ADF data to the GDLST value of C_{L0} would yield ADF C_{LMAX} values greater than the GDLST values.

The pitching moment curves (Figure 12-4) compare well in the low- AOA region ($AOA < 30$ deg). The LARC data are more nose-up than the other data in this region. The BAR data are the most nose-down at low AOA . The ADF data are well within the scatter at low AOA and compares well with the GDLST and LASC results.

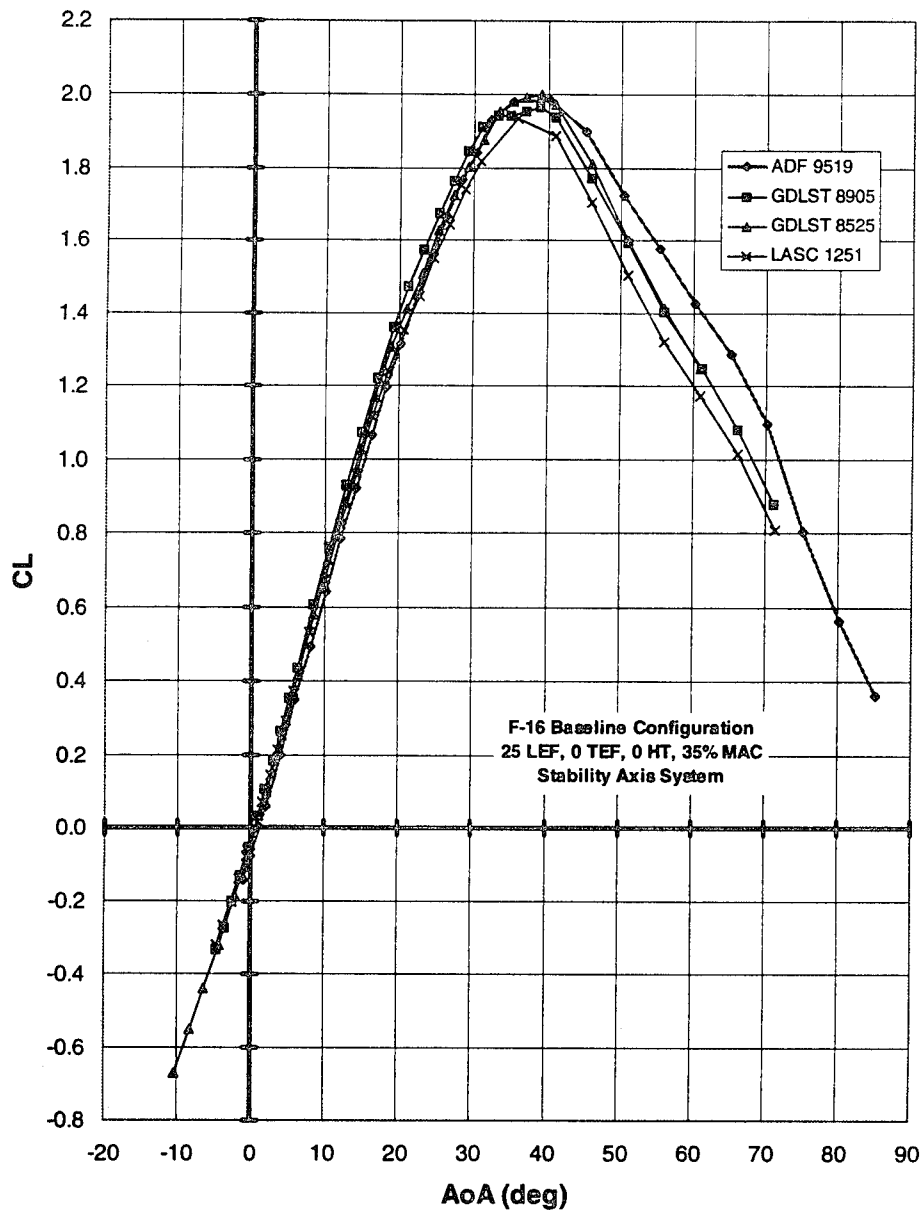


Figure 12-3: Facility to Facility Lift Comparison

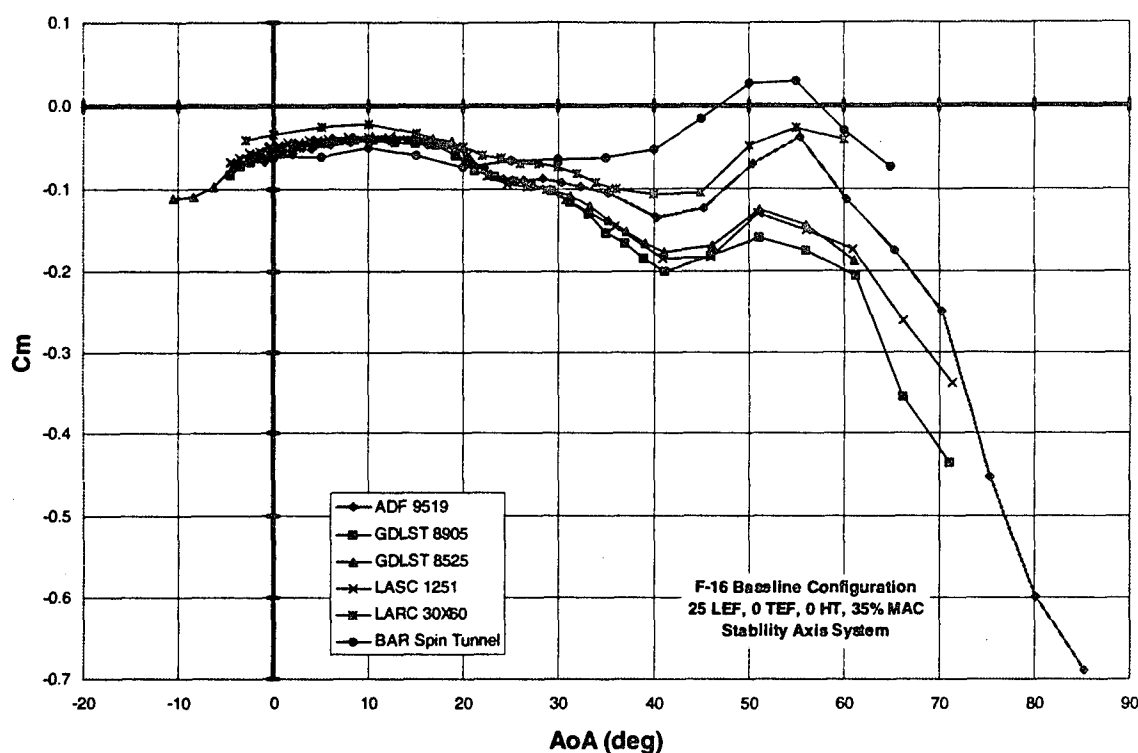


Figure 12-4 Facility to Facility Comparison -- Pitching Moment

There are significant discrepancies in the pitching moment curves at higher AOA's. The lower Reynolds Number tunnels (BAR, LARC, ADF) consistently show more nose up pitching moment at higher AOA's than the other three runs. These results are consistent with F-16 wind tunnel test experience; pitching moment data from low Reynolds number tunnels tend to correctly match full-scale F-16 flight characteristics^{B1}. The ADF results match fairly well with the results from the LaRC 30' X 60' tunnel.

12.2.2 Lateral-Directional

The two plots in this section, Figure 12-5 and Figure 12-6, compare lateral-directional derivatives. Data are included from four of the six tests used in the previous section. Neither the BAR runs nor the LaRC 30' X 60' data were used in this evaluation. Static lateral-directional stability derivatives were calculated by computing the slope of the linear least squares fit between ± 5 deg of sideslip. The results shown in this section are for a 25 deg LEF deflection with no other control surfaces deflected. All data are shown in the

body axis coordinate system (as opposed to stability axis for the longitudinal data) and referenced to 35% MAC.

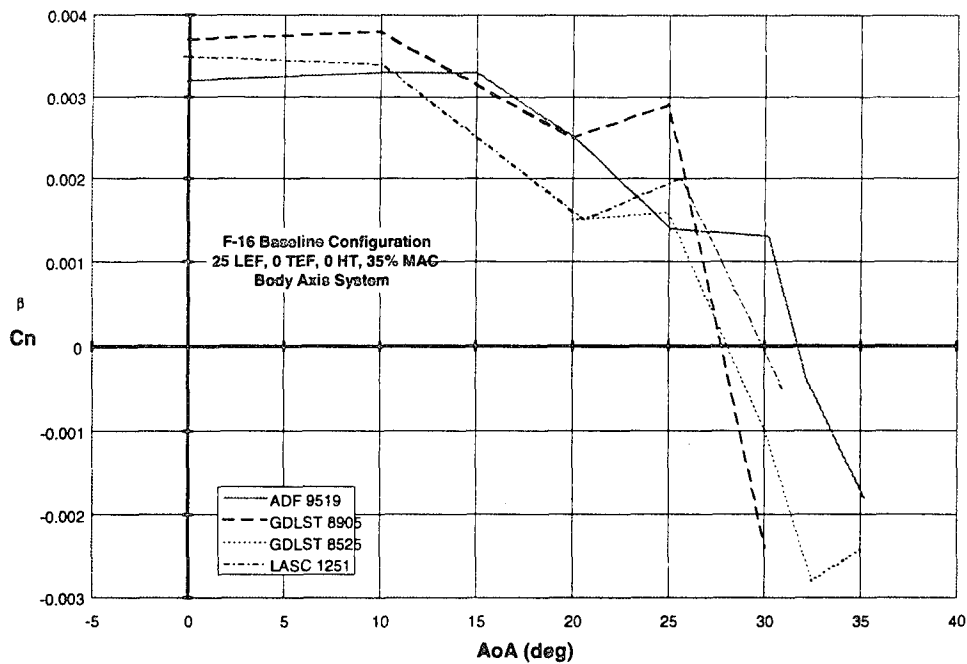


Figure 12-5 Facility-to-Facility Comparison - Directional Stability

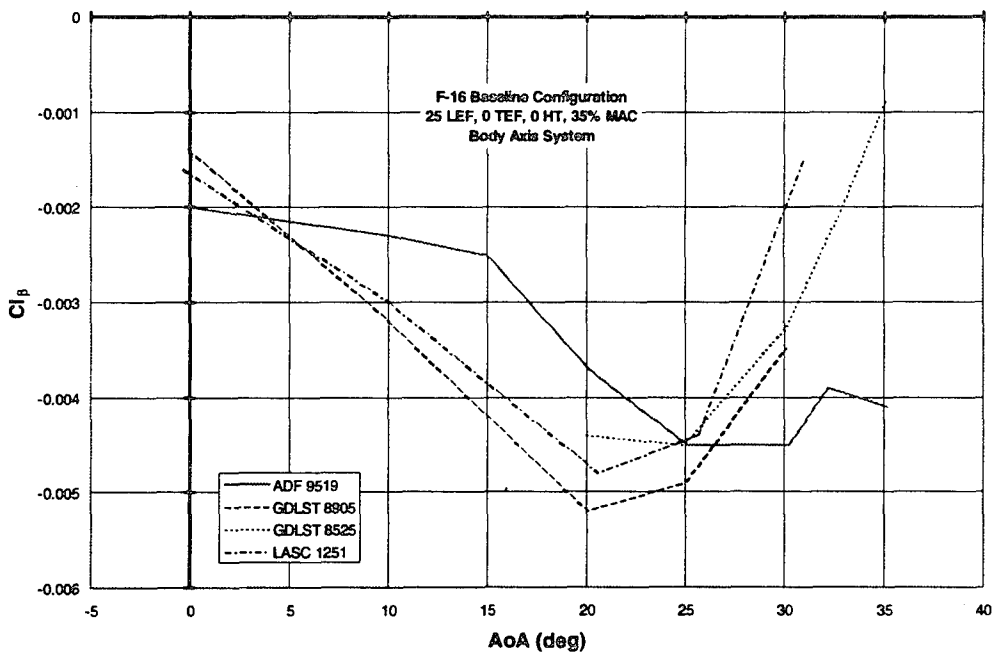


Figure 12-6 Test-to-Test Comparison - Lateral Stability

Figure 12-5 contains a comparison of directional stability. All four of the curves show the directional stability becoming negative between 27 deg AOA and 32 deg AOA. Both of the GDLST curves go unstable around 28 deg AOA. The ADF gives a more optimistic result, going unstable around 32 deg AOA. There is also a trend of increasing directional stability slightly between 20 deg and 25 deg AOA for all of the runs except those from the ADF. This trend is somewhat apparent in the ADF data between 25 deg and 30 deg AOA.

Figure 12-6 contains a comparison of the lateral stability derivatives. $C_{l\beta}$ is less negative for the ADF tunnel than the other tests up until 25 deg AOA. At this point the ADF $C_{l\beta}$ values become more negative than the other data.

Figures 12-7 through 12-10 show comparisons of the yawing moment and rolling moment with sideslip. ADF sideslip cuts compare favorably with data from the other tunnels at the four AOA shown. Slight differences in the lateral and directional slopes are apparent; however, the ADF does a reasonable job predicting the trends with sideslip. There is substantial scatter in the 30 deg AOA directional data (Figure 12-10). The ADF data lie within the scatter predicted by the other wind tunnels. F-16 lateral-directional aerodynamics change rapidly in this AOA region. It is not surprising to observe scatter in the data from test-to-test.

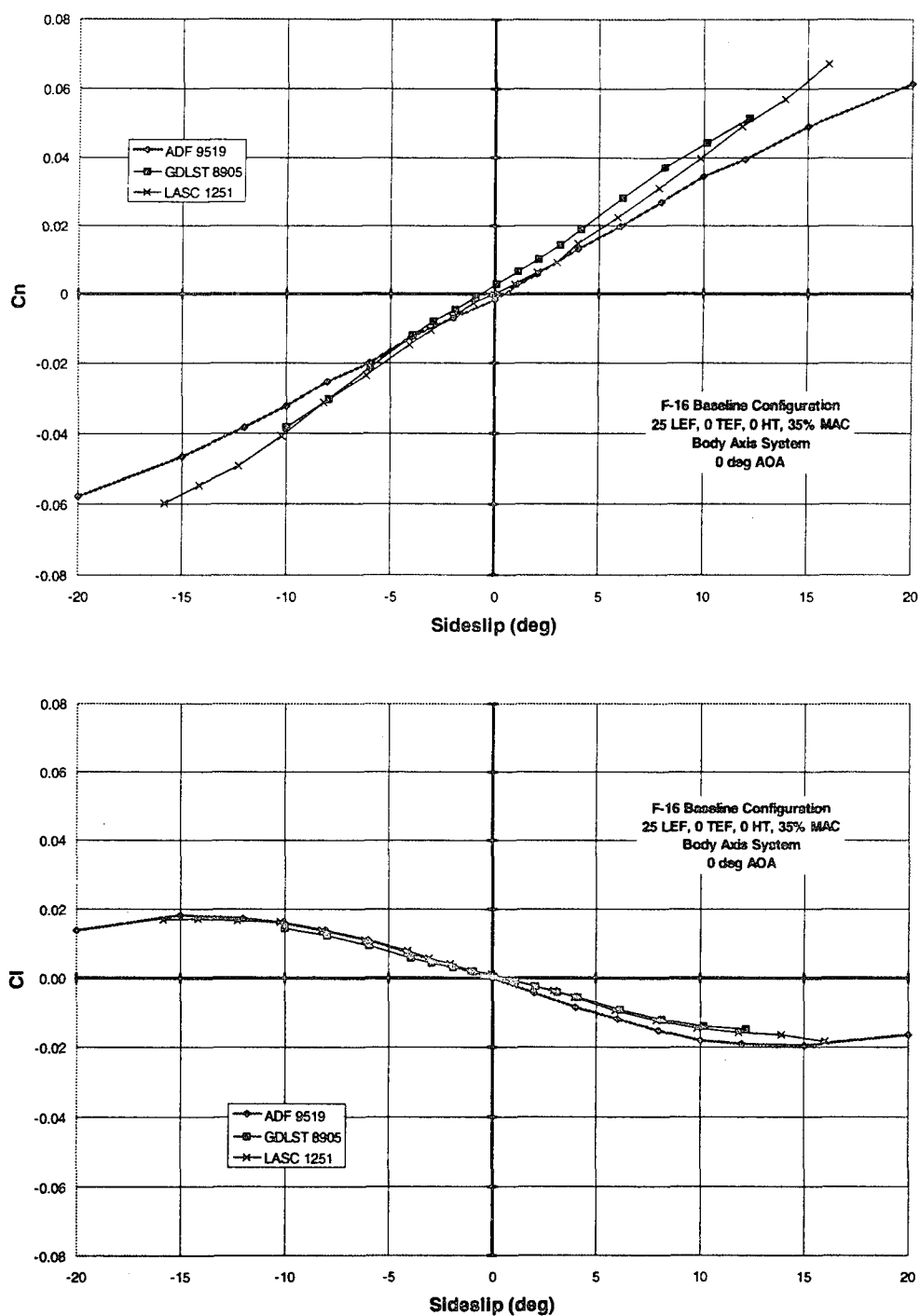


Figure 12-7 Facility-to-Facility Comparison - Sideslip Cuts at 0 deg AOA

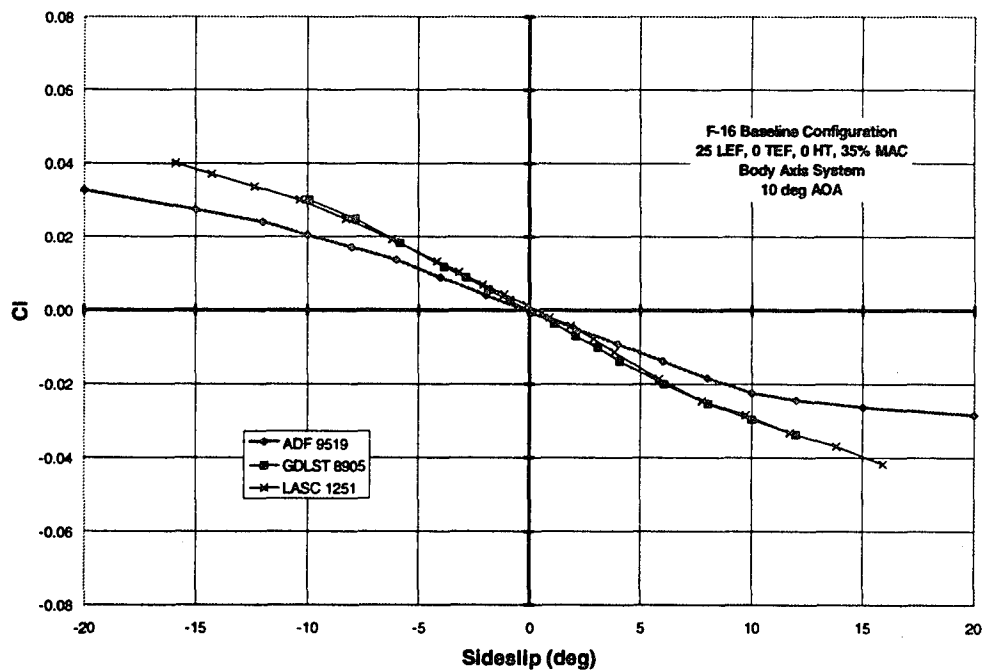
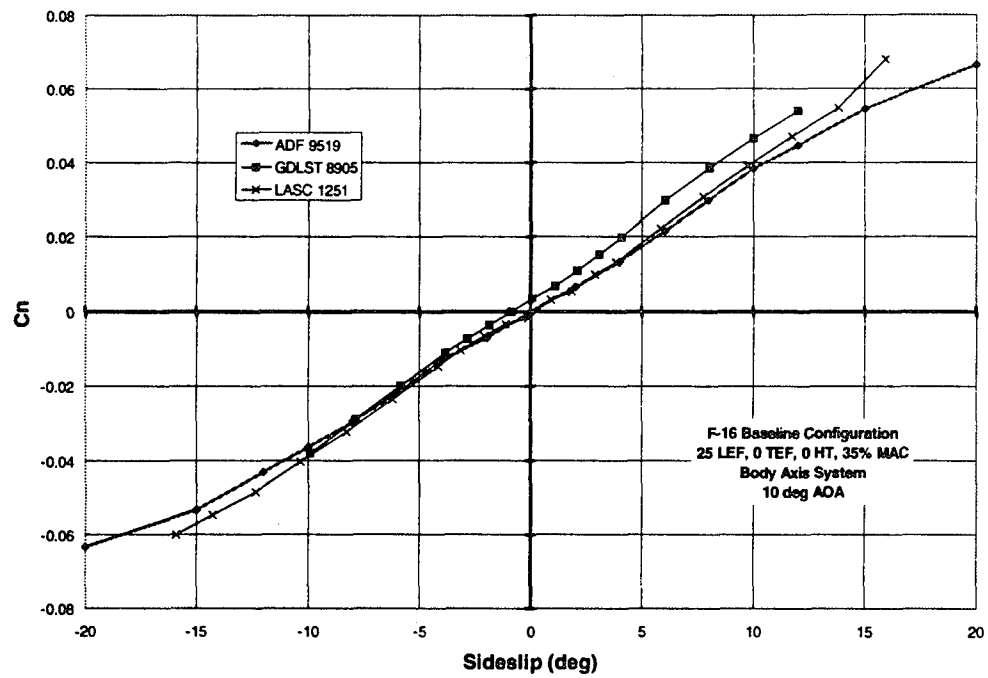


Figure 12-8 Facility to Facility Comparison -- Sideslip Cuts at 10 deg AOA

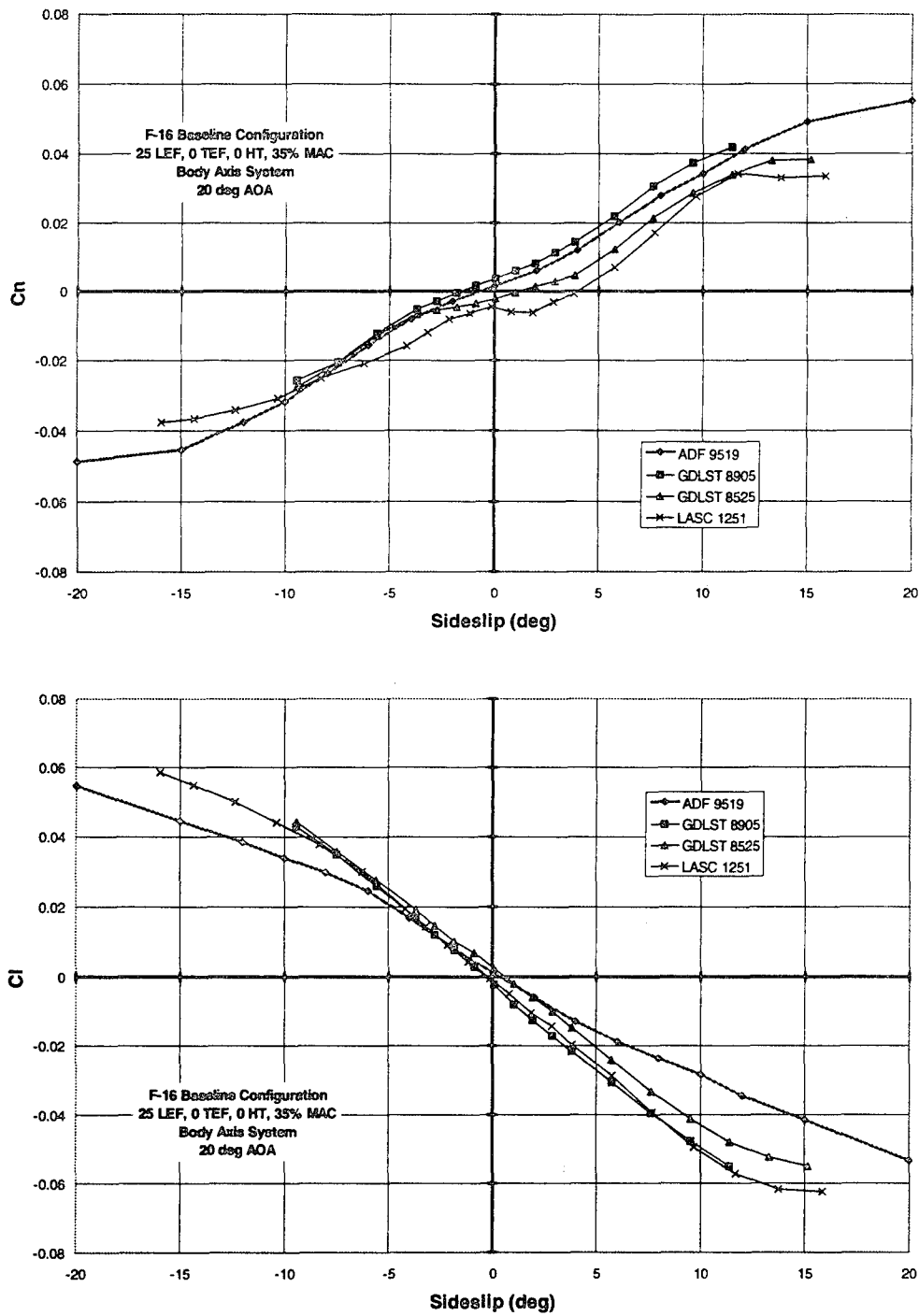


Figure 12-9 Facility to Facility Comparison -- Sideslip Cuts at 20 deg AOA

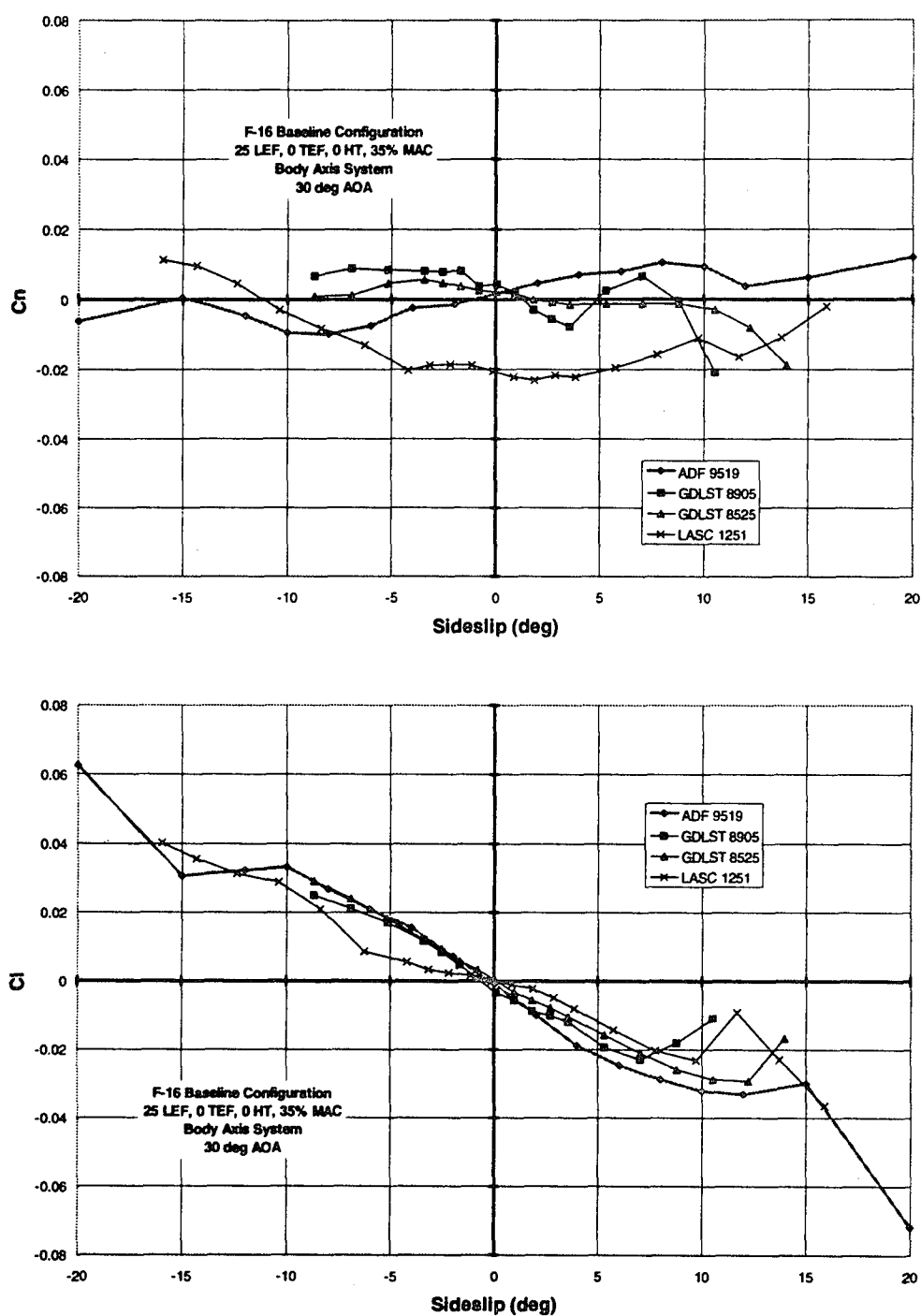


Figure 12-10 Facility-to-Facility Comparison - Sideslip Cuts at 30 deg AOA

12.2.3 Nose-Down Control Power

This section includes results from five of the six tests used in the longitudinal comparison section. Results are available from five different wind tunnel tests at four different facilities. The first run on the plot is taken from the LMTAS ADF 9519 test.

Figure 12-11 contains the comparison data for maximum nose-down pitch control power. The results from the comparison match well up to around 30 deg AOA. Above 30 deg AOA the results from the different facilities begin to diverge. The results from the BAR test are consistently more nose-up than the results from the other facilities. The ADF results are consistent with trends from other low-Reynolds number wind tunnels. Nose-down pitch control power available determined from F-16 flight test results are more consistent with the low R_N wind tunnel results.

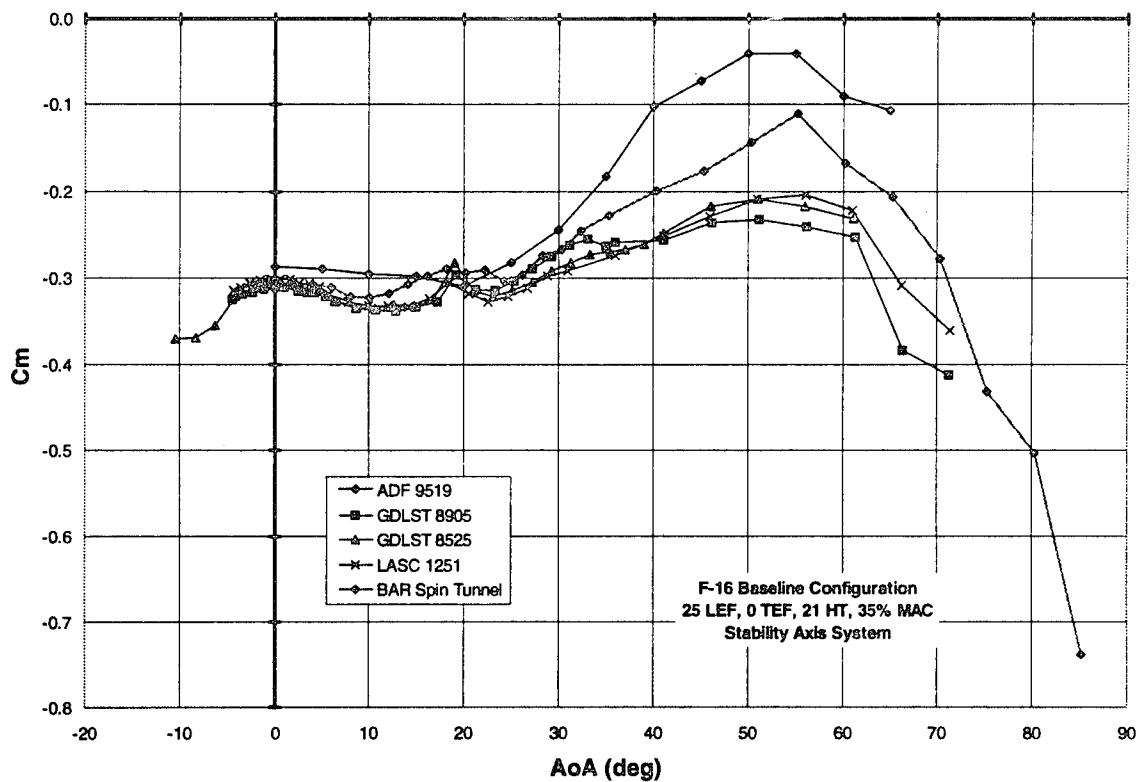


Figure 12-11 Test-to-Test Comparison - Nose-Down Control Power

12.3 Summary

A summary of comparisons of F-16 force and moment results from the LMTAS ADF wind tunnel to results from other wind tunnel facilities is provided below.

In test and test-to-test repeatability of the ADF data is adequate. Maximum lift coefficient values are slightly lower for wings horizontal runs than for wings vertical runs. The differences may be due to blockage effects. (No corrections were made to the ADF data prior to this evaluation.)

Lift coefficient data match the data from the other facilities very well.

Pitching moment data from the ADF wind tunnel are consistent with results from other low R_N facilities. The ADF low-AOA results are within the scatter of the results from the other facilities. At high-AOA, the ADF results are more nose-up than the results from higher R_N facilities. F-16 flight test experience has shown the aircraft to exhibit more nose-up pitching moments (and less nose-down control power) than the data obtained from wind tunnels operating in the R_N range of GDLST and LASC. The LaRC 30' x 60' and BAR pitching moment data are generally more representative of the real aircraft; the low R_N ADF data are consistent with data from these two wind tunnels.

Prediction of directional stability from the ADF tunnel is adequate. For the F-16, the cross-over point from positive to negative body axis directional stability occurred at a slightly higher AOA than that predicted by the GDLST and LASC low-speed wind tunnels. At low to moderate AOA, directional stability magnitudes were consistent with results from the other facilities.

Body axis lateral stability was underpredicted at low AOA, and over-predicted at high AOA. Lateral-directional trends with sideslip are consistent with data from other wind tunnels.

Overall, the ADF wind tunnel does a credible job of predicting static stability and control aerodynamic data considering the model scale and detail and the low operating R_N . The facility is suitable for conducting low-cost screening for preliminary design configuration evaluations.

12.4 References

- B1. Hammet, L.N., An Investigation of the F-16 High Angle-of-Attack Pitching Moment Discrepancy", AFWAL-TR-81-3107, September 1981.

13 APPENDIX C: Configuration 201 Aerodynamic Data Analysis

Two wind tunnel test entries of the 201-series configuration were conducted in January 1995 at the LMTAS ADF wind tunnel. This facility is an open circuit tunnel designed for low-cost screening of configuration concepts. It operates at a Reynolds number of 0.8×10^6 1/ft, and a dynamic pressure of 18 psf. Discussion of data accuracy from this tunnel is included in Appendix B.

A 1/40th scale model of Configuration 201 was constructed using LMTAS funds in 1994. The model is modular, and can support three different wing planforms, canards, horizontal, and vertical tails on a common fuselage. The vertical tailless canard variant was tested during ADF entries 9502 and 9505. Figure 13-1 shows a photograph of the model.

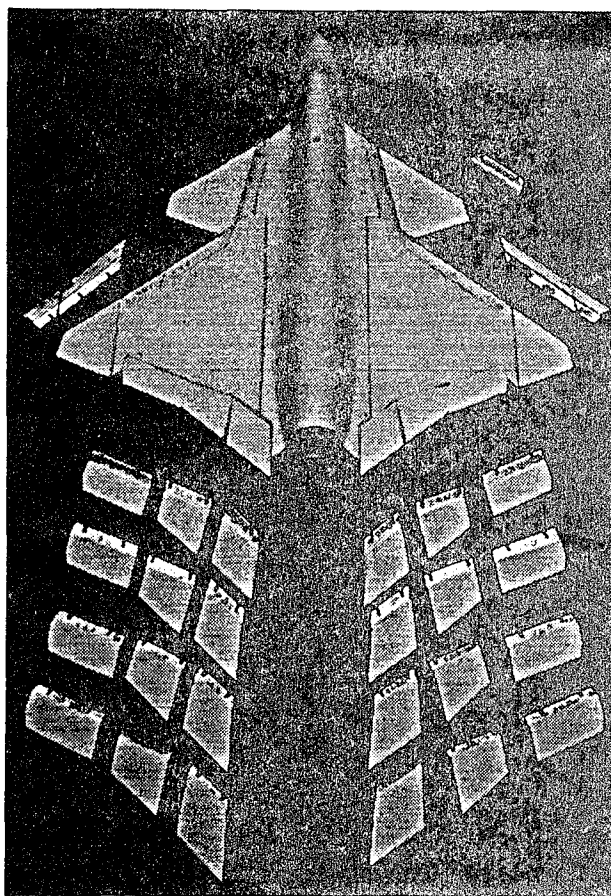


Figure 13-1 Configuration 201-Series 1/40th Scale Wind Tunnel Model

Data reduction constants are shown in Table 13-1.

Table 13-1 Configuration 201 Data Reduction Constants (Full Scale)

Parameter	Value
Reference Area (ft ²)	705.6
Span (ft)	42.9
MAC (in)	249.13
FSLEMAC (in)	333.65
MRC (%MAC)	20.0
Waterline MRC (in)	91.0
Model Scale	1/40
Test R_N ($\times 10^6$ 1/ft)	0.8
Mach Number	0.1

A five-component balance was used to measure normal force, side force, pitch, roll and yawing moments. Axial force data were not available.

The model's inlets exited the bottom of the model (Figure 13-2). No flow exited the aft end of the model. Tufts attached to the model indicated flow through the inlets throughout the range of AOA and sideslip tested. It is unknown whether the airflow exiting the lower surface of the model had any effect on the force and moment data.

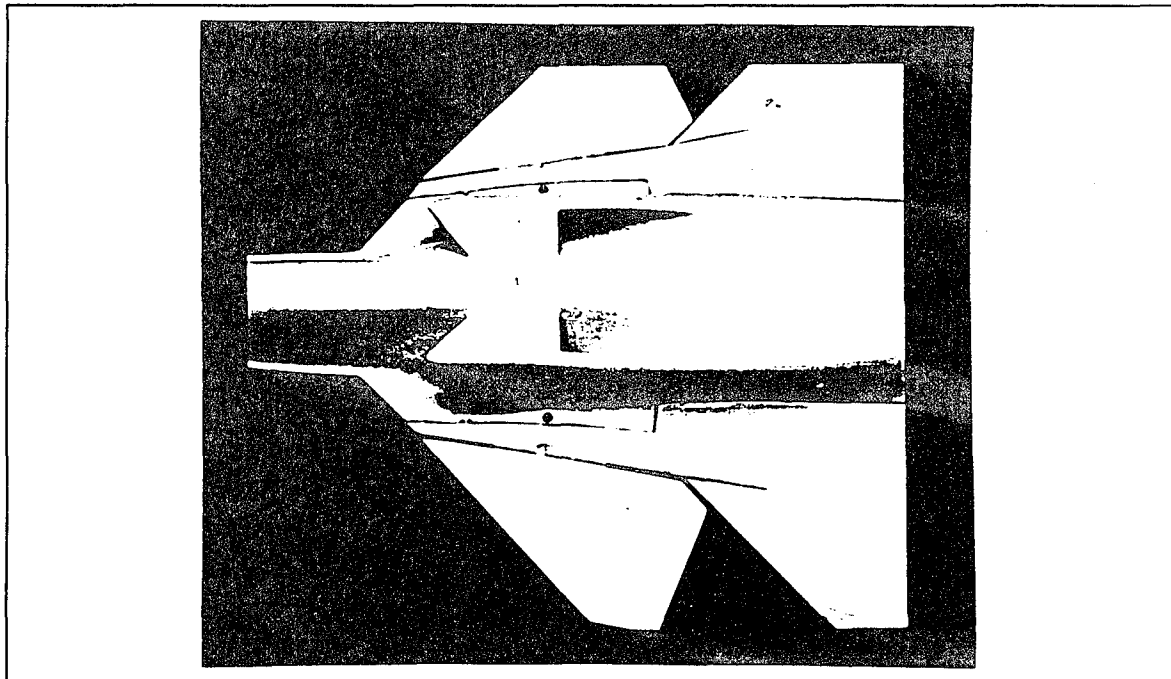


Figure 13-2 The Inlet Flow Exited at the Bottom of the Model

13.1 Longitudinal Data Analysis

Component build-up runs were conducted to determine the effect of the canard on the configuration. Two canard sizes at various canard deflections were tested as well. The small canard had a movable area approximately 9% of the wing reference area. Figure 13-3 shows the effect of the small canard with the LEF set to zero. The canard-off pitching moment data shows the configuration to be approximately neutrally stable without the canard at the test MRC. Canard-on pitching moments are linear up to approximately 20 deg AOA depending on the deflection. A 10 deg canard deflection breaks stable at 18 deg AOA.

Figure 13-4 shows large deflections of the small canard at high AOA. The LEF was set to 25 deg for these runs. The configuration exhibits a very stable break in the pitching moment curves at 40 deg AOA.

Large canard control effectiveness is shown in Figure 13-5 with LEF at 25 deg. This canard had a controllable area approximately 12.7% of the wing reference area. The effect of canard size at zero deflection on longitudinal characteristics is shown in Figure 13-6.

Table 13-2 lists aerodynamic centers computed by sloping the data over the linear portion of the normal force curve.

Table 13-2 Effect of Canard on Aerodynamic Center Location

Canard	AC Location (% MAC)
Off	21.73
Small	11.38
Large	8.48

Small Canard Control Effectiveness
 $LEF = 0$; $MRC = 20\%$ MAC; ADF 9502

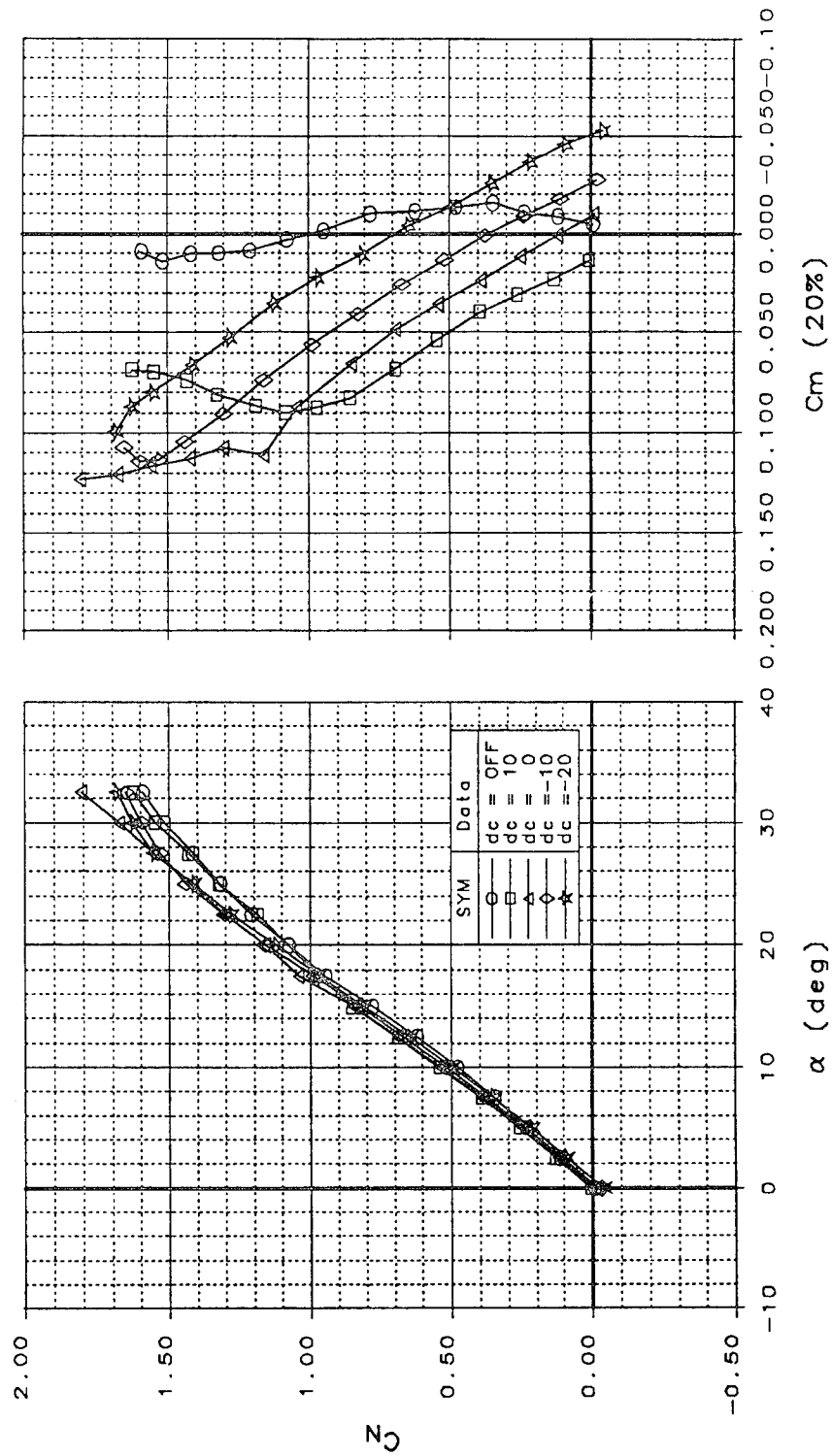


Figure 13-3 Longitudinal Data with Varying Small Canard Deflection ($LEF = 0$ deg)

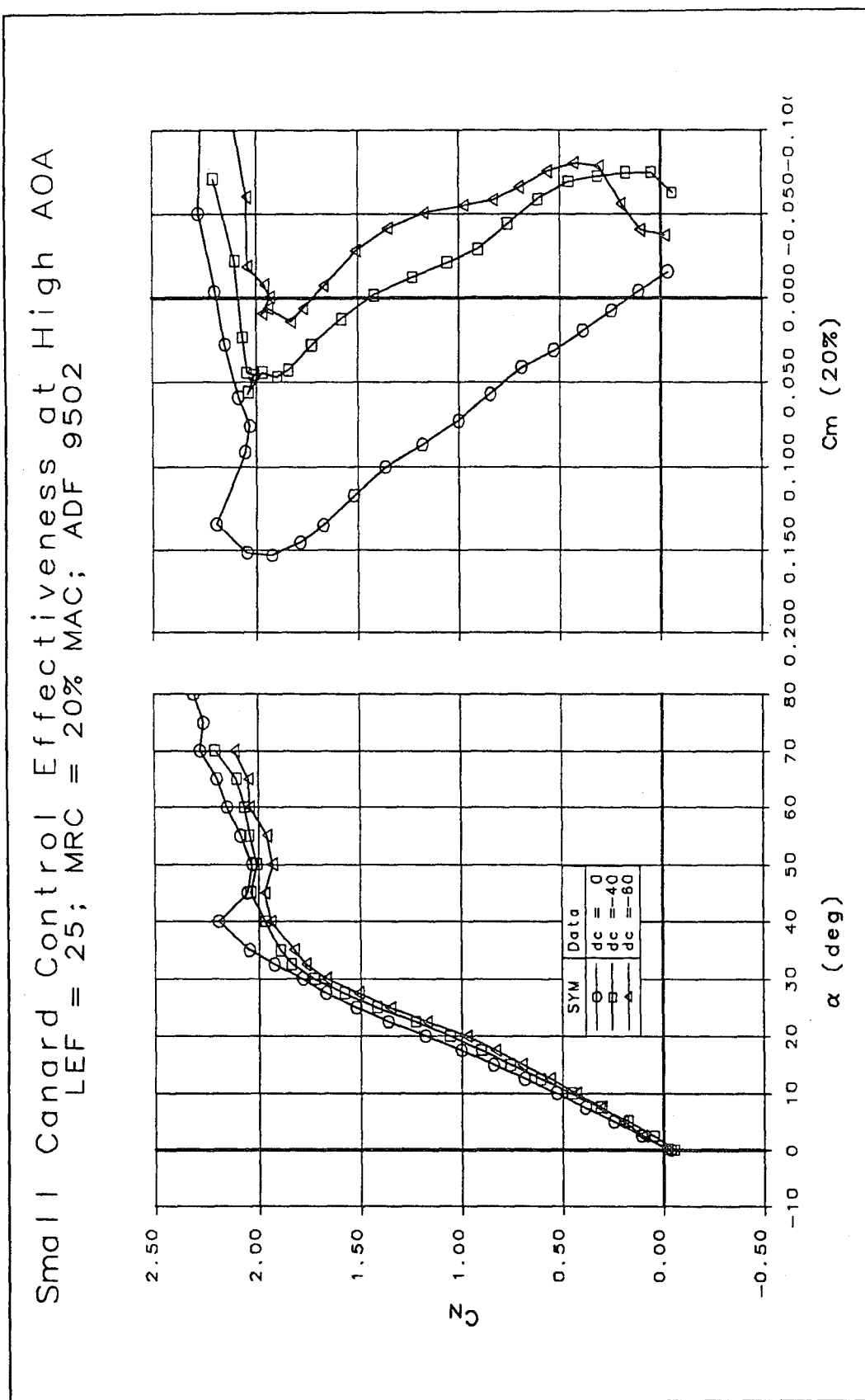


Figure 13-4 High AOA Longitudinal Results with Small Canard (LEF = 25 deg)

Large Canard Control Effectiveness LEF = 25; MRC = 20% MAC; ADF 9502

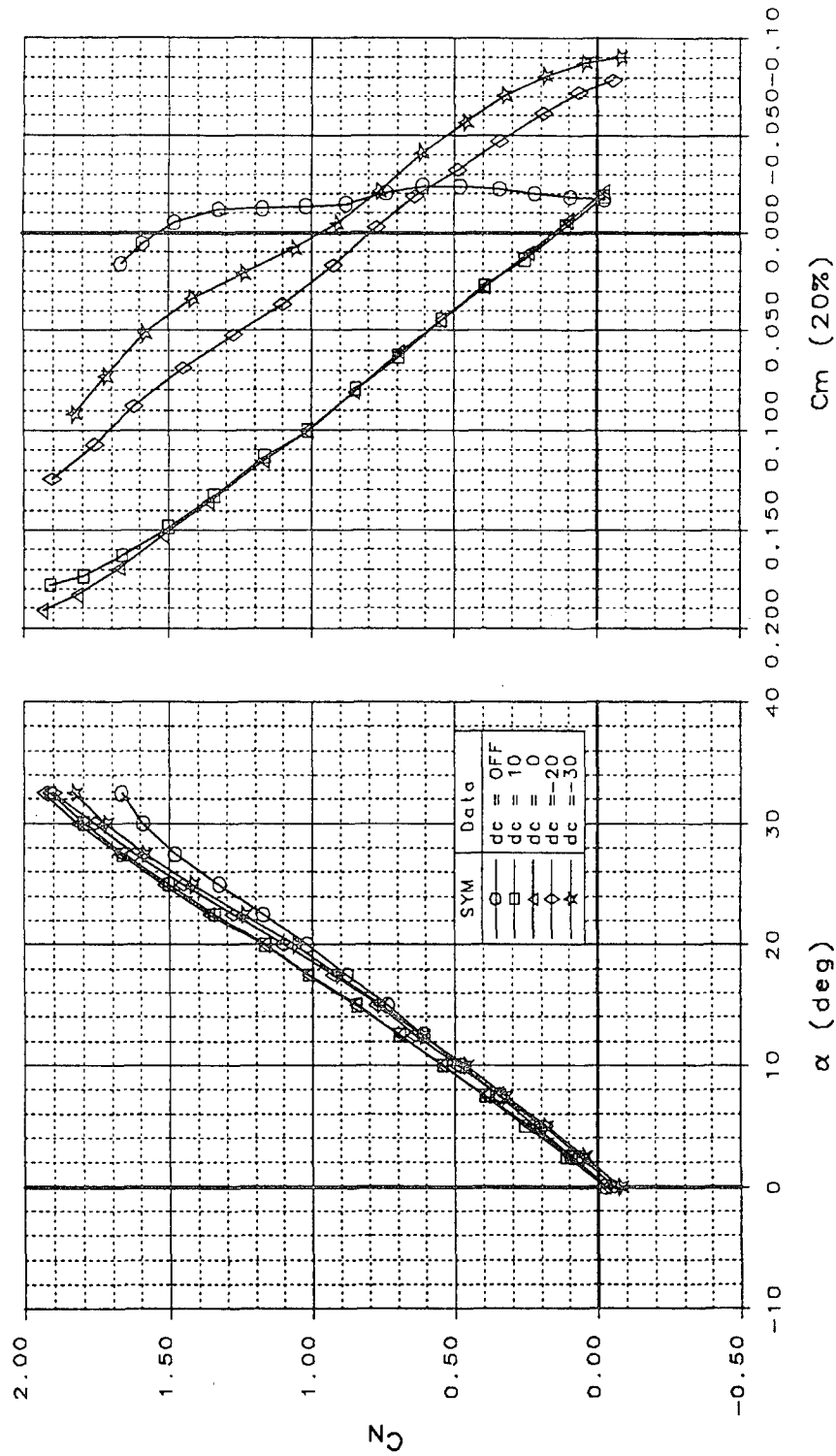


Figure 13-5 Large Canard Longitudinal Data (LEF = 25 deg)

EFFECT OF CANARD SIZE
LEF = 25; MRC = 20% MAC

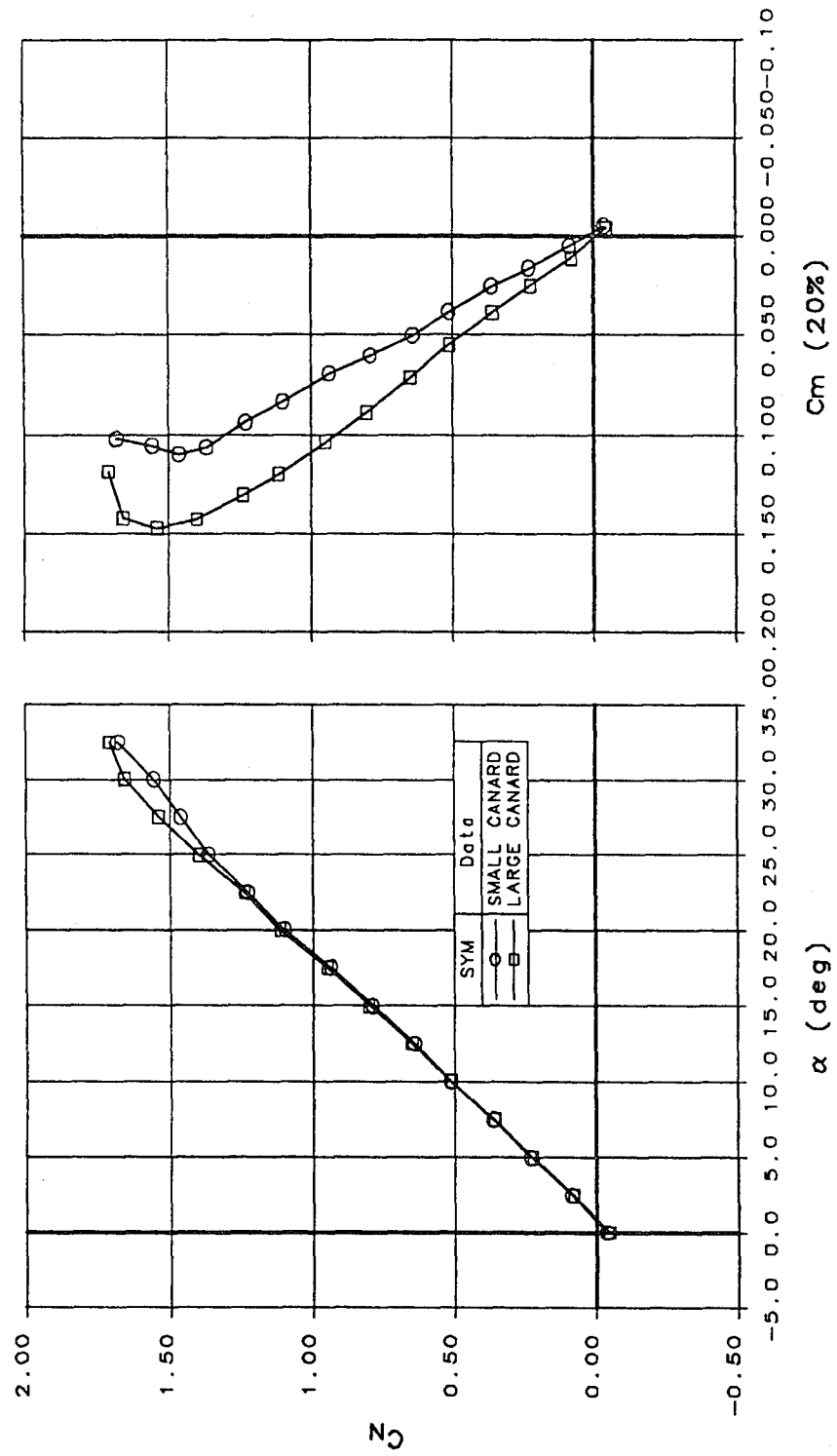


Figure 13-6 Effect of Canard Size on Longitudinal Stability

Leading edge flap effects on longitudinal stability are shown in Figure 13-7. The LEF linearizes the pitching moment curve near 20 deg AOA, and results in reduced normal force up to 22 deg AOA. Slightly higher normal forces are achievable with the LEF at 25 deg above 22 deg AOA.

Nose-down control power is shown in Figure 13-8. All trailing edge flaps are set to 20 deg TED. The AMT is set to zero. A -60 deg deflection of the large canard resulted in greater nose-down control power in the 5 to 30 deg AOA region than a -60 deg small canard deflection. At high AOA (45 deg), the canard off provided slightly more nose-down control power than the small canard at -60. The large canard at -60 generated less control power at this condition. A -40 deg deflection of the small canard resulted in no nose-down pitch control power near 60 deg AOA at the test MRC. Greater nose-down control capabilities are probably achievable with larger trailing edge flap deflections.

The effect of the AMT on nose-down control power is shown in Figure 13-9. Deflecting the AMT 20 deg TED provides small additional control power at high AOA. These data represent canard-off with LEF set at 25 deg. A summary of aft limit data are shown in Table 13-3. A nose-down control margin of -0.07 rad/sec^2 was added to these data assuming a pitch inertia (I_{yy}) of 89,000 slug-ft².

Effect of LEF On Longitudinal Stability
ADF 9502; MRC = 20% MAC; Canard = 0

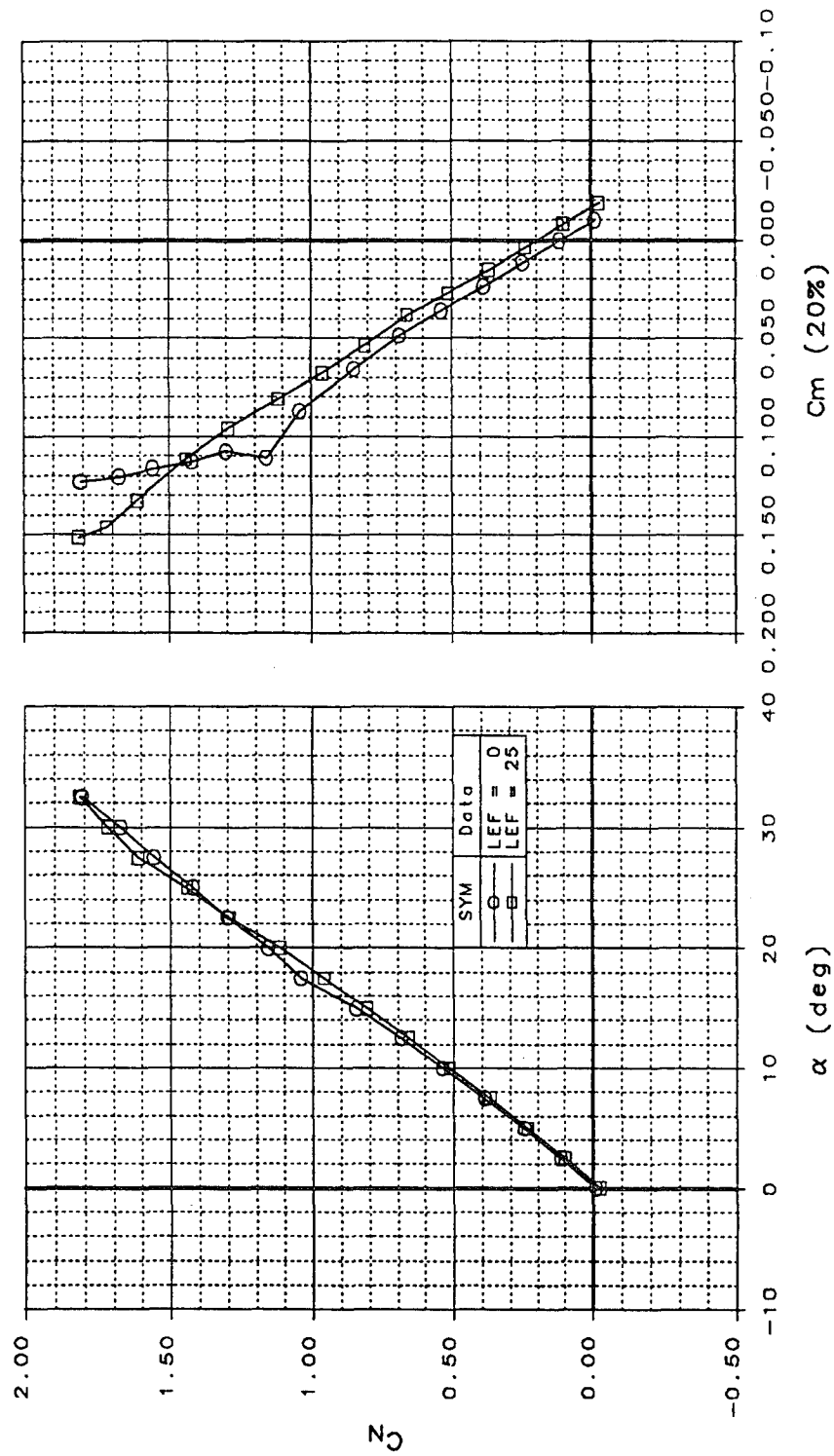


Figure 13-7 25 deg LEF Deflections Linearize the Pitching Moment Data

LEF = 25; Max Nose-Down Control Power
TE Controls = 20; MRC = 20% MAC; ADF 9502

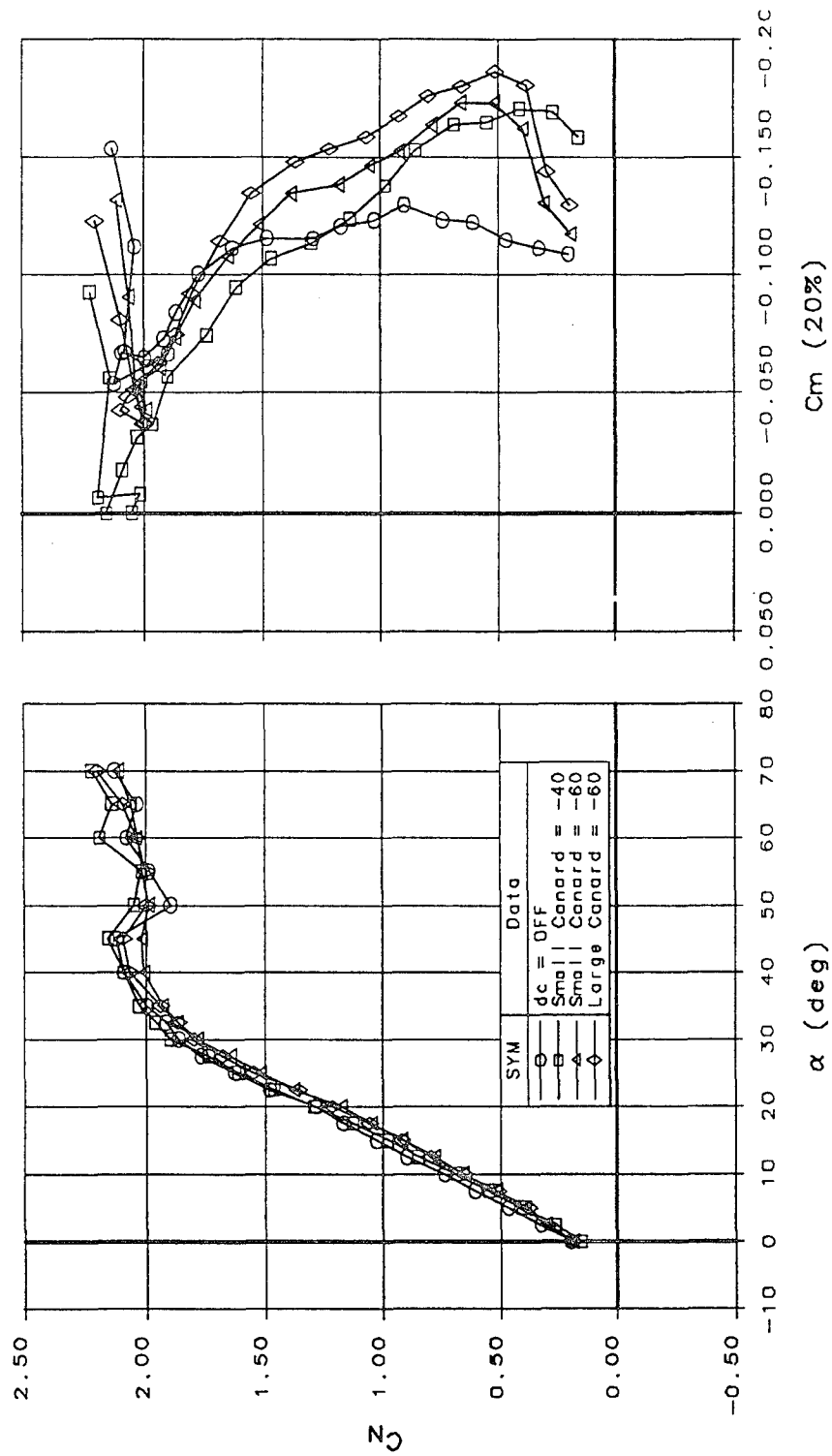


Figure 13-8 Maximum Nose-Down Control Power (LEF = 25 deg)

Effect of AMT on Max Nose-Down Control Power Canard Off; LEF = 25; TE Controls = 20

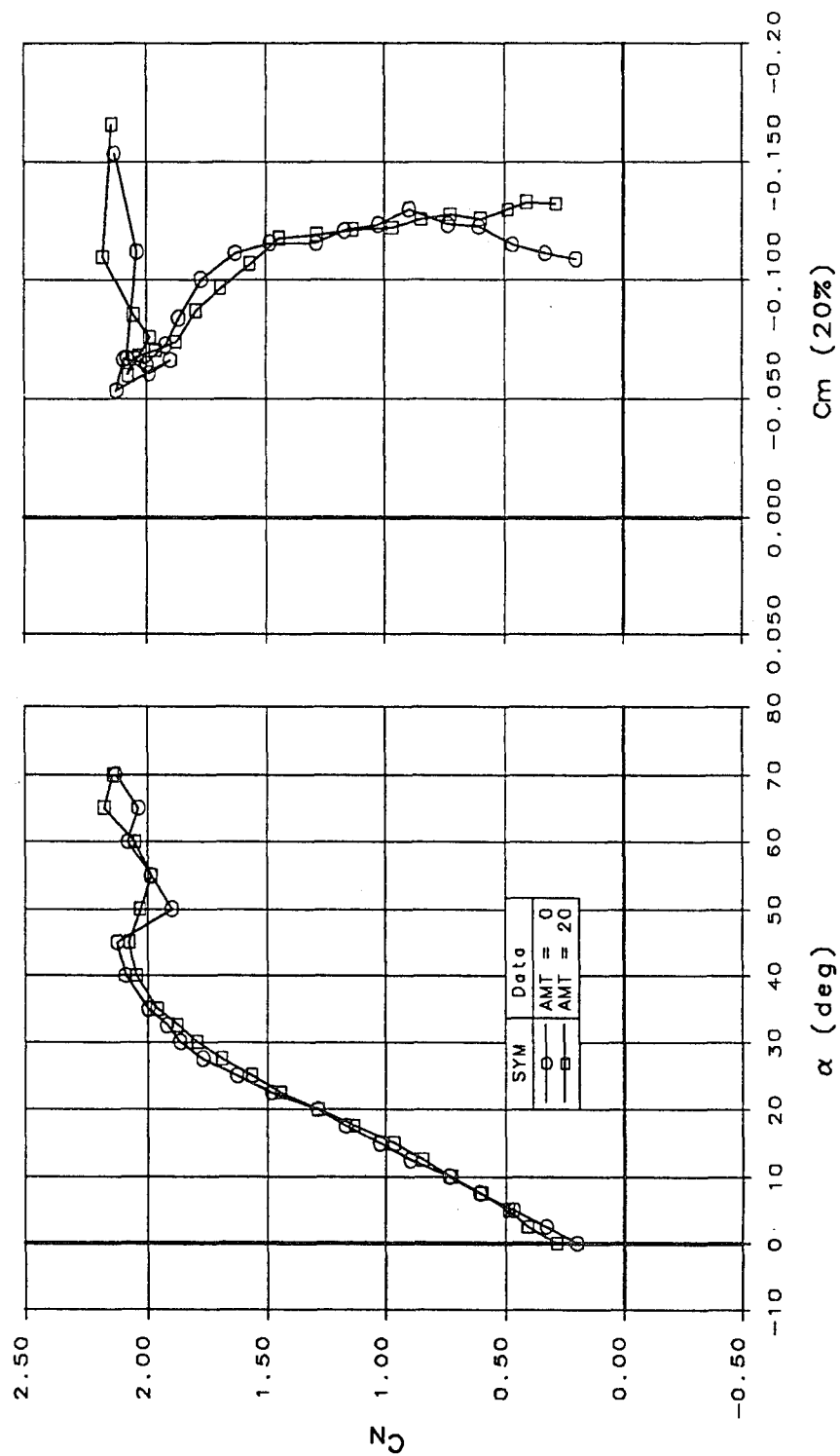


Figure 13-9 The AMT Provides Additional Nose-Down Control Power at High AOA

**Table 13-3 Deep Stall Aft CG Limit Capabilities (LEF = 25 deg; All TEF = 20 deg;
 \dot{q} Margin = -0.07 rad/sec²)**

Configuration	Aft Limit (%MAC)
Canard Off	22.03
Canard Off & AMT = 20 deg	22.39
Small Canard @ -40 deg	19.50
Small Canard @ -60 deg	21.64
Large Canard @ -60 deg	21.31

The AMT provides an additional 0.36 % MAC aft limit capability at 20 deg deflection. The large canard aft limit is 0.33% MAC forward of the small canard limit at the same deflection.

13.2 Comparison of Wind Tunnel Data with HASC Predictions

The vortex lattice routine HASC^{C1, C2} was used to make predictions of the original 201 configuration. These predictions were used to guide the decision-making process while setting up the wind tunnel test matrix. Comparisons of HASC results with longitudinal test data are shown in Figures 13-10 through 13-12.

Figure 13-10 shows that HASC did a reasonable job of predicting normal-force curve slope and longitudinal stability in the linear AOA range with LEF deflected 25 deg. HASC underpredicted normal force, and indicated a non-linearity in the pitching moment curve at 25 deg AOA.

Figure 13-11 shows HASC predictions of canard control effectiveness compared with the ADF data. In this comparison, the HASC data represent 25 deg LEF deflections, while the ADF data have the LEF set to zero. Nevertheless, the pitch control effectiveness of the canard is predicted reasonably well up to 15 deg AOA.

COMPARISON OF ADF WITH HASC PREDICTIONS
LEF=25; ADF 9502; Low Speed

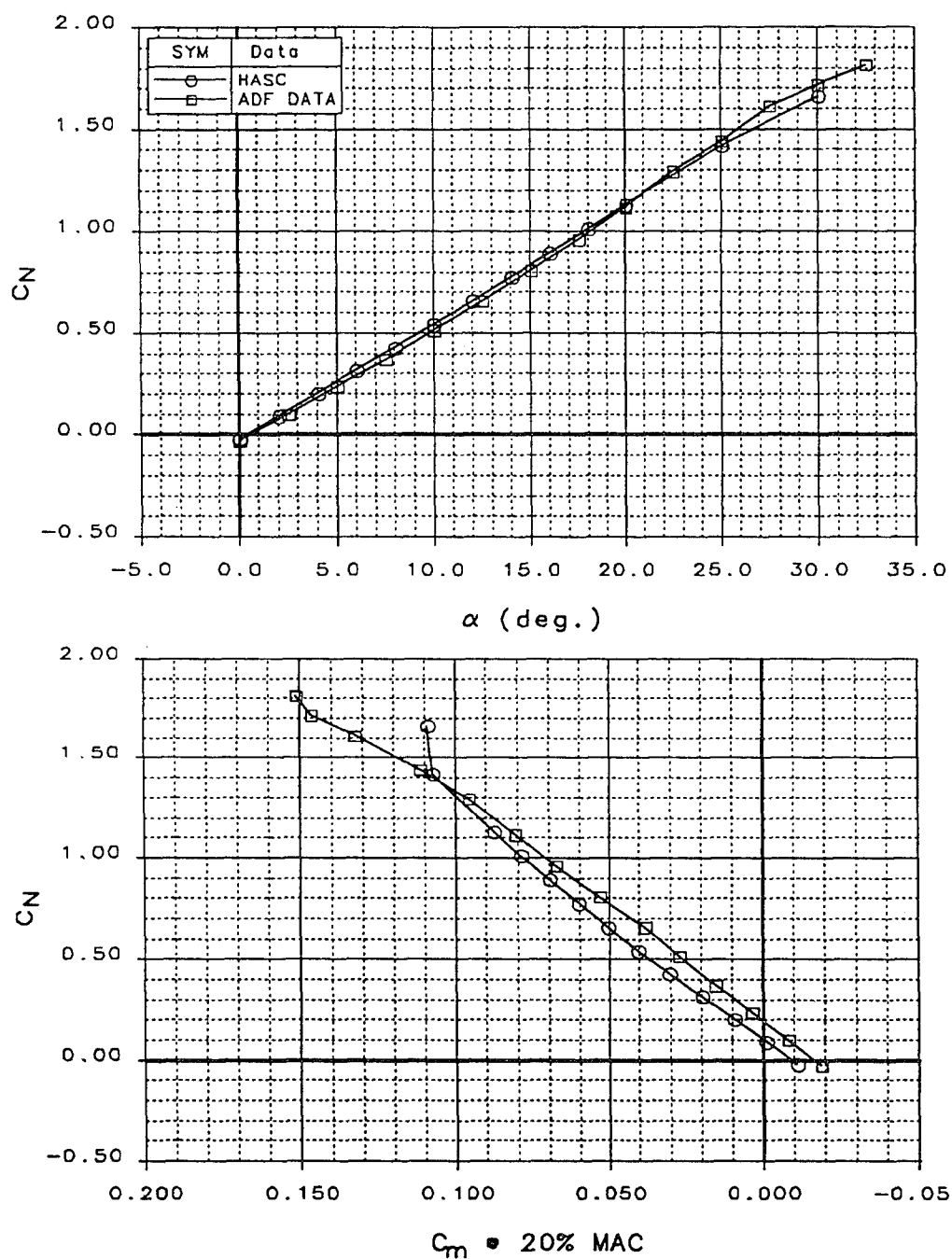


Figure 13-10 Comparison of Longitudinal Data with HASC Predictions

COMPARISON OF ADF WITH HASC PREDICTIONS

Canard Control Effectiveness

HASC Data: LEF=25; ADF Data: LEF=0

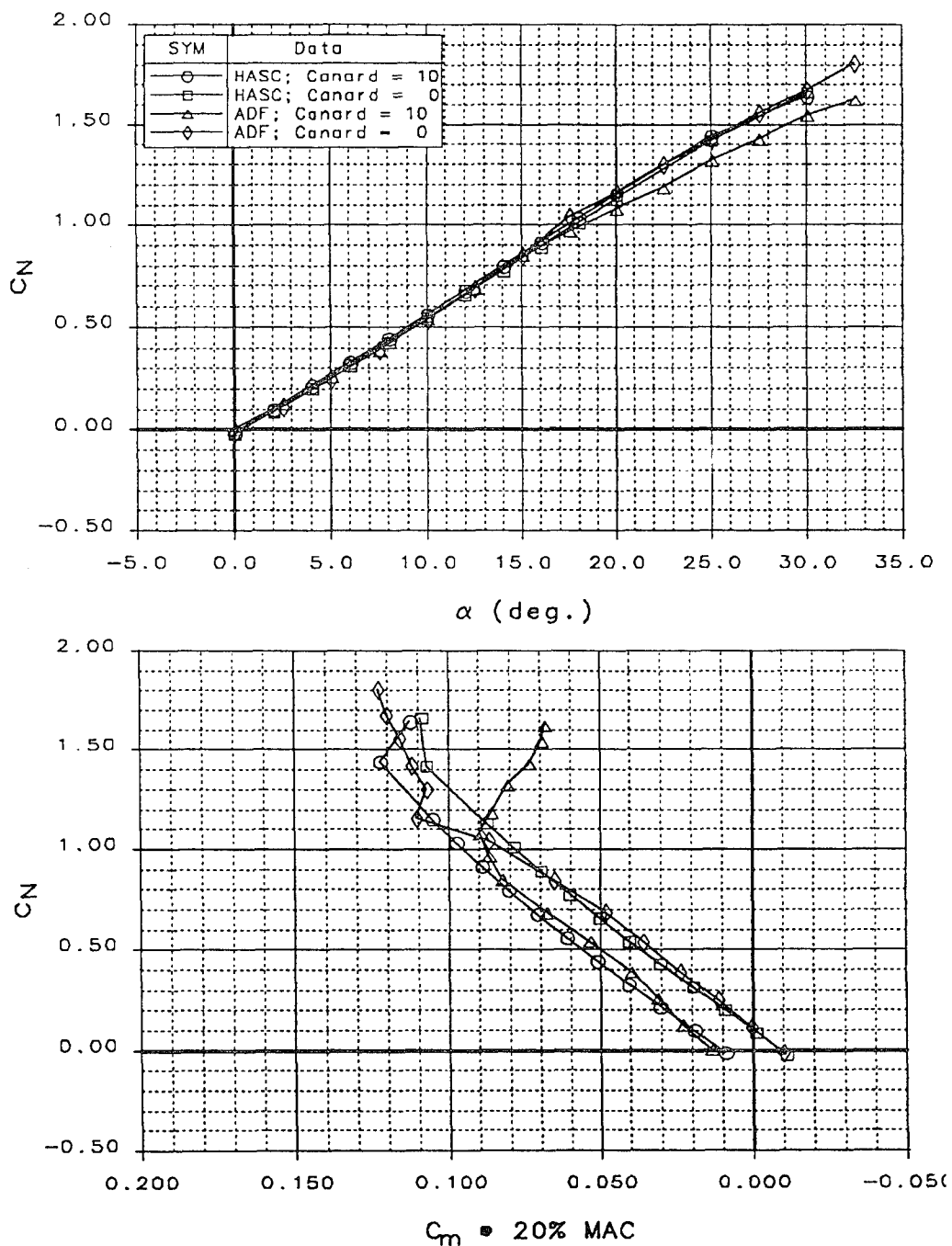


Figure 13-11 HASC Correctly Predicted Low AOA Canard Control Effectiveness

Figure 13-12 shows HASC vs wind tunnel data at LEF set to zero. The HASC results were empirically corrected above 17.5 deg AOA to represent a nose-up pitch increment due to the sharp-edged forebody chine. Comparisons with the wind tunnel data indicate that such a correction should not have been applied. With the LEF down, no significant nose-up nonlinearities are apparent due to the forebody chine. Further study would be required to justify this conclusion.

COMPARISON OF ADF WITH HASC PREDICTIONS
LEF=0; ADF 9502; Low Speed

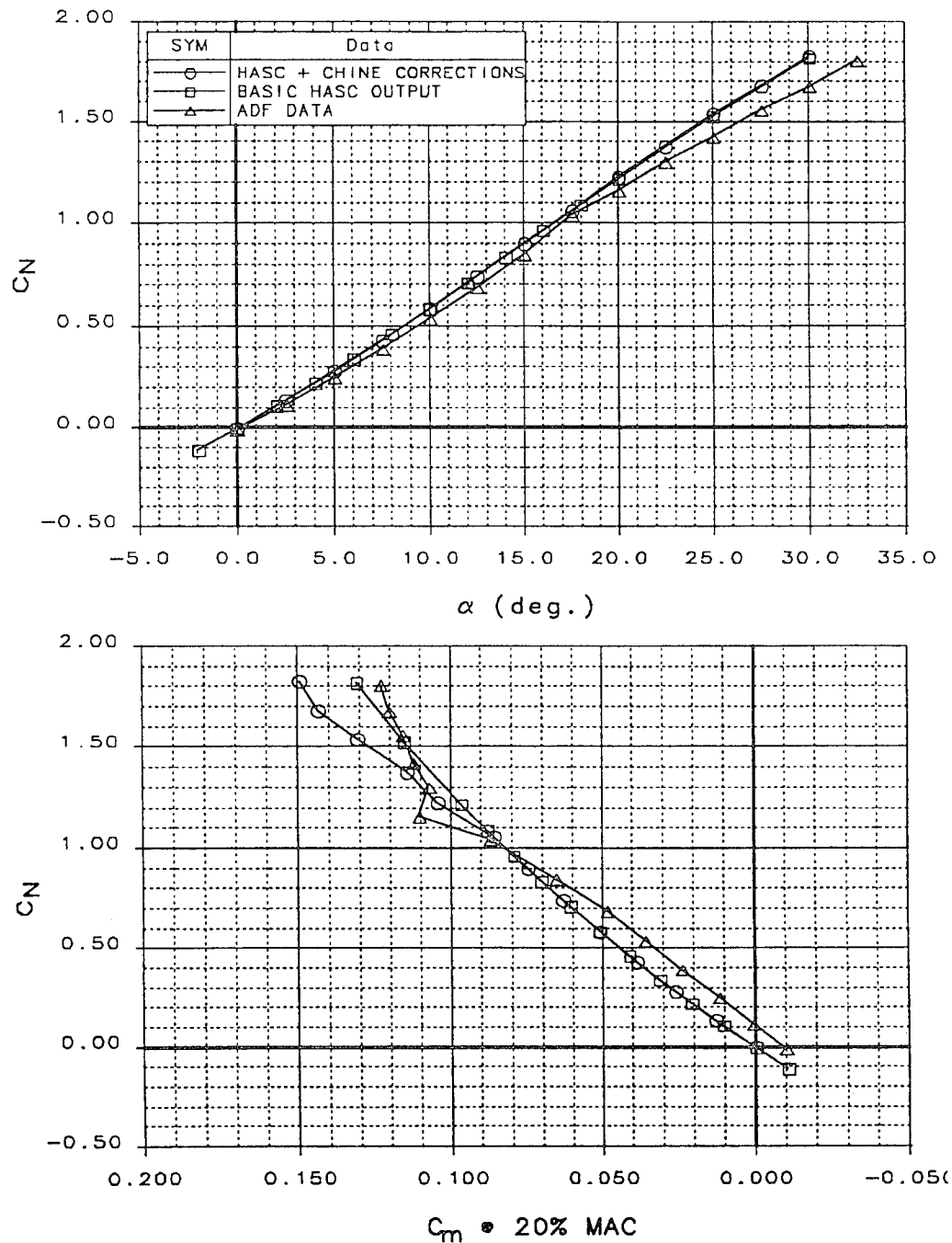


Figure 13-12 The Empirical Increment Added to HASC Results to Account for the Chined Forebody was not Required

13.3 Longitudinal Trim Analysis

Based on conclusions drawn as a result of studying HASC predictions (not shown here), and Reference C3, for maximum trimmed lift at the approach condition, the canard should be set at an optimum high lift condition, and the configuration trimmed with trailing edge flaps (TEF). The canard should be scheduled to unload at higher AOA to avoid saturating the trailing edge surfaces.

Figure 13-13 shows the effect of canard deflection on the TEF at three different settings. The LEF was set at 25 deg. (For this figure, TEF deflections represent equal elevon and pitch flap settings.) Up to 25 deg AOA, canard deflection has no appreciable affect on normal force. Leading edge up canard deflections result in slight nose-up pitch increments with the TEF neutral or down at power approach AOA's. TEF up deflections show relative insensitivity to canard deflections in the 12 deg to 22 deg AOA range. The slight nose-up increments provided by nose-up canard deflections will require greater TED flap deflections to trim, resulting in higher trimmed lift coefficients at the approach condition. As a result, 10 deg nose-up canard was chosen for the take-off and PA setting.

Low-speed canard schedules vs AOA are shown in Figure 13-14 for both the small and large canards. The canard is scheduled to maintain TEF deflections ≤ 15 deg. This provides a 15 deg TEF deflection margin for pitch and rolling maneuvers with the canard fixed. If greater nose-down control power is required, the canard can be further unloaded (deflected leading edge down).

Figure 13-15 shows lift and moment curves for a scheduled canard, LEF down and symmetric ailerons fixed 15 deg TED. Deflecting the ailerons provides a small benefit in trimmed normal force at approach conditions (Figure 13-16).

Effect of Canard Deflection on TEF Effectiveness $LEF = 25$; TEF = Elevon & Pitch Flap

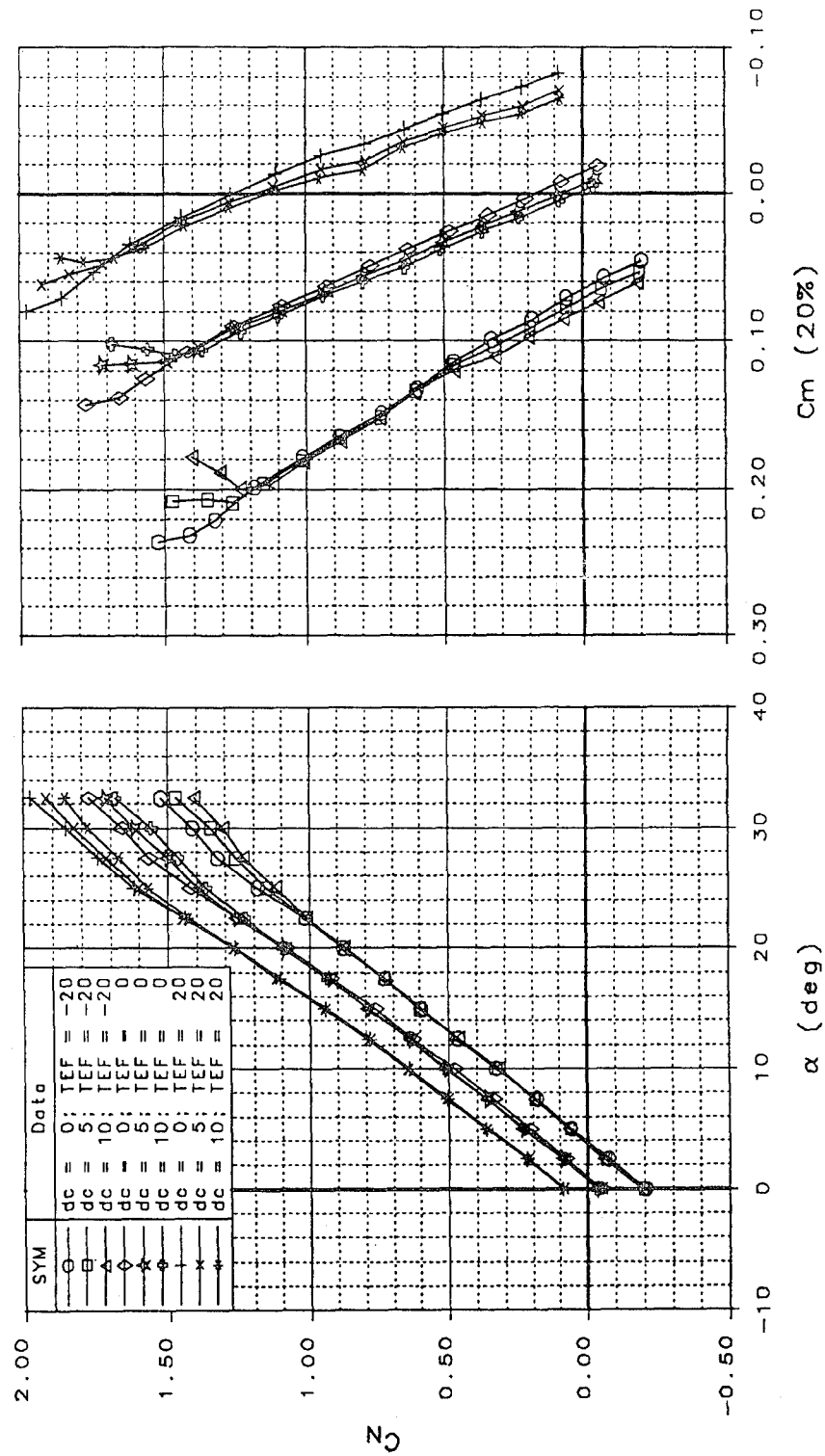


Figure 13-13 Canard/TEF Aerodynamic Interactions ($LEF = 25$ deg)

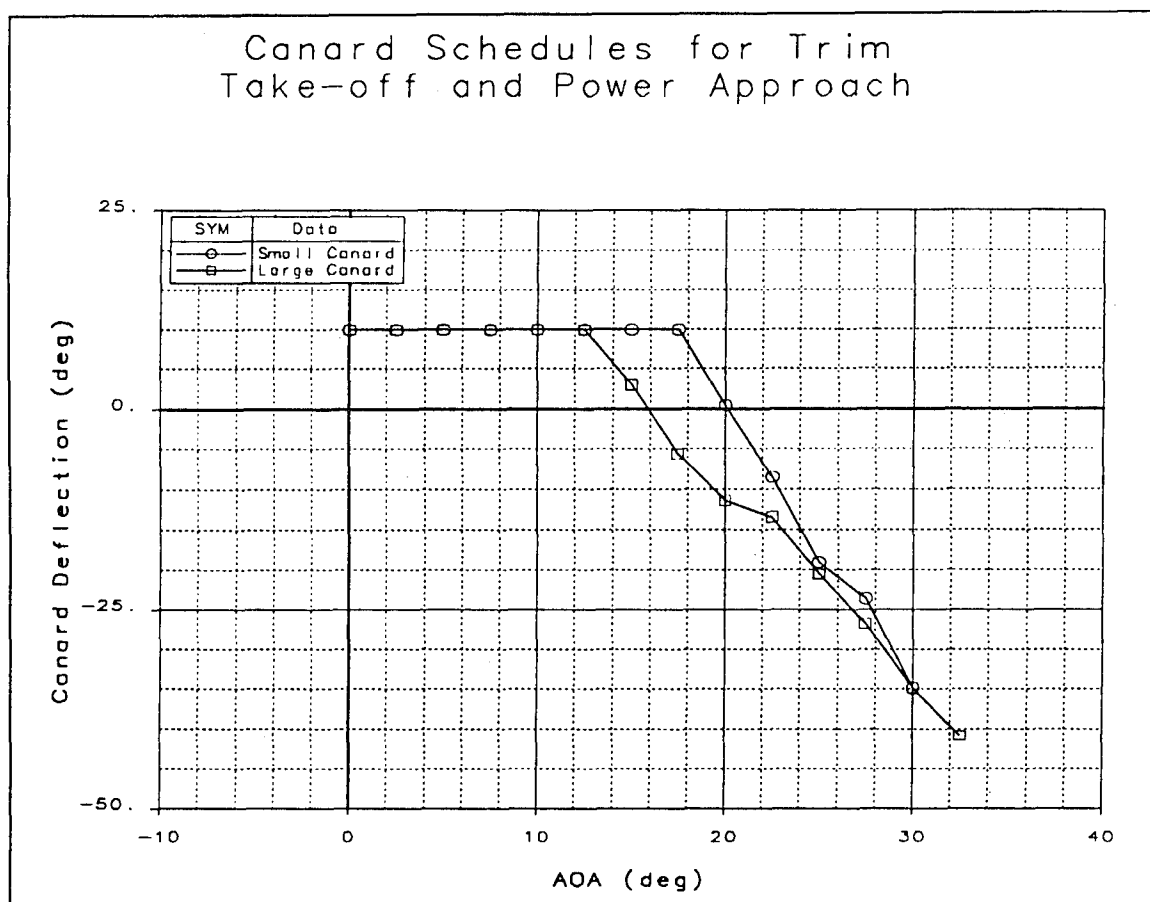


Figure 13-14 Canard Schedules for Takeoff and Power Approach

Longitudinal Control Effectiveness
 LEF = 25; Large Canard Scheduled; MRC = 20% MAC
 TEF = Elevon & Pitch Flap; Aileron = 15 deg

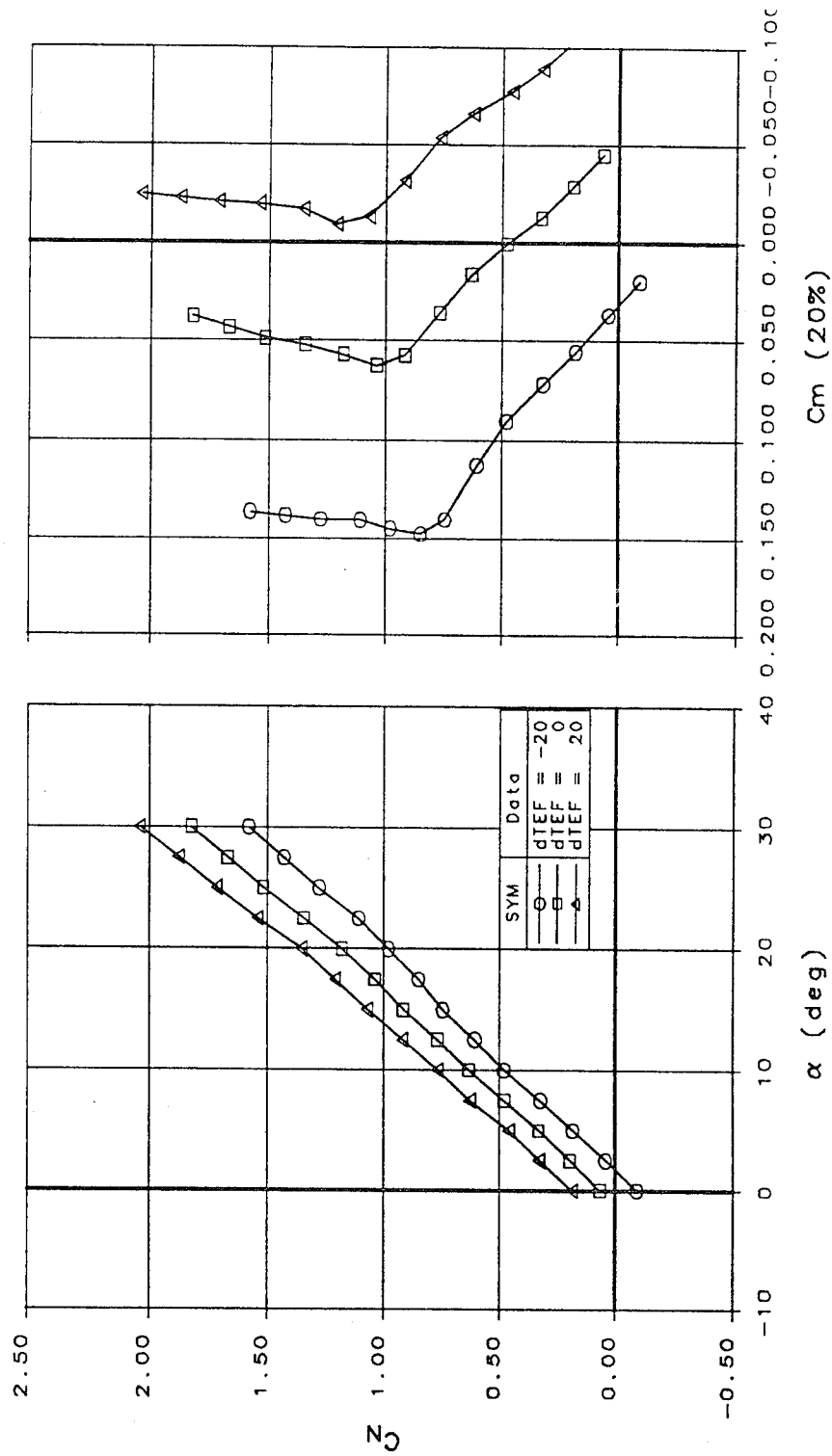


Figure 13-15 Untrimmed Longitudinal Data with Canard Scheduled (LEF/Aileron = 25/15 deg)

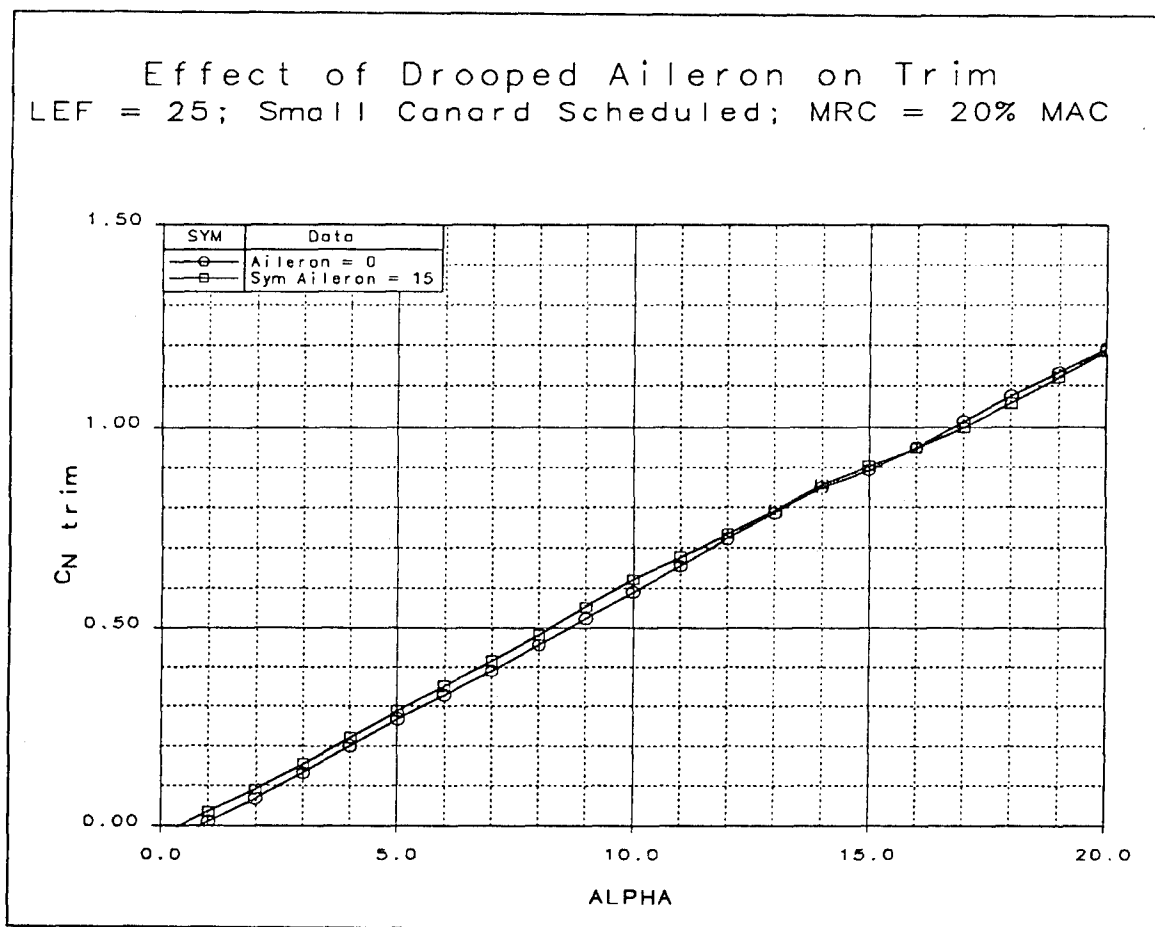


Figure 13-16 Drooping the Aileron Improves Trimmed Lift Values at PA Conditions

13.4 Lateral-Directional Stability

Lateral-directional stability data were collected by sweeping the sting in pitch at constant sideslip angles. At the time of the test, mechanical problems prevented the sting from exceeding 32.5 deg AOA at any yaw angle other than zero. Unless otherwise stated, all lateral-directional data shown are in body axes.

Canard-off lateral-directional characteristics are shown in Figure 13-17. Some asymmetry is evident in the data at high AOA. The airframe is slightly unstable in yaw at low AOA. Lateral-stability is good, representing typical delta wing characteristics with increasing AOA. The canard-off airframe becomes laterally unstable in body axes above 20 deg AOA. Directional stability is degraded above 25 deg AOA.

Lateral-directional stability derivatives were determined using the secant method between zero and 10 deg AOA. Derivatives were determined for both positive and negative sideslips, and the results averaged. Figure 13-18 shows the effect on lateral-directional stability of adding the small canard. Leading edge flaps were set at zero. The canard had a 5 deg dihedral to place the tips above the wing reference plane at zero deflection. As a result, lateral stability was improved at low to moderate AOA, and the magnitude of instability above 20 deg AOA was reduced. Directional stability was degraded above 20 deg AOA.

Figure 13-19 shows the same two configurations, only with LEF deflected 25 deg normal to hingeline. Comparing figures 13-18 and 13-19, one can see the significant improvement in stability afforded by simply deflecting the LEF. Lateral stability is improved dramatically with the cross-over to instability being delayed from 20 deg to 28 deg AOA. The magnitude of instability is not as severe. Directional instabilities at high AOA are reduced as well. A similar result was achieved with the canard on and LEF down 25 deg.

Canard-Off Lateral-Directional Characteristics Body Axis; ADF 9502

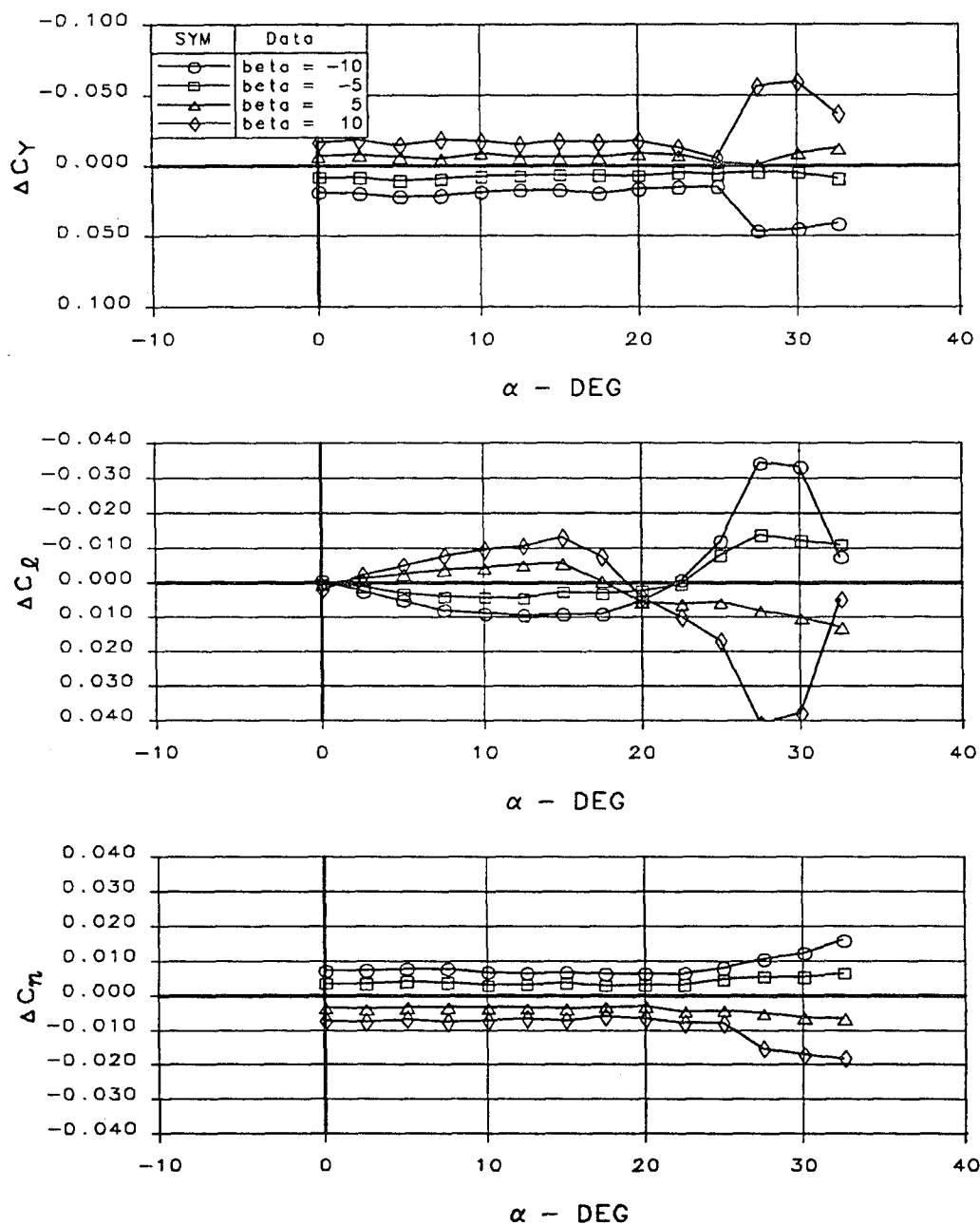


Figure 13-17 Canard-Off Lateral-Directional Stability ($LEF = 0$ deg)

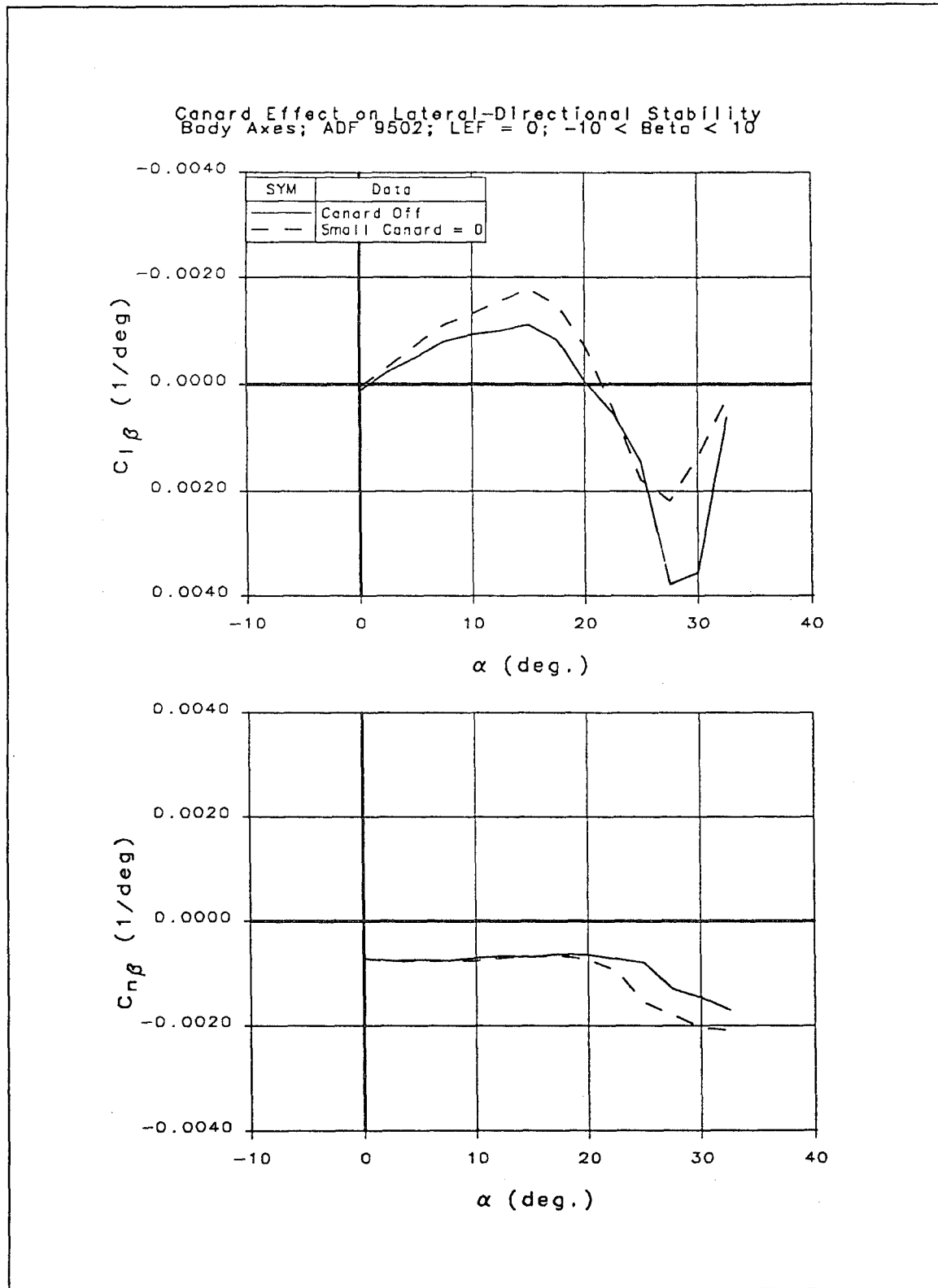


Figure 13-18 Effect of Small Canard on Lateral-Directional Stability (LEF = 0 deg)

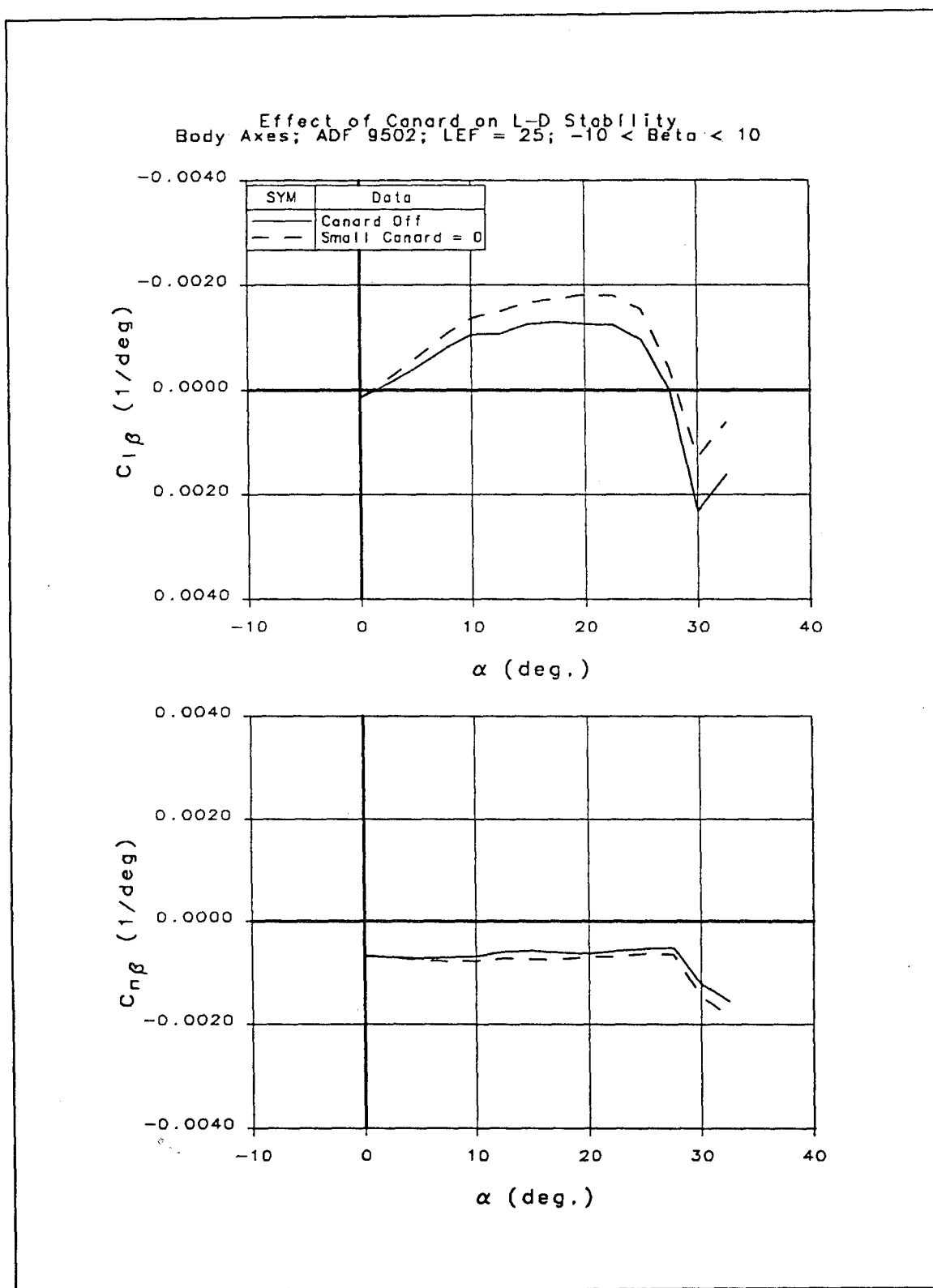


Figure 13-19 Effect of Small Canard on Lateral-Directional Stability (LEF = 25 deg)

Canard deflections affect lateral-directional stability due to the variations in location of the trailing tip vortices off of the canard with respect to the wing. Changing the canard incidence changes the location of the trailing vortices with respect to the wing. The effects of canard deflections on stability can be seen in Figure 13-20. In general, positive (leading edge up) canard deflections degrade stability, and negative deflections improve stability. For $AOA > 25$ deg, negative deflections increase the magnitude of lateral instability. Fortunately, canard deflection effects on lateral-directional stability are synergistic with the canard positions required for pitch trim.

Figure 13-21 shows the effect of large canard deflections on stability in conjunction with a 25 deg LEF deflection. Characteristics are similar to those shown Figure 13-20; although, the LEF provides favorable influence on the derivatives at high AOA. Finally, Figure 13-22 shows lateral-directional characteristics with the LEF down 25 deg, and the canard operating on the schedules shown in Figure 13-14. There is essentially no difference in lateral-directional stability due to canard size with the canards on their appropriate schedules for pitch trim.

Effect of Small Canard Deflections on L-D Stability
Body Axes; ADF 9502; LEF = 0; $-10 < \text{Beta} < 10$

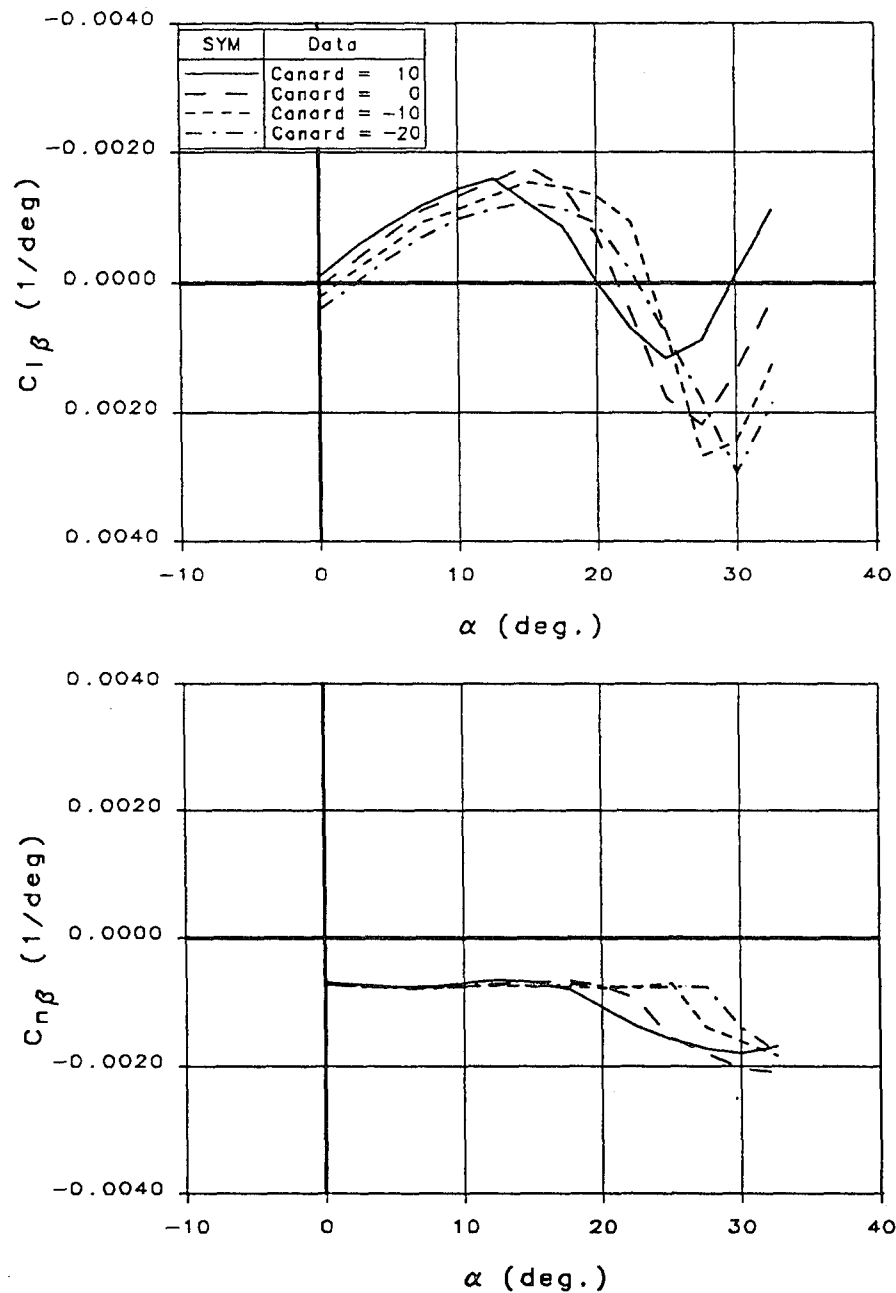
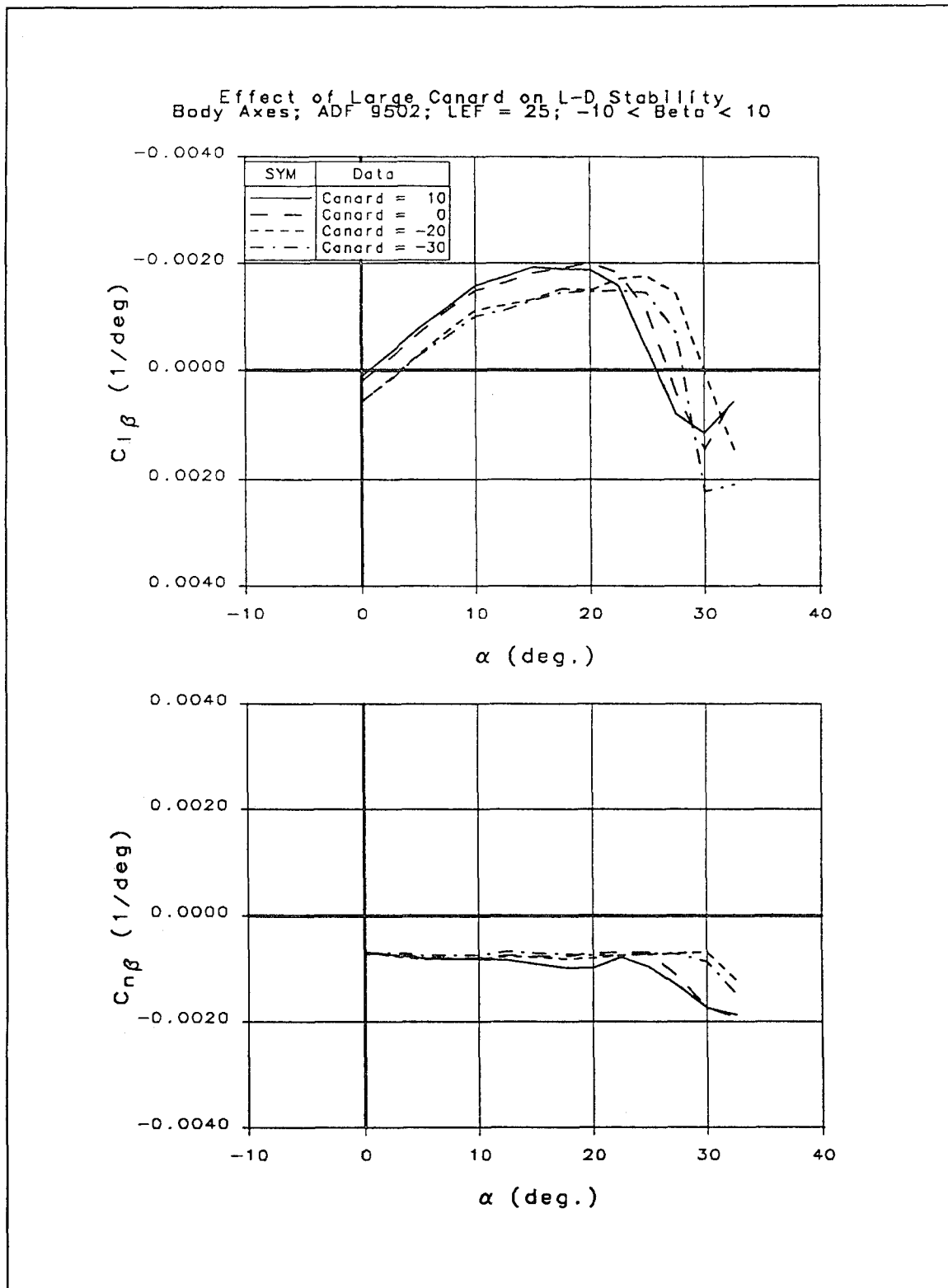


Figure 13-20 Effect of Canard Deflection of Lateral-Directional Stability (LEF=0)



**Figure 13-21 Effect of Large Canard Deflections on Lateral-Directional Stability
(LEF = 25)**

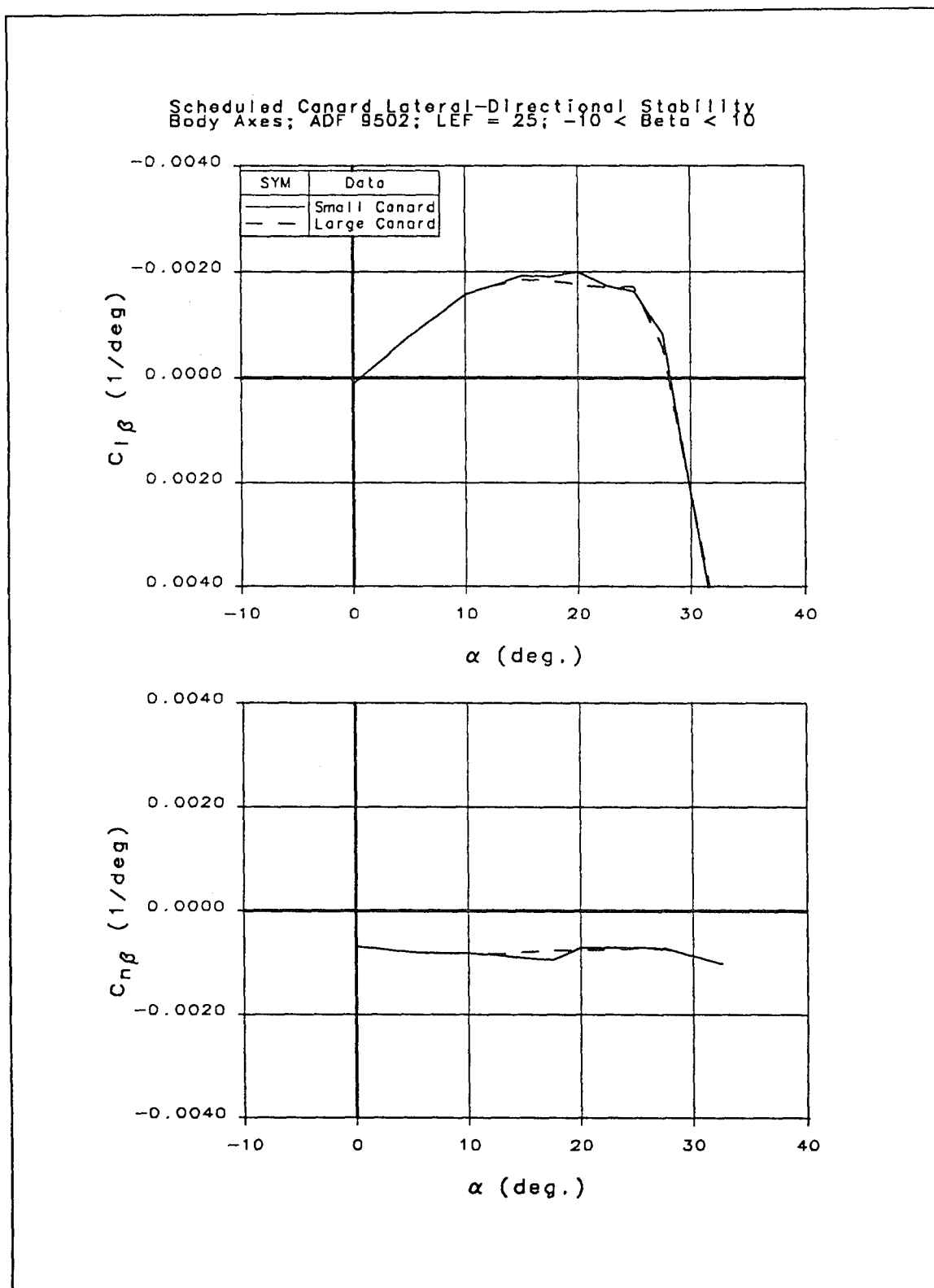


Figure 13-22 Lateral-Directional Stability (Canard/LEF = Scheduled/25 deg)

13.5 Control Effectiveness

Control effectiveness plots were derived by interpolating the raw data to even AOA, and subtracting off the appropriate baseline runs. All data are in body axes referenced to 20% MAC.

13.5.1 Pitch Flaps

Figure 13-23 shows control increments due to symmetric deflection of the inboard trailing edge flap (pitch flaps). This surface provides good pitch control effectiveness throughout the AOA range, a trait typical of pitch flaps.

13.5.2 Elevons

Elevon (middle trailing edge flap) control effectiveness is shown in Figure 13-24. Data from left-side deflections are shown. Nose-down pitch effectiveness is lost above 45 deg AOA. A corresponding loss in roll control power can also be observed.

The effect of a 10 deg canard deflection on elevon control power is shown in Figure 13-25. Positive canard deflections generally decreased pitch effectiveness, and slightly increased roll effectiveness.

13.5.3 Ailerons

Aileron control effectiveness is shown in Figure 13-26. As with the elevon, nose-down pitch effectiveness is degraded above 45 deg AOA. Significant body axis adverse yaw is created by TED aileron deflections.

The effect of spoiler deflections on aileron effectiveness are shown in Figure 13-27. Not surprisingly, maximum spoiler deflections adversely impact aileron control power -- especially TED aileron deflections.

Two canard deflections were tested with the ailerons deflected. A 10 deg canard deflection had a small impact on aileron control effectiveness, with most of the effect in the pitch axis (Figure 13-28).

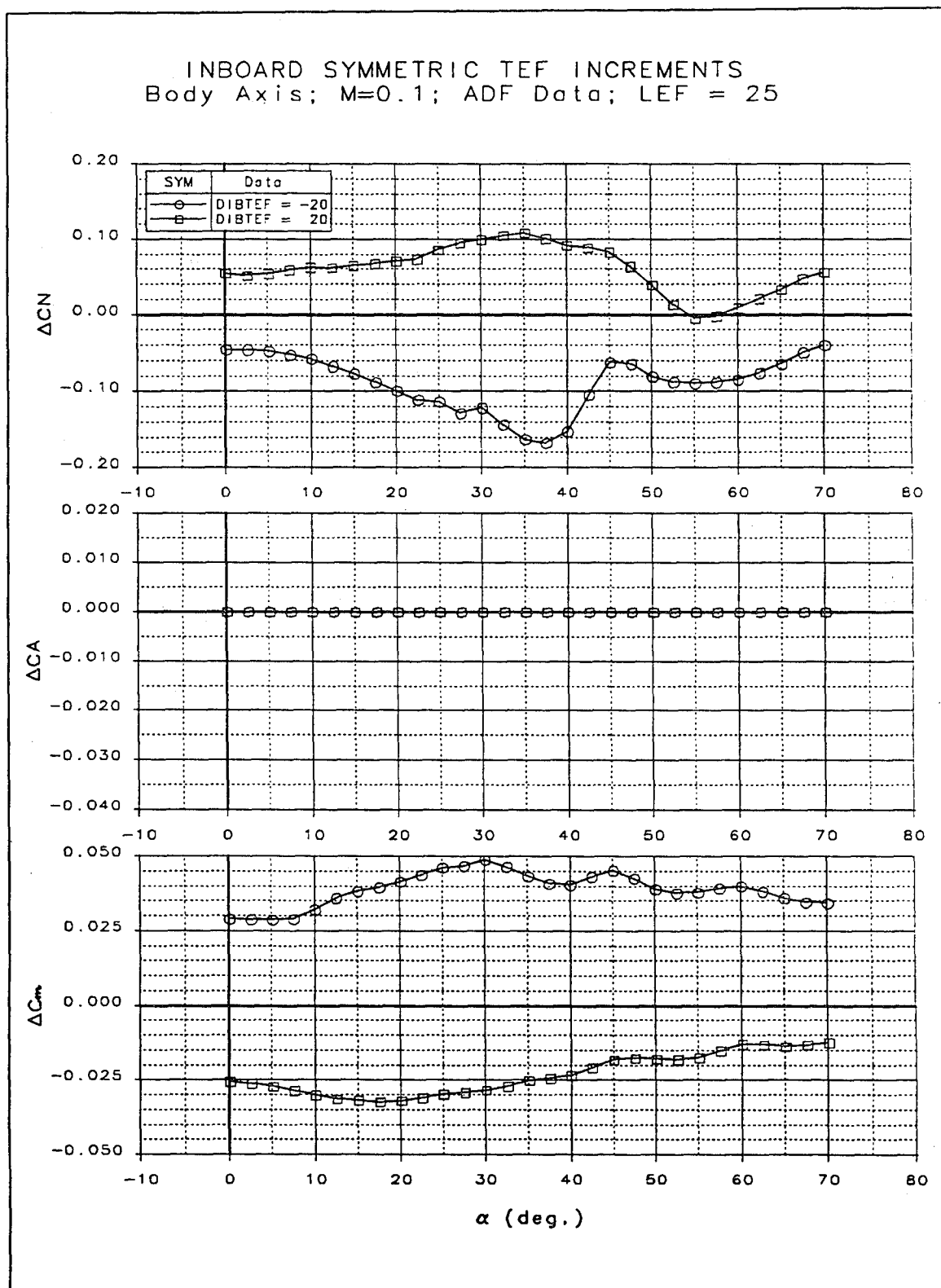


Figure 13-23 Pitch Flap Control Effectiveness

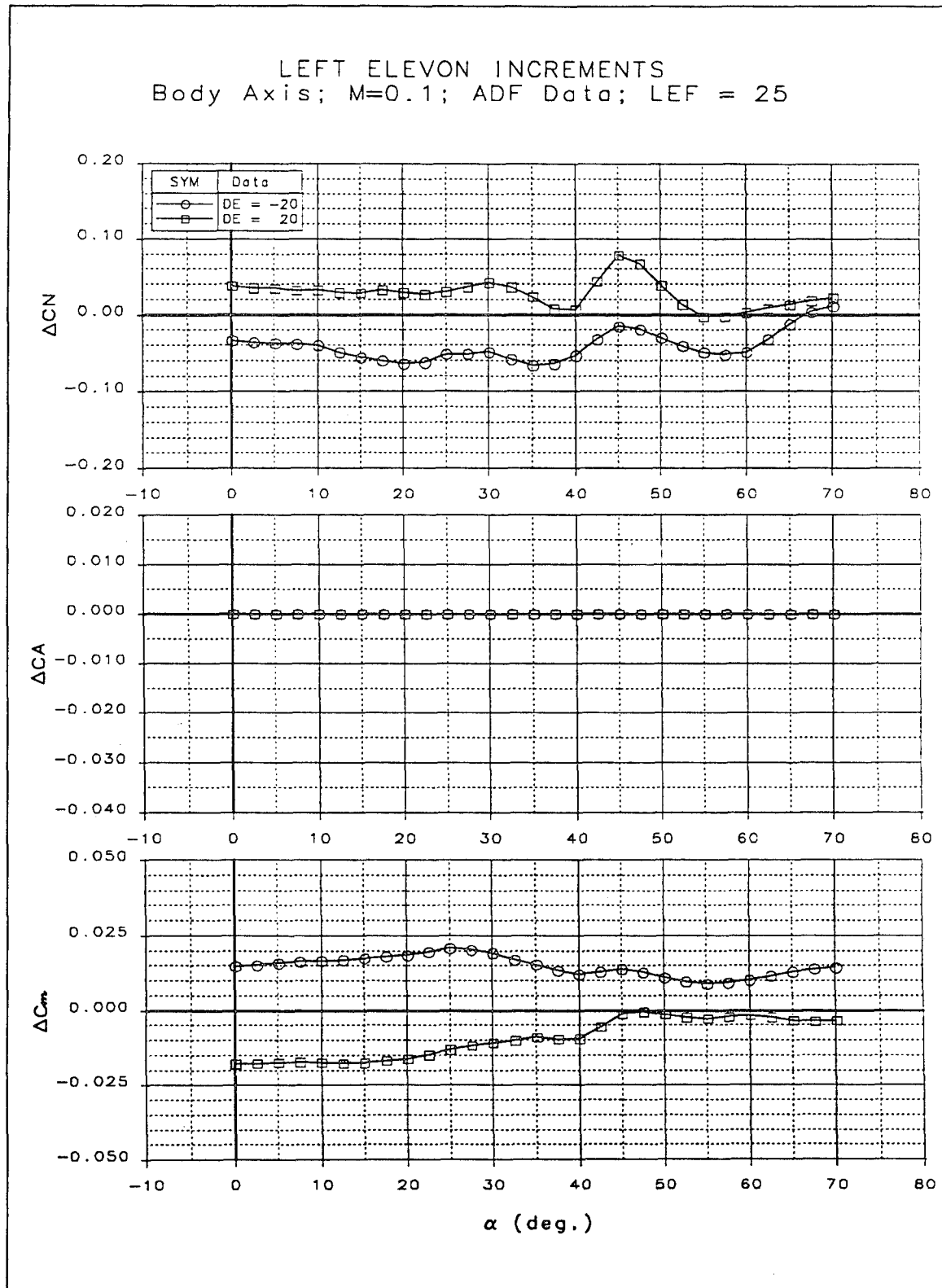


Figure 13-24 Left Elevon Control Effectiveness

LEFT ELEVON INCREMENTS
Body Axis; $M=0.1$; ADF Data; $LEF = 25$

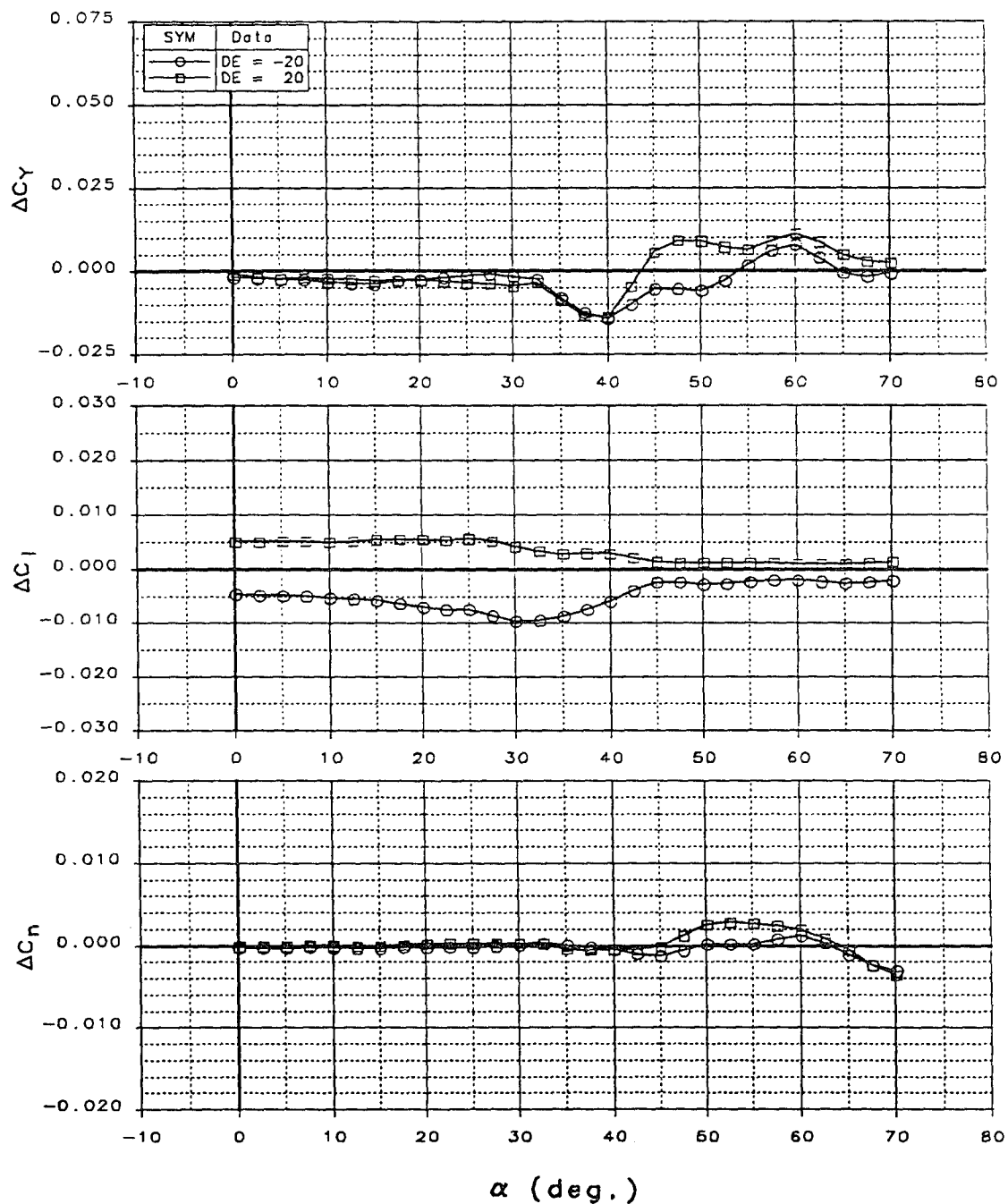


Figure 13-24 Left Elevon Control Effectiveness (Concluded)

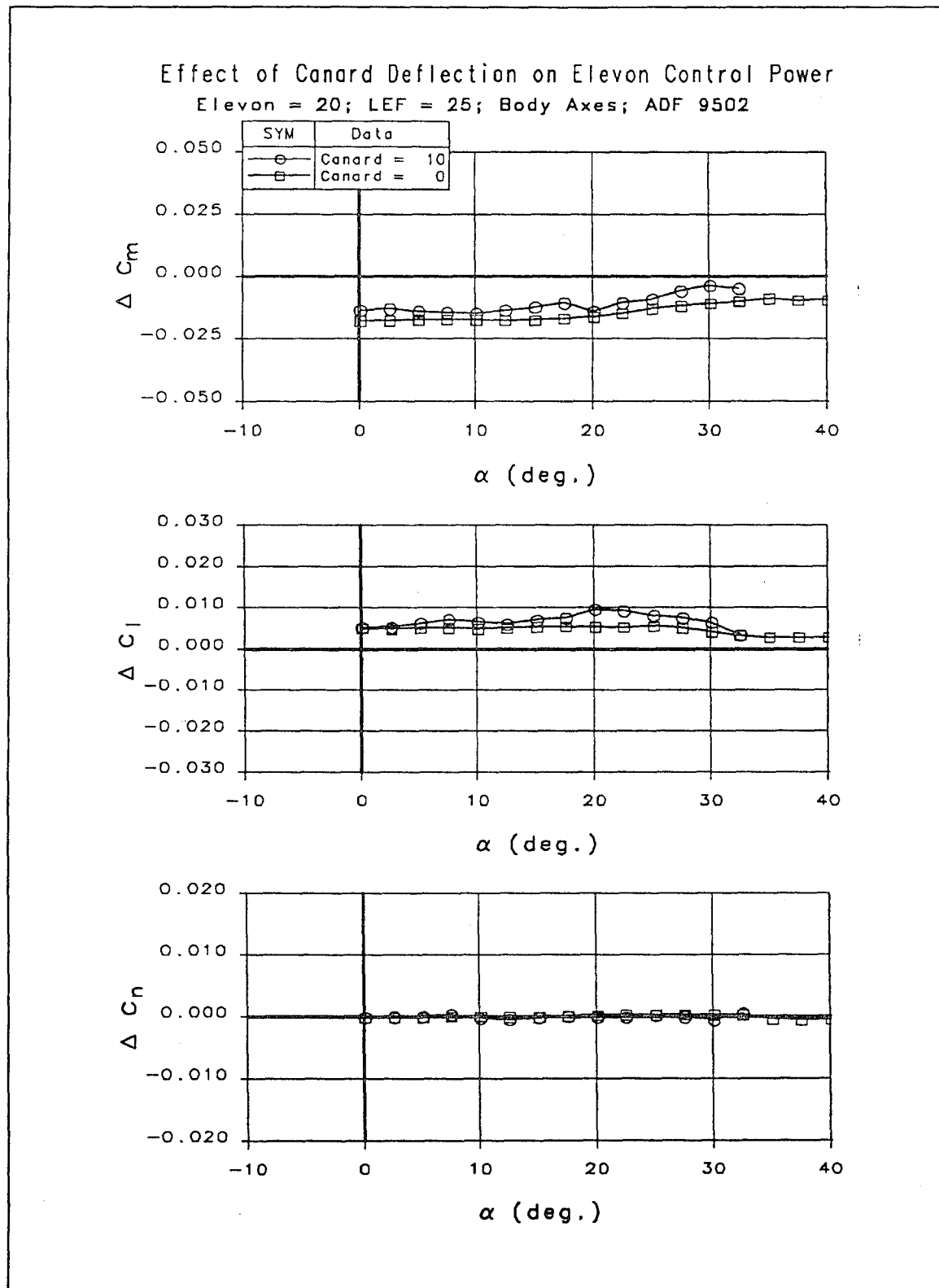


Figure 13-25 Effect of a 10 deg Canard Deflection of Elevon Control Effectiveness

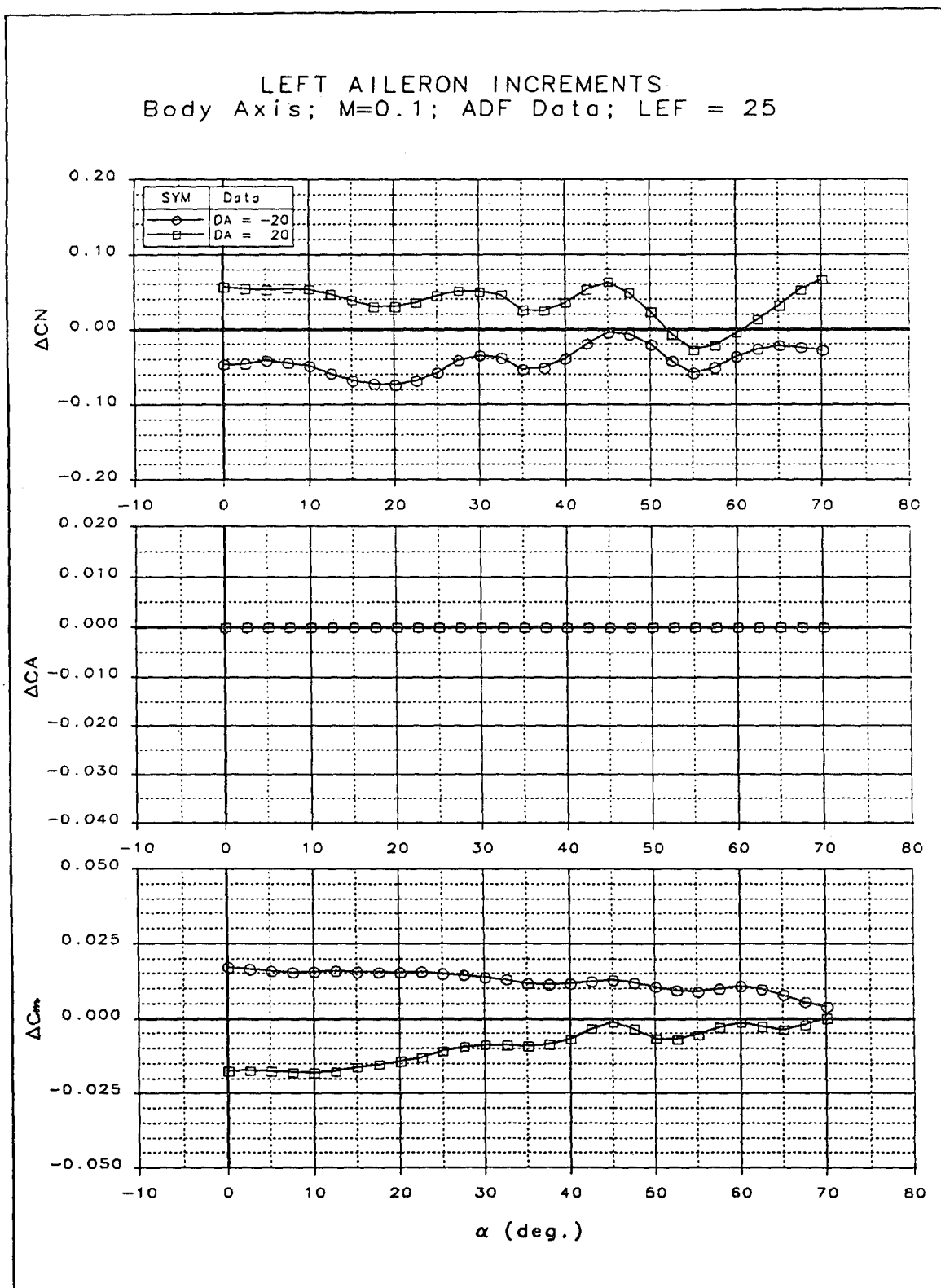


Figure 13-26 Left Aileron Control Effectiveness

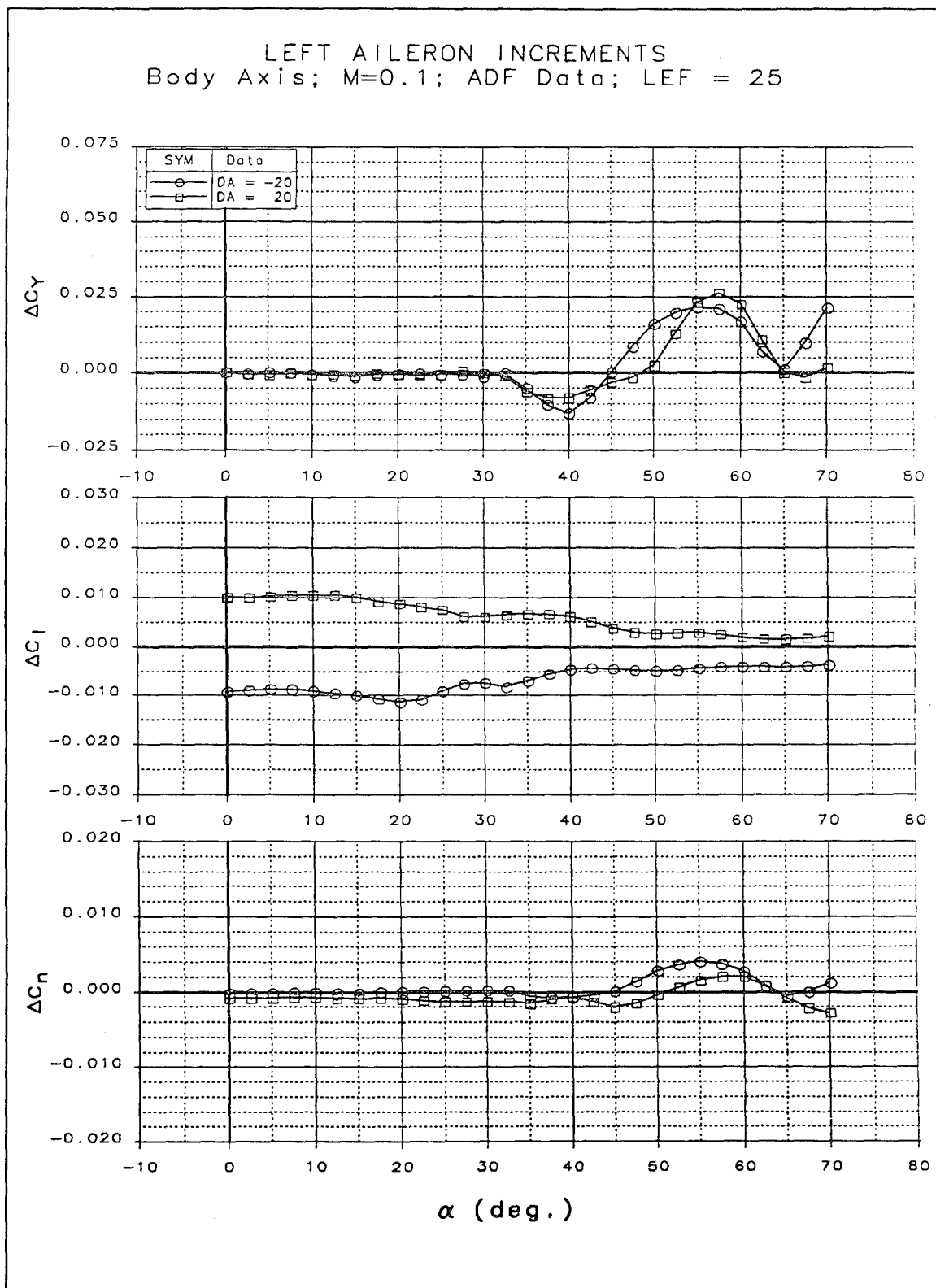


Figure 13-26 Left Aileron Control Effectiveness (Concluded)

Effect of Spoiler Deflection on Aileron Control Power
 LEF = 25; Body Axes; ADF 9502

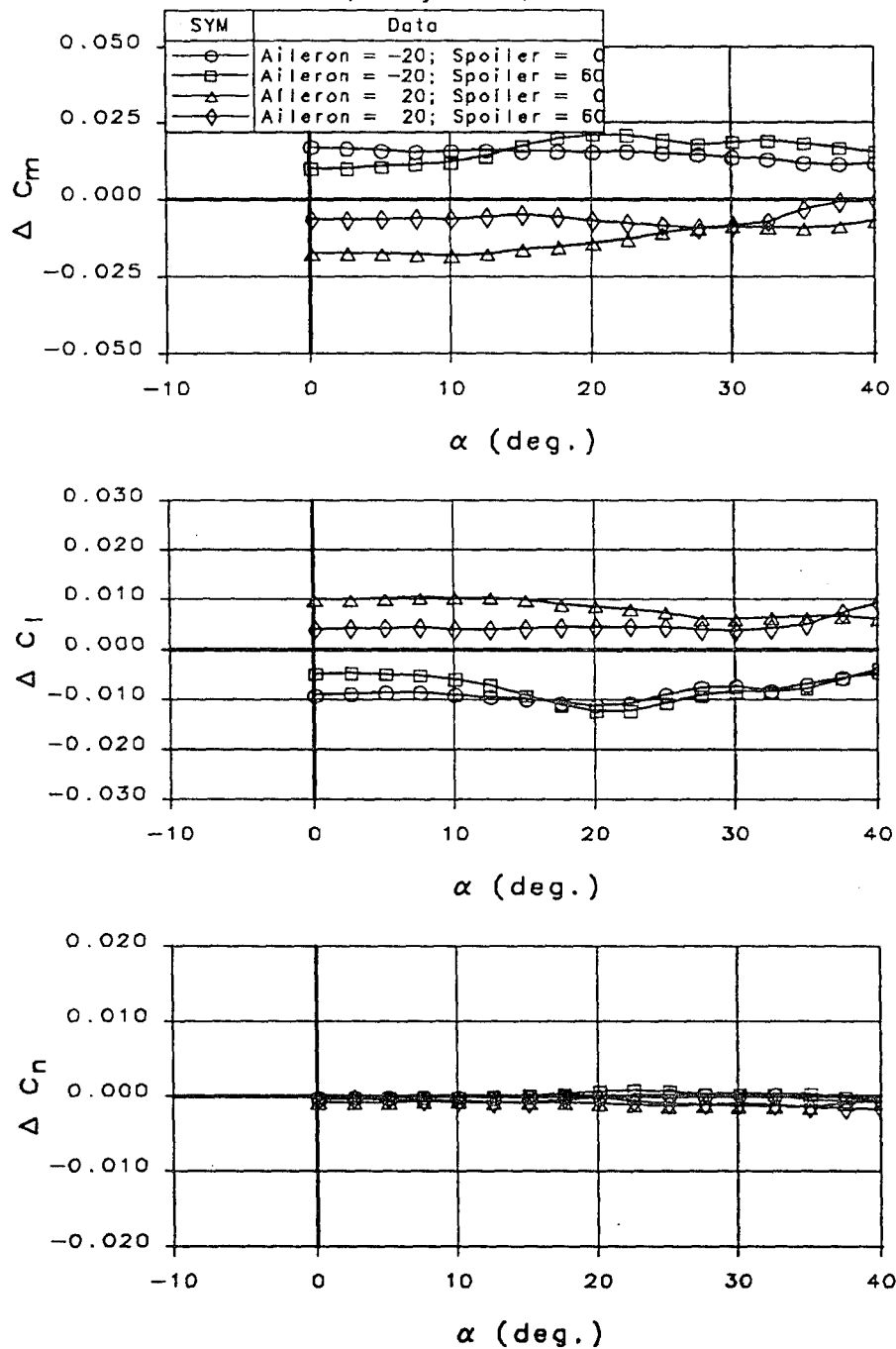


Figure 13-27 Effect of Spoiler on Aileron Control Power

Effect of Canard Deflection on Aileron Control Power

Aileron = 20; LEF = 25; Body Axes; ADF 9502

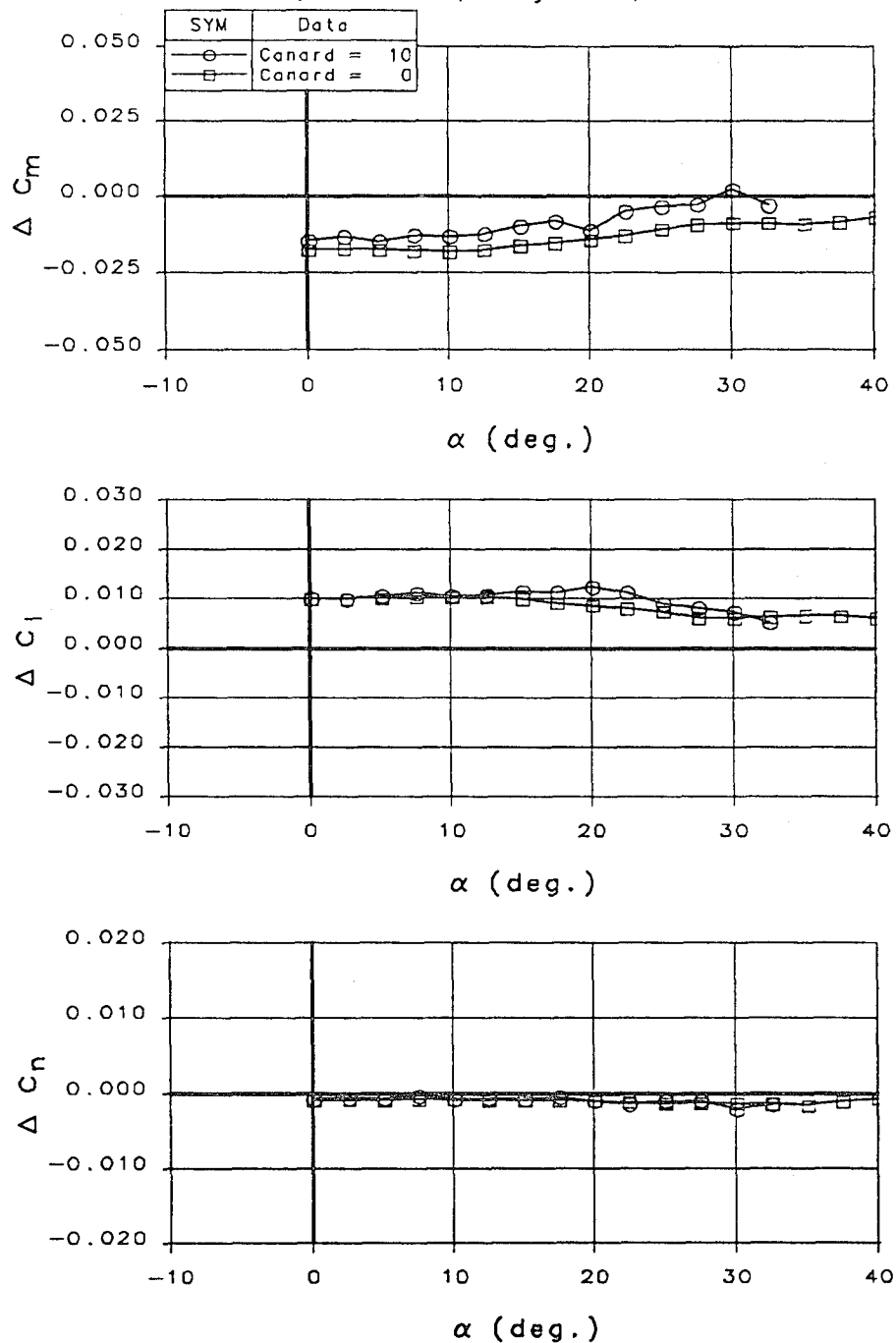


Figure 13-28 Effect of Canard Deflection on Aileron Control Power

AMT interaction with the adjacent aileron is shown in Figure 13-29. TEU AMT deflections had little impact on aileron effectiveness. TED tip deflections degraded aileron pitch effectiveness. TEU aileron roll power was degraded by a TED AMT deflection at nearly all AOA.

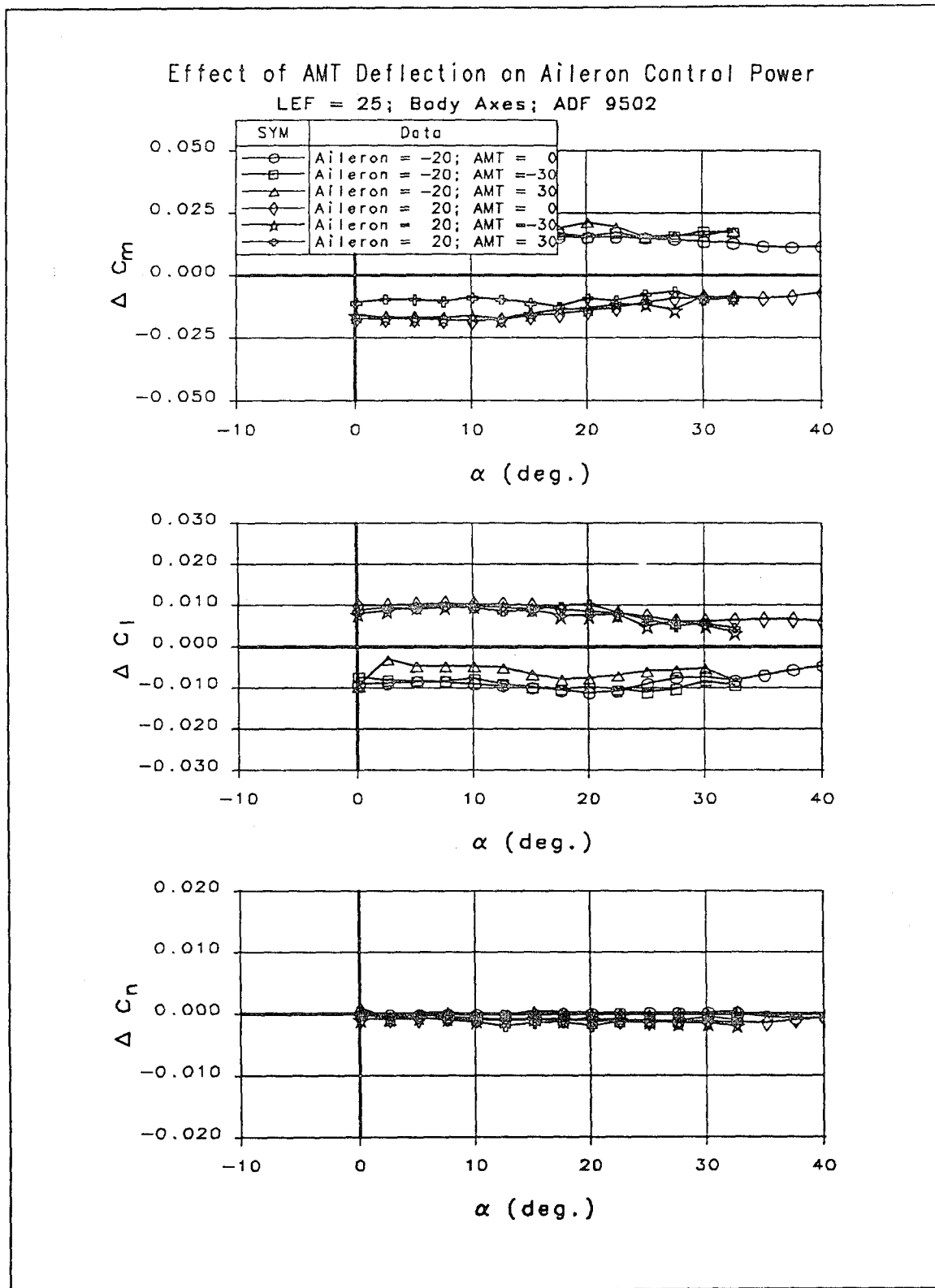


Figure 13-29 AMT Interaction with Aileron Effectiveness

13.5.4 All-Moving Tips

All moving tip control effectiveness data are shown in Figure 13-30. A complete analysis of this and other AMT control data are presented in the main body of this report.

13.5.5 Spoilers

Spoiler control effectiveness data are shown for various canard positions in Figure 13-31. Canard deflections have a small influence on spoiler effectiveness, with negative deflections generally having a favorable interaction in roll at moderate AOA.

Effect of spoiler hingeline sweep is shown in Figure 13-32. Forward swept hingelines provide good high AOA roll control at the expense of poor yaw characteristics. The aft-swept hingeline resulted in good high AOA yaw characteristics with reduced roll control power.

Additionally, the aft-swept spoiler resulted in nose-down pitch at moderate AOA -- a favorable characteristic.

Figure 13-33 shows the effect on spoiler control power due to the addition of the small canard. Small degradations in roll and yaw power were apparent. Pitch due to spoiler deflection was more nose-up with the canard off.

LEFT ALL MOVING TIP INCREMENTS
Body Axis; $M=0.1$; ADF Data; LEF = 25

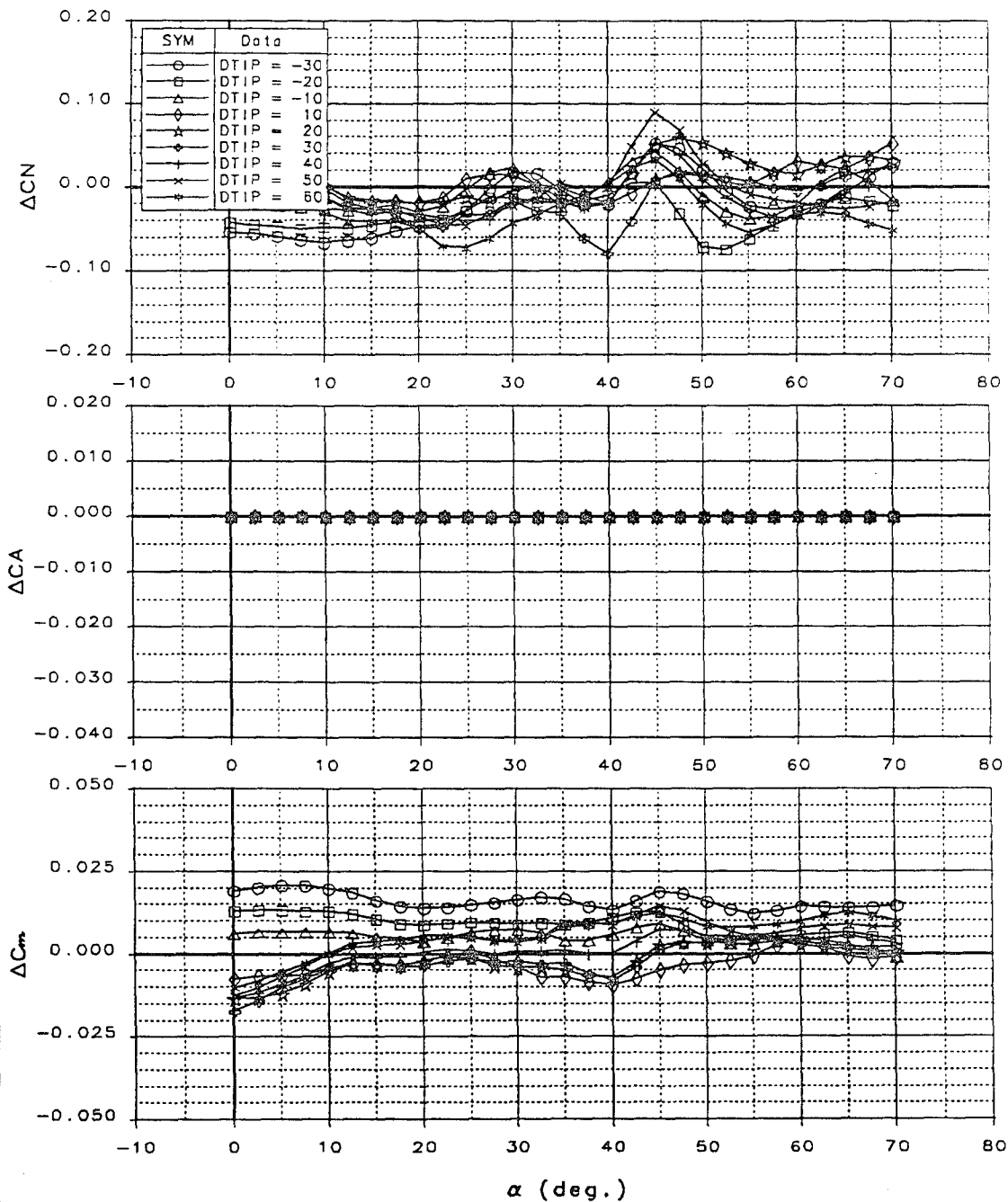


Figure 13-30 All-Moving Wing Tip Control Effectiveness

LEFT ALL MOVING TIP INCREMENTS
Body Axis; $M=0.1$; ADF Data; LEF = 25

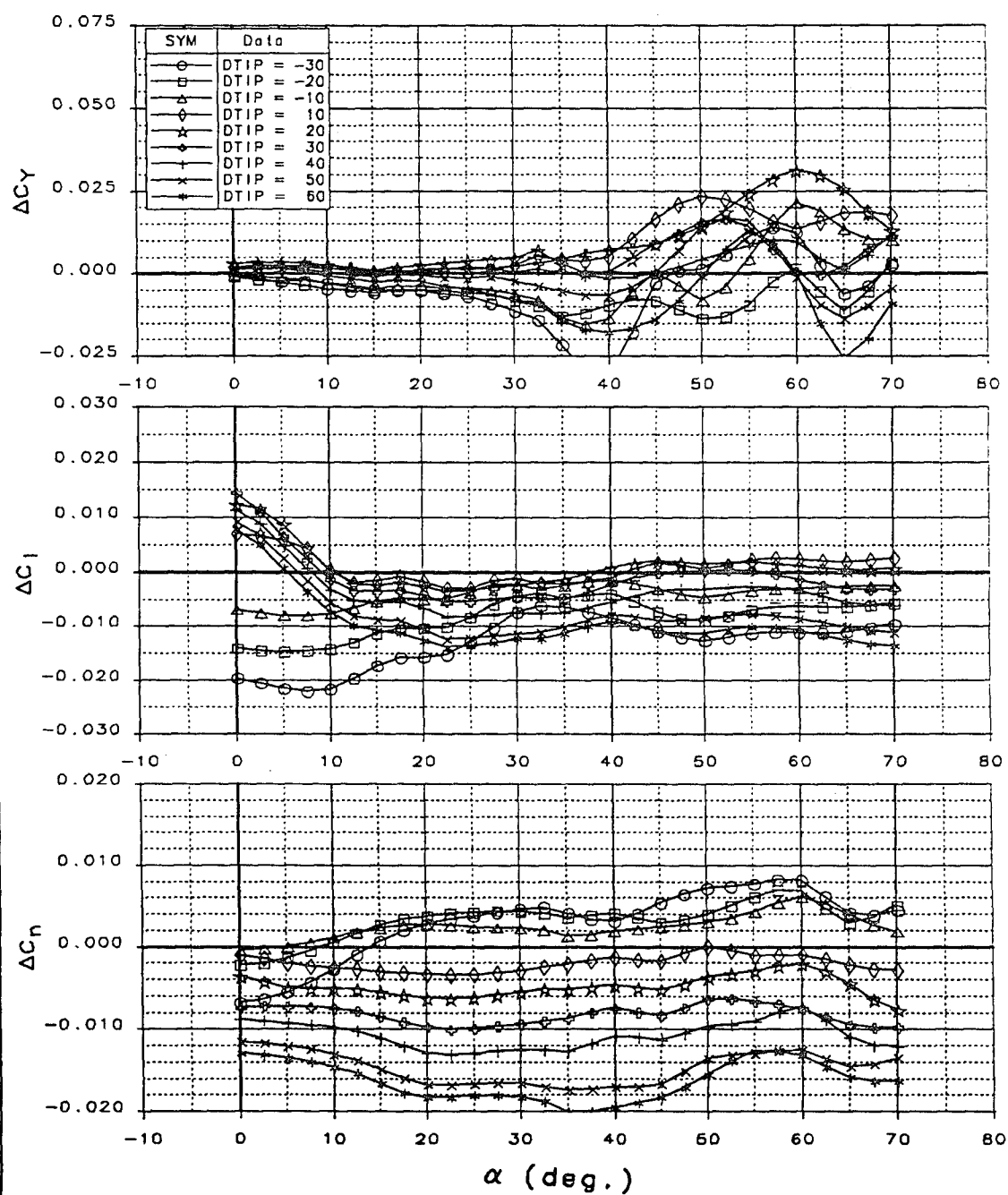


Figure 13-30 All Moving Wing Tip Control Effectiveness (Concluded)

LEFT SPOILER INCREMENTS
Body Axis; $M=0.1$; ADF Data; LEF = 25

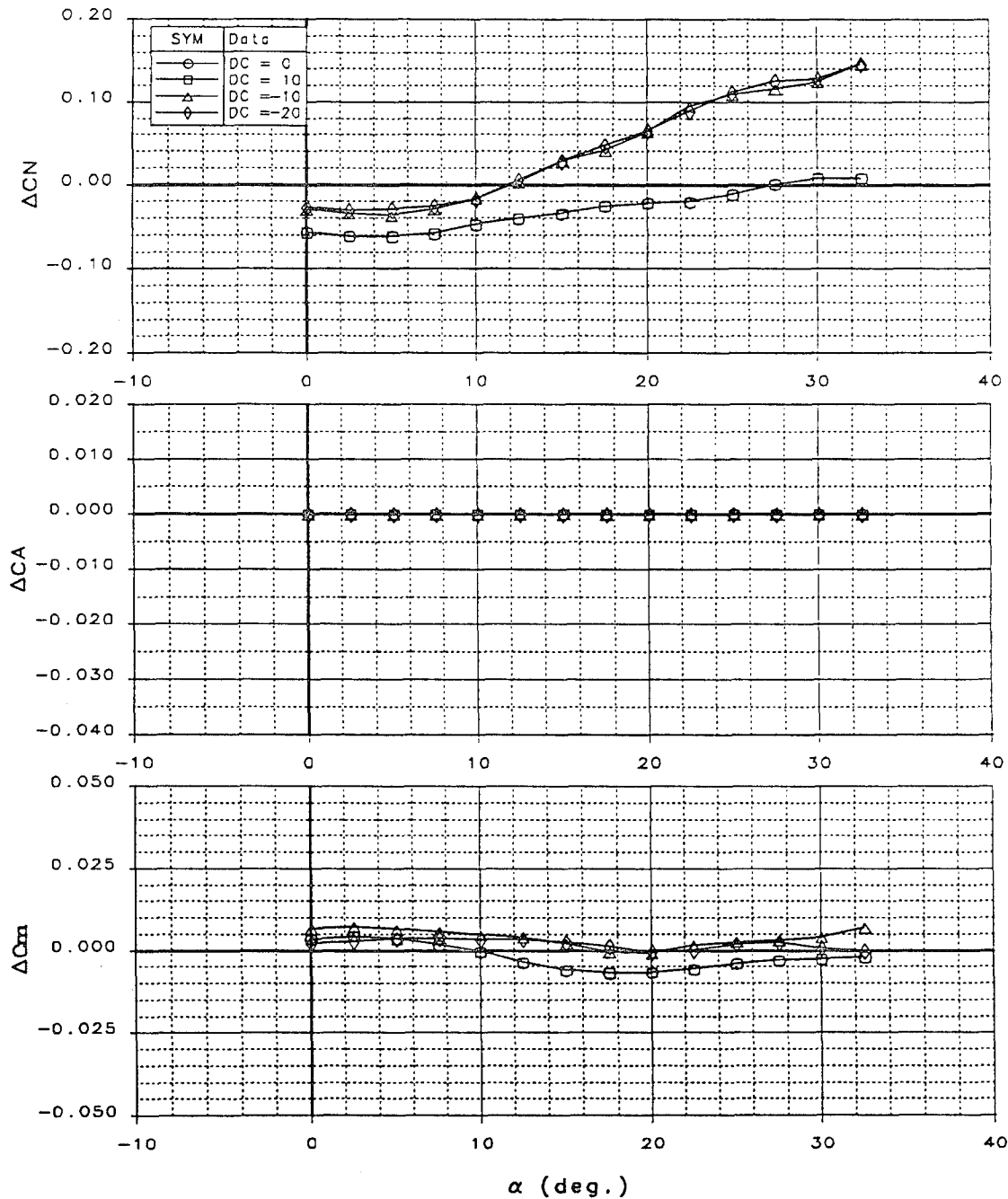


Figure 13-31 Effect of Canard Deflection on Spoiler Control Effectiveness

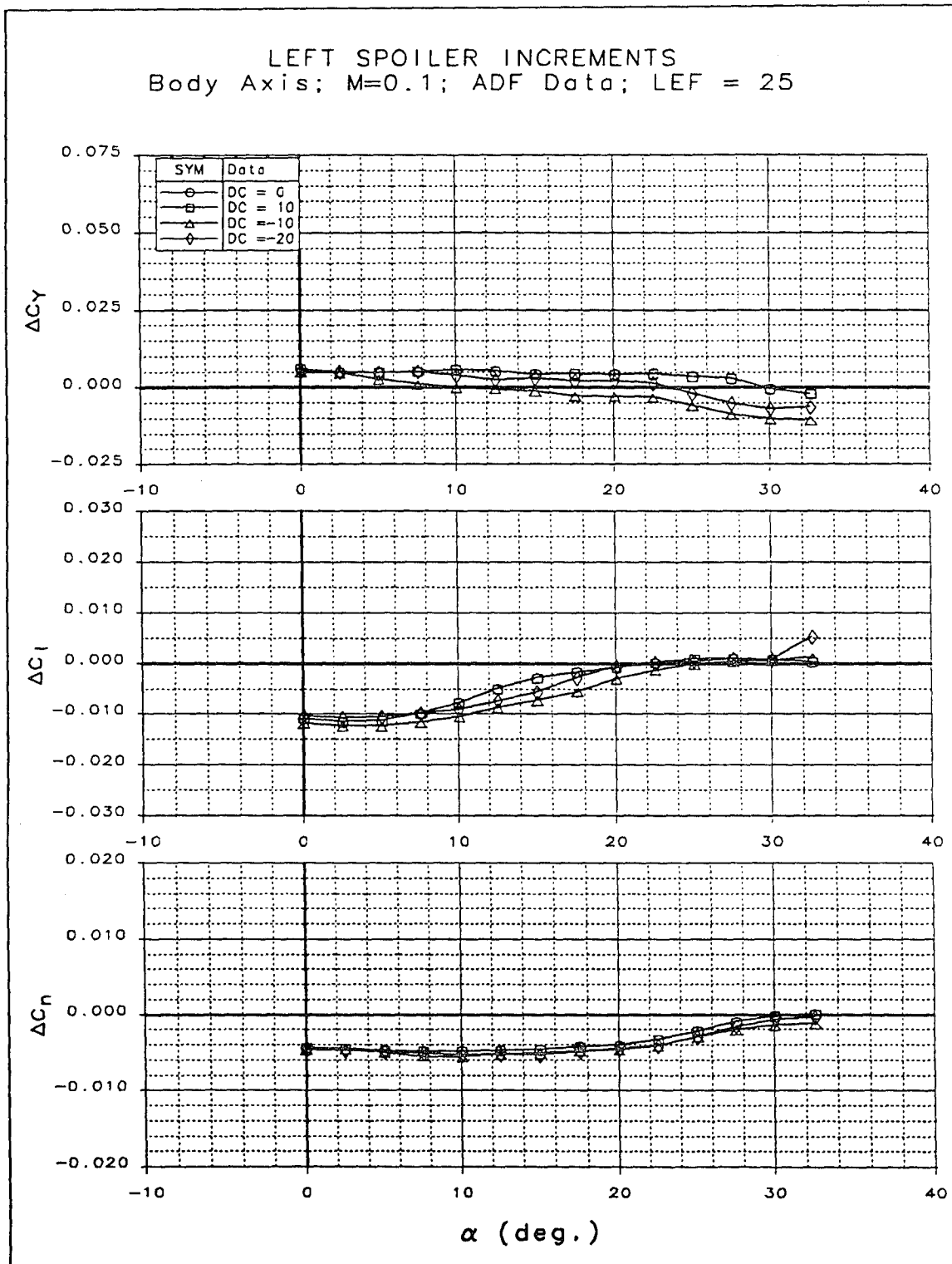


Figure 13-31 Effect of Canard Deflection on Spoiler (Concluded)

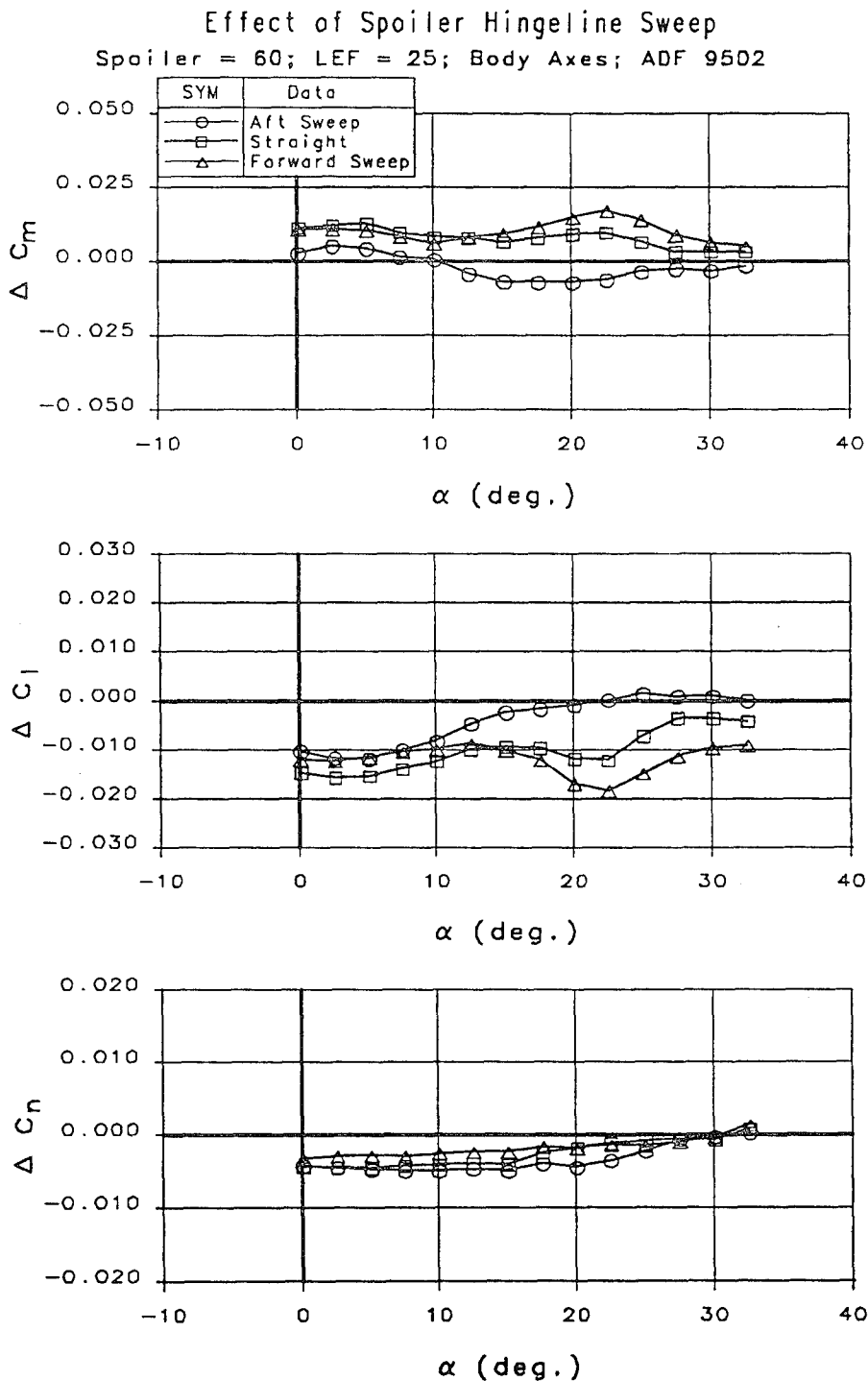


Figure 13-32 Effect of Spoiler Hingeline Sweep on Control Power

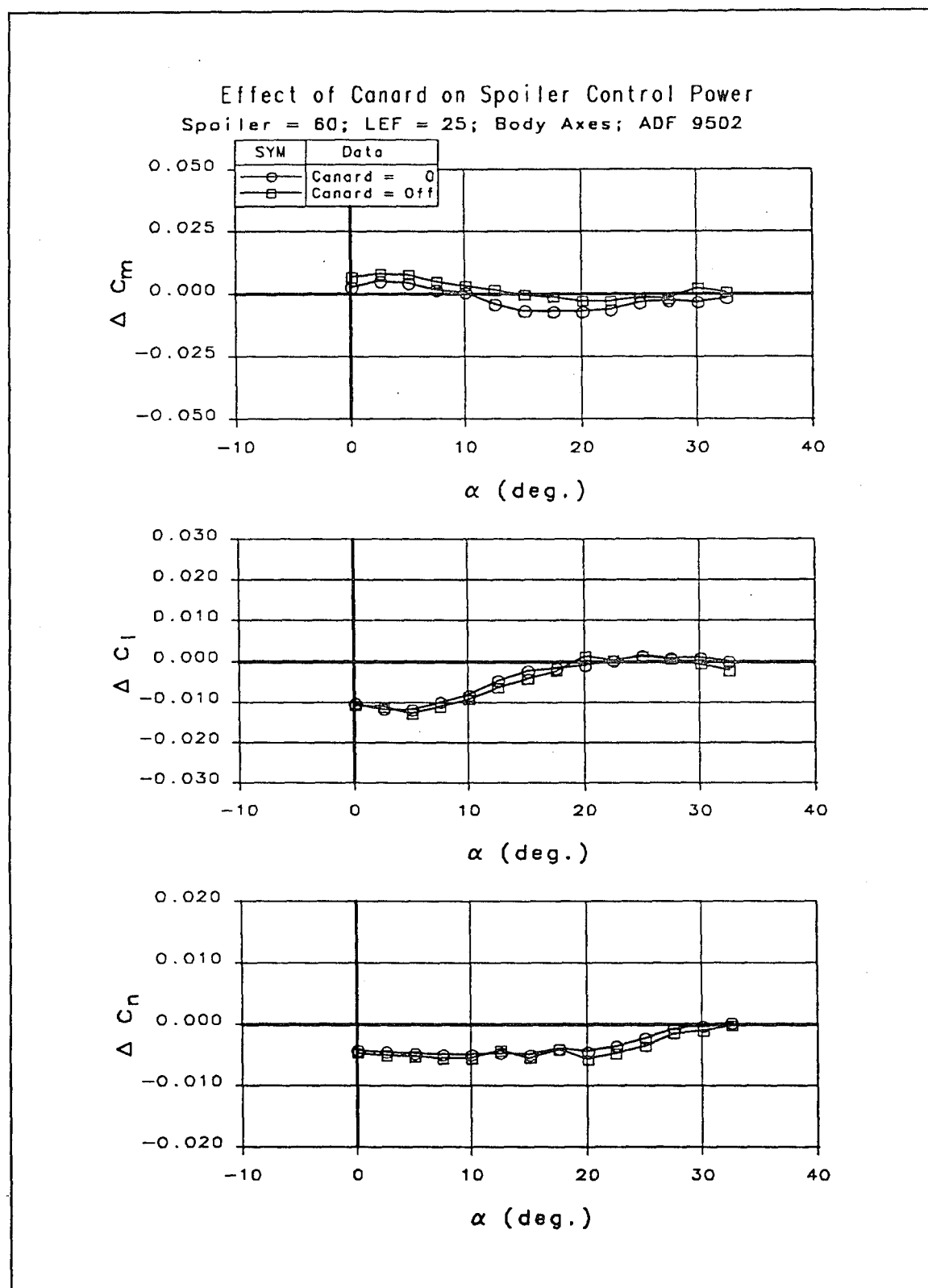


Figure 13-33 Effect of the Small Canard on Spoiler Control Power

13.6 References

- C1. Adler, C.O., Dixon, C.J., "High Angle-of-Attack Stability and Control -- Prediction Methods and Code", WL-TR-92-3050, October 1992.
- C2 Albright, A.E., Dixon, C.J., Hegedus, M.C., "Modification of Conceptual Design Aerodynamic Prediction Method HASC95 with VTXCHN", Draft Report to NASA Langley Research Center, November 1995.
- C3. Behrbohm, H., "Basic Low-Speed Aerodynamics of the Short-Coupled Canard Configuration of Small Aspect Ratio", SAAB Technical Note SAAB TN60, July 1965.

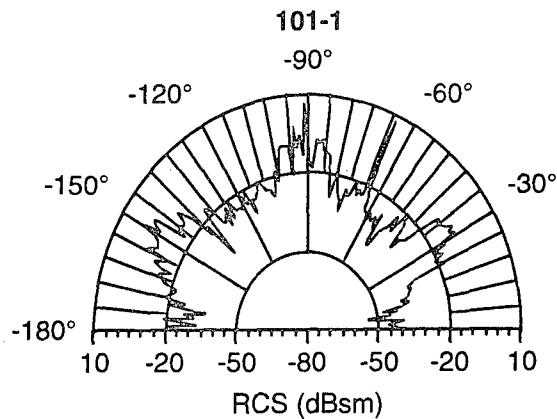
14 Appendix D: RCS Data

RCS polar plots are provided for each case analyzed during the ICE study. Data are provided for each configuration at 5.4 GHz, 9.7 GHz, and 16 GHz at -10 deg, 0 deg and 10 deg elevation angles. Both gaps analysis (MESSAGE) and deflected surface analysis (VISAGE) results are shown. Beneath each plot, the frontal, beam and aft sector and PCUM50 averages are tabulated.

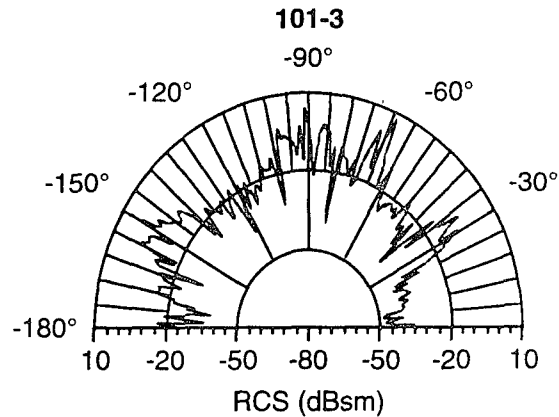
Sector average plots for the beam and aft sector are included at the end of this section. The frontal sector average data are shown in the main body of this report (see Section 7).

Gap Data

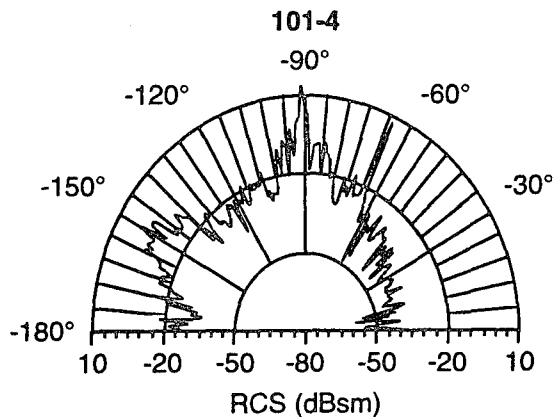
• 5.4 GHz • 0° Elevation • V/V Pol



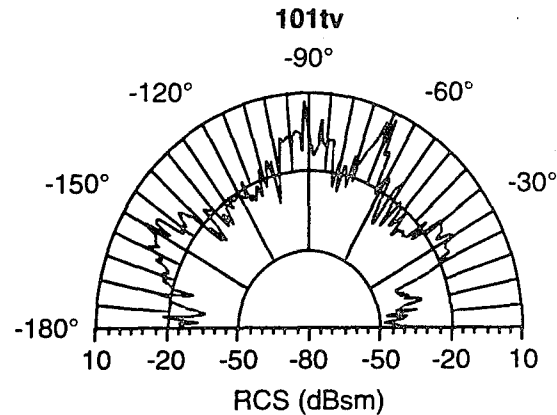
0° to -60° Sector Avg. (dBsm): -29.5
 0° to -60° PCUM50 (dBsm): -30.6
 -60° to -120° Sector Avg. (dBsm): -19.3
 -60° to -120° PCUM50 (dBsm): -21.8
 -120° to -180° Sector Avg. (dBsm): -19.3
 -120° to -180° PCUM50 (dBsm): -19.7



0° to -60° Sector Avg. (dBsm): -29.0
 0° to -60° PCUM50 (dBsm): -28.7
 -60° to -120° Sector Avg. (dBsm): -14.0
 -60° to -120° PCUM50 (dBsm): -13.8
 -120° to -180° Sector Avg. (dBsm): -18.5
 -120° to -180° PCUM50 (dBsm): -18.7



0° to -60° Sector Avg. (dBsm): -40.0
 0° to -60° PCUM50 (dBsm): -39.8
 -60° to -120° Sector Avg. (dBsm): -18.2
 -60° to -120° PCUM50 (dBsm): -21.5
 -120° to -180° Sector Avg. (dBsm): -19.8
 -120° to -180° PCUM50 (dBsm): -21.0

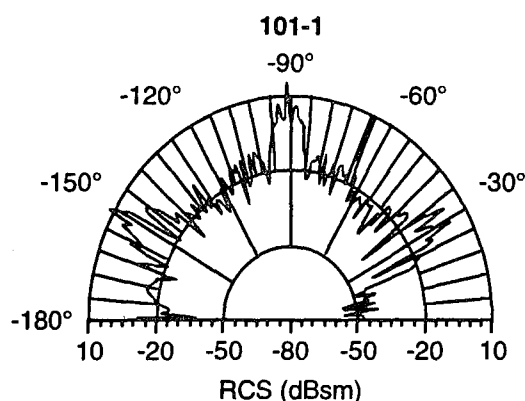


0° to -60° Sector Avg. (dBsm): -27.4
 0° to -60° PCUM50 (dBsm): -26.9
 -60° to -120° Sector Avg. (dBsm): -13.7
 -60° to -120° PCUM50 (dBsm): -14.0
 -120° to -180° Sector Avg. (dBsm): -18.8
 -120° to -180° PCUM50 (dBsm): -19.0

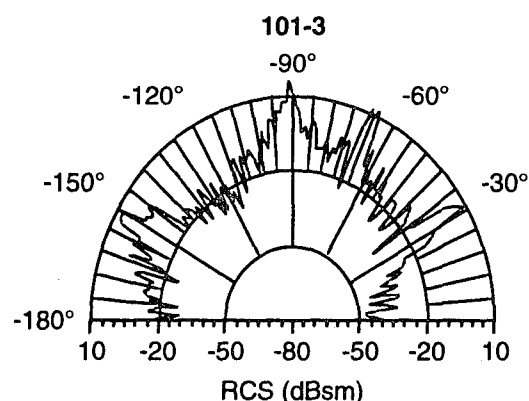
Figure 14-1: RCS Gap Data; 5.4 GHz; 0 deg Elevation

Gap Data

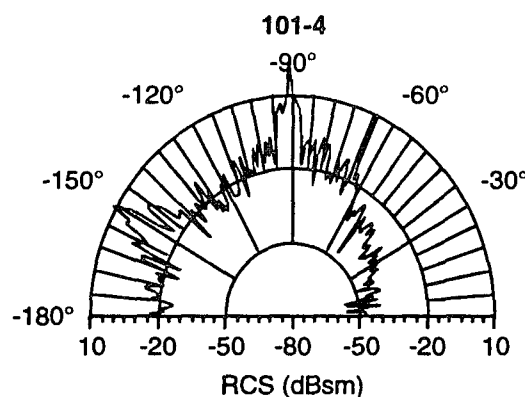
• 9.7 GHz • 0° Elevation • V/V Pol



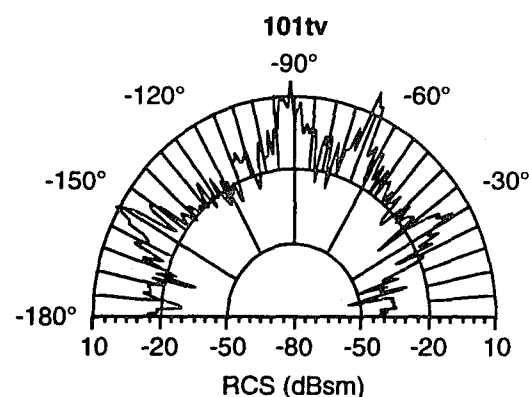
0° to -60° Sector Avg. (dBsm): -28.5
 0° to -60° PCUM50 (dBsm): -24.4
 -60° to -120° Sector Avg. (dBsm): -14.1
 -60° to -120° PCUM50 (dBsm): -15.4
 -120° to -180° Sector Avg. (dBsm): -15.6
 -120° to -180° PCUM50 (dBsm): -17.2



0° to -60° Sector Avg. (dBsm): -23.7
 0° to -60° PCUM50 (dBsm): -24.8
 -60° to -120° Sector Avg. (dBsm): -7.1
 -60° to -120° PCUM50 (dBsm): -8.4
 -120° to -180° Sector Avg. (dBsm): -14.1
 -120° to -180° PCUM50 (dBsm): -15.7



0° to -60° Sector Avg. (dBsm): -39.3
 0° to -60° PCUM50 (dBsm): -40.0
 -60° to -120° Sector Avg. (dBsm): -12.6
 -60° to -120° PCUM50 (dBsm): -14.4
 -120° to -180° Sector Avg. (dBsm): -15.6
 -120° to -180° PCUM50 (dBsm): -17.2

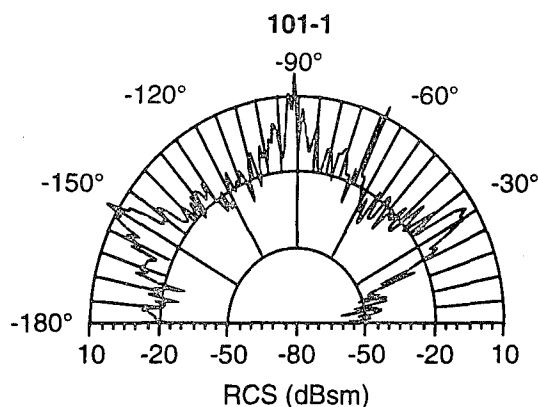


0° to -60° Sector Avg. (dBsm): -23.1
 0° to -60° PCUM50 (dBsm): -19.5
 -60° to -120° Sector Avg. (dBsm): -8.0
 -60° to -120° PCUM50 (dBsm): -8.7
 -120° to -180° Sector Avg. (dBsm): -14.6
 -120° to -180° PCUM50 (dBsm): -15.9

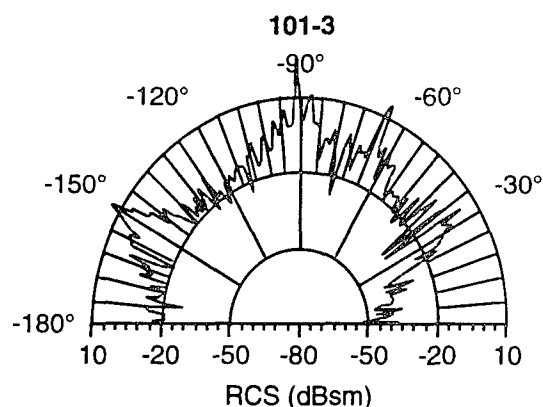
Figure 14-2: RCS Gap Data; 9.7 GHz; 0 deg Elevation

Gap Data

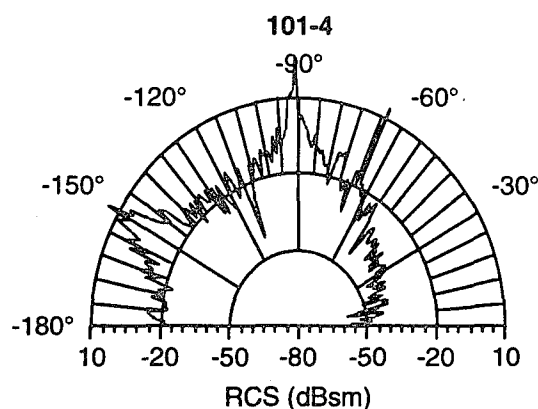
• 16.0 GHz • 0° Elevation • V/V Pol



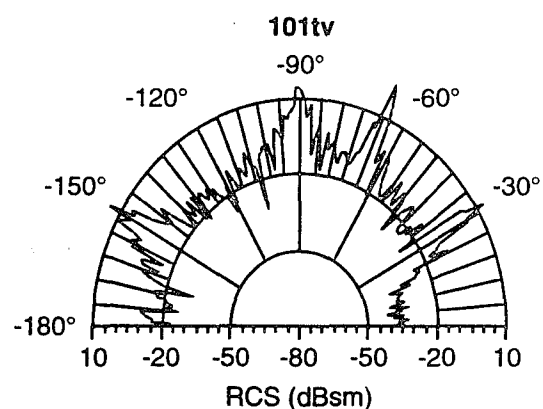
0° to -60° Sector Avg. (dBsm): -28.8
 0° to -60° PCUM50 (dBsm): -26.4
 -60° to -120° Sector Avg. (dBsm): -12.4
 -60° to -120° PCUM50 (dBsm): -13.1
 -120° to -180° Sector Avg. (dBsm): -13.1
 -120° to -180° PCUM50 (dBsm): -14.6



0° to -60° Sector Avg. (dBsm): -24.4
 0° to -60° PCUM50 (dBsm): -22.4
 -60° to -120° Sector Avg. (dBsm): -6.0
 -60° to -120° PCUM50 (dBsm): -6.5
 -120° to -180° Sector Avg. (dBsm): -12.1
 -120° to -180° PCUM50 (dBsm): -13.7



0° to -60° Sector Avg. (dBsm): -39.9
 0° to -60° PCUM50 (dBsm): -39.6
 -60° to -120° Sector Avg. (dBsm): -12.6
 -60° to -120° PCUM50 (dBsm): -12.3
 -120° to -180° Sector Avg. (dBsm): -13.4
 -120° to -180° PCUM50 (dBsm): -15.1

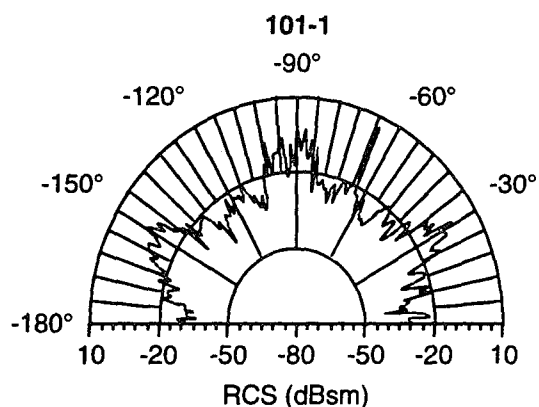


0° to -60° Sector Avg. (dBsm): -21.7
 0° to -60° PCUM50 (dBsm): -22.2
 -60° to -120° Sector Avg. (dBsm): -6.7
 -60° to -120° PCUM50 (dBsm): -8.1
 -120° to -180° Sector Avg. (dBsm): -12.7
 -120° to -180° PCUM50 (dBsm): -15.3

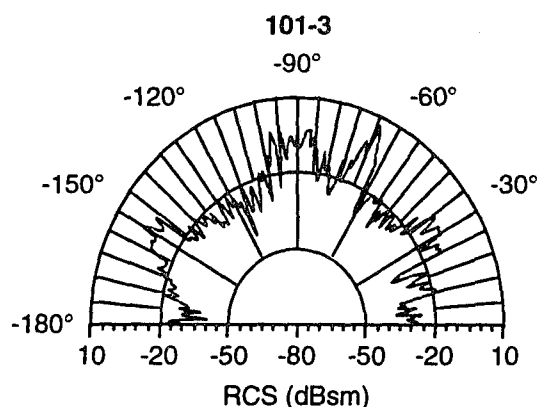
Figure 14-3: RCS Gap Data; 16 GHz; 0 deg Elevation

Gap Data

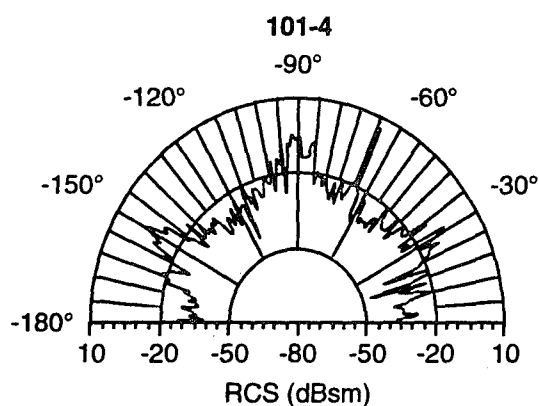
• 5.4 GHz • 10° Elevation • V/V Pol



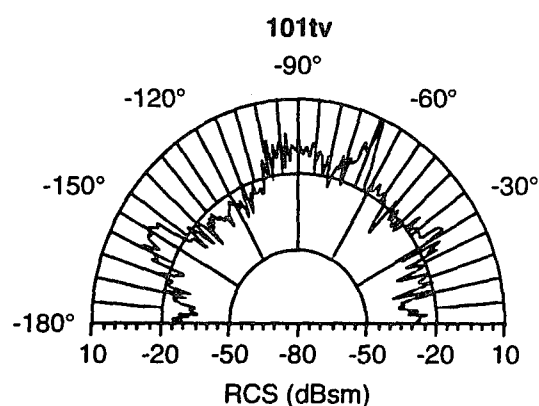
0° to -60° Sector Avg. (dBsm): -22.8
 0° to -60° PCUM50 (dBsm): -23.1
 -60° to -120° Sector Avg. (dBsm): -20.1
 -60° to -120° PCUM50 (dBsm): -22.5
 -120° to -180° Sector Avg. (dBsm): -22.2
 -120° to -180° PCUM50 (dBsm): -22.9



0° to -60° Sector Avg. (dBsm): -22.0
 0° to -60° PCUM50 (dBsm): -21.5
 -60° to -120° Sector Avg. (dBsm): -16.5
 -60° to -120° PCUM50 (dBsm): -16.8
 -120° to -180° Sector Avg. (dBsm): -22.2
 -120° to -180° PCUM50 (dBsm): -22.6



0° to -60° Sector Avg. (dBsm): -26.1
 0° to -60° PCUM50 (dBsm): -27.1
 -60° to -120° Sector Avg. (dBsm): -20.8
 -60° to -120° PCUM50 (dBsm): -22.5
 -120° to -180° Sector Avg. (dBsm): -25.5
 -120° to -180° PCUM50 (dBsm): -27.5

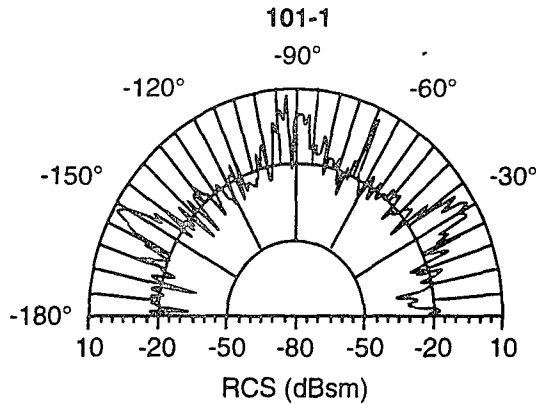


0° to -60° Sector Avg. (dBsm): -21.5
 0° to -60° PCUM50 (dBsm): -20.2
 -60° to -120° Sector Avg. (dBsm): -15.3
 -60° to -120° PCUM50 (dBsm): -13.8
 -120° to -180° Sector Avg. (dBsm): -22.4
 -120° to -180° PCUM50 (dBsm): -24.4

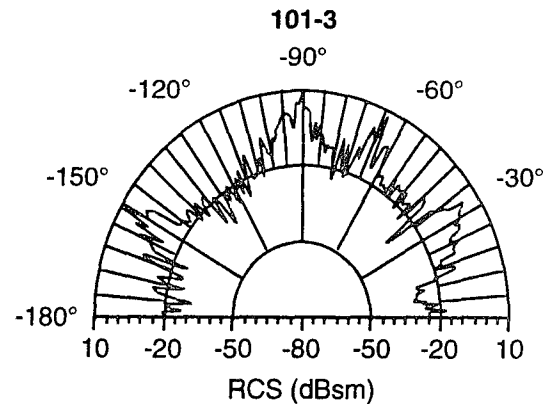
Figure 14-4: RCS Gap Data; 5.4 GHz; 10 deg Elevation

Gap Data

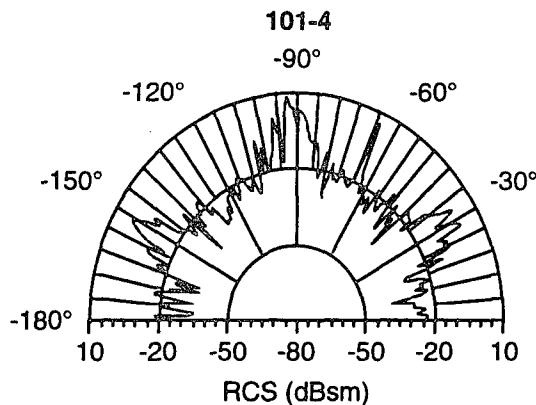
• 9.7 GHz • 10° Elevation • V/V Pol



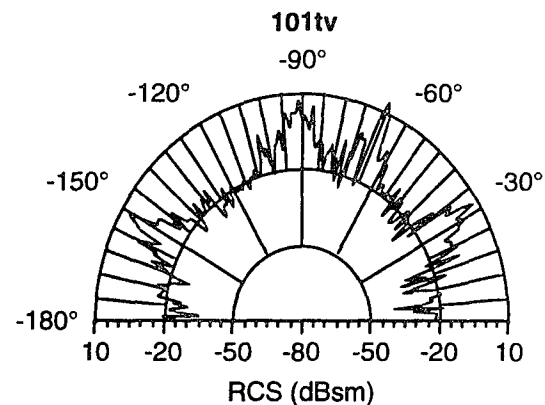
0° to -60° Sector Avg. (dBsm): -16.8
 0° to -60° PCUM50 (dBsm): -18.1
 -60° to -120° Sector Avg. (dBsm): -15.3
 -60° to -120° PCUM50 (dBsm): -16.2
 -120° to -180° Sector Avg. (dBsm): -17.4
 -120° to -180° PCUM50 (dBsm): -18.6



0° to -60° Sector Avg. (dBsm): -15.7
 0° to -60° PCUM50 (dBsm): -15.6
 -60° to -120° Sector Avg. (dBsm): -10.7
 -60° to -120° PCUM50 (dBsm): -11.5
 -120° to -180° Sector Avg. (dBsm): -17.4
 -120° to -180° PCUM50 (dBsm): -18.7



0° to -60° Sector Avg. (dBsm): -19.5
 0° to -60° PCUM50 (dBsm): -21.7
 -60° to -120° Sector Avg. (dBsm): -15.3
 -60° to -120° PCUM50 (dBsm): -19.2
 -120° to -180° Sector Avg. (dBsm): -20.7
 -120° to -180° PCUM50 (dBsm): -20.9

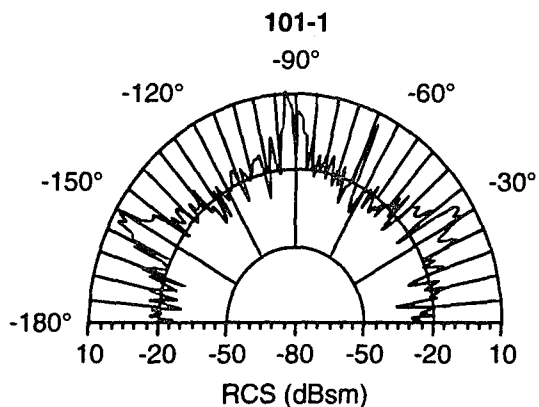


0° to -60° Sector Avg. (dBsm): -17.3
 0° to -60° PCUM50 (dBsm): -18.3
 -60° to -120° Sector Avg. (dBsm): -10.3
 -60° to -120° PCUM50 (dBsm): -10.6
 -120° to -180° Sector Avg. (dBsm): -17.2
 -120° to -180° PCUM50 (dBsm): -18.7

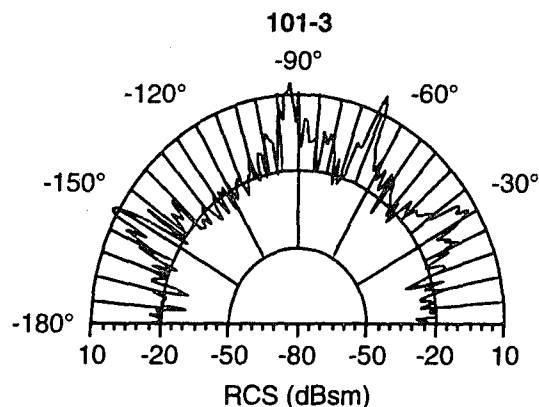
Figure 14-5: RCS Gap Data; 9.7 GHz; 10 deg Elevation

Gap Data

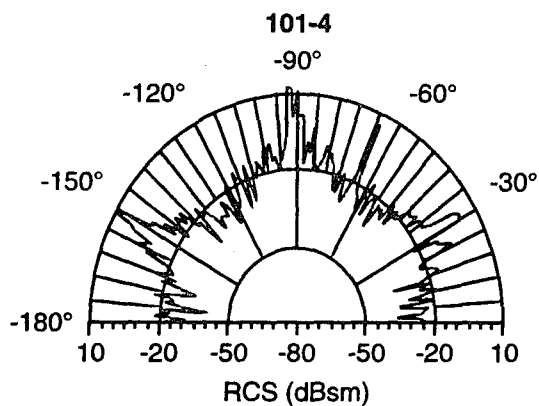
• 16.0 GHz • 10° Elevation • V/V Pol



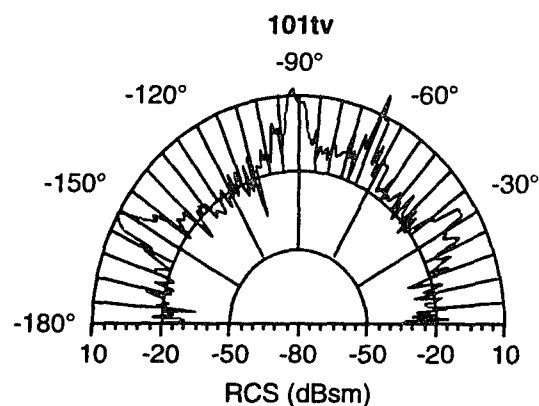
0° to -60° Sector Avg. (dBsm): -16.8
 0° to -60° PCUM50 (dBsm): -18.4
 -60° to -120° Sector Avg. (dBsm): -15.4
 -60° to -120° PCUM50 (dBsm): -16.9
 -120° to -180° Sector Avg. (dBsm): -16.3
 -120° to -180° PCUM50 (dBsm): -17.4



0° to -60° Sector Avg. (dBsm): -14.6
 0° to -60° PCUM50 (dBsm): -15.1
 -60° to -120° Sector Avg. (dBsm): -9.3
 -60° to -120° PCUM50 (dBsm): -9.1
 -120° to -180° Sector Avg. (dBsm): -16.2
 -120° to -180° PCUM50 (dBsm): -19.1



0° to -60° Sector Avg. (dBsm): -19.7
 0° to -60° PCUM50 (dBsm): -20.4
 -60° to -120° Sector Avg. (dBsm): -15.7
 -60° to -120° PCUM50 (dBsm): -17.3
 -120° to -180° Sector Avg. (dBsm): -20.1
 -120° to -180° PCUM50 (dBsm): -22.4

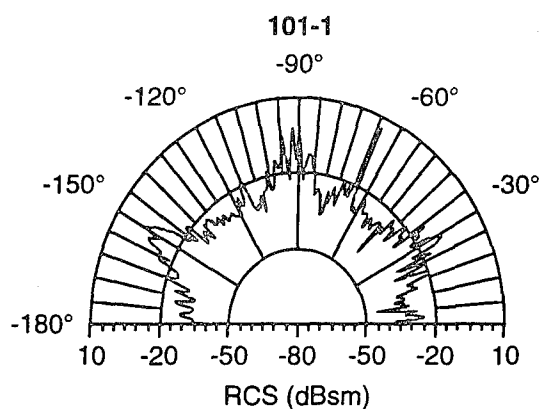


0° to -60° Sector Avg. (dBsm): -15.1
 0° to -60° PCUM50 (dBsm): -15.4
 -60° to -120° Sector Avg. (dBsm): -8.7
 -60° to -120° PCUM50 (dBsm): -10.1
 -120° to -180° Sector Avg. (dBsm): -16.5
 -120° to -180° PCUM50 (dBsm): -18.7

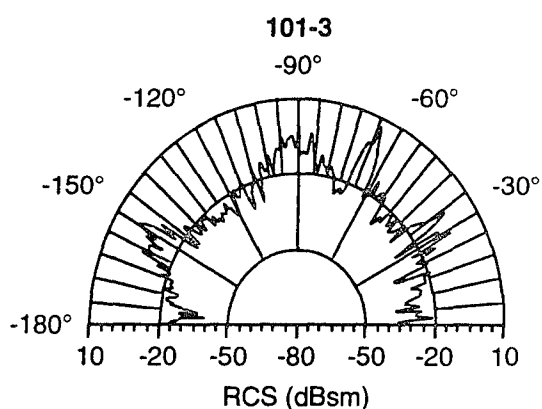
Figure 14-6: RCS Gap Data; 16 GHz; 10 deg Elevation

Gap Data

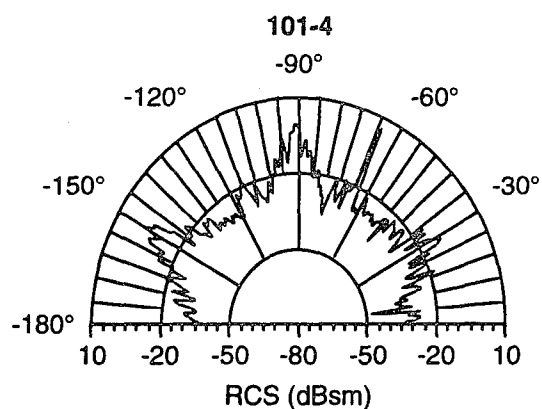
• 5.4 GHz • -10° Elevation • V/V Pol



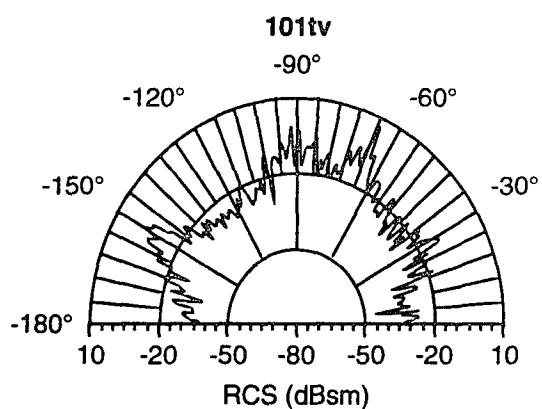
0° to -60° Sector Avg. (dBsm): -26.7
 0° to -60° PCUM50 (dBsm): -27.1
 -60° to -120° Sector Avg. (dBsm): -22.6
 -60° to -120° PCUM50 (dBsm): -24.3
 -120° to -180° Sector Avg. (dBsm): -24.6
 -120° to -180° PCUM50 (dBsm): -26.3



0° to -60° Sector Avg. (dBsm): -22.2
 0° to -60° PCUM50 (dBsm): -23.2
 -60° to -120° Sector Avg. (dBsm): -15.3
 -60° to -120° PCUM50 (dBsm): -15.8
 -120° to -180° Sector Avg. (dBsm): -21.6
 -120° to -180° PCUM50 (dBsm): -23.4



0° to -60° Sector Avg. (dBsm): -26.2
 0° to -60° PCUM50 (dBsm): -26.9
 -60° to -120° Sector Avg. (dBsm): -20.6
 -60° to -120° PCUM50 (dBsm): -21.5
 -120° to -180° Sector Avg. (dBsm): -24.3
 -120° to -180° PCUM50 (dBsm): -25.7

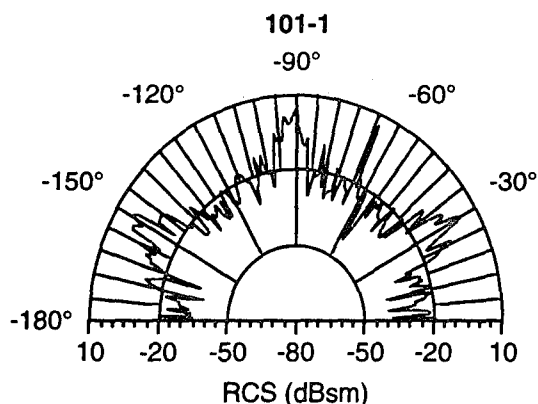


0° to -60° Sector Avg. (dBsm): -24.1
 0° to -60° PCUM50 (dBsm): -24.3
 -60° to -120° Sector Avg. (dBsm): -15.4
 -60° to -120° PCUM50 (dBsm): -15.7
 -120° to -180° Sector Avg. (dBsm): -24.0
 -120° to -180° PCUM50 (dBsm): -25.7

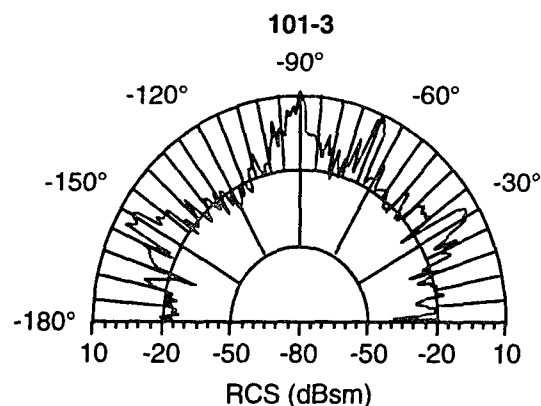
Figure 14-7: RCS Gap Data; 5.4 GHz; -10 deg Elevation

Gap Data

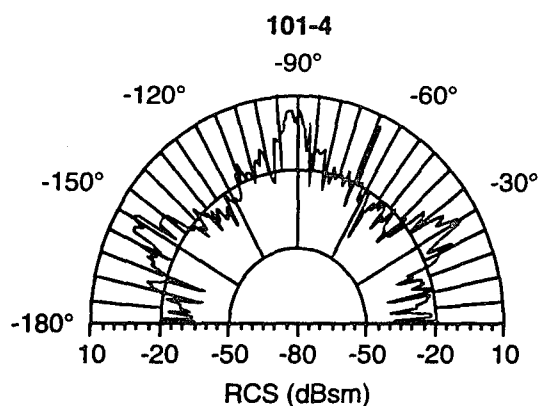
• 9.7 GHz • -10° Elevation • V/V Pol



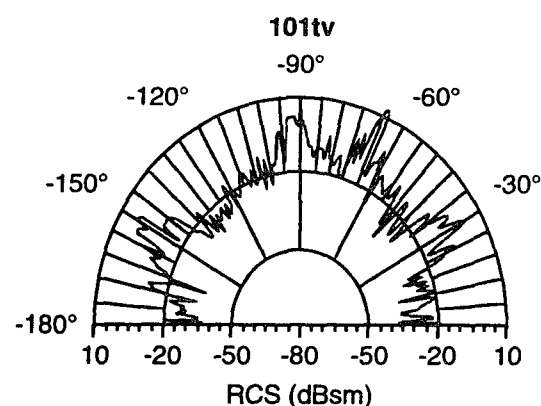
0° to -60° Sector Avg. (dBsm): -21.5
 0° to -60° PCUM50 (dBsm): -22.0
 -60° to -120° Sector Avg. (dBsm): -18.0
 -60° to -120° PCUM50 (dBsm): -20.0
 -120° to -180° Sector Avg. (dBsm): -20.0
 -120° to -180° PCUM50 (dBsm): -20.5



0° to -60° Sector Avg. (dBsm): -16.2
 0° to -60° PCUM50 (dBsm): -16.9
 -60° to -120° Sector Avg. (dBsm): -10.7
 -60° to -120° PCUM50 (dBsm): -11.5
 -120° to -180° Sector Avg. (dBsm): -16.4
 -120° to -180° PCUM50 (dBsm): -19.0



0° to -60° Sector Avg. (dBsm): -21.1
 0° to -60° PCUM50 (dBsm): -22.0
 -60° to -120° Sector Avg. (dBsm): -15.3
 -60° to -120° PCUM50 (dBsm): -16.9
 -120° to -180° Sector Avg. (dBsm): -19.9
 -120° to -180° PCUM50 (dBsm): -20.5

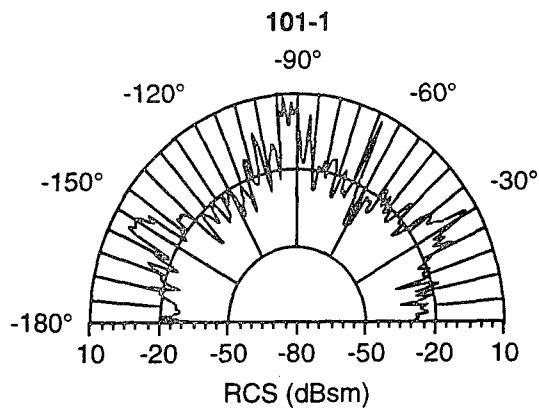


0° to -60° Sector Avg. (dBsm): -18.7
 0° to -60° PCUM50 (dBsm): -19.1
 -60° to -120° Sector Avg. (dBsm): -11.8
 -60° to -120° PCUM50 (dBsm): -13.4
 -120° to -180° Sector Avg. (dBsm): -19.8
 -120° to -180° PCUM50 (dBsm): -21.1

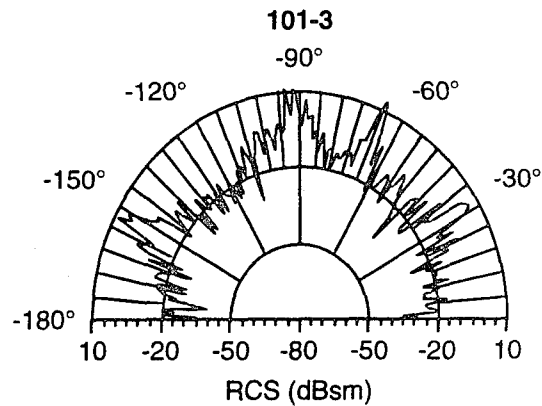
Figure 14-8: RCS Gap Data; 9.7 GHz; -10 deg Elevation

Gap Data

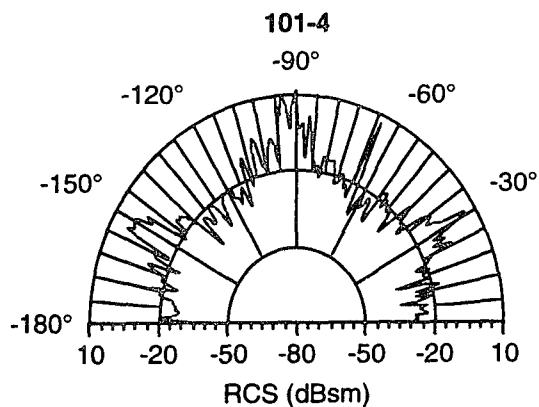
• 16.0 GHz • -10° Elevation • V/V Pol



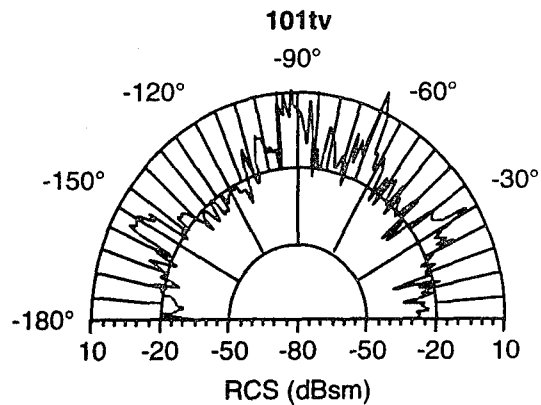
0° to -60° Sector Avg. (dBsm): -19.7
 0° to -60° PCUM50 (dBsm): -21.3
 -60° to -120° Sector Avg. (dBsm): -17.0
 -60° to -120° PCUM50 (dBsm): -18.9
 -120° to -180° Sector Avg. (dBsm): -19.6
 -120° to -180° PCUM50 (dBsm): -20.8



0° to -60° Sector Avg. (dBsm): -16.4
 0° to -60° PCUM50 (dBsm): -17.1
 -60° to -120° Sector Avg. (dBsm): -8.6
 -60° to -120° PCUM50 (dBsm): -10.2
 -120° to -180° Sector Avg. (dBsm): -17.8
 -120° to -180° PCUM50 (dBsm): -18.3



0° to -60° Sector Avg. (dBsm): -19.7
 0° to -60° PCUM50 (dBsm): -21.1
 -60° to -120° Sector Avg. (dBsm): -14.5
 -60° to -120° PCUM50 (dBsm): -16.8
 -120° to -180° Sector Avg. (dBsm): -19.4
 -120° to -180° PCUM50 (dBsm): -20.7

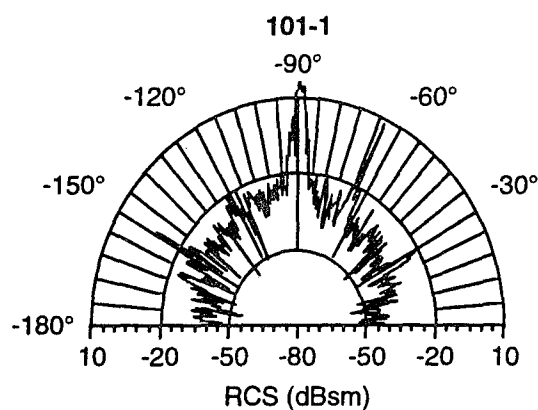


0° to -60° Sector Avg. (dBsm): -17.9
 0° to -60° PCUM50 (dBsm): -19.3
 -60° to -120° Sector Avg. (dBsm): -10.3
 -60° to -120° PCUM50 (dBsm): -12.0
 -120° to -180° Sector Avg. (dBsm): -19.3
 -120° to -180° PCUM50 (dBsm): -21.0

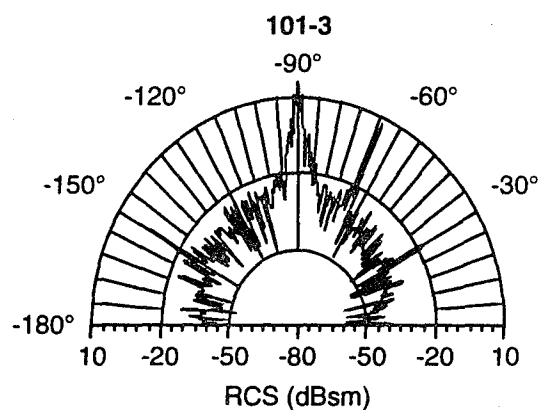
Figure 14-9: RCS Gap Data; 16 GHz; -10 deg Elevation

Deflected Effectors Data (Physical Optics)

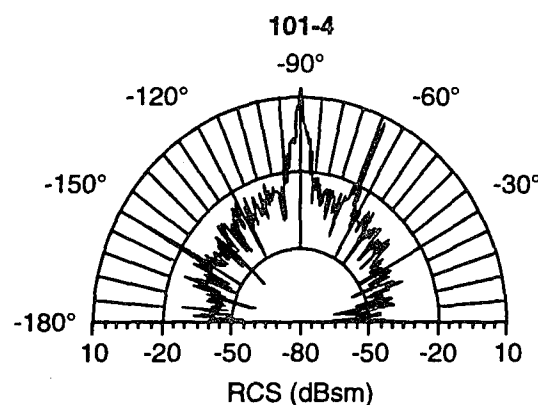
• 5.4 GHz • 0° Elevation



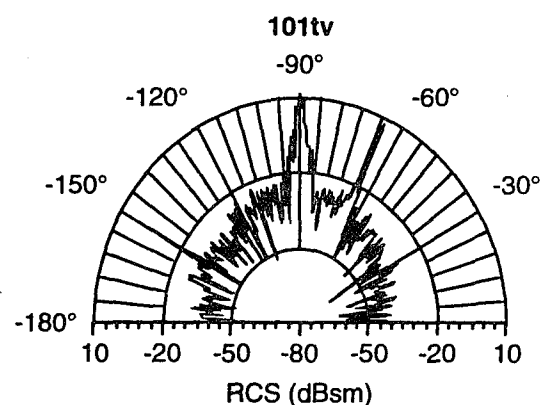
0° to -60° Sector Avg. (dBsm): -38.1
 0° to -60° PCUM50 (dBsm): -37.5
 -60° to -120° Sector Avg. (dBsm): -24.0
 -60° to -120° PCUM50 (dBsm): -26.7
 -120° to -180° Sector Avg. (dBsm): -34.6
 -120° to -180° PCUM50 (dBsm): -34.6



0° to -60° Sector Avg. (dBsm): -39.1
 0° to -60° PCUM50 (dBsm): -39.2
 -60° to -120° Sector Avg. (dBsm): -24.4
 -60° to -120° PCUM50 (dBsm): -26.7
 -120° to -180° Sector Avg. (dBsm): -34.8
 -120° to -180° PCUM50 (dBsm): -35.3



0° to -60° Sector Avg. (dBsm): -40.1
 0° to -60° PCUM50 (dBsm): -39.1
 -60° to -120° Sector Avg. (dBsm): -24.9
 -60° to -120° PCUM50 (dBsm): -27.2
 -120° to -180° Sector Avg. (dBsm): -37.0
 -120° to -180° PCUM50 (dBsm): -36.6

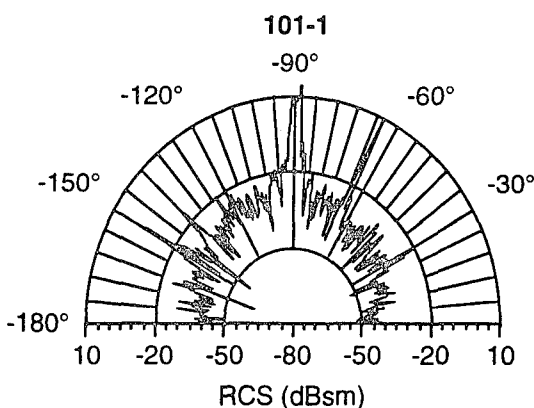


0° to -60° Sector Avg. (dBsm): -40.9
 0° to -60° PCUM50 (dBsm): -39.7
 -60° to -120° Sector Avg. (dBsm): -25.5
 -60° to -120° PCUM50 (dBsm): -27.7
 -120° to -180° Sector Avg. (dBsm): -36.6
 -120° to -180° PCUM50 (dBsm): -36.3

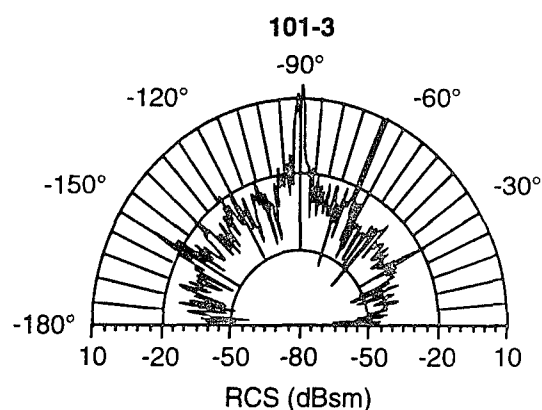
Figure 14-10: RCS Physical Optics Data; 5.4 GHz; 0 deg Elevation

Deflected Effectors Data (Physical Optics)

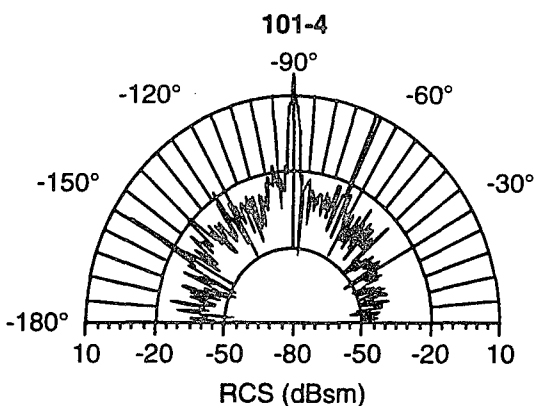
• 9.7 GHz • 0° Elevation



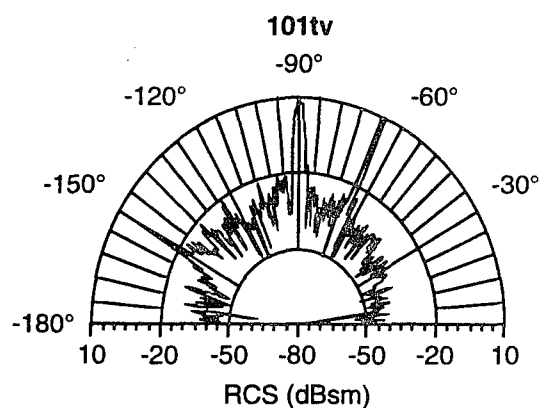
0° to -60° Sector Avg. (dBsm): -38.6
 0° to -60° PCUM50 (dBsm): -38.8
 -60° to -120° Sector Avg. (dBsm): -25.4
 -60° to -120° PCUM50 (dBsm): -27.3
 -120° to -180° Sector Avg. (dBsm): -34.6
 -120° to -180° PCUM50 (dBsm): -34.8



0° to -60° Sector Avg. (dBsm): -39.4
 0° to -60° PCUM50 (dBsm): -38.4
 -60° to -120° Sector Avg. (dBsm): -25.3
 -60° to -120° PCUM50 (dBsm): -26.3
 -120° to -180° Sector Avg. (dBsm): -33.1
 -120° to -180° PCUM50 (dBsm): -32.9



0° to -60° Sector Avg. (dBsm): -41.1
 0° to -60° PCUM50 (dBsm): -41.4
 -60° to -120° Sector Avg. (dBsm): -26.4
 -60° to -120° PCUM50 (dBsm): -28.1
 -120° to -180° Sector Avg. (dBsm): -35.5
 -120° to -180° PCUM50 (dBsm): -35.5

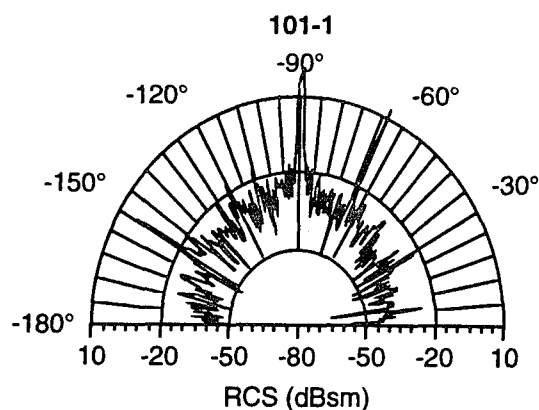


0° to -60° Sector Avg. (dBsm): -40.8
 0° to -60° PCUM50 (dBsm): -40.3
 -60° to -120° Sector Avg. (dBsm): -28.6
 -60° to -120° PCUM50 (dBsm): -31.0
 -120° to -180° Sector Avg. (dBsm): -35.0
 -120° to -180° PCUM50 (dBsm): -34.6

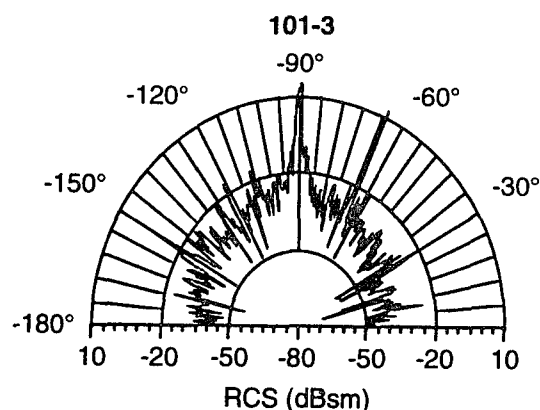
Figure 14-11: RCS Physical Optics Data; 9.7 GHz; 0 deg Elevation

Deflected Effectors Data (Physical Optics)

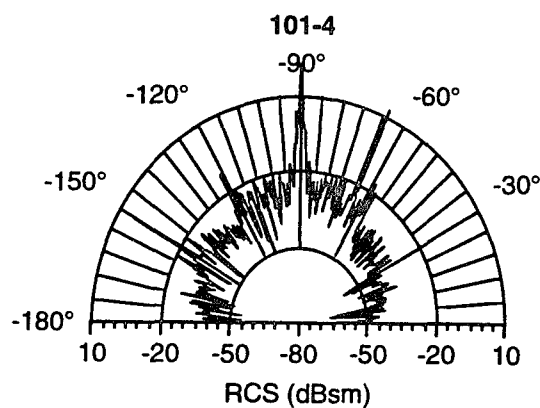
• 16.0 GHz • 0° Elevation



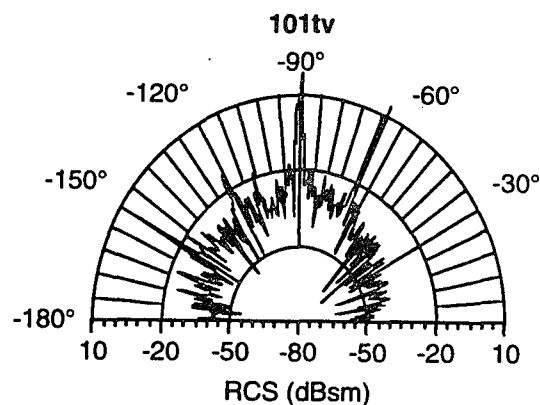
0° to -60° Sector Avg. (dBsm): -38.5
 0° to -60° PCUM50 (dBsm): -37.5
 -60° to -120° Sector Avg. (dBsm): -26.2
 -60° to -120° PCUM50 (dBsm): -27.9
 -120° to -180° Sector Avg. (dBsm): -33.7
 -120° to -180° PCUM50 (dBsm): -33.7



0° to -60° Sector Avg. (dBsm): -39.1
 0° to -60° PCUM50 (dBsm): -38.5
 -60° to -120° Sector Avg. (dBsm): -25.5
 -60° to -120° PCUM50 (dBsm): -27.3
 -120° to -180° Sector Avg. (dBsm): -32.7
 -120° to -180° PCUM50 (dBsm): -33.7



0° to -60° Sector Avg. (dBsm): -41.8
 0° to -60° PCUM50 (dBsm): -41.8
 -60° to -120° Sector Avg. (dBsm): -25.5
 -60° to -120° PCUM50 (dBsm): -26.2
 -120° to -180° Sector Avg. (dBsm): -35.3
 -120° to -180° PCUM50 (dBsm): -34.9

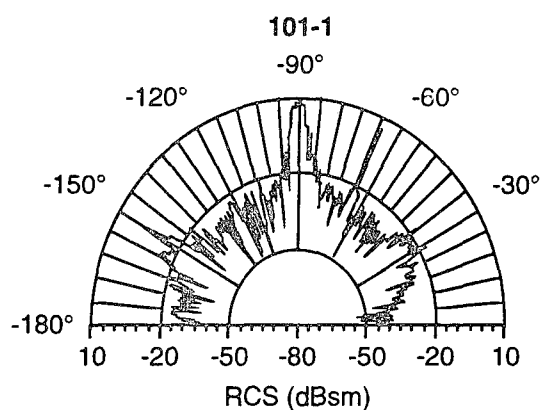


0° to -60° Sector Avg. (dBsm): -43.9
 0° to -60° PCUM50 (dBsm): -42.5
 -60° to -120° Sector Avg. (dBsm): -27.4
 -60° to -120° PCUM50 (dBsm): -29.5
 -120° to -180° Sector Avg. (dBsm): -35.2
 -120° to -180° PCUM50 (dBsm): -35.2

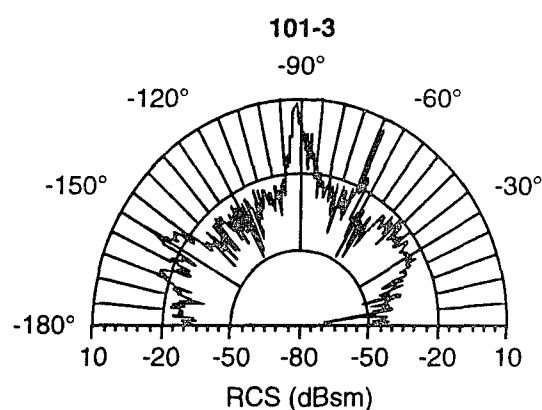
Figure 14-12: RCS Physical Optics Data; 16 GHz; 0 deg Elevation

Deflected Effectors Data (Physical Optics)

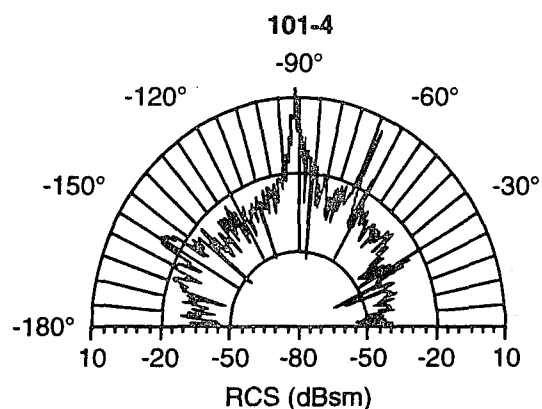
• 5.4 GHz • 10° Elevation



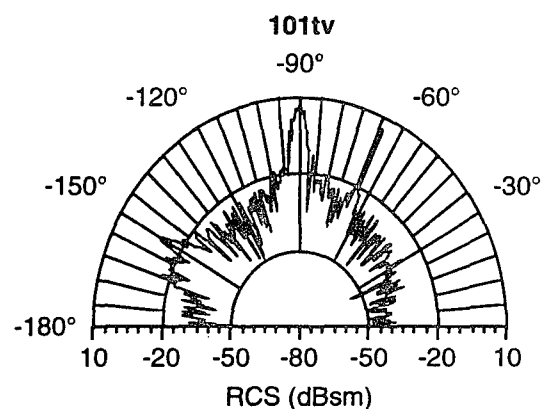
0° to -60° Sector Avg. (dBsm): -31.6
 0° to -60° PCUM50 (dBsm): -30.4
 -60° to -120° Sector Avg. (dBsm): -23.5
 -60° to -120° PCUM50 (dBsm): -26.0
 -120° to -180° Sector Avg. (dBsm): -27.0
 -120° to -180° PCUM50 (dBsm): -26.7



0° to -60° Sector Avg. (dBsm): -33.8
 0° to -60° PCUM50 (dBsm): -32.0
 -60° to -120° Sector Avg. (dBsm): -23.7
 -60° to -120° PCUM50 (dBsm): -25.4
 -120° to -180° Sector Avg. (dBsm): -26.6
 -120° to -180° PCUM50 (dBsm): -26.8



0° to -60° Sector Avg. (dBsm): -37.7
 0° to -60° PCUM50 (dBsm): -37.8
 -60° to -120° Sector Avg. (dBsm): -24.2
 -60° to -120° PCUM50 (dBsm): -25.8
 -120° to -180° Sector Avg. (dBsm): -29.9
 -120° to -180° PCUM50 (dBsm): -29.4

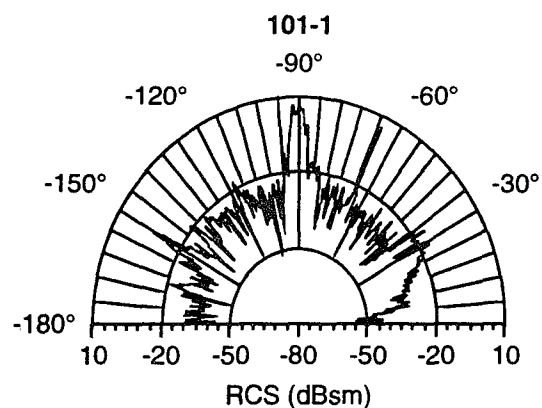


0° to -60° Sector Avg. (dBsm): -38.0
 0° to -60° PCUM50 (dBsm): -37.8
 -60° to -120° Sector Avg. (dBsm): -23.3
 -60° to -120° PCUM50 (dBsm): -24.2
 -120° to -180° Sector Avg. (dBsm): -28.3
 -120° to -180° PCUM50 (dBsm): -28.1

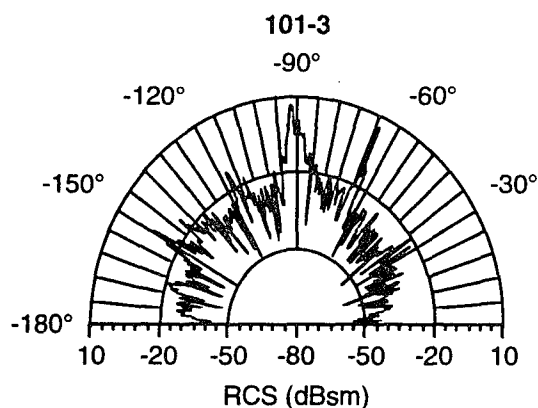
Figure 14-13: RCS Physical Optics Data; 5.4 GHz; 10 deg Elevation

Deflected Effectors Data (Physical Optics)

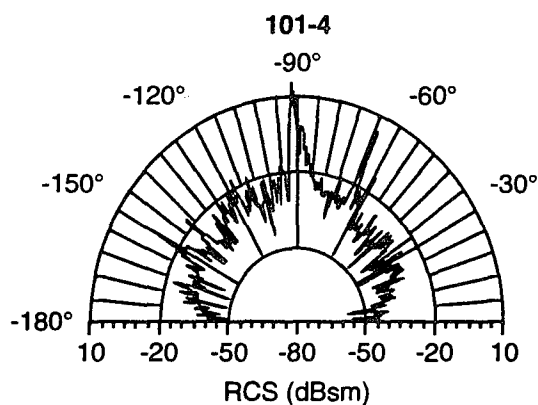
• 9.7 GHz • 10° Elevation



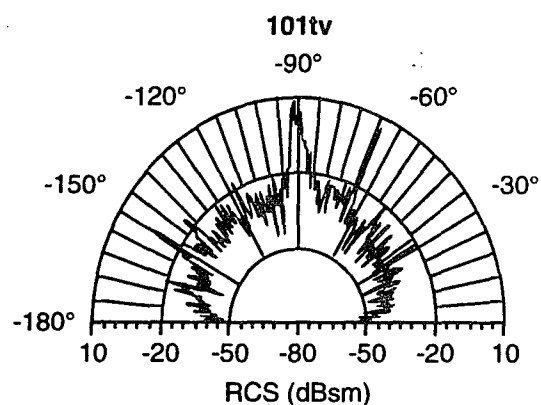
0° to -60° Sector Avg. (dBsm): -31.4
 0° to -60° PCUM50 (dBsm): -30.8
 -60° to -120° Sector Avg. (dBsm): -23.9
 -60° to -120° PCUM50 (dBsm): -25.4
 -120° to -180° Sector Avg. (dBsm): -30.0
 -120° to -180° PCUM50 (dBsm): -29.7



0° to -60° Sector Avg. (dBsm): -38.4
 0° to -60° PCUM50 (dBsm): -38.2
 -60° to -120° Sector Avg. (dBsm): -22.8
 -60° to -120° PCUM50 (dBsm): -24.7
 -120° to -180° Sector Avg. (dBsm): -29.0
 -120° to -180° PCUM50 (dBsm): -27.9



0° to -60° Sector Avg. (dBsm): -37.4
 0° to -60° PCUM50 (dBsm): -36.9
 -60° to -120° Sector Avg. (dBsm): -22.6
 -60° to -120° PCUM50 (dBsm): -24.9
 -120° to -180° Sector Avg. (dBsm): -32.0
 -120° to -180° PCUM50 (dBsm): -32.0

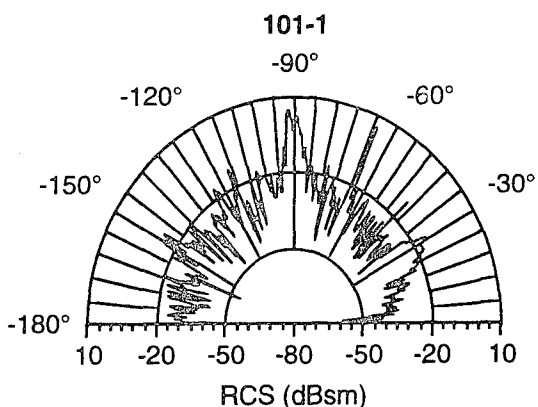


0° to -60° Sector Avg. (dBsm): -37.7
 0° to -60° PCUM50 (dBsm): -37.4
 -60° to -120° Sector Avg. (dBsm): -24.5
 -60° to -120° PCUM50 (dBsm): -26.3
 -120° to -180° Sector Avg. (dBsm): -31.6
 -120° to -180° PCUM50 (dBsm): -32.2

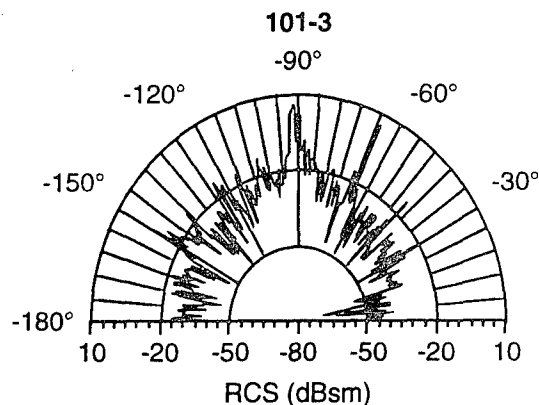
Figure 14-14: RCS Physical Optics Data; 9.7 GHz; 10 deg Elevation

Deflected Effectors Data (Physical Optics)

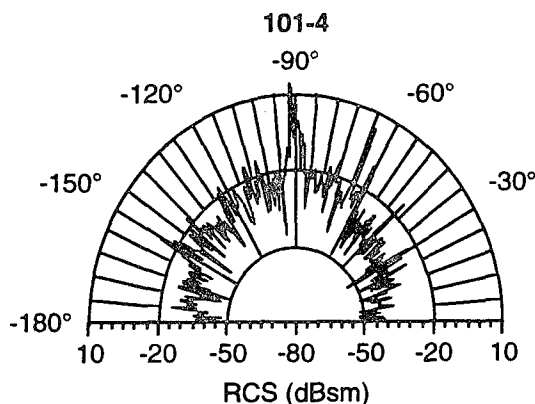
• 16.0 GHz • 10° Elevation



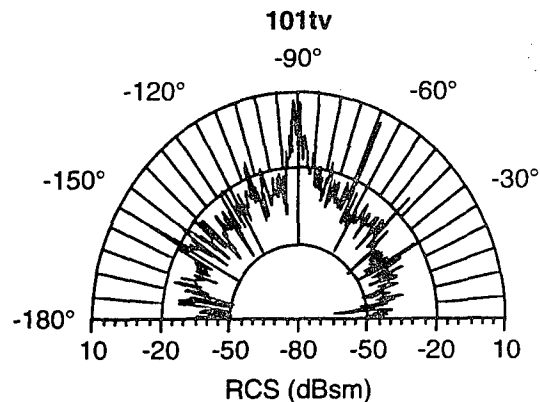
0° to -60° Sector Avg. (dBsm): -31.7
 0° to -60° PCUM50 (dBsm): -31.5
 -60° to -120° Sector Avg. (dBsm): -23.3
 -60° to -120° PCUM50 (dBsm): -25.3
 -120° to -180° Sector Avg. (dBsm): -29.6
 -120° to -180° PCUM50 (dBsm): -29.5



0° to -60° Sector Avg. (dBsm): -38.8
 0° to -60° PCUM50 (dBsm): -38.3
 -60° to -120° Sector Avg. (dBsm): -22.1
 -60° to -120° PCUM50 (dBsm): -22.8
 -120° to -180° Sector Avg. (dBsm): -29.1
 -120° to -180° PCUM50 (dBsm): -28.1



0° to -60° Sector Avg. (dBsm): -38.4
 0° to -60° PCUM50 (dBsm): -37.6
 -60° to -120° Sector Avg. (dBsm): -22.2
 -60° to -120° PCUM50 (dBsm): -22.7
 -120° to -180° Sector Avg. (dBsm): -31.4
 -120° to -180° PCUM50 (dBsm): -31.1

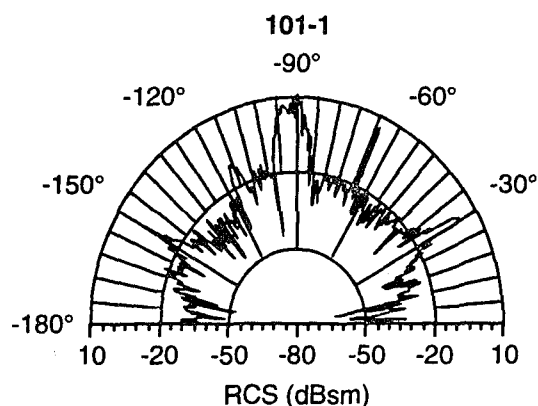


0° to -60° Sector Avg. (dBsm): -38.1
 0° to -60° PCUM50 (dBsm): -37.3
 -60° to -120° Sector Avg. (dBsm): -24.6
 -60° to -120° PCUM50 (dBsm): -26.3
 -120° to -180° Sector Avg. (dBsm): -32.2
 -120° to -180° PCUM50 (dBsm): -31.7

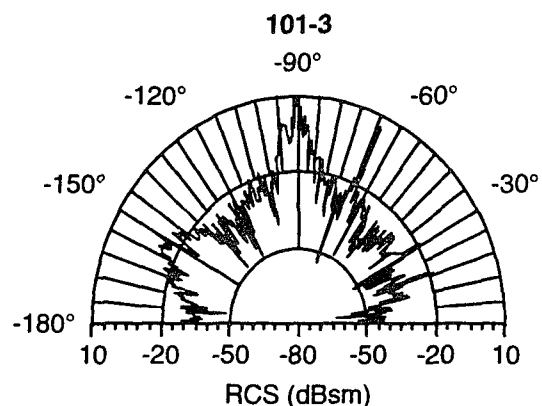
Figure 14-15: RCS Physical Optics Data; 16 GHz; 10 deg Elevation

Deflected Effectors Data (Physical Optics)

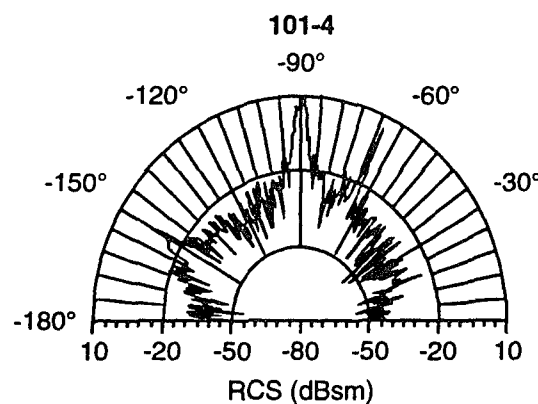
• 5.4 GHz • -10° Elevation



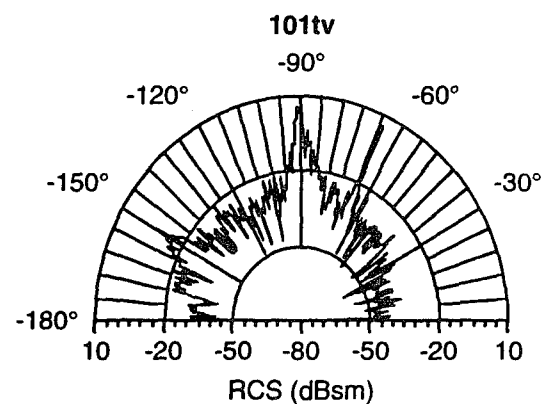
0° to -60° Sector Avg. (dBsm): -27.5
 0° to -60° PCUM50 (dBsm): -26.0
 -60° to -120° Sector Avg. (dBsm): -16.6
 -60° to -120° PCUM50 (dBsm): -20.0
 -120° to -180° Sector Avg. (dBsm): -29.2
 -120° to -180° PCUM50 (dBsm): -28.9



0° to -60° Sector Avg. (dBsm): -36.0
 0° to -60° PCUM50 (dBsm): -35.1
 -60° to -120° Sector Avg. (dBsm): -20.2
 -60° to -120° PCUM50 (dBsm): -22.7
 -120° to -180° Sector Avg. (dBsm): -27.2
 -120° to -180° PCUM50 (dBsm): -26.6



0° to -60° Sector Avg. (dBsm): -38.1
 0° to -60° PCUM50 (dBsm): -37.3
 -60° to -120° Sector Avg. (dBsm): -23.4
 -60° to -120° PCUM50 (dBsm): -25.5
 -120° to -180° Sector Avg. (dBsm): -30.2
 -120° to -180° PCUM50 (dBsm): -30.1

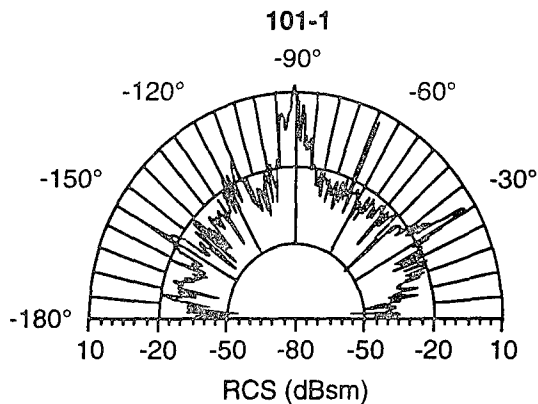


0° to -60° Sector Avg. (dBsm): -40.4
 0° to -60° PCUM50 (dBsm): -39.9
 -60° to -120° Sector Avg. (dBsm): -25.2
 -60° to -120° PCUM50 (dBsm): -26.9
 -120° to -180° Sector Avg. (dBsm): -28.6
 -120° to -180° PCUM50 (dBsm): -29.1

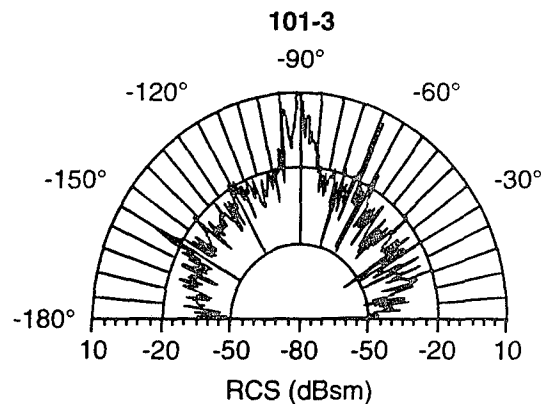
Figure 14-16: RCS Physical Optics Data; 5.4 GHz; -10 deg Elevation

Deflected Effectors Data (Physical Optics)

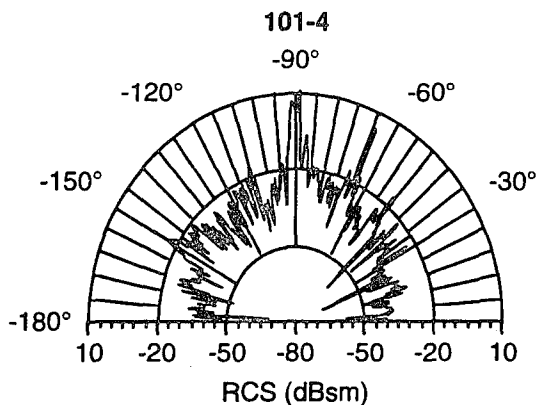
• 9.7 GHz • -10° Elevation



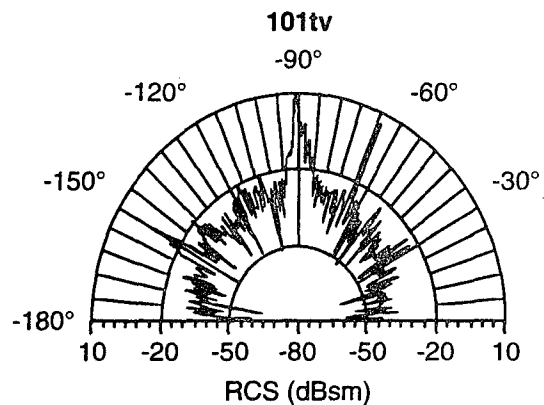
0° to -60° Sector Avg. (dBsm): -27.1
 0° to -60° PCUM50 (dBsm): -26.5
 -60° to -120° Sector Avg. (dBsm): -19.7
 -60° to -120° PCUM50 (dBsm): -22.8
 -120° to -180° Sector Avg. (dBsm): -30.3
 -120° to -180° PCUM50 (dBsm): -29.9



0° to -60° Sector Avg. (dBsm): -35.2
 0° to -60° PCUM50 (dBsm): -34.9
 -60° to -120° Sector Avg. (dBsm): -20.0
 -60° to -120° PCUM50 (dBsm): -21.9
 -120° to -180° Sector Avg. (dBsm): -30.6
 -120° to -180° PCUM50 (dBsm): -30.7



0° to -60° Sector Avg. (dBsm): -36.1
 0° to -60° PCUM50 (dBsm): -36.5
 -60° to -120° Sector Avg. (dBsm): -23.2
 -60° to -120° PCUM50 (dBsm): -24.4
 -120° to -180° Sector Avg. (dBsm): -32.9
 -120° to -180° PCUM50 (dBsm): -33.2

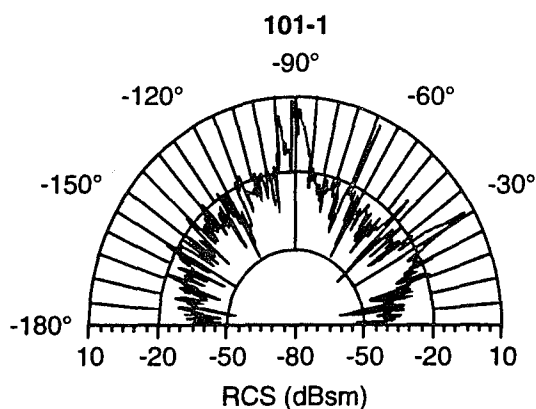


0° to -60° Sector Avg. (dBsm): -40.2
 0° to -60° PCUM50 (dBsm): -40.5
 -60° to -120° Sector Avg. (dBsm): -25.1
 -60° to -120° PCUM50 (dBsm): -26.5
 -120° to -180° Sector Avg. (dBsm): -33.7
 -120° to -180° PCUM50 (dBsm): -33.1

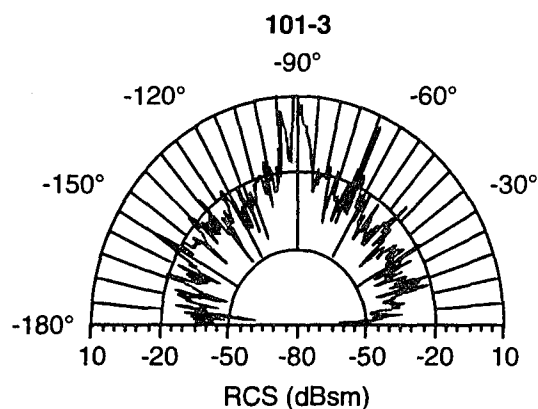
Figure 14-17: RCS Physical Optics Data; 9.7 GHz; -10 deg Elevation

Deflected Effectors Data (Physical Optics)

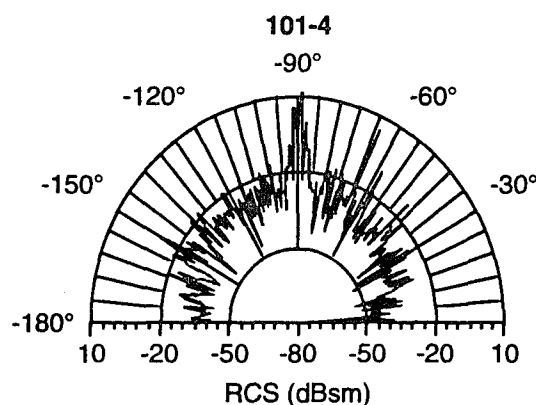
• 16.0 GHz • -10° Elevation



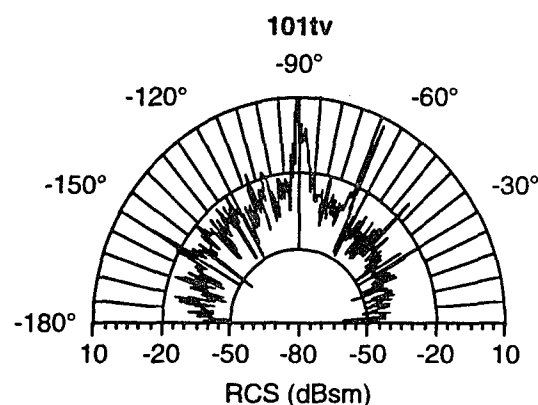
0° to -60° Sector Avg. (dBsm): -29.4
 0° to -60° PCUM50 (dBsm): -28.2
 -60° to -120° Sector Avg. (dBsm): -21.1
 -60° to -120° PCUM50 (dBsm): -22.3
 -120° to -180° Sector Avg. (dBsm): -30.5
 -120° to -180° PCUM50 (dBsm): -30.0



0° to -60° Sector Avg. (dBsm): -33.7
 0° to -60° PCUM50 (dBsm): -33.2
 -60° to -120° Sector Avg. (dBsm): -19.9
 -60° to -120° PCUM50 (dBsm): -21.2
 -120° to -180° Sector Avg. (dBsm): -30.1
 -120° to -180° PCUM50 (dBsm): -29.1



0° to -60° Sector Avg. (dBsm): -35.6
 0° to -60° PCUM50 (dBsm): -35.7
 -60° to -120° Sector Avg. (dBsm): -24.2
 -60° to -120° PCUM50 (dBsm): -24.9
 -120° to -180° Sector Avg. (dBsm): -31.0
 -120° to -180° PCUM50 (dBsm): -30.6



0° to -60° Sector Avg. (dBsm): -40.1
 0° to -60° PCUM50 (dBsm): -40.9
 -60° to -120° Sector Avg. (dBsm): -26.5
 -60° to -120° PCUM50 (dBsm): -28.3
 -120° to -180° Sector Avg. (dBsm): -32.9
 -120° to -180° PCUM50 (dBsm): -31.9

Figure 14-18: RCS Physical Optics Data; 16 GHz; -10 deg Elevation

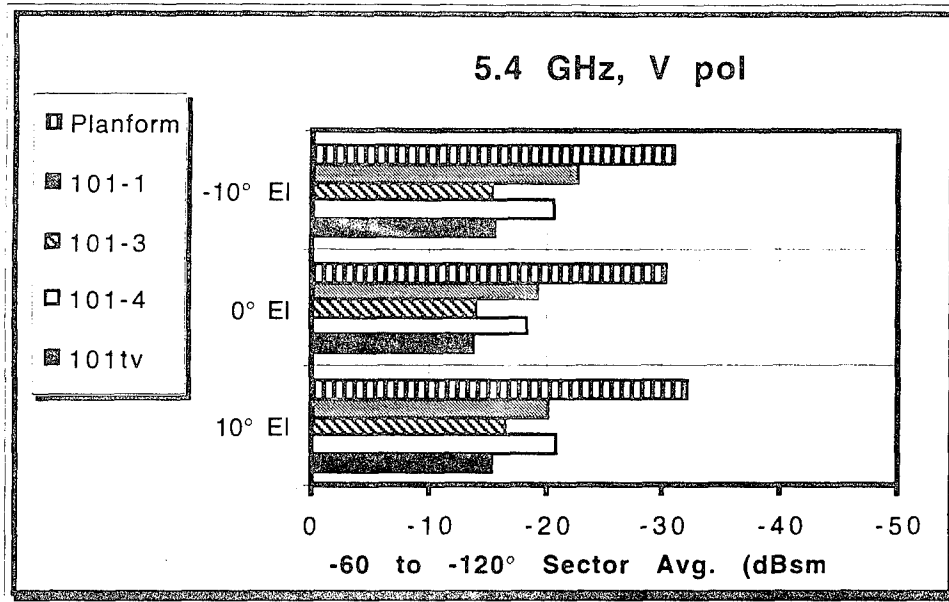


Figure 14-19: Beam Sector Averages; 5.4 GHz; Gap Effects

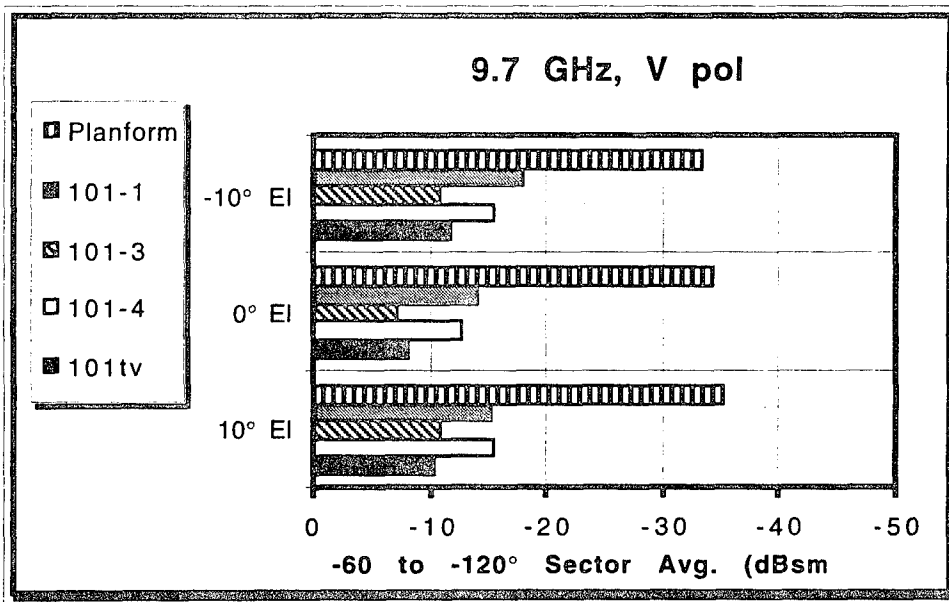


Figure 14-20: Beam Sector Averages; 9.7 GHz; Gap Effects

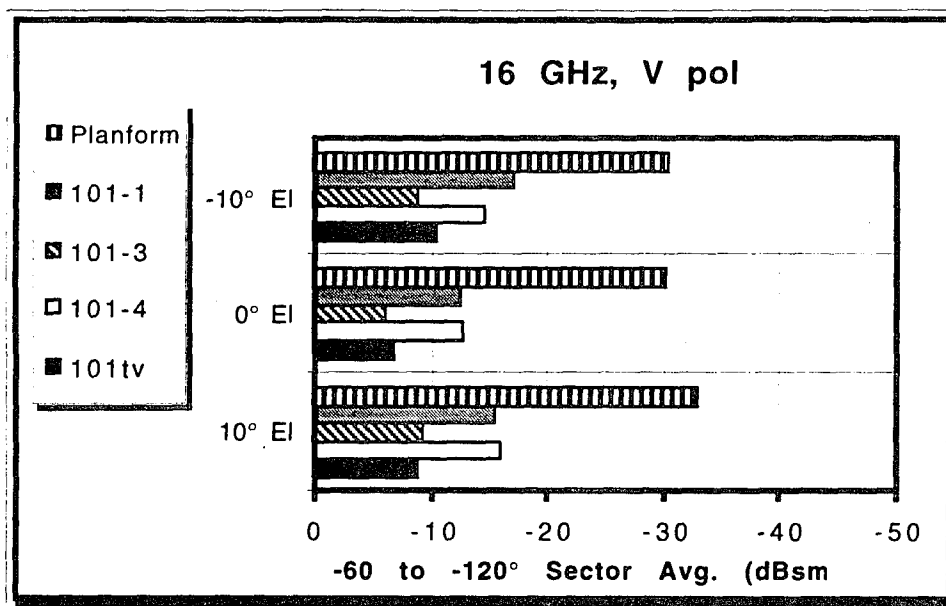


Figure 14-21: Beam Sector Averages; 16 GHz; Gap Effects

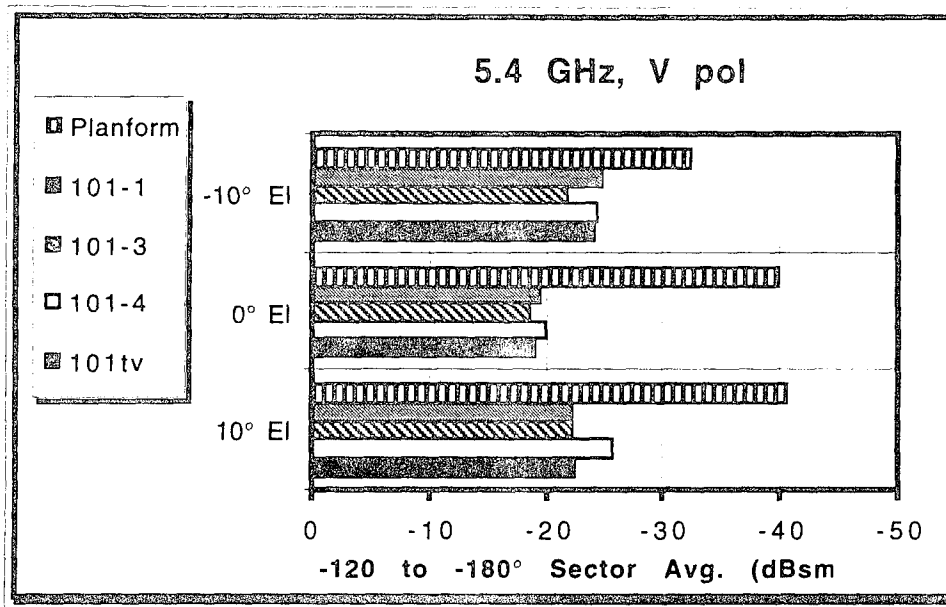


Figure 14-22: Aft Sector Averages; 5.4 GHz; Gap Effects

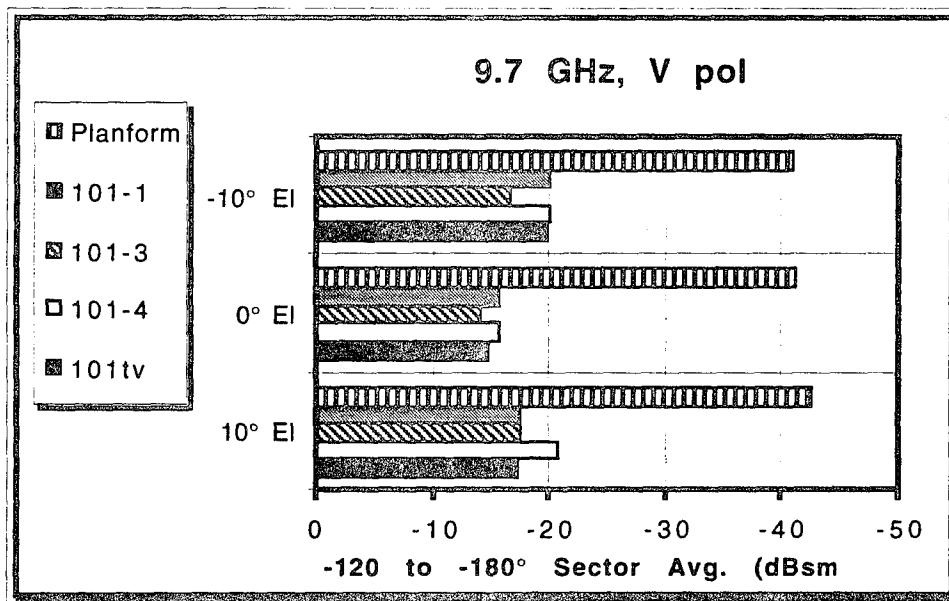


Figure 14-23: Aft Sector Averages; 9.7 GHz; Gap Effects

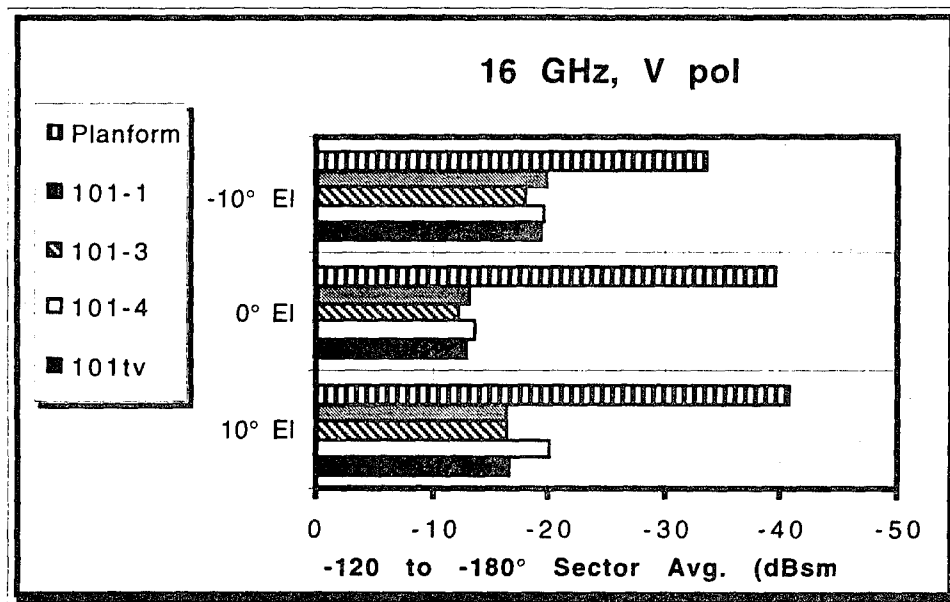


Figure 14-24: Aft Sector Averages; 16 GHz; Gap Effects

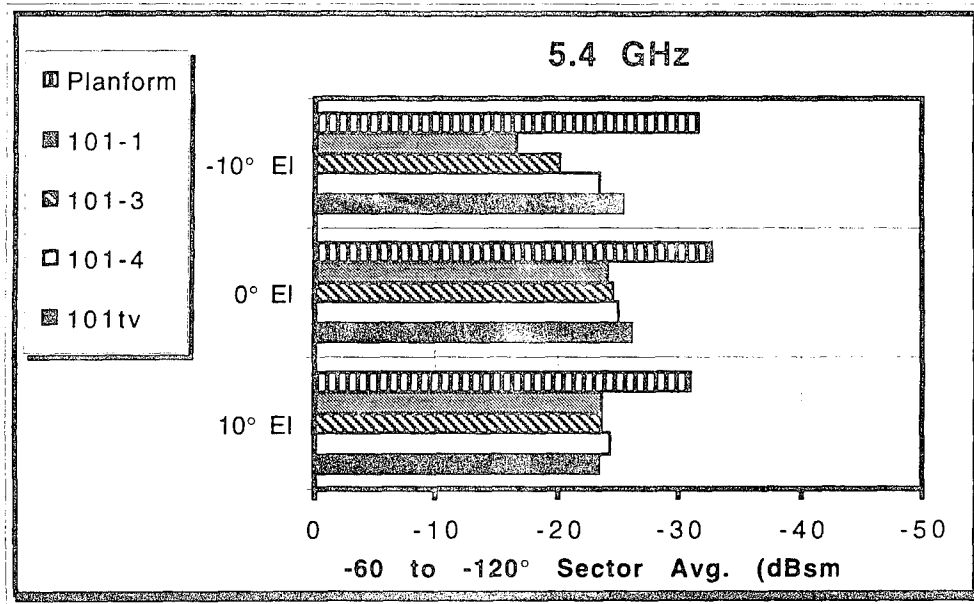


Figure 14-25: Beam Sector Averages; 5.4 GHz; Deflected Controls Effects

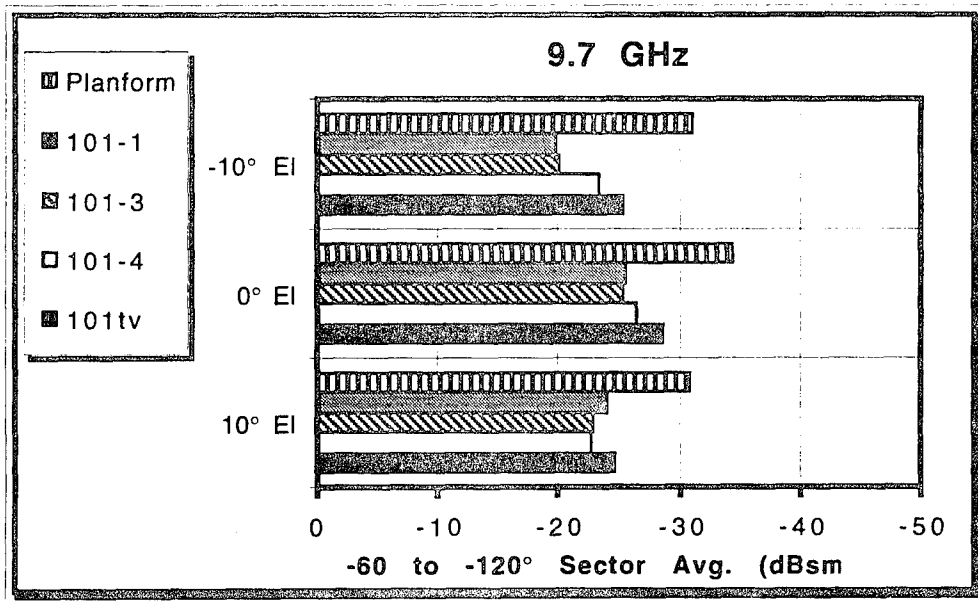


Figure 14-26: Beam Sector Averages; 9.7 GHz; Deflected Controls Effects

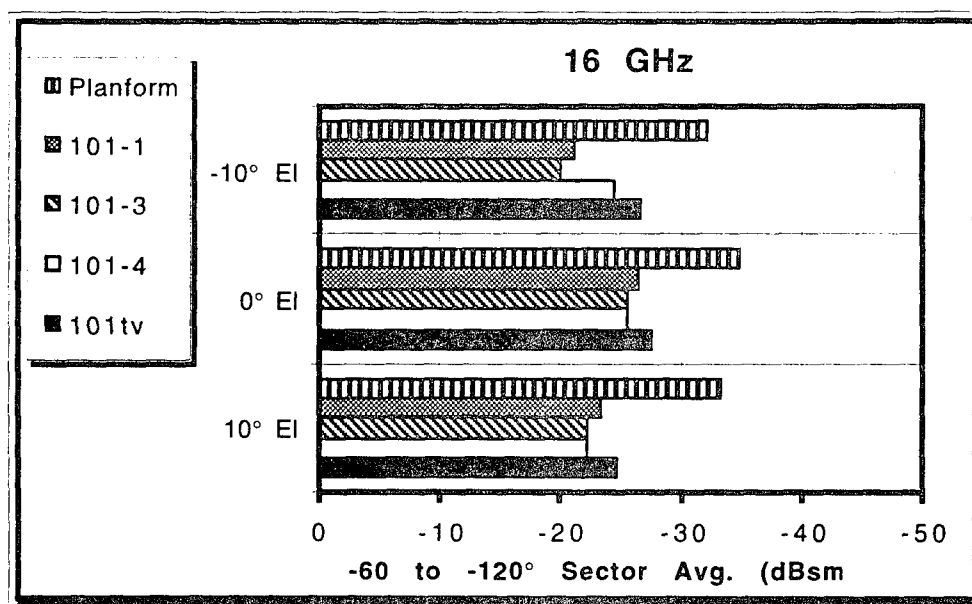


Figure 14-27: Beam Sector Averages; 16 GHz; Deflected Controls Effects

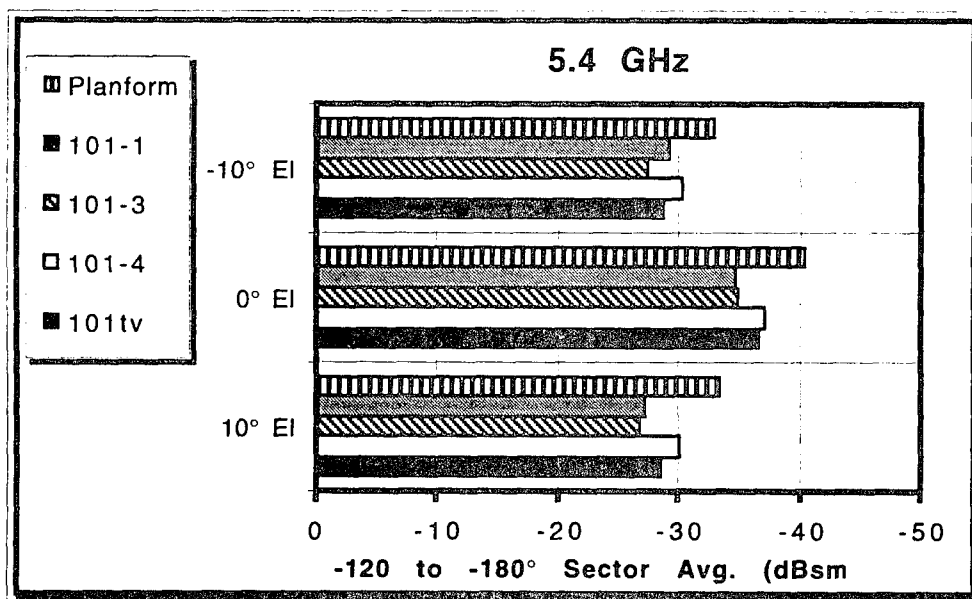


Figure 14-28: Aft Sector Averages; 5.4 GHz; Deflected Controls Effects

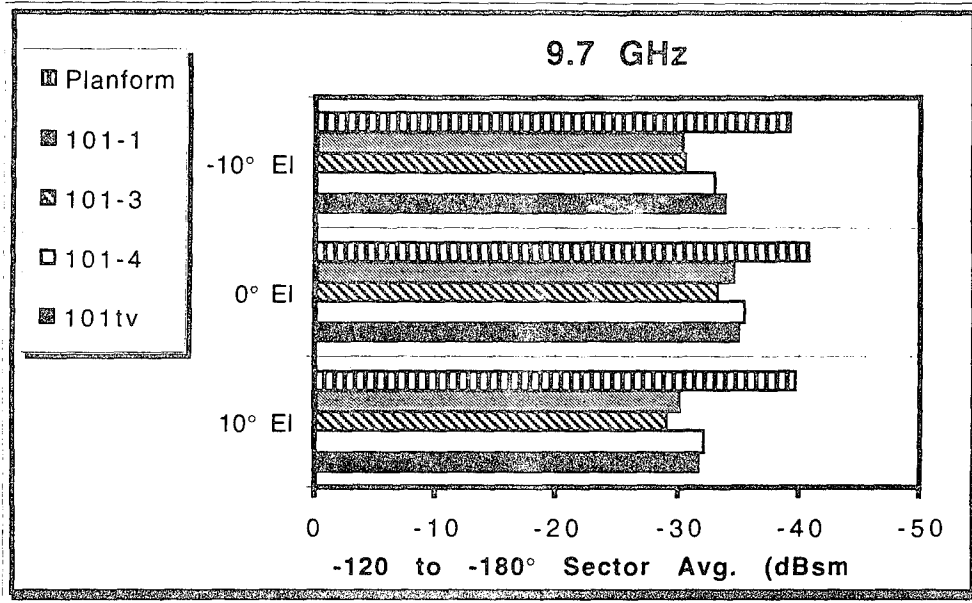


Figure 14-29: Aft Sector Averages; 9.7 GHz; Deflected Controls Effects

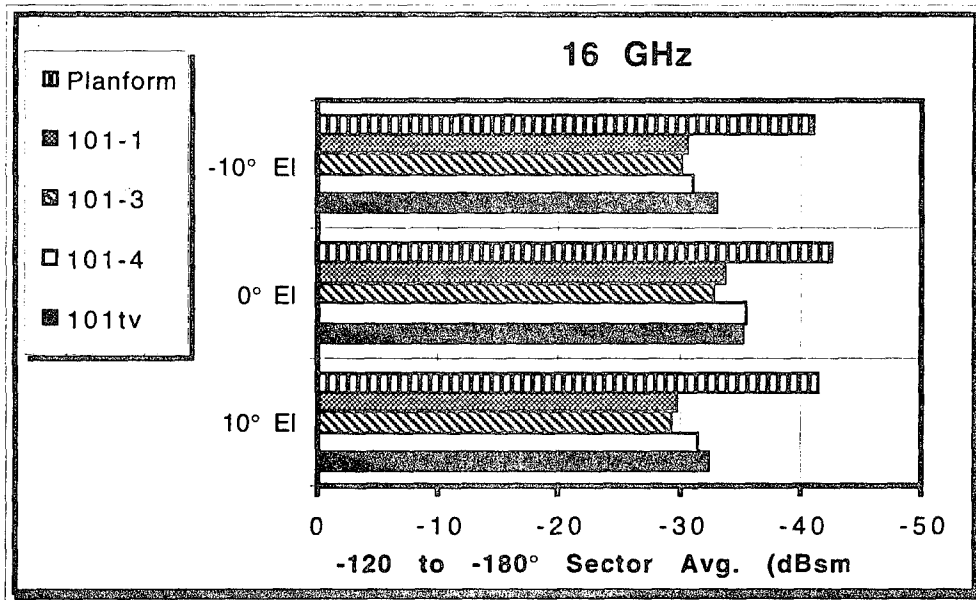


Figure 14-30: Aft Sector Averages; 16 GHz; Deflected Controls Effects



Air Force Research Laboratory
Technical Information Division-STINFO

WRIGHT-PATTERSON AFB, OH

STINFO/Technical Editing Section
ATTN: Joe Burke
Det 1 AFRL/WST (STINFO)
Bldg 640, Rm 60
2331 12th St
WPAFB OH 45433-7950

Tel.# 937-255-5766, DSN 785-5766
FAX# 937-255-5383, DSN 785-5383

Email: joseph.burke@ws.wpafb.af.mil

FAX COVER SHEET

TO:

NAME: Bill Bush
ADDRESS: DTIC/OC
VOICE: 427-0011
FAX: ~~427-9075~~ 9244

PAGE 1 OF 3

MESSAGE/COMMENTS:

Please make the following changes
to rpts.

DATE: 9-15-99 TIME 1100



DEPARTMENT OF THE AIR FORCE
AIR FORCE RESEARCH LABORATORY
WRIGHT-PATTERSON AIR FORCE BASE OHIO 45433

9-14-99

MEMORANDUM FOR: Defense Technical Information Center/OMI
8725 John J. Kingman Rd, Suite 0944
Ft Belvoir, VA 22060-6218

FROM: Det 1 AFRL/WST
Bldg 640 Rm 60
2331 12th Street
Wright-Patterson AFB OH 45433-7950

SUBJECT: Notice of Changes in Technical Report(s) (see below)

Please change subject report(s) as follows:

The following have all been approved for public release, distribution is unlimited:

AFWAL-TR-83-3072,
WRDC-TR-90-3081,
WL-TR-96-3043,
WL-TR-96-3074,
WL-TR-97-3059,

AD B955 265✓
AD B 166 585✓

AD B212 813 - OK ST-A

~~AD B 212 361 ST-A~~

AD B 232 172 ✓ ~~OK ST-A~~

B212361

Joseph A. Burke
JOSEPH A. BURKE, Team Leader
STINFO and Technical Editing
Technical Information Division